



Universiteit  
Leiden  
The Netherlands

## Monitoring the immune responses to vaccination and pertussis: bordetella pertussis and beyond

Diks, A.M.

### Citation

Diks, A. M. (2022, December 21). *Monitoring the immune responses to vaccination and pertussis: bordetella pertussis and beyond*. Retrieved from <https://hdl.handle.net/1887/3503582>

Version: Publisher's Version

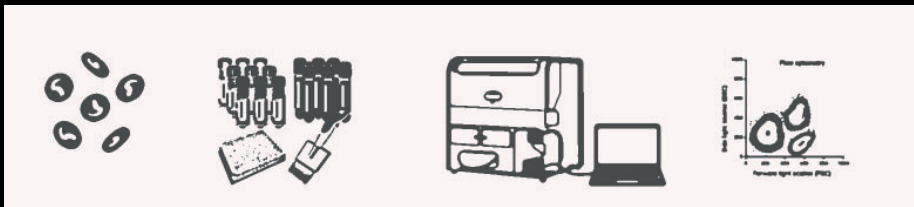
License: [Licence agreement concerning inclusion of doctoral thesis in the Institutional Repository of the University of Leiden](#)

Downloaded from: <https://hdl.handle.net/1887/3503582>

**Note:** To cite this publication please use the final published version (if applicable).

# Monitoring the immune responses to vaccination and infection: *Bordetella pertussis* and beyond

Annieck M. Diks



## **Stellingen behorende bij het proefschrift: Monitoring the immune responses to vaccination and infection – *Bordetella pertussis* and beyond**

1. To ensure data quality and reproducibility, it is important that protocols and phenotypic descriptions are standardized between different laboratories & clinical sites (this thesis).
2. Understanding the cellular mechanisms underlying protective immunity will help guiding future vaccine design (this thesis).
3. Mucosal immunity and blocking of transmission should always be considered when evaluating the efficacy of vaccination against an infectious respiratory pathogen (this thesis).
4. Before we can decide whether PLC $\gamma$ 2 – or any other protein- is a suitable therapeutic target, we should understand how much we can influence its functional range (e.g. by stabilizing or amplifying the signaling) without causing side effects (this thesis).
5. The in- and exclusion criteria of a vaccination cohort can heavily influence the final results and should therefore be carefully considered and described in the study protocol.
6. Certain infections (e.g. helminth infections) can influence vaccination responsiveness; therefore, the environmental triggers of the target population should be kept in mind during the development and evaluation of a vaccine candidate.
7. To improve vaccine-induced immunity, we should consider making the vaccination route more similar to the infection route.
8. Adding exploratory methods to the established ‘standard’ methods may ultimately speed up the search for new (surrogate) biomarkers.
9. The moment you stop learning is the moment your knowledge becomes outdated.
10. Vaak bu’j te bang (a common saying in the “Achterhoek” region of the Netherlands).  
Both in Science and ‘real life’, it is a lot easier to stay within your comfort zone. I believe that we progress in science and real life by working on (and over) the edge of our comfort zones.
11. The importance of social inclusivity and contact with nature is reflected by their positive association with reduced feelings of loneliness (Hammoud et al., Scientific Reports, 2021, 11:24134).

MONITORING THE IMMUNE RESPONSES TO  
VACCINATION AND INFECTION-  
*BORDETELLA PERTUSSIS* AND BEYOND

Annieck Margo Diks



Printed by: Universitair Facilitair Bedrijf [Universiteit Leiden]  
Cover: Design by A.M. Diks  
Basis for cover figures created in Biorender.com

© A.M. Diks, 2022

All rights reserved. No parts of this thesis may be reproduced in any matter or means without prior written permission from the author.

Monitoring the immune responses to vaccination  
and infection-  
*Bordetella pertussis* and beyond

**Proefschrift**

ter verkrijging van  
de graad van doctor aan de Universiteit Leiden,  
op gezag van rector magnificus prof.dr.ir. H. Bijl,  
volgens besluit van het college voor promoties  
te verdedigen op woensdag 21 december 2022  
klokke 10:00 uur

door

**Annieck Margo Diks**

geboren te Doetinchem  
in 1992

Promotor: Prof. dr. J.J.M. van Dongen

Copromotor: Dr. M.A. Berkowska

Overige leden: Prof. dr. A. Orfao, University of Salamanca (Spain)

Prof. dr. M. Roestenberg

Prof. dr. N.A. Bos, University of Groningen

Dr. H. Holstege, Amsterdam UMC

voor papa en mama



# Table of contents

|                    |  |     |
|--------------------|--|-----|
| <b>Chapter 1</b>   | General Introduction   | 9   |
| <b>Chapter 2</b>   | The importance of standardization in the pre- and post-analytical phase for reliable immune monitoring in clinical trials        |     |
| <b>Chapter 2.1</b> | Impact of blood storage and sample handling on quality of high dimensional flow cytometric data in multicenter clinical research | 41  |
| <b>Chapter 2.2</b> | Improved standardization of flow cytometry diagnostic screening of primary immunodeficiency by software-based automated gating   | 67  |
| <b>Chapter 3</b>   | Monitoring immune responses to <i>Bordetella pertussis</i>   |     |
| <b>Chapter 3.1</b> | Highly sensitive flow cytometry allows monitoring of changes in circulating immune cells in blood after Tdap booster vaccination | 89  |
| <b>Chapter 3.2</b> | Age and primary vaccination background influence the plasma cell response to pertussis booster vaccination                       | 115 |
| <b>Chapter 3.3</b> | Longitudinal dynamics of human B-cell response at single-cell level in response to Tdap vaccination                              | 147 |
| <b>Chapter 3.4</b> | Distinct cellular kinetics in participants protected from colonization upon <i>B.pertussis</i> challenge                         | 177 |
| <b>Chapter 4</b>   | <i>PLCG2</i> variant p.P522R -associated with healthy aging- may reduce the aging of the human immune system                     | 209 |
| <b>Chapter 5</b>   | General Discussion   | 239 |
| <b>Appendices</b>  | Appendix 1   | 262 |
|                    | Appendix 2   | 274 |
|                    | Summary  | 281 |
|                    | Samenvatting   | 284 |
|                    | Curriculum vitae   | 288 |
|                    | List of publications   | 289 |
|                    | Acknowledgements   | 290 |



# **Chapter 1**

## **General Introduction**

NB: parts of this chapter have been published in 'B-cell immunophenotyping to predict vaccination outcome in the immunocompromised - a systematic review' by Diks & Overduin et al.[1]





### 1.1 The human immune system– general overview

The primary task of our immune system is to protect our body from pathogens. To do so, the immune system utilizes several lines of defense. The first line of defense comprises physical and chemical barriers, such as the epithelium, mucosal surfaces, and secreted antimicrobial products (**Figure 1**). The next line of defense is the innate immune system, which consists of blood proteins (such as the complement system), cytokines, and innate immune cells such as phagocytes (which can eliminate the pathogen by engulfing and digesting it (phagocytosis)), dendritic cells (which can activate the cells of the adaptive immune system via a process called antigen presentation), and natural killer cells (which can kill infected cells). Innate immunity is already present before an infection occurs or can be generated within hours and is therefore able to respond fast upon infection/pathogen invasion.

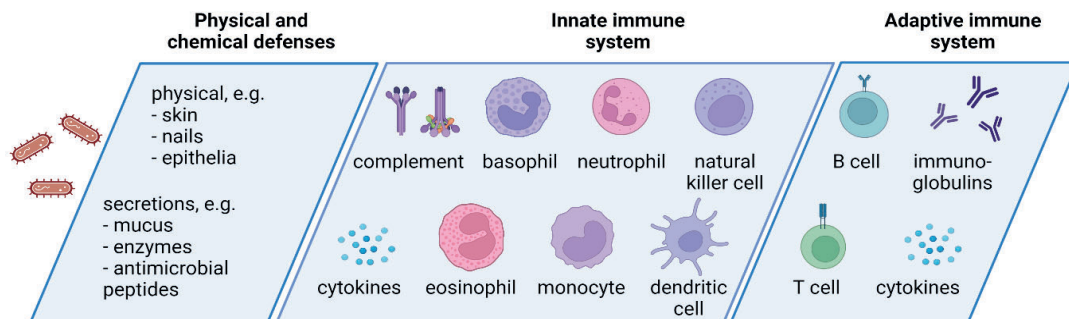


**Figure 1. Simplified overview of the three lines of defense that protect the human body from pathogens.** The first line comprises physical and chemical defenses, such as skin, nails and epithelial lining, and secretions such as mucus, enzymes, and antimicrobial peptides. The second layer of defense consists out of the cells of the innate immune system. These are phagocytes (neutrophils, monocytes, and dendritic cells), eosinophils, basophils, and natural killer cells. In addition to immune cells, proteins from the complement system and cytokines are part of the innate immune system. The last layer of defense consists of the adaptive immune system, which is characterized by unique receptors and the ability to create memory cells, which leads to a more robust and specific response upon a second encounter with the pathogen. Like in innate immunity, cytokines play an important role in adaptive immunity. The adaptive immune system consists out of B- and T cells, which both exist in various activation and maturation stages. The last part of the adaptive immune system are the immunoglobulins, which are antigen-specific products secreted by the terminally differentiated B cells (plasma cells). Of note, only immune cells that generally can be detected in the periphery are shown. Figure created in Biorender.com.

Although innate responses provide effective initial defenses against infections, many pathogens have evolved mechanisms to escape the innate immune system. To eliminate these pathogens, an adaptive immune response is required. The adaptive immune system is the third line of defense. It is characterized by the presence of unique receptors on the cell surface and the generation of immunological memory. These receptors specifically distinguish parts of microbes and molecules, called antigens. The adaptive immune system launches more vigorous responses upon repeated encounters and comprises B- and T-lymphocytes (B and T cells), and immunoglobulins (also frequently referred to as ‘antibodies’). Like in innate immunity, cytokines play an important role in adaptive immunity.[2]

The components of the innate and adaptive immune system are inter-connected and work together to provide optimal protection against pathogens. For example, the innate and adaptive immune system are connected via antigen-presenting cells. These are innate cells that present an antigen to a naive T cell (or pre-existing memory T cells) in a process called ‘antigen presentation’. When the presented antigen is recognized by the unique receptor on the naive T cell, this T cell can become activated.[3,4] Moreover, T cells can instruct innate immune cells by means of cytokine secretions, and the products of B cells (immunoglobulins) can neutralize a pathogen and enhance its degradation by innate immune cells. Thus, there is a continuous interplay between the different components of the immune system.

Immune cells can be found in all tissues in the body, such as the blood, bone marrow, thymus, spleen, and secondary lymphoid organs, but also in the epithelial layers or in mucosa-associated lymphoid tissue (MALT).[2] In addition, released cytokines and chemokines can attract immune cells to specific locations, for example a site of tissue damage or infection. Some types of immune cells are found primarily in the tissues, such as tissue-resident T cells, Langerhans cells, dendritic cells (DCs), mast cells and macrophages.[2] In this thesis, we focus on immune cells that can generally be detected in peripheral blood.

### 1.2 The innate immune system

The innate immune system consists out of several immune cell types and is responsible for the control or removal of encountered pathogens by starting inflammation and/or the antiviral defense. The main types of innate immune cells found in the periphery are phagocytes (neutrophils, monocytes, and dendritic cells (DCs)), eosinophils, basophils, and natural killer (NK) cells. Upon inflammation or tissue damage, the first cells to arrive are neutrophils and monocytes. When migrating from the blood into the tissue, monocytes differentiate into macrophages. Neutrophils, monocytes and macrophages express receptors on their surface that can sense pathogens via different mechanisms.[3,5] For example, via detection of specific conserved patterns on the outside of the pathogen (‘pathogen-associated molecular patterns; PAMP’s), complement proteins attached to the pathogen and marking it for degradation, or specific immunoglobulins – often generated in a previous response- bound to the pathogen (a process known as opsonization). As **Chapter 4** of this thesis discusses the phagocytosis of opsonized pathogens, this process will be explained in more detail (**Figure 2**).

Opsonized particles are covered in immunoglobulins that recognized and bound to the particle. Phagocytes express receptors on their surface that can recognize the Fc-part of these immunoglobulins, these receptors are called Fc-Receptor (FcR). Although inhibitory FcRs do exist (FcγRIIB; CD32), the majority of FcRs has activator properties, such as FcγRIII (CD16) and FcγRI (CD64). Binding of multiple immunoglobulins can lead to FcR cross-linking. This results in signal transduction events, which leads to mobilization of the cytoskeleton. One important player in this signaling cascade is phospholipase C gamma 2 (PLCγ2) (we go

more in depth into this in **Chapter 4**).[6] The mobilization of the cytoskeleton enables the phagocyte to engulf the pathogen while keeping it concealed from the rest of the cell in a so-called phagosome. The phagosome then fuses with other vesicles (lysosomes) present in the cell, which contain substances that are harmful for the pathogen. The fusion with the lysosomes leads to a controlled release of enzymes and chemicals, such as reactive oxygen and nitrogen species, which are all meant to destroy and digest the engulfed pathogen (**Figure 2**).[2,5,7]

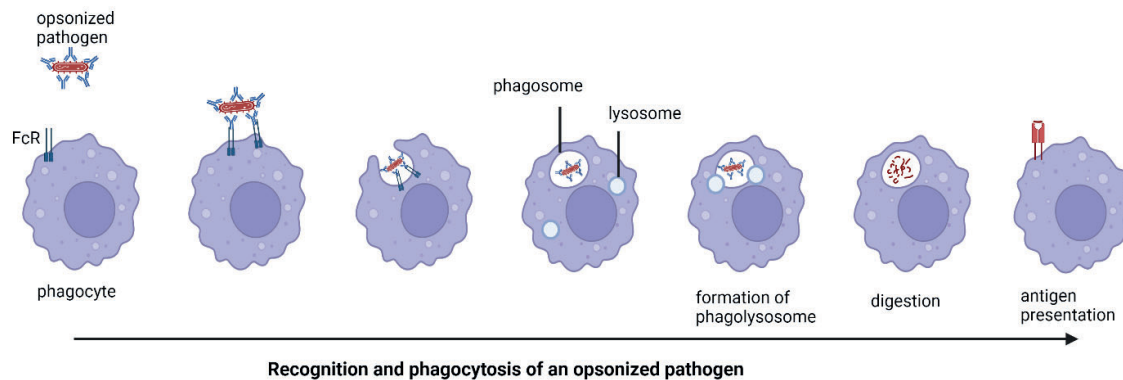


**Figure 2. Simplified representation of the phagocytosis of an opsonized pathogen.** From left to right: phagocytes express Fc-receptors (FcR), which can recognize the Fc-tail of the immunoglobulins that have opsonized the pathogen. Cross-linking of the FcRs leads to cell activation. The phagocyte adjusts its cytoskeleton to engulf the pathogen. When the pathogen is engulfed, it is contained in a vesicle: the phagosome. Next, the phagosome is fused with lysosomes, resulting in phagolysosomes, which are vesicles filled with substances that are meant to destroy the pathogen. Upon destruction of the pathogen, the phagocyte can present parts of the pathogen on its surface to activate the adaptive immune cells. Figure created in BioRender.com.

Within the monocyte compartment, several subsets can be defined based on phenotypic and functional differences. Monocytes mature from classical monocytes (cMos, CD14++CD16-), via intermediate (iMos, CD14++CD16+) to nonclassical monocytes (ncMos, CD14+CD16++) and can be further subdivided into different functional subsets or activation stages (**Figure 3**).[8,9] cMos play an important role in the initiation and progression of the inflammatory response, whereas ncMos are involved in the resolution of inflammation and have the ability to clear dead cells.[9] The function of iMos seems to be intermediate, combining both pro- and anti-inflammatory properties.[9] Within the cMos, two subpopulations can be defined based on expression of surface marker CD62L+ (also known as L-selectin) and FcεR1.[10,11] The CD62L+ cMos are thought to be recent bone marrow emigrants, whereas CD62L- cMos most likely have been activated, and have shed the CD62L upon activation. Within the ncMos, several subpopulations can be defined based on markers such as CD9, CD36 and SLAN.[9-11] Within these ncMo subsets, it was shown that SLAN+ ncMos had higher efferocytosis (removal of apoptotic cells by phagocytes) capacities compared to SLAN- ncMos, suggesting they play a role in clearance of apoptotic cells.[9]

Another important set of innate cells that can be found in the circulation are DCs. Although a large part of the DCs resides within the tissues, they can be detec-

ted in low quantities in the circulation. DCs can be subdivided into myeloid DCs (mDCs) and plasmacytoid DCs (pDCs) with different functional properties.[8] In short, mDCs are considered ‘the classical DCs’: immature DCs that circulate through the body in search of antigens. Upon encounter of antigens, these antigens are taken up via several mechanisms such as phagocytosis, macropinocytosis or receptor-mediated endocytosis.[4] Next, the DCs migrate to the lymph node. During this process, the DC matures, and its main function becomes antigen presentation via MHC molecules (major histocompatibility complex) on the cell surface to engage the adaptive immune system.[4] Although pDCs can also present antigen to T cells, they are considered to specialize in the production of type 1 Interferon and promote antiviral immune responses.[12]

Eosinophils are innate immune cells known to have a role in defense against parasite infections, but their numbers are also known to increase in allergic diseases, drug reactions and in hypereosinophilic syndrome.[13] Basophils play a role in allergic responses and in the host defense against parasites.[13] Lastly, NK cells respond to viral infections in a non-antigen specific way and play a role in the elimination of malignant cells from the body.[5]

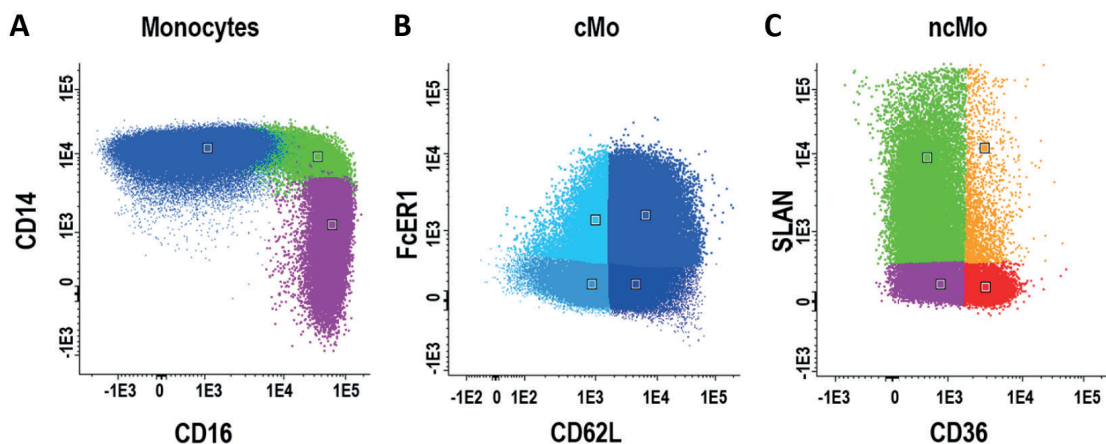


**Figure 3. Different monocyte subsets discriminated based on differential expression of surface markers.** (A) Based on expression of CD14 and CD16, classical monocytes (cMo), intermediate monocytes (iMo), and non-classical monocytes (ncMo) can be defined. (B) Within cMo, four subpopulations can be defined based on expression of CD62L (L-selectin) and the FcER1. (C) Within ncMo, four subpopulations can be defined based on expression of SLAN and CD36.

### 1.3 The adaptive immune system

#### 1.3.1 Generation of unique receptors

The adaptive immune system consists out of two main players: T cells and B cells. Both are generated in the bone marrow from common lymphoid progenitor cells. However, T cells mature in the thymus, and B cells mature in the bone marrow. Both B and T cells express a unique receptor on their surface (the B- and T-cell receptor, BCR and TCR, respectively).[14] The genes encoding these unique receptors are generated by the rearrangement of the different variable (V) genes with the diversity (D) and joining (J) genes. An example of this recombination is shown for the BCR heavy chain- encoding genes (IGH) in **Figure 4** (adapted from

[15]). IGHV, IGHD and IGHJ genes are present in the DNA of every cell in the body (germline genes) but only when a single random V gene, D gene and J gene have rearranged to form a functional V(D)J exon, the DNA can be transcribed into a functional receptor.[16,17] Of note, the D gene is not included in every recombination; the BCR Ig heavy chain (IgH), TCR  $\beta$  and TCR  $\delta$  chains are encoded by a V, D and J gene, while the BCR Ig light chain (IgL), TCR  $\alpha$  and TCR  $\gamma$  chains are encoded by a V and J gene only.[17,18] This rearrangement of genes— called V(D)J recombination- results in an exon encoding a unique receptor. In addition to the use of different V(D)J combinations, junctional diversity (caused by non-homologous end joining; NHEJ) is an important contributor to the generation of unique receptors.[17] In this process, there is a random removal and addition of nucleotides at the joints where double stranded DNA breaks were introduced and where the DNA pieces were ligated together to form the functional V(D)J exon. Moreover, the heavy and light chains are paired randomly. The combination of

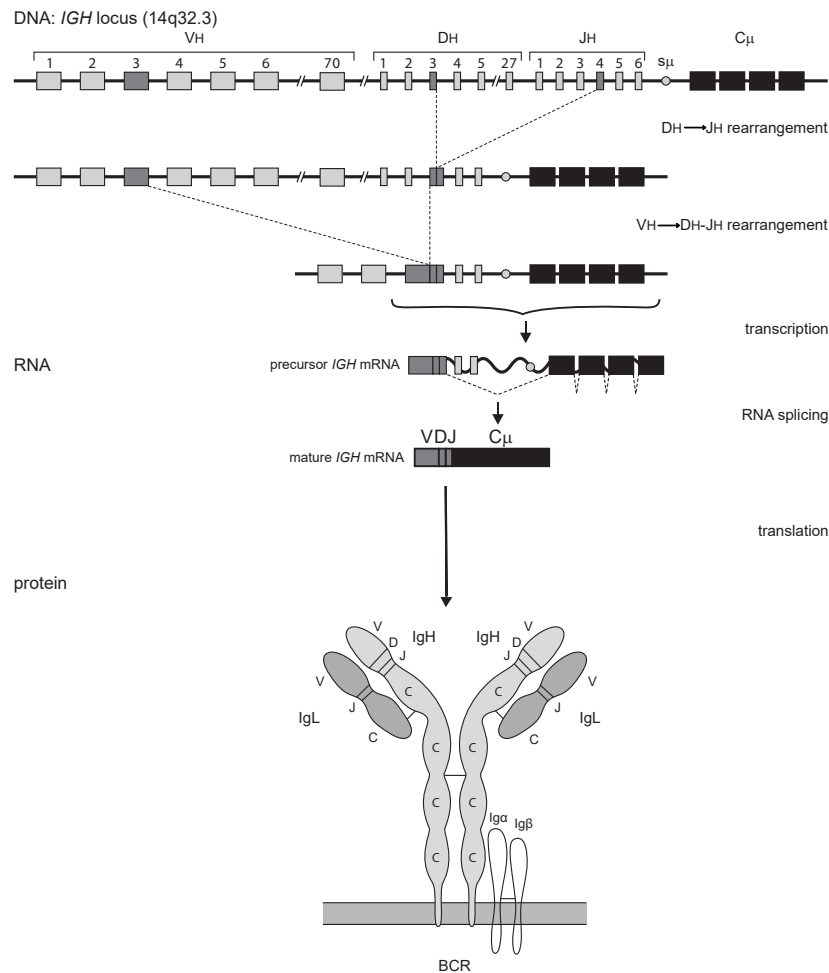


**Figure 4. Schematic representation of IGH gene rearrangement.** In the first step of V(D)J recombination in the IGH a D gene is coupled to a J gene. Subsequently, a V gene is coupled to the DJ joint. The VDJ exon is transcribed and spliced to the IGHM exons. A functional IgM protein is transported to the plasma membrane with anchoring molecules Ig $\alpha$  and Ig $\beta$  (also known as CD79Aa and CD79b, respectively) and a functional Ig light chain protein in immature and mature B cells. Adapted from van Dongen et al, 1991.



V(D)J recombination, introduction of junctional diversity, and random pairing of the heavy and light chains occurs in individual lymphocytes during their maturation process, and results in a large variety of BCRs and TCRs expressed.[17] Importantly, not every successful receptor rearrangement will lead to a naive B or T cell being released into the circulation. There are extensive selection processes ongoing to prevent release of potentially harmful B- and T cells into the circulation. Continuous production of new B- and T cells (naive cells) leads to a constant renewal of the available repertoire. Only cells that encountered a matching antigen become activated and can further develop into memory or effector cells. Cells that did not find a matching antigen will not receive activation or survival signals and will generally go into programmed cell death, thereby creating space for newly generated B- and T cells to enter the circulation. It is estimated that at any given moment, the available repertoire (i.e., the number of unique receptors) present in an individual is approximately  $10^7$ , although it should be noted that this depends on the age of the given individual (higher in younger individuals, lower in the elderly).[2,19-21]

### 1.3.2 T-cell subsets and functions

When a T cell has successfully generated a unique TCR and has passed the selection processes, it is released in the circulation as a naive T cell. Of note, most T cells generate a TCR consisting of  $\alpha$  and  $\beta$  chain (TCR $\alpha\beta$ ), and a small part of T cells generates a TCR consisting of a  $\gamma$  and  $\delta$  chain (TCR $\gamma\delta$ ). The main goal of the naive T cell is to encounter antigen, which occurs via antigen presentation on MHC I or MHC II molecules on other cells. Upon antigen recognition the naive T cell will get activated and start proliferating and differentiating into effector T cells and memory T cells. The effector T cells are short-lived, whereas the memory T cells stay in the body for a longer time, providing immunological memory in case of antigen re-encounter.[22] Aside from naive, effector and memory cells, there are many subsets defined within the T-cell compartment, each with specific characteristics.[22] Although many T-cell subsets can be monitored in the blood, most T cells are present in the bodily tissues, and only part of T cells is thought to be (re)circulating.[23]

In healthy adults, majority of T cells found in the blood are of the CD4 'helper' T (Th) cell or CD8 'cytotoxic' T cell phenotype. CD4 T cells recognize MHC II-antigen complexes, and CD8 T cells recognize MHC I-antigen complexes. Cytotoxic T cells scan the surface of cells in the tissues. When a cell is damaged or infected, the CD8 T cell gets activated and induces apoptosis of the damaged/infected cell. [2] The CD4 Th cells play a role in the activation of innate immune cells and -in the case of follicular Th (Tfh) cells- in the activation and shaping of the B-cell and immunoglobulin response.[24] There are different subtypes of Th cells, each of which is directed to the defense against specific types of pathogens (**Table 1**, based on ref [2,23,25,26]). Importantly, although we can distinguish many different Th cell subsets, there seems to be a high plasticity between them. Likewise, each Th subset has signature cytokines, yet there is overlap between the cytokine production in different Th subsets.[23]

**Table 1. Overview of main helper T-cell subsets, their signature cytokines, and functions.** Table based on ref [2,23,25,26].

| Type Th cell | Signature cytokine expression | Associated with  |
|--------------|-------------------------------|--|
| Th1          | IFN- $\gamma$                 | Defense against intracellular microbes                       |
| Th2          | IL-4, IL-5, IL-13             | Defense against helminthic parasites                         |
| Th17         | IL-17, IL-22, (IL-10)         | Defense against extracellular bacteria; fungi; Tissue repair |
| Th22         | IL-22                         | Tissue repair  |

The most well-known Th subsets are Th1, Th2, Th17 and Th22 cells, which are generated in different responses and can each be identified by the secretion of signature cytokines, or by the expression of specific surface markers (**Table 1**). A recent study by Botafogo et al. (2020) described a flow cytometry panel in which many of these T-cell subsets can be identified based on the surface expression of various markers.[27] This flow cytometry approach identified an even larger heterogeneity within the Th subsets, and has defined several new possible Th subsets, primarily described by their marker expression pattern (based on expression of CXCR3, CCR4, CCR6 and CCR10).

Aside from cytotoxic T cells and Th cells, other T-cell subsets can be found in the blood too. Examples hereof are the Tfh cells, regulatory T cells (Tregs) and TCR $\gamma\delta$  T cells.[27-31]

Tfh cells are primarily present in the secondary lymphoid organs (especially in germinal centers), but can also be detected in the blood, albeit in lower quantities. Like in Th cells, there is a heterogeneity within the Tfh cells.[30] Based on marker expression patterns, subpopulations similar to Th cells can be defined, e.g. Th1-like cells, Th2-like cells, etc.[27] Next are the Tregs, which are thought to play an important role in the development and maintenance of immune tolerance. In a healthy situation, they regulate ongoing immune responses and prevent autoimmunity. Like Th and Tfh cells, Tregs have been shown to be a heterogeneous population.[29] Lastly, TCR $\gamma\delta$  T cells can be identified in the circulation. TCR $\gamma\delta$  T cells are a small distinct T-cell subset/lineage and although their exact function in immunity is not fully understood, it is known that TCR $\gamma\delta$  T cells have features of innate and adaptive immune cells and seem to have a multifaceted role in immunity.[28] And— in contrast to TCR  $\alpha\beta$  T cells- these cells are not completely restricted by MHC presentation for antigen recognition.[31]

In this thesis, we used the flow cytometry panel as published by Botafogo et



al.[27] to monitor the CD4 T-cell compartment and describe the kinetics of CD4 T-cell populations that can be defined with that marker combination.

### 1.3.3 B-cell functions and subsets- general overview

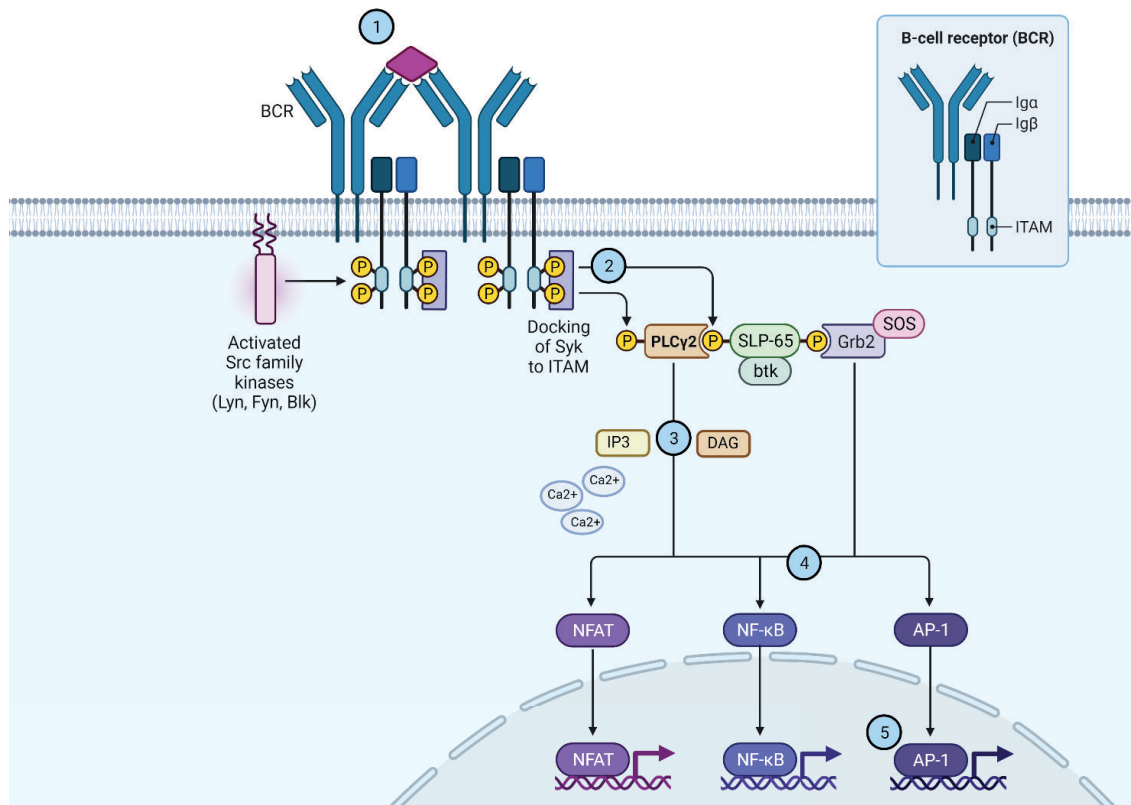
As explained in §1.3.1, the BCR is formed during a process called V(D)J recombination. First the genes encoding the immunoglobulin heavy chain (IgH), and then the genes encoding the immunoglobulin light chain (Igk or Igλ) rearrange to form a unique BCR.[15,32,33] From the immunoglobulin light chain genes, each developing B cell will first initiate recombination of the Igk light chain. When this does not result in a functional light chain, the cell will initiate recombination of the Igλ light chain. If both Igk and Igλ rearrangements fail, the cell will go into programmed cell death.

After generation of a functional BCR the B cell leaves the bone marrow and enters the blood as a naive B cell in search for antigen. As each generated B cell expresses a unique BCR, there is a large variety in the available repertoire. Upon encounter of an antigen that matches the BCR, the naive B cell gets activated and develops into an effector cell (known as plasma cell) or a memory cell. Dependent on the type of antigen, this process can be T-cell dependent (in case of protein antigens) or T-cell independent (in case of nucleic acid, lipid, and polysaccharide antigens).[34]

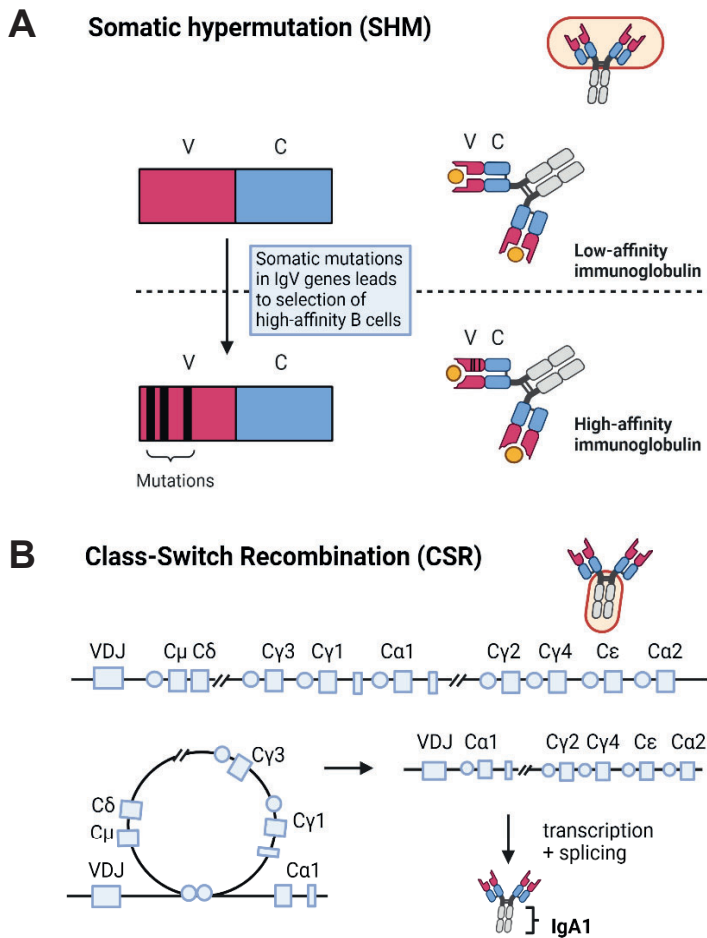
### 1.3.4 B-cell functions - Activation of the BCR

The BCR forms a complex with the Igα and Igβ molecules. The Igα and Igβ molecules contain an immunoreceptor tyrosine-based activation motif (ITAM) in the cytoplasmic tail. Upon binding of antigen, the involved BCRs start cross-linking (**Figure 5**). This leads to phosphorylation of the ITAMs in the Igα and Igβ molecules, which triggers subsequent signaling events downstream of the BCR.[35] For example, the PLCγ2 protein gets activated, which leads to the production of second messengers such as diacylglycerol (DAG) and inositol-1, 4, 5-trisphosphate (IP3).[35,36] IP3 generation leads to the increase in intracellular calcium, whereas DAG is an activator of protein kinase C (PKC).[37,38] The production of second messenger molecules and the increased calcium levels result in enzyme activation. These enzymes activate several transcription factors, such as NFAT and NF-κB, which results in activation of genes whose products are required for functional B-cell responses, such as proliferation and differentiation.[35]

Upon activation, the B cell starts proliferating and actively modifying its BCR to generate a BCR with a better fit to the antigen. This modification occurs via the introduction of mutations in the regions of the BCR that come into direct contact with the antigen. This process is called ‘Somatic Hypermutation’ (SHM) (**Figure 6A**).[24] Moreover, the B cell can change the isotype of their heavy chain in order to alter the effector functions of the BCR and secreted immunoglobulins in a process called ‘Class-Switch Recombination’ (CSR) (**Table 2**, based on [39-42]).[24] As this process involves the removal of genomic fragments, this is an irreversible process that goes in one direction (**Figure 6B**, based on [2,15,43]).



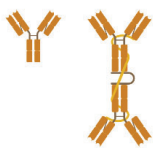




**Figure 5. Simplified representation of the major steps in BCR activation.** (1) Cross-linking of the BCRs by means of antigen binding (or via use of Fab-binding fragments). (2) Phosphorylation of the ITAM parts of the Igα and Igβ chain by the activation Src family kinases. (3) Release of secondary messenger molecules/biochemical intermediates, such as DAG or the release of calcium. These lead to the activation of (Ca-dependent) enzymes. (4) Activation of transcription factors. (5) Activation/transcription of genes whose products are required for functional B-cell responses. Adapted from 'BCR downstream signaling' by BioRender.com (2022). Retrieved from <https://app.biorender.com/biorender-templates>.



**Figure 6. Simplified representation of the processes of Somatic Hypermutations (SHM) and Class-Switch Recombination (CSR).** (A). Introduction of somatic hypermutations can lead to structural changes in the V-region of the immunoglobulin, which can lead to increased or decreased affinity, or no change in affinity. Immunoglobulins with higher affinity are preferentially selected, and thus SHM leads to the generation of higher affinity immunoglobulins. V; Variable region, C; Constant region (B) The human IGH locus contains nine constant regions (IGHC). When an antigen-activated B cell gets T-cell help, the B cell will undergo switching to another isotype, depending on the T-cell help. In this figure, the proximal genes  $C_{\mu}$ ,  $C_{\delta}$ , and  $C_{\gamma 3}$  are deleted in a circle of DNA, which leads to recombination of the VDJ with the  $Ca1$  gene. Transcription of the newly formed exon results in generation of immunoglobulin with the IgA1 constant region. As part of the DNA is deleted, next class switching events can only go in one direction. Adapted from ‘Somatic Hypermutation allows for generation of higher affinity BCRs’ by BioRender.com (2022). Retrieved from <https://app.biorender.com/biorender-templates>.

**Table 2. General overview of different immunoglobulin (sub)classes.** In the left column, simplified representations of the immunoglobulin format(s) present are indicated. The primary known binding receptors and effector functions are indicated per immunoglobulin subclass.[39-42] Immunoglobulin representations generated in BioRender.com.

| Immunoglobulin  | format         | binding receptor | function  |
|---|----------------|------------------|---|
| IgM    | Pentamer       | FcμR             | Complement fixation; opsonization; primary adaptive responses   |
| IgG   | Monomer        | FcγR             | <b>IgG1-4:</b> secondary adaptive responses<br><b>IgG1, IgG3:</b> complement fixation, strong opsonization, strong FcγR binding<br><b>IgG2:</b> no complement binding or opsonization capacity, reduced binding to most FcγRs<br><b>IgG4:</b> no complement binding, reduced binding to most FcγRs, <i>in vivo</i> Fab exchange resulting in bispecific immunoglobulins |
| IgA  | Monomer, dimer | FcαR             | <b>IgA1:</b> mainly mucosal immunity, immune protection of newborns, larger distances between Fab tips allows binding that are further apart<br><b>IgA2:</b> mainly mucosal immunity, immune protection of newborns   |
| IgD  | Monomer        | FcδR             | Function not defined, possibly involved in regulation of B-cell fate and shaping of B-cell repertoire   |
| IgE  | Monomer        | FcεR             | Involved in allergies, hypersensitivity and worm infections   |

### 1.3.5 Generation of kappa-deleting recombination circles (KRECs)

Each developing B cell will first initiate recombination of the Igκ light chain and will only initiate recombination of the Igλ light chain if Igκ is not successfully recombined. This knowledge can be used to our advantage in immune monitoring. We know that when the Jκ-Cκ intron recombination signal sequence (intron RSS) rearranges to the kappa-deleting element (Kde), the Igκ locus is not rearranged any further (thus rendering this locus ‘non-functional’).[44,45] In humans, this rearrangement is quite common in mature B cells with an Igκ light chain, and present in almost all B cells with an Igλ light chain.[46-48] During this specific rearrangement, part of the DNA is excised and remains as an ‘excision circle’ in the cell (**Figure 7**, duplicated with permission from [46]). These excision circles – also known as kappa-deleting recombination circles; KRECs- are stable elements which do not replicate during cell divisions. This means that on the

## Chapter 1

cell population level they dilute upon each cell division. Thus, by calculating the ratio between the ‘coding joint’, which is left in the genome and the ‘signal joint’ on the KREC, the average number of cell divisions that a B-cell population has undergone since generation of the BCR ( $\approx$  since they left the bone marrow) can be determined.[46] This concept and the first results are described in the patent filed by van Dongen and Szczepanski in 2004 (PCT/NL2005/00761, priority date 25.10.2004).[49] For T cells, a similar approach can be used when detecting the T cell receptor excision circles (TRECs).[50,51] In terms of immune monitoring the number of detected KRECs or TRECs could give insight in the dynamics of

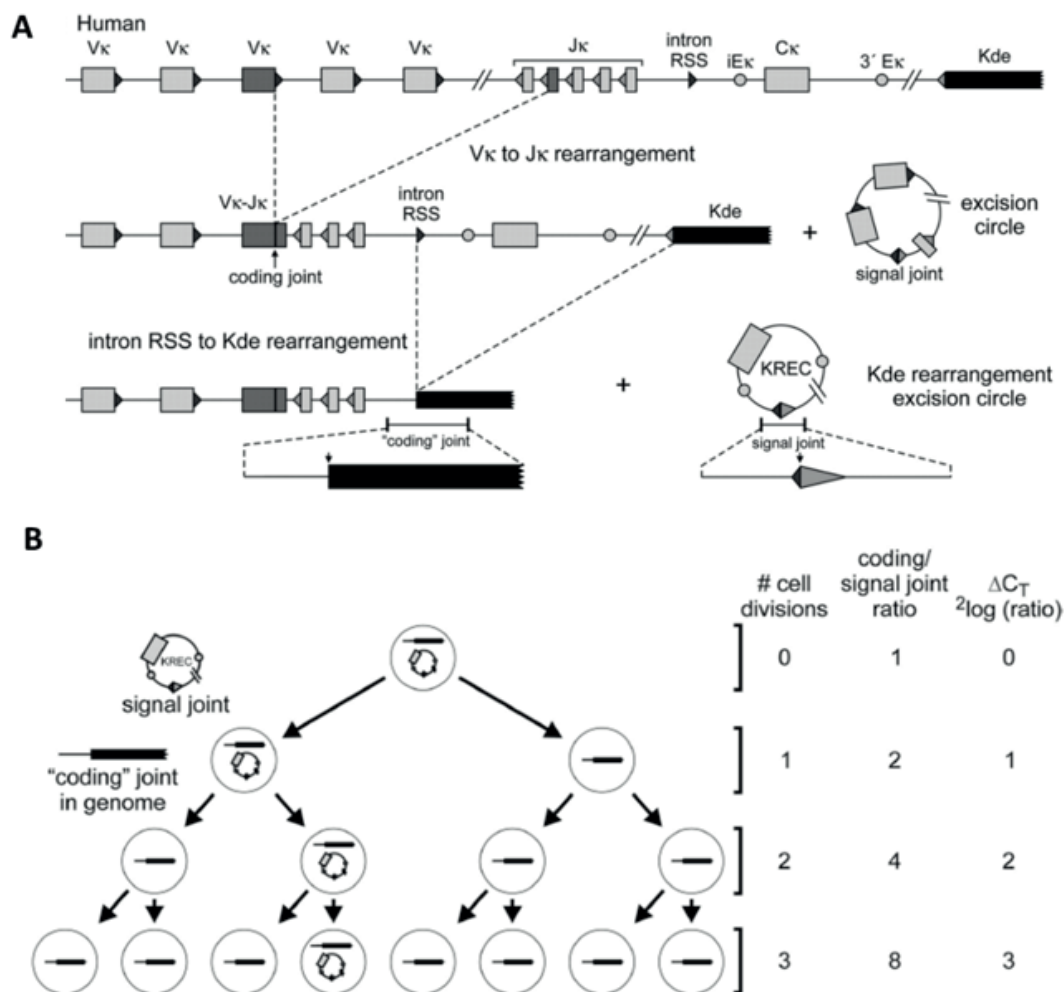


**Figure 7. Formation of kappa-deleting recombination circles during the generation of the human B-cell receptor.** (A) V(D)J recombination of the IGK locus results in a  $V\kappa$ - $J\kappa$  coding joint. Subsequent rearrangement between the intron RSS and the  $Kde$  elements can make the IGK allele nonfunctional by deleting the  $c\kappa$  exons and the enhancer. Consequently, the coding joint precludes any further rearrangements in the IGK locus and therefore remains present in the genome. The KREC with the corresponding signal joint is a stable double-stranded, circular DNA structure, which will not be degraded, but neither be duplicated during the cell cycle. (B) Therefore, upon each cell division, the number of KRECs will be diluted. The coding joint in the genome and the signal joint on the KREC can be quantified via RQ-PCR and their ratio can be used to determine the number of cell divisions a B-cell subset has undergone since they left the bone marrow. Figure and legend duplicated with permission from Van Dongen (2004).

B- and T-cell subsets. One example is the case of severe combined immunodeficiency (SCID) or primary immunodeficiencies (PID), where the level of TREC and KREC numbers can aid the diagnosis. In fact, this approach has implemented in newborn screening programs in several countries.[52,53]

As indicated earlier in this introduction, naive B cells differentiate into memory B cells (that can persist in the body for many years) and plasma cells, which produce large quantities of immunoglobulins to neutralize antigen. In the blood, several maturation stages of plasma cells can be observed based on expression of several cellular markers. The surface marker CD20 (its exact function is not known, but CD20 interacts with the BCR and may be involved in B-cell activation [54]) and CD138 (a proteoglycan that is considered a hallmark of (mature) plasma cells [55]) play an important role in defining the plasma cell maturation stage. Immature plasma cells express CD20 but not CD138. During maturation, CD20 is downregulated and CD138 is upregulated. Most mature plasma cells are CD20 negative, and CD138 positive (**Figure 8A**).[56] Plasma cells of all these maturation stages can be detected in circulation, and thus a heterogenous expression of CD138 is observed. As CD138 expression is considered a hallmark of plasma cells, this mixed circulating plasma cell population is often referred to as plasmablasts. In this thesis, we will refer to the circulating plasmablast/plasma cell populations simply as plasma cells.

Aside from the changes in CD20/CD138 expression, maturing plasma cells gradually lose the expression of surface immunoglobulins (the BCR) and various other surface markers (**Figure 8B**) and initiate massive immunoglobulin production (production and secretion of BCRs).[55] After their generation in follicles or germinal centers, plasma cells migrate via the blood stream to find a niche that supports their survival (bone marrow, spleen, MALT, lymph node).[55] Although most generated plasma cells are short-lived, the plasma cells that find a niche become long-lived plasma cells and can stay in the body for many years. It is thought that, upon antigen-challenge, a fraction of the newly generated plasma cells will compete with the long-lived plasma cells for a place in the niches, pro-

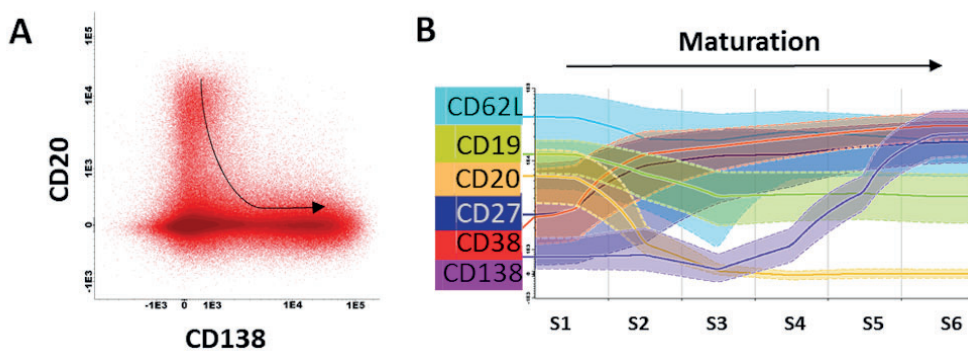


**Figure 8.** (A) Heterogenous expression of CD20 and CD138 in plasma cells, depending on their maturation status. (B) Gradual loss or gain of expression of various surface markers in plasma cells upon their maturation.



bably expelling some of these plasma cells from their location. As a result hereof, the pool of long-lived plasma cells is a dynamic entity.[57] The immunoglobulins secreted by plasma cells play an important role in the neutralization of the pathogen/antigen. Depending on the type of antigen, the type of encounter and the location in the body (e.g., mucosal vs. systemic), different BCRs are generated, and thus different types of immunoglobulins are generated.

### **1.3.6 B-cell functions and subsets- distribution in the general population**

In healthy adults, majority of B cells are of the naive mature or memory B-cell phenotype (**Figure 9**, modified from [1,46,48]). Additionally, low numbers of transitional/immature B cells (recent bone marrow migrants) and plasma cells can be detected in peripheral blood.[58] While the breadth of the naive B-cell repertoire (number of naive B cells carrying a unique BCR) is crucial in the response to neoantigens, the diversity within the memory B-cell compartment, shaped by previous antigen encounters, plays an important role in recall responses, such as to a booster vaccination. Within memory B cells, two major subpopulations can be defined: the non class-switched memory B cells and class-switched memory B cells. Most non class-switched memory B cells are believed to be (partly) derived from T-cell independent immune responses. In contrast, formation of class-switched memory B cells is mostly T-cell dependent and takes place in germinal centers upon recognition of protein antigens.[34] However, it should be noted that several exceptions to these general observations have been described, such as T-cell independent IgA responses in the MALT or T-cell dependent origin of a part of IgM+ memory B cells.[59]

### **1.4 Immune monitoring**

All the immune cells mentioned so far can be detected in the peripheral blood, which is considered the 'highway' for immune cells to make their way through our body.[60,61] The blood can be sampled in a minimally invasive manner, making it suitable to use for immune monitoring. Immune monitoring is a process where the immune system is monitored at one or several timepoints to gain more information about its status or composition. Detailed monitoring of the immune system and ongoing processes can be a valuable source of information, both when the system is in homeostasis and when it is not, e.g. in case of infection, disease, or when an individual is receiving treatment or medication.[62-64] Immune monitoring can be performed *in vivo* and *in vitro*, with a functional or phenotypic assessment or a combination of both, and at different levels; the cellular level, the molecular level, or by means of e.g. serum analysis or repertoire studies.[65-70] The preferred method of immune monitoring may be influenced by the available material, equipment, timeframe, funding and knowledge.

In this thesis, we primarily used flow cytometry-based immune monitoring tools to assess baseline and ongoing cellular immune kinetics, with peripheral blood as source of material. Therefore, we will further explain this method in the following paragraph (§1.5). To a lesser extent, serology, ELISpot, qPCR, activation/

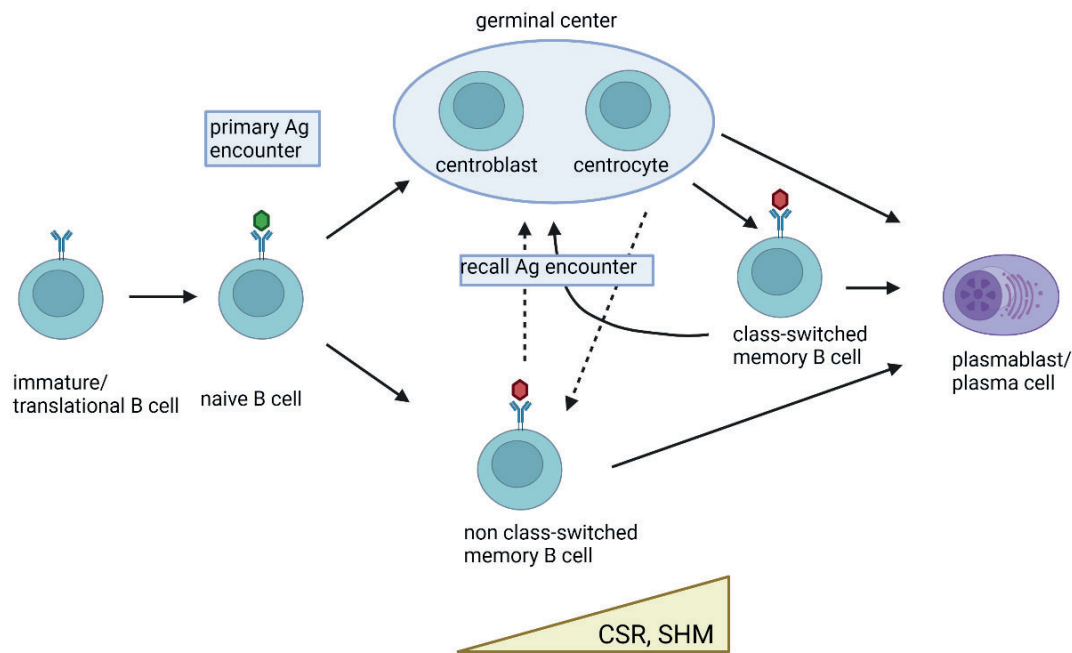


**Figure 9. Simplified representation of major B-cell subsets detectable in blood.** From left to right: Immature/Transitional B cells are recent bone marrow migrants and present in low numbers in the peripheral blood. They mature into naive B cells, which constitute a major part of the circulating B-cell population. The number of naive B cells with unique B-cell receptors forms the naive B-cell repertoire, which is crucial for recognition of neoantigens (primary antigen encounters). Naive B cells which encountered T-cell dependent antigens (e.g., a protein), will enter germinal centers to receive T-cell help. Consequently, they will upregulate AID (Activation Induced Cytidine Deaminase) and subsequently improve affinity for antigen by initiating Somatic Hypermutation (SHM) and change effector functions in the process of Class-Switch Recombination (CSR). Only B cells that express receptors with increased affinity to the encountered antigen survive and can leave the germinal center as class-switched memory B cells or as plasma cells. When a B cell is activated by a T-cell independent antigen (e.g., a polysaccharide, nucleic acid or lipid), it does not enter the germinal center, but differentiates into a non class-switched memory B cell instead. Class-switched and non class-switched memory B cells make up a large part of the circulating B-cell compartment, and are present in other parts of the peripheral lymphoid system, such as the spleen or lymph nodes. These memory B cells are important during recall responses (recall antigen encounter) when they can re-enter germinal centers and undergo further processes of affinity maturation and class-switching. Lastly, plasma cells are the terminal effector B cells and responsible for massive immunoglobulin production after antigen encounter. Upon infection or vaccination, a transient peak of plasma cell numbers is observed, but in steady state, plasma cell numbers are low. Figure created in Bio-Render.com. Modified from Diks et al., 2021, van Zelm et al., 2005, van Zelm et al., 2007. 1,46,48

stimulation assays and single cell-sequencing technologies were used for immune monitoring, again using peripheral blood as source of material.

Serology, or the detection of antigen-specific serum immunoglobulins is considered a golden standard when it comes to assessing vaccine effectiveness; the (increased) levels of vaccine-specific immunoglobulins in the serum are known to correlate with protection against disease in numerous cases.[71] To detect and quantify the number of antigen-specific B cells, the ELISpot method was applied in this thesis. Significant correlations between the number of Ag-specific B cells and the Ag-specific Ig serum levels have been reported for multiple vaccines.[72]



The qPCR-based methods that we use in this thesis are related to the detection of KRECs. The number of KRECs detected in a B-cell population can give information about the number of cell divisions that a B-cell population has undergone since it left the bone marrow.[46] Activation and stimulation assays were used in this thesis to determine the ‘fitness’ of cells. We evaluated the activation of cells upon stimulation at various locations during the activation pathway, such as phosphorylation events, calcium release, and phagocytosis/ROS production (upon stimulation with opsonized particles).

Lastly, we made use of single cell sequencing techniques to investigate the B-cell repertoire during an immune response. By investigating the B-cell repertoire, we can get insight in the selection processes that occur upon antigen encounter. This way we may identify structures that are most immunogenic during natural pathogen encounter and evaluate if these are also present in current vaccines or vaccine candidates.

### **1.5 Flow cytometry as a tool for immune monitoring**

Flow cytometry is a frequently used immune monitoring method which allows identification of cells/particles in (single cell) suspensions. Cell identification is based on the detection of cellular markers by fluorescently labelled (monoclonal) antibodies or detection of nucleic acids by fluorescent dyes (**Figure 10**).[73] Frequently used cell suspensions for flow cytometry include, but are not limited to, mechanically or enzymatically digested tissues, cell lines and/or co-cultures, bone marrow, cerebrospinal fluid, saliva, urine and (peripheral) blood.

In the early days, the number of cellular markers that could be detected was rather limited. However, over time the number of fluorescent labels and the ability of flow cytometers to pick up multiple signals has increased significantly, leading to the development and publication of several high-dimensional/multicolor flow cytometry panels (van der Pan et al, manuscript accepted).[27,74,75] Such panels allow identification of many different cell entities, such as subsets, maturation stages or different activation stages. Aside from the detection of surface/intracellular markers, the availability of bioparticles coupled to a sensor dye or sensor dyes in general, such as pHrodo, DHR123 or calcium-sensor dyes, allow for detection of processes such as phagocytosis, generation of reactive oxygen species (ROS) or calcium release. Thus, the use of (intra)cellular markers, bioparticles and sensor dyes can be a valuable source of information about the function of evaluated cells. Additionally, the introduction of high-throughput flow cytometers allows analysis of high cell numbers, and when counting beads are used, one can retain information about absolute numbers. The large availability of fluorochrome-linked detection antibodies, number of fluorescent dyes and the opportunity to adjust the optical configuration of the machine result in great flexibility. Lastly, the introduction of spectral flow cytometers has resulted in an even higher number of marker combinations that can be used simultaneously. Spectral flow cytometers differ from conventional flow cytometers regarding their optics and detectors, resulting in detection of the complete emission spectrum from a

fluorochrome/dye instead of only the light passing a set of filters, as is the case in conventional flow cytometers.[76] The combination of high-throughput, flexibility and the relatively fast acquisition of cells make flow cytometry a very suitable tool for exploratory research.

Although much information can be retrieved from such complex flow cytometry panels and large cell numbers, this increased complexity of antibody panels has resulted in an increased subjectivity when it comes to data analysis and interpretation.[74] To ensure data quality and reproducibility, it is important that protocols and phenotypic descriptions are standardized between laboratories/clinical sites. To this end, several groups and consortia proposed the use of harmonized or standardized protocols for sample collection, acquisition, and (automated) analysis.[77-80] In this thesis, the guidelines and protocols as proposed by the EuroFlow Consortium have been applied to all experiments executed on

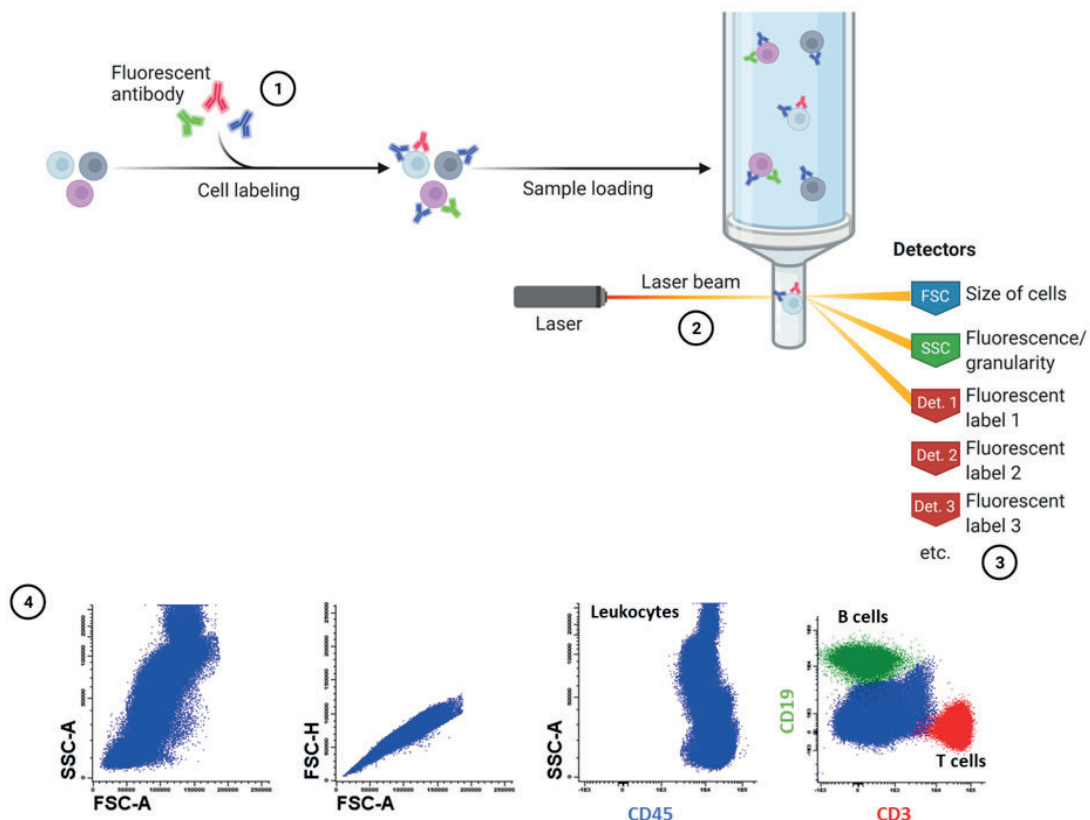


**Figure 10. Simplified overview of flow cytometry principles.** The main steps are indicated and labeled sequentially. (1) A mixture of cells is fluorescently labeled with antibodies specific for each cell type. (2) In the flow cytometer, the labeled cell mixture is passing a laser beam in a stream of fluid. The laser beam strikes the stream and the cells that are passing by at that moment. Based on the type of cell that is hit at that moment, different light signals are hitting the detectors. The FSC detector identifies the cell size. The SSC detector identifies the (auto)fluorescence and the granularity of the cell. The other detectors identify signals originating from the fluorescently labeled antibodies that bound to the cells. (3) For each interrogated cell (also called “event”), the outcome of each detector is saved as a separate parameter. (4) Using flow cytometry analysis software, each cell type can be identified based on its unique combination of parameters. Adapted from ‘Fluorescence-activated Cell Sorting (FACS)’ by BioRender.com (2022). Retrieved from <https://app.biorender.com/biorender-templates>.

## Chapter 1

a BD FACS Canto II 3L or a BD FACS LSR (X-20) Fortessa 4L (BD Biosciences, San Jose, CA, USA).[77,81] In short, this means that standardized protocols were used whenever available, and that machine performance was monitored daily with CS&T beads (BD Biosciences) as well as SPHERO™ Rainbow calibration particles (Cytognos, Salamanca, Spain).

**Figure 11** shows an overview of different aspects in the preanalytical, analytical and postanalytical process that can influence the results and should ideally be decided before start of large experiments, such as a clinical trial. In short, the type of anticoagulant can influence cell distribution over time.[82] The presence of a fixation agent can influence cell identification markers (e.g. altered scatter properties), but allows for extended sample stability.[83,84] The amount of blood used for sample processing and acquisition (and thus cell numbers evaluated) determines depth of analysis, moreover, protocol adjustment may be needed when sample volume changes. With increased sample age (time since donation), quality reduces, but this differs per evaluated cell type and is influenced by type of anti-coagulant, storage temperature, storage time and mode of storage (e.g. full blood, cell suspension, or fixed cells).[84-86] During sample acquisition, the type of flow cytometer used (including configuration and calibration), the used protocols, and the antibody cocktail can influence the generated flow cytometry files.[81] Lastly, the analysis of the flow cytometry files is dependent on the (experience of the) operator and population definition. Thus, standardization of these aspects leads to increased data quality and reproducibility.

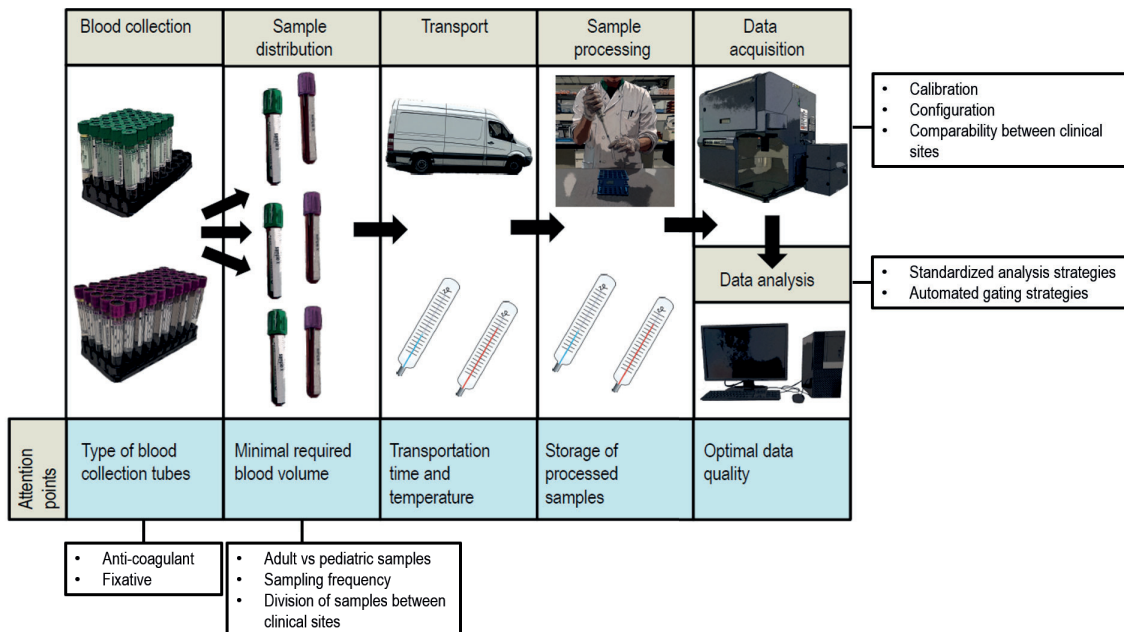


**Figure 11.** Different aspects in the preanalytical, analytical and postanalytical process that can influence the quality of results and should ideally be decided before start of large experiments, such as a clinical trial. Figure modified from Diks et al (this thesis).

### 1.6 Immune response to antigen – vaccines

Exposure to a pathogen or vaccine component initiates an immune response which effectiveness depends on the cooperation of multiple cell types. During the immune response, innate immune cells are rapidly recruited to the place of damage or infection.[62,87,88] They initiate the immune response by means of local inflammation, but also act as antigen (Ag)-presenting cells.[87,88] The innate response is followed by activation of adaptive immune cells (T and B cells), which results in the formation of effector and memory cells.[24] The generation of immunological memory is the basis for vaccine-induced protection. By actively exposing the immune system to a part of a pathogen, or a weakened/dead pathogen, the immune system is triggered and generates an immune response against the pathogen, while induction of disease is avoided. In this process, immunological memory is built, and when the pathogen is encountered in real-life, the tools required to neutralize/destroy the pathogen are already present. This leads to a more efficient immune response and can prevent (major) disease. The efficacy of vaccines has been demonstrated by the reduced number of infectious-disease related deaths since their introduction.[89]

However, the use of vaccines is often based on empirical data, and not all underlying (protective) mechanisms are fully understood. Moreover, the vaccine composition such as type of adjuvant, variety and concentration of antigen, and type of antigen (e.g., peptide, polysaccharide-conjugates, or whole pathogen) can lead to differences between generated immunity versus optimal protective immunity.

### 1.7 The difference between vaccine-induced and natural infection-induced immunity- *Bordetella pertussis*

The main immune response monitored in this thesis is the response launched against *Bordetella pertussis* (Bp), a gram-negative bacterium responsible for the respiratory tract disease pertussis, also known as whooping cough. Infection with Bp occurs via airways and transmission of the bacterium occurs via respiratory droplets. Although the introduction of vaccines against pertussis (1940s/1950s) have resulted in a great reduction in reported cases, there is still a high disease burden (**Figure 12**). In 2018, there were 35.627 reported pertussis cases in Europe, of which 10 had a fatal outcome.[90] However, it is generally assumed that there is an underreporting of pertussis cases, and thus that actual number of cases is higher. Worldwide, an estimated 300.000-400.000 pertussis related deaths occur annually, mostly affecting infants and people in developing countries. [91,92]

The initial pertussis vaccines were whole cell pertussis vaccines (wP vaccines), which contained inactivated Bp. However, due to the unfavorable reactogenicity profile of the wP vaccine, many countries switched to acellular pertussis vaccines (aP vaccines).[93,94] The aP vaccines contain one or more Bp antigens, such as pertussis toxin, pertactin, filamentous hemagglutinin and fimbriae2/3, and are adjuvanted with aluminum hydroxide. Vaccines against pertussis are generally combined vaccines that also provide protection against diphtheria, tetanus and

in some cases also *Haemophilus influenzae* type B, polio or hepatitis B.[95] In the US, the first aP vaccine was licensed in 1996, and in Europe, transition towards aP vaccines started in 1995 (Netherlands: 2005).[96]

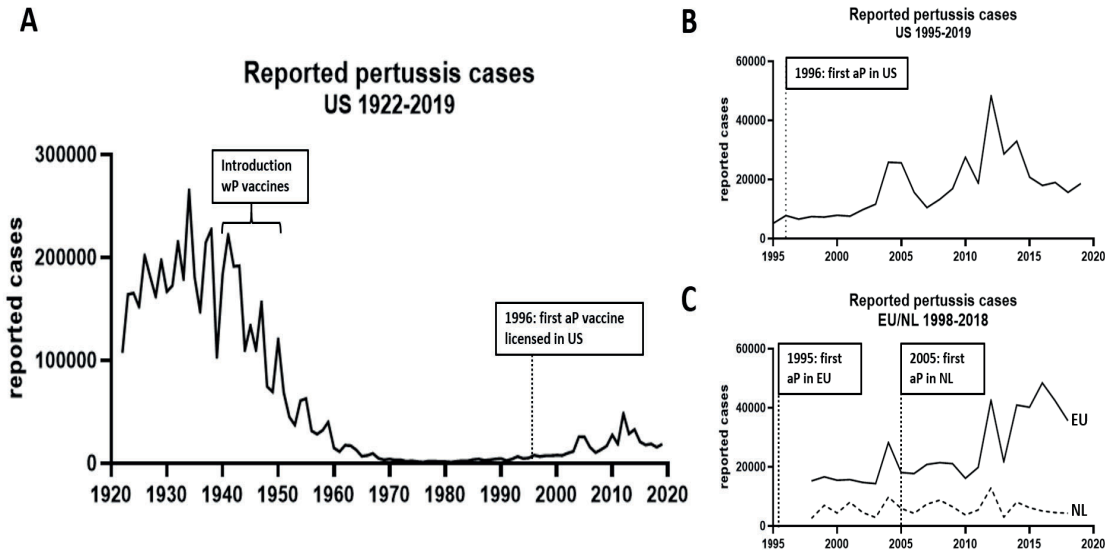


**Figure 12.** Number of reported pertussis cases in (A) the US (1922-2019), (B) the US (1995-2019), and (C) Europe (EU) and the Netherlands (1998-2018, timeline starts at 1995). Reported pertussis cases were retrieved from the Center for Disease Control.[99] Reported pertussis cases for Europe/Netherlands were retrieved from the European surveillance atlas for infectious diseases.[100]

Nowadays, most high income countries use aP vaccines, whereas several low- and middle income countries still use the wP vaccine.[96,97] Although the introduction of pertussis vaccines in 1940s/1950s resulted in a strong reduction of the number of cases, the incidence of pertussis has increased in the past decennia with a shift in reported cases from young children to adolescents and adults (**Figure 12**).[92,98-100] This may be explained by the fact that protection against Bp is not life-long. Moreover, several studies suggested that aP-induced immunity wanes faster than wP vaccine-induced immunity.[92,93] Dependent on the type of vaccine (wP or aP vaccine), different cellular and serological responses were detected, such as skewing of the Th-response and differences in induced vaccine-specific serum immunoglobulin subclasses.[101-103] In addition, baboon studies have shown that wP and aP vaccines do not prevent transmission of Bp (with wP vaccines being more efficient in reducing colonization and transmission than aP vaccines).[104] Thus, although vaccinated individuals were protected from disease, they could still transmit the pathogen upon infection. Indeed, most pertussis cases with severe outcome are found in unprotected individuals, especially unvaccinated or incompletely vaccinated infants.[92,98] Thus, it is of importance to develop new pertussis vaccines that protect against colonization and transmission.

To develop new vaccination strategies, it is important to gain a thorough understanding of differences and similarities in the immune response induced by per-



tussis vaccines and natural infection. Previous studies showed that the cellular and serological responses post-vaccination differed from cellular and serological responses measured in patients with a natural infection.[101] However, patient settings are not optimal due to heterogeneity in the cohort and the number of unknown factors (for example, time since infection, time since symptoms, baseline parameters). In contrast, human challenge studies allow for safe and controlled infection, with the option to monitor/predefine many parameters, and with standardized clinical readout. Therefore, such studies can be an immense source of new information regarding immune responses to “natural infection” and the induction of protective immunity.

In the case of pertussis, there are several differences between vaccination and natural infection that can influence the induced immune response. The major differences between current Bp vaccines and natural infection are the site of antigen encounter (deltoid muscle vs respiratory tract) and the variety/concentration of antigens (as indicated above; pertussis vaccines are combination vaccines). Upon vaccination, a high load of Bp (and other) antigens is injected in the muscle (skipping the first line of defense), whereas upon natural infection, the antigenic load of Bp may be a lot lower and more gradually encountered, as the Bp initially encounters the first line of defense (physical and mechanical defenses, mucosal tract). The encounter of bacteria in mucosal areas may initiate immune processes (mucosal responses) that are not induced upon primary vaccination but may be of importance for the induction of protective immunity against infection and transmission. Prevention of transmission is not only of importance to pertussis vaccines but may play a role in other infectious respiratory diseases, such as SARS-CoV-2.

### **1.8 Immune monitoring outside the healthy adult population**

Aside from vaccine evaluation (generally occurring in healthy adults), immune monitoring can be applied in many other situations. In the field of diagnostics, immune monitoring is a valuable tool that can help with the identification or exclusion of hematological malignancies or immune deficiencies. Moreover, the reconstitution of immune system after hematopoietic stem cell transplantation or immunosuppressive treatments and targeted immunotherapies can be subjected to immune monitoring. Thus, immune monitoring has many applications.

One specific group in which monitoring is becoming more important is the aging population. Increased welfare, because of economical and medical improvements, has resulted in people all around the globe living longer. The WHO has estimated that in the coming 25-30 years, the number of individuals aged 60 or older will double, from 1 billion in 2020 to about 2.1 billion in 2050.[105] In majority of people, aging goes hand in hand with a decline in cognitive and/or physical health. There are many age-related impairments, such as lowered resistance to infection, dementia, osteoporosis, atherosclerosis and diabetes, which are directly or indirectly related to the aging immune system, especially to the low grade inflammation that is often observed in older individuals (inflammaging).[20,106]

## Chapter 1

---

This overall increase in age creates new challenges for our medical system and the way we monitor the immune system of these individuals (for example; when a population is reaching older age, should we adjust the parameters defining 'healthy reference values' in such individuals?).

Upon aging, the numbers and distribution of circulating immune cells and the functioning of immune cells change. The output of naive B and T cells into the periphery decreases, which leads to a decrease in naive cells in the circulation. This, in combination with the reported increase in oligoclonality in older adults results in a decreased B and T-cell repertoire.[19-21] Moreover, impaired germinal center formation, reduced affinity maturation, memory B-cell formation and lowered levels of plasma cells in the bone marrow have been reported in both human and animal models.[19] Additionally, the functioning of innate immune cells declines. Several studies reported a lowered capacity to phagocytose opsonized particles and produce ROS in neutrophils derived from aged individuals.[21,107] Moreover, reduced phagocytic capacity, lowered ROS production and lower anti-tumor properties were reported for monocytes derived from older adults.[20,108,109] Lastly, immune cells with unusual phenotypes can get a more prominent place during the aging process, as was shown for the so-called 'age-associated B cells'.[1,110,111] Altogether, these processes indicate that upon aging, individuals become less equipped to deal with infection and inflammation. This does not only influence 'natural encounters' but may also negatively impact the induction of protective immunity by means of vaccination.

Indeed, several studies evaluating vaccine responses in the elderly have shown reduced vaccination responses, such as reduced Ag-specific serum immunoglobulins, immunoglobulin functioning (neutralizing or inhibiting capacity), and plasma cell counts.[1] Of note, although reduced immune responses were observed in several of these studies, there was still an expected benefit of the vaccination. However, the impact of aging was not consistent between these studies. A possible explanation is the stringency of the inclusion criteria. As indicated above, majority of individuals experience a cognitive and physical decline upon aging. However, we know from studies that this decline varies between individuals and can be influenced by several factors, such as lifestyle, stress factors and genetics. Depending on these factors, a person can age well or poorly. Therefore, not only the age in years, but also the 'biological age' influences the ability of an individual to respond to antigen-challenge. Thus, when a study has stringent health-related inclusion criteria, it may automatically select for individuals that are aging well, and thus reduce the impact of the age in years. In order to harmonize the study cohorts in immunogerontological studies, protocols have been composed to better select and describe the elderly cohort, for example the SENI-EUR protocol.[112]

Although majority of individuals show physical and cognitive decline upon aging, there is a selected group of individuals that ages well. Although their successful aging is most likely a combination of several factors, multiple studies have sear-

ched for factors that are associated with good or poor aging.[113,114] The ApoE4 allele is a well-known genetic factor negatively associated with longevity, but there are many more gene variants associated with increased or decreased likelihood of longevity. Examples of gene variants positively associated with longevity are the 1082GG polymorphism in the gene encoding IL-10, the Asp299Gly polymorphism in the gene encoding TLR4, and the P522R polymorphism in the gene encoding PLC $\gamma$ 2.[114,115] As indicated before, aging is in part an immunological process. Therefore, it is relevant to understand the impact of these factors associated with successful aging/increased resilience against aging. Better insight in these processes may help guide and design future therapies for age-related complications.

### 1.9 Outline of this thesis

Standardization in clinical trials is crucial to obtain data that is reliable and comparable in-between study locations. Therefore, we first evaluated the influence of pre- and post-analytical procedures on the quality of flow-cytometric immunophenotyping in blood. In **Chapter 2**, we assessed the impact of delayed sample processing and acquisition, storage temperature and fixating agents on quantity and distribution of leukocyte subsets (**2.1**). We showed that blood samples stored for <24h at room temperature before processing and staining seem most suitable for reliable immunophenotyping, despite observed losses in absolute cell numbers. Next, we measured the impact of delayed sample processing on the performance of a database-driven analysis (**2.2**). Here, we showed that automated analysis is superior to manual analysis regarding reproducibility and robustness, although expert revision of these automated files remains necessary in samples with numerical alterations and aberrant B- and T-cell maturation and/or marker expression profiles.

Knowledge gathered in studies presented in **Chapter 2** was utilized in several clinical trials where we aimed to dissect the cellular immune responses following controlled pertussis infection or vaccination. These clinical trials were initiated locally at the LUMC or within the IMI-2 PERISCOPE Consortium and their major outcomes are summarized in **Chapter 3**. Initially, within LUMC, we performed an extensive trial, in which we investigated kinetics of multiple leukocyte subsets over time following vaccination (**3.1**). This allowed us to determine the most relevant timepoints and populations for the follow up analysis. Additionally, this set of data could be used as a ‘framework’, on which we projected data of subsequent vaccination study, where we collected samples from fewer timepoints, but from more diverse cohorts (different ages and priming backgrounds) (**3.2**). There, we showed that the plasma cell response initiated after Tdap booster vaccination differed with age and priming background. Cellular analysis of the immune response to pertussis vaccination was further extended by molecular studies using single cell sequencing technologies on highly enriched plasma cell samples from one vaccinated individual (**3.3**). In this study, we developed a pipeline for analysis of such samples, including hallmarks of antigen exposure, such as somatic hypermutation and clonal expansion. Additionally, we established a query tool to



identify B-cell receptors related to anti-tetanus and anti-pertussis toxoid responses. Finally, in **3.4**, we compared the findings from the vaccination studies with the kinetics found in individuals that were or were not protected against colonization in a controlled bacterial challenge with the same pathogen (*B. pertussis*). Here, we showed that donors that were protected from colonization showed distinct early cellular kinetics. Moreover, we showed that the plasma cell response generated after booster vaccination or bacterial challenge differed with regards to timing, magnitude, maturation, and polarization to specific Ig subsets. With this information we can better understand immunity against pertussis and use this knowledge for future pertussis vaccine evaluations.

In **Chapter 4** we evaluated the SARS-CoV-2 vaccination responses in a cohort of older adults/elderly with or without a specific variant of the *PLCG2* gene. This variant is associated with cognitively healthy aging and longevity, but its impact on the immune system remains unknown. Therefore, we extended this study by an in-depth analysis of the quantity and functionality of the circulating immune cells. Although no differences were observed in the responses against SARS-CoV-2 vaccination, carriers of this variant tended to show less signs of immunosenescence compared to age-matched non-carriers.

Lastly, in **Chapter 5**, we discuss the general findings of this thesis and outline future directions that, we believe, should be pursued to reliably gain more insights in the human immune system.

### References

1. Diks AM, Overduin LA, Van Leenen LD, et al. B-Cell Immunophenotyping to Predict Vaccination Outcome in the Immunocompromised-A Systematic Review. *Frontiers in immunology*. 2021;3524.
2. Abbas AK, Lichtman AH, Pillai S. Cellular and molecular immunology. 7th ed: Elsevier Saunders; 2012.
3. Medzhitov R, Janeway Jr CA. Innate immune recognition and control of adaptive immune responses. Paper presented at: Seminars in immunology1998.
4. Banchereau J, Briere F, Caux C, et al. Immunobiology of dendritic cells. *Annual review of immunology*. 2000;18(1):767-811.
5. Tosi MF. Innate immune responses to infection. *Journal of Allergy and Clinical Immunology*. 2005;116(2):241-249.
6. Wang D, Feng J, Wen R, et al. Phospholipase C $\gamma$ 2 is essential in the functions of B cell and several Fc receptors. *Immunity*. 2000;13(1):25-35.
7. Underhill DM, Ozinsky A. Phagocytosis of microbes: complexity in action. *Annual review of immunology*. 2002;20(1):825-852.
8. Ziegler-Heitbrock L, Ancuta P, Crowe S, et al. Nomenclature of monocytes and dendritic cells in blood. *Blood*. 2010;116(16):e74-e80.
9. Hamers AA, Dinh HQ, Thomas GD, et al. Human monocyte heterogeneity as revealed by high-dimensional mass cytometry. *Arteriosclerosis, thrombosis, vascular biology*. 2019;39(1):25-36.
10. Damasceno D, Almeida J, Teodosio C, et al. Monocyte Subsets and Serum Inflammatory and Bone-Associated Markers in Monoclonal Gammopathy of Undetermined Significance and Multiple Myeloma. *Cancers*. 2021;13(6):1454.
11. Damasceno D, Teodosio C, van den Bossche WB, et al. Distribution of subsets of blood monocytic cells throughout life. *Journal of Allergy Clinical Immunology*. 2019;144(1):320-323. e326.
12. Segura E. Review of mouse and human dendritic cell subsets. *Dendritic Cell Protocols*. 2016:3-15.

13. Stone KD, Prussin C, Metcalfe DD. IgE, mast cells, basophils, and eosinophils. *Journal of Allergy Clinical Immunology*. 2010;125(2):S73-S80.
14. Van Zelm MC, Van Der Burg M, Langerak AW, Van Dongen JJ. PID comes full circle: applications of V (D) J recombination excision circles in research, diagnostics and newborn screening of primary immunodeficiency disorders. *Frontiers in immunology*. 2011;2:12.
15. van Dongen JJ, Wolvers-Tettero IL. Analysis of immunoglobulin and T cell receptor genes. Part I: Basic and technical aspects. *Clinica Chimica Acta*. 1991;198(1-2):1-92.
16. Oettinger MA. V (D) J recombination: on the cutting edge. *Current opinion in cell biology*. 1999;11(3):325-329.
17. Schatz DG, Ji Y. Recombination centres and the orchestration of V (D) J recombination. *Nature Reviews Immunology*. 2011;11(4):251-263.
18. Chien Y-H, Bonneville M. Gamma delta T cell receptors. *Cellular Molecular Life Sciences CMLS*. 2006;63(18):2089-2094.
19. Cancro MP, Hao Y, Scholz JL, et al. B cells and aging: molecules and mechanisms. *Trends in immunology*. 2009;30(7):313-318.
20. Castelo-Branco C, Soveral I. The immune system and aging: a review. *Gynecological Endocrinology*. 2014;30(1):16-22.
21. Frasca D, Diaz A, Romero M, Garcia D, Blomberg BB. B cell immunosenescence. *Annual review of cell developmental biology*. 2020;36:551-574.
22. Mahnke YD, Brodie TM, Sallusto F, Roederer M, Lugli E. The who's who of T-cell differentiation: human memory T-cell subsets. *European journal of immunology*. 2013;43(11):2797-2809.
23. Eyerich S, Zielinski CE. Defining Th-cell subsets in a classical and tissue-specific manner: examples from the skin. *European journal of immunology*. 2014;44(12):3475-3483.
24. Gatto D, Brink R. The germinal center reaction. *Journal of Allergy and Clinical Immunology*. 2010;126(5):898-907.
25. Eyerich S, Eyerich K, Pennino D, et al. Th22 cells represent a distinct human T cell subset involved in epidermal immunity and remodeling. *The Journal of clinical investigation*. 2009;119(12):3573-3585.
26. Stockinger B, Veldhoen M. Differentiation and function of Th17 T cells. *Current opinion in immunology*. 2007;19(3):281-286.
27. Botafogo V, Pérez-Andres M, Jara-Acevedo M, et al. Age distribution of multiple functionally relevant subsets of CD4+ T cells in human blood using a standardized and validated 14-color EuroFlow immune monitoring tube. *Frontiers in immunology*. 2020;11:166.
28. Fichtner AS, Ravens S, Prinz I. Human  $\gamma\delta$  TCR repertoires in health and disease. *Cells*. 2020;9(4):800.
29. Dasgupta A, Saxena R. Regulatory T cells: a review. *Natl Med J India*. 2012;25(6):341-351.
30. King C. New insights into the differentiation and function of T follicular helper cells. *Nature Reviews Immunology*. 2009;9(11):757-766.
31. Vermijlen D, Gatti D, Kouzeli A, Rus T, Eberl M.  $\gamma\delta$  T cell responses: How many ligands will it take till we know? Paper presented at: Seminars in cell & developmental biology 2018.
32. Ghia P, Ten Boekel E, Sanz E, De La Hera A, Rolink A, Melchers F. Ordering of human bone marrow B lymphocyte precursors by single-cell polymerase chain reaction analyses of the rearrangement status of the immunoglobulin H and L chain gene loci. *The Journal of experimental medicine*. 1996;184(6):2217-2230.
33. Van Zelm MC, Van Der Burg M, Van Dongen JJ. Homeostatic and maturation-associated proliferation in the peripheral B-cell compartment. *J Cell Cycle*. 2007;6(23):2890-2895.
34. Abbas AK, Lichtman AH, Pillai S. *Cellular and Molecular Immunology 7e-11 - B cell activation and antibody production*. In: Philadelphia, PA, USA: Elsevier Saunders; 2012:243-268.
35. Kurosaki T, Shinohara H, Baba Y. B cell signaling and fate decision. *Annual review of immunology*. 2009;28:21-55.
36. Hikida M, Kurosaki T. Regulation of phospholipase C- $\gamma$ 2 networks in B lymphocytes. *J Advances in immunology*. 2005;88:73-96.
37. Sugawara H, Kurosaki M, Takata M, Kurosaki T. Genetic evidence for involvement of type 1, type 2 and type 3 inositol 1, 4, 5-trisphosphate receptors in signal transduction through the B-cell antigen receptor. *The EMBO journal*. 1997;16(11):3078-3088.
38. Toker A. Signaling through protein kinase C. *Frontiers in Bioscience*. 1998;3(1):1134-1147.
39. Vidarsson G, Dekkers G, Rispens T. IgG subclasses and allotypes: from structure to effector

## Chapter 1

---

functions. *Frontiers in immunology*. 2014;5:520.

40. Geisberger R, Lamers M, Achatz G. The riddle of the dual expression of IgM and IgD. *Immunology*. 2006;118(4):429-437.
41. Woof JM, Kerr MA. The function of immunoglobulin A in immunity. *The Journal of Pathology: A Journal of the Pathological Society of Great Britain Ireland*. 2006;208(2):270-282.
42. Schroeder Jr HW, Cavacini L. Structure and function of immunoglobulins. *Journal of Allergy Clinical Immunology*. 2010;125(2):S41-S52.
43. Berkowska M. PhD thesis: Generation of an immunocompetent B-cell repertoire 2012.
44. Siminovitch KA, Bakhshi A, Goldman P, Korsmeyer SJ. A uniform deleting element mediates the loss of  $\kappa$  genes in human B cells. *Nature immunology*. 1985;316(6025):260-262.
45. Inlay M, Alt FW, Baltimore D, Xu Y. Essential roles of the  $\kappa$  light chain intronic enhancer and 3' enhancer in  $\kappa$  rearrangement and demethylation. *Nature immunology*. 2002;3(5):463-468.
46. Van Zelm MC, Szczepański T, Van Der Burg M, Van Dongen JJ. Replication history of B lymphocytes reveals homeostatic proliferation and extensive antigen-induced B cell expansion. *The Journal of experimental medicine*. 2007;204(3):645-655.
47. van der Burg M, Tümkaya T, Boerma M, de Bruin-Versteeg S, Langerak AW, van Dongen JJ. Ordered recombination of immunoglobulin light chain genes occurs at the IGK locus but seems less strict at the IGL locus. *Blood, The Journal of the American Society of Hematology*. 2001;97(4):1001-1008.
48. Van Zelm MC, Van Der Burg M, De Ridder D, et al. Ig gene rearrangement steps are initiated in early human precursor B cell subsets and correlate with specific transcription factor expression. *The Journal of Immunology*. 2005;175(9):5912-5922.
49. Dongen JJMv, Szczepanski T, Inventors. Determining the replicative history of lymphocytes. 2004.
50. Hazenberg MD, Verschuren MC, Hamann D, Miedema F, van Dongen JJ. T cell receptor excision circles as markers for recent thymic emigrants: basic aspects, technical approach, and guidelines for interpretation. *Journal of molecular medicine*. 2001;79(11):631-640.
51. Breit TM, Verschuren M, Wolvers-Tettero I, Van Gastel-Mol E, Hählen K, Van Dongen J. Human T cell leukemias with continuous V (D) J recombinase activity for TCR-delta gene deletion. *The Journal of Immunology*. 1997;159(9):4341-4349.
52. Blom M, Bredius RG, Weijman G, et al. Introducing newborn screening for severe combined immunodeficiency (SCID) in the Dutch neonatal screening program. *International Journal of Neonatal Screening*. 2018;4(4):40.
53. Shinwari K, Bolkov M, Tuzankina IA, Chereshev VA. Newborn Screening through TREC, TREC/KREC System for Primary Immunodeficiency with limitation of TREC/KREC. *Comprehensive Review. Anti-Inflammatory Anti-Allergy Agents in Medicinal Chemistry*. 2021;20(2):132-149.
54. Pavlasova G, Mraz M. The regulation and function of CD20: an "enigma" of B-cell biology and targeted therapy. *Haematologica*. 2020;105(6):1494.
55. Caraux A, Klein B, Paiva B, et al. Circulating human B and plasma cells. Age-associated changes in counts and detailed characterization of circulating normal CD138<sup>-</sup> and CD138<sup>+</sup> plasma cells. *haematologica*. 2010;95(6):1016.
56. Perez-Andres M, Paiva B, Nieto WG, et al. Human peripheral blood B-cell compartments: a crossroad in B-cell traffic. *Cytometry Part B: Clinical Cytometry*. 2010;78(S1):S47-S60.
57. Oracki SA, Walker JA, Hibbs ML, Corcoran LM, Tarlinton DM. Plasma cell development and survival. *Immunological reviews*. 2010;237(1):140-159.
58. Blanco E, Pérez-Andrés M, Arriba-Méndez S, et al. Age-associated distribution of normal B-cell and plasma cell subsets in peripheral blood. *Journal of Allergy and Clinical Immunology*. 2018;141(6):2208-2219. e2216.
59. Berkowska MA, Driessen GJ, Bikos V, et al. Human memory B cells originate from three distinct germinal center-dependent and-independent maturation pathways. *Blood, The Journal of the American Society of Hematology*. 2011;118(8):2150-2158.
60. Butcher EC, Picker LJ. Lymphocyte homing and homeostasis. *Science*. 1996;272(5258):60-67.
61. Springer TA. Traffic signals for lymphocyte recirculation and leukocyte emigration: the multistep paradigm. *Cells*. 1994;76(2):301-314.
62. van den Bossche WB, Rykov K, Teodosio C, et al. Flow cytometric assessment of leukocyte kinetics for the monitoring of tissue damage. *Clinical Immunology*. 2018;197:224-230.

63. Odendahl M, Mei H, Hoyer BF, et al. Generation of migratory antigen-specific plasma blasts and mobilization of resident plasma cells in a secondary immune response. *Blood*. 2005;105(4):1614-1621.
64. Van Dongen JJM, Van Der Burg M, Kalina T, et al. EuroFlow-based flowcytometric diagnostic screening and classification of primary immunodeficiencies of the lymphoid system. *Frontiers in immunology*. 2019;10:1271.
65. Clay TM, Hobeika AC, Mosca PJ, Lyerly HK, Morse MA. Assays for monitoring cellular immune responses to active immunotherapy of cancer. *Clinical Cancer Research*. 2001;7(5):1127-1135.
66. van Zelm MC, McKenzie CI, Varese N, Rolland JM, O'Hehir RE. Recent developments and highlights in immune monitoring of allergen immunotherapy. *Allergy*. 2019;74(12):2342-2354.
67. Edwards KM, Berbers GA. Immune responses to pertussis vaccines and disease. *The Journal of infectious diseases*. 2014;209(suppl\_1):S10-S15.
68. Mollers M, Vossen JM, Scherpenisse M, van der Klis FR, Meijer CJ, de Melker HE. current knowledge on the role of HPV antibodies after natural infection and vaccination: implications for monitoring an HPV vaccination programme. *Journal of medical virology*. 2013;85(8):1379-1385.
69. van Beers JJ, Damoiseaux JG. Immune Monitoring upon Treatment with Biologics in Sjögren's Syndrome: The What, Where, When, and How. *Biomolecules*. 2021;11(1):116.
70. Kalina T, Bakardjieva M, Blom M, et al. EuroFlow standardized approach to diagnostic immunophenotyping of severe PID in newborns and young children. *Frontiers in immunology*. 2020;11:371.
71. Plotkin SA. Correlates of protection induced by vaccination. *Clinical vaccine immunology*. 2010;17(7):1055-1065.
72. Buisman A, De Rond C, Öztürk K, Ten Hulscher H, Van Binnendijk R. Long-term presence of memory B-cells specific for different vaccine components. *Vaccine*. 2009;28(1):179-186.
73. Brown M, Wittwer C. Flow cytometry: principles and clinical applications in hematology. *Clinical chemistry*. 2000;46(8):1221-1229.
74. Sanjabi S, Lear S. New cytometry tools for immune monitoring during cancer immunotherapy. *Cytometry Part B: Clinical Cytometry*. 2021;100(1):10-18.
75. Jensen HA, Wnek R. Analytical performance of a 25-marker spectral cytometry immune monitoring assay in peripheral blood. *Cytometry Part A*. 2021;99(2):180-193.
76. Adan A, Alizada G, Kiraz Y, Baran Y, Nalbant A. Flow cytometry: basic principles and applications. *Critical reviews in biotechnology*. 2017;37(2):163-176.
77. Kalina T, Flores-Montero J, Van Der Velden V, et al. EuroFlow standardization of flow cytometer instrument settings and immunophenotyping protocols. *Leukemia*. 2012;26(9):1986-2010.
78. Finak G, Langweiler M, Jaimes M, et al. Standardizing flow cytometry immunophenotyping analysis from the human immunophenotyping consortium. *Scientific reports*. 2016;6(1):1-11.
79. Pedreira C, da Costa ES, Lecrevisse Q, et al. From big flow cytometry datasets to smart diagnostic strategies: The EuroFlow approach. *Journal of immunological methods*. 2019;475:112631.
80. Streitz M, Miloud T, Kapinsky M, et al. Standardization of whole blood immune phenotype monitoring for clinical trials: panels and methods from the ONE study. *Transplantation research*. 2013;2(1):1-15.
81. Kalina T, Flores-Montero J, Lecrevisse Q, et al. Quality assessment program for Euro Flow protocols: Summary results of four-year (2010–2013) quality assurance rounds. *Cytometry Part A*. 2015;87(2):145-156.
82. Nicholson JK, Green TA. Selection of anticoagulants for lymphocyte immunophenotyping: effect of specimen age on results. *Journal of immunological methods*. 1993;165(1):31-35.
83. Davis C, Wu X, Li W, Fan H, Reddy M. Stability of immunophenotypic markers in fixed peripheral blood for extended analysis using flow cytometry. *Journal of immunological methods*. 2011;363(2):158-165.
84. Ng AA, Lee BT, Teo TS, Poidinger M, Connolly JE. Optimal cellular preservation for high dimensional flow cytometric analysis of multicentre trials. *Journal of immunological methods*. 2012;385(1-2):79-89.
85. Hodge G, Flower R, Han P. Optimal storage conditions for preserving granulocyte viability as monitored by Annexin V binding in whole blood. *Journal of immunological methods*. 1999;225(1-2):27-38.
86. Ekong T, Hill AM, Gompels M, Brown A. The effect of the temperature and duration of sample storage on the measurement of lymphocyte subpopulations from HIV-1-positive and control



## Chapter 1

---

- subjects. *Journal of immunological methods*. 1992;151(1-2):217-225.
87. Liang F, Loré K. Local innate immune responses in the vaccine adjuvant-injected muscle. *Clinical translational immunology*. 2016;5(4):e74.
88. Coffman RL, Sher A, Seder RA. Vaccine adjuvants: putting innate immunity to work. *Immunity*. 2010;33(4):492-503.
89. Roush SW, Murphy TV, Group V-PDTW. Historical comparisons of morbidity and mortality for vaccine-preventable diseases in the United States. *JAMA*. 2007;298(18):2155-2163.
90. European Centre for Disease Prevention and Control ECDC. Surveillance Atlas of Infectious Diseases Reported pertussis cases and pertussis-related deaths - Dataset provided by ECDC based on data provided by WHO and Ministries of Health from the affected countries. Available at: <http://atlas.ecdc.europa.eu/public/index.aspx>. Accessed 05-08-2021.
91. Crowcroft N, Stein C, Duclos P, Birmingham M. How best to estimate the global burden of pertussis? *The Lancet infectious diseases*. 2003;3(7):413-418.
92. Wood N, McIntyre P. Pertussis: review of epidemiology, diagnosis, management and prevention. *J Paediatric respiratory reviews*. 2008;9(3):201-212.
93. Burdin N, Handy LK, Plotkin SA. What is wrong with pertussis vaccine immunity? The problem of waning effectiveness of pertussis vaccines. *Cold Spring Harbor perspectives in biology*. 2017;9(12):a029454.
94. Lambert LC. Pertussis vaccine trials in the 1990s. *The Journal of infectious diseases*. 2014;209(suppl\_1):S4-S9.
95. Rijksinstituut voor Volksgezondheid En Milieu RIVM. Rijksvaccinatieprogramma [EN: National Immunization Programme]. <https://rijksvaccinatieprogramma.nl/english>. Accessed 06-08-2021.
96. Therre H, Baron S. Pertussis immunisation in Europe—the situation in late 1999. *Eurosurveillance*. 2000;5(1):6-10.
97. Forsyth KD, Tan T, von König C-HW, Heininger U, Chitkara AJ, Plotkin S. Recommendations to control pertussis prioritized relative to economies: A Global Pertussis Initiative update. *Vaccine*. 2018;36(48):7270-7275.
98. Bamberger ES, Srugo I. What is new in pertussis? *European journal of pediatrics*. 2008;167(2):133-139.
99. Center for Disease Control CDC. reported pertussis cases by year since 1922. 2022; [www.cdc.gov/pertussis/surv-reporting/cases-by-year.html](http://www.cdc.gov/pertussis/surv-reporting/cases-by-year.html). Accessed 19-01-2022.
100. European Centre for Disease Prevention and Control ECDC. Reported pertussis cases ECDC. 2022; reported pertussis cases Europe/Netherlands. Available at: [www.atlas.ECDC.Europe.com](http://www.atlas.ECDC.Europe.com). Accessed 19-01-2022.
101. Higgs R, Higgins S, Ross P, Mills K. Immunity to the respiratory pathogen *Bordetella pertussis*. *Mucosal immunology*. 2012;5(5):485-500.
102. Hendriks LH, Schure R-M, Öztürk K, et al. Different IgG-subclass distributions after whole-cell and acellular pertussis infant primary vaccinations in healthy and pertussis infected children. *Vaccine*. 2011;29(40):6874-6880.
103. Van Der Lee S, Hendriks LH, Sanders EA, Berbers GA, Buisman AM. Whole-cell or acellular pertussis primary immunizations in infancy determines adolescent cellular immune profiles. *Frontiers in immunology*. 2018;9:51.
104. Warfel JM, Zimmerman LI, Merkel TJ. Acellular pertussis vaccines protect against disease but fail to prevent infection and transmission in a nonhuman primate model. *Proceedings of the National Academy of Sciences*. 2014;111(2):787-792.
105. WHO. Ageing and Health - Key Facts. [WHO web page]. 2021; Home/Newsroom/Fact sheets/Detail/Ageing and health. Available at: <https://www.who.int/news-room/fact-sheets/detail/ageing-and-health>. Accessed November, 9th 2021.
106. Franceschi C, Bonafè M, Valensin S, et al. Inflamm-aging: an evolutionary perspective on immunosenescence. *Annals of the new York Academy of Sciences*. 2000;908(1):244-254.
107. Fortin CF, McDonald PP, Lesur O, Fülöp Jr T. Aging and neutrophils: there is still much to do. *Rejuvenation research*. 2008;11(5):873-882.
108. McLachlan JA, Serkin CD, Morrey KM, Bakouche O. Antitumoral properties of aged human monocytes. *The Journal of Immunology*. 1995;154(2):832-843.
109. Hearps AC, Martin GE, Angelovich TA, et al. Aging is associated with chronic innate immune activation and dysregulation of monocyte phenotype and function. *Aging cell*. 2012;11(5):867-875.

110. Nipper AJ, Smithey MJ, Shah RC, Canaday DH, Landay AL. Diminished antibody response to influenza vaccination is characterized by expansion of an age-associated B-cell population with low PAX5. *Clinical Immunology*. 2018;193:80-87.
111. Frasca D, Diaz A, Romero M, Blomberg BB. Human peripheral late/exhausted memory B cells express a senescent-associated secretory phenotype and preferentially utilize metabolic signaling pathways. *Experimental gerontology*. 2017;87:113-120.
112. Ligthart GJ, Corberand JX, Fournier C, et al. Admission criteria for immunogerontological studies in man: the SENIEUR protocol. *Mechanisms of ageing development*. 1984;28(1):47-55.
113. Wagner K-H, Cameron-Smith D, Wessner B, Franzke B. Biomarkers of aging: from function to molecular biology. *J Nutrients*. 2016;8(6):338.
114. van der Lee SJ, Conway OJ, Jansen I, et al. A nonsynonymous mutation in PLCG2 reduces the risk of Alzheimer's disease, dementia with Lewy bodies and frontotemporal dementia, and increases the likelihood of longevity. *Acta neuropathologica*. 2019;138(2):237-250.
115. Capri M, Salvioli S, Sevini F, et al. The genetics of human longevity. *Annals of the New York Academy of Sciences*. 2006;1067(1):252-263.



## Chapter 2.1

# Impact of blood storage and sample handling on quality of high dimensional flow cytometric data in multicenter clinical research

A.M. Diks<sup>1</sup>, C. Bonroy<sup>2 3</sup>, C. Teodosio<sup>1</sup>, R.J. Groenland<sup>1</sup>, B. de Mooij<sup>1</sup>, E. De Maertelaere<sup>3</sup>, J. Neiryck<sup>3</sup>, J. Philippé<sup>2 3</sup>, A. Orfao<sup>4</sup>, J.J.M. van Dongen<sup>1</sup>, M.A. Berkowska<sup>1</sup>

<sup>1</sup> Department of Immunohematology and Blood Transfusion, Leiden University Medical Center, Albinusdreef 2, 2333 ZA Leiden, Netherlands

<sup>2</sup> Department of Diagnostic Sciences, Ghent University, Ghent, Belgium

<sup>3</sup> Department of Laboratory Medicine, Ghent University Hospital, Ghent, Belgium

<sup>4</sup> Cancer Research Centre (IBMCC, USAL-CSIC; CIBERONC CB16/12/00400), Institute for Biomedical Research of Salamanca (IBSAL) and Department of Medicine and Cytometry Service (NUCLEUS Research Support Platform), University of Salamanca (USAL), Salamanca, Spain

**Journal of Immunological Methods, December 2019**  
**<https://doi.org/10.1016/j.jim.2019.06.007>**



### **Abstract**

Obtaining reliable and reproducible high quality data in multicenter clinical research settings requires design of optimal standard operating procedures. While the need for standardization in sample processing and data analysis is well-recognized, the impact of sample handling in the pre-analytical phase remains underestimated. We evaluated the impact of sample storage time ( $\approx$  transport time) and temperature, type of anticoagulant, and limited blood volume on reproducibility of flow cytometric studies.

EDTA and Na-Heparin samples processed with the EuroFlow bulk lysis protocol, stained and stored at 4°C showed fairly stable expression of cell surface markers and distribution of the major leukocyte populations for up to 72h. Additional sample fixation (1% PFA, Fix & Perm) did not have any beneficial effects. Blood samples stored for <24h at room temperature before processing and staining seemed suitable for reliable immunophenotyping, although losses in absolute cell numbers were observed. The major losses were observed in myeloid cells and monocytes, while lymphocytes seemed less affected. Expression of cell surface markers and population distribution were more stable in Na-Heparin blood than in EDTA blood. However, storage of Na-Heparin samples was associated with faster decrease in leukocyte counts over time. Whole blood fixation strategies (Cyto-Chex, TransFix) improved long-term population distribution, but were detrimental for expression of cellular markers. The main conclusions from this study on healthy donor blood samples were successfully confirmed in EDTA clinical (patient) blood samples with different time delays until processing. Finally, we recognized the need for adjustments in bulk lysis in case of insufficient blood volumes.

Despite clear overall conclusions, individual markers and cell populations had different preferred conditions. Therefore, specific guidelines for sample handling should always be adjusted to the clinical application and the main target leukocyte population.

**Keywords:** Flow cytometry, Immunophenotyping, Clinical trial, Blood storage, Sample fixation, Anticoagulant

## Introduction

Standardized sample processing, immunostaining procedures, and calibration of instruments assure quality and reproducibility of flow cytometric data [1, 2]. Still, limited guidelines are available for sample handling in the pre-analytical phase. Parameters such as sample volume, storage time and temperature, and type of anticoagulant seem crucial for optimal data quality, reproducibility, and correct data interpretation.

In multicenter studies transportation of samples is often required. Whenever granulocytes are not studied [3] and selective loss of leukocyte subsets can be afforded [4], batch shipment of cryopreserved mononuclear cells might be used. However, if precise quantification and detailed immunophenotyping of all leukocyte subsets is required, peripheral blood (PB) needs to be analyzed fresh prior to any substantial sample manipulation. Whenever sample collection and analysis cannot be performed at the same location, either fresh blood or stained blood samples are shipped for central data acquisition. Depending on the distance, availability of personnel and equipment, such shipment may cause serious delays.

Prolonged blood storage leads to selective loss of cell populations with a short half-life time, such as eosinophils and neutrophils [5, 6]. Additionally, biochemical changes, such as decrease in pH, changes in blood gases [7], alterations in the contents of amino acids, carbohydrates, lipids and cofactors [8, 9], might further influence cell viability. The magnitude of these changes partly depends on the temperature [10, 11]. Ng et al. reported that certain monocytes and natural killer (NK) cell subsets are relatively stable at 4°C [12], while Hodge et al. showed a delayed apoptosis of granulocytes in refrigerated blood [12, 13]. In contrast, lymphocyte stability is affected by low temperature, with optimal temperature for T cells being 14-16°C [14]. Thus, both time and temperature of blood storage need to be optimized for specific research questions.

Reagents like Cyto-Chex, TransFix and formaldehyde extend the storage time of whole blood prior to flow cytometric analysis [12, 15]. However, they might have some unwanted effects. Davis et al. and Ng et al. found that while Cyto-Chex is more effective in preserving cell counts, TransFix is more potent in preserving cell identity [12, 16]. The loss of signal intensity, especially in Cyto-Chex, was further confirmed by others [17].

The Fix & Perm reagent Kit (Nordic MUBio, Susteren, the Netherlands), Becton Dickinson Perm/Wash buffer (BD Biosciences, San Jose CA), paraformaldehyde (PFA), glutaraldehyde or ethanol are frequently used to stabilize processed and labeled samples [2, 18-21]. Still, these reagents may affect the detection of cell surface markers by reducing the availability of the targeted antigen epitopes [22, 23] and thereby hamper optimal discrimination between cell populations. So far, no extensive comparative study of the impact of these techniques on the quality of stained samples after storage has been performed.

## Chapter 2.1

Combining flow cytometry with functional assays may influence the choice of anticoagulant. Ethylene diamine tetra-acetate (EDTA) is generally preferred in immunophenotyping, but it retains calcium for enzymatic reactions which hampers functional studies; thus, for the latter assays EDTA should preferably be replaced by heparin [8]. Several studies have evaluated the impact of anticoagulant on sample stability. Heparin was found superior to EDTA in preserving granulocytes [13], while data on lymphocyte stability remains controversial [24, 25]. So far, little is known about the impact of anticoagulant on the stability of cellular markers over time.

Standardized protocols (e.g. the EuroFlow bulk lysis protocol [26]) are designed for predefined large blood volumes. If, for example in pediatric settings, sample volume is insufficient, protocol adjustments might improve the quality of the final data.

Here we evaluated the impact of different blood storage conditions and potential protocol adjustments on the quality of flow cytometric data in multicenter clinical research settings (**Figure 1**). For this purpose the highly standardized EuroFlow “primary immunodeficiency orientation tube” (PIDOT)[27], which allows identification of all major cell populations in blood, was used as a model to assess stability of cells and cell surface markers in healthy and clinical samples.

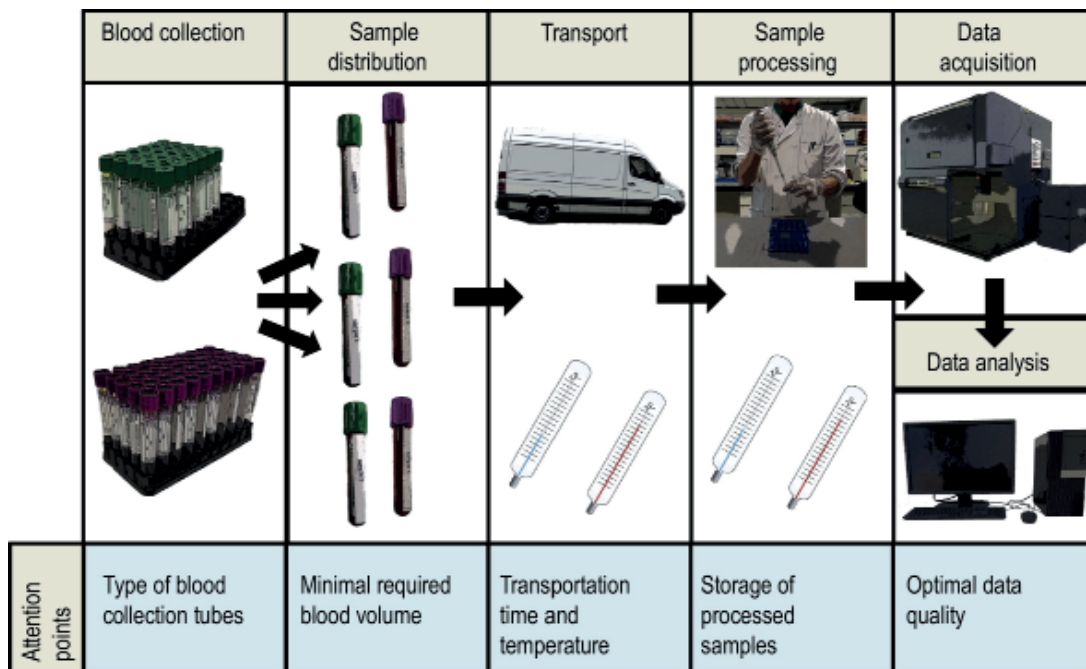


**Figure 1. Critical decision steps involving the sample pre-analytical phase in clinical trial design.** Depending on the design of the trial several decisions need to be made concerning (1) the choice of the blood collection tubes (anti-coagulant), (2) the distribution of samples based on the minimal volumes required per assay, (3) the time and temperature of sample transportation, and (4) storage of processed samples prior to data acquisition and data analysis.

## Materials and methods

### Samples

PB samples were obtained from healthy adult volunteers after they had given their informed consent to participate (n=15; m/f ratio: 5/10; age range: 23-62y, mean age: 36y). K<sub>3</sub>EDTA blood collection tubes (Vacuette®, Greiner Bio-One, Alphen aan den Rijn, the Netherlands) were used in all experiments, unless indicated otherwise. To evaluate the effect of anticoagulant on sample quality and stability, Na-Heparin blood collection tubes (Vacuette®, Greiner Bio-One) were used in parallel.

### Blood processing and staining with PIDOT

All PB samples were processed according to the EuroFlow bulk lysis standard operating protocol (SOP) (available at [www.EuroFlow.org](http://www.EuroFlow.org)). In brief, up to 2ml of blood was incubated with 50ml of ammonium chloride (NH<sub>4</sub>Cl) at room temperature (RT) on a roller bank to lyse non-nucleated red blood cells. After a washing step, nucleated cells were counted on an automated hematological analyzer (Sysmex XP-300, Sysmex Europe GmbH, Norderstedt, Germany), and  $2.5 \times 10^6$  cells were stained for 30min in the dark with the PIDOT antibody combination (Cytognos SL, Salamanca, Spain) according to the instructions of the manufacturer ([www.cytognos.com](http://www.cytognos.com))[27]. Finally, cells were incubated for 10min (in the dark; RT) with 2ml of BD FACS™ Lysing Solution (BD Biosciences), washed once and re-suspended in 200µl PBS prior to acquisition. A liquid format of the antibody combination was used [28], unless indicated otherwise. In the latter cases a dried version of PIDOT was used. Previous studies showed similar performance in samples stained using liquid and dried PIDOT [28].

In the experiments with limited sample volume, a modified version of the bulk lysis protocol was used where 100 or 200µl of K<sub>3</sub>EDTA PB sample was lysed in 3ml or 50ml of NH<sub>4</sub>Cl without cell counting prior to acquisition on the flow cytometer.

### Storage of stained samples (delayed acquisition)

Bulk-lysed PB samples stained with the PIDOT antibody combination were acquired directly or stored at 4°C for delayed acquisition (0h, 6h, 18h, 24h, 30h, 42h, 48h, 66h and 72h). In addition, part of the samples was treated with Reagent A of Fix & Perm® (F&P) or PFA (Merck, Darmstadt, Germany) to evaluate the effect of additional sample fixation on the stability of stained surface markers and leukocyte subset distribution. Treatment with Reagent A (F&P) was performed according to the manufacturer's protocol. In brief, after treatment with 1x BD FACS™ Lysing Solution and a washing step, 100µl of sample was incubated with 100µl of Reagent A for 15min in the dark (RT). Afterwards, samples were washed and stored in 200µl of PBS at 4°C for up to 72h. Treatment with PFA was performed in a comparable way, except for the incubation that was performed on ice. After initial evaluation of PFA concentration (0.5%, 1% and 2% final concentration), 1% PFA was used.

### **Storage of whole blood samples (delayed processing and staining)**

To investigate the effect of prolonged blood storage on data quality, K3EDTA and Na-Heparin blood samples were stored at RT or 4°C for up to 72h prior to processing and staining. Additionally, treatment with TransFix (Cytomark, Leeds, UK) and Cyto-Chex blood collection tubes (Streck Cyto-Chex™, La Vista, NE) were evaluated.

TransFix was added to PB in K3EDTA collection tubes according to manufacturer's protocol (Revision 3 US, 2016-11). Both storage at RT (for up to 4 days) and at 4°C (for up to 14 days) were investigated. Cyto-Chex blood collection tubes were used according to manufacturer's protocol (Version 2017-02) and stored at RT for evaluation for up to 14 days.

### **Evaluation of absolute cell numbers**

Two alternative approaches were used to determine absolute cell counts in (aged) K3EDTA and Na-Heparin blood samples. First, absolute leukocyte counts were measured on an automated hematological analyzer (Sysmex XP-300) at 0h, 6h, 12h, 24h, 30h, 36h, 48h, 54h, 60h and 72h after blood drawing. Then, analyses were repeated with Perfect-Count Microspheres™ (Cytognos) on BD LSRFortessa™ flow cytometer according to the EuroFlow SOP ([www.EuroFlow.org](http://www.EuroFlow.org)). Leukocytes were discriminated based on the expression of CD45 (CD45-OC515, Cytognos).

### **Evaluation of clinical samples**

To extrapolate the results of the storage experiments to diagnostic settings, flow cytometric data on 88 peripheral blood samples from primary immunodeficiency (PID) suspected individuals were evaluated retrospectively (age range: 0-79y, mean age: 30y). Flow cytometric data were obtained in a diagnostic context and approval for inclusion in the study was obtained by the Ghent University Hospital Ethics Committee (approval 2016/1137). In the diagnostic setting, samples were processed locally according to the EuroFlow guidelines. In all cases K2EDTA (BD Vacutainer®, Becton Dickinson Benelux, Erembodegem, Belgium) was used as anticoagulant, and whole blood was stored at RT for variable time periods before analysis with PIDOT (liquid format).

### **Flow cytometer set up and data acquisition**

PIDOT stained samples were measured on FACSCanto™ II (BD Biosciences) instruments while Perfect-Count tubes were measured on LSRFortessa™ flow cytometer (BD Biosciences). Flow cytometers were calibrated daily according to the EuroFlow guidelines. In short, photomultiplier tube (PMT) voltages of the flow cytometer were set using BD™ Setup and Tracking (CS&T) beads (BD Biosciences) and SPHERO™ Rainbow calibration particles (Cytognos), as previously described[2, 29].

### **Data analysis**

Samples were mostly analyzed manually or manually checked after automated analysis with the EuroFlow PIDOT reference database (Infinicyt™ Software v2.0,



Cytognos) with respect to both marker stability and distribution of the major cell populations. Most positive and negative reference populations were defined as previously described [28]. For each reference population, mean fluorescence intensity (MFI) was determined. A deviation of 30% from the original MFI value (MFI-baseline) was set as the acceptance limit. The difference compared to MFI-baseline was determined by the following formula in which MFI<sub>x</sub> represents the MFI of a sample in a given condition:  $(\text{MFI}_{\text{baseline}} - \text{MFI}_x) / \text{MFI}_{\text{baseline}} * 100$ . The distribution of a cell population was calculated as its relative frequency in the sample after excluding debris and doublets.

Determination of the degree of correlation between variables was performed using a Spearman correlation, after assessment of the normality of the distribution using the Shapiro Wilks test. For all statistical analyses the GraphPad Prism 8.0 software (GraphPad, San Diego, CA, USA), was used.

## Results

### Stable expression of cell surface markers and distribution of major cell populations after delayed acquisition of stained samples

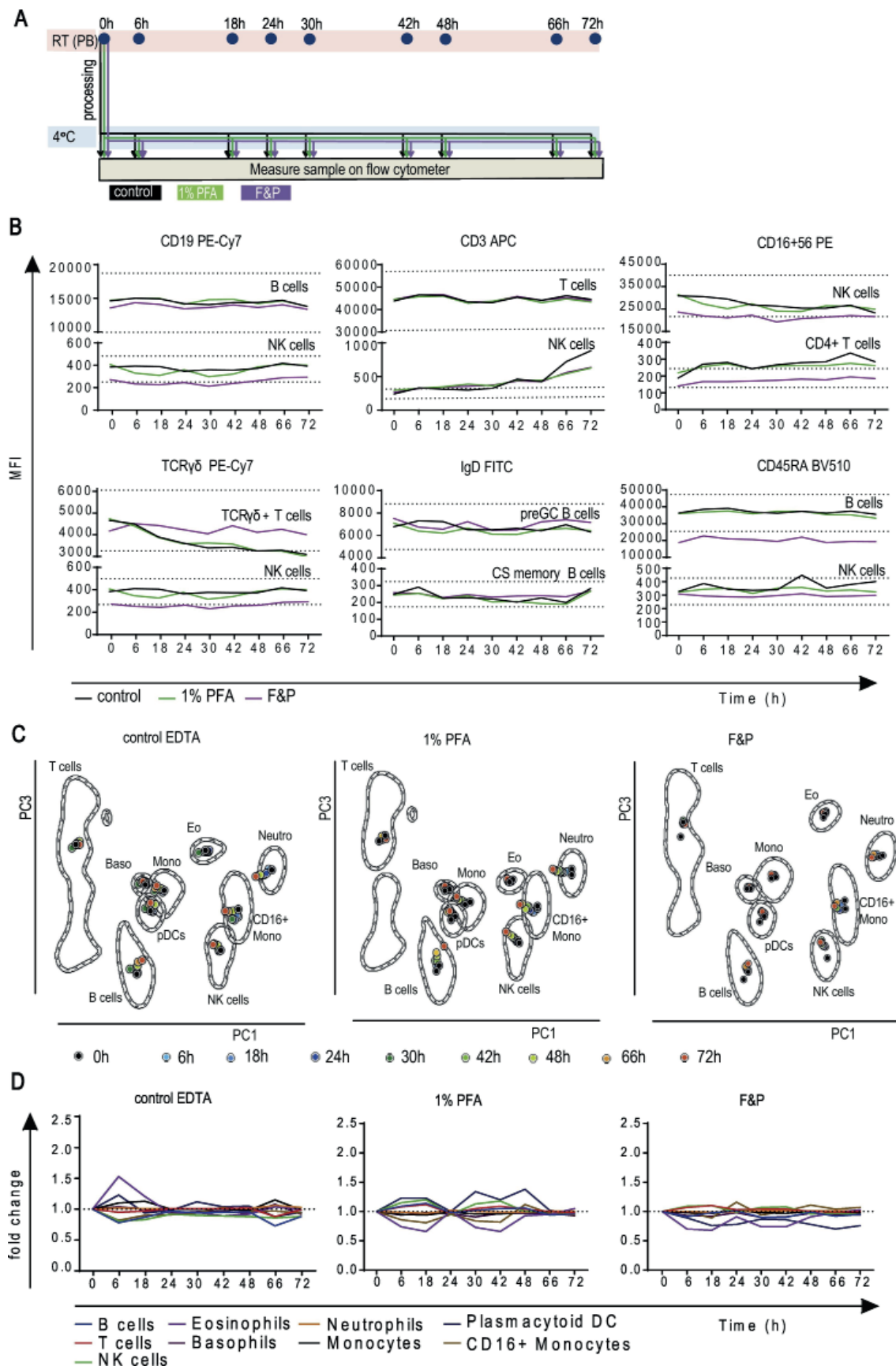
The PIDOT SOP (Cytognos PIDOT manual: revision 16-02-2018) recommends acquiring cells immediately after staining, or at most after 1h of storage at 4°C. To determine the effect of delayed acquisition of stained samples, PIDOT tubes were analyzed fresh or after they had been stored at 4°C for 6h, 18h, 24h, 30h, 42h, 48h, 66h and 72h (**Figure 2A**).

The impact of sample storage on the expression of cell surface markers was evaluated by analysis of their MFI on both positive and negative reference populations (**Supplemental Table 1, Figure 2B**). Most markers remained stable on positive reference populations for up to 72h with the exception of CD16+CD56 PE (> 10% loss of MFI after 24h), and TCR $\gamma\delta$  PE-Cy7 (>10% loss of MFI after 18h, >30% loss after 48h). Despite the stable MFI on positive reference populations, background staining increased for most markers, in particular for CD16+CD56 PE (>30% after 6h), but in no case this hampered the discrimination of cell populations stained with PIDOT.

The Automatic Population Separator (APS) tool, based on the principal component analysis algorithms, was used to demonstrate overall segregation of populations in the multidimensional space. With the exception of neutrophils at 72h, all medians of populations in aged blood fell within one standard deviation (SD) line of the reference baseline population, and outside of one standard deviation lines of other populations (**Figure 2C**). Although basophils, monocytes and plasmacytoid dendritic cells (pDCs) were positioned closely together, they were clearly separable in other APS views (not shown).

To evaluate which of the major lymphoid and myeloid populations are the most affected by storage, their distribution was compared in stained samples stored for different time periods (**Supplemental Table 2**). Remarkably, the distribution

# Chapter 2.1





of the major cell subsets remained quite stable for up to 72h (**Supplemental Table 2, Figure 2D**). The largest variation from baseline was observed for the eosinophils, mainly due to substantial changes in one donor.

### No beneficial effect of additional fixation of stained samples

The lysing solution utilized in the PIDOT SOP already contains a low concentration of fixative (<15% formaldehyde and <50% diethylene glycol in BD FACS™ Lysing Solution; 10x concentrated). To evaluate whether usage of an additional fixation step would have a positive impact on the quality of the data, freshly stained samples were treated with 1% PFA or with Solution A from F&P and evaluated after 0h, 6h, 18h, 24h, 30h, 42h, 48h, 66h and 72h storage at 4°C (**Figure 2A**).

Fixation with 1% PFA had no additional beneficial effect on the stability of cell surface markers (**Supplemental Table 1, Figure 2B**), whereas treatment with Solution A of F&P mainly had detrimental effects such as decreased MFI values for CD45RA BV510, IgM PerCP-Cy5.5 (>30%) and to a lesser extent for CD16+56 PE, CD4 PerCP-Cy5.5, CD27 BV421 and TCRγδ PE-Cy7 (>10%). After the initial decrease in MFI, signal remained relatively stable over time. Moreover, the discrimination among the distinct cell populations identified with PIDOT was not hampered by the additional fixation step. Evaluation of population phenotype in the APS view revealed that in stored samples fixed with 1% PFA, aged neutrophils (>42h), CD16+ monocytes (<48h) and NK cells (>66 h) showed the biggest variation from baseline, deviating >1SD line of the reference population (**Figure 2C**). F&P treated samples stayed within 1SD of the reference population at all times, but at the early time points fixed sample differed from baseline more than unfixed stored samples. In both PFA and F&P-treated samples, all populations were clearly separable.

The distribution of cell populations in fixed samples should reflect the distribution of the same cell populations in fresh samples and remain stable over time. However, directly after fixation with 1% PFA, the frequency of lymphocytes (B, T, NK cells) and CD16+ monocytes decreased by >10% (**Supplemental Table 2, Figure 2D**). Additionally, the frequency of basophils and eosinophils decreased by >10% after 6h. These changes were mainly compensated by the relative increase in neutrophils. Afterwards, the distribution of populations remained stable

**Figure 2 (previous page). Longitudinal analysis of stained samples stored without or with additional fixative.** Peripheral blood samples were collected into K3EDTA tubes stained and stored at 4°C for delayed acquisition. Additional stained samples were treated with 1% paraformaldehyde (PFA) or Fix&Perm Solution A (F&P) directly after staining and prior to the storage at 4 °C, n ≥ 3. (A) Flow chart showing the different storage conditions tested in this experiment (B) Mean fluorescence intensity (MFI) of selected cell surface markers on positive and negative reference populations. Each point indicates a mean value from ≥3 individual experiments. Dashed lines depict a 30% deviation from the MFI value at baseline (fresh sample without an additional fixative). (C) Individual populations from different time points separated by an automated population separator (APS) and visualized in 2D projections of the first and third principal components. Each dot represents a median value and each dashed line represent 1 standard deviation line of the indicated population at t = 0 h. Data of one representative donor is shown. Obtained data were analyzed with Infinicyt™ Software. (D) Changes in the frequency of individual cell populations over time relative to baseline.

over time. Fixation with Solution A resulted in a similar pattern, but with less impact on T cells and NK cells (**Supplemental Table 2**).

### **Hampered expression of cell surface markers and gradual loss of myeloid cells after prolonged whole blood storage**

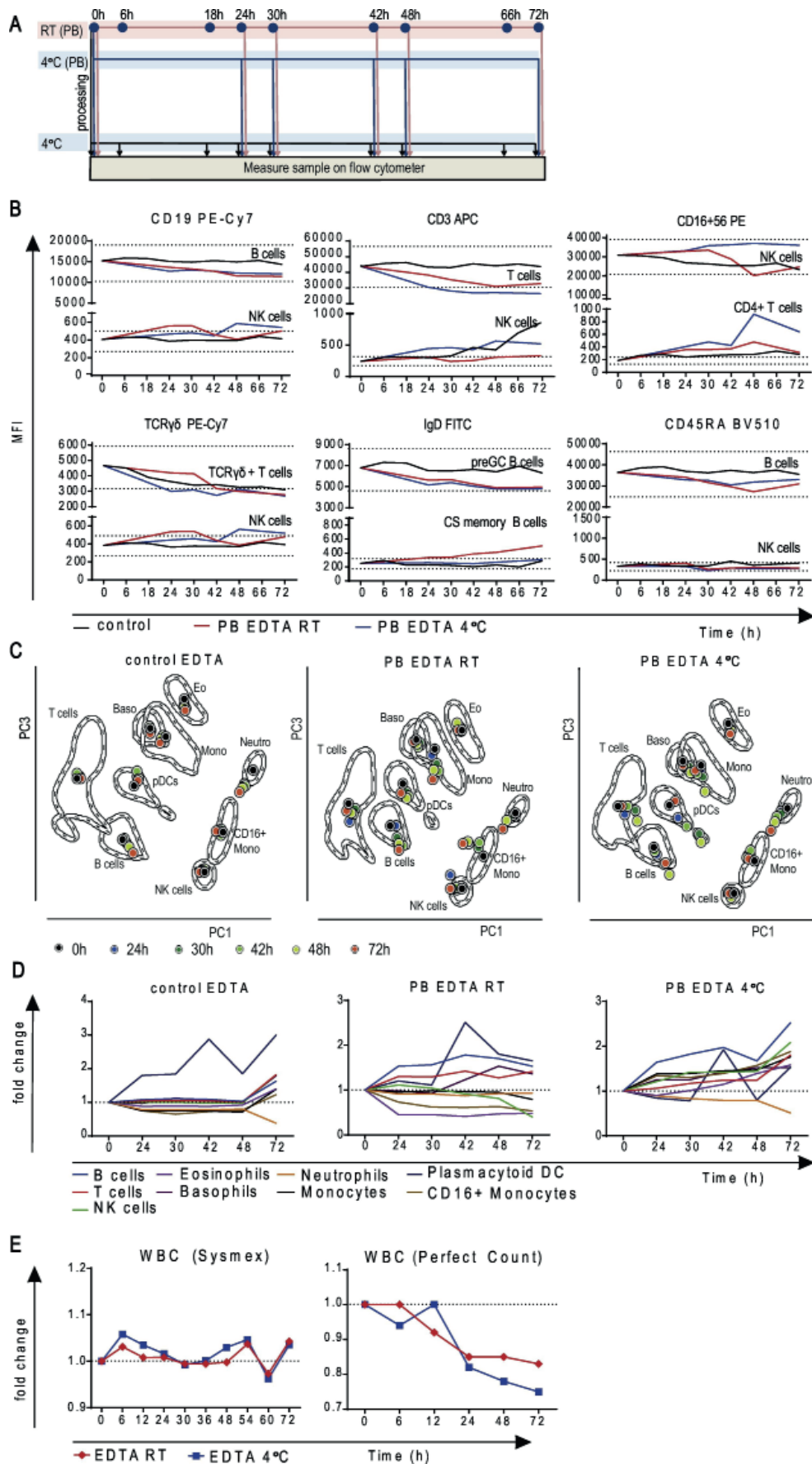
To mimic the delay caused by sample transportation, PB collected in EDTA tubes was analyzed at 0h or stored as whole blood either at RT or at 4°C, for delayed processing, staining and acquisition at 24h, 30h, 42h, 48h and 72h (**Figure 3A**).

In order to assess the impact of prolonged blood storage on detection of cell surface markers, MFIs of individual markers were analyzed on both positive and negative reference populations. Irrespective of storage temperature, already at 24h most markers showed >10% decrease in MFI on the positive reference cell populations, together with an increased unspecific staining on negative cells (**Supplemental Table 1, Figure 3B**). At RT the MFI signal was the least stable for CD27 BV421 and TCR $\gamma\delta$  PE-Cy7 (>30% decrease in MFI from 42h onwards), while at 4°C the most affected markers were CD3 APC and TCR $\gamma\delta$  PE-Cy7 (>30% decrease in MFI after 24h). Despite all the above, most populations could still be identified for up to 72h, but discrimination among them was clearly impaired over time.

In the APS view, (CD16+) monocytes, NK cells, neutrophils and B cells deviated >1SD of the reference population when blood was stored at RT from more than 30h (**Figure 3C**). Whereas in PB stored at 4°C the phenotype of B cells, T cells, and pDCs was impaired at later time points (>24h), CD16+ monocytes and NK cells showed limited deviation from baseline.

Several blood cell populations, mainly those of myeloid origin, have half-life times equal or shorter than 24h (6-8h for neutrophils, 18h for eosinophils, 1-2d for monocytes) [5, 6, 30]. Indeed, in blood stored for 24h at RT the frequency of eosinophils was reduced by 55% and the frequency of CD16+ monocytes by 27% (**Figure 3D, Supplemental Table 2**). Although the relative loss of neutrophils reached only 9%, a substantial part of these latter cells already showed early signs of apoptosis (lower FSC, SSC, CD45 and CD16 expression, without a clear separation from the viable population). The most overrepresented populations were long-living pDCs (+20%) and lymphocytes, with B cells being more overes-

**Figure 3 (next page). Longitudinal analysis of blood samples stored in K3EDTA tubes.** Peripheral blood samples were collected into K3EDTA tubes and stored either at RT or at 4°C for delayed staining. All results were compared to freshly stained K3EDTA samples,  $n \geq 3$ . (A) Flow chart showing different storage conditions tested in this experiment (B) Mean fluorescence intensity (MFI) of selected cell surface markers on positive and negative reference populations. Each point indicates a mean value from  $\geq 3$  individual experiments. Dashed lines depict a 30% deviation from the MFI value at baseline. (C) Individual populations from different time points separated by an automated population separator (APS) and visualized in 2D projections of the first and third principal components. Each dot represents a median value and each dashed line represent 1 standard deviation line of the indicated population at  $t = 0$  h. Data of one representative donor is shown. Obtained data were analyzed with Infinicyt™ Software. (D) Changes in the frequency of individual cell populations over time relative to baseline. (E) Changes in leukocyte count over time relative to baseline as measured by two independent methods.



estimated (+53%) than T cells (+29%) and NK cells (+11%). In blood stored at 4°C for 24h, both eosinophils and neutrophils were underestimated by around 11%, which was mainly compensated by a relative increase in both lymphocytes and monocytes (**Supplemental Table 2**). Thus, monocytes were better preserved at 4°C than at RT. Nevertheless, samples stored at RT were overall more stable than samples stored at 4°C.

Cell death not only influences the distribution of cell populations in a sample, but also their absolute counts. Interestingly, at later time points, analysis on Sysmex XP-300 was more robust than analysis with the Perfect-Count Microspheres™, which showed progressive loss of cells of up to 17% (RT) and 25% (4°C) at 72h (**Figure 3E**). These differences may be caused by less extensive sample handling or the less stringent exclusion of dying cells on Sysmex XP-300.

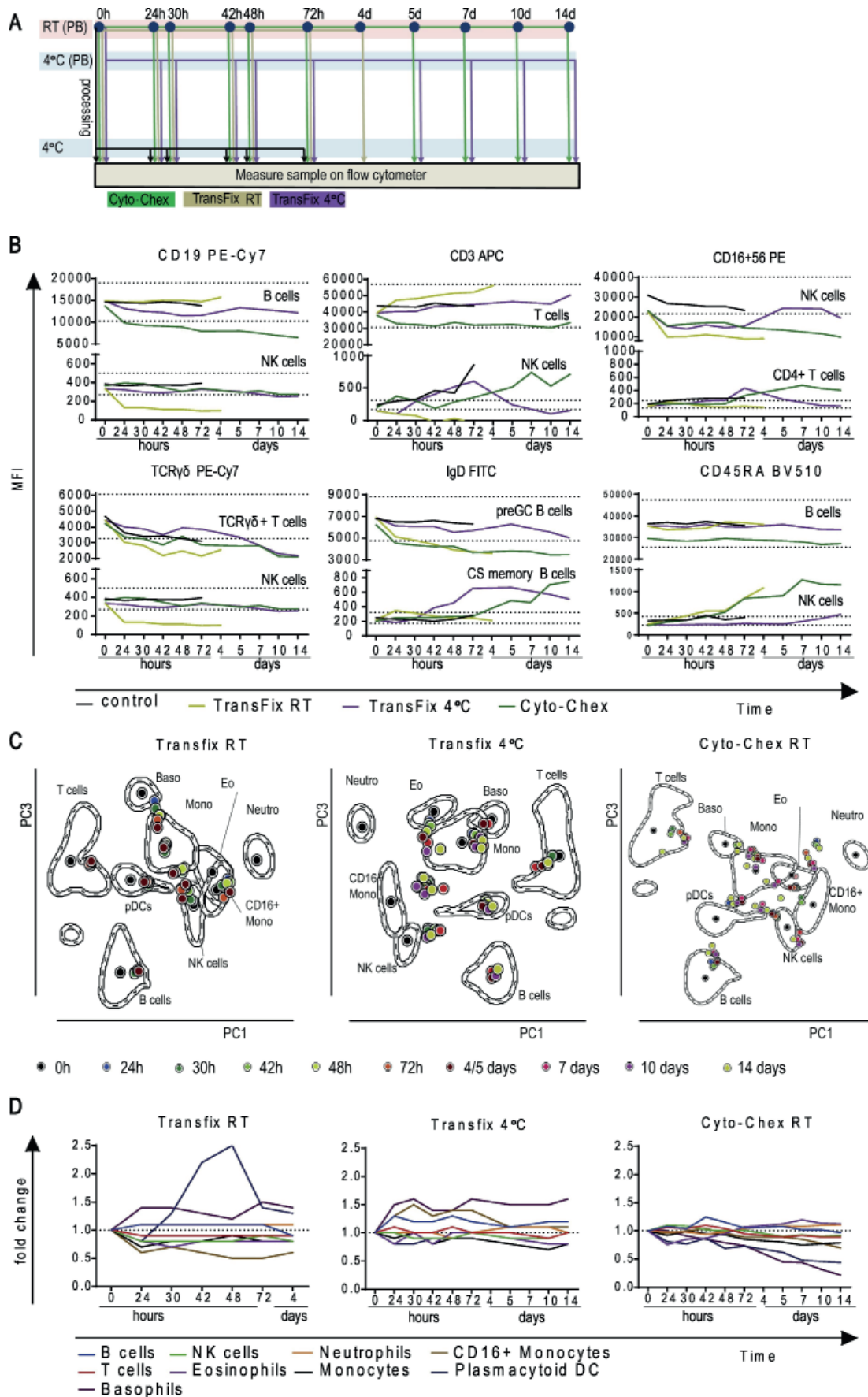
### **Hampered expression of cell surface markers and initial changes in the distribution of cell populations after whole blood fixation**

Two alternative whole blood fixation strategies were evaluated in parallel: TransFix for up to 4 days at RT and up to 14 days at 4°C and Cyto-Chex for up to 14 days at RT (**Figure 4A**). Both fixation methods resulted in an initial decrease in MFI (>10%) for approximately half of the markers tested (**Supplemental Table 1, Figure 4B**). In all cases the most affected markers were CD16+CD56 PE and CD27 BV421 (>30% MFI loss), followed by CD8 FITC and TCRγδ PE-Cy7 (>10% decreased MFI values). Additionally, TransFix led to changes in signal intensity of CD45RA BV510 (>10% increase at 4°C) and IgM PerCP-Cy5-5 (>10% decrease at RT), and Cyto-Chex fixation was associated with decreased signal intensity of CD4 PerCP-Cy5-5 (>10%). Further decrease in MFI over time occurred for all markers in Cyto-Chex tubes and for most markers in TransFix-treated samples. Decreased MFIs, increased background and affected cell scatter hampered discrimination of several cell subsets. Finally, the number of cell doublets and debris was increased, most likely due to an increased cell death and as a side effect of fixation (data not shown).

TransFix-treated samples stored at RT showed the best preservation of population phenotype of all whole blood-fixed samples. Nevertheless, in the APS view

**Figure 4 (next page). Longitudinal analysis of blood samples stored in K3EDTA tubes with a whole blood fixative.** Peripheral blood samples were collected into K3EDTA tubes, treated with TransFix and stored for delayed staining either at RT or at 4°C or collected into Cyto-Chex blood collection tubes and stored for delayed staining at RT. All results were compared to freshly stained K3EDTA samples,  $n \geq 3$ . (A) Flow chart showing different storage conditions tested in this experiment (B) Mean fluorescence intensity (MFI) of selected cell surface markers on positive and negative reference populations. Each point indicates a mean value from  $\geq 3$  individual experiments. Dashed lines depict a 30% deviation from the MFI value at baseline (fresh sample without an additional fixative). (C) Individual populations from different time points separated by an automated population separator (APS) and visualized in 2D projections of the first and third principal components. Each dot represents a median value and each dashed line represent 1 standard deviation line of the indicated population at  $t = 0$  h. Data of one representative donor is shown. Obtained data were analyzed with Infinicyt™ Software. (D) Changes in the frequency of individual cell populations over time relative to baseline.





basophils, neutrophils and eosinophils at multiple time points deviated more than 1SD from their reference population (**Figure 4C**). In TransFix-treated samples stored at 4°C, myeloid cells were heavily affected from the start. Already at 24h time point neutrophils, CD16+ monocytes and NK cells deviated >1SD from baseline samples. Deviations in eosinophils, monocytes and basophils showed a gradual increase in time. Evaluation of Cyto-Chex treated samples revealed a hampered identification of pDCs, neutrophils, basophils, CD16+ monocytes and eosinophils at most time points. Thus, whole blood fixation seemed to have the biggest detrimental impact on cells of myeloid origin.

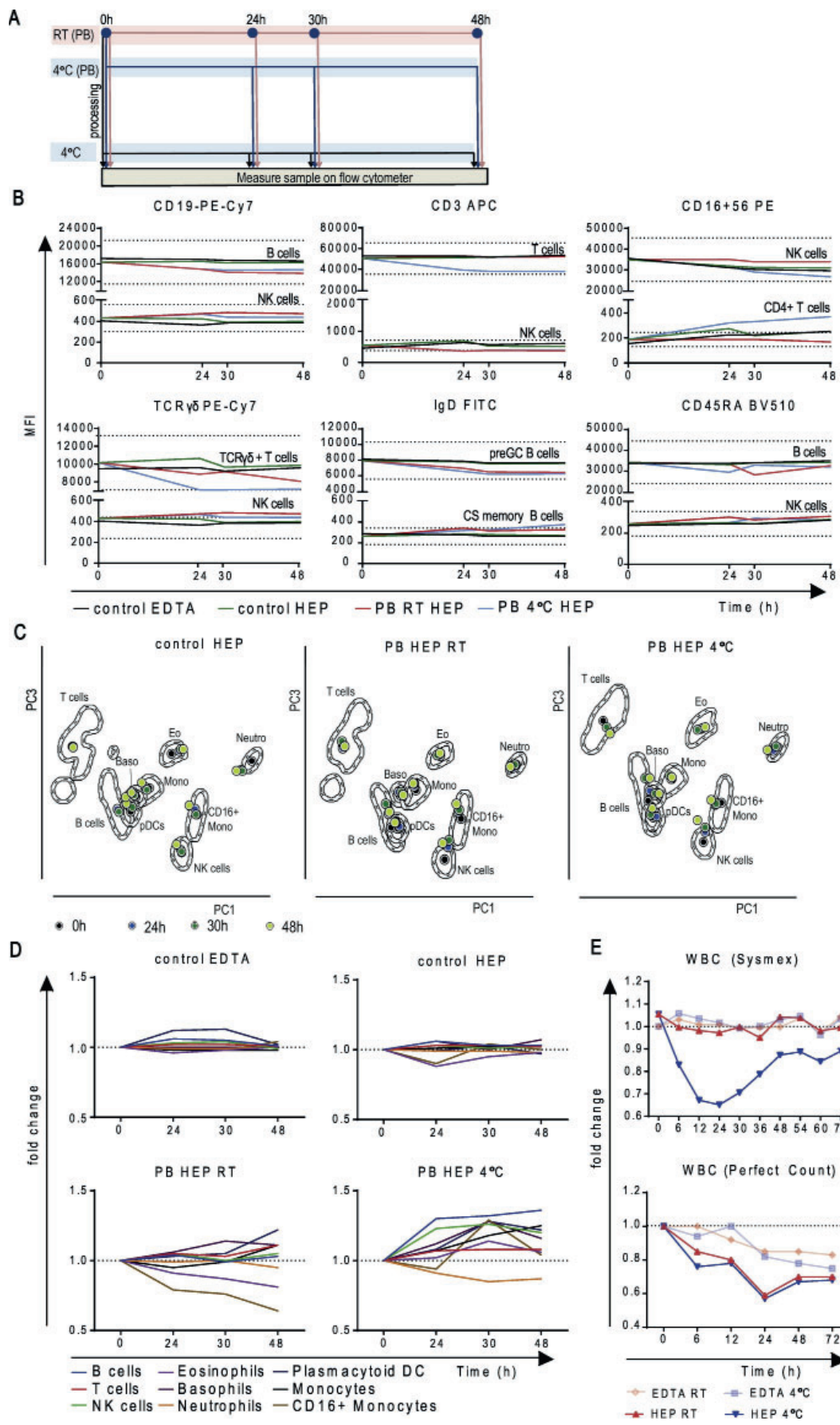
Although at most of the time points populations of cells in Cyto-Chex and TransFix samples cluster together in the multidimensional space, the initial deviation from baseline samples renders them unsuitable for comparison with baseline samples and use for detailed immunophenotyping.

Both Cyto-Chex and TransFix affected the relative distribution of multiple cell populations. Lymphocytes and monocytes were overrepresented at the expense of granulocytes, similar to what was observed in blood samples stored at 4°C (**Supplemental Table 2, Figure 4D**). Decrease in neutrophil numbers was especially prominent in samples treated with TransFix. After these initial changes, the distribution of cell populations remained relatively stable over time. Overall, samples stored at RT performed slightly better than samples stored at 4°C.

### **Good performance of PIDOT in Na-Heparin blood**

Heparin is often the anticoagulant of choice when immunophenotyping needs to be combined with functional assays. To compare EDTA and Na-Heparin blood samples, Na-Heparin and EDTA anticoagulated blood was stained directly and stored at 4°C for acquisition at 0h, 24h, 30h and 48h. Additionally, samples in Na-Heparin tubes were stored at RT or at 4°C for delayed staining and acquisition at 24h, 30h and 48h (**Figure 5A**).

**Figure 5 (next page). Longitudinal analysis of blood samples collected into Na-Heparin tubes.** Peripheral blood samples were collected into Na-Heparin tubes, stained and acquired directly or stored at 4°C for delayed acquisition. Additional samples were collected into Na-Heparin tubes and stored either at RT or at 4°C for delayed staining. All results were compared to freshly stained K3EDTA samples of the same donors,  $n \geq 3$ . In 1 donor, the PIDOT in dried format was used, in all others, the liquid format was used for staining. (A) Flow chart showing different storage conditions tested in this experiment (B) Mean fluorescence intensity (MFI) of selected cell surface markers on positive and negative reference populations. Each point indicates a mean value from  $\geq 3$  individual experiments. Dashed lines depict a 30% deviation from the MFI value at baseline (fresh sample without an additional fixative). (C) Individual populations from different time points separated by an automated population separator (APS) and visualized in 2D projections of the first and third principal components. Each dot represents a median value and each dashed line represent 1 standard deviation line of the indicated population at  $t = 0$  h. Data of one representative donor is shown. Obtained data were analyzed with Infinicyt™ Software. (D) Changes in the frequency of individual cell populations over time relative to baseline. (E) Changes in leukocyte count over time relative to baseline as measured by two independent methods.





## Chapter 2.1

---

Stained and stored EDTA and Na-Heparin samples performed equally well with regards to marker stability and cell population distribution (**Figure 5B-D, Supplemental Table 3, Supplemental Table 4**). None of the markers in samples collected in Na-Heparin tubes, besides CD16+56 PE showed a >10% decrease in MFI signal, and the increase in background staining was limited (>30% for only CD16+CD56 PE and CD27 BV421). None of the analyzed cell populations were clearly over- or underestimated over time. When looking at a representative donor in the APS plot, baseline samples showed a smaller standard deviation in directly stained Na-Heparin samples compared to directly stained EDTA samples. For neutrophils and CD16+ monocytes, >1SD difference was seen after 24h and 48h, respectively. Nevertheless, stored samples closely represented baseline samples (**Figure 5C**).

Samples stored at RT in Na-Heparin tubes prior to staining showed stable expression of most of the evaluated cell surface markers (none showed decreased MFI values of >30%) and outperformed samples stored at RT in EDTA tubes (**Supplemental Table 1**). Sample storage at 4°C had a more detrimental effect on marker expression in both EDTA and Na-Heparin. While CD3 APC and CD27 BV421 performed better in Na-Heparin tubes, CD8 FITC was more stable in EDTA.

Na-Heparin samples stored at RT showed virtually no deviations >1SD in the multidimensional space up to 48h of PB storage. Na-Heparin samples stored at 4°C showed deviations >1SD from 30h onwards for NK cells, B cells and neutrophils (**Figure 5C**).

The relative distribution of distinct cell populations was more stable when samples were stored at RT, and Na-Heparin tubes were associated with more stable results than EDTA tubes (**Figure 5D**). Up to 24h no major deviations were observed in Na-Heparin samples stored at RT, while at later time points lymphocytes (mainly T cells), monocytes and basophils were slightly overrepresented at the expense of eosinophils, CD16+ monocytes and neutrophils. These changes were more prominent in Na-Heparin blood stored at 4°C, where almost all cell populations deviated from baseline by >10% already at 30h. Again, lymphocytes (mainly B cells), monocytes and basophils were overrepresented at the expense of neutrophils.

In contrast to the expression of cell surface markers and the distribution of cell populations, absolute leukocyte numbers were less stable in samples stored in Na-Heparin than in EDTA (**Figure 5E**). After 24h, in samples measured by Perfect-Count Microspheres™, absolute cell counts decreased by ~40% in Na-Heparin and by ~20% in EDTA. Remarkably, all samples were stable over time when measured on Sysmex XP-300 except for Na-Heparin samples stored at 4°C. Na-Heparin samples stored at 4°C showed a strong initial drop in absolute cell counts in all donors (>30% after 12h), followed by gradual recovery from 30h onwards.

**Bulk lysis protocol should be adjusted for limited sample volume**

Bulk lysis SOP is optimized for 1.5-2ml of blood, which results in more than the  $2.5 \times 10^6$  cells required for PIDOT. As different lysis protocols may impact sample properties like scatter and marker expression, it is recommended to use the same protocol for all samples that are compared to one another, especially when automated analysis is used. In case too little sample volume is available for bulk lysis, the protocol may need to be adjusted. To evaluate the procedure for limited blood volumes, 100 $\mu$ l and 200 $\mu$ l of blood were lysed either with 50ml of NH<sub>4</sub>Cl (bulk lysis SOP) or 3ml of NH<sub>4</sub>Cl (blood/NH<sub>4</sub>Cl ratio similar to official EuroFlow SOP; **Supplemental Table 5**) and stained with PIDOT. If a reduced NH<sub>4</sub>Cl volume was used, lysis was performed directly in the staining tube to minimize cell loss during transfer of sample between tubes.

If the original blood/NH<sub>4</sub>Cl ratio was maintained, the distribution of cell populations in small volume samples was more comparable to the distribution of such cell populations in samples processed according to the SOP. In small volume samples lysed with 50ml of NH<sub>4</sub>Cl most B-cell subsets were underestimated by >20%, mainly in favor of granulocytes and monocytes. In all tested conditions, the fluctuations of plasma cell percentages were large (>50%), most likely due to the small population size at the detection limit of the method.

**Prolonged storage of diagnostic samples affects data analysis**

To evaluate the impact of sample storage in diagnostic settings, 88 EDTA blood samples from PID-suspected individuals were stored for up to 8 days at RT and analyzed with PIDOT. As all samples were sent for routine diagnostics, no baseline measurements were available. For analysis purposes samples were anonymized and divided into five categories based on storage duration: 0-12h, 12-24h, 24-48h, 48-72h and >72h.

As in the whole blood storage experiments with healthy controls, most markers showed >10% decrease in MFI on the positive reference population already 12-24h after collection (**Supplemental table 6, Figure 6**). In accordance with the previous findings in PB stored at RT, the most dramatic decrease in signal was observed for TCR $\gamma\delta$  PE-Cy7 and CD27 BV421, which showed >30% and 28% decrease in MFI in samples acquired >48h after drawing, respectively. Furthermore, control and diagnostic samples shared some common features regarding relative changes in population distribution over time, i.e. a gradual loss of eosinophils and NK cells (**Figure 6, Supplemental table 7**). Although in both control and diagnostic samples most populations could be identified in aged blood, the situation in PID-suspected individuals was complicated by the unknown diagnosis. Therefore, the absence or an aberrant phenotype of a given population could be

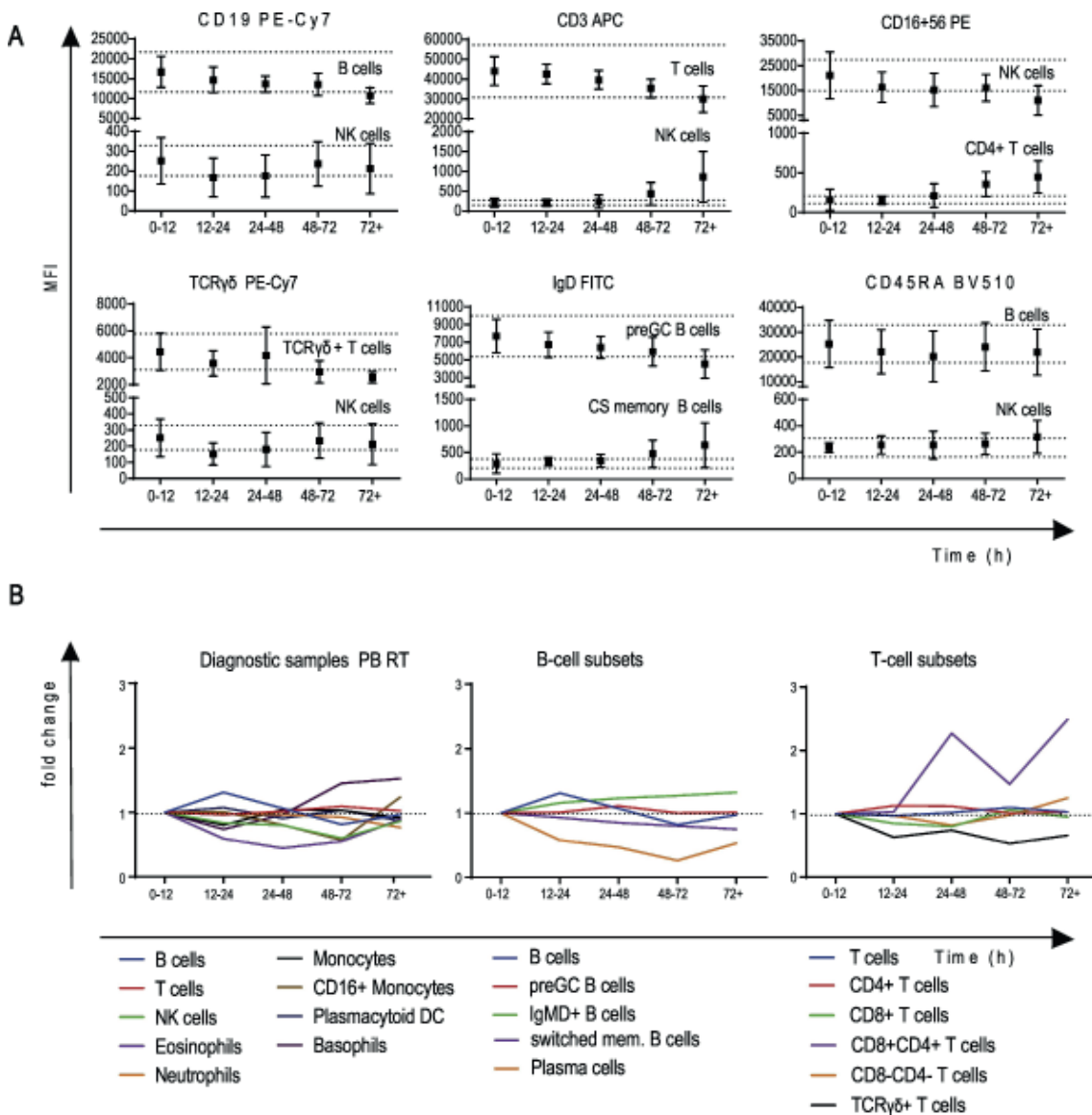


**Figure 6. Impact of sample storage on diagnostic samples collected in K3EDTA tubes.** Peripheral blood samples were collected into K3EDTA tubes and stored at RT until staining (n = 88). Mean age and range per group: 0–12 h (20.1; 1–67.4), 12–24 h (23.0; 0.4–71.3), 24–48 h (36.5; 0.4–78.8), 48–72 h (39.9; 5.9–68.7), 72 h + (28.6; 1.2–76.8) (A) Mean fluorescence intensity (MFI) of selected cell surface markers on positive and negative reference populations. Each point indicates a mean value of all diagnostic samples collected within that timeframe (n ≥ 11). Dashed lines depict a 30% deviation from the MFI value from the samples acquired 0–12 h after collection. (B) Changes in the frequency of individual cell populations over time relative to the samples acquired 0–12 h after collection.

attributed either to prolonged sample storage or to the underlying disease.

## Discussion

Complex sample logistics in multicenter clinical studies require careful alignment of working procedures among participating laboratories. Extra challenges are caused by limited sample volume (e.g. in case of infants or young children) and the need of sample transportation to another (e.g. reference) laboratory.

Here we evaluated several critical steps in the process of obtaining high quality flow cytometry data from peripheral blood samples. We showed how the choice of anticoagulant influences the stability of cell surface markers and cell populations, and tested a range of possibilities to preserve whole blood and stained samples for delayed acquisition. These results were translated to clinical settings by retrospective analysis of routine diagnostic samples. Finally, we recognized the need for adjusting working procedures in case of insufficient sample volumes. Enumeration of white blood cells is one of the most frequently requested routine diagnostic tests. Here we evaluated two alternative strategies to determine absolute cell counts: flow cytometry-based Perfect-Count Microsphere™ measurements and the Sysmex XP-300 hematological analyzer. Overall, results obtained with Sysmex XP-300 in aged blood better reflected results from fresh samples. Analysis with Perfect-Count Microspheres™ was preceded by sample treatment for 10 min with NH<sub>4</sub>Cl. This lysis step can have a detrimental effect on the – already vulnerable- aging cells which then become classified as debris or dead cells rather than viable cells; alternatively speed of analysis and electronic-digital signal processing, together with different rates of doublet formation might contribute to explain such differences. Furthermore, the potential inclusion or exclusion of apoptotic cells by different counting methods could result in different blood cell counts. Irrespective of the blood storage temperature, measurement of Na-Heparin samples resulted in lower absolute cell counts than those obtained for EDTA anticoagulated samples. Therefore, whenever longitudinal analyses are required, or subtle changes in cell numbers are expected, it is crucial to always use the same blood collection tubes, preferably EDTA tubes if samples will be processed immediately (<24-30h).

Reliable analysis of absolute cell counts by Sysmex XP-300 was not possible in Na-Heparin samples stored at 4°C. For these samples leukocyte numbers showed an apparently rapid initial decrease followed by a slow gradual recovery after 24h. These changes were positively correlated with the platelet counts (Spearman correlation  $P < 0.0001$ , correlation coefficient of 0.65). A likely explanation is that in Na-Heparin samples stored at 4°C platelets become activated and start to form aggregates [31, 32] including platelet-leukocyte aggregates. This formation and disintegration may explain fluctuations in the absolute leucocyte count.

Total white blood cell numbers can be reliably determined in a limited volume of blood. However, if infrequent cell populations need to be quantified, analysis might reach the detection limit. Here, we stained  $2.5 \times 10^6$  cells (resulting in acquisition of  $\sim 1-1.5 \times 10^6$  cells) and observed that small populations like plasma cells, eosinophils and specific T-cell subsets showed a greater variation than larger cell populations, implying that the enumeration of less represented cell populations has to be more critically assessed. Increasing the number of cells evaluated will most likely improve accurate quantitation of such rare cells. As stated by Oldaker et al., and proven by Theunissen et al., and Flores Montero et al., detection of low represented abnormal cell populations is possible as long as an adequate number of events is acquired [26, 33, 34].

## Chapter 2.1

---

In fact, the limit of detection of one or more cell populations becomes an important problem when limited blood volumes are available. Here we found that the distribution of populations analyzed in the small volume samples better reflects the distribution of populations in large volume samples when the volumes of reagent are adjusted to maintain the same blood/reagents volume ratio. Fewer transfer steps between tubes in the protocol with adjusted blood/reagents volume may further influence better preservation of initial population distribution. Consequently, reagent volumes and protocols need to be adapted to sample volumes. In any case, the total number of acquired white blood cells should always be acknowledged to indicate the reliability of the data.

Populations of cells are defined based on the presence or absence of specific markers and their expression levels (especially of importance if these are modulated during cell activation and/or maturation)[35-38]. Therefore, each marker should not only provide a proper discrimination between strong and dim positive cells and between positive and negative cells, but it should also provide an adequate resolution to detect more subtle changes. Here we confirmed and extended previous observations [12-17, 22-25] by showing that the type of anticoagulant, storage time, storage conditions and treatment all had an impact on marker expression levels and background staining. Similar findings on the impact of anticoagulant on sample stability have recently been published by Kárai et al. in the context of bone marrow and PB processing [39].

None of the two tested anticoagulants (Na-Heparin, EDTA) had a clear advantage over the other with regard to stability of marker expression levels. However, individual markers performed better in one of the conditions. Therefore, if MFIs are to be compared, it is crucial to be consistent with the choice of anticoagulant.

For most markers the resolution of signal decreased over time. The decrease in signal and increase in background staining was more prominent in stored whole blood than in stored processed and stained samples. This is likely because the signal intensity can be influenced by unspecific binding of mAbs to dying cells and shedding or internalization of markers due to e.g. apoptosis or (in)activation [38, 40]. Furthermore, sample (including whole blood) fixation (Solution A from F&P, Cyto-Chex, TransFix) had a negative impact on marker expression. In these circumstances the most prominent loss of signal occurred directly after addition of a fixative, possibly due to conformational changes of the antibody targeted epitopes or impact of the fixative on the fluorochromes [41].

Certain fluorochromes, e.g. some of the tandem-dyes, are known to be less stable [42]. Despite a broad range of antibodies assessed, we have not observed antibodies conjugated with any specific dye to be more affected. At the same time, we found that antibodies with lower affinity for the antigen, such as TCR $\gamma\delta$ , were especially sensitive to prolonged sample storage. This is in line with what has been reported by Davis et al., who showed that CD4 PE conjugates from different clones showed great variability in both avidity and antibody stability [43] and by



Van der Velden et al., who showed that TCR $\gamma\delta$  PE-Cy7 showed greater variability when used in different formats (freeze-dried or liquid antibodies) [28].

In whole blood samples the largest differences in cell distribution were caused by progressive cell death (mainly granulocytes), which appeared to be associated with both changes in the cell phenotype and an increase in doublets and debris. Although whole blood fixation had a detrimental effect on the relative distribution of distinct cell populations directly after treatment, it stabilized the relative distribution afterwards, making this condition more beneficial at the later time points. Thus, if blood cannot be processed within 24-30h, and the distribution of cell populations is of primary interest, whole blood fixation might be an option. However, we would not recommend it for general immunophenotyping. Of note, it has been reported that PB fixation may preserve leukocyte counts compared to untreated PB [44, 45]. Again, here we show that additional fixation of processed samples provides better results than fixation of whole blood samples.

Processing of diagnostic samples can be delayed by transportation as well as by personnel and equipment availability. This can have several consequences for the outcome of flow cytometric analysis. First, we showed in healthy controls that, depending on the storage conditions, absolute cell counts can decrease by up to 40% already 24h after collection. Since absolute cell count is one of the diagnostic criteria for immunodeficiencies, cell loss in aged samples can affect proper diagnosis. Secondly, several immunodeficiencies are characterized by the absence or reduced number of cell populations or their aberrant phenotype [27, 46]. A recent study by van der Burg et al. showed reduced numbers of memory B cells in confirmed SCID patients. The markers used in PIDOT to separate memory B cells from pre-germinal center cells are mainly CD27 and IgM. Thus, the observed decrease in CD27 BV421 and increased background in the PerCP-Cy5.5 channel (which harbors both IgM and CD4) can eventually hamper discrimination of memory B cells. Analogical problem can arise in identification of TCR $\gamma\delta$  T cells, as TCR $\gamma\delta$  PE-Cy7 was one of the most storage-affected markers, and lack of these cells can be associated with immune deficiency. Thus, prolonged storage (>24h) of diagnostic samples should be avoided and, if not possible, they should be evaluated critically, keeping in mind that changes may be attributed to sample aging. In this study we used a <30% deviation from baseline MFI as a measure of marker stability. In many cases, samples could be reliably analyzed by experienced personnel despite greater signal changes. This was at least in part based on the software used for data analysis (Infinicyt™ Software v2.0, Cytognos), which allows for simultaneous multidimensional gating rather than 2-dimensional consecutive gating. In this multidimensional approach changes in expression of cellular markers over time were absorbed by other markers in such a way that population separation was still possible. Recently, a database has been released for automated analysis of PIDOT (Infinicyt™ Software 2.0, Cytognos). Although during the construction of a database high quality samples are required [47], it would be of great interest to evaluate how aged and differently treated samples can be run through such a database.

### **Concluding remarks**

This intricate set of data presented here was based on the analysis of a single antibody combination: PIDOT. Therefore, it cannot provide universal guidelines. Still, certain conclusions can be drawn about what can and should not be done in the pre-analytical phase of multicenter clinical trials:

- Delay from blood collection to blood processing should be minimized, especially in a diagnostic setting.
- PB samples stored for <24h at RT seem suitable for reliable immunophenotyping, although losses in absolute cell numbers should be taken into account.
- PB samples stored for 24-48h at RT may be used for immunophenotyping, but results will be less reliable. Again, losses in absolute cell numbers should be taken into account.
- In whole PB samples, most populations are more stable when stored in Na-Heparin than in EDTA tubes at RT.
- However, storage of processed and stained samples is usually more beneficial than storage of whole blood.
- B and T cells are the most stable populations, followed by NK cells, whereas myeloid cells and monocytes are more sensitive to storage. Thus, based on cell type of interest, different delays are acceptable.
- The impact of anticoagulant and potential fixation steps on the expression of individual cell markers varied significantly; thus, it is crucial to be consistent in the use of anticoagulant, storage time and temperature.
- Any deviations from standard operating procedures should be recorded.
- When determining absolute counts, minimize storage or aim for consistent delays. Be consistent with the method used. In our experience an automated hematological analyzer is more stable than flow cytometric determination of absolute counts.

Specific recommendations for individual types of cells are summarized in **Supplemental Figure 1**.

### **Acknowledgments**

The authors thank Fenna de Bie and Demi van den Blink for their support during experimental work. Furthermore, we would like to thank the blood donors for their participation.

### **Declaration of interests**

The authors declare no conflict of interest apart from J.J.M. van Dongen and A. Orfao, who are chairman and co-chairman of the EuroFlow scientific consortium, which receives royalties from licensed patents; this income is solely used for continuation of the collaboration within the EuroFlow consortium. In addition, J.J.M. van Dongen and A. Orfao have an Educational Service Agreement with BD Biosciences; income from this agreement goes to LUMC and USAL respectively.



**Supplemental Figures and Tables can be found in the online article:**

<https://www.sciencedirect.com/science/article/pii/S0022175919301140>

or by scanning the following QR code:



2.1

**References**

1. Owens, M.A., et al., Validation and quality control of immunophenotyping in clinical flow cytometry. *Journal of immunological methods*, 2000. 243(1-2): p. 33-50.
2. Kalina, T., et al., EuroFlow standardization of flow cytometer instrument settings and immunophenotyping protocols. *Leukemia*, 2012. 26(9): p. 1986-2010.
3. Lionetti, F.J., et al., Cryopreservation of human granulocytes. *Cryobiology*, 1975. 12(3): p. 181-191.
4. Reimann, K.A., et al., Preservation of lymphocyte immunophenotype and proliferative responses in cryopreserved peripheral blood mononuclear cells from human immunodeficiency virus type 1-infected donors: implications for multicenter clinical trials. *Clinical and diagnostic laboratory immunology*, 2000. 7(3): p. 352-359.
5. Park, Y.M. and B.S. Bochner, Eosinophil survival and apoptosis in health and disease. *Allergy, asthma & immunology research*, 2010. 2(2): p. 87-101.
6. Summers, C., et al., Neutrophil kinetics in health and disease. *Trends in immunology*, 2010. 31(8): p. 318-324.
7. Kelman, G. and J. Nunn, Nomograms for correction of blood Po<sub>2</sub>, Pco<sub>2</sub>, pH, and base excess for time and temperature. *Journal of Applied Physiology*, 1966. 21(5): p. 1484-1490.
8. Kamlage, B., et al., Impact of Prolonged Blood Incubation and Extended Serum Storage at Room Temperature on the Human Serum Metabolome. *Metabolites*, 2018. 8(1): p. 6.
9. Nishiumi, S., et al., Differences in metabolite profiles caused by pre-analytical blood processing procedures. *Journal of bioscience and bioengineering*, 2017.
10. Tanner, M., et al., Substantial changes in gene expression level due to the storage temperature and storage duration of human whole blood. *International Journal of Laboratory Hematology*, 2002. 24(6): p. 337-341.
11. Thavasu, P., et al., Measuring cytokine levels in blood. Importance of anticoagulants, processing, and storage conditions. *Journal of immunological methods*, 1992. 153(1-2): p. 115-124.
12. Ng, A.A., et al., Optimal cellular preservation for high dimensional flow cytometric analysis of multicentre trials. *Journal of immunological methods*, 2012. 385(1): p. 79-89.
13. Hodge, G.L., R. Flower, and P. Han, Optimal storage conditions for preserving granulocyte viability as monitored by Annexin V binding in whole blood. *Journal of immunological methods*, 1999. 225(1-2): p. 27-38.
14. Ekong, T., et al., The effect of the temperature and duration of sample storage on the measurement of lymphocyte subpopulations from HIV-1-positive and control subjects. *Journal of immunological methods*, 1992. 151(1-2): p. 217-225.
15. Chow, S., et al., Whole blood fixation and permeabilization protocol with red blood cell lysis for flow cytometry of intracellular phosphorylated epitopes in leukocyte subpopulations. *Cytometry Part A*, 2005. 67(1): p. 4-17.
16. Davis, C., et al., Stability of immunophenotypic markers in fixed peripheral blood for extended analysis using flow cytometry. *Journal of immunological methods*, 2011. 363(2): p. 158-165.
17. Schumacher, A., Effect of ex vivo storage and Cyto-Chex on the expression of P-selectin glycoprotein ligand-1 (PSGL-1) on human peripheral leukocytes. *Journal of immunological methods*, 2007. 323(1): p. 24-30.
18. Schmid, I., C.H. Uittenbogaart, and J.V. Giorgi, A gentle fixation and permeabilization method for combined cell surface and intracellular staining with improved precision in DNA quantification. *Cytometry Part A*, 1991. 12(3): p. 279-285.
19. Gerner, W., et al., Detection of intracellular antigens in porcine PBMC by flow cytometry: a comparison of fixation and permeabilisation reagents. *Veterinary immunology and immunopathology*

## Chapter 2.1

---

- logy, 2008. 121(3-4): p. 251-259.
20. Carayon, P. and A. Bord, Identification of DNA-replicating lymphocyte subsets using a new method to label the bromo-deoxyuridine incorporated into the DNA. *Journal of immunological methods*, 1992. 147(2): p. 225-230.
  21. Liu, Z., N. Braunstein, and N. Suci-Foca, T cell recognition of allopeptides in context of syngeneic MHC. *The Journal of Immunology*, 1992. 148(1): p. 35-40.
  22. Lal, R.B., L.J. Edison, and T.M. Chused, Fixation and long-term storage of human lymphocytes for surface marker analysis by flow cytometry. *Cytometry Part A*, 1988. 9(3): p. 213-219.
  23. Maecker, H.T., et al., A model for harmonizing flow cytometry in clinical trials. *Nature immunology*, 2010. 11(11): p. 975.
  24. Nicholson, J.K. and T.A. Green, Selection of anticoagulants for lymphocyte immunophenotyping: effect of specimen age on results. *Journal of immunological methods*, 1993. 165(1): p. 31-35.
  25. Paxton, H., et al., Results of the flow cytometry ACTG quality control program: analysis and findings. *Clinical immunology and immunopathology*, 1989. 52(1): p. 68-84.
  26. Flores-Montero, J., et al., Next Generation Flow for highly sensitive and standardized detection of minimal residual disease in multiple myeloma. *Leukemia*, 2017. 31(10): p. 2094.
  27. van der Burg, M., et al., The EuroFlow PID orientation tube for flow cytometric diagnostic screening of primary immunodeficiencies of the lymphoid system. *Frontiers in Immunology*, 2019. 10: p. 246.
  28. van der Velden, V.H., et al., Optimization and testing of dried antibody tube: The EuroFlow LST and PIDOT tubes as examples. *Journal of immunological methods*, 2017. DOI: 10.1016/j.jim.2017.03.011.
  29. Kalina, T., et al., Quality assessment program for EuroFlow protocols: Summary results of four-year (2010–2013) quality assurance rounds. *Cytometry Part A*, 2015. 87(2): p. 145-156.
  30. Ziegler-Heitbrock, L., Reprint of: Monocyte subsets in man and other species. *Cellular immunology*, 2014. 291(1-2): p. 11-15.
  31. Zucker, M.B. and J. BORRELLI, Reversible alterations in platelet morphology produced by anticoagulants and by cold. *Blood*, 1954. 9(6): p. 602-608.
  32. WHITE, J.G. and W. KRIVIT, An ultrastructural basis for the shape changes induced in platelets by chilling. *Blood*, 1967. 30(5): p. 625-635.
  33. Oldaker, T.A., P.K. Wallace, and D. Barnett, Flow cytometry quality requirements for monitoring of minimal disease in plasma cell myeloma. *Cytometry Part B: Clinical Cytometry*, 2016. 90(1): p. 40-46.
  34. Theunissen, P., et al., Standardized flow cytometry for highly sensitive MRD measurements in B-cell acute lymphoblastic leukemia. *Blood*, 2017. 129(3): p. 347-357.
  35. Sallusto, F., A. Lanzavecchia, and C.R. Mackay, Chemokines and chemokine receptors in T-cell priming and Th1/Th2-mediated responses. *Immunology today*, 1998. 19(12): p. 568-574.
  36. Nopp, A., J. Lundahl, and G. Hallden, Quantitative, rather than qualitative, differences in CD69 upregulation in human blood eosinophils upon activation with selected stimuli. *Allergy*, 2000. 55(2): p. 148-156.
  37. Bachmann, M.F., et al., Functional properties and lineage relationship of CD8+ T cell subsets identified by expression of IL-7 receptor  $\alpha$  and CD62L. *The Journal of Immunology*, 2005. 175(7): p. 4686-4696.
  38. Reddy, M., et al., Comparative analysis of lymphocyte activation marker expression and cytokine secretion profile in stimulated human peripheral blood mononuclear cell cultures: an in vitro model to monitor cellular immune function. *Journal of immunological methods*, 2004. 293(1-2): p. 127-142.
  39. Kárai, B., et al., The impact of delayed sample handling and type of anticoagulant on the interpretation of dysplastic signs detected by flow cytometry. *Biochemia medica: Biochemia medica*, 2018. 28(2): p. 1-13.
  40. Dransfield, I., et al., Neutrophil apoptosis is associated with a reduction in CD16 (Fc gamma RIII) expression. *The Journal of Immunology*, 1994. 153(3): p. 1254-1263.
  41. McCarthy, D., et al., Effect of fixation on quantification of the expression of leucocyte function-associated surface antigens. *Cytometry: The Journal of the International Society for Analytical Cytology*, 1994. 17(1): p. 39-49.
  42. Hulspas, R., et al., Flow cytometry and the stability of phycoerythrin-tandem dye conjugates. *Cytometry Part A: The Journal of the International Society for Advancement of Cytometry*,

2009. 75(11): p. 966-972.

43. Davis, K.A., et al., Determination of CD4 antigen density on cells: role of antibody valency, avidity, clones, and conjugation. *Cytometry*, 1998. 33(2): p. 197-205.

44. Springer, W., et al., Evaluation of a new reagent for preserving fresh blood samples and its potential usefulness for internal quality controls of multichannel hematology analyzers. *American journal of clinical pathology*, 1999. 111(3): p. 387-396.

45. Canonico, B., et al., Evaluation of leukocyte stabilisation in TransFix®-treated blood samples by flow cytometry and transmission electron microscopy. *Journal of immunological methods*, 2004. 295(1-2): p. 67-78.

46. van Zelm, M.C., et al., An antibody-deficiency syndrome due to mutations in the CD19 gene. *New England Journal of Medicine*, 2006. 354(18): p. 1901-1912.

47. Lhermitte, L., et al., Automated database-guided expert-supervised orientation for immunophenotypic diagnosis and classification of acute leukemia. *Leukemia*, 2018. 32(4): p. 874.



## Chapter 2.2

# Improved standardization of flow cytometry diagnostic screening of primary immunodeficiency by Software-based automated gating

Eleni Linskens<sup>1</sup>, Annieck M. Diks<sup>2</sup>, Jana Neirinck<sup>3</sup>, Martin Perez-Andres<sup>4,5</sup>, Emilie De Maertelaere<sup>1</sup>, Magdalena A. Berkowska<sup>2</sup>, Tessa Kerre<sup>6</sup>, Mattias Hofmans<sup>1</sup>, Alberto Orfao<sup>4 5</sup>, Jacques J. M. van Dongen<sup>2</sup>, Filomeen Haerynck<sup>7</sup>, Jan Philippe<sup>1 3</sup> and Carolien Bonroy<sup>1 3\*</sup>

<sup>1</sup> Department of Laboratory Medicine, Ghent University Hospital, Ghent, Belgium

<sup>2</sup> Department of Immunohematology and Blood Transfusion, Leiden University Medical Center, Leiden, Netherlands

<sup>3</sup> Department of Diagnostic Science, Ghent University, Ghent, Belgium

<sup>4</sup> Cancer Research Centre (IBMCC, USAL-CSIC; CIBERONC CB16/12/00400), Department of Medicine and Cytometry Service (NUCLEUS Research Support Platform), Institute for Biomedical Research of Salamanca (IBSAL), University of Salamanca (USAL), Salamanca, Spain

<sup>5</sup> Translational and Clinical Research Program, Centro de Investigacion del Cancer and Instituto de Biologia Molecular y Celular del Cancer, Consejo Superior de Investigaciones Cientificas (CSIC)-University of Salamanca (USAL), Department of Medicine, IBSAL and CIBERONC, University of Salamanca, Salamanca, Spain

<sup>6</sup> Department of Hematology, Ghent University Hospital, Ghent, Belgium

<sup>7</sup> Department of Pediatric Pulmonology and Immunology and PID Research Laboratory, Ghent University Hospital, Ghent, Belgium

**Frontiers in Immunology, November 2020**  
**doi: 10.3389/fimmu.2020.584646**

### **Abstract**

**Background:** Multiparameter flow cytometry (FC) is essential in the diagnostic work-up and classification of primary immunodeficiency (PIDs). The EuroFlow PID Orientation tube (PIDOT) allows identification of all main lymphocyte subpopulations in blood. To standardize data analysis, tools for Automated Gating and Identification (AG&I) of the informative cell populations, were developed by EuroFlow. Here, we evaluated the contribution of these innovative AG&I tools to the standardization of FC in the diagnostic work-up of PID, by comparing AG&I against expert-based (EuroFlow-standardized) Manual Gating (MG) strategy, and its impact on the reproducibility and clinical interpretation of results.

**Methods:** FC data files from 44 patients (13 CVID, 12 PID, 19 non-PID) and 26 healthy donor (HD) blood samples stained with PIDOT were analyzed in parallel by MG and AG&I, using Infinicyt™ software (Cytognos). For comparison, percentage differences in absolute cell counts/ $\mu\text{L}$  were calculated for each lymphocyte subpopulation. Data files showing differences  $>20\%$  were checked for their potential clinical relevance, based on age- matched percentile (p5-p95) reference ranges. In parallel, intra- and inter-observer reproducibility of MG vs AG&I were evaluated in a subset of 12 samples.

**Results:** The AG&I approach was able to identify the vast majority of lymphoid events ( $>99\%$ ), associated with a significantly higher intra- and inter-observer reproducibility compared to MG. For most HD (83%) and patient (68%) samples, a high degree of agreement ( $<20\%$  numerical differences in absolute cell counts/ $\mu\text{L}$ ) was obtained between MG and the AG&I module. This translated into a minimal impact ( $<5\%$  of observations) on the final clinical interpretation. In all except three samples, extended expert revision of the AG&I approach revealed no error. In the three remaining samples aberrant maturation and/or abnormal marker expression profiles were seen leading in all three cases to numerical alarms by AG&I.

**Conclusion:** Altogether, our results indicate that replacement of MG by the AG&I module would be associated with a greater reproducibility and robustness of results in the diagnostic work-up of patients suspected of PID. However, expert revision of the results of AG&I of PIDOT data still remains necessary in samples with numerical alterations and aberrant B- and T-cell maturation and/or marker expression profiles.

**Keywords:** flow cytometry, immunophenotyping, primary immunodeficiencies, automated gating, standardization, EuroFlow

## Introduction

Primary immunodeficiency (PIDs) comprises a clinically heterogeneous group of rare disorders with defects in the innate and/or adaptive immune system. Due to the dysfunctional immune system, patients can suffer from a wide variety of clinical manifestations, including severe, recurrent, and opportunistic infections, auto-inflammation and auto-immunity [1–3]. Since delayed diagnosis causes higher morbidity and mortality, fast and efficient PID diagnosis, classification and risk assessment is critically important.

Multicolor flow cytometric (FC) immunophenotyping has become a key tool in the diagnostic work-up and classification of PID [1, 3–7]. FC has the advantage of providing fast, widely accessible and relatively low-cost diagnostic screening [8] based on a wide range of assays devoted to immunophenotypic identification and enumeration of specific (sub)populations of blood lymphocytes (e.g. B, T and NK cell subsets), quantitative evaluation of disease-associated protein expression profiles—e.g. Wiskott-Aldrich syndrome protein screen (WASP), CD40/CD40Ligand expression for hyper IgM syndromes-, functional assays (e.g. lymphocyte/T-cell proliferation) and analysis of specific signaling pathways (e.g. phosphorylation of STAT proteins) [2, 7–9].

Despite the clinical relevance of FC in the diagnosis and classification of PID, standardization of specific FC assays across distinct laboratories still remains a challenge. Thus, most published FC data on PID are limited to single center datasets which may not be directly applicable in other centers. Generation of reproducible and comparable data in multicenter settings is required for (inter)national data exchange and integration, creation of larger datasets of patient samples and better identification and definition of the altered immunophenotypic patterns associated with specific PID diagnostic categories.

In the past years, the EuroFlow consortium developed a diagnostic algorithm together with fully standardized antibody combinations (preferably used as dried format reagent mixes) [10] and analytical FC procedures for the diagnostic screening and classification of PID of the lymphoid system [6]. In the proposed EuroFlow approach, the PID orientation tube (PIDOT) plays a central role in case of suspicion of PID, as recently validated in a selected cohort of genetically defined PID patients [4]. Overall, PIDOT allows unequivocal and reproducible identification of >20 different leucocyte populations (including 15 T, B and NK lymphoid subpopulations) in blood, when more than a million cells are evaluated. Interpretation of such data using the classical (2-dimensional-based) expert-guided Manual Gating (MG) approaches (i.e. Boolean gating strategies) is time-consuming and highly subjective, as it relies on the operator's gating decisions, knowledge and expertise. Thereby, MG strategies may result in disturbing levels of variability and more limited reproducibility of FC data analysis, depending on the knowledge and experience of each individual expert [11–14]. In order to avoid such variability introduced during data analysis, the EuroFlow consortium has developed innovative Automated Gating and Identification (AG&I) approaches



and software tools [14], which can be directly applied to the analysis of FC standard data files of blood samples stained with the PIDOT. This tool is based on the combined use of clustering algorithms and big data-based classification approaches, including direct comparison of individual clusters of events per interrogated sample against i) a fully annotated database of FC data files from healthy individuals stained according to the same standard operating procedures (SOPs), and ii) reference values based on a large dataset of hundreds of age-matched healthy donors that includes samples from controls between 0 days (neonatal) and 89 year-old subjects [4, 14].

In this study, we evaluated the contribution of the AG&I module available in the Infinicyt software (Cytognos Sl, Salamanca, Spain), in combination with the PIDOT antibody panel and database, for an increased reproducibility and standardization of multiparameter FC analysis of lymphocyte populations in blood of patients suspected of PID, compared to the classical EuroFlow- standardized MG strategy. In parallel, we also evaluated the potential impact of the new AG&I tool vs. the classical MG approach on the clinical interpretation of PIDOT results.

### **Materials and Methods**

#### **Sample Collection**

FC PIDOT data files of peripheral blood (PB) samples from 44 patients, collected in a routine context of PID suspicion at the Hematology Laboratory of the Ghent University Hospital between November 2016 and March 2018, were included in this study. From these patients, 13 were diagnosed with common variable immunodeficiency (CVID) according to the ESID criteria [9] (M/F ratio: 8/5; age range: 7–67y), and 12 with other PID (M/F ratio: 5/7; age range: 1–12y; two patients with Shwachman–Bodian–Diamond Syndrome [SBDS]; two with KMT2A deficiency; two with myeloperoxidase (MPO) deficiency; one patient with tumor necrosis factor receptor- associated periodic syndrome [TRAPS]; one with KMT2D deficiency; one with adenosine deaminase (ADA) deficiency; one with IRAK4 deficiency and two with mannose-binding lectin (MBL) deficiency); the other 19 cases corresponded to non-PID patients with PID suspicion at time of sampling in whom the diagnosis of PID was ruled out ([non PID]; M/F ratio: 12/7; age range: 11m–50y). In addition, FC PIDOT data files from 26 healthy donors (HD) (M/F ratio: 10/16; age range: 20–58y) collected at Leiden University Medical Center (n=16) and at the Hematology Laboratory of the Ghent University Hospital (n=10) were included in the study [15]. The study was approved by the local ethics committee of the Ghent University Hospital, Belgium (approval 2016/1137). Informed consent from the adult healthy volunteers included in the study was obtained at the time of blood sampling at the participating centers[(15)].

#### **Staining Procedures, Instrument Set-Up, and Data Acquisition**

PB samples were collected in BD Vacutainer tubes containing K<sub>2</sub>EDTA (Becton/Dickinson, San Jose, CA). For each sample, a white blood cell (WBC) count was determined on a Sysmex XP-300 hematology analyzer (Sysmex Corporation, Kobe, Japan). For the immunophenotypic studies non-nucleated red cells were

lysed prior to staining, strictly following the EuroFlow bulk lyse SOP (available at [www.EuroFlow.org](http://www.EuroFlow.org)), as described elsewhere [16, 17]. Subsequently, a stain-wash protocol was performed. Thus, the remaining cell pellet in a volume of 100 $\mu$ L, was stained for 30 minutes in the dark (room temperature [RT]) with the EuroFlow PIDOT monoclonal antibody combination, as previously described (liquid format) [4]. Afterwards, 2mL of BD FACS™ Lysing solution –Becton/Dickinson Biosciences (BD)- diluted 1/10 (v/v) in distilled water, was added and the cell suspension was incubated for another 10 minutes at RT in the dark. Afterwards, cells were washed and the cell pellet was re-suspended in 300 $\mu$ L of washing buffer. Staining and data acquisition of all samples were performed within 24h after blood collection. Data were acquired on BD FACSCanto™ II flow cytometers (BD) at the collection sites. In both centers, instrument settings and data acquisition were performed according to the EuroFlow guidelines available at [www.EuroFlow.org](http://www.EuroFlow.org) [11]. Standard instrument settings were monitored by BD™ Cytometer Setup and Tracking (CS&T) beads (BD) and eight-peak Rainbow bead calibration particles (Spherotech, Lake Forest, IL). For each sample at least 10<sup>6</sup> total events were acquired at low-medium speed. Subsequently, data were exported as an FC standard-file for further analysis. As per the EuroFlow standard instrument setting and calibration SOPs, further manual compensation for optimization of measurements of individual samples was not required.

### Data Analysis

All FC standard data files were analyzed using Infinicyt™ Software (version 2.0.1b, Cytognos SL, Salamanca, Spain) both manually (MG strategy) and automatically (AG&I) using the Infinicyt™ AG&I module and the EuroFlow PIDOT database, with a special focus on the lymphoid populations. MG was based on the previously published EuroFlow PIDOT guidelines [4, 6]. Briefly, gating of the lymphoid populations was performed after excluding debris and cell doublets based on sideward light scatter area (SSC-A)/forward light scatter area (FSC-A) and FSC Height (FSC-H)/FSC-A bivariate dotplots, respectively. B-cells were identified based on their unique CD45hi CD19+ CD3- CD45RA+ phenotype and FSClo SSClo characteristics. Further identification of B-cell subpopulations was based on the levels of expression of CD27, IgM and IgD. In turn, T-cells were identified based on a CD45hi CD3+ and FSClo SSClo phenotype. After gating TCR $\gamma\delta$ + T-cells, the CD4+, CD8+ and CD4- CD8- TCR $\gamma\delta$ - T-cell subpopulations were identified. Subsequently, the distinct maturation-associated subsets of CD4+ and CD8+ TCR $\gamma\delta$ - T-cell subpopulations were further identified based on their unique levels of expression of CD27 and CD45RA. Finally, NK-cells were defined as CD45hiCD19-CD3- CD16&CD56hiCD45RAlo/+ FSC-Alo SSC-Alo cells. More details on the MG strategy used for the identification of the lymphoid populations are provided in **Table 1**.

In parallel with the MG strategy, all FC standard data files were also analyzed with the AG&I module of Infinicyt™. The AG&I module compares each FC standard data file with a reference database of healthy controls using the automated gating and classification algorithms, as previously described in detail [18, 19].

**Table 1. Phenotypic features used in the Manual Gating (MG) strategy for the identification of lymphoid populations in blood according to the EuroFlow guidelines for analysis of blood samples stained with PIDOT.**

| Population   | Gating strategy <sup>(1)</sup>  |
|--|---|
| B-cells  | FSC <sup>lo</sup> SSC <sup>lo</sup> CD45 <sup>hi</sup> CD19 <sup>+</sup> CD3 <sup>-</sup> CD45RA <sup>+</sup>                                 |
| Pre-germinal center B-cells                                  | CD27 <sup>+</sup> IgD <sup>+</sup> IgM <sup>+</sup>   |
| Post-germinal center B-cells/<br>plasmacells (MBC/PC)        |   |
| Unswitched MBC/PC <sup>(2)</sup>                             | IgD <sup>+</sup> IgM <sup>+</sup> CD27 <sup>+</sup>   |
| Switched MBC/PC <sup>(2)</sup>                               | IgD <sup>-</sup> IgM <sup>-</sup> CD27 <sup>-</sup>   |
| IgD <sup>+</sup> IgM <sup>-</sup> post-GC                    | IgD <sup>+</sup> IgM <sup>-</sup> CD27 <sup>+</sup>   |
| T-cells  | FSC <sup>lo</sup> SSC <sup>lo</sup> CD45 <sup>hi</sup> CD3 <sup>+</sup> CD19 <sup>-</sup><br>CD16&CD56 <sup>-</sup>                           |
| TCRγδ <sup>+</sup> T-cells                                   | TCRγδ <sup>+</sup> CD4 <sup>-</sup> CD8 <sup>-</sup>  |
| TCRγδ <sup>-</sup> CD4 <sup>+</sup> CD8 <sup>-</sup> T-cells | TCRγδ <sup>-</sup> CD4 <sup>+</sup> CD8 <sup>-</sup>  |
| CD4 <sup>+</sup> T-cells                                     | TCRγδ <sup>-</sup> CD4 <sup>+</sup> CD8 <sup>-</sup>  |
| CD4 <sup>+</sup> naive T-cells                               | CD27 <sup>+</sup> CD45RA <sup>+</sup>   |
| CD4 <sup>+</sup> central memory T-cells                      | CD27 <sup>+</sup> CD45RA <sup>-</sup>   |
| CD4 <sup>+</sup> effector memory T-cells                     | CD27 <sup>-</sup> CD45RA <sup>-</sup>   |
| CD4 <sup>+</sup> terminal effector T-cells                   | CD27 <sup>-</sup> CD45RA <sup>+</sup>   |
| CD8 <sup>+</sup> T-cells                                     | TCRγδ <sup>-</sup> CD4 <sup>-</sup> CD8 <sup>+</sup>  |
| CD8 <sup>+</sup> naive T-cells                               | CD27 <sup>+</sup> CD45RA <sup>+</sup>   |
| CD8 <sup>+</sup> central memory T-cells                      | CD27 <sup>+</sup> CD45RA <sup>-</sup>   |
| CD8 <sup>+</sup> effector memory T-cells                     | CD27 <sup>-</sup> CD45RA <sup>-</sup>   |
| CD8 <sup>+</sup> effector CD27 <sup>+</sup> T-cells          | CD27 <sup>lo</sup> CD45RA <sup>+</sup>  |
| CD8 <sup>+</sup> terminal effector T-cells                   | CD27 <sup>-</sup> CD45RA <sup>+</sup>   |
| CD4 <sup>+</sup> CD8 <sup>+</sup> T-cells                    | TCRγδ <sup>-</sup> CD4 <sup>+</sup> CD8 <sup>+</sup>  |
| Natural Killer cells   | SSC-A <sup>lo</sup> FSC-A <sup>lo</sup> CD45 <sup>hi</sup> CD19 <sup>-</sup> CD3 <sup>-</sup><br>CD16&CD56 <sup>hi</sup> CD45RA <sup>lo</sup> |

<sup>(1)</sup>In addition to the classical two-dimensional gating based on the listed markers, automatic population separator (APS) plots were used for fine-tune the gating of the listed cell populations as described elsewhere (4); <sup>(2)</sup>Most MBC/PC, but not all, are CD27<sup>+</sup>.

This automated analysis included a first clustering step of all individual events in the data file, followed in a second step by classification of the resulting clusters of events into the cell populations identified a priori in the database, according to their characteristics in the multidimensional space generated by all the parameters evaluated. Input of patient's age and WBC counts was required before the automated process could be started. During automated data processing, most events are automatically assigned to the different cell populations with only a few remaining unassigned clusters of events (= "checks"). For these latter groups of alarmed events, the AG&I module proposes one or more populations to which they might correspond, but definitive assignment to a given cell population must be done manually by an expert. Once the alarmed events have been checked by the expert, the software provides an automated report indicating the normal range in age-matched controls, with a "remark" for each cell population with values out of the normal range, using previously published reference values [4, 6].

In this study, those events automatically assigned to a given cell population were not re-evaluated or re-classified manually to mimic the optimal routine situation, unless stated otherwise. Following the automated gating process, the percentage of each cell population from both its parent population and all WBC, was automatically calculated, recorded, and stored by the Infinicyt™ software. Absolute cell counts/μL were calculated according to the white blood cell count (dual platform) as follows:

$$\frac{\text{Relative WBC (\%)}}{100} \times \text{WBC/mL} = \text{Absolute count/mL}$$

### Comparison Between the MG Strategy and the AG&I Approach

Absolute cell counts/ $\mu\text{L}$  obtained with the MG and AG&I strategies were compared for each cell population. The percentage difference between the counts for each cell population obtained with the two strategies was calculated by the following formula:

$$\frac{(\text{absolute count/mL})_{MG} - (\text{absolute count/mL})_{AG\&I}}{(\text{absolute count/mL})_{MG}} \times 100$$

According to the International Standard EN ISO 15189 [20], the two gating methods were considered to be equivalent whenever the percent difference was <20%. Nevertheless, for the less abundant subpopulations with relatively wide reference intervals, the application of the <20% difference criterion may be clinically irrelevant. Because of this, for all lymphoid subpopulations with >20% differences we applied an additional criterion that relied on the impact on the final clinical interpretation, based on comparison of each of the two values against age-matched reference percentile (p5–p95) ranges as determined on a group of 250 HD [4]. Differences in interpretation of the results after application of these age-matched reference values were considered as ‘clinically relevant’ and triggered a more detailed revision of both the AG&I (including a revision of the automatically assigned events whenever necessary) and MG analyses.

### Intra- and Inter-Observer Reproducibility

Twelve samples (three samples from each patient group and the HD group) out of the 70 samples analyzed were randomly chosen to document the impact of the use of the AG&I software tools vs MG, on intra-observer and inter-observer reproducibility of data analysis.

For evaluation of intra-observer reproducibility, MG and AG&I were performed five times by the same observer (EL) on those 12 samples selected as described above. For inter-observer reproducibility, MG and AG&I were performed on the same 12 samples by five different observers (EL, MH, CB, PB, JDW). All five observers were trained individuals with strong expertise in gating the EuroFlow PIDOT tube and (routine) users of Infinicyt™. Standard deviation (SD) and coefficient of variation (CV) values were calculated for each cell population as obtained by both gating strategies.

### Statistical Methods

For comparison of the analysis strategies, Spearman rank correlation was used. For comparison between groups for continuous variables, the Chi-squared test with the Yates’ correction for continuity, was applied. Statistical comparison of the CVs was performed by the variance ratio F-test. Two-sided p-values <0.05 were considered to be associated with statistical significance. In case of multiple testing, the Bonferroni correction was applied. Statistical evaluation was performed using MedCalc Statistical Software (version 15.6.1; MedCalc Software bvba, Ostend, Belgium) and GraphPad Prism (version 5.04 for Windows; GraphPad Software, San Diego, CA).

### Results

#### Comparison Between MG and AG&I Approaches on Healthy Donor Blood Samples

When considering all observations for the HD samples (n=520 observations; 20 cell populations in 26 samples), the vast majority of the events in the HD FC standard data files—median of 99.85% (range: 99.30–99.95%)—that corresponded to lymphoid cells were classified into one of the lymphocyte populations of the database with the AG&I module. In contrast, for a minor fraction of events—median 0.15% (range 0.0–0.70%)—the AG&I module induced an alarm due to phenotypic deviations from the reference populations in the PIDOT database and required revision by an expert.

Differences greater than 20% on absolute cell counts (/ $\mu$ L) as calculated via MG vs AG&I were observed in 17% of all HD observations. An overview of these differences per cell population is shown in **Table 2**. Briefly, no differences >20% between both analytical strategies (MG and AG&I) were observed for 9/20 lymphoid populations (i.e., total lymphocytes, B-cells, pre-GC B-cells, T-cells, CD4+ T-cells, CD4+ naïve and central memory T-cells, CD8+ T-cells, and TCR $\gamma$  $\delta$ + T-cells). In turn, a limited number of HD samples showed >20% differences between MG and AG&I counts for NK-cells (n=3/26), unswitched memory B-cells/plasma cells (MBC/PC) (n=8/26), switched MBC/PC (n=2/26), CD4+ effector memory T-cells (n= 2/26), CD8+ naïve T-cells (n=2/26), CD8+ central memory T-cells (n=5/26) and CD4-CD8- TCR $\gamma$  $\delta$ - T-cells (n=6/26). In contrast, differences were more frequently observed [60% of the observations (n=62/104)] for other less abundant T-cell subpopulations [CD4+ terminal differentiated (TD) T-cells (n=20/26), CD8+ effector memory T-cells (n=11/26), CD8+ TD27+ T-cells (n=19/26) and CD8+ TD T-cells], as might have been expected for these populations which typically represent <1% of all WBC. Of note, CD4+CD8+ double-positive T-cells were not assigned as a separate population with the AG&I module. Spearman rank correlation coefficients for cell populations mandatory for PID screening and classification according to the ESID criteria (i.e. total lymphocytes, total B-cells, pre-GC B-cells, unswitched and switched MBC/PC, total T-cells, CD4+ and CD8+ T-cells, CD4+ and CD8+ naïve and central memory T-cells, TCR $\gamma$  $\delta$ + and TCR $\gamma$  $\delta$ - CD4-CD8- T-cells, NK-cells) are shown in **Table 3**. For healthy donor samples correlation coefficients of >0.90 were obtained for most populations.



**Table 2. Comparison of the Manual Gating (MG) strategy versus the AG&I module.** CVID, Common Variable Immunodeficiency Disorder patients; PID, Other PID patients; Non PID: patients with diseases other than PID; HD, healthy donors; Pre-GC-B-cells, pre-germinal center B-cells; TD, terminal differentiated; NK-Cells, natural killer cells; NA, not applicable.

| Population   | n of samples (%) with > 20% numerical differences |                           |                |                |                   | n of samples (%) with clinically relevant differences vs age-matched (p5 - p95) normal reference values |                         |                           |                 |                 |                   |                |
|--|---|---------------------------|----------------|----------------|-------------------|---|-------------------------|---------------------------|-----------------|-----------------|-------------------|----------------|
|  | Total samples<br>n = 70                           | Patient samples<br>n = 44 | CVID<br>n = 13 | PID<br>n = 12  | Non PID<br>n = 19 | HD<br>n = 26  | Total samples<br>n = 70 | Patient samples<br>n = 44 | CVID<br>n = 13  | PID<br>n = 12   | Non PID<br>n = 19 | HD<br>n = 26   |
| Lymphocytes  | 1<br>(1.4)  | 1<br>(2.3)                | 1<br>(7.7)     | 0<br>(0)       | 0<br>(0)          | 0<br>(0)  | 0<br>(0)                | 0<br>(0)                  | NA              | NA              | NA                | 0<br>(0)       |
| B-cells  | 1<br>(1.5)  | 1<br>(3.8)                | 1<br>(7.7)     | 0<br>(0)       | 0<br>(0)          | 0<br>(0)  | 0<br>(0)                | 0<br>(0)                  | NA              | NA              | NA                | 0<br>(0)       |
| Pre-GC B-cells   | 6<br>(8.6)  | 6<br>(14)                 | 4<br>(31)      | 2<br>(17)      | 0<br>(0)          | 0<br>(0)  | 1<br>(1.4)              | 1<br>(2.3)                | 1<br>(7.7)      | 0<br>(0)        | 0<br>(0)          | 0<br>(0)       |
| Unswitched   | 35<br>(50)  | 27<br>(61)                | 9<br>(69)      | 10<br>(83)     | 8<br>(42)         | 8<br>(31)   | 6<br>(8.6)              | 6<br>(14)                 | 2<br>(15)       | 4<br>(33)       | 0<br>(0)          | 0<br>(0)       |
| MBC/PC   | 15<br>(21)  | 13<br>(30)                | 3<br>(23)      | 5<br>(42)      | 5<br>(26)         | 2<br>(7.7)  | 5<br>(7.1)              | 5<br>(11)                 | 2<br>(15)       | 2<br>(17)       | 1<br>(5.3)        | 0<br>(0)       |
| Switched   | 1<br>(1.5)  | 1<br>(3.8)                | 1<br>(7.7)     | 0<br>(0)       | 0<br>(0)          | 0<br>(0)  | 0<br>(0)                | 0<br>(0)                  | NA              | NA              | NA                | 0<br>(0)       |
| MBC/PC T-cells   | 2<br>(2.9)  | 2<br>(4.5)                | 1<br>(7.7)     | 0<br>(0)       | 1<br>(5.3)        | 0<br>(0)  | 1<br>(1.4)              | 1<br>(2.3)                | 1<br>(7.7)      | 0<br>(0)        | 0<br>(0)          | 0<br>(0)       |
| CD4+ T-cells   | 6<br>(8.6)  | 6<br>(14)                 | 3<br>(23)      | 1<br>(8.3)     | 2<br>(11)         | 0<br>(0)  | 0<br>(0)                | 0<br>(0)                  | NA              | NA              | NA                | 0<br>(0)       |
| CD4+ naive T-cells   | 10<br>(14)  | 10<br>(23)                | 1<br>(7.7)     | 4<br>(33)      | 5<br>(26)         | 0<br>(0)  | 3<br>(4.3)              | 3<br>(6.8)                | 0<br>(0)        | 1<br>(8.3)      | 2<br>(11)         | 0<br>(0)       |
| CD4+ central memory T-cells  | 8<br>(11)   | 8<br>(18)                 | 3<br>(23)      | 3<br>(25)      | 2<br>(11)         | 2<br>(7.7)  | 3<br>(4.3)              | 3<br>(6.8)                | 1<br>(7.7)      | 1<br>(8.3)      | 1<br>(5.3)        | 0<br>(0)       |
| CD4+ effector memory T-cells                                       | 57<br>(81)  | 37<br>(84)                | 11<br>(85)     | 11<br>(92)     | 15<br>(79)        | 20<br>(77)  | 1<br>(1.4)              | 1<br>(2.3)                | 0<br>(0)        | 0<br>(0)        | 1<br>(5.3)        | 0<br>(0)       |
| CD4+ TD T-cells  | 5<br>(7.1)  | 5<br>(11)                 | 1<br>(7.7)     | 1<br>(8.3)     | 3<br>(16)         | 0<br>(0)  | 0<br>(0)                | 0<br>(0)                  | NA              | NA              | NA                | 0<br>(0)       |
| CD8+ T-cells   | 11<br>(16)  | 9<br>(20)                 | 5<br>(38)      | 1<br>(8.3)     | 3<br>(16)         | 2<br>(7.7)  | 2<br>(2.9)              | 2<br>(4.5)                | 0<br>(0)        | 0<br>(0)        | 2<br>(11)         | 0<br>(0)       |
| CD8+ naive T-cells   | 29<br>(41)  | 24<br>(55)                | 5<br>(38)      | 8<br>(67)      | 11<br>(58)        | 5<br>(19)   | 4<br>(5.7)              | 4<br>(9.1)                | 0<br>(0)        | 2<br>(17)       | 2<br>(11)         | 0<br>(0)       |
| CD8+ central memory T-cells  | 44<br>(63)  | 33<br>(75)                | 9<br>(69)      | 9<br>(75)      | 15<br>(79)        | 11<br>(42)  | 9<br>(13)               | 7<br>(16)                 | 1<br>(7.7)      | 2<br>(17)       | 4<br>(21)         | 2<br>(7.7)     |
| CD8+ effector memory T-cells                                       | 60<br>(86)  | 41<br>(93)                | 12<br>(92)     | 12<br>(100)    | 17<br>(89)        | 19<br>(73)  | 14<br>(20)              | 12<br>(27)                | 2<br>(15)       | 3<br>(25)       | 7<br>(37)         | 2<br>(7.7)     |
| CD8+ TD27+ T-cells   | 44<br>(63)  | 32<br>(73)                | 10<br>(77)     | 8<br>(67)      | 14<br>(74)        | 12<br>(46)  | 5<br>(7.1)              | 3<br>(6.8)                | 1<br>(7.7)      | 2<br>(17)       | 0<br>(0)          | 2<br>(7.7)     |
| CD8+ TD27- T-cells   | 20<br>(29)  | 14<br>(32)                | 4<br>(31)      | 5<br>(42)      | 5<br>(26)         | 6<br>(23)   | 6<br>(8.6)              | 6<br>(14)                 | 4<br>(31)       | 1<br>(8.3)      | 1<br>(5.3)        | 0<br>(0)       |
| CD4 CD8 TCRgd T-cells  | 6<br>(8.6)  | 6<br>(14)                 | 4<br>(31)      | 0<br>(0)       | 2<br>(11)         | 0<br>(0)  | 1<br>(1.4)              | 1<br>(2.3)                | 1<br>(7.7)      | 0<br>(0)        | 0<br>(0)          | 0<br>(0)       |
| TCRgd+ T-cells   | 9<br>(13)   | 6<br>(14)                 | 4<br>(31)      | 2<br>(17)      | 0<br>(0)          | 3<br>(12)   | 1<br>(1.4)              | 0<br>(0)                  | 0<br>(0)        | 0<br>(0)        | 0<br>(0)          | 1<br>(3.8)     |
| NK-cells   | 372/1400<br>[27]                                  | 282/880<br>[32]           | 92/260<br>[35] | 81/240<br>[34] | 108/380<br>[28]   | 90/520<br>[17]  | 62/1400<br>[4.4]        | 55/880<br>[6.3]           | 16/260<br>[6.2] | 18/240<br>[7.5] | 21/380<br>[5.5]   | 7/520<br>[1.3] |
| Total number of observations with deviations on total [% on total] |   |                           |                |                |                   |   |                         |                           |                 |                 |                   |                |

CVID, Common Variable Immunodeficiency Disorder patients; PID, Other PID patients; Non PID: patients with diseases other than PID; HD, healthy donors; Pre-GC-B-cells, pre-germinal center B-cells; TD, terminal differentiated; NK-Cells, natural killer cells; NA, not applicable.





**Table 3. Correlation between absolute counts obtained by manual gating (MG) versus automated gating and identification (AG&I).**

|  | Healthy donors | Patients | Total |
|--|----------------|----------|-------|
| Lymphocytes  | 0.996          | 0.994    | 0.994 |
| B-cells  | 0.996          | 0.998    | 0.998 |
| Pre-GC B-cells   | 0.997          | 0.992    | 0.995 |
| Unswitched MBC/PC  | 0.955          | 0.845    | 0.877 |
| Switched MBC/PC  | 0.983          | 0.963    | 0.956 |
| T-cells  | 0.997          | 0.992    | 0.992 |
| CD4 <sup>+</sup> T-cells                                     | 0.998          | 0.989    | 0.990 |
| CD4 <sup>+</sup> naive T-cells                               | 0.976          | 0.988    | 0.989 |
| CD4 <sup>+</sup> central memory T-cells                      | 0.960          | 0.933    | 0.923 |
| CD8 <sup>+</sup> T-cells                                     | 0.995          | 0.980    | 0.991 |
| CD8 <sup>+</sup> naive T-cells                               | 0.987          | 0.978    | 0.983 |
| CD8 <sup>+</sup> central memory T-cells                      | 0.779          | 0.933    | 0.893 |
| TCRgd <sup>+</sup> T-cells                                   | 0.999          | 0.925    | 0.942 |
| TCRgd <sup>-</sup> CD4 <sup>-</sup> CD8 <sup>-</sup> T-cells | 0.951          | 0.915    | 0.955 |
| Natural killer cells   | 0.883          | 0.983    | 0.973 |

*Results expressed as Spearman rank correlation coefficient values for those cell populations that are mandatory for PID screening and classification according to the ESID criteria. For all correlations p-values < 0.001 were detected.*

In order to further evaluate the impact of AG&I on both intra- and inter-observer reproducibility of data analysis on HD samples, SDs and median %CVs for MG and AG&I data, were compared (see **Figure 1A**). As a result, a lower overall median % CV was observed with the AG&I approach compared to MG (5.8 vs 0.2% for intra-observer and 8.0 vs 0.3% for inter-observer reproducibility, respectively). A more detailed analysis of the impact of AG&I for the individual cell populations is given in **Supplementary Table 1A**.

### **Comparison of the MG Strategy Versus the AG&I Module on Samples of Patients Suspected of PID**

A rather limited median percentage of checks (% of total events) was observed with the AG&I module (median 0.54%; range: 0.02–41.5%) for all observations recorded on the patient samples (n=880 observations for 20 cell populations in 44 samples) (**Supplementary Figure 1**).

Around one third (32%) of all patient samples showed >20% differences on the absolute cell counts (/μL) of at least one cell population as obtained with MG vs the AG&I module, with similar frequencies (p>0.05) in each of the three patient groups (CVID 35%, other PID 34%, and non-PID 28%). Despite this, differences >20% between both analytical strategies involving one or more of the major lymphocyte populations in blood (total lymphocytes, B-cells, T-cells, CD4<sup>+</sup> and CD8<sup>+</sup> T-cells) were restricted to a minority (<15%) of all patient samples. Thus, >20% differences were observed for total lymphocytes in 1/44 patients, B-cells in 1/44 cases, T-cells in 1/44, CD4<sup>+</sup> T-cells in 2/44, and CD8<sup>+</sup> T-cells in 5/44 cases. More than 20% differences between MG vs AG&I observed in the patient sam-

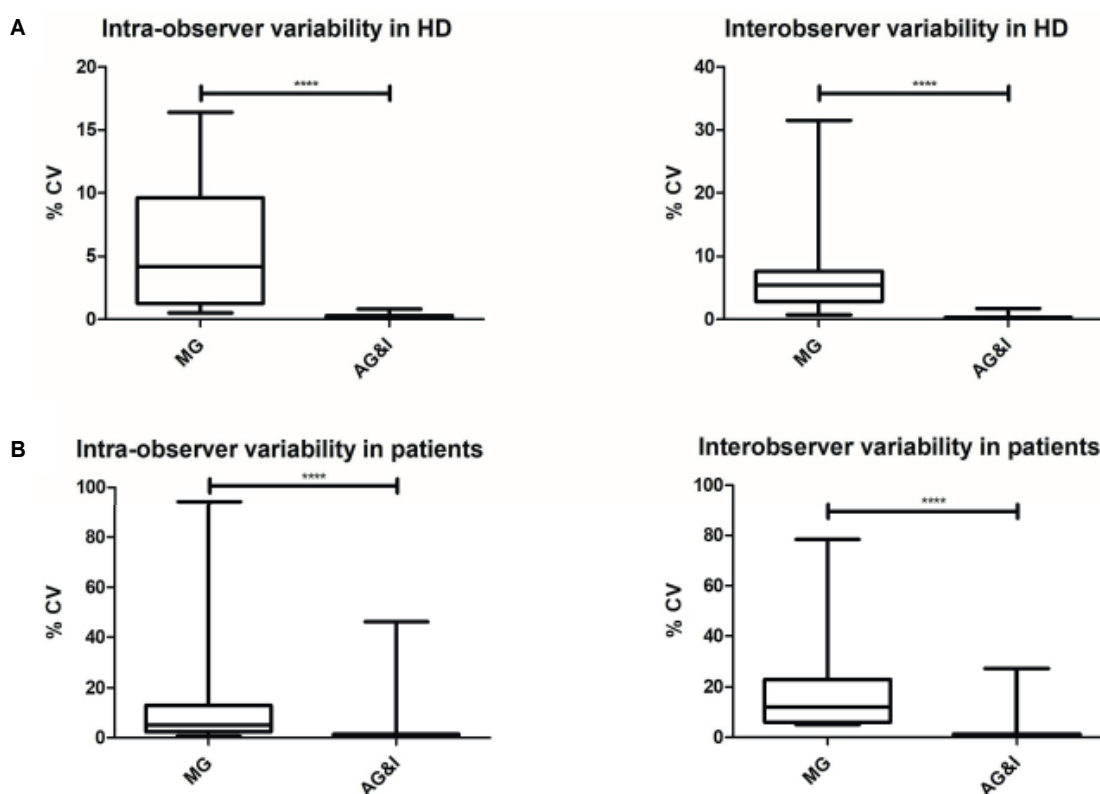


**Figure 1. Intra- and inter-observer reproducibility of Manual Gating (MG) versus Automated Gating and Identification (AG&I).** (A; top figure) Box-and-Whisker plots of CVs (%) for all lymphoid populations in HD blood samples. (B; bottom figure) Box-and-Whisker plots of CVs (%) for all lymphoid populations in patient samples. \*\*\*\*Statistically significant differences ( $P < 0.0001$ ) based on the variance ratio F-test.

ples were mostly documented for the less abundant B- and T-cell subpopulations (counts  $<1\%$  of all WBC). An overview of the results obtained per cell population is shown in **Table 2**. Spearman rank correlation coefficients for patient samples were calculated, showing correlation coefficients of  $>0.90$  for most subset populations mandatory for PID screening and classification according to the ESID criteria (see **Table 3**).

The AG&I approach showed a greater intra- and inter- observer reproducibility than MG also on patient samples with lower median %CV (5.1 vs 0.4% for intra-observer and 12.1 vs. 0.6% for inter-observer reproducibility for AG&I vs MG, respectively) for all 20 lymphoid populations identified (see **Figure 1B** and **Supplementary Table 1B**).

### Impact of AG&I vs MG on Clinical Interpretation of Results

The possible impact of differences on clinical interpretation of cell counts obtained with the AG&I tool vs the MG strategy was evaluated by comparing each of the paired counts against age- matched reference percentile (p5–p95) ranges, assessed on a group of 250 HD [4]. Data are summarized in **Table 2**. Overall, comparison of the results obtained with each of the two data analysis approaches against age-matched reference values, translated into different clinical interpre-

## Chapter 2.2

---

tations for MG and AG&I in only 4.4% (n=62/1,400) of all paired observations [1.3% (n=7/ 520) for HD and 6% (n=55/880) for the patient samples].

Looking at the major lymphocyte populations (total lymphocytes, B-cells and T-cells) in both HD and patient samples, no difference in clinical interpretation was observed after evaluating the results against the age-matched p5–p95 reference values. The clinically relevant differences were also limited for the NK-cells, a different interpretation being restricted to a single HD sample (absolute NK-cell counts below p5 for MG while within the p5–p95 range for AG&I).

No differences in clinical interpretation related to the B-cell populations were observed in HD. In contrast, several differences in clinical interpretation were observed among the patients. Thus, clinically relevant differences in pre-germinal center B-cell counts were observed for one CVID patient sample for which differences against age-matched reference values were also detected for the memory B-cell populations as discussed in more detail below (Sample 1). Differences in clinical interpretation for unswitched and switched MBC/PC were mostly observed among CVID (n=2) and other PID samples (n=4; 2 KMT2A deficiencies, 1 IRAK4 deficiency, and 1 MBL). For the two KMT2A deficiency patients, who typically display a CVID-like phenotype with deviations in B-cell maturation and low absolute counts of different B-cell populations, the absolute counts obtained with MG were within age-matched reference ranges for both unswitched and switched MBC/PC, while AG&I provided decreased absolute counts for both memory B-cell populations below the p5. The IRAK4 deficiency sample and MBL deficiency sample (both conditions for which no lymphoid deviations are usually expected) also showed clinically relevant differences for the unswitched MBC/PC subpopulation, with abnormal values for the MG approach (below p5 for the IRAK4 deficiency and above p95 for the MBL deficiency), but normal absolute counts for all B-cell subpopulations when analyzed with the AG&I tool. In addition, another CVID patient sample (not Sample 1, see above), showed a clinically relevant difference in the absolute number of unswitched MBC/PC: decreased below p5 with MG while within the normal range with the AG&I approach. In another CVID sample, different clinical interpretation for switched MBC/PC was made with AG&I (absolute values below p5 as is expected for a CVID phenotype) and MG (absolute values within the p5–p95 range).

Differences in clinical interpretation related to CD4+ T-cell populations (including the less abundant CD4+ T cell populations) were also absent in HD and very limited in patient samples (0–7% of samples depending on the specific CD4+ T-cell population). No clinically relevant differences were found in HD for naive and central memory CD8+ T-cells, with only a few discrepancies in patient samples (between 5% and 9% of the samples depending on the specific CD8+ T-cell population). More differences in clinical interpretation (compared with age-matched normal p5–p95 reference ranges) were observed for the CD8+ effector T-cell populations (range: 7–27% of samples depending on the specific cell population). Despite all the above, detailed analysis of all clinically relevant

differences observed for the distinct T-cell populations identified with PIDOT, showed no recurrent pattern (or cause) in all but one sample. This latter sample corresponded to a non-PID sample (Sample 2) which showed a combined pattern of clinically relevant differences in both CD4<sup>+</sup> memory effector T-cells and CD4-CD8- TCR $\gamma\delta$ - T-cells, as discussed in more detail below.

Different clinical interpretation for the TCR $\gamma\delta$ <sup>+</sup> and CD4-CD8- TCR $\gamma\delta$ - T-cells were observed for a limited number of samples (1 and 6, respectively). One of these samples was already described above (Sample 2). In addition, one CVID sample (Sample 3) showed clinically relevant differences for both TCR $\gamma\delta$ <sup>+</sup> and CD4-CD8- TCR $\gamma\delta$ - T-cells, triggering further investigations (see below). For the remaining four discrepant samples, no underlying cause could be identified to clarify the difference.

### Detailed Analyses of Clinically Relevant Discrepancies

Detailed revision of both MG and AG&I data analysis was performed for all samples showing “clinically relevant” differences on the interpretation of the results obtained (once compared with age-matched reference values) for at least one lymphoid cell population (differences in 62 observations corresponding to 37 samples). In 34/37 samples (92%) AG&I results were confirmed during the expert review. In the remaining three samples (8%) corresponding to two CVID samples [Sample 1 and 3] and one non-PID patient sample [Sample 2] AG&I results were questionable. In more detail, in one of these two CVID samples [Sample 1], different absolute counts were observed for all B-cell populations identified by MG vs AG&I. Plots corresponding to the (unchecked) AG&I analysis for this sample are shown in **Figure 2A**. This was due to the fact that by AG&I a large proportion of the B-cells was automatically assigned to the memory IgD+IgM-B-cell population. MG confirmed that phenotypically this population was indeed CD27<sup>+</sup>; however, its phenotype was not fully compatible with the classically high IgD expression (MFI of between 104 – 105 using the EuroFlow instrument settings in combination with the EuroFlow PIDOT reagents) on memory IgD+IgM-B-cells, making their distinction from switched MBC/PC (CD27<sup>+</sup>/ IgM-/IgD-) a challenge, also with MG that assigned them to switched MBC/PC. Despite this uncommon phenotype, AG&I analysis did not classify these events as ‘checks’. In the other two discordant samples (Samples 2 and 3) clinically relevant differences for the CD4-CD8- TCR $\gamma\delta$ - T-cell population were observed and confirmed after revision of the AG&I data. In the latter CVID sample (Sample 3), a large TCR $\gamma\delta$ <sup>+</sup> population was automatically assigned to the CD4-CD8- TCR $\gamma\delta$ - population by AG&I (unchecked AG&I plots shown in **Figure 2B**). In the non- PID sample (Sample 2), events classified by MG as CD4<sup>+</sup> effector memory T-cells and CD4<sup>+</sup> naive T-cells had been incorrectly classified by the AG&I module as CD4-CD8- TCR $\gamma\delta$ - due to an abnormally low CD4-signal because of a technical (staining) issue (unchecked AG&I plots shown in **Figure 2C**). Despite all the above, these wrongly identified cell populations were systematically alarmed as “numerically altered” by the AG&I software tool, pointing out the need for review by the expert prior to final reporting.

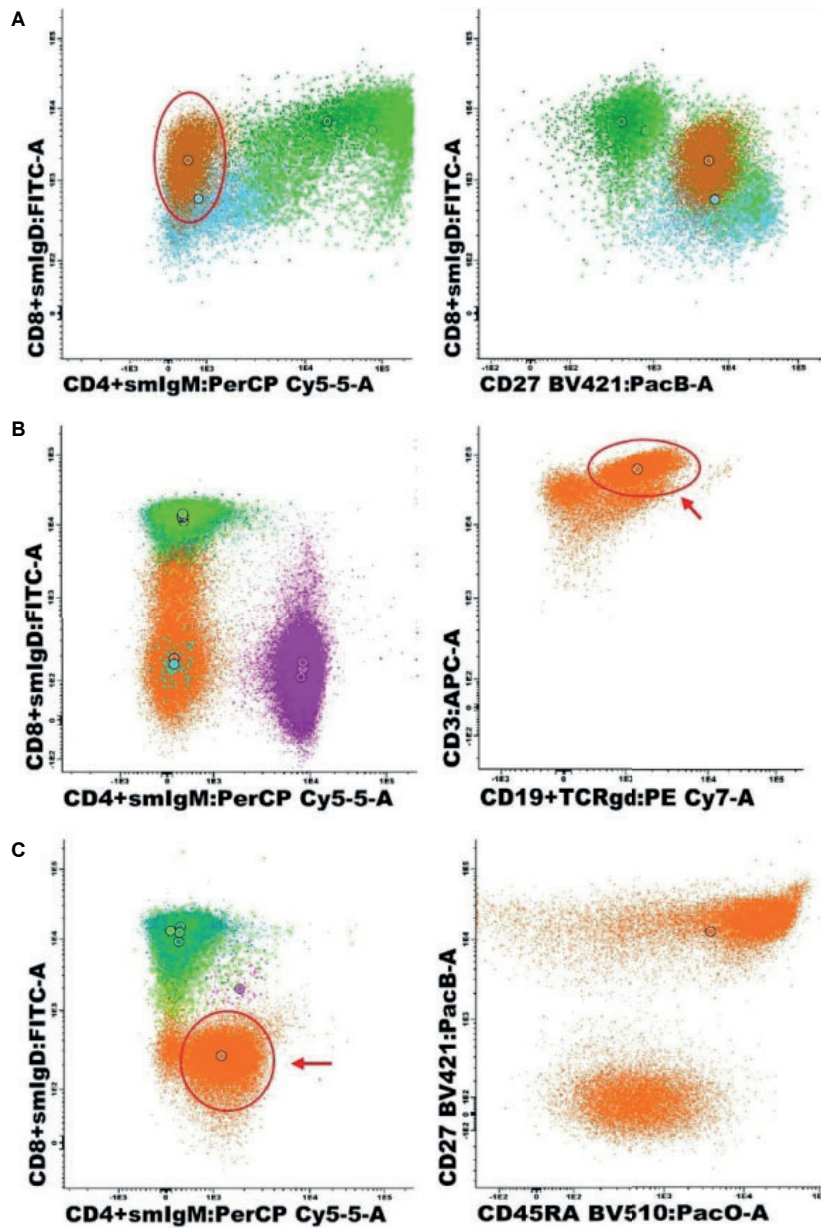


**Figure 2. Representative (unchecked) AG&I bivariate dot-plots corresponding to the specific cell populations present in those 3 cases with altered phenotypes identified during detailed expert revision.** (A) CVID sample (Sample 1) with a B-cell population showing abnormally dim expression of IgD on IgM-negative B-cells, classified by the AG&I tool as IgD+IgM-MBC/PC (brown) with need for expert revision based on their aberrant expression pattern, in addition to pre-germinal center B-cells (dark green), unswitched MBC/PC (bright green) and switched MBC/PC (blue). (B) CVID sample with a large population of TCR $\gamma\delta$ + T-cells (see arrow) incorrectly assigned CD4-CD8- TCR $\gamma\delta$ - events (orange) (sample 3) in addition to CD8+ T-cells (green), CD4+ T-cells (purple) and TCR $\gamma\delta$ + T-cells (blue). (C) Non PID patient with a large population of dim CD4+ events (see arrow) automatically classified as CD4-CD8- TCR $\gamma\delta$ - T-cells (orange) (sample 2), in addition to CD8+ T-cells (green) and CD4+ T-cells (pink).



## Discussion

Due to major technological advances in multiparameter FC, data analysis has become increasingly complex and time-consuming [13, 18, 21–23]. This also implies higher variability and more subjectivity, as it is influenced by the observer's expertise. Thus, the increased complexity associated with greater numbers of cells measured for an increasingly high number of parameters with the ability of identifying greater numbers of cell populations, has fostered the development of automated algorithms and tools for the analysis of complex multiparameter FC datasets [14, 18, 21–23]. In this study, we evaluated the contribution of the EuroFlow AG&I module implemented in the Infinicyt software for analysis of PB samples stained with PIDOT in the standardization of the FC diagnostic work-up of PID.

Overall, our results showed that compared to MG, the use of the AG&I approach was associated with a significantly lower intra- and inter-observer variability of data analysis (and also interpretation) for all lymphoid populations identified with the PIDOT. In fact, the use of the AG&I tool systematically provided for most lymphoid populations identified a high intra- and inter-observer reproducibility with <20% CVs according to the EN ISO 15189 criterion applied in most European medical diagnostics laboratories [20]. Altogether, these results indicate that replacement of MG by the AG&I module would be associated with a greater reproducibility and robustness of results.

In turn, a high degree of agreement (defined as <20% numerical differences in absolute cell counts/ $\mu\text{L}$ ) was obtained between expert-based MG and the AG&I module, for most lymphocyte populations in both HD (83% of all observations) and routine diagnostic patient samples (68% of all observations), most discrepancies occurring for cell populations present at low (<1%) frequencies in blood. This translated into a minimal possible impact (4.4% of all observations, 6.3% of patient observations, 1.3% of HD observations) on the final clinical interpretation (e.g. normal vs increased or decreased cell counts) resulting from the comparison of the results obtained with each analytical approach with (p5–p95) age-matched reference values. Thereby, only a limited number of discordant observations between MG and AG&I was detected for those lymphoid populations that are mandatory for PID screening according to the ESID criteria (i.e. total lymphocytes, total B-cells, pre-GC B-cells, unswitched and switched MBC/PC, total T-cells, CD4+ and CD8+ T-cells, CD4+ and CD8+ naïve and central memory T-cells, TCR $\gamma\delta$ + and TCR $\gamma\delta$ - CD4-CD8- T-cells, NK-cells). For those lymphoid populations, discrepant observations were restricted to 4.4% of patients observations (n=29/660 observations) and 0.2% of HD observations (n=1/390). This was due to the fact that most differences were observed for the less abundant T-cell populations (e.g. CD4+ and CD8+ effector memory and terminally differentiated T-cells), that are currently not considered in the (routine) diagnostic work-up of PID.

Looking into potential reasons for the discrepancies here reported between AG&I and MG, we identified three different variables to contribute to such differences:



low absolute counts, suboptimal light scatter measurements and the use of single heterogeneously expressed markers for the distinction between two lymphoid populations. Thus, several of the less abundant T- cell subpopulations had low absolute counts for those samples with a >20% difference between AG&I and MG (Mann-Whitney U,  $p < 0.05$ , see **Supplementary Data Table 2**). Besides, EuroFlow recommends well defined intervals for median FSC-A and/or SSC-A values for lymphocytes (median FSC-A of >50,000/<60,000 and median SSC-A of >11,000/<13,000). Here we observed that when these criteria were violated, an increased number of samples with >20% differences between AG&I and MG was found (see **Supplementary Data Tables 2 and 3**). For B- cells, the high number of >20% AG&I vs. MG differences observed for unswitched memory B-cells (and pre-GC B cells) could be related to the fact that these two B-cell populations are discriminated among them based upon a single marker/ parameter with heterogeneous expression levels (i.e. CD27). This was confirmed by the significant lower delta MFI for CD27 between pre-GC and unswitched memory B-cells in the discrepant FC standard data file cases (median MFI values of 999 vs. 2441 arbitrary fluorescence channel values, Mann-Whitney U  $p = 0.043$ ) and vice versa (**Supplementary Data Figure 2**). Overall, these results indicate that AG&I is more reproducible and more accurate than MG in detecting abnormal values for individual cell populations (see below) due to technical issues, including those populations that are mainly discriminated based on a single, heterogeneously expressed marker (e.g. CD27 in unswitched memory B-cells vs pre-germinal center B-cells).

Thus, these data indicate that strict adherence to the EuroFlow SOPs and criteria for instrument setup and calibration is mandatory, including a systematic check of the light scatter characteristics of lymphocytes for individual samples before final data storage, in parallel to careful evaluation of cell populations with low absolute count results.

Taken together, our results indicate that compared to conventional expert-based MG, routine use of the AG&I tool is associated with both a greater reproducibility of data analysis and a more robust interpretation of the numerical alterations detected for those lymphoid cell populations that are relevant in the diagnostic work-up of PID of the lymphoid system. However, for PID diagnosis, FC results should not be interpreted based on alterations involving single cell populations, but rather on the combination of altered patterns that typically affect >1 cell population within a sample.

As indicated above, numerical clinically relevant differences between AG&I and MG were more frequently observed among the patient samples than in HD samples. These results might be due to the fact that abnormal B- and T-cell maturation patterns and/or marker expression profiles are virtually restricted to patient samples and such altered profiles frequently represent a challenge during data analysis, even when MG is performed by an experienced operator. Indeed, clinically relevant differences within the B-cell subpopulations were found in several

PID patients included in this study. For these PID patient-associated differences, it remains difficult to define which gating approach is correct due to the lack of a reference standard and the limited number of patients analyzed. Nevertheless, our results suggest a more accurate gating of B-cell populations using AG&I vs MG, since using the AG&I approach, B-cell alterations were only detected in the KMT2A-deficient patients, which are expected to have a CVID-like phenotype [24], but not in the IRAK4-deficient and MBL-deficient patients for whom no lymphoid deviations are usually expected [2, 9]. Altogether, these findings underline the need for robust reference databases of PIDOT-stained blood samples from well-defined PID patients, in addition to normal HD blood, for unequivocal and accurate classification of cell events in PID suspicious patient blood samples, ideally generated in multi-center settings, as initiated by the EuroFlow PID consortium [4, 6, 13, 14, 25]. Moreover, the availability of reference images of PID patients to the database might also contribute to a better classification of the more challenging cell populations and cases.

Despite all the above, the AG&I approach used here, based on the PIDOT database composed of HD blood samples stained with PIDOT at multiple centers, separately classifies all clusters of events that show phenotypic deviations from normal as groups of events that need to be checked by an expert. For HD samples, only a minor proportion of all events contained in the individual FC data files (<1% events) were classified as “checks”, i.e. events mimicking lymphoid cells that required expert revision following the AG&I classification tool. This observation is in line with previously published data on HD blood samples stained with other EuroFlow antibody combinations, that typically showed <2% checks of the total events [14]. In contrast, some cell populations which are either absent or present at very low frequency in normal blood, such as activated B- and T-cells, might require expert revision, particularly for patient samples, as confirmed here. Optimal use of the AG&I module for PIDOT would imply that in a first step, only unclassified clusters of events should be checked by an expert. Subsequently, all cell populations that carry phenotypic and/or numerical alarm should be revised, as done in this study for 37 samples that showed >20% differences in the absolute cell counts obtained for at least one cell population with the AG&I approach vs MG, that led to a distinct clinical interpretation after comparison with p5–p95 age-matched reference ranges (normal vs altered cell population). In all except three of these 37 samples, extended expert revision of the AG&I gating approach revealed no error. In the three remaining samples aberrant maturation and/or abnormal marker expression profiles were seen which might have induced an arguable classification of specific cell populations by the AG&I tool leading in all three cases to numerical alarms (i.e. absolute counts of the corresponding cell populations falling outside age-matched normal reference ranges). Thus, in a routine clinical laboratory setting, these latter deviations would trigger expert revision of the immunophenotypic results prior to their integration with other laboratory data and clinical findings. Although the underlying reason for these phenotypic deviations could not be fully identified, they might be due, at least in part to technical issues related with the quality of staining with single liquid for-

## Chapter 2.2

---

mat reagents (e.g. CD4 staining in one case, IgD staining in another patient and TCR $\gamma\delta$  staining in third patient). In order to limit the impact of reagent variability and minimize pipetting issues, EuroFlow encourages the use of the lyophilized format of the PIDOT reagents [10].

In summary, here we show that the AG&I tool contributes to the standardization of FC data analysis in the diagnostic work-up of PID suspected patients, mostly due to its improved reproducibility vs conventional expert-based MG approaches and a more robust definition of numerical alterations against age-matched reference ranges. However, expert revision of the results of AG&I of PIDOT data still remains necessary in samples with numerical alterations and aberrant B- and T-cell maturation and/or abnormal marker expression profiles. Importantly, diagnosis of PID requires integration of FC results with other laboratory data (e.g. serum immunoglobulin levels, functional assays, molecular diagnostics, vaccination response), clinical findings and clinical history (e.g. history of infections), according to both the ESID and IUIS criteria [2, 6, 9]. Of note, this study specifically focused on the evaluation of the technical performance of the new AG&I module for analysis of PIDOT data in a rather limited cohort of healthy donor and patient samples. Therefore, the overall impact of the new AG&I approach on the final PID diagnosis still remains to be fully defined in larger patient cohorts that include a wide variety of PID patients, preferably in a multi-center setting.

### **Data availability statement**

The raw data supporting the conclusions of this article will be made available by the authors, without undue reservation.

### **Ethics statement**

The studies involving human participants were reviewed and approved by the local ethics committee of the Ghent University Hospital, Belgium (approval 2016/1137). Written informed consent to participate in this study was provided by the participants' legal guardian/next of kin.

### **Author contributions**

EL, AD, JN, MP-A, EM, MB, MH, AO, JD, JP, and CB contributed to the conception and design of the study. EL, AD, JN, EM, MB, TK, MH, and FH performed data acquisition and data analysis. MP-A provided the reference values. EL, AO, MP, JP, and CB wrote the manuscript. All authors contributed to the article and approved the submitted version.

### **Funding**

The coordination and innovation processes of this study were supported by the EuroFlow Consortium. The EuroFlow Consortium received support from the FP6-2004- LIFESCIHEALTH-5 program of the European Commission (grant LSHB-CT-2006-018708) as Specific Targeted Research Project (STREP). The EuroFlow Consortium is part of the European Scientific Foundation for Hemato-Oncology (ESLHO), a Scientific Working Group (SWG) of the European He-

matology Association (EHA). JN is granted by the Fund for Scientific Research, TBM Funding, Belgium (T000119N). This work was also supported by a grant of the Grand Challenges Program of VIB.

### Acknowledgements

All members of the EuroFlow PID Workpackage (chaired by M. van der Burg) are greatly acknowledged for their contribution, critical insights and helpful discussions. We would like to thank all laboratory technicians for the excellent technical support. We gratefully acknowledge Pauline Breughe (PB) and Jana De Wolf (JDW) for their contribution in the inter-observer variability project of this study.

2.2

### Conflict of Interest

JD, MP-A, and AO each report being one of the inventors on the EuroFlow-owned patent PCT/NL 2015/050762 (Diagnosis of primary immunodeficiencies). The Infinicyt software is based on intellectual property (IP) of the EuroFlow laboratories (University of Salamanca in Spain and Federal University of Rio de Janeiro in Brazil) and the scientific input of other EuroFlow members. All above mentioned intellectual property and related patents are licensed to Cytognos (Salamanca, ES) and BD Biosciences (San Jose, CA), which companies pay royalties to the EuroFlow Consortium. These royalties are exclusively used for continuation of the EuroFlow collaboration and sustainability of the EuroFlow consortium. JD and AO report an Educational Services Agreement from BD Biosciences and a Scientific Advisory Agreement from Cytognos; all related fees and honoraria are for the involved university departments at Leiden University Medical Center and University of Salamanca.

The remaining authors declare that the research was conducted in the absence of any commercial or financial relationships that could be construed as a potential conflict of interest.

### Supplementary Material

The Supplementary Material for this article can be found online at: <https://www.frontiersin.org/articles/10.3389/fimmu.2020.584646/full#supplementary-material>

Or using the following QR code:



### References

1. Rezaei N, Bonilla FA, Seppänen M, De Vries E, Bousfiha AA, Puck J. Introduction on Primary Immunodeficiency Diseases. Berlin: Springer (2017).
2. Bousfiha A, Jeddane L, Picard C, Ailal F. The 2017 IUIS Phenotypic Classification for Primary Immunodeficiencies. *J Clin Immunol* (2018) 38:129–43. doi: 10.1007/s10875-017-0465-8
3. Shields AM. The primary immunodeficiency disorders Key points. *Med (Baltimore)* (2017) 45(10):1–8. doi: 10.1016/j.mpmed.2017.07.011
4. Van Der Burg M, Kalina T, Perez-andres M, Vlkova M. The EuroFlow PID Orientation Tube for Flow Cytometric Diagnostic Screening of Primary Immunodeficiencies of the Lymphoid System. *Front Immunol* (2019) 10:1–11. doi: 10.3389/fimmu.2019.00246
5. Blanco E, Perez-Andres M, Arriba-Mendez S, Serrano C, Criado I, Pino-molina D, et al.

## Chapter 2.2

---

- Defects in memory B-cell and plasma cell subsets expressing different immunoglobulin-subclasses in patients with CVID and immunoglobulin subclass deficiencies. *J Allergy Clin Immunol* (2019) 144 (3):809–24. doi: 10.1016/j.jaci.2019.02.017
6. van Dongen JJM, Van Der Burg M, Kalina T. EuroFlow-Based Flowcytometric Diagnostic Screening and Classification of Primary Immunodeficiencies of the Lymphoid System. *Front Immunol* (2019) 10 (1271):1–21. doi: 10.3389/fimmu.2019.01271
  7. Takashima T, Okamura M, Yeh T, Okano T, Yamashita M, Tanaka K. Multicolor Flow Cytometry for the Diagnosis of Primary Immunodeficiency Diseases. *J Clin Immunol* (2017) 37:486–95. doi: 10.1016/j.alit.2017.06.003
  8. Richardson AM, Moyer AM, Hasadsri L, Abraham RS. Diagnostic Tools for Inborn Errors of Human Immunity (Primary Immunodeficiencies and Immune Dysregulatory Diseases). *Curr Allergy Asthma Rep* (2018) 18 (19):1–17. doi: 10.1007/s11882-018-0770-1
  9. ESID. European Society for Immunodeficiencies: ESID Registry - Working definitions for clinical diagnosis of PID. [cited 2019 Aug 8]. (2019). Available at: <https://esid.org/Working-Parties/Registry-Working-Party/Diagnosis-criteria>.
  10. van der Velden VHJ, Flores-Montero J, Perez-Andres M, Martin-Ayuso M, Crespo O, Blanco E, et al. Optimization and testing of dried antibody tube: The EuroFlow LST and PIDOT tubes as examples. *J Immunol Methods* (2019) 475:112287. doi: 10.1016/j.jim.2017.03.011
  11. Kalina T, Flores-Montero J, Van Der Velden VHJ, Martin-Ayuso M, Böttcher S, Ritgen M, et al. EuroFlow standardization of flow cytometer instrument settings and immunophenotyping protocols. *Leukemia* (2012) 26(9):1986–2010. doi: 10.1038/leu.2012.122
  12. Kalina T, Brdickova N, Glier H, Fernandez P, Bitter M, Flores-Montero J, et al. Frequent issues and lessons learned from EuroFlow QA. *J Immunol Methods* (2019) 475:112520. doi: 10.1016/j.jim.2018.09.008
  13. Pedreira CE, Costa ES, Lecrevisse Q, van Dongen JJM, Orfao A. Overview of clinical flow cytometry data analysis: Recent advances and future challenges. *Trends Biotechnol* (2013) 31(7):415–25. doi: 10.1016/j.tibtech.2013.04.008
  14. Pedreira CE, Sobral E, Lecrevisse Q, Grigore G, Fluxa R, Verde J, et al. From big flow cytometry datasets to smart diagnostic strategies: The EuroFlow approach. *J Immunol Methods* (2019) 475:112631. doi: 10.1016/j.jim.2019.07.003
  15. Diks AM, Bonroy C, Teodosio C, Groenland RJ, De Mooij B, De Maertelaere E. Impact of blood storage and sample handling on quality of high dimensional flow cytometric data in multicenter clinical research. *J Immunol Methods* (2019) 475:112631. doi:10.1016/j.jim.2019.07.003
  16. Flores-Montero J, Sanoja-Flores L, Paiva B, Puig N, Garcia-Sanchez O, Böttcher S, et al. Next Generation Flow for highly sensitive and standardized detection of minimal residual disease in multiple myeloma. *Leukemia* (2017) 31:2094–103. doi: 10.1038/leu.2017.29
  17. Theunissen P, Mejstrikova E, Sedek L, Van Der Sluijs-gelling AJ, Gaipa G, Bartels M, et al. Standardized flow cytometry for highly sensitive MRD measurements in B-cell acute lymphoblastic leukemia. *Blood* (2017) 129 (3):347–57. doi: 10.1182/blood-2016-07-726307
  18. Flores-montero J, Grigore G, Fluxa R, Fernandez P, Almeida J, Muñoz N, et al. EuroFlow Lymphoid Screening Tube (LST) database for automated identification of blood lymphocyte subsets. *J Immunol Methods* (2019) 475:112662. doi: 10.1016/j.jim.2019.112662
  19. Rodriguez F. Method of digital information classification. United States (2018).
  20. DIN EN ISO 15189. Medical laboratories - Particular requirements for quality and competence (ISO 15189:2007). (2007).
  21. Modell V, Quinn J, Orange J, Notarangelo L, Modell F. Primary immunodeficiencies worldwide: an updated overview from the Jeffrey Modell Centers Global Network. *Immunol Res* (2016) 64:736–53. doi: 10.1007/s12026-016-8784-z
  22. Verschoor CP, Lelic A, Bramson JL, Bowdish DME, Maecker H. An introduction to automated flow cytometry gating tools and their implementation. *Front Immunol* (2015) 6(380):1–9. doi: 10.3389/fimmu.2015.00380
  23. Mair F, Hartmann FJ, Mrdjen D, Tosevski V. The end of gating? An introduction to automated analysis of high dimensional cytometry data. (2016) 46:34–43. doi: 10.1002/eji.201545774
  24. Bogaert DJ, Dullaers M, Kuehn HS, Leroy BP, Julie E. Early-onset primary antibody deficiency resembling common variable immunodeficiency challenges the diagnosis of Wiedeman-Steiner and Roifman syndromes. *Sci Rep* (2017) 7(January):1–12. doi: 10.1038/s41598-017-02434-4
  25. Costa ES, Pedreira CE, Barrena S, Lecrevisse Q, Flores J, Quijano S, et al. Automated pat-



tern-guided principal component analysis vs expert-based immunophenotypic classification of B-cell chronic lymphoproliferative disorders: a step forward in the standardization of clinical immunophenotyping. *Leukemia* (2010) 24:1927–33. doi: 10.1038/leu.2010.160





## Chapter 3.1

### **Highly sensitive flow cytometry allows monitoring of changes in circulating immune cells in blood after Tdap booster vaccination**

Annieck M. Diks<sup>1</sup>, Indu Khatri<sup>1,2†</sup>, Liesbeth E.M. Oosten<sup>1†</sup>, Bas de Mooij<sup>1</sup>, Rick J. Groenland<sup>1</sup>, Cristina Teodosio<sup>1</sup>, Martin Perez-Andres<sup>3</sup>, Alberto Orfao<sup>3</sup>, Guy A.M. Berbers<sup>4</sup>, Jaap Jan Zwaginga<sup>5</sup>, Jacques J.M. van Dongen<sup>1</sup> (corresponding), Magdalena A. Berkowska<sup>1</sup>

<sup>1</sup> Department of Immunology, Leiden University Medical Center, Albinusdreef 2, 2333 ZA, Leiden, the Netherlands

<sup>2</sup> Leiden Computational Biology Center, Leiden University Medical Center, 2333 ZC Leiden, The Netherlands

<sup>3</sup> Cancer Research Centre (IBMCC, USAL-CSIC; CIBERONC CB16/12/00400), Institute for Biomedical Research of Salamanca (IBSAL) and Department of Medicine and Cytometry Service (NUCLEUS Research Support Platform), University of Salamanca (USAL), Salamanca, Spain

<sup>4</sup> Center for Infectious Disease Control, National Institute of Public Health and the Environment, Antonie van Leeuwenhoeklaan 9, 3721 MA Bilthoven, The Netherlands

<sup>5</sup> Department of Hematology, Leiden University Medical Center, Albinusdreef 2, 2333 ZA, Leiden, the Netherlands

† These authors have contributed equally to this work

**Frontiers in Immunology, June 2021**

**<https://doi.org/10.3389/fimmu.2021.666953>**

### **Abstract**

Antigen-specific serum immunoglobulin (Ag-specific Ig) levels are broadly used as correlates of protection. However, in several disease and vaccination models these fail to predict immunity. In these models, in-depth knowledge of cellular processes associated with protective versus poor responses may bring added value. We applied high-throughput multicolor flow cytometry to track over-time changes in circulating immune cells in 10 individuals following pertussis booster vaccination (Tdap, Boostrix®, GlaxoSmithKline). Next, we applied correlation network analysis to extensively investigate how changes in individual cell populations correlate with each other and with Ag-specific Ig levels. We further determined the most informative cell subsets and analysis time points for future studies. Expansion and maturation of total IgG1 plasma cells, which peaked at day 7 post-vaccination, was the most prominent cellular change. Although these cells preceded the increase in Ag-specific serum Ig levels, they did not correlate with the increase of Ig levels. In contrast, strong correlation was observed between Ag-specific IgGs and maximum expansion of total IgG1 and IgA1 memory B cells at days 7 to 28. Changes in circulating T cells were limited, implying the need for a more sensitive approach. Early changes in innate immune cells, i.e. expansion of neutrophils, and expansion and maturation of monocytes up to day 5, most likely reflected their responses to local damage and adjuvant. Here we show that simultaneous monitoring of multiple circulating immune subsets in blood by flow cytometry is feasible. B cells seem to be the best candidates for vaccine monitoring.

**Keywords:** pertussis vaccine, flow cytometry, immune monitoring, plasma cells, correlation networks

## Introduction

Determination of antigen-specific immunoglobulin (Ag-specific Ig) levels in serum is routinely used as readout for vaccine efficacy and/or protective immunity [1-3]. Besides Ag-specific Igs, immunological memory is preserved in the form of circulating memory B and T cells, which are more difficult to measure. These cells are preserved even when Ag-specific Ig levels have waned. Therefore, the cellular compartment may harbor potential for more accurate correlates of protection and provide insights into the mechanism of protection. Whereas serology provides insight in Ag-specific Ig levels and function, analysis of circulating immune cells may result in a deeper understanding of the processes induced by the vaccine and the cellular changes preceding Ig production. These additional insights can support the evaluation of novel vaccination strategies, such as addition of new adjuvants, antigens or changing the route of administration.

Cellular processes and their kinetics can be evaluated with different methods, such as ELISpot, cytokine production, tetramer staining or cell proliferation assays [4]. These techniques have resulted in identification of several cellular correlates of protection. For example, Sridhar et al. reported that for flu a higher frequency of (pre-existing) cross-reactive IFN $\gamma$ +IL-2- CD8 T cells was associated with decreased disease symptoms, and CD45RA+CCR7- late effector T cells within the above-mentioned cross-reactive T cells were a cellular correlate of protection [5]. Furthermore, Wilkinson et al. showed increased numbers of influenza-specific CD4 T cells before the detectable increase in antibody levels [6]. Despite their (generally) high sensitivity, such approaches may be laborious and require additional steps like pre-existing knowledge of HLA-type, prolonged incubation with or without culturing and stimulation, or isolation of cell subsets. Moreover, they mostly focus on a small part of the immune system and are therefore less suitable as an exploratory tool. Many of these limitations can be overcome with the use of flow cytometry or mass cytometry.

However, conventional flow and mass cytometry do have some limitations with regards to the monitoring of cellular processes and their kinetics in the blood. First, cells of interest can be present in low numbers in the peripheral blood (PB) (such as plasma cells, <5 cells/ $\mu$ L [7]), which may hamper their detection. This can be overcome by increasing sample volume, as applied in minimal residual disease monitoring [8]. With the introduction of the new generation of high-speed flow cytometers, measuring increased cell numbers is becoming less of a hurdle. Second, cellular changes in PB may not directly reflect cellular changes in specific tissues. However, the blood stream is thought to be a 'crossroad' for cell trafficking. Leukocytes continuously circulate via blood through the body in search of damage or infection [9-11]. This implies that when analyzed at the right time points, PB can contain valuable information about processes ongoing in the body [11-14]. Flow cytometry can be an important tool in exploratory research, because it allows in-depth phenotyping and monitoring of millions of cells, while retaining information about absolute cell numbers. Finally, Ag-specific approaches are valuable tools, but not all antigens are commercially available, and associated

costs can be high. Thus, it can be of interest to know which general changes can be observed post-vaccination.

A deeper understanding of cellular processes associated with vaccination may be of great value for pertussis research. The current acellular pertussis vaccine (aP) is a combined multivalent vaccine used to protect against tetanus, diphtheria and pertussis (Tdap) and, in some cases, additional diseases such as polio, Hib and hepatitis [15]. It is mandatory or highly recommended in many countries, including the Netherlands [16,17]. Despite good vaccine coverage, the incidence of pertussis cases has increased over the past decennia [18]. Therefore, an improved vaccination strategy or vaccine formulation based on in-depth understanding of cellular processes is of a great interest.

In this study, we used a pertussis booster vaccine (Tdap, Boostrix®, GlaxoSmith-Kline) as a model to extensively monitor cellular kinetics in the immune system of 10 healthy adults. Using high-dimensional flow cytometry, we investigated longitudinal changes in PB immune cell subsets before and after detectable increase in Ag-specific serum Igs. Moreover, we tested for correlations between total population kinetics and Ag-specific serum Ig levels. The exploratory nature of this study generated a vast amount of complex data, which is challenging to interpret without automated strategies. Therefore, we developed a top-down approach which starts with correlation network analysis to identify shared patterns between and within different immune cell populations. As the use of correlation network analysis yielded many correlations, we next evaluated the fluctuations of individual populations. Using this two-step approach, we assessed the complete dataset and identified most informative cell populations and time points post-Tdap booster vaccination. These can be further employed in larger scale studies, in order to e.g. evaluate candidate correlates of protection.

### **Materials and methods**

#### **Study design and sample collection**

This study was approved by the Medical Ethics Committee of Leiden University Medical Center (LUMC) (registration number: P16-214 EUDRACT: 2016-002011-18) and performed in competent adults after signing an informed consent form. Only volunteers who were (1) healthy, as evaluated by a questionnaire, (2) had blood hemoglobin levels and leukocyte differential counts within normal range, (3) had no suspected exposure to Bp in the past, (4) had a completed vaccination scheme according to Dutch National Immunization Program ([www.rivm.nl/en/national-immunisation-programme](http://www.rivm.nl/en/national-immunisation-programme)) were eligible. Exclusion criteria are listed in **Supplementary Table 1**. Between June and December 2017, 10 individuals were included (m/f ratio: 1/9; age range: 25-55y, mean age: 37y), and completed the study. After initial blood collection (day 0), volunteers were vaccinated intramuscularly with the Boostrix® vaccine (GlaxoSmithKline). This reduced-antigen, combined Tdap booster vaccine contains diphtheria toxoid (Diph) (2.5Lf (limit of flocculation)), tetanus toxoid (Tet) (5Lf), three Bp proteins -i.e. pertussis toxoid (PT) (8µg), filamentous hemagglutinin (FHA) (8µg), pertactin

(Prn) (2.5µg) and aluminum hydroxide as adjuvant 19. PB samples were collected in K2EDTA blood collection tubes (BD Vacutainer, BD Biosciences, San Jose, CA, USA) and serum collection tubes (BD Vacutainer, BD Biosciences) at baseline (day 0) and subsequently at nine pre-defined time points i.e. day 3, 5, 7, 10, 14, 21 (20-21), 28 (28-31), 90 (90-95) and 1 year (day 363-371) post-vaccination. One donor was not eligible at the last time point.

### **Evaluation of total and Ag-specific serum Ig levels**

Serological analyses were performed in all collected samples. Levels of the three major Ig classes (IgM, IgA and IgG) were determined by turbidimetry, and IgG subclass (IgG1, IgG2, IgG3 and IgG4) levels were determined by nephelometry at the certified Clinical Chemistry laboratory at LUMC. Levels of IgG directed against Tet, Diph, PT, FHA, Prn and Fimbriae 2/3 (Fim2/3), and levels of IgA directed against PT, FHA, Prn and Fim2/3 were determined by multiplex immune assay (MIA) at the Dutch National Institute for Public Health and the Environment (RIVM, The Netherlands) [20].

### **Longitudinal flow cytometric analysis of up to 250 circulating immune cells subsets in blood**

All blood samples were subjected to high-throughput flow cytometric immunophenotyping with a panel of four recently developed multicolor immune monitoring antibody combinations (or their prototypes). In brief, the dendritic cell-monocyte panel (DC-monocyte) allows analysis of up to 19 different (sub) populations within the myeloid compartment, including several subsets of monocytes and dendritic cells [21] (van der Pan et al., manuscript in preparation). The CD4 T-cell tube (CD4T) allows identification of at least 89 (up to 161) populations within the CD4 T-cell compartment with different functionalities and maturation stages, and longitudinal use of this tube may provide insight in the activation/maturation of T-cell subsets [21,22]. The CD8 cytotoxic T-cell tube (CYTOX) allows identification of up to 50 (sub)populations within the CD8 T-cell and the natural killer (NK) cell compartments [21]. Lastly, the B-cell and plasma cell tube (BIGH) allows identification of up to 115 populations of B and plasma cells distinguished based on their maturation stage-associated phenotypic profile and the expressed Ig subclasses [7,21].

Depending on the antibody combination, samples were either processed according to the bulk lysis protocol, for staining of  $10 \times 10^6$  cells (DC-Monocyte and BIGH) or prepared using the EuroFlow stain-lyse-wash protocol (CD4T, CYTOX; both protocols available on [www.EuroFlow.org](http://www.EuroFlow.org)). For BIGH and CYTOX tubes, surface staining was followed by intracellular staining with the Fix & Perm reagent kit (Nordic MUBio, Susteren, The Netherlands) according to manufacturer's protocol. In brief, 100µl of washed sample was fixed with 100µl of Solution A (15min in the dark at RT), washed, and permeabilized by adding 100µl of Solution B (15min in the dark at RT) and antibodies against intracellular markers. Next, samples were washed and re-suspended in PBS for immediate acquisition (or stored for max ~3h at 4°C). Additionally, BD TruCount tubes (BD Biosci-



ences) were used according to manufacturer's protocol for precise enumeration of cell subsets. By adding HLA-DR Pacific Blue, CD3 FITC, CD45 PerCP-Cy5.5, CD16 PE, CD56 PE, CD19 PE-Cy7, CD300e (IREM2) APC and CD14 APC-H7, we could determine absolute cell count of total leukocytes, eosinophils, neutrophils, monocytes (including classical, intermediate and non-classical monocytes (cMo, iMo and ncMo, respectively [23])), dendritic cells, basophils, total lymphocytes, B cells, natural killer (NK) cells and T cells. For each immune monitoring panel, a representative population was selected (e.g. total B-cell count as reference point in the BIGH panel) and used to determine absolute cell counts of all other populations in that panel. Immune monitoring tubes were measured on a BD FACS LSRFortessa 4L or BD FACS LSR Fortessa x20 4L flow cytometer (BD Biosciences, San Jose, CA, USA), while TruCount samples were measured on a BD FACS Canto™ II 3L (BD Biosciences) instrument. Flow cytometers were calibrated daily according to EuroFlow guidelines, as previously described [24,25]. All data were analyzed manually with Infinicyt software (Infinicyt™ Software v2.0, Cytognos) according to the gating strategies proposed for these panels as proposed by EuroFlow [7,22] [van der Pan et al., manuscript in preparation].

### **Correlation network analysis**

A sliding window of 3 time points was used to evaluate correlating changes between and within all immune subsets and Ag-specific Ig levels. To identify patterns shared by different individuals, the ratio over baseline was used as input. Pearson correlations were calculated using Hmisc library in R. The correlations were filtered based on their presence in at least 8/10 donors and the edges >90% positive and negative mean correlations were considered for visualization. To approach the data in a completely unbiased manner, we did not incorporate any adjustments or corrections for expected or implied correlations (e.g. when population A-B and B-C correlate strongly, a correlation between A-C is implied). For initial interpretation, the correlations were visualized in the open source software Cytoscape (version 3.7.1; Cytoscape Consortium [26]) (**Fig. 1A**). To select the most informative time points, each timeframe was inspected individually (**Fig. 1B**). The most relevant networks were selected and dynamic networks were generated using the open source Gephi software (version 0.9.2; Gephi.org [27]) and are attached to this manuscript as supplementary videos.

### **Statistical analysis of independent comparisons**

Correlations of baseline levels of B cells, naive B cells, memory B cells (total, IgG1 and IgA1), plasma cells (total, IgG1, IgG4 and IgA1), total T cells, CD4 T cells, CD8 T cells, T follicular helper cells (TFHs), TCR $\gamma\delta$  T cells, regulatory T cells (Tregs), naive CD4 T cells, NK cells, total leukocytes, neutrophils, monocytes, myeloid and plasmacytoid DCs (mDCs and pDCs) with the level (IU/mL) of vaccine-specific serum IgG at days 14, 21, 28, 90 and 365 were calculated using Spearman's rank correlation.

For other statistical analyses (indicated in figure legends) the GraphPad Prism 8.1.1 software (GraphPad, San Diego, CA, USA), was used. Correlation coefficients

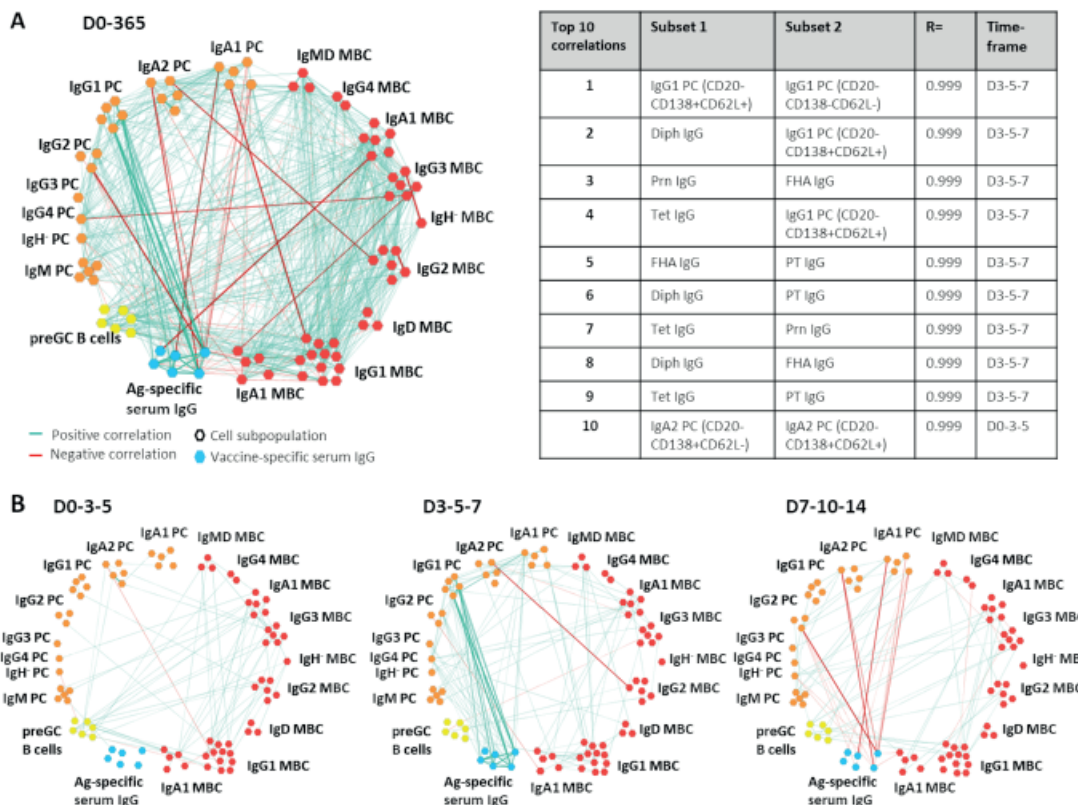


**Figure 1. Example of Cytoscape network analysis between B-cell subsets and/or antigen-specific serum IgGs.** In this example, correlations between and within the B-cell compartment and Ag-specific serum IgGs are shown. All positive and negative correlations with an  $R > 0.90$  or  $R < -0.90$  over 3 sequential time points and present in at least 8/10 donors were visualized. Only subsets that had at least 1 correlation were shown in the network. For ease of interpretation, subset names have been removed and group names have been added. Of note, the most informative correlation networks found in this study were visualized in the Gephi software and are added as supplementary movies to this manuscript. MBC= Memory B cells (red), PC= plasma cells (orange), preGC B cells= pre-germinal center B cells (yellow), Ag-specific serum IgG= antigen-specific serum IgG (blue). D= Days after vaccination. A. All correlations found within and between the B-cell compartment and Ag-specific serum IgGs at all time points. The table presents an overview of the 10 strongest correlations of the visualized network. B. The most relevant correlations visualized per timeframe.

(Spearman  $r$ )  $> 0.8$  were classified as strong correlations, and  $r$ -values  $< 0.8$  were classified as weak correlation. When multiple correlations were tested between two variables, but at several timepoints (e.g. maximum plasma cell expansion (day 7) and the level of vaccine-specific IgG (“Boostrix-IgG”) at days 14, 21 and 28), correction for multiple testing was done using the false discovery rate (FDR) approach method of Benjamini and Hochberg with an FDR of 5%.

## Results

### All donors reached protective serum Ig levels 14 days post-vaccination

Seven out of ten donors reported a painful/sore arm after receiving the vaccine. One serious adverse event, unrelated to this study, was reported.

## Chapter 3.1

Increase in Ag-specific serum Ig levels is the primary read-out of vaccine efficacy. To follow changes in serum Ig levels post-Boostrix® vaccination and determine whether and when study participants reached protective levels, major Ig classes and IgG subclasses were measured at baseline and at all consecutive time points. In most donors, the levels of major Ig classes at baseline were within the normal reference ranges and followed subtle changes upon Boostrix® vaccination (donor ranges: IgG 7.95-14.20 g/L, IgA 1.31-5.04 g/L, IgM 0.85-1.60 g/L, IgG1 4.35-8.87 g/L, IgG2 1.95-5.40 g/L, IgG3 0.30-0.53 g/L, IgG4 0.15-3.15 g/L) (Suppl. Fig.1) [28,29].

Ag-specific responses were analyzed separately for serum IgGs and IgAs (Fig. 2A+B). Baseline serum IgGs directed against Diph (median: 0.12 IU/mL, range: 0.007-0.65 IU/mL) were above protective levels (0.01-0.1 IU/mL [30-32]) in 5/10 donors, while baseline serum IgGs directed against Tet (median: 2.07 IU/mL, range: 0.29-9.30 IU/mL) were above protective levels (0.1 IU/mL [33]) in all donors. Baseline anti-PT serum IgGs (median: 11 IU/mL, range: 1-121 IU/mL) were at arbitrary protective levels of >20 IU/mL [34-36] in 3/10 donors. Baseline anti-FHA, anti-Prn and anti-Fim2/3 IgG levels were highly variable between donors (median anti-FHA: 33.5 IU/mL, range: 8-188 IU/mL, median anti-Prn: 20.5 IU/mL, range: 2-161 IU/mL, and lastly, median anti Fim2/3: 30 IU/mL, range: 1-83 IU/mL).

Baseline anti-PT and anti-Prn IgA levels (median anti-PT IgA: 0.56 IU/mL, range: 0.25-14.3 IU/mL, median anti-Prn IgA: 2.7 IU/mL, range: 0.67-12.7 IU/mL)

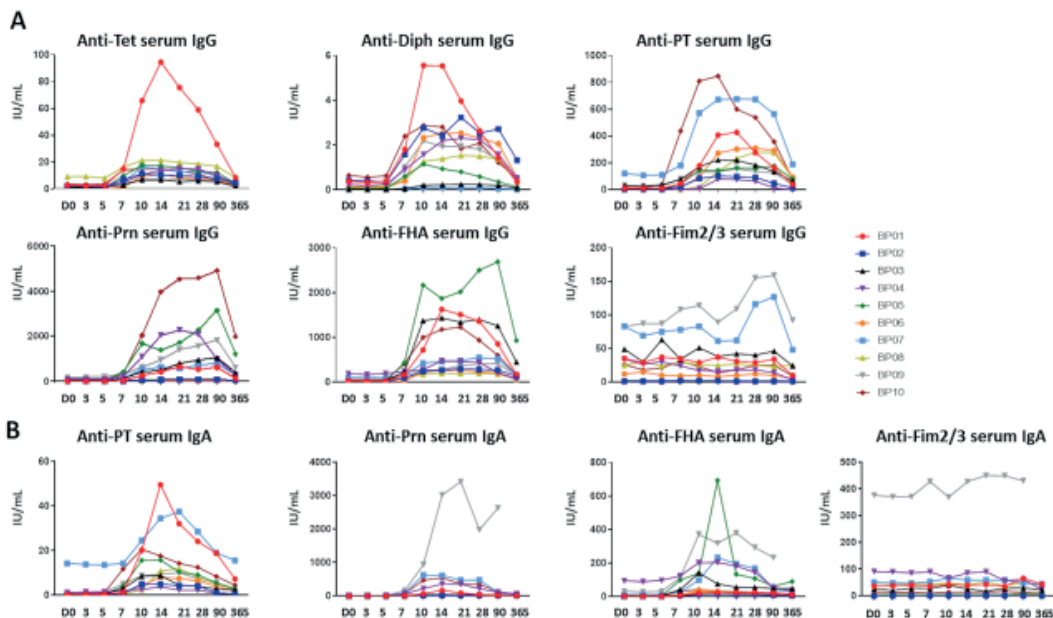


**Figure 2. Ag-specific serum Ig levels prior to and post-aP booster vaccination.** A. Ag-specific serum IgG levels (IU/mL) directed against the 5 vaccine components (Diphtheria toxoid (Diph), tetanus toxoid (Tet), PT, FHA, and Prn). Fim2/3 was not present in the vaccine and considered a negative control in A and B. B. Ag-specific serum IgA levels (IU/mL) directed against the Bp vaccine components (PT, FHA, Prn). For Diph and Tet no quantitative read-out was available. D= Days after vaccination.

were similar in most donors, whereas baseline anti-FHA and anti-Fim2/3 IgAs were detected at variable levels (median anti-FHA IgA: 4.0 IU/mL, range: 0.25-94.4 IU/mL, median anti-Fim2/3 IgA: 31.7 IU/mL, range 0.37-377.0 IU/mL). Elevated baseline levels of anti-PT IgG (121 IU/mL) and anti-PT IgA (14.3 IU/mL) in donor BP07 were either remaining high from previous vaccination or potential (subclinical) infection [37]. In donor BP09, elevated anti-Prn and anti-Fim2/3, but no anti-PT IgAs were observed at baseline, indicative of previous contact with another microorganism, for example another *Bordetella* species [36].

In all donors, Ag-specific serum Ig levels started to rise from ~day 7 post-vaccination. Among Bp antigens the IgG level range at the peak was 79-847 IU/mL for anti-PT, 261-2688 IU/mL for anti-FHA and 39-4928 IU/mL for anti-Prn. For IgA the level range at the peak was 4-50 IU/mL for anti-PT, 14-693 IU/mL for anti-FHA and 6-3421 IU/mL for anti-Prn. As expected, for both Ig isotypes serum levels of anti-Fim2/3 Igs showed limited variation over time (max. ratio of 3x over baseline), since Fim2/3 was not a component of this vaccine. Although both Ig responses showed some heterogeneity in-between donors with regards to magnitude and number of targeted antigens, all donors reached arbitrary protective anti-PT IgG levels at day 14 post-vaccination the latest (>20 IU/mL). For diphtheria, all donors reached 0.01 IU/mL IgG levels (basic protection) the latest at day 7, and 0.1 IU/mL IgG levels (full protection) at day 10 [30-32]. Waning was observed after 1 year for all vaccine-specific Ig responses. Nevertheless, 8/10 donors maintained protective anti-PT (>20 IU/mL) IgG and anti-Diph IgG (>0.1 IU/ml) serum levels at 1 year post-vaccination. All donors maintained protective anti-Tet IgG levels (>0.1 IU/ml) [33].

### **Early expansion of plasma cells preceded the increase in vaccine-specific serum Ig levels**

All donors responded to vaccination by reaching protective IgG levels. To determine whether vaccination also triggered cellular changes which could be traced in circulation, we monitored the kinetics of over 250 immune cell populations in blood. Thereafter, we used correlation networks to investigate which cellular changes were associated with the change in Ag-specific Ig levels. Since not all identified correlations were biologically relevant (e.g. between two populations constant over time), we critically assessed these networks and used observed correlations as a guide to interpret the data.

Igs are the secretory product of terminally differentiated B cells (plasma cells). Therefore, we first focused on B-cell and plasma cell subsets and compared their kinetics with Ag-specific Igs within any 3-visit timeframes (**Dynamic network video: B-serology**). Plasma cells and Ag-specific serum Igs at multiple timeframes followed similar kinetics, as reflected by positive correlations between them. These correlations were the strongest between IgG1 and IgA1 plasma cells, and vaccine-specific Igs at day 3-5-7 (**Dynamic network video: B-serology**) due to the simultaneous rise of both Ig and plasma cell levels (**Fig. 2, Fig. 3A**).



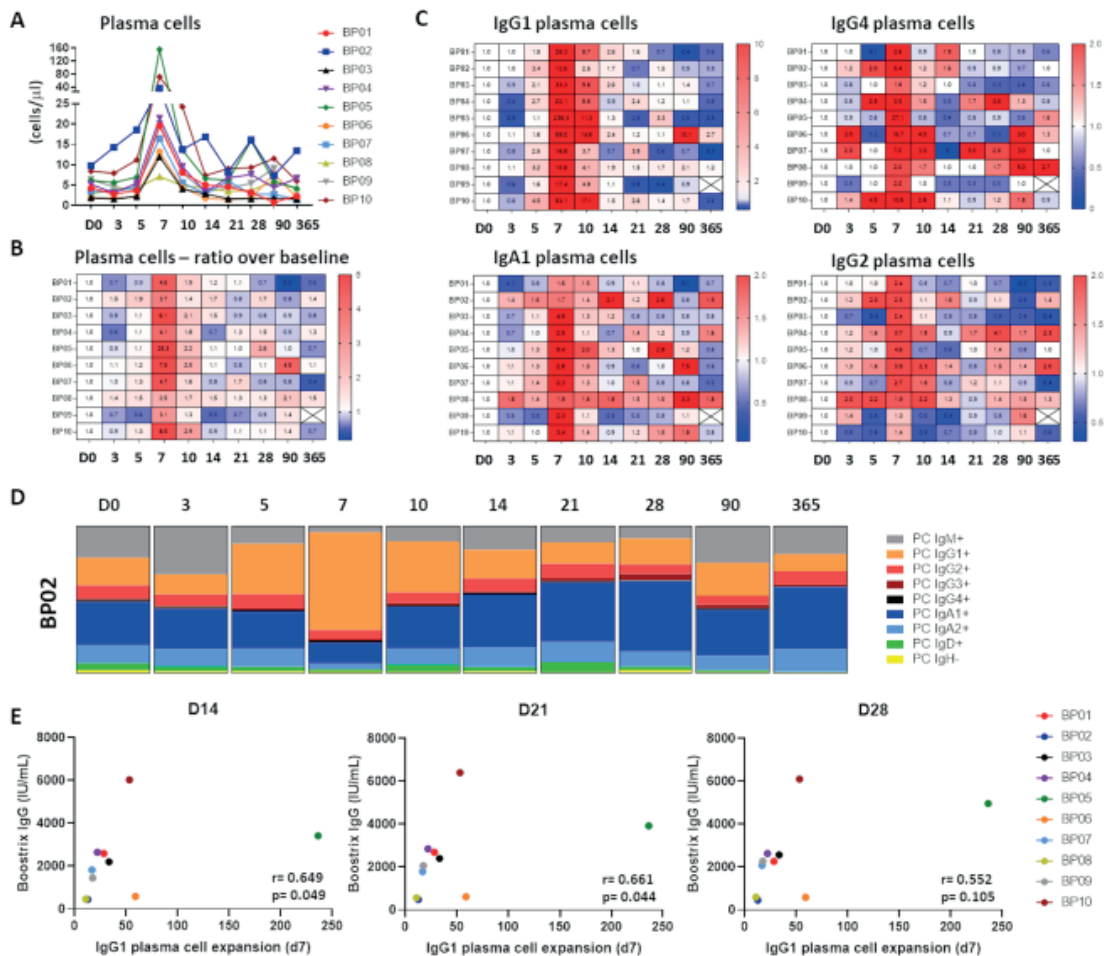


**Figure 3. Kinetics in the plasma cell compartment upon immunization with aP booster.** A. Maximum expansion of plasma cells at day 7 (up to 156 cells/ $\mu$ l). Expansion started at day 5, peaked at day 7 and returned to baseline afterwards. B. Heatmap representing the expansion of plasma cells in ratio over baseline. C. Heatmaps representing the expansion of different plasma cell subsets. Only the most prominent expansions were visualized: IgG1 plasma cells (11-236x), IgG4 plasma cells (2-27x), IgA1 plasma cells (1.6-10.4x) and IgG2 plasma cells (1.3-4.6x). D. Fluctuations in the distribution of the plasma cell compartment over time. One representative donor is shown. Majority of the expanded plasma cells was of IgG1 phenotype (min-max in donors: 44% -76%). E. Correlation between maximum plasma cell expansion (day 7) and the level of vaccine-specific IgG (“Boostrix-IgG”) at days 14, 21 and 28 as determined by Spearman’s rank correlation. An FDR-corrected p-value of  $<0.0075$  was considered significant. D= Days after vaccination.

Interestingly, the more mature IgG1 plasma cells (CD20-CD138-) and IgA1 plasma cells (CD20-138- and CD20-138+) showed stronger correlations with serum IgGs (anti-Tet, anti-Diph) and serum IgAs (anti-PT, anti-Prn and anti-FHA) (**Dynamic network video: B-Serology**) than their less mature counterparts. Furthermore, strong positive correlations were found between IgG4 plasma cells and Ag-specific serum IgGs (anti-Tet, anti-Diph, anti-Prn and anti-FHA) and IgAs (anti-FHA and anti-PT). At day 7-10-14, a negative correlation was observed between decreasing plasma cell numbers and increasing serum Ig levels (**Dynamic network video: B-Serology**). No correlations between plasma cells and Ag-specific Igs were observed at later time points i.e. day 21-365. Thus, correlations between kinetics of IgG1, IgA1 and IgG4 plasma cells and vaccine-specific se-

rum Igs were not restricted to one particular vaccine antigen, but mainly limited to early timeframes post-vaccination.

Based on the change in the direction of correlation, we hypothesized that changes in plasma cell numbers precede changes in Ag-specific serum Igs. To test this hypothesis, we shifted the timeframes in Ag-specific Ig kinetics by 1, 2 or 3 time points later and earlier as compared to the plasma cells (**Suppl. Fig. 2**). By shifting one timeframe later for serum Ig levels, strong positive correlations were found between IgG1 plasma cells (day 0-3-5) and vaccine-specific serum Ig levels (day 3-5-7), and between IgA1, IgG1 and IgG4 plasma cells (day 3-5-7) and vaccine-specific serum Ig levels (day 5-7-10), respectively (**Dynamic network video: B-Serology+1**). The number of edges and the correlation strength were similar as found when correlating within the same timeframes (**B-serology +1 versus B-serology network**). Shifting the timeframe later by 2 visits resulted in fewer correlations. A strong positive correlation was observed between IgG1 plasma cells (day 0-3-5) and serum IgAs (anti-Prn and anti-PT; day 5-7-10), and between IgG4 plasma cells (day 7-10-14) and serum IgAs (anti-FHA; day 14-21-28), respectively (**Dynamic network video: B-Serology +2**). Other timeframe comparisons i.e. 3 later and 1, 2 and 3 earlier timeframes did not reveal any relevant correlations. Thus, increasing plasma cell levels preceded for most of antigens the increase in serum Ig levels by 1-2 time points.

### **Strong increase in IgG1 plasma cell levels did not explain quantitative changes in Ag-specific Ig levels**

Strong correlations between plasma cell levels and Ag-specific Igs implied dynamic changes in the plasma cell compartment. Indeed, plasma cells showed a clear expansion from day 5 to day 14 post-vaccination, with a sharp peak at day 7 (ratio over baseline: 2.5-25x) (**Fig. 3A+B**). This was predominantly due to expansion of IgG1 plasma cells (ratio over baseline: 11-236x), followed by IgG4 plasma cells (ratio over baseline: 2-27x), IgA1 plasma cells (ratio over baseline: 1.6-9.4x), and IgG2 plasma cells (ratio over baseline: 1.3-4.6x) (**Fig. 3C**). Expansion in other plasma cell subclasses was limited and restricted to individual donors (**Suppl. Fig. 3**). Irrespective of the magnitude of changes, the distribution of plasma cells at day 7 was strongly skewed towards IgG1, which constituted 44%-76% of all plasma cells at the peak of expansion (**Fig. 3D**).

Increase in plasma cell numbers in blood preceded and strongly correlated with an increase in Ag-specific serum Ig levels. Still, it remains unclear to what extent these circulating plasma cells are responsible for the entire vaccine-specific Ig production. To address this issue, we correlated the maximum IgG1 plasma cell expansion (day 7) with the vaccine-specific IgG levels measured at later time points (**Fig. 3E**). Although donors with higher changes (ratio) in IgG1 plasma cells showed somewhat greater vaccine-specific IgG levels, no significant (strong) correlation was observed. Similarly, no statistical significance was reached between IgA1 or IgG4 plasma cell expansion (day 7) and vaccine-specific IgG levels (data not shown), or between any of the plasma cell subsets and vaccine-specific



IgA levels.

### **Circulating plasma cells matured in time upon immunization**

Although plasma cell expansion preceded the increase in Ag-specific serum Ig levels, the magnitude of this expansion failed to explain quantitative changes in vaccine-specific serum Igs. This suggested that expanding plasma cells may be newly generated cells on their way to bone marrow or tissues (e.g. mucosal tissues). Newly generated plasma cells have high expression of CD20 and lack CD138. During maturation, CD20 is downregulated, which is followed by upregulation of CD138 at later stages [38] (**Fig. 4A**). To investigate which other markers change their expression during plasma cell maturation, we drew a maturation pathway with the Infinicyt™ software maturation tool [21]. Downregulation of CD20 was accompanied by milder downregulation of CD19 and CD62L, while upregulation of CD138 was preceded by increase in expression of CD38 and CD27 (**Fig. 4B**). We used this information about the expression of all six markers to draw a new maturation pathway for IgG1 plasma cells and distinguished 6 consecutive maturation stages (S1-S6). Finally, the distribution of IgG1 plasma cells over the maturation stages was analyzed for samples collected at all 10 time points. At baseline and at day 3 IgG1 plasma cells were low in number, and relatively evenly distributed over all maturation stages (**Fig. 4C**). From day 5 onwards, plasma cells expanded in numbers and more frequently belonged to more mature stages (S3-S6). At day 7, the peak of plasma cell expansion, the majority of IgG1 plasma cells reached the most mature phenotypes (~70% in S5+S6). In principle, the higher expansion of plasma cells, the more cells belonged to the most mature stages (**Suppl. Fig. 4**). After day 7, plasma cell numbers and their distribution over maturation stages were gradually returning to baseline, which for individual donors was reached between days 14-28. The same phenomenon was observed in multiple other plasma cell subsets despite their overall lower expansion (IgG2, IgG3, IgG4, IgA1) (data not shown). Therefore, expanding plasma cells seem to be newly generated cells on their way to bone marrow, and this maturation observed in the periphery may be a hallmark of recent antigen encountering, such as vaccination. We further investigated this by correlating the absolute increase (cell count day 7 – baseline cell count) in IgG1 and IgA1 plasma cells (using the classical 3 maturation stages based on CD20 and CD138 expression) with the levels of Ag-specific Igs from day 7 onwards. In general, no strong correlations were found, with exception of the correlation between the absolute increase in CD20-CD138- IgA1 plasma cells and the vaccine-specific IgG levels at day 7 (**Suppl. Fig. 5**).

### **Longitudinal changes in serum Ig levels did not correlate with longitudinal changes in the memory B-cell compartment**

Despite clear expansion and maturation of circulating plasma cells, these failed to quantitatively explain expansion in Ag-specific Ig levels (**Fig. 3E**), suggesting that most of the Ag-specific Igs are derived from memory responses (represented by long-lived plasma cells in bone marrow and memory B cells in periphery). Overall, fluctuations of memory B-cell numbers were limited over the time of analysis (ratio over baseline: 0.36-1.75x), as were fluctuations of total B cells and

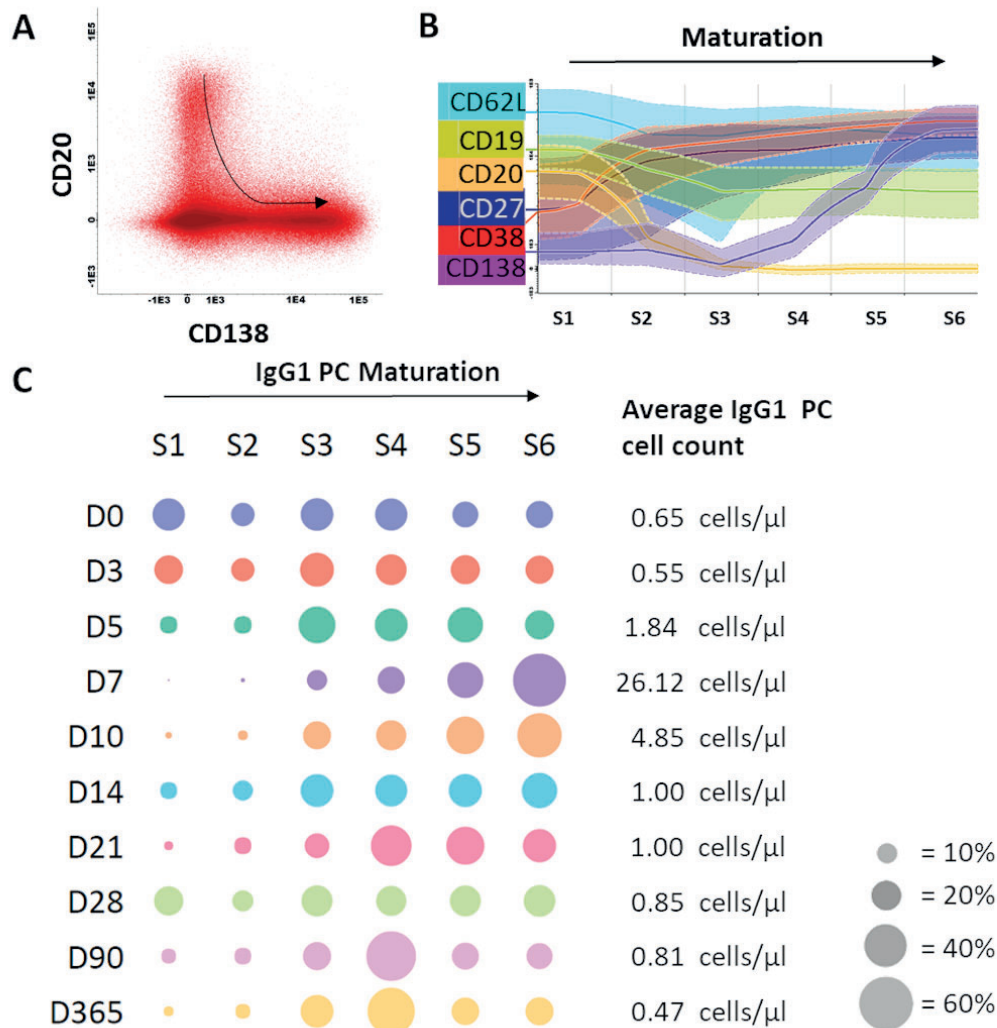


**Figure 4. Maturation of IgG1 plasma cells was observed upon immunization with aP booster.** A. Flow cytometry files containing the plasma cells of all donors at all time points were merged in the Infinicyt software to visualize plasma cell maturation. The plasma cell maturation, defined by downregulation of CD20 and upregulation of CD138, is shown in the dot plot. The arrow indicates the direction of the maturation pathway. B. Based on this CD20-CD138 maturation pathway, the Infinicyt software maturation tool identified 4 additional markers in the flow cytometry panel that were up- or downregulated upon plasma cell maturation. Based on the 6 identified markers (CD19, CD20, CD27, CD62L, CD38, CD138), 6 maturation stages were defined. C. Per time point the percentage of plasma cells in each maturation stage was plotted (total IgG1 plasma cells of all donors, grouped per time point). The size of the dot indicates the percentage of plasma cells in a given maturation stage (average of 10 donors). Cell count is shown at the right side of the plot (average of 10 donors). The bubble plot was generated using plotly python graphing library. D= Days after vaccination.

naive B cells (**Suppl. Fig. 6**). In contrast to the plasma cell compartment, no skewing towards a particular memory B-cell subset was observed (data not shown). Kinetics of IgG1 and IgA1 memory B-cell subsets strongly correlated with each other and, to a lesser extent, with IgG3 memory B-cell subsets. In contrast to plasma cells, correlations between Ag-specific Ig levels and memory B cells were absent both within and in-between timeframes (**Dynamic network videos: B-Serology, B-Serology +1, B-Serology +2**). Lastly, no correlation of base-

line values of major B-cell populations and the vaccine-specific IgG levels at days 14, 21, 28, 90 or 365 was found (data not shown).

### **Maximum expansion of IgG1 and IgA1 memory B cells correlated strongly with the increase in Ag-specific serum IgG**

Lack of correlations between Ag-specific serum Ig kinetics and memory B-cell kinetics is likely a consequence of the low frequency of expanding Ag-specific memory B cells in blood [39,40]. Furthermore, memory B-cell expansion may be less unified in time than plasma cell expansion. To address this second possibility, we correlated the levels of Ag-specific serum Igs at days 14-365 with the maximum observed expansion of total and individual memory B-cell subsets between days 7 and 28 (in majority of donors this maximum expansion was reached between days 7 and 14). In donors with a higher memory B-cell expansion there was a trend towards higher Ag-specific serum Ig, but no strong positive correlation ( $r > 0.8$ ) was found (data not shown). However, further investigation of memory B-cell subsets confirmed a strong positive correlation between IgG1 and IgA1 memory B-cell expansion (max. expansion d7-28) and Ag-specific serum Ig. After correction for multiple testing, we found a strong positive correlation between total Ag-specific serum IgG levels at day 21 and maximum expansion of IgG1 memory B cells ( $r = 0.8061$ ,  $p = 0.0072$ ) (**Fig. 5A**). Furthermore, the maximum expansion of IgA1 memory B cells strongly correlated with serum IgG levels at days 14 and 21 ( $r = 0.8303$ ,  $p = 0.0047$  and  $r = 0.8788$ ,  $p = 0.0016$ , respectively) (**Fig. 5B**). These strong correlations between IgG1 and IgA1 memory B-cell expansions and the increased Ag-specific serum IgG levels could not simply be explained by changes in total B-cell or leukocyte numbers (**Suppl. Fig. 7**) and were stronger than any correlation between serum IgG levels and the day 7 IgG1 plasma cell peak (**Fig. 3E**). As the rise in Ag-specific Igs was mostly caused by Bp-specific Igs, the abovementioned correlations held true when correlating only to Bp-specific Ig levels, but not for Diph-specific or Tet-specific serology (data not shown).

### **Minor changes in circulating T cells showed limited correlations with B cells and Ag-specific Igs**

T-cell help in the germinal centers results in the generation of high affinity B cells [41]. For Tdap vaccination, polarization of CD4 T-cell responses towards Th2 has been described [42]. However, recent studies indicated that in donors who were wP-primed, T-cell responses upon aP booster vaccinations were skewed towards a Th1/Th17 response [43,44]. Within CD4 T cells, we evaluated both kinetics of different T-helper cell types (including TFHs and Tregs) and of different effector stages within these subsets (e.g. naive, central-, transitional-, peripheral- and effector memory).

Analysis of correlation networks revealed multiple correlations in-between CD4 T-cell subsets within the same timeframes. These correlations were especially prominent between T helper and TFH cells of the TH17, TH1/17 and CXCR3+CCR4+CCR6+CCR10- phenotype. At the same time, no consistent strong correlations were found between CD4 T cells and Ag-specific Igs, and correlations be-

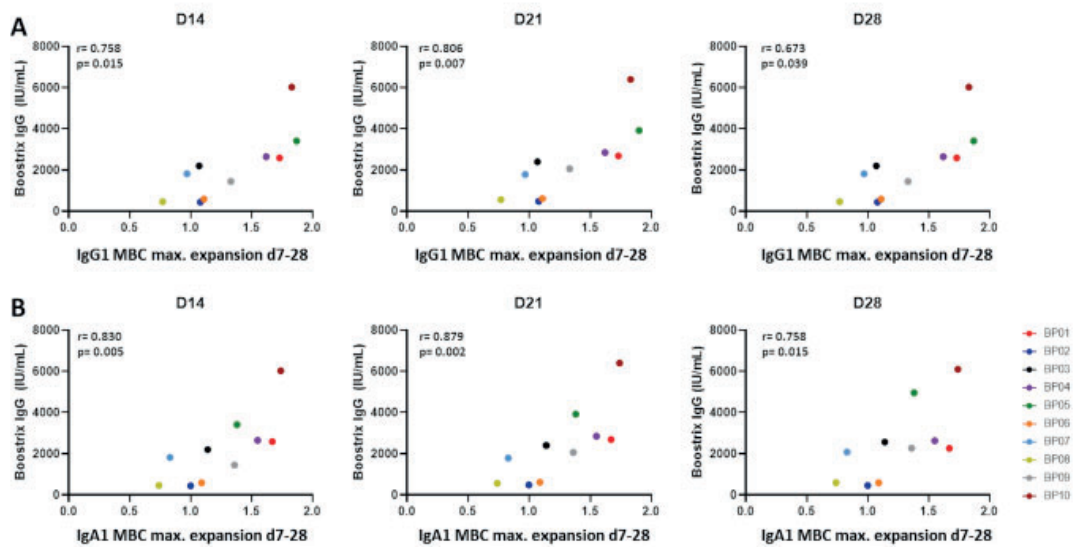


**Figure 5. Correlation between maximum expansion of memory B-cell subsets and vaccine-specific IgGs as determined by Spearman's rank correlation.** A. Correlation between the maximum expansion of IgG1 memory B cells (ratio over baseline at days 7-28) and vaccine-specific IgGs ("Boostrix-IgG") at days 14, 21 and 28. B. Correlation between the maximum expansion of IgA1 memory B cells (ratio over baseline at days 7-28) and vaccine-specific IgGs at days 14, 21 and 28. An FDR-corrected p-value of  $<0.0075$  was considered significant. D= Days after vaccination.

tween CD4 T cells and B cells were limited and restricted to minor populations (**Dynamic network video: B-CD4**). Despite several correlations, changes in absolute T-cell subset numbers over time were limited (**Supplementary Table 2**). Likewise, no consistent changes were observed in maturation of T helper subsets. Thus, in this case, monitoring of T-cell kinetics in the periphery may require an Ag-specific approach.

Additionally, we correlated CD8 T-cell and NK-cell kinetics with changes in B cells and Ag-specific Ig levels. Within the CD8 T-cell and NK-cell compartments correlations were limited and inconsistent, suggesting no shared response pattern. Likewise, hardly any correlations were observed between both Ag-specific Igs and NK or CD8 T cells, and between B cells and NK or CD8 T cells (mostly restricted to CD8 or TCR $\gamma\delta$  T-cell subsets). When comparing CD4 T-cell kinetics with NK and CD8 T-cell kinetics, very limited or no correlations were observed. Lastly, no correlation of baseline values of major cell populations and the vaccine-specific IgG levels at days 14, 21, 28, 90 or 365 was found (data not shown). Changes in innate immune cells preceded, but poorly correlated with changes in the T- or B-cell compartments

So far, post-vaccination kinetics of serum Igs, B cells and T cells were evaluated over time, but not the kinetics of innate immune cells. Local damage, antigens and adjuvant introduced by the vaccine lead to the recruitment of innate immune cells, which serve an important role in initiating the immune response by means of local inflammation and antigen presentation [45-48].



## Chapter 3.1

---

Overall, correlations between kinetics of innate immune cells and the change in Ag-specific serum Ig levels were limited and mostly restricted to monocyte subsets (cMo, iMo and ncMo, further subdivided into different functional subsets/activation stages, e.g. based on expression of CD62L, FcER1, CD36 or SLAN [49,50] [van den Bossche & Damasceno et al., manuscript in preparation]). Likewise, correlations between kinetics in the innate immune cell compartment and the B-compartment were sparse, both within and in-between timeframes. No correlations were found between T-cell and innate immune cell fluctuations within the same timeframes (**Dynamic network video: CD4- DC Monocyte**), and only limited correlations were present upon shifting timeframes (early monocyte changes with later Treg changes). Lastly, no correlations between baseline values of major innate immune cell populations and the vaccine-specific IgG levels at days 14, 21, 28, 90 or 365 were found (data not shown).

In terms of absolute cell counts, in approximately half of the donors, an increase in total leukocyte count was observed at the earliest evaluated time points post-vaccination (days 3-5, **Suppl. Fig. 8A**). This was mainly due to an increase in both mature and immature neutrophils (total neutrophils: max. ratio over baseline: 2.6x) (**Suppl. Fig. 8B**). At the same time – mostly in donors that showed neutrophil expansion - total monocyte numbers showed a max. ratio over baseline of 2x and at day 3 predominantly belonged to the more mature iMos and ncMos. No increase was observed for cMos.

### Discussion

In this study we showed that flow cytometry is a sensitive tool to monitor cellular changes upon vaccination. Although most of these changes occur locally in the tissue, many cells can be traced during their passage in PB, if sufficiently sensitive methods are applied. Up to 5 days post-Tdap-vaccination, fluctuations were predominantly found in the levels of neutrophils and monocytes and were associated with gradual maturation of monocytes. Afterwards, plasma cells started expanding from day 5 onwards with a sharp peak in (predominantly IgG1) plasma cell levels at day 7, simultaneously with plasma cell maturation. Despite limited changes in memory B-cell numbers, these changes strongly correlated with increase in Ag-specific serum IgG levels, which occurred from day 7 onwards. Although memory B cells seem better correlated with serological responses, strong homogenous plasma cell increase and clear plasma cell maturation over time can play a valuable role in immune response timing. Despite in-depth analysis, no uniform changes were detected in circulating T-cell subsets. We summarize our findings and their potential role in immune monitoring in **Fig. 6**.

Correlation networks are frequently used in systems biology to model kinetic relationships between different types of omics data [51-53]. Analysis of correlation networks is suited for large, multidimensional datasets, and can aid in finding shared or correlating patterns in exploratory studies. Such results should be analyzed cautiously as two interacting pairs that remain constant over time will correlate as well, which may be irrelevant for the posed research question. Therefore,

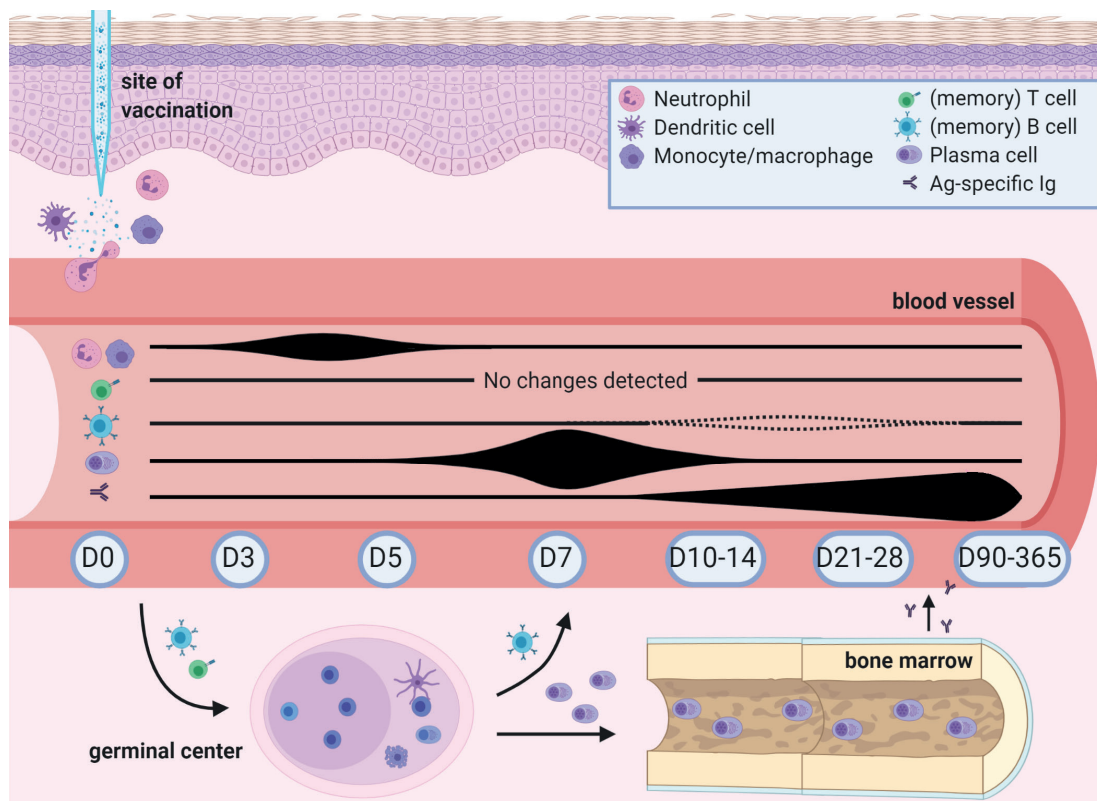


**Figure 6. Overview of changes detected in human peripheral blood post-Boostrix vaccination in this study.** Created with BioRender.com. Up to 5 days post-vaccination, fluctuations were found in the levels of circulating neutrophils and monocytes, with a change in total monocyte composition (based on expression of CD14 and CD16, with increased levels of intermediate and non-classical monocytes). Circulating plasma cells started expanding from day 5 onwards with a sharp peak in (predominantly IgG1) plasma cell levels at day 7 simultaneous with plasma cell maturation. Changes in circulating memory B-cell numbers were limited. Increase in Ag-specific IgG serum levels occurred from day 7 onwards and only showed signs of waning at d365. Despite in-depth analysis, no uniform changes were detected in circulating T-cell subsets. Baseline cell count and Ag-specific serum Ig levels did not seem to influence the levels of Ag-specific IgGs.

identified correlations should be confirmed by experimental data or in another group of samples. In our study, we correlated longitudinal changes in circulating immune cells and serology readouts over a 3 time point window.

Increase in number of neutrophils, iMo and ncMo was the earliest signs of immune response to Boostrix. In fact, innate immune cell kinetics might be even more prominent than observed as we did not study cellular changes before day 3. Mouse models have shown increased numbers of neutrophils and monocytes at the site of vaccination already within hours [54]. Moreover, upon Ebola vaccination, a significant increase in frequency and activation state of DCs and monocyte subsets was observed after 1 and 3 days, and a gene enrichment set analysis after flu vaccination pointed towards gene signatures from innate immunity modules after 1 day [55,56]. The changes observed in our study may not be vaccine specific, but rather related to the local damage or adjuvant [11]. It has been shown in man and mouse that the type of adjuvant used and the route of administration



## Chapter 3.1

---

can influence the innate response [54,57]. Lastly, Rechten et al showed a correlation between innate markers and post-vaccination antibody levels (days 28 and later) [55]. Therefore, flow cytometric evaluation of innate immune cells at early time points (days 1-3) may be a valuable tool to evaluate different adjuvants as well as different routes of vaccine administration.

Increase in plasma cell numbers started at day 5 and peaked at day 7 post-vaccination. In steady state, numbers of circulating plasma cells in blood are low, with median values in adults of  $<5$  cells/ $\mu$ L [7], in contrast, plasma cell counts expand rapidly upon infection or vaccination. This highly dynamic behavior brings both challenges and opportunities. Because of low baseline numbers, reliable detection of circulating plasma cells has only become possible upon introduction of high-throughput flow cytometry. In turn, the system is relatively 'clean' and easy to study without the need of introducing an antigen-specific approach. It has been shown in an influenza model that at the peak of expansion up to 80% of the generated IgG plasma cell peak can be antigen specific [12,58]. The same is likely to be true in our Tdap booster study. This is in contrast to memory B cells, where cells raised in response to the vaccine or infection may constitute  $<0.1\%$  of all B cells [59,60]. Currently, we are evaluating which of the components of the multivalent Boostrix vaccine are recognized by most Ag-specific B cells, and whether there are phenotypical differences in-between plasma cells with different specificities. At the peak of expansion majority of plasma cells was of the IgG1 phenotype. Ag-specific serum Igs were mostly IgGs and correlated well with the max. expansion of IgG1 memory B cells (max. ratio over baseline between days 7-28). In fact, IgGs (mainly IgG1) are the most frequently raised in response to vaccination and for many vaccines Ag-specific serum IgGs are considered correlates of protection [61,62]. IgG1 plays an important role in complement activation and antibody dependent cell-mediated cytotoxicity [63]. Moreover, IgG1 can be transferred to the placenta to protect fetus and newborns, which can be highly relevant for maternal vaccination programs [64,65].

Increase in Ag-specific serum IgA levels and IgA B cells was less pronounced. This can be related to the fact that -in contrast to IgG- IgA responses are mostly associated with natural infections and occur locally in the mucosa-associated lymphoid tissue. Moreover, the monomeric serum IgAs -generated upon vaccination- are metabolized at a faster rate than serum IgGs [66]. Therefore, serum IgA levels are rarely considered a read-out of vaccine efficacy, i.e. in case of rotavirus [67]. The volunteers in this study were adults. As Bp carriage within the population is high, it is likely that they have encountered Bp earlier in life and had pre-existing IgA memory B cells which became activated upon antigen encounter [68,69]. Indeed, several studies showed an age-dependent increase in Bp-specific serum IgA levels [70,71]. Alternative vaccine administration routes, such as the intranasal delivery of a live-attenuated bacterium in the BPZE1 vaccine, can also result in robust Ag-specific IgA responses [57].

The composition of the plasma cell compartment in steady state is a mixture of

plasma cells of different maturation stages [72], and over the course of an immune response, the contribution of the most mature plasma cells (CD20-CD138+) increases. Since the magnitude of plasma cell expansion differs between donors, knowledge of these maturation stages may be useful when assessing the progress of an immune response. Although up to 80% of total plasma cells at the peak of expansion can be Ag-specific and derived from the ongoing response, the origin of remaining plasma cells may be somewhat different. Odendahl and colleagues showed that upon vaccination with tetanus toxoid a considerable amount of circulating plasma cells, not specific to the used vaccine, were long-lived plasma cells forced to leave their niche in the bone marrow upon competition with newly generated plasma cells [13]. These cells may further contribute to the observed shift in plasma cell maturation. Moreover, the competition for the bone marrow niche prolongs retention of the newly generated plasma cells in the blood, which may start maturing before leaving circulation.

The early expansion of plasma cells at days 5-7 was closely followed by an increase in Ag-specific serum Igs from day 7 onwards. This rise in serum Igs continued even when plasma cell numbers had returned to baseline. However, magnitude of plasma cell expansion did not reflect quantitative changes in serum Ig levels. One of the potential explanations of this phenomenon is that, at the peak of response, part of the circulating plasma cells may be derived from the “expelled” long-lived plasma cells in bone marrow rather than from the ongoing immune response [13]. Further explanation may have to do with plasma cell affinity. If affinity of the newly produced Abs is low, they may not be detected in Ag-specific assays, such as MIA. Finally, it remains unclear whether all produced plasma cells will be able to successfully home to bone marrow and start Ig production. To shed more light on these issues, it would be of value to compare the B-cell receptors (BCR) of circulating plasma cells with the structure of Ag-specific Igs.

Despite minor quantitative changes, and in contrast to circulating plasma cells, total IgG1 memory B cells at the peak of expansion (max. ratio over baseline between days 7-28) correlated well with Ag-specific serum Ig levels (IU/mL). Correlations between Ag-specific memory B cells and serum Ig levels, have been observed for tetanus toxoid and rotavirus, but were not corroborated by other studies on tetanus toxoid and wasp venom [59,60]. The different techniques used in-between those studies may account for the different findings. A study on pertussis by Hendrikx et al showed correlations between circulating memory B cells as measured by ELISPOT and Bp-specific serum Igs (at baseline with FHA, post-vaccination with FHA, PT and Prn) [73]. Although these techniques yield valuable data, they are laborious and difficult to apply in daily practice. Our non-Ag-specific approach, when confirmed in a larger cohort, would be more convenient in a way that it is not dependent on the availability and costs of (labeled) antigens.

Although the CD4 T-cell panel used in this study allowed us to monitor different maturation and activation stages of (minor) T-cell subsets in a highly sensitive manner, no consistent kinetics or maturation of T cells were detected in this stu-

## Chapter 3.1

---

dy. However, a recent study by Lamberts et al, showed that their recently developed T-cell assay enabled relatively fast detection of Ag-specific T-cell kinetics upon aP vaccination [44]. Similarly, Da Silva and colleagues were able to monitor an Ag-specific CD4 T-cell response upon aP vaccination [43]. Still, both studies showed low prevalence of Ag-specific T cells, which could explain the limited cellular changes observed in the T-cell compartment in our approach.

Of note, the magnitude of cellular changes differed between donors. This may be due to individual differences in the immune system responsiveness and previous (natural) Bp exposure, as also visible from diverse Ig levels generated post-vaccination. Furthermore, it can be related to differences in timing of the response. In our study, we included days 5, 7 and 10 and observed a clear plasma cell peak at day 7. This is in line with previous studies using rabies, tetanus and influenza vaccination, which reported detection of plasma cells 6-7 days after secondary immunization [12,14,74]. However, somewhat delayed responses in some of the donors cannot be excluded. Moreover, timing may differ in case of a primary immunization or when using a different route of delivery, therefore the findings presented in this study may not directly be extrapolated to all types of vaccination [14,57].

Lastly, 2/10 donors in this study did not have protective anti-PT serum IgG levels (>20 IU/mL) 1 year after vaccination. These two donors did not show a deviating cellular response as compared to the other donors. Moreover, a decrease in Ag-specific Ig levels 1 year after vaccination was observed for all donors. Whether these donors are still protected, may not only depend on the Ag-specific antibodies, but also on the presence of memory cells [75].

In this study, we implemented a broad in-depth flow-cytometric approach to determine the most relevant time points for cellular immune analysis in vaccination studies and to identify candidate populations for novel cellular correlates of protection. This approach could be useful in early evaluation of e.g. vaccine candidates, altered routes of vaccine/antigen administration or the setup of disease models. Currently, we are comparing cellular kinetics post-Boostrix vaccination in this cohort and additional in four cohorts of different ages and priming backgrounds, with cellular kinetics post-bacterial challenge in humans, as recently described by De Graaf and colleagues [76,77]. This work is done within the framework of the IMI (Innovative Medicines Initiative) PERISCOPE Consortium (<https://periscope-project.eu/>). In these studies, additional analyses are performed by different IMI PERISCOPE partners providing insights into Ag-specific immunity, local (mucosal) immunity, cytokine and chemokine production [44,78,79]. This should yield novel insights into the extent to which current vaccines mimics naturally obtained immunity.

### **Conflict of Interest**

AMD, CT, JJMvD, AO, MAP and MAB report inventorship of the patent “Means and methods for multiparameter cytometry-based leukocyte subsetting”

(NL2844751, filing date 5 November 2019)<sup>21</sup>, owned by the EuroFlow Consortium. In addition, JJMvD and AO reports to be chairman and co-chairman of the EuroFlow scientific foundation, which receives royalties from licensed patents, which are collectively owned by the participants of the EuroFlow Foundation. These royalties are exclusively used for continuation of the EuroFlow collaboration and sustainability of the EuroFlow consortium. In addition, JJMvD and AO report an Educational Services Agreement from BD Biosciences (San José, CA) and a Scientific Advisor Agreement with Cytognos; all related fees and honoraria go to LUMC and USAL, respectively.

### Author Contributions

MAB, JJMvD, LEMO designed the study. LEMO and JJZ coordinated the clinical part of this study. GAMB coordinated the Ag-specific serology work at RIVM. BdM, RJG, AMD, CT and MAB performed the experimental work and data analysis. AO and MPA provided conceptual input. IK performed bioinformatics analysis and constructed the correlation networks. AMD and MAB wrote the manuscript. All authors read and commented on the manuscript. All authors contributed to the article and approved the submitted version.

### Funding

IK is supported by the European Union's Horizon 2020 research and innovation program under the Marie Skłodowska-Curie grant agreement No 707404. The here presented study is a pilot study for the Innovative Medicines Initiative (IMI) PERISCOPE program, a Joint Undertaking under grant agreement No 115910. This Joint Undertaking receives support from the European Union's Horizon 2020 Research and Innovation Programme, the European Federation of Pharmaceutical Industries and Associations (EFPIA), and the Bill and Melinda Gates Foundation (BMGF). The flow cytometric studies in this study were supported by the EuroFlow Consortium. The EuroFlow Consortium received support from the FP6-2004-LIFESCIHEALTH-5 program of the European Commission (grant LSHB-CT-2006-018708) as Specific Targeted Research Project (STREP).

### Acknowledgements

The authors would like to thank the personnel of the Unit Hemapheresis (Dept. of Immunology, LUMC), for their help with the clinical part of this study, Marieke Bitter for her help with the financial management of this study, and Pieter van Gageldonk from National Institute of Public Health and the Environment for analysis of Ag-specific serum Ig levels. Moreover, we acknowledge the LUMC Flow cytometry Core Facility (FCF) and the help of the FCF operators. We are grateful to all subjects, who volunteered to contribute to our vaccination study.

### Supplementary Material

The Supplementary Material for this article can be found online at: <https://www.frontiersin.org/articles/10.3389/fimmu.2021.666953/full#supplementary-material>

Or using the following QR code:



### References

1. Plotkin SA. Complex correlates of protection after vaccination. *Journal of Clinical infectious diseases*. 2013;56(10):1458-1465.
2. Whittle H, Inskip H, Hall A, Mendy M, Downes R, Hoare S. Vaccination against chronic viral carriage in The Gambia. *The Lancet*. 1991;337(8744):747-750.
3. Plotkin SA. Correlates of protection induced by vaccination. *Clin Vaccine Immunol*. 2010;17(7):1055-1065.
4. Clay TM, Hobeika AC, Mosca PJ, Lyerly HK, Morse MA. Assays for monitoring cellular immune responses to active immunotherapy of cancer. *Journal of Clinical Cancer Research*. 2001;7(5):1127-1135.
5. Sridhar S, Begom S, Bermingham A, et al. Cellular immune correlates of protection against symptomatic pandemic influenza. *Nature medicine*. 2013;19(10):1305.
6. Wilkinson TM, Li CK, Chui CS, et al. Preexisting influenza-specific CD4+ T cells correlate with disease protection against influenza challenge in humans. *Nature medicine*. 2012;18(2):274.
7. Blanco E, Pérez-Andrés M, Arriba-Méndez S, et al. Age-associated distribution of normal B-cell and plasma cell subsets in peripheral blood. *Journal of Allergy and Clinical Immunology*. 2018;141(6):2208-2219. e2216.
8. Theunissen P, Mejstrikova E, Sedek L, et al. Standardized flow cytometry for highly sensitive MRD measurements in B-cell acute lymphoblastic leukemia. *Blood, The Journal of the American Society of Hematology*. 2017;129(3):347-357.
9. Springer TA. Traffic signals for lymphocyte recirculation and leukocyte emigration: the multistep paradigm. *Cell*. 1994;76(2):301-314.
10. Butcher EC, Picker LJ. Lymphocyte homing and homeostasis. *Science*. 1996;272(5258):60-67.
11. van den Bossche WB, Rykov K, Teodosio C, et al. Flow cytometric assessment of leukocyte kinetics for the monitoring of tissue damage. *Clinical Immunology*. 2018;197:224-230.
12. Ellebedy AH, Jackson KJ, Kissick HT, et al. Defining antigen-specific plasmablast and memory B cell subsets in human blood after viral infection or vaccination. *Nature immunology*. 2016;17(10):1226.
13. Odendahl M, Mei H, Hoyer BF, et al. Generation of migratory antigen-specific plasma blasts and mobilization of resident plasma cells in a secondary immune response. *Blood*. 2005;105(4):1614-1621.
14. Blanchard-Rohner G, Pulickal AS, Jol-van der Zijde CM, Snape MD, Pollard AJ. Appearance of peripheral blood plasma cells and memory B cells in a primary and secondary immune response in humans. *Blood*. 2009;114(24):4998-5002.
15. CDC. Vaccines & Preventable diseases Home. [CDC website]. 2020; About Diphtheria, Tetanus, and Pertussis Vaccines. Available at: <https://www.cdc.gov/vaccines/vpd/dtap-tdap-td/hcp/about-vaccine.html>. Accessed 23-07, 2020.
16. Schurink-van't Klooster T, De Melker H. The national immunisation programme in the Netherlands: surveillance and developments in 2015-2016. RIVM open repository. 2016.
17. Girard DZ. Recommended or mandatory pertussis vaccination policy in developed countries: does the choice matter? *Public Health*. 2012;126(2):117-122.
18. Tan T, Dalby T, Forsyth K, et al. Pertussis across the globe: recent epidemiologic trends from 2000 to 2013. *The Pediatric infectious disease journal*. 2015;34(9):e222-e232.
19. GSK. Boostrix- Highlights of prescribing information. Information leaflet Boostrix vaccine. Available at: [https://www.gsksource.com/pharma/content/dam/GlaxoSmithKline/US/en/Prescribing\\_Information/Boostrix/pdf/BOOSTRIX.PDF](https://www.gsksource.com/pharma/content/dam/GlaxoSmithKline/US/en/Prescribing_Information/Boostrix/pdf/BOOSTRIX.PDF). Accessed May 19, 2020.
20. van Gageldonk PG, van Schaijk FG, van der Klis FR, Berbers GA. Development and validation of a multiplex immunoassay for the simultaneous determination of serum antibodies to Bordetella pertussis, diphtheria and tetanus. *Journal of immunological methods*. 2008;335(1-2):79-89.
21. van Dongen JJM, Orfao de Matos Correia E, Vale JA, Goncalves Grunho Teodosio CI, et al., Inventors. Means and methods for multiparameter cytometry-based leukocyte subsetting. US patent PCT/NL2020/050688. priority date: 05-11-2019, 2019.
22. Botafogo V, Pérez-Andrés M, Jara-Acevedo M, et al. Age Distribution of Multiple Functionally Relevant Subsets of CD4+ T Cells in Human Blood Using a Standardized and Validated 14-Color EuroFlow Immune Monitoring Tube. *Frontiers in Immunology*. 2020;11:166.
23. Ziegler-Heitbrock L, Ancuta P, Crowe S, et al. Nomenclature of monocytes and dendritic



- cells in blood. *Blood*. 2010;116(16):e74-e80.
24. Kalina T, Flores-Montero J, Lecrevisse Q, et al. Quality assessment program for EuroFlow protocols: Summary results of four-year (2010–2013) quality assurance rounds. *Cytometry Part A*. 2015;87(2):145-156.
  25. Kalina T, Flores-Montero J, Van Der Velden V, et al. EuroFlow standardization of flow cytometer instrument settings and immunophenotyping protocols. *Leukemia*. 2012;26(9):1986-2010.
  26. Shannon P, Markiel A, Ozier O, et al. Cytoscape: a software environment for integrated models of biomolecular interaction networks. *Genome research*. 2003;13(11):2498-2504.
  27. Bastian M, Heymann S, Jacomy M. Gephi: an open source software for exploring and manipulating networks. Paper presented at: Third international AAAI conference on weblogs and social media 2009.
  28. Schauer U, Stemberg F, Rieger CH, et al. IgG subclass concentrations in certified reference material 470 and reference values for children and adults determined with the binding site reagents. *Clinical chemistry*. 2003;49(11):1924-1929.
  29. der Deutschen Gesellschaft für Klinische Chemie und des Verbandes der Diagnostica-Industrie e.V. V. Konsensuswerte der Deutschen Gesellschaft für Laboratoriumsmedizin. *Clinical Laboratory*. 1995;41:743-748.
  30. Ipsen J. Circulating antitoxin at the onset of diphtheria in 425 patients. *Journal of Immunology*. 1946;54(4):325-347.
  31. Edmunds W, Pebody R, Aggerback H, et al. The sero-epidemiology of diphtheria in Western Europe. *Epidemiology & Infection*. 2000;125(1):113-125.
  32. Galazka A. Diphtheria: the immunological basis for immunisation. Geneva: World Health Organization, 1993. WHO/EPI/GEN/93.12.
  33. Edsall G. Specific prophylaxis of tetanus. *Journal of the American Medical Association*. 1959;171(4):417-427.
  34. Hendrikx LH, Felderhof MK, Öztürk K, et al. Enhanced memory B-cell immune responses after a second acellular pertussis booster vaccination in children 9 years of age. *Vaccine*. 2011;30(1):51-58.
  35. Long SS, Welton CJ, Clark JL. Widespread silent transmission of pertussis in families: antibody correlates of infection and symptomatology. *Journal of Infectious Diseases*. 1990;161(3):480-486.
  36. Guiso N, Berbers G, Fry NK, He Q, Riffelmann M, von König CW. What to do and what not to do in serological diagnosis of pertussis: recommendations from EU reference laboratories. *European Journal of Clinical Microbiology & Infectious Diseases*. 2011;30(3):307-312.
  37. de Melker H, Versteegh F, Conyn-van Spaendonck M, et al. Specificity and sensitivity of high levels of immunoglobulin G antibodies against pertussis toxin in a single serum sample for diagnosis of infection with *Bordetella pertussis*. *Journal of clinical microbiology*. 2000;38(2):800-806.
  38. Perez-Andres M, Paiva B, Nieto WG, et al. Human peripheral blood B-cell compartments: a crossroad in B-cell traffic. *Cytometry Part B: Clinical Cytometry*. 2010;78(S1):S47-S60.
  39. Nanan R, Heinrich D, Frosch M, Kreth HW. Acute and long-term effects of booster immunisation on frequencies of antigen-specific memory B-lymphocytes. *Vaccine*. 2001;20(3-4):498-504.
  40. Buisman A, De Rond C, Öztürk K, Ten Hulscher H, Van Binnendijk R. Long-term presence of memory B-cells specific for different vaccine components. *Vaccine*. 2009;28(1):179-186.
  41. Gatto D, Brink R. The germinal center reaction. *Journal of Allergy and Clinical Immunology*. 2010;126(5):898-907.
  42. Bancroft T, Dillon MB, da Silva Antunes R, et al. Th1 versus Th2 T cell polarization by whole-cell and acellular childhood pertussis vaccines persists upon re-immunization in adolescence and adulthood. *Cellular immunology*. 2016;304:35-43.
  43. da Silva Antunes R, Babor M, Carpenter C, et al. Th1/Th17 polarization persists following whole-cell pertussis vaccination despite repeated acellular boosters. *The Journal of clinical investigation*. 2018;128(9).
  44. Lambert EE, Corbière V, van Gaans-van den Brink J, et al. Uncovering Distinct Primary Vaccination-Dependent Profiles in Human *Bordetella Pertussis* Specific CD4+ T-Cell Responses Using a Novel Whole Blood Assay. *Vaccines*. 2020;8(2):225.
  45. Li H, Nookala S, Re F. Aluminum hydroxide adjuvants activate caspase-1 and induce IL-1 $\beta$  and IL-18 release. *The Journal of Immunology*. 2007;178(8):5271-5276.
  46. Coffman RL, Sher A, Seder RA. Vaccine adjuvants: putting innate immunity to work. *Im-*



## Chapter 3.1

---

- munity. 2010;33(4):492-503.
47. Lu F, HogenEsch H. Kinetics of the inflammatory response following intramuscular injection of aluminum adjuvant. *Vaccine*. 2013;31(37):3979-3986.
  48. Lindblad EB. Aluminium compounds for use in vaccines. *Immunology and cell biology*. 2004;82(5):497-505.
  49. Hamers AA, Dinh HQ, Thomas GD, et al. Human monocyte heterogeneity as revealed by high-dimensional mass cytometry. *Arteriosclerosis, thrombosis, and vascular biology*. 2019;39(1):25-36.
  50. Damasceno D, Almeida J, Teodosio C, et al. Monocyte Subsets and Serum Inflammatory and Bone-Associated Markers in Monoclonal Gammopathy of Undetermined Significance and Multiple Myeloma. *Cancers*. 2021;13(6):1454.
  51. Adourian A, Jennings E, Balasubramanian R, et al. Correlation network analysis for data integration and biomarker selection. *Molecular BioSystems*. 2008;4(3):249-259.
  52. Hood L, Perlmutter RM. The impact of systems approaches on biological problems in drug discovery. *Nature biotechnology*. 2004;22(10):1215-1217.
  53. Kelder T, Stroeve J, Bijlsma S, Radonjic M, Roeselers G. Correlation network analysis reveals relationships between diet-induced changes in human gut microbiota and metabolic health. *Nutrition & diabetes*. 2014;4(6):e122-e122.
  54. Liang F, Loré K. Local innate immune responses in the vaccine adjuvant-injected muscle. *Clinical translational immunology*. 2016;5(4):e74.
  55. Rechten A, Richert L, Lorenzo H, et al. Systems vaccinology identifies an early innate immune signature as a correlate of antibody responses to the Ebola vaccine rVSV-ZEBOV. *Cell reports*. 2017;20(9):2251-2261.
  56. Nakaya HI, Clutterbuck E, Kazmin D, et al. Systems biology of immunity to MF59-adjuvanted versus nonadjuvanted trivalent seasonal influenza vaccines in early childhood. *Proceedings of the National Academy of Sciences*. 2016;113(7):1853-1858.
  57. Lin A, Apostolovic D, Jahnmatz M, et al. Live attenuated pertussis vaccine BPZE1 induces a broad antibody response in humans. *The Journal of Clinical Investigation*. 2020;130(5).
  58. Wrämmert J, Smith K, Miller J, et al. Rapid cloning of high-affinity human monoclonal antibodies against influenza virus. *Nature*. 2008;453(7195):667.
  59. Rojas OL, Narváez CF, Greenberg HB, Angel J, Franco MA. Characterization of rotavirus specific B cells and their relation with serological memory. *Virology*. 2008;380(2):234-242.
  60. Leyendeckers H, Odendahl M, Löhndorf A, et al. Correlation analysis between frequencies of circulating antigen-specific IgG-bearing memory B cells and serum titers of antigen-specific IgG. *European journal of immunology*. 1999;29(4):1406-1417.
  61. Schure R-M, Hendrikx LH, de Rond LG, et al. Differential T-and B-cell responses to pertussis in acellular vaccine-primed versus whole-cell vaccine-primed children 2 years after preschool acellular booster vaccination. *Clin Vaccine Immunol*. 2013;20(9):1388-1395.
  62. Robbins JB, Schneerson R, Szu SC. Perspective: hypothesis: serum IgG antibody is sufficient to confer protection against infectious diseases by inactivating the inoculum. *Journal of Infectious Diseases*. 1995;171(6):1387-1398.
  63. Parham P. The immune system; Ch.9 Immunity mediated by B cells and antibodies. Garland Science; 2014.
  64. Safadi MAP. Control of pertussis in infants: time has finally come? In: Taylor & Francis; 2015.
  65. RIVM. Pertussis- 22-week vaccination. [website of the RIVM]. [rivm.nl/en/22-week-vaccination](http://rivm.nl/en/22-week-vaccination). Available at. Accessed June 23, 2020.
  66. Woof JM, Kerr MA. The function of immunoglobulin A in immunity. *The Journal of Pathology: A Journal of the Pathological Society of Great Britain and Ireland*. 2006;208(2):270-282.
  67. Franco MA, Angel J, Greenberg HB. Immunity and correlates of protection for rotavirus vaccines. *Vaccine*. 2006;24(15):2718-2731.
  68. Cherry JD. Epidemic pertussis in 2012—the resurgence of a vaccine-preventable disease. *New England Journal of Medicine*. 2012;367(9):785-787.
  69. N. van der Maas HdM, K. Heuvelman, M. van Gent, F.R. Mooi. Kinhoestsurveillance in 2013 en 2014 - RIVM Brieffrapport 2014-0165. 2014.
  70. Subissi L, Rodeghiero C, Martini H, et al. Assessment of IgA anti-PT and IgG anti-ACT reflex testing to improve Bordetella pertussis serodiagnosis in recently vaccinated subjects. *Clinical*

Microbiology and Infection. 2020;26(5):645. e641-645. e648.

71. Hendrikx LH, Öztürk K, De Rond LG, et al. Serum IgA responses against pertussis proteins in infected and Dutch wP or aP vaccinated children: an additional role in pertussis diagnostics. *PLoS One*. 2011;6(11):e27681.
72. Caraux A, Klein B, Paiva B, et al. Circulating human B and plasma cells. Age-associated changes in counts and detailed characterization of circulating normal CD138<sup>-</sup> and CD138<sup>+</sup> plasma cells. *haematologica*. 2010;95(6):1016-1020.
73. Hendrikx LH, de Rond LG, Öztürk K, et al. Impact of infant and preschool pertussis vaccinations on memory B-cell responses in children at 4 years of age. *Vaccine*. 2011;29(34):5725-5730.
74. Frölich D, Giesecke C, Mei HE, et al. Secondary immunization generates clonally related antigen-specific plasma cells and memory B cells. *The Journal of Immunology*. 2010;185(5):3103-3110.
75. Hendrikx LH, Öztürk K, De Rond LG, et al. Identifying long-term memory B-cells in vaccinated children despite waning antibody levels specific for *Bordetella pertussis* proteins. *Vaccine*. 2011;29(7):1431-1437.
76. De Graaf H, Gbesemete D, Gorringe AR, et al. Investigating *Bordetella pertussis* colonisation and immunity: protocol for an inpatient controlled human infection model. *BMJ open*. 2017;7(10):e018594.
77. de Graaf H, Ibrahim M, Hill AR, et al. Controlled human infection with *Bordetella pertussis* induces asymptomatic, immunising colonisation. *Clinical Infectious Diseases*. 2019.
78. Versteegen P, Pinto MV, Barkoff AM, et al. Responses to an acellular pertussis booster vaccination in children, adolescents, and young and older adults: A collaborative study in Finland, the Netherlands, and the United Kingdom. *EBioMedicine*. 2021;65:103247.
79. Diavatopoulos DA, Mills KH, Kester KE, et al. PERISCOPE: road towards effective control of pertussis. *The Lancet Infectious Diseases*. 2019;19(5):e179-e186.



## Chapter 3.2

### **Age and primary vaccination background influence the plasma cell response to pertussis booster vaccination**

Annieck M. Diks<sup>1</sup>, Pauline Versteegen<sup>2</sup>, Cristina Teodosio<sup>1</sup>, Rick J. Groenland<sup>1</sup>, Bas de Mooij<sup>1</sup>, Anne-Marie Buisman<sup>2</sup>, Alba Torres-Valle<sup>3 4</sup>, Martín Pérez-Andrés<sup>3 4</sup>, Alberto Orfao<sup>3 4</sup>, Guy A.M. Berbers<sup>2</sup>, Jacques J.M. van Dongen<sup>1 3 4\*</sup>, and Magdalena A. Berkowska<sup>1</sup> on behalf of the IMI-2 PERISCOPE Consortium

<sup>1</sup>Department of Immunology, Leiden University Medical Center, Albinusdreef 2, 2333 ZA, Leiden, The Netherlands; A.M.Diks@lumc.nl (A.M.D.), C.I.Teodosio@lumc.nl (C.T.), R.J.Groenland@lumc.nl (R.J.G.), demooij.bas@gmail.com (B.d.M.), J.J.M.van\_Dongen@lumc.nl (J.J.M.v.D.), M.A.Berkowska@lumc.nl (M.A.B.)

<sup>2</sup>Center for Infectious Disease Control, National Institute of Public Health and the Environment, Antonie van Leeuwenhoeklaan 9, 3721 MA Bilthoven, The Netherlands; pauline.versteegen@rivm.nl (P.V.), annemarie.buisman@rivm.nl (A.-M.B.), guy.berbers@rivm.nl (G.A.M.B.)

<sup>3</sup>Cancer Research Centre (IBMCC, USAL-CSIC; CIBERONC CB16/12/00400), Institute for Biomedical Research of Salamanca (IBSAL), Salamanca 37007, Spain; albatordesvalle@usal.es (A.T.-V.), mmmar@usal.es (M.P.-A.), orfao@usal.es (A.O.)

<sup>4</sup>Department of Medicine and Cytometry Service (NUCLEUS Research Support Platform), University of Salamanca (USAL), Salamanca 37007, Spain

**Vaccines, January 2022**

**<https://doi.org/10.3390/vaccines10020136>**

### **Abstract**

Pertussis is a vaccine-preventable disease caused by the bacterium *Bordetella pertussis*. Over the past years, the incidence and mortality of pertussis increased significantly. A possible cause is the switch from whole cell to acellular pertussis vaccines, although other factors may also contribute. Here, we applied high-dimensional flow cytometry to investigate changes in B cells in individuals of different ages and distinct priming backgrounds upon administration of an acellular pertussis booster vaccine. Participants were divided over four age cohorts. We compared longitudinal kinetics within each cohort and between the different cohorts. Changes in the B-cell compartment were correlated to numbers of vaccine-specific B- and plasma cells and serum Ig levels. Expansion and maturation of plasma cells 7 days postvaccination was the most prominent cellular change in all age groups and was most pronounced for more mature IgG1+ plasma cells. Plasma cell responses were stronger in individuals primed with whole-cell vaccine than in individuals primed with acellular vaccine. Moreover, IgG1+ and IgA1+ plasma cell expansion correlated with FHA-, Prn-, or PT- specific serum IgG or IgA levels. Our study indicates plasma cells as a potential early cellular marker of an immune response and contributes to understanding differences in immune responses between age groups and primary vaccination backgrounds.

**Keywords:** Tdap; flow cytometry; acellular pertussis vaccine (aP); whole-cell pertussis vaccine (wP); plasma cells; ELISpot; vaccine priming effect; plasma cell expansion

## Introduction

Pertussis is a vaccine-preventable respiratory disease caused by the bacterium *Bordetella pertussis* (Bp). Since the introduction of the first pertussis vaccines in the 1940s and 1950s containing whole inactivated bacteria (whole-cell pertussis; wP), the incidence and mortality of pertussis have dramatically decreased [1]. However, the wP vaccine itself has a relatively high reactogenicity profile [2,3]. Therefore, from the early 1980s onwards, many (developed) countries started to replace the wP vaccine by an acellular pertussis (aP) vaccine, which had a more favorable reactogenicity profile [3,4]. In the Netherlands, this change took place on 1 January 2005. The aP vaccines contain purified Bp components, such as pertussis toxoid (PT), filamentous hemagglutinin (FHA), pertactin (Prn), and Fimbriae 2 and 3 (Fim2/3). In the Netherlands, the combined DTaP-IPV-Hib-HepB vaccine (providing protection against diphtheria, tetanus, pertussis, polio, *Haemophilus influenzae* type b (Hib), and hepatitis B) is used for primary vaccination. The booster vaccinations given at a later age are often Tdap vaccines [5]. Immune surveillance data have shown that despite high vaccination coverage in many countries, there has been an increase in pertussis cases in the past decennia [6,7]. This increase is not only seen in aP-using countries but was also reported in countries that primarily used wP vaccines at the time of investigation [6,8]. Several explanations for this increase have been proposed. First of all, improved awareness, surveillance, and diagnostics may increase the detection rate [9]. Furthermore, several new Bp strains have been described. These strains lack antigens present in the aP vaccine (such as FHA- or Prn-deficient strains), or PtxP3 strains that have adapted to suppress host immunity by producing higher levels of PT [10–13]. Lastly, there may be increased carriership within the population as well as faster waning of protective immunity in aP-primed individuals. Initial studies comparing the efficacy of aP vs. wP vaccines showed a similar short-term protection [14,15]. However, later long-term studies showed that protection lasted shorter when using aP vaccines [16–19]. Further, baboon models have shown that aP-induced immunity does not prevent transmission, immunity induced by wP vaccines leads to a faster clearance of bacteria, and immunity generated by infection prevents colonization [20]. These combined data point at the need for mucosal immunity to prevent or reduce colonization and carriership.

An improved vaccine, immunization program, and/or route of administration seem necessary to combat pertussis. This implies a need to first understand the mechanism underlying protection induced by aP and wP vaccines (their differences and similarities). So far, no true correlate of protection (neither serological nor cellular) has been established for pertussis, and this would greatly aid evaluation of newly developed vaccines. This is one of the pillars of the Innovative Medicines Initiative (IMI)-2 PERISCOPE Consortium (PERTussIS CORrelates of Protection Europe), which aims to increase the scientific understanding of pertussis-related immunity in humans, identify new biomarkers of protection, and generate technology and infrastructure for the future development of improved pertussis vaccines [21].



## Chapter 3.2

---

Several (recent) studies within and outside the IMI-2 PERISCOPE Consortium have shown that initial priming against pertussis (aP or wP vaccine) influences protection against disease as well as the immune response to (future) booster vaccinations [16,18,22–25]. For example, Hendrikx et al. found that in aP-primed children, antigen (Ag)-specific IgG4 serum levels were higher compared with those in wP-primed children [23]. Furthermore, Da Silva et al. showed that, even after receiving aP booster vaccinations, initial priming (wP or aP vaccine) determined the Ag-specific CD4 T-cell response [24]. Similarly, Lambert et al. showed that CD4 T cells isolated from recently aP-boosted individuals could be separated in a principal component analysis (PCA) view based on priming background. Here, an aP priming background resulted in a more Th2-related response compared to a wP priming background [22].

Neither vaccine-induced nor infection-induced immunity leads to lifelong protection against pertussis. Thus, the use of booster vaccinations later in life is a topic relevant for public health, as people with waned immunity can become carriers and, thus, a source of transmission. Moreover, older adults can be more vulnerable to severe disease outcomes [26]. Several studies have shown that aP boosters are effective and well-tolerated in (older) adults [27,28]. Recently, Versteegen et al. investigated the specific serological response to an aP booster vaccination in four cohorts of different ages and primary vaccination backgrounds in the Netherlands, Finland, and the UK (IMI-2 PERISCOPE study acronym: BERT, Booster pertussis vaccination study) [29]. Here, they found that all age cohorts showed a good response upon booster vaccination, with only limited differences between the different age cohorts for the Bp-specific IgG levels. However, Ag-specific serum IgA (both pre- and postvaccination) increased with age, likely caused by (mild) exposures to Bp over time.

Previous studies on influenza have shown that up to 80% of the circulating IgG plasma cells 7 days after vaccination can be vaccine-specific [30,31]. This, combined with the low numbers of circulating plasma cells at baseline (median counts <5cells/ $\mu$ L [32]), implies that the plasma cell system is a relatively ‘clean’ system to monitor. Thus, flow cytometry may serve as a faster and less laborious approach to study vaccination-elicited plasma cells than typical Ag-specific approaches such as Enzyme-Linked Immunospot (ELISpot). Recently, our team used high-dimensional flow cytometry to investigate over-time cellular kinetics in 10 healthy (wP-primed) adults upon aP vaccination. We were able to demonstrate a clear expansion and maturation of plasma cells (especially IgG1+), and a strong correlation between IgG1+ memory B-cell expansion and the magnitude of the Ag-specific IgG serum response [33]. Here, we extended our exploratory study by the analysis of participants of different ages and different priming backgrounds after receiving an aP booster (Boostrix-IPV, GlaxoSmithKline (GSK), Wavre, Belgium). We included 48 individuals enrolled in the Dutch cohort used in the IMI-2 PERISCOPE–BERT study ([periscope-project.eu/patients/study-2-bert/](http://periscope-project.eu/patients/study-2-bert/)) at predefined time points, with the primary objective of describing the kinetics of circulating B-cell populations in four cohorts of different ages and with different

priming backgrounds.

## Materials and Methods

### Study Design and Sample Collection

This study comprises one of the exploratory objectives of the Dutch ‘BERT study’, which was initiated by the IMI-2 PERISCOPE Consortium. It was approved by Medical Research Ethics Committees United (MEC-U, NL60807.100.17-R17.039) and registered at the EU Clinical trial registry (EudraCT number 2016-003678-42). To be eligible for this study, participants had to (1) be generally healthy; (2) have no recent evidence of serious disease—i.e., requiring the use of immunosuppressive or immunomodulating medication—within the 3 months prior to inclusion; (3) received all regular vaccines according to Dutch National Immunization Program ([www.rivm.nl/en/national-immunisation-programme](http://www.rivm.nl/en/national-immunisation-programme), accessed on 18-11-2020) as appropriate for their age. An extensive description of the cohort and a complete overview of all inclusion and exclusion criteria was published recently by Versteegen and colleagues [29]. For convenience, an overview of inclusion and exclusion criteria specific for this study is provided in **Supplementary Materials, Supplemental Table S1**. A fraction of the participants of this aP vaccination study was subjected to additional exploratory analysis, such as mass cytometry, evaluation of mucosal antibodies, NGS, or in-depth flow cytometry. The exploratory substudy monitoring the fluctuations in circulating B-cell subsets at baseline and days 7, 14, and 28 after vaccination is discussed in this manuscript. Here, 48 individuals were selected from four cohorts of different ages and distinct priming backgrounds at infancy: children, 7–10 y/o, aP-primed; adolescents, 11–15 y/o, aP- or wP-primed (aiming for equal distribution of priming background); young adults, 20–34 y/o, wP-primed; older adults 60–70 y/o, in whom vaccination history was unknown (presumably, wP-primed or not vaccinated). Participants were selected from the study cohort of the overarching ‘BERT study’. For each cohort, the first 12 participants to be included for the BERT study were also included in this flow cytometric study. Dropouts were replaced by individuals that were included but had not yet started the BERT study. As we aimed for an equal distribution of priming background in the adolescent cohort, inclusion of participants for this cohort was guided by priming background and order of inclusion in the BERT cohort.

The study was conducted by the Spaarne Academy (Spaarne Hospital, Hoofddorp, the Netherlands). Written informed consent was obtained at the start of the study. Participants were vaccinated intramuscularly with the Boostrix-IPV vaccine after their first blood donation (baseline). Boostrix-IPV is a reduced-antigen Tdap-IPV booster vaccine, which contains diphtheria toxoid (Diph) ( $\geq 2.5$  Limit of flocculation (Lf)); tetanus toxoid (Tet) ( $\geq 5$  Lf); three *Bordetella pertussis* proteins, PT (8 $\mu$ g), FHA (8 $\mu$ g), Prn (2.5 $\mu$ g); and inactivated poliovirus (Mahoney strain, 40 D-Antigen units (DU); MEF-1 strain, 8 DU; Saukett strain, 32 DU) and aluminum hydroxide as adjuvant [34]. Peripheral blood samples were collected in blood collection tubes using heparin as anticoagulant and in serum collection tubes at baseline, day 7, and day 28 after vaccination. An additional peripheral

blood sample was taken at day 14 in participants aged 20–34 and aged 60–70. Individuals were excluded and replaced by a new participant if a blood sample at day 0 or 28 could not be obtained.

### **Evaluation of Antigen-Specific Immunoglobulin Levels in Serum**

Serological analysis was performed in all collected samples. Levels of IgG directed against Tet, PT, FHA, Prn, and Fim2/3, and levels of IgA directed against PT, FHA, Prn, and Fim2/3 were determined by multiplex immunoassay (MIA) at the Dutch National Institute for Public Health and the Environment (RIVM, The Netherlands) [35]. The serum antibody responses raised against Bp-antigens during the PERISCOPE–BERT study have been extensively discussed by Versteegen and colleagues [29].

### **Detection of Vaccine-Specific Antibody-Producing Plasma Cells and Memory B Cells**

Analysis of numbers of IgG and IgA producing plasma cells and memory B cells was performed in the majority of the samples included in this study. B cells producing IgG directed against PT, FHA, Prn, and Tet, and B cells producing IgA directed against PT, FHA, and Prn were measured using ELISpot assay at the RIVM. This procedure has been described previously [36]. In short, peripheral blood mononuclear cells (PBMCs) were isolated using a density gradient. For antibody-producing plasma cells, PBMCs at day 7 postvaccination were directly transferred to Ag-coated ELISpot filter plates (duplicates). For the detection of vaccine-specific memory B cells, PBMCs collected at day 0 and day 28 were collected and stored at  $-135^{\circ}\text{C}$ . Thawed PBMCs were stimulated for 5 days using a culture medium containing CpG, IL-2, and IL-10. Next, cells were transferred to Ag-coated plates (duplicates). Numbers of Ag-specific antibody-producing cells—appearing as spots—were measured using an ImmunoSpot S6 Ultra-V analyzer (Cellular Technology Limited, Cleveland, OH). Uncoated wells filled with PBS served as negative control and were used to subtract background signal. Wells with a signal below the limit of quantification were set at  $0.1 \text{ cell}/10^5 \text{ PBMCs}$ . Cumulative IgG and IgA spot counts for all antigens measured were used for analyses.

### **Longitudinal Flow Cytometric Analysis of Circulating B-cell Subsets**

All peripheral blood samples were subjected to high-throughput flow cytometric immunophenotyping of the B-cell compartment. Here, we used a recently developed BIGH-tube: the B-cell and plasma cell tube (BIGH) allows identification of  $>100$  populations of B and plasma cells distinguished based on their maturation stage and expressed Ig subclasses [32,37] (Antibody panel and phenotypic description of the identified B-cell subsets: **Supplemental Table S2 and S3**).

Samples were processed according to the bulk lysis protocol using  $10 \times 10^6$  cells followed by intracellular staining, as described before [33] (protocols available on [www.EuroFlow.org](http://www.EuroFlow.org)), with the addition of membrane staining with CD45-AlexaFluor700.

In short, based on the white blood cell count (as determined by an automated

hematological analyzer (Sysmex XP-300, Sysmex Europe GmbH, Norderstedt, Germany)), one or multiple tubes were filled with up to 2 mL of blood, after which ammonium chloride was added up to a total volume of 50 mL. After a 15 min incubation at room temperature on a roller bank to lyse non-nucleated red blood cells, cells were washed, counted on a Sysmex XP-300, and pooled to a total of  $10 \times 10^6$  cells. Next, cells were stained with an antibody cocktail directed against surface markers for 30 min in the dark with the BIGH panel (**Supplemental Table S2**). This was followed by a cytoplasmic staining for intracellular Igs using the Fix & Perm reagent kit (Nordic MUBio, Susteren, The Netherlands) according to the manufacturer's protocol. Finally, samples were washed and resuspended in PBS for immediate acquisition (or stored for max ~3 h at 4 °C).

For precise enumeration of cell numbers, we used Perfect-Count Microspheres™ (Cytognos) according to the EuroFlow SOP (protocol available on [www.EuroFlow.org](http://www.EuroFlow.org), accessed on 09-10-2017). In short, exactly 50 µL of well-mixed Perfect-Count Microspheres™ were added to exactly 50 µL of peripheral blood. Then, antibodies directed against CD19, CD3, and CD45 were added and the sample was incubated for 30 min in the dark. Next, 500 µL of NH<sub>4</sub>Cl was added and after 10 min incubation, samples were ready for immediate acquisition. Using this tube, we could identify and quantify total leukocytes and lymphocytes, B, T, and NK cells in each sample. All samples were acquired at the Flow cytometry Core Facility of LUMC, using a BD FACS LSR Fortessa 4L (BD Biosciences, San Jose, CA, USA) or a BD FACS LSR Fortessa X-20 flow cytometer (BD Biosciences), which were calibrated daily according to EuroFlow guidelines, as previously described [38,39].

### Data Analysis and Statistics

To ensure objective data analysis and minimize operator-induced variability, all data were analyzed using the automated gating and identification (AGI) module of the Infinicyt software (Infinicyt™ Software v2.0, Cytognos). This AGI module makes use of clustering algorithms and comparison with fully annotated reference flow cytometry (FCS) data files of healthy individuals to assign clusters of events to a population [40]. Importantly, when there was no perfect fit for a cluster of events, this was marked as a 'check' population and the software indicated to which populations this cluster may correspond. These check events were assigned manually according to the proposed gating strategies for the BIGH panel (**Supplemental Table S3**) [32,37].

For visualization and statistical analysis, the GraphPad Prism 8.1.1 software (GraphPad, San Diego, CA, USA) was used. First, normality of distribution of major cell populations at baseline was evaluated using D'Agostino–Pearson Normality test. As not all major cell populations were normally distributed, a nonparametric approach was applied. To test longitudinal changes within each cohort, the Wilcoxon signed-rank test for paired samples was used. This was corrected for multiple testing by Bonferroni correction (in case of three sampling timepoints,  $p < 0.0167$ ; in case of four sampling timepoints,  $p < 0.0083$  was con-



sidered significant). To compare differences between the four cohorts at days 0, 7, and 28, the Kruskal–Wallis approach was used, followed by Dunn’s test. At day 14, only samples from the two adult cohorts were collected; therefore, the Mann–Whitney test was used instead of Kruskal–Wallis at day 14. This was corrected for multiple testing by Bonferroni correction ( $p < 0.0125$  was considered significant). Correlations were determined using Spearman’s Ranking Correlation. Correlation coefficients with a  $p < 0.05$  were considered significant. Within these significant correlations, correlation coefficients  $< 0.6$  or—in case of negative correlation,  $> -0.6$ —were considered weak correlations, whereas correlation coefficients  $> 0.6$  or  $< -0.6$  were considered strong correlations. In Supplemental Tables S5 and S6, where many correlations were analyzed, we corrected for multiple testing by Bonferroni correction ( $p < 0.01$  was considered significant). Lastly, in the comparison between aP- and wP-primed individuals (comparison of ratio over baseline at days 7 and 28), we performed Mann–Whitney, followed by Bonferroni correction ( $p < 0.025$  was considered significant).

### Results

#### Study Cohorts

All participants enrolled in the study between October 2017 and March 2018. In total, 12 children (age: 7–10, aP-primed, m/f ratio: 6/6), 12 adolescents (age: 11–15, 7 individuals wP-primed, m/f ratio: 2/5; 5 individuals aP-primed, m/f ratio: 4/1), 12 young adults (age 20–34, wP-primed, m/f ratio: 7/5), and 12 older adults (age 60–70, presumably wP-primed or not vaccinated, m/f ratio: 4/7) completed this study (as part of the PERISCOPE–BERT study). Three children who were initially enrolled dropped out and were replaced by three new participants. From all acquired samples, two baseline B-cell samples were lost due to technical problems (one child and one young adult). Finally, one older adult was excluded due to (potentially) clonal expansion of B cells and replaced by a new participant.

For most participants, the leukocyte, lymphocyte, T-cell, B-cell, and NK-cell counts at baseline were within the normal age-matched range (**Table 1, Supplemental Table S4**), or, in case of minor deviations, fell into the normal range at later time points [41,42]. Leukocytes, lymphocytes, and T cells remained mostly stable over the time of analysis. Although NK-cell numbers showed a minor decrease at day 28, this was most likely not related to the vaccination response (day 0 vs. 28,  $p \leq 0.01$ ; day 7 vs. 28,  $p \leq 0.05$ , **Supplemental Figure S1**). There were no statistically significant differences in absolute leukocyte, lymphocyte, T-cell, and NK-cell counts at baseline between age cohorts. Thus, regarding the numbers of leukocytes, lymphocytes, B cells, T cells, and NK cells, our participants were healthy representatives of the general population.

**Table 1. (next page, continues several pages) Baseline distribution of normal B-cell and plasma cell subsets (cells/ $\mu$ L) in each age cohort.** Ages of the cohorts of which reference values were used: children 5–9 y/o, adolescents 10–17 y/o, young adults 18–39 y/o, older adults 60–79 y/o. The reference values as indicated in this table were selected from the study performed by Blanco et al. [32]. In the before-mentioned study, reference values for B-cell subsets are provided for all age ranges (from cord blood until older adults  $> 80$  y/o). When referring to the reference values indicated here, please refer to the original source data.

| Cohort                    | Children (ch) |       |       | Adolescents (ad) |       |       | Young Adults (yo) |       |       | Older Adults (ol)   |      |       | Statistical Differences Between Cohorts   |           |           |           |
|---------------------------|---------------|-------|-------|------------------|-------|-------|-------------------|-------|-------|---|------|-------|---|-----------|-----------|-----------|
|                           | 7-10 y/o      |       |       | 11-15 y/o        |       |       | 20-34 y/o         |       |       | 60-70 y/o   |      |       | No vaccination history available (presumably WP-primed or not vaccinated) (yo vs. ol) |           |           |           |
| Age                       |               |       |       |                  |       |       | WP                |       |       |   |      |       |   |           |           |           |
| Priming background        | aP            |       |       | Mixed aP and wP  |       |       | wP                |       |       | No vaccination history available (presumably WP-primed or not vaccinated) |      |       | No significant differences found within the other combination (yo vs. ol)             |           |           |           |
|                           | median        | min.  | max.  | median           | min.  | max.  | median            | min.  | max.  | median  | min. | max.  | ch vs. yo   | ch vs. ol | ad vs. yo | ad vs. ol |
| N=                        | 11 †          |       |       | 12               |       |       | 11 †              |       |       | 12  |      |       |   |           |           |           |
| <b>total B-cell</b>       |               |       |       |                  |       |       |                   |       |       |   |      |       |   |           |           |           |
| reference cell counts     | 451           | 157   | 725   | 360              | 174   | 630   | 220               | 41    | 470   | 173   | 36   | 384   | **  | ***       | ns        | *         |
| cell counts               | 496.0         | 346.0 | 966.0 | 430.0            | 133.0 | 667.0 | 279.0             | 141.0 | 481.0 | 244.0   | 53.5 | 396.0 |   |           |           |           |
| <b>pre-GC B-cell</b>      |               |       |       |                  |       |       |                   |       |       |   |      |       |   |           |           |           |
| reference cell counts     | NI            | NI    | NI    | NI               | NI    | NI    | NI                | NI    | NI    | NI  | NI   | NI    | **  | **        | ns        | **        |
| cell counts               | 391.0         | 173.0 | 731.0 | 326.5            | 96.3  | 529.0 | 194.0             | 53.2  | 342.0 | 195.0   | 31.5 | 273.0 |   |           |           |           |
| <b>immature B-cell</b>    |               |       |       |                  |       |       |                   |       |       |   |      |       |   |           |           |           |
| reference cell counts     | 41            | 12    | 84    | 37               | 11    | 111   | 5.6               | 0.25  | 24    | 6.1   | 0.69 | 36    | **  | ****      | ns        | **        |
| cell counts               | 26.6          | 9.5   | 70.4  | 20.8             | 1.6   | 43.7  | 5.9               | 1.1   | 19.8  | 4.7   | 0.6  | 9.2   |   |           |           |           |
| <b>CD5+ naive B-cell</b>  |               |       |       |                  |       |       |                   |       |       |   |      |       |   |           |           |           |
| reference cell counts     | NI            | NI    | NI    | NI               | NI    | NI    | NI                | NI    | NI    | NI  | NI   | NI    | *   | ***       | ns        | *         |
| cell counts               | 89.7          | 25.0  | 248.0 | 49.8             | 5.2   | 166.0 | 30.9              | 7.8   | 152.0 | 15.3  | 2.4  | 47.0  |   |           |           |           |
| <b>naive B-cell</b>       |               |       |       |                  |       |       |                   |       |       |   |      |       |   |           |           |           |
| reference cell counts     | 265           | 68    | 505   | 189              | 75    | 401   | 111               | 13    | 288   | 109   | 20   | 280   | **  | *         | ns        | *         |
| cell counts               | 260.0         | 124.0 | 483.0 | 238.5            | 89.4  | 335.0 | 160.0             | 44.0  | 186.0 | 150.0   | 24.9 | 250.0 |   |           |           |           |
| <b>memory B-cell</b>      |               |       |       |                  |       |       |                   |       |       |   |      |       |   |           |           |           |
| reference cell counts     | 123           | 64    | 282   | 68               | 31    | 160   | 91                | 23    | 221   | 56  | 13   | 128   | ns  | **        | ns        | ns        |
| cell counts               | 160.0         | 76.1  | 252.0 | 96.2             | 33.6  | 193.0 | 85.7              | 31.3  | 282.0 | 63.8  | 21.1 | 171.0 |   |           |           |           |
| <b>IgMD+ memory cells</b> |               |       |       |                  |       |       |                   |       |       |   |      |       |   |           |           |           |
| reference cell counts     | 54            | 23    | 147   | 29               | 17    | 78    | 38                | 7.9   | 122   | 27  | 7.4  | 72    | *   | ****      | ns        | ns        |
| cell counts               | 65.7          | 30.7  | 129.0 | 48.8             | 16.0  | 141.0 | 37.4              | 10.0  | 121.0 | 20.8  | 8.6  | 93.2  |   |           |           |           |
| <b>IgG1+ memory cells</b> |               |       |       |                  |       |       |                   |       |       |   |      |       |   |           |           |           |
| reference cell counts     | 30            | 12    | 86    | 18               | 7     | 42    | 18                | 3.2   | 40    | 9.1   | 1.3  | 22    | *   | ****      | ns        | **        |
| cell counts               | 47.8          | 15.2  | 81.7  | 17.3             | 6.8   | 44.7  | 13.2              | 5.4   | 72.5  | 16.5  | 2.8  | 27.8  |   |           |           |           |

3.2



|                           | median | min.  | max. | median | min.  | max. | median | min.  | max. | median | min.  | max. | ch vs. yo | ch vs. ol | ch ad vs. ad yo |
|---------------------------|--------|-------|------|--------|-------|------|--------|-------|------|--------|-------|------|-----------|-----------|-----------------|
| <b>IgG2+ memory cells</b> |        |       |      |        |       |      |        |       |      |        |       |      |           |           |                 |
| reference cell counts     | 4.4    | 0.7   | 15   | 3.0    | 0.7   | 10   | 5.9    | 1.6   | 30   | 3.6    | 1.0   | 11   | *         | ***       | ns ns           |
| cell counts               | 3.8    | 1.6   | 10.3 | 2.8    | 1.4   | 4.4  | 3.1    | 1.1   | 12.3 | 2.8    | 0.6   | 13.4 |           |           |                 |
| <b>IgG3+ memory cells</b> |        |       |      |        |       |      |        |       |      |        |       |      |           |           |                 |
| reference cell counts     | 7.4    | 2.4   | 16   | 3.0    | 1.1   | 8.3  | 3.0    | 0.5   | 8.4  | 2.3    | 0.4   | 8.1  | *         | **        | ns ns           |
| cell counts               | 7.9    | 3.2   | 13.0 | 3.1    | 0.6   | 7.1  | 1.8    | 0.8   | 6.4  | 2.1    | 0.5   | 7.4  |           |           |                 |
| <b>IgG4+ memory cells</b> |        |       |      |        |       |      |        |       |      |        |       |      |           |           |                 |
| reference cell counts     | 0.4    | <0.01 | 2.0  | 0.2    | <0.01 | 2.9  | 0.4    | <0.01 | 2.4  | 0.4    | <0.01 | 2.1  | ns        | ***       | ns ns           |
| cell counts               | 0.2    | <0.05 | 2.2  | 0.3    | <0.05 | 1.0  | 0.5    | 0.1   | 6.1  | 0.3    | 0.1   | 1.2  |           |           |                 |
| <b>IgA1+ memory cells</b> |        |       |      |        |       |      |        |       |      |        |       |      |           |           |                 |
| reference cell counts     | 12     | 4.5   | 24   | 9.0    | 2.9   | 21   | 11     | 2.1   | 43   | 6.2    | 2.2   | 22   | ns        | ns        | ns ns           |
| cell counts               | 16.3   | 6.4   | 34.7 | 11.4   | 4.4   | 14.7 | 8.0    | 3.8   | 42.4 | 11.2   | 4.2   | 30.4 |           |           |                 |
| <b>IgA2+ memory cells</b> |        |       |      |        |       |      |        |       |      |        |       |      |           |           |                 |
| reference cell counts     | 3.2    | 1.0   | 13   | 2.7    | 0.8   | 5.9  | 4.1    | 1.2   | 18   | 3.4    | 0.7   | 9.0  | ns        | **        | ns ns           |
| cell counts               | 4.8    | 1.4   | 10.3 | 2.7    | 0.5   | 6.2  | 3.1    | 0.7   | 17.5 | 2.7    | 0.8   | 9.6  |           |           |                 |
| <b>IgD+ memory cells</b>  |        |       |      |        |       |      |        |       |      |        |       |      |           |           |                 |
| reference cell counts     | 1.1    | <0.01 | 2.9  | 0.3    | <0.01 | 1.7  | 0.2    | <0.01 | 2.4  | 0.01   | <0.01 | 1.2  | *         | **        | ns ns           |
| cell counts               | 1.0    | 0.3   | 2.1  | 0.4    | <0.05 | 1.4  | 0.2    | <0.05 | 2.7  | 0.2    | <0.05 | 0.8  |           |           |                 |
| <b>IgH- memory cells</b>  |        |       |      |        |       |      |        |       |      |        |       |      |           |           |                 |
| reference cell counts     | 2.2    | 0.6   | 4.4  | 1.5    | 0.4   | 2.7  | 1.2    | 0.5   | 1.8  | 0.9    | 0.3   | 3.0  | ns        | ns        | ns ns           |
| cell counts               | NI     | NI    | NI   | NI     | NI    | NI   | NI     | NI    | NI   | NI     | NI    | NI   |           |           |                 |
| <b>total plasma cells</b> |        |       |      |        |       |      |        |       |      |        |       |      |           |           |                 |
| reference cell counts     | 13     | 3.5   | 45   | 8.5    | 1.3   | 27   | 4.4    | 1.1   | 25   | 1.2    | 0.3   | 7.1  | ns        | *         | ns ns           |
| cell counts               | 8.5    | 3.8   | 12.9 | 3.4    | 1.6   | 13.1 | 2.6    | 1.2   | 8.5  | 1.6    | 0.2   | 6.1  |           |           |                 |
| <b>IgM+ plasma cells</b>  |        |       |      |        |       |      |        |       |      |        |       |      |           |           |                 |
| reference cell counts     | 1.4    | 0.6   | 14   | 0.8    | 0.2   | 5.7  | 0.4    | 0.05  | 4.7  | 0.1    | 0.01  | 0.8  | ns        | ns        | ns ns           |
| cell counts               | 1.3    | 0.3   | 2.9  | 0.6    | 0.4   | 2.0  | 0.4    | 0.1   | 2.8  | 0.1    | <0.05 | 0.8  |           |           |                 |
| <b>IgG1+ plasma cells</b> |        |       |      |        |       |      |        |       |      |        |       |      |           |           |                 |
| reference cell counts     | 1.9    | 0.1   | 7.7  | 1.1    | 0.1   | 4.8  | 0.4    | 0.05  | 4.4  | 0.1    | 0.01  | 0.6  | **        | **        | ns ns           |
| cell counts               | 1.5    | 0.2   | 2.7  | 0.4    | 0.1   | 5.6  | 0.4    | 0.1   | 1.3  | 0.2    | 0.1   | 0.6  |           |           |                 |
| <b>IgG2+ plasma cells</b> |        |       |      |        |       |      |        |       |      |        |       |      |           |           |                 |
| reference cell counts     | 0.7    | 0.07  | 2.3  | 0.5    | 0.08  | 0.8  | 0.2    | <0.01 | 2.6  | 0.09   | <0.01 | 1.6  | ns        | ns        | ns ns           |
| cell counts               | 0.8    | 0.2   | 1.1  | 0.3    | 0.1   | 1.5  | 0.2    | <0.05 | 0.6  | 0.1    | <0.05 | 1.2  |           |           |                 |

|                           | median | min.  | max. | median | min.  | max. | median | min.  | max. | median | min.  | max.  | ch vs. yo | ch vs. ol | ch vs. ad | ad vs. ol |
|---------------------------|--------|-------|------|--------|-------|------|--------|-------|------|--------|-------|-------|-----------|-----------|-----------|-----------|
| <b>IgG3+ plasma cells</b> |        |       |      |        |       |      |        |       |      |        |       |       |           |           |           |           |
| reference cell counts     | 0.2    | <0.01 | 1.3  | 0.08   | <0.01 | 0.4  | 0.03   | <0.01 | 0.3  | <0.01  | <0.01 | 0.2   | *         | **        | ns        | ns        |
| cell counts               | 0.2    | <0.05 | 0.5  | <0.05  | <0.05 | 0.9  | <0.05  | <0.05 | 0.1  | <0.05  | <0.05 | 0.1   |           |           |           |           |
| <b>IgG4+ plasma cells</b> |        |       |      |        |       |      |        |       |      |        |       |       |           |           |           |           |
| reference cell counts     | 0.02   | <0.01 | 0.2  | <0.01  | <0.01 | 0.2  | <0.01  | <0.01 | 0.4  | <0.01  | <0.01 | 0.1   | ns        | ns        | ns        | ns        |
| cell counts               | <0.05  | <0.05 | 0.2  | <0.05  | <0.05 | 0.2  | <0.05  | <0.05 | 0.7  | <0.05  | <0.05 | 0.1   |           |           |           |           |
| <b>IgA1+ plasma cells</b> |        |       |      |        |       |      |        |       |      |        |       |       |           |           |           |           |
| reference cell counts     | 4.4    | 0.6   | 16   | 3.1    | 0.5   | 14   | 1.7    | 0.3   | 6.9  | 0.4    | 0.04  | 3.3   | ns        | ns        | ns        | ns        |
| cell counts               | 3.4    | 0.6   | 5.6  | 1.3    | 0.4   | 4.1  | 1.1    | 0.4   | 3.3  | 0.7    | 0.1   | 3.0   |           |           |           |           |
| <b>IgA2+ plasma cells</b> |        |       |      |        |       |      |        |       |      |        |       |       |           |           |           |           |
| reference cell counts     | 1.5    | 0.3   | 3.5  | 1.0    | 0.3   | 3.6  | 0.7    | 0.2   | 4.2  | 0.3    | 0.06  | 1.2   | ns        | ns        | ns        | ns        |
| cell counts               | 1.0    | 0.3   | 2.7  | 2.7    | 0.5   | 6.2  | 0.3    | 0.1   | 1.1  | 0.2    | 0.1   | 1.2   |           |           |           |           |
| <b>IgD+ plasma cells</b>  |        |       |      |        |       |      |        |       |      |        |       |       |           |           |           |           |
| reference cell counts     | 0.04   | <0.01 | 0.8  | <0.01  | <0.01 | 2.0  | <0.01  | <0.01 | 1.1  | <0.01  | <0.01 | 0.2   | **        | **        | *         | ns        |
| cell counts               | 0.1    | <0.05 | 0.6  | <0.05  | <0.05 | 0.1  | <0.05  | <0.05 | 0.1  | <0.05  | <0.05 | <0.05 | <0.05     | <0.05     | <0.05     | <0.05     |

† in children and young adults, for one included donor no baseline B-cell data was available.

NI= not indicated

\*  $p < 0.05$  \*\*  $p \leq 0.01$  \*\*\*  $p \leq 0.001$  \*\*\*\*  $p \leq 0.0001$

3.2

### **Higher Counts of Naive B Cells and Plasma Cells in Children**

B-cell numbers are known to decrease over time from an average of 1400 cells/ $\mu\text{L}$  in children <2 years to 200 cells/ $\mu\text{L}$  in adults [32,41]. This trend was also visible in our dataset, where children had more B cells than the adult groups (**Table 1**). This difference was mainly due to high numbers of pre-germinal center (naive) B cells in children. Although memory B-cell numbers were also higher in children than in adults (160 cells/ $\mu\text{L}$  in children vs. 85.7 cells/ $\mu\text{L}$  in young adults, n.s., and 160 cells/ $\mu\text{L}$  in children vs. 63.8 cells/ $\mu\text{L}$  in older adults,  $p \leq 0.01$ ), these differences were less prominent, and mainly restricted to IgG1+ and IgG3+ memory B cells. Finally, several plasma cell subsets were significantly more abundant in children than in adults (IgG1+, IgG3+, and IgD+ plasma cells), but due to their overall low frequencies, this did not have a major impact on total B-cell numbers. Limited differences in B-cell subset numbers were observed between adolescents and adults (**Table 1**). These differences were predominantly found in pre-germinal center (naive) B cells and individual plasma cell subsets. Thus, baseline cell numbers of B-cell subsets differed between the cohorts, which was in line with previously published data of age-matched individuals [32].

### **Expansion of Plasma Cells as the Most Prominent Cellular B-cell Change after Vaccination**

We have recently shown that aP booster vaccination in (wP-primed) adults triggers several cellular changes, of which the expansion of (predominantly) IgG1+ plasma cells at day 7 is most prominent [33]. Now, we set out to determine whether the same types of changes occur in vaccinated individuals, irrespective of age and primary vaccination background.

Total B cells, pre-germinal center B cells, and memory B cells remained relatively stable and did not show any consistent fluctuations over time following vaccination. However, in all participants, plasma cells underwent significant expansion between baseline and day 7 ( $p \leq 0.01$  for children, and  $p \leq 0.001$  for adolescents and the adult cohorts, **Figure 1**). The magnitude of this expansion was highly similar in children, adolescents, and young adults (ratio to baseline: 2.6–3.4) and was significantly higher in older adults compared with children (ratio: 2.6 in children vs. 5.7 in older adults,  $p \leq 0.01$ ). Total plasma cell numbers returned to baseline at day 14 or, if day 14 was not measured, day 28 ( $p \leq 0.001$  for adolescents, young and older adults; in the children cohort, plasma cell counts were still slightly elevated at day 28). Thus, the expansion of plasma cells 7 days postvaccination was the most prominent change in all age groups.

### **Despite Individual Differences, Skewing towards IgG1+ Plasma Cell Responses in all Cohorts**

Cell expansion at day 7 was not equally pronounced in all plasma cell subsets. It was most prominent in IgG1+ plasma cells (ratio to baseline: 5.7–17.6, depending on cohort,  $p \leq 0.001$  in all cohorts, with a higher increase in older adults compared with children,  $p < 0.05$ ). This was followed by IgG3+ plasma cells (ratio: 3.6–6.5,  $p \leq 0.01$  in children and adolescents, and  $p \leq 0.001$  in young and older

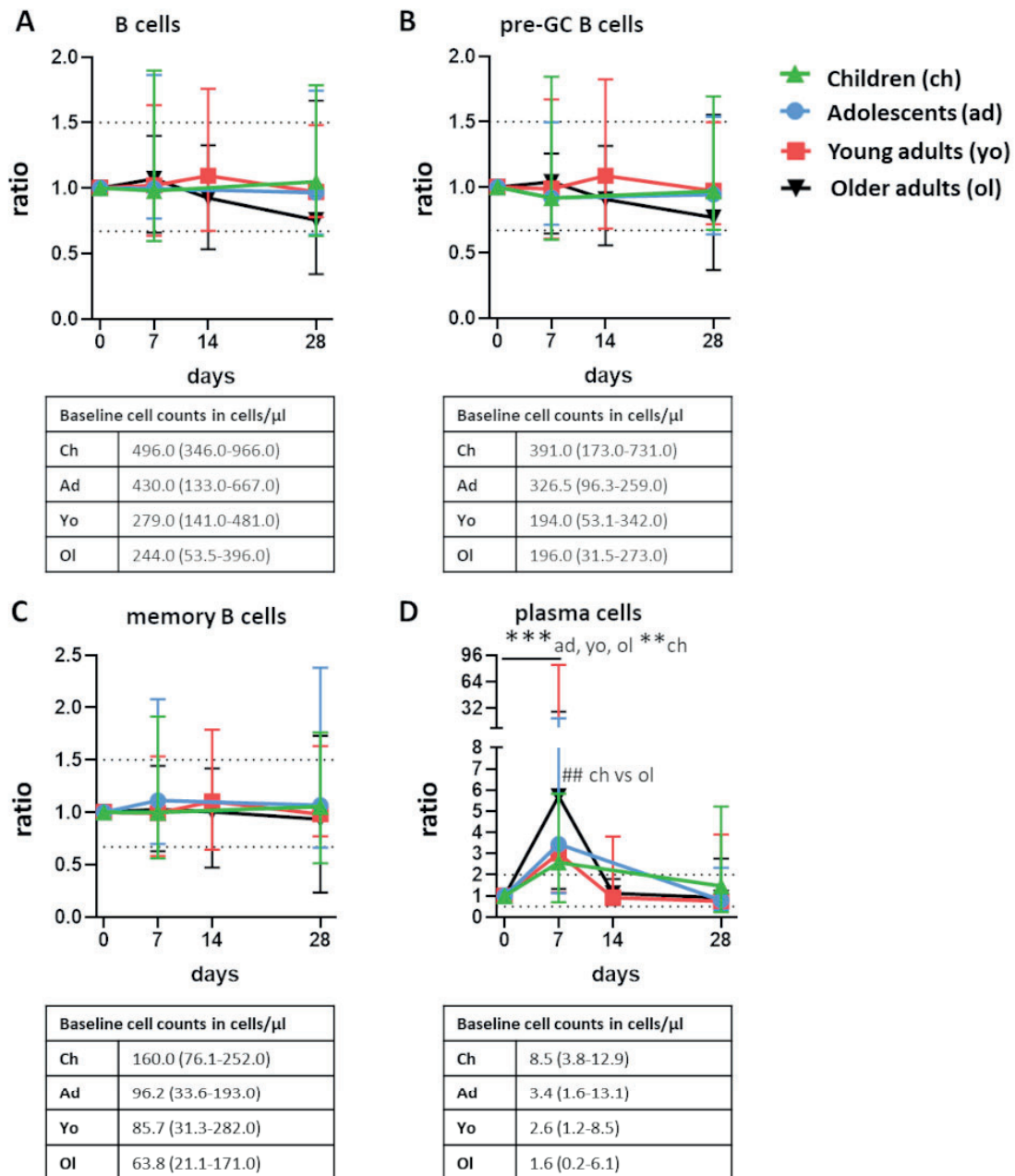


**Figure 1. Postvaccination fluctuations of major B-cell subsets. Fluctuations of (A) total B cells (B) pre-germinal center (pre-GC) B cells, (C) memory B cells, and (D) plasma cells postvaccination presented as ratio over baseline (median, min-max).** For total B cells, pre-GC B cells, and memory B cells, the dashed lines indicate a ratio over baseline of 0.67 and 1.5. For plasma cells, the dashed lines indicate a ratio over baseline of 0.5 and 2.0. Underneath each graph, the baseline cell counts per cohort are presented in cells/ $\mu$ L (median, min-max). To assess longitudinal changes within each cohort, Wilcoxon matched pair signed-rank test followed by Bonferroni correction was used. To test differences between cohorts at one timepoint, Kruskal–Wallis followed by Dunn’s test was used, with exception of the comparison at day 14. At day 14, only blood samples from the adult cohorts were collected; here, the Mann–Whitney test followed by Bonferroni correction was used. For longitudinal changes, only significant differences compared with baseline are shown. Significant longitudinal differences within a cohort are indicated as \*\*,  $p \leq 0.01$ ; \*\*\*,  $p \leq 0.001$ . Significant differences between cohorts at the same time point are indicated as ##,  $p \leq 0.01$ .

adults, **Figure 2A**). IgG4+ plasma cells were significantly increased in children and adolescents (ratio: 5.1 and 7.2, respectively,  $p \leq 0.01$ ). IgG2+ plasma cells were significantly increased in adolescents only (ratio: 1.8,  $p \leq 0.001$ ). IgA1+ plasma cells were significantly increased in both adult cohorts (ratio: 2.1 and 3.9 in younger and older adults,  $p \leq 0.01$  and  $p \leq 0.001$ , respectively). Although IgM+ plasma cells seemed to expand at day 7 in older adults, there was a large variation between individuals and the difference was not statistically significant.

Despite individual changes in response patterns between the cohorts, IgG1+ plasma cells were the most expanded subset. They constituted between 43% (young adults) and 61% (adolescents) of all plasma cells at the peak of expansion, while only at most 18% at baseline (**Figure 2B**). Although the ratio (to baseline) of plasma cells was often higher in adults than in children, children had higher baseline IgG1+ plasma cell numbers, and also higher IgG1+ plasma cell numbers at day 7 (median cell count at day 7: 7.64 cells/ $\mu$ L in children vs. 3.81 cells/ $\mu$ L in older adults, ns). Thus, the expansion of IgG1+ plasma cells was the most prominent in all cohorts. Both an increase over baseline (ratio) and in absolute cell numbers were observed.

### **Maturation of Plasma Cells over Time Following Vaccination**

Newly generated plasma cells migrate from germinal centers via the blood stream to become long-lived antibody-secreting plasma cells in the bone marrow and other peripheral tissues. Over time, they gradually lose expression of CD20 and gain expression of CD138 [43] (**Figure 3A**). We used this information to divide plasma cells into consecutive maturation stages and to trace their maturation over time after booster vaccination.

Plasma cells representing all maturation stages were expanded at day 7 (**Supplemental Figure S2** for total plasma cells, **Figure 3** for IgG1+ plasma cells). This expansion was limited in the least mature CD20+CD138- plasma cells (ratio to baseline: up to 3.1 in IgG1+ plasma cells in children, **Figure 3B**), clearer in intermediate CD20-CD138- plasma cells (ratio to baseline: up to 22.7 in IgG1+ plasma cells in young adults, in all cohorts  $p \leq 0.01$  or  $p \leq 0.001$ ), and most prominent in the most mature CD20-CD138+ plasma cells (ratio to baseline: up to of 115.6 in young adults, in all cohorts  $p \leq 0.01$  or  $p \leq 0.001$ ). Similar to what was observed for total plasma cells, expansion of IgG1+ plasma cells belonging to different maturation stages was least prominent in children. In all cohorts, a significant increase in the percentage of the most mature plasma cells was observed, except for the adolescent cohort, showing just a trend. At day 7 postvaccination, most mature plasma cells constituted between 42% and 53% of IgG1+ plasma cells (**Figure 3C**). Thus, the expansion of plasma cells at day 7 postvaccination was accompanied by a shift towards a more mature plasma cell phenotype in all cohorts.

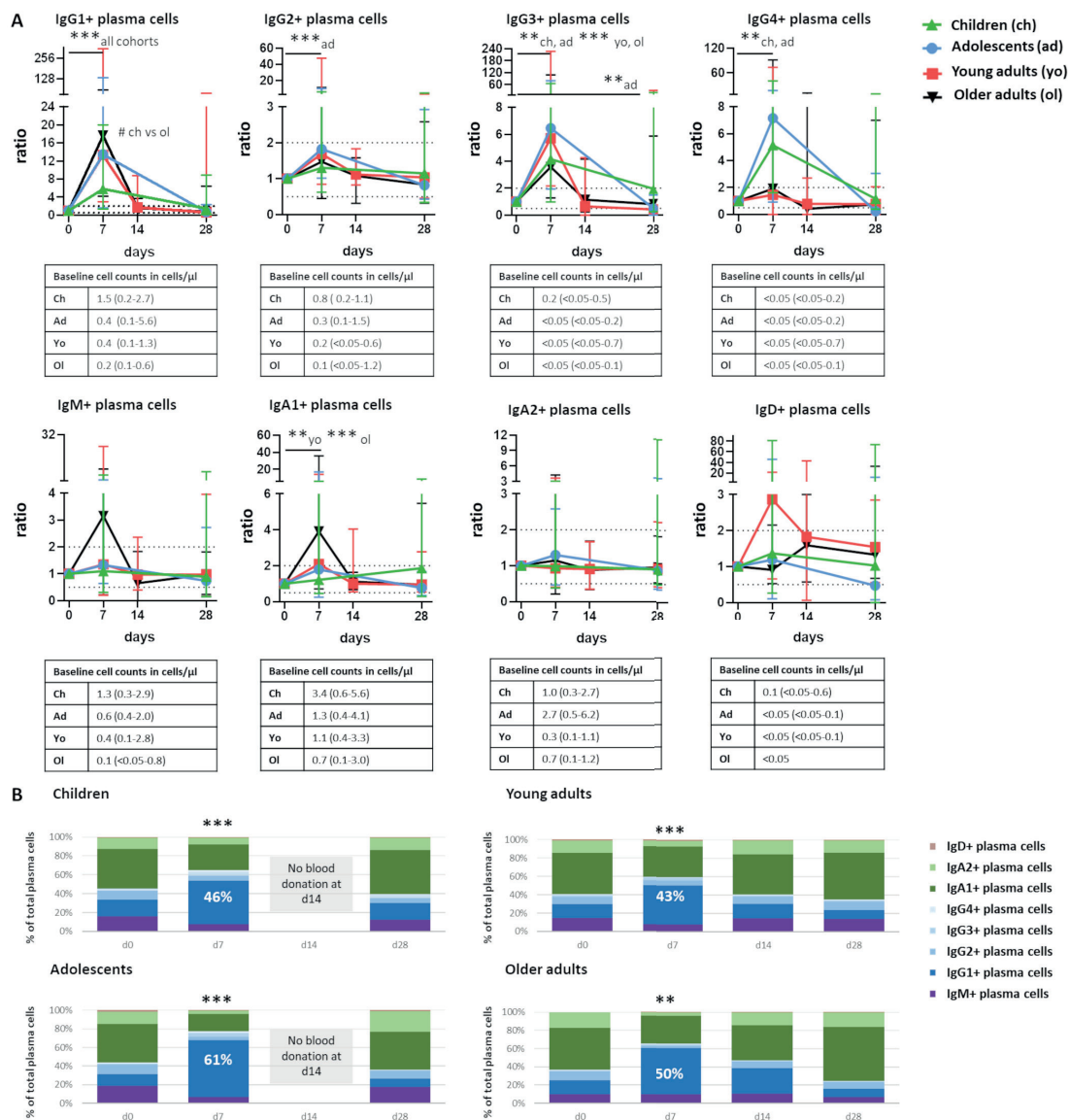


**Figure 2. Individuals of all age groups underwent expansion of IgG1+ plasma cells at day 7 postvaccination.** (A) Quantitative changes in plasma cells expressing different Ig subclasses, presented as ratio over baseline (median, min-max). Each symbol represents a median value with range. Dashed lines indicate a ratio over baseline of 0.5 and 2. Underneath each graph, the baseline cell counts per cohort are presented in cells/μL (median, min-max). Wilcoxon matched pair signed-rank test followed by Bonferroni correction was used to assess longitudinal differences within each cohort. Differences in ratio at day 7 between cohorts were assessed using Kruskal–Wallis followed by Dunn’s test. (B) Over-time distribution of plasma cells expressing different Ig subclasses. Median values for each population were used to construct the plots. Wilcoxon matched pair signed-rank test followed by Bonferroni correction was used to assess longitudinal differences in the percentage of IgG1+ cells in the total plasma cell compartment within each cohort. Differences in the percentage of IgG1+ cells in total plasma cell compartment between cohorts were assessed using Kruskal–Wallis followed by Dunn’s test but did not yield significant differences. For pediatric cohorts, no blood samples were collected at day 14; the Mann–Whitney test followed by Bonferroni correction was used. For longitudinal changes, only significant differences compared with baseline are shown. Significant longitudinal differences within a cohort are indicated as \*\*,  $p \leq 0.01$ ; \*\*\*,  $p \leq 0.001$ . Significant differences between cohorts at the same time point are indicated as #,  $p < 0.05$ . d = days after vaccination.



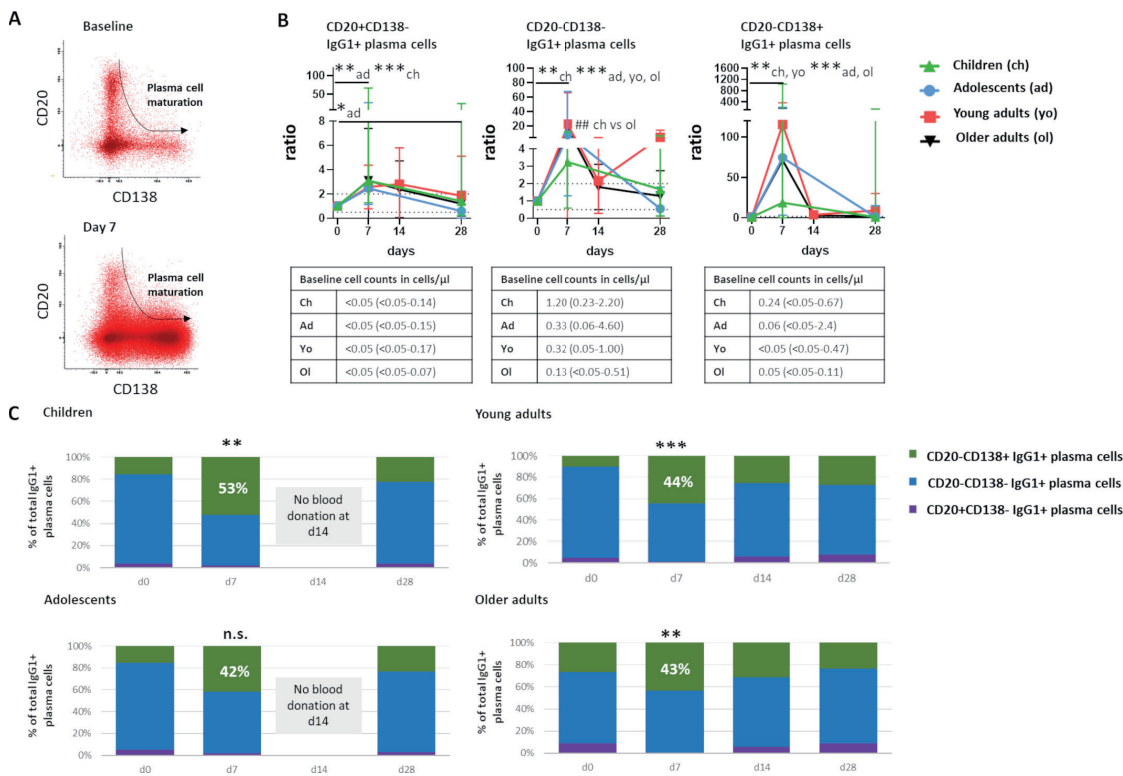


**Figure 3. Over-time maturation of IgG1+ plasma cells.** (A) Representative dot plots showing the phenotypical changes during plasma cell maturation. The top plot shows a baseline situation and the bottom plot shows a situation at day 7 postvaccination. Each dot represents an individual cell. The arrow indicates the direction of changes during maturation. (B) Over-time quantitative changes in IgG1+ plasma cells belonging to different maturation stages, presented as ratio over baseline (median, min-max). Dashed lines indicate a ratio over baseline of 0.5 and 2. Underneath each graph, a table shows the baseline cell counts of that population in cells/ $\mu$ L (median, min-max). (C) Over-time distribution of IgG1+ plasma cells representing different maturation stages with total IgG1+ plasma cells based on expression of CD20 and CD138. Median values for each population were used to construct the plots. Wilcoxon matched pair signed-rank test followed by Bonferroni correction was used to assess longitudinal differences in percentage of CD20-CD138+ cells in total IgG1+ plasma cells within each cohort. Differences in the percentage of CD20-CD138+ cells in total IgG1+ plasma cells between cohorts were assessed using Kruskal–Wallis followed by Dunn’s test but did not yield significant differences. For pediatric cohorts, no blood samples were collected at day 14; the Mann–Whitney test followed by Bonferroni correction was used. For longitudinal changes, only significant differences compared with baseline are shown. Significant longitudinal differences within a cohort are indicated as \*,  $p < 0.05$ ; \*\*,  $p \leq 0.01$ ; \*\*\*,  $p \leq 0.001$ . Significant differences between cohorts at the same time point are indicated as ##,  $p \leq 0.01$ . d = days after vaccination.

As an expansion of IgA1+ plasma cells was observed in the adult cohorts, we evaluated maturation of IgA1+ plasma cells at the peak of expansion as well. In children, no increase in more mature (CD20-CD138- and CD20-CD138+) IgA1+ plasma cells was observed at the peak of expansion. In adolescents, a small increase of the most mature (CD20-CD138+) IgA1+ plasma cells was observed, and in both adult cohorts, an increase in both intermediate and the most mature (CD20-CD138- and CD20-CD138+) IgA1+ plasma cells was observed at the peak of plasma cell expansion (adolescent cohort:  $p < 0.05$ , adult cohorts:  $p \leq 0.01$ ). When comparing all cohorts at 7 days postvaccination, a higher expansion of the most mature IgA1+ plasma cells was observed in older adults compared with children

( $p \leq 0.01$ ). Thus, the expansion and maturation of IgA1+ plasma cells seemed to increase with the age of the cohort. However, within the oldest cohort, no correlation was found between total IgA plasma cells, IgA1+ plasma cells, or vaccine-specific IgA cells, and age.

### **No Clear Changes in the Memory B-cell Compartment over Time Following Vaccination**

While mature antibody-secreting plasma cells predominantly reside in bone marrow and only transiently appear in blood, memory B cells form the circulating component of immunological memory. In the steady state, memory B cells (directed against various antigens) are known to be abundant in blood of both children and adults, and undergo limited quantitative changes following antigen exposure [44,45]. Still, memory B cells with specific reactivities can be detected in the blood stream [45–47]. In our previous study, we showed that even minor expansions in circulating memory B cells can strongly correlate with a postvaccination increase in Bp-specific serum Ig levels [33]. Therefore, we set out to determine whether any quantitative changes can be observed at selected time points and whether the same pattern is shared by different cohorts.

Neither total memory B cells nor any of the major memory B-cell subsets underwent consistent quantitative changes over time following vaccination (**Figure 4A**). One exception was the IgG4+ memory B-cell subset in adolescents, which showed a minor but significant increase at day 28 compared with baseline levels. Moreover, at 14 days postvaccination, there was a minor but significant difference between the number of IgG3+ memory B cells between young and older adults, although there were no significant longitudinal changes within any of the groups. Within each cohort, the distribution of memory B-cell subsets was stable over the time of analysis (**Figure 4B**). However, upon further subdivision of memory B cells based on the expression of CD20, CD21, CD24, and CD27, two memory B-cell subsets underwent significant fluctuations over time (Supplemental Figure S3). In adolescents, there was a significant increase in IgG1+ CD20++CD21-CD24+ memory B cells at day 28 after vaccination. Moreover, in adolescents and older adults, there was a significant increase in IgG1+ CD20++CD21-CD24-CD27+ memory B cells at days 14 or 28 after vaccination compared with baseline. Therefore, it is possible that memory B cells specific to Boostrix-IPV vaccine reside within these CD20++CD21- memory B cells. Here, the use of an Ag-specific approach should lead to additional insights. No significant differences were observed between the cohorts. Although most of subsets defined within IgG1+ memory B cells were significantly more numerous in children than in both adult cohorts (data not shown), this was mainly due to higher numbers of IgG1+ memory B cells in children at baseline. Thus, except for a few minor fluctuations, no differences in the number of memory B cells were observed after Tdap booster vaccination.

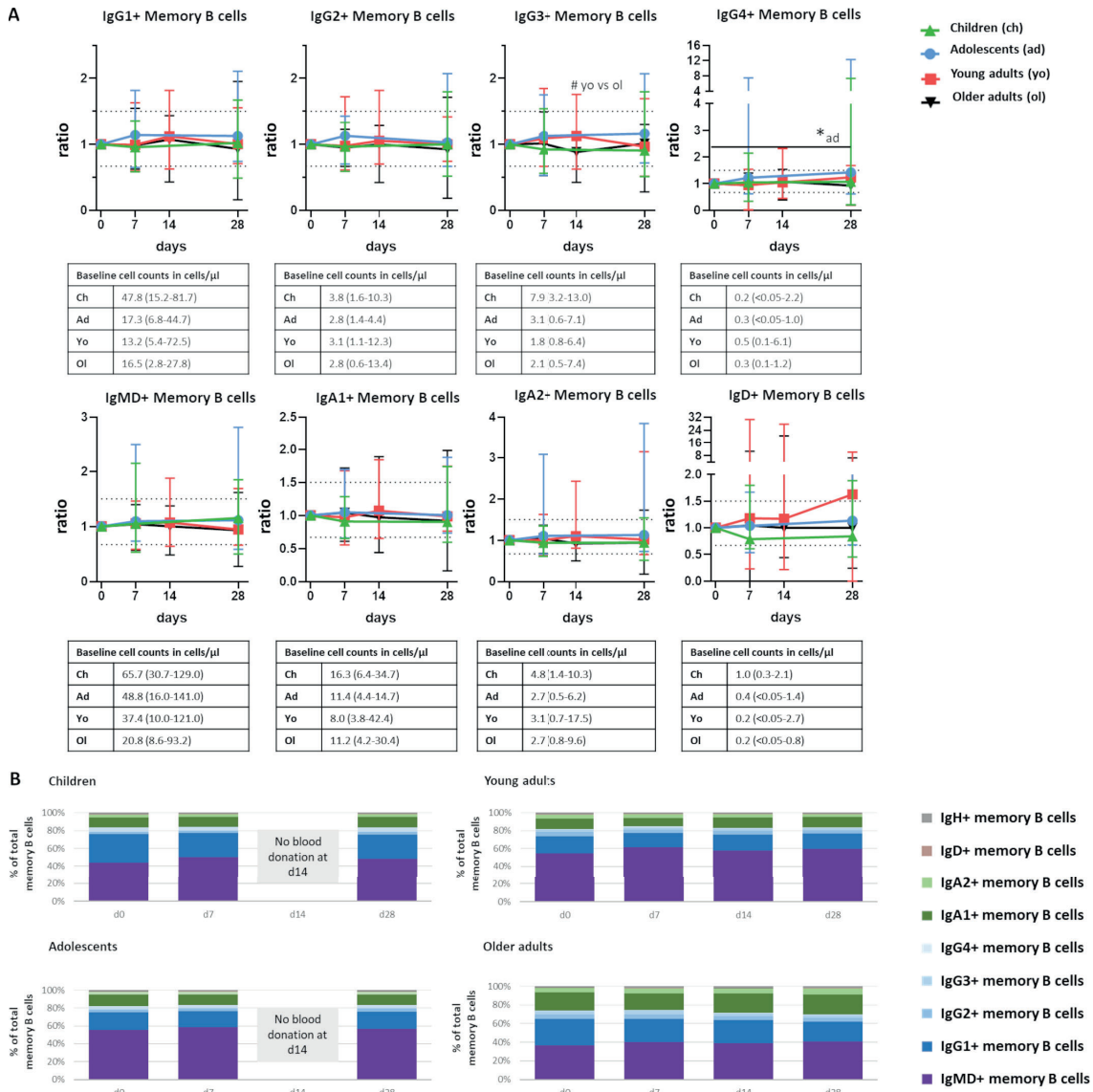


**Figure 4. Stable distribution of memory B-cell subsets over time after vaccination.** (A) Quantitative changes in memory B cells expressing different Ig subclasses, presented as ratio over baseline (median, min-max). Dashed lines indicate a ratio over baseline of 0.67 and 1.5. Underneath each graph, a table shows the baseline cell counts of that population in cells/ $\mu$ L (median, min-max). (B) Over-time distribution of memory B cells expressing different Ig subclasses within the total memory B-cell compartment. Median values for each population were used to construct the plots. Wilcoxon matched pair signed-rank test followed by Bonferroni correction was used to assess longitudinal differences within each cohort. Differences between cohorts were assessed using Kruskal–Wallis followed by Dunn’s test but did not yield significant differences. For pediatric cohorts, no blood samples were collected at day 14; the Mann–Whitney test followed by Bonferroni correction was used. For longitudinal changes, only significant differences compared with baseline are shown as \*,  $p < 0.05$ . Significant differences between cohorts at the same time point are indicated as #,  $p < 0.05$ . d = days after vaccination.

### Good Correlation between the Increase in Plasma Cell Numbers with the Vaccine-Specific Antibody-Producing Cells

Plasma cells are the main producers of antibodies, and, in a recall response, are mainly generated from Ag-specific memory B cells originating from a previous encounter. To support our flow cytometry-based monitoring of memory B- and plasma cell fluctuations, we determined the increase in numbers of vaccine-specific plasma and memory B cells upon vaccination via ELISpot.

Previous studies on influenza have found that Ag-specific plasma cells generated after vaccination represent up to 80% of the total plasma cell pool [30,31]. Therefore, we correlated numbers of total plasma cells (non-Ag-specific) as determined by flow cytometry to those specific for the vaccine components as determined by ELISpot analysis. In our Tdap-IPV vaccination study, the absolute increase in IgG and IgA plasma cell numbers from baseline to day 7 and the number of vaccine-specific IgG- and IgA-producing plasma cells at day 7 showed a positive correlation, indicating that the increase in total IgG and IgA plasma cells is explained by the increase in Ag-specific IgG and IgA plasma cells (IgG:  $r = 0.59$ ,  $p < 0.0001$ ; IgA:  $r = 0.60$ ,  $p < 0.0001$ ) (**Figure 5**).

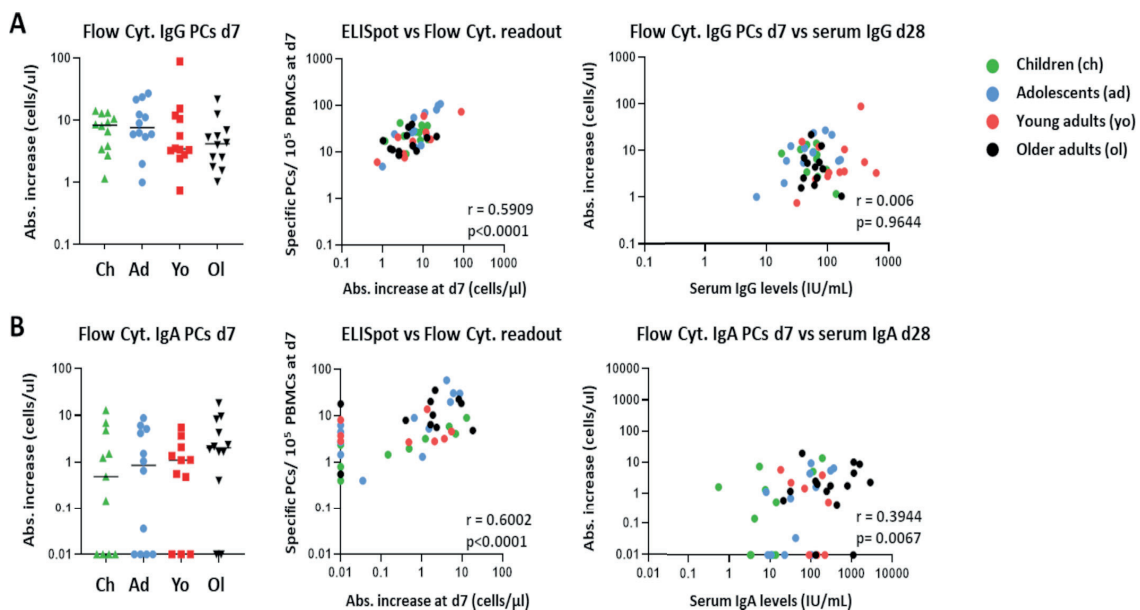


**Figure 5. Correlation between cellular changes as measured by flow cytometry and ELISpot, and the correlation between plasma cell expansion and vaccine-specific serum Igs 28 days postvaccination.** (A) Left panel: expansion of IgG+ plasma cells (day 7) per individual, expressed as absolute increase in cells/ $\mu$ L. Middle panel: correlation between the ELISpot and flow cytometry readout for IgG+ plasma cells. Right panel: correlation between the increase in plasma cells (as measured by flow cytometry) and the vaccine-specific serum IgG levels (day 28). (B) Left panel: expansion of IgA1+ plasma cells (day 7) per individual, expressed as absolute increase in cells/ $\mu$ L. Middle panel: correlation between the ELISpot and flow cytometry readout for IgA+ plasma cells. Right panel: correlation between the increase in plasma cells (as measured by flow cytometry) and the vaccine-specific serum IgA levels (day 28). Each dot represents a single donor. Of note, for visualization purposes, all absolute increases lower than 0.01 were set to 0.01. The original values were used to calculate the Spearman correlations. Flow Cyt. = flow cytometry; PCs = plasma cells; d = days after vaccination; Abs. = absolute.

## Chapter 3.2

---

Next, we evaluated whether the expansion of circulating IgG<sup>+</sup> and IgA<sup>+</sup> plasma cells at day 7 could predict the increase in serum IgG and IgA at day 28 and year 1 postvaccination. We correlated the increase in IgG<sup>+</sup> and IgA<sup>+</sup> plasma cells (measured by flow cytometry) with the levels of vaccine-specific serum IgG and IgA at day 28 and year 1. Although plasma cells had no predictive value for serum IgG levels, a positive correlation was found for serum IgA levels ( $r = 0.3944$ ,  $p = 0.0067$ ). Although weaker, this correlation was still present at year 1 postvaccination ( $r = 0.3403$ ,  $p = 0.0207$ ).

For memory B cells, no correlation was observed between the ELISpot readout and flow cytometry readout (**Supplemental Figure S4**). Neither flow cytometry IgG nor IgA memory readout correlated with vaccine-specific serum Igs at day 28 or year 1 (data not shown). These findings indicate that for analysis of memory B cells by flow cytometry, an Ag-specific approach is required. As differences in cellular changes could be found between the different age groups, we also tested for correlations between cell expansion (ratio over baseline) and vaccine-specific serum Ig (IU/mL) within each age group (**Supplemental Figure S5**). No correlations between cell expansion and serum Ig levels were found.

Thus, the expansion of total plasma cells measured by flow cytometry correlated with the expansion of Ag-specific plasma cells measured by ELISpot. In this regard, flow cytometry and ELISpot can provide complementary data. This is not observed for memory B cells.

### **Weak Positive Correlation between Plasma Cell Expansion and Vaccine-Component-Specific Ig Levels**

As the response to individual vaccine components may differ, we next correlated the IgG<sup>1+</sup> and IgA<sup>1+</sup> plasma cell expansions at day 7 postvaccination with the levels of serum IgG and IgA directed against individual pertussis vaccine components. Additionally, we tested whether the degree of maturation correlated with vaccine-component-specific IgG or IgA levels. Within the IgG<sup>1+</sup> plasma cells, the strongest correlations (with a correlation coefficient between 0.3–0.5) were found between PT- or Prn-specific IgG levels and total IgG<sup>1+</sup> plasma cells or CD20-CD138- IgG<sup>1+</sup> plasma cells (**Supplemental Table S5** (IgG)). No correlations were observed between IgG<sup>1+</sup> memory B-cell expansion and vaccine-component-specific serum IgG. Correlations between IgA<sup>1+</sup> plasma cells and serum IgAs against individual pertussis components were higher and more frequent (ranging between 0.3–0.6, **Supplemental Table S6**). Most correlations were found between FHA-specific serum IgAs and the increase in total IgA<sup>1+</sup> plasma cells, CD20-CD138- IgA<sup>1+</sup> plasma cells, and CD20-CD138+ IgA<sup>1+</sup> plasma cells. Considerably fewer correlations were found between PT- and Prn-specific serum IgAs and the increase in IgA<sup>1+</sup> plasma cells. Interestingly, a positive correlation was found between the maximum expansion of IgA<sup>1+</sup> memory B cells and the FHA-specific serum IgAs at year 1 postvaccination (ratio over baseline).



### More Prominent Cellular Responses in Participants Primed with wP Vaccine

Due to the change in the National Immunization Program on 1 January 2005, all children and 5 out of 12 adolescents were primed with an aP vaccine, while 7 adolescents and all young adults received the Dutch wP vaccine in childhood (presumably, older adults were vaccinated with wP or had received no pertussis vaccination during childhood). It has been previously shown that the primary vaccine can impact both T-cell and antibody responses [16,18,22–24]. As antibodies are the product of plasma cells, we studied whether B-cell and plasma cell responses are also influenced by the primary vaccine. To avoid the effect of age, we first compared both subgroups of adolescents.

Over-time changes in numbers of total, naive, and memory B cells were minor and comparable between wP- and aP-primed adolescents (**Figure 6A**). In contrast, changes in plasma cell numbers were much more prominent in adolescents who were primed with the Dutch wP vaccine vs. aP-primed adolescents (ratio to baseline: 4.8 vs. 1.5 at day 7 in total plasma cell numbers). From all plasma cells, the differences were the clearest for IgG1+ (ratio: 23.9 vs. 4.5 at day 7), IgG3+ (ratio: 19.7 vs. 3.7 at day 7), and IgG4+ (ratio: 9.2 vs. 3.2 at day 7) plasma cells. Only the difference in IgG1+ plasma cell expansion reached statistical significance ( $p \leq 0.01$ ), possibly due to the low number of participants in both groups. Moreover, plasma cell maturation at the peak of expansion was more prominent in wP-primed adolescents in whom the most mature CD20-CD138+ plasma cells constituted 46% of IgG1+ plasma cells in contrast to 39% in aP-primed adolescents (**Figure 6A,B**). Thus, the type of primary vaccination background seems to influence the plasma cell response to later booster vaccinations. In our study, the plasma cell response was stronger and more diverse in wP-primed adolescents.

To exclude that differences observed in the adolescent cohort were caused by the different sex distribution between aP- and wP-primed individuals, we assessed the impact of sex on the cell expansion in the young adult cohort and extrapolated this to the adolescent cohort. The young adult cohort was well sex-balanced and had a homogenous priming background. We evaluated the expansion of total B cells, plasma cells, IgG1–3+ plasma cells, and IgA1+ plasma cells in males and females. No significant differences were observed between male and female responses (**Supplemental Figure S6**). Therefore, we concluded that the sex imbalance in the adolescent cohort did not influence the plasma cell expansion as found in this study.

The adolescent cohort only consisted of 12 individuals, which is rather small for statistical analysis. Therefore, although we found some age-dependent differences in cellular responses, we grouped all aP-primed individuals (children and adolescents) and all wP-primed individuals (adolescents and young adults; not the older adults, because of their uncertain vaccination background status) to increase the size of the aP- vs. wP-primed study cohorts (**Supplemental Figure S7A**). In this comparison, expansions of total and IgG1+ plasma cells were again



## Chapter 3.2

more pronounced in wP-primed participants. Differences in other plasma cell subsets did not reach statistical significance. Finally, based on ratio to baseline, the (total) plasma cell maturation was more prominent in wP-primed individuals compared with aP-primed individuals, and differed significantly for intermediate mature plasma cells. The percentage of the most mature cells in the IgG1+ plasma cell population did not significantly differ between the two groups (**Supplemental Figure S7**).

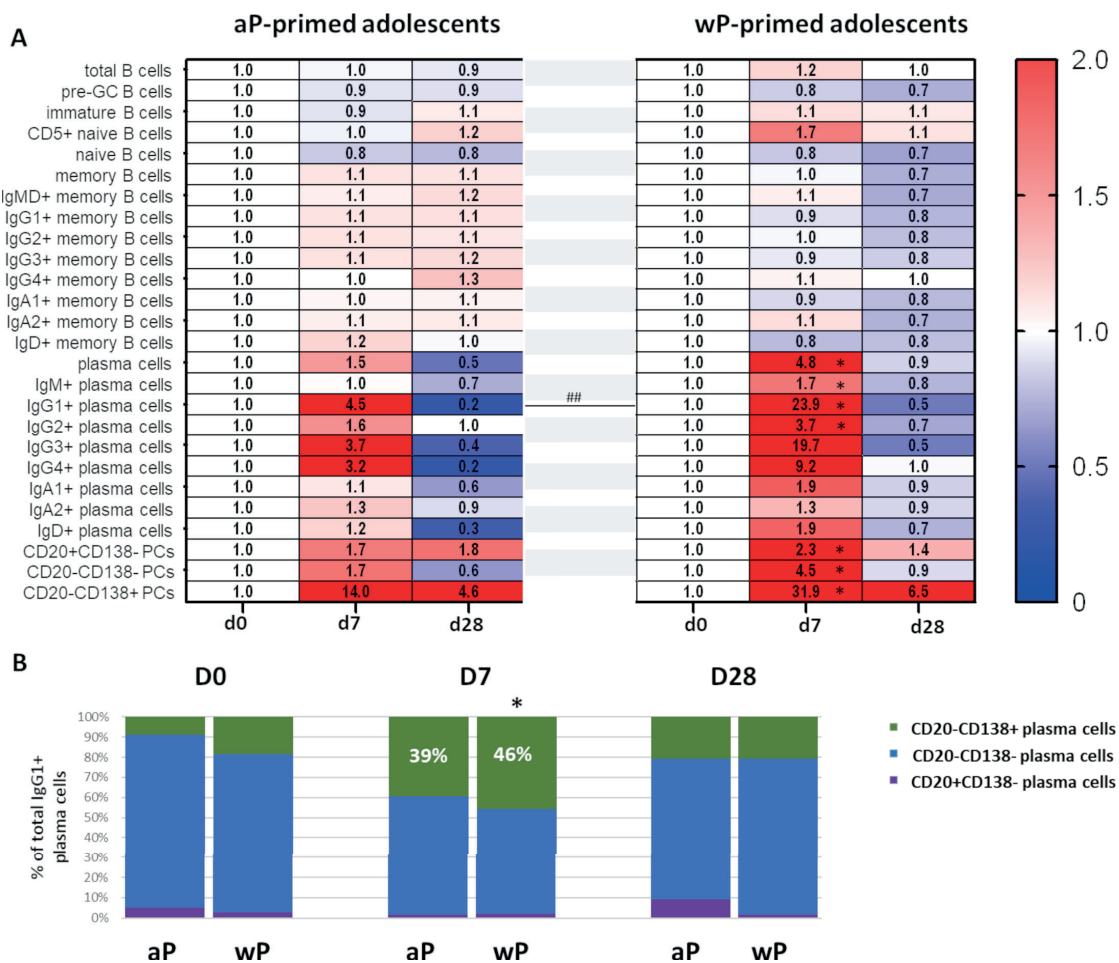


**Figure 6. IgG1+ plasma cell expansion and maturation are more prominent in age-matched participants after wP priming.** (A) Heatmap showing over-time changes in memory B-cell and plasma cell subsets in aP-primed ( $n = 5$ ) or wP-primed ( $n = 7$ ) adolescents (median values). (B) Over-time distribution of IgG1+ plasma cells representing different maturation stages within total IgG1+ plasma cells. Median values for each population were used to construct the plots. Wilcoxon matched pair signed-rank test followed by Bonferroni correction was used to assess longitudinal differences in percentage of CD20-CD138+ cells in total IgG1+ plasma cells within each cohort. Differences in the percentage CD20-CD138+ cells in total IgG1+ plasma cells between cohorts were assessed using Kruskal-Wallis followed by Dunn's test but did not yield significant differences. For longitudinal changes, only significant differences compared to baseline are shown. Significant longitudinal differences within a cohort are indicated as \*,  $p < 0.05$ . Significant differences between cohorts at the same time point are indicated as ##,  $p \leq 0.01$ . d = days after vaccination; aP = acellular pertussis vaccine; wP = whole-cell pertussis vaccine; pre-GC = pre-Germinal Center.

In summary, we showed that, irrespective of the age of vaccinated individuals, the most prominent cellular changes occurred in the numbers of circulating plasma cells. Despite some age-related differences, the expansion and maturation of IgG1+ plasma cells at day 7 postvaccination are a shared phenomenon. This expansion of plasma cells measured by flow cytometry was complementary to the increase of vaccine-specific plasma cell numbers determined by ELISpot. Positive correlations between plasma cell expansion and postvaccination Ag-specific serum Ig levels were observed, mainly when correlating with the individual Bp components (Bp: FHA, Prn, and PT). Finally, plasma cell responses were stronger in individuals who were wP-primed.

### Discussion

In this study, we applied high-dimensional flow cytometry to investigate changes in B cells in individuals of different ages and primary vaccination backgrounds upon administration of an aP booster vaccine and correlated these findings with vaccine-specific Ig levels in serum. In all age groups, expansion and maturation of plasma cells 7 days postvaccination was the most prominent cellular change. Although in children the expansion of plasma cells was less prominent than in adults (ratio to baseline), they had more plasma cells at peak levels due to their initially high plasma cell numbers. Furthermore, total and IgG1+ plasma cell responses were stronger in individuals primed with the Dutch wP vaccine than in individuals who were primed with aP vaccines. No consistent over-time memory B-cell fluctuations were observed. No strong correlation between plasma cell expansion or memory B-cell expansion with vaccine-specific serum Ig levels was observed, yet the absolute increase in IgA plasma cells at day 7 correlated weakly with the IgA serum levels at day 28 (IU/mL). Furthermore, weak positive correlations were observed between the expansion of IgG1+ and IgA1+ plasma cells and FHA-, Prn-, and PT-specific serum IgG or IgA levels postvaccination. Although serology provides insight into Ag-specific Ig levels and function, analysis of circulating immune cells may result in a deeper understanding of the processes induced by the vaccine and the cellular changes preceding Ig production. Our study points at plasma cells as a potential cellular marker of an immune response and contributes to a better understanding of the immune responses (to booster vaccinations) between different age groups and different primary vaccination backgrounds.

To ensure objective data analysis, we used the automated gating and identification (AGI) tool in the Infinicyt software. This tool was shown to reduce intra- and inter-operator variability and increase reproducibility of the analysis [40,48–50]. This is especially important for studies with big data from multiple samples, which cannot be analyzed by a single operator within a reasonable timeframe. Irrespective of the new analysis strategy, these data corroborated major findings from our previous study, where data were subjected to manual analysis [33]. This automated analysis approach, in combination with the standardized EuroFlow sample processing and acquisition procedures, allows for identification of fluctuations in small populations of cells such as different plasma cell maturation stages.

## Chapter 3.2

---

Levels of Ag-specific serum Igs are routinely used as readout for vaccine efficacy. In many cases, a rise in Ag-specific IgG levels is associated with response to vaccination, and for several vaccines—e.g., against rotavirus—an increase in IgA levels has been indicated as a correlate of protection [23,45,51–53]. As Igs are the product of terminally differentiated B cells (plasma cells), the B-cell compartment may harbor new correlates or biomarkers of ongoing immune responses. Indeed, we found that expansion and maturation of circulating plasma cells 7 days after booster vaccination was the most prominent cellular change. The generation of mainly IgG1+ plasma cells is in line with previous serology-based studies, where within Bp-specific serum IgGs mostly IgG1 antibodies were found, with minor contribution of IgG2, -3, and -4 [51,54]. The positive correlation between the numbers of total plasma cells with the vaccine-specific plasma cell numbers supports the assumption that most of the plasma cells at the peak of expansion are vaccine-specific.

The IgA response, observed mostly in the adult cohorts, is likely a result of immunological memory generated by previous (subclinical) infection of the respiratory tract, where a mucosal response against Bp was launched. As Bp circulates within the population, causing outbreaks every 2–5 years, the adult cohorts have likely encountered Bp multiple times during life, which explains the more prominent IgA1+ plasma cell response in these groups [55–58]. In contrast, the expansion of IgG4+ plasma cells was mostly seen in the pediatric cohorts, which may be explained by the predominant aP priming in these cohorts; this has been shown to induce a more Th2-related response as well as increased vaccine-specific serum IgG4 [23,24].

In addition to the expansion of IgG1+ and IgA1+ plasma cells in adults, and the IgG1+ and IgG4+ response in the pediatric cohorts, which are in line with previous (cellular and serology-based) studies, we also observed a prominent increase in IgG3+ plasma cells in all cohorts [23,33,51,54]. A potential explanation for this phenomenon might be that, in addition to the memory B cells, there are naive B cells that recognize the antigens and undergo first-step IgG3 class switching and affinity maturation [59].

The difference in plasma cell—and thus, antibody—production can have consequences for the type and efficacy of the launched immune response. IgG1 and IgG3 antibodies have stronger opsonizing capacities compared with IgG4 antibodies [60]. The mixed IgG1-IgG3-IgG4 response observed in the mostly aP-primed pediatric cohorts may lead to competition for Bp antigens in future encounters, possibly leading to less efficient bacterial clearance compared with the IgG1-IgG3 (and IgA1) response observed in the adult cohorts [59,61]. Lastly, the prominent contribution of IgA1+ plasma cells to responses observed in the adult cohorts, which is likely an indicator of previous pertussis encounters, may imply existence of effective mucosal defense mechanisms, and more efficient protection against bacterial translocation in IgA-producing individuals. Comparison of repertoires and reactivities of IgA in mucosa and in circulation could provide better insights

into this phenomenon and value of IgA as a biomarker of protection.

Maturation of plasma cells (total and IgG1+) was observed irrespective of age and priming background. The clear expansion and maturation of total and IgG1+ plasma cells are in line with our previous findings and may be explained by the prolonged retention of newly generated plasma cells in the periphery as well as the competition for bone marrow niches with pre-existing long-lived plasma cells [33,62].

In this study, several differences between the aP- and wP-primed cohorts were observed. Although the sizes of the age-matched adolescent cohorts were too limited to reach statistically significant conclusions, major observations were confirmed by analysis of all individuals with known primary vaccination background. Remarkably, this difference based on primary vaccination background was not observed in the overarching part of the BERT study, where the Bp-specific Ig responses of 85 Dutch and Finnish adolescents pre- and postvaccination were evaluated [29].

The formulation of aP and wP vaccines differs with regards to number of antigens and the total antigenic load, with wP vaccines containing the broad variety of pertussis antigens and aP vaccines containing high concentrations of a restricted number of antigens. In consequence, wP priming is likely to trigger a more diverse antibody response. Since consecutive boosters lead to a more specific, but also more restricted response, this initial broad priming can be beneficial in case of encountering future (mutated) bacterial strains [10,12,13]. Interestingly, in this study, we showed that compared to aP-primed individuals, individuals primed with the Dutch wP vaccine have a stronger response upon aP booster vaccination. It would be of interest to visualize potential differences in breadth of an immune response against Bp antigens. Moreover, since the initial type of priming vaccine seems to imprint future responses to given antigens, it should be carefully considered in the design of future vaccines and vaccination strategies. This may also hold true for diseases other than pertussis, such as COVID-19.

To identify unique and shared patterns between groups, we primarily focused on normalized data (represented as the ratio to baseline). However, we also showed that, in line with published studies, children had overall higher leukocyte and B-cell counts compared with (older) adults [32,41]. Specifically, the cell count of naive B and T cells—and thus, the available naive repertoire—is substantially higher in youth [32,48]. Therefore, despite a lower increase in cells expressed as ratio to baseline, children and adolescents may still produce a stronger and more diverse immune responses than adults.

In this study, memory B-cell fluctuations were limited. As the frequencies of Ag-specific memory B cells are low, as demonstrated by previous studies using ELISpot assays, an increase in only these Ag-specific memory B cells may not have an impact on the total memory B-cell population [36,63]. Indeed, in this study,

no correlation was found between the memory B-cell fluctuations measured by flow cytometry and the vaccine-specific memory B cells by ELISpot. However, we observed an increase in CD20<sup>++</sup>CD21<sup>-</sup> IgG1<sup>+</sup> memory B cells in older adults and adolescents at days 14 and 28 after vaccination, respectively. Interestingly, several studies reported an increased percentage of Ag-specific CD27<sup>+</sup>CD21<sup>-</sup>/dim B cells 14 days after influenza vaccination [64,65]. There is no consensus about the exact function of these CD21<sup>-</sup>/dim B cells, but it has been suggested that CD21<sup>-</sup>/dim B cells are exhausted cells or, as described in autoimmunity and chronic infection, are anergic [66,67]. In this context, it is not unlikely that cells that have responded to an antigen multiple times would acquire this phenotype. However, Lau and colleagues suggest that CD21<sup>-</sup>/dim B cells are primed for plasma cell differentiation [64]. Ag-specific flow cytometry studies should give insight into the exact function of this B-cell subset.

No correlation was found between expansion of memory B cells and Ag-specific serum IgG levels at day 28. Previously, we observed a clear correlation between the expansion of IgG1<sup>+</sup> memory B cells and the vaccine-specific IgG levels at day 21 in a cohort of 10 healthy adults [33]. Moreover, we found that although in the majority of participants memory B cells showed maximum expansion at 14 days after vaccination, the expansion of memory B cells was not as synchronized in time as the plasma cell expansion, implying that, in some participants, we may not have sampled at the most optimal timepoint [33], especially in the children and adolescent cohorts, where the sampling times were limited to days 0, 7, and 28. This difference in timing of memory B-cell responses might be related to the immune status of each individual at baseline and makes the use of memory B cells as correlates of protection more difficult.

Neither aP nor wP vaccination yield a response that fully mimics natural infection; especially, the IgA response seems to be limited upon vaccination and mostly relies upon previous encounters with Bp. To overcome this limitation, multiple novel pertussis vaccines and alternative delivery routes are being developed, such as nasal delivery of a vaccine or the use of life-attenuated Bp strains (BPZE1) [68–70]. It would be of interest to evaluate how (cellular) immune responses induced by these vaccine candidates compare with cellular kinetics induced by intramuscular aP and wP vaccines, as well as (controlled) human infection. Such comparison between aP booster vaccination and (controlled) human infection is currently ongoing within the IMI-2 PERISCOPE program [71,72]. These studies will create a solid basis for evaluation of novel vaccination approaches.

### **Conclusions**

Analysis of circulating immune cells results in a deeper understanding of the processes induced by vaccination and the cellular changes preceding Ig production. Irrespective of the age of vaccinated individuals, the most prominent cellular changes occurred in the numbers of circulating plasma cells. The expansion and maturation of IgG1<sup>+</sup> plasma cells at day 7 postvaccination were a shared phenomenon. Plasma cell expansion, as determined by flow cytometry, was comple-



mentary to the increase of vaccine-specific plasma cell numbers as determined by ELISpot. Positive correlations between plasma cell expansion and postvaccination Ag-specific serum Ig levels were observed, mainly when correlating with the individual Bp components. Finally, plasma cell responses were stronger in individuals who were wP-primed. Thus, our study contributes to a better understanding of the immune responses (to booster vaccinations) between different age groups and different primary vaccination backgrounds.

**Author Contributions:** Conceptualization, C.T., A.-M.B., M.P.-A., A.O., G.A.M.B., J.J.M.v.D., and M.A.B.; methodology, A.T.-V., M.P.-A., and A.O.; validation, R.J.G. and B.d.M.; formal analysis, A.M.D., P.V., C.T., R.J.G., B.d.M., and M.A.B.; investigation, A.M.D., P.V., C.T., R.J.G., B.d.M., and M.A.B.; data curation, A.M.D., P.V., and G.A.M.B.; writing – original draft preparation, A.M.D. and M.A.B.; writing – review & editing, A.M.D., P.V., C.T., R.J.G., B.d.M., A.-M.B., A.T.-V., M.P.-A., A.O., G.A.M.B., J.J.M.v.D., and M.A.B.; visualization, A.M.D.; supervision, A.-M.B., M.P.-A., A.O., G.A.M.B., J.J.M.v.D., and M.A.B.; project administration, P.V., A.-M.B., G.A.M.B., J.J.M.v.D., and M.A.B.; funding acquisition, A.O., G.A.M.B., and J.J.M.v.D. All authors have read and agreed to the published version of the manuscript.

**Funding:** This PERISCOPE project has received funding from the Innovative Medicines Initiative 2 Joint Undertaking under grant agreement No 115910. This Joint Undertaking receives support from the European Union's Horizon 2020 research and innovation program and EFPIA and BMGF. The Joint Undertaking is not responsible for any use that may be made of the information this manuscript contains.

**Institutional Review Board Statement:** The study was conducted according to the guidelines of the Declaration of Helsinki and approved by the Medical Research Ethics Committees United (MEC-U, NL60807.100.17-R17.039) on 2017-09-01 and registered at the EU Clinical trial registry (EudraCT number 2016-003678-42).

**Informed Consent Statement:** Written informed consent was obtained from all subjects (or their parent/guardian) involved in the study.

**Data Availability Statement:** The data presented in this study are available on request from the corresponding author.

**Acknowledgments:** The authors would like to thank all research nurses and clinical trial staff, especially J. Zonneveld and G. van Asselts (Spaarne Gasthuis), for their support in sample collection, performing home visits, and management of the clinical data. We also acknowledge M. van Houten (Spaarne Gasthuis) for her help with the trial coordination, clinical trial management, and clinical sample collection. We thank P. van Gageldonk, N. Kaagman and L. de Rond from National Institute of Public Health and the Environment for measuring the



## Chapter 3.2

---

Ag-specific serum Ig levels and antibody producing cells. We express gratitude to all participants and their families for their participation in this study. Moreover, the authors gratefully acknowledge the Flow cytometry Core Facility at LUMC (coordinated by K. Schepers, M. Hameetman, run by operators S. van de Pas, D. Lowie, J. Jansen, IJ. Reyneveld, and former operators E. de Haas and G. de Roo) for their support.

**Conflicts of Interest:** A.M.D., C.T., M.P.-A., A.O., J.J.M.v.D. and M.A.B. report inventorship of the patent “Means and methods for multiparameter cytometry-based leukocyte subsetting” (NL2844751, filing date 5 November 2019) [37], owned by the EuroFlow Consortium. In addition, J.J.M.v.D. and A.O. report to be chairman and co-chairman of the EuroFlow scientific foundation, which receives royalties from licensed patents, which are collectively owned by the participants of the EuroFlow Foundation. These royalties are exclusively used for continuation of the EuroFlow collaboration and sustainability of the EuroFlow consortium. Lastly, J.J.M.v.D. and A.O. report an Educational Services Agreement from BD Biosciences (San José, CA) and a Scientific Advisor Agreement with Cytognos; all related fees and honoraria go to LUMC and USAL, respectively.

**Supplementary Materials:** The Supplementary Material for this article can be found online at: <https://www.mdpi.com/article/10.3390/vaccines10020136/s1>

Or using the following QR code:



### References

1. Atkinson, W. *Epidemiology and Prevention of Vaccine-Preventable Diseases*; Department of Health & Human Services, Centers for Disease Control and Prevention: Washington DC, 2006.
2. Cherry, J.D. Historical review of pertussis and the classical vaccine. *J. Infect. Dis.* 1996, 174, S259–S263.
3. Lambert, L.C. Pertussis vaccine trials in the 1990s. *J. Infect. Dis.* 2014, 209, S4–S9.
4. Decker, M.D.; Edwards, K.M.; Steinhoff, M.C.; Rennels, M.B.; Pichichero, M.E.; Englund, J.A.; Anderson, E.L.; Deloria, M.A.; Reed, G.F. Comparison of 13 acellular pertussis vaccines: Adverse reactions. *Pediatrics* 1995, 96, 557–566.
5. Rijksvaccinatieprogramma [EN: National Immunization Programme]. Available online: <https://rijksvaccinatieprogramma.nl/english> (accessed on 18 November 2020).
6. Tan, T.; Dalby, T.; Forsyth, K.; Halperin, S.A.; Heininger, U.; Hozbor, D.; Plotkin, S.; Ulloa-Gutierrez, R.; Von König, C.H.W. Pertussis across the globe: Recent epidemiologic trends from 2000 to 2013. *Pediatric Infect. Dis. J.* 2015, 34, e222–e232.
7. Versteegen, P.; Berbers, G.A.; Smits, G.; Sanders, E.A.; van der Klis, F.R.; de Melker, H.E.; van der Maas, N.A. More than 10 years after introduction of an acellular pertussis vaccine in infancy: A cross-sectional serosurvey of pertussis in the Netherlands. *Lancet Reg. Health-Eur.* 2021, 10, 100196.
8. Heininger, U.; André, P.; Chlibek, R.; Kristufkova, Z.; Kutsar, K.; Mangarov, A.; Mészner, Z.; Nitsch-Osuch, A.; Petrović, V.; Prymula, R. Comparative epidemiologic characteristics of pertussis in 10 central and eastern European countries, 2000–2013. *PLoS ONE* 2016, 11, e0155949.
9. Berbers, G.A.; de Greeff, S.C.; Mooi, F.R. Improving pertussis vaccination. *Hum. Vaccines* 2009, 5, 497–503.
10. Bart, M.J.; van der Heide, H.G.; Zeddeman, A.; Heuvelman, K.; van Gent, M.; Mooi, F.R. Complete genome sequences of 11 *Bordetella pertussis* strains representing the pandemic ptxP3 lineage. *Genome Announc.* 2015, 3, e01394-15.

11. Mooi, F.R.; van Loo, I.H.; Van Gent, M.; He, Q.; Bart, M.J.; Heuvelman, K.J.; De Greeff, S.C.; Diavatopoulos, D.; Teunis, P.; Nagelkerke, N. Bordetella pertussis strains with increased toxin production associated with pertussis resurgence. *Emerg. Infect. Dis.* 2009, 15, 1206.
12. Martin, S.W.; Pawloski, L.; Williams, M.; Weening, K.; DeBolt, C.; Qin, X.; Reynolds, L.; Kenyon, C.; Giambrone, G.; Kudish, K. Pertactin-negative Bordetella pertussis strains: Evidence for a possible selective advantage. *Clin. Infect. Dis.* 2015, 60, 223–227.
13. Lam, C.; Octavia, S.; Ricafort, L.; Sintchenko, V.; Gilbert, G.L.; Wood, N.; McIntyre, P.; Marshall, H.; Guiso, N.; Keil, A.D. Rapid increase in pertactin-deficient Bordetella pertussis isolates, Australia. *Emerg. Infect. Dis.* 2014, 20, 626.
14. Sato, Y.; Kimura, M.; Fukumi, H. Development of a pertussis component vaccine in Japan. *Lancet* 1984, 323, 122–126.
15. Gustafsson, L.; Hallander, H.O.; Olin, P.; Reizenstein, E.; Storsaeter, J. A controlled trial of a two-component acellular, a five-component acellular, and a whole-cell pertussis vaccine. *N. Engl. J. Med.* 1996, 334, 349–356.
16. Liko, J.; Robison, S.G.; Cieslak, P.R. Priming with whole-cell versus acellular pertussis vaccine. *N. Engl. J. Med.* 2013, 368, 581–582.
17. Klein, N.P.; Bartlett, J.; Fireman, B.; Baxter, R. Waning Tdap effectiveness in adolescents. *Pediatrics* 2016, 137, e20153326.
18. Sheridan, S.L.; Ware, R.S.; Grimwood, K.; Lambert, S.B. Number and order of whole cell pertussis vaccines in infancy and disease protection. *Jama* 2012, 308, 454–456.
19. Klein, N.P.; Bartlett, J.; Fireman, B.; Rowhani-Rahbar, A.; Baxter, R. Comparative effectiveness of acellular versus whole-cell pertussis vaccines in teenagers. *Pediatrics* 2013, 131, e1716–e1722.
20. Warfel, J.M.; Zimmerman, L.I.; Merkel, T.J. Acellular pertussis vaccines protect against disease but fail to prevent infection and transmission in a nonhuman primate model. *Proc. Natl. Acad. Sci. USA* 2014, 111, 787–792.
21. Diavatopoulos, D.A.; Mills, K.H.; Kester, K.E.; Kampmann, B.; Silerova, M.; Heininger, U.; van Dongen, J.J.; van der Most, R.G.; Huijnen, M.A.; Siena, E. PERISCOPE: Road towards effective control of pertussis. *Lancet Infect. Dis.* 2019, 19, e179–e186.
22. Lambert, E.E.; Corbière, V.; van Gaans-van den Brink, J.; Duijst, M.; Venkatasubramanian, P.B.; Simonetti, E.; Huynen, M.; Diavatopoulos, D.D.; Versteegen, P.; Berbers, G.A. Uncovering Distinct Primary Vaccination-Dependent Profiles in Human Bordetella Pertussis Specific CD4+ T-Cell Responses Using a Novel Whole Blood Assay. *Vaccines* 2020, 8, 225.
23. Hendrikx, L.H.; Schure, R.-M.; Öztürk, K.; de Rond, L.G.; de Greeff, S.; Sanders, E.A.; Berbers, G.A.; Buisman, A.-M. Different IgG-subclass distributions after whole-cell and acellular pertussis infant primary vaccinations in healthy and pertussis infected children. *Vaccine* 2011, 29, 6874–6880.
24. da Silva Antunes, R.; Babor, M.; Carpenter, C.; Khalil, N.; Cortese, M.; Mentzer, A.J.; Seumo, G.; Petro, C.D.; Purcell, L.A.; Vijayanand, P. Th1/Th17 polarization persists following whole-cell pertussis vaccination despite repeated acellular boosters. *J. Clin. Investig.* 2018, 128, 3853–3865.
25. Van Der Lee, S.; Hendrikx, L.H.; Sanders, E.A.; Berbers, G.A.; Buisman, A.-M. Whole-cell or acellular pertussis primary immunizations in infancy determines adolescent cellular immune profiles. *Front. Immunol.* 2018, 9, 51.
26. Kandeil, W.; Atanasov, P.; Avramioti, D.; Fu, J.; Demartean, N.; Li, X. The burden of pertussis in older adults: What is the role of vaccination? A systematic literature review. *Expert Rev. Vaccines* 2019, 18, 439–455.
27. Van Damme, P.; McIntyre, P.; Grimprel, E.; Kuriyakose, S.; Jacquet, J.-M.; Hardt, K.; Messier, M.; Van Der Meeren, O. Immunogenicity of the reduced-antigen-content dTpa vaccine (Boostrix®) in adults 55 years of age and over: A sub-analysis of four trials. *Vaccine* 2011, 29, 5932–5939.
28. Theeten, H.; Rümke, H.; Hoppener, F.J.; Vilatimó, R.; Narejos, S.; Van Damme, P.; Hoet, B. Primary vaccination of adults with reduced antigen-content diphtheria-tetanus-acellular pertussis or dTpa-inactivated poliovirus vaccines compared to diphtheria-tetanus-toxoid vaccines. *Curr. Med. Res. Opin.* 2007, 23, 2729–2739.
29. Versteegen, P.; Pinto, M.V.; Barkoff, A.M.; van Gageldonk, P.G.; van de Kasstele, J.; van Houten, M.A.; Sanders, E.A.; de Groot, R.; Diavatopoulos, D.A.; Bibi, S. Responses to an acellular pertussis booster vaccination in children, adolescents, and young and older adults: A collaborative

## Chapter 3.2

---

- study in Finland, the Netherlands, and the United Kingdom. *EBioMedicine* 2021, 65, 103247.
30. Ellebedy, A.H.; Jackson, K.J.; Kissick, H.T.; Nakaya, H.I.; Davis, C.W.; Roskin, K.M.; McElroy, A.K.; Oshansky, C.M.; Elbein, R.; Thomas, S. Defining antigen-specific plasmablast and memory B cell subsets in human blood after viral infection or vaccination. *Nat. Immunol.* 2016, 17, 1226–1234.
31. Wrammert, J.; Smith, K.; Miller, J.; Langley, W.A.; Kokko, K.; Larsen, C.; Zheng, N.-Y.; Mays, I.; Garman, L.; Helms, C. Rapid cloning of high-affinity human monoclonal antibodies against influenza virus. *Nature* 2008, 453, 667–671.
32. Blanco, E.; Pérez-Andrés, M.; Arriba-Méndez, S.; Contreras-Sanfeliciano, T.; Criado, I.; Pelak, O.; Serra-Caetano, A.; Romero, A.; Puig, N.; Remesal, A. Age-associated distribution of normal B-cell and plasma cell subsets in peripheral blood. *J. Allergy Clin. Immunol.* 2018, 141, 2208–2219. e2216.
33. Diks, A.M.; Khatri, I.; Oosten, L.E.M.; de Mooij, B.; Groenland, R.J.; Teodosio, C.; Perez-Andres, M.; Orfao, A.; Berbers, G.A.M.; Zwaginga, J.J.; et al. Highly Sensitive Flow Cytometry Allows Monitoring of Changes in Circulating Immune Cells in Blood After Tdap Booster Vaccination. *Front. Immunol.* 2021, 12, 2091. <https://doi.org/10.3389/fimmu.2021.666953>.
34. GlaxoSmithKline. Boostrix Polio; Product Summary. Available online: <https://www.geeniesmiddeleninformatiebank.nl/Bijsluiters/h35123.pdf> (accessed on 7 July 2020).
35. van Gageldonk, P.G.; van Schaijk, F.G.; van der Klis, F.R.; Berbers, G.A. Development and validation of a multiplex immunoassay for the simultaneous determination of serum antibodies to *Bordetella pertussis*, diphtheria and tetanus. *J. Immunol. Methods* 2008, 335, 79–89.
36. Buisman, A.; De Rond, C.; Öztürk, K.; Ten Hulscher, H.; Van Binnendijk, R. Long-term presence of memory B-cells specific for different vaccine components. *Vaccine* 2009, 28, 179–186.
37. van Dongen, J.J.M.; Orfao de Matos Correia E Vale, J.A.; Goncalves Grunho Teodosio, C.I.; Perez Y Andres, M.; Almeida Parra, J.M.; Van den Bossche, W.B.L.; Botafogo Goncalves, V.D.; Berkowska, M.A.; Van der Pan, K.; Blanco Alvarez, E.; et al. Means and Methods for Multiparameter Cytometry-Based Leukocyte Subsetting; 2019.
38. Kalina, T.; Flores-Montero, J.; Lecrevisse, Q.; Pedreira, C.E.; Velden, V.H.; Novakova, M.; Mejstrikova, E.; Hrusak, O.; Böttcher, S.; Karsch, D. Quality assessment program for EuroFlow protocols: Summary results of four-year (2010–2013) quality assurance rounds. *Cytom. Part A* 2015, 87, 145–156.
39. Kalina, T.; Flores-Montero, J.; Van Der Velden, V.; Martin-Ayuso, M.; Böttcher, S.; Ritgen, M.; Almeida, J.; Lhermitte, L.; Asnafi, V.; Mendonca, A. EuroFlow standardization of flow cytometer instrument settings and immunophenotyping protocols. *Leukemia* 2012, 26, 1986–2010.
40. Pedreira, C.; da Costa, E.S.; Lecrevisse, Q.; Grigore, G.; Fluxa, R.; Verde, J.; Hernandez, J.; van Dongen, J.; Orfao, A. From big flow cytometry datasets to smart diagnostic strategies: The EuroFlow approach. *J. Immunol. Methods* 2019, 475, 112631.
41. Comans-Bitter, W.M.; de Groot, R.; van den Beemd, R.; Neijens, H.J.; Hop, W.C.; Groeneveld, K.; Hooijkaas, H.; van Dongen, J.J. Immunophenotyping of blood lymphocytes in childhood: Reference values for lymphocyte subpopulations. *J. Pediatrics* 1997, 130, 388–393.
42. Kumar, P.; CM, C. *Clinical Medicine*, 8th ed.; Saunders Elsevier: Edinburgh, UK, 2012; p. 373.
43. Perez-Andres, M.; Paiva, B.; Nieto, W.G.; Caraux, A.; Schmitz, A.; Almeida, J.; Vogt, R., Jr.; Marti, G.; Rawstron, A.; Van Zelm, M. Human peripheral blood B-cell compartments: A crossroad in B-cell traffic. *Cytom. Part B: Clin. Cytom.* 2010, 78, S47–S60.
44. Tangye, S.G.; Tarlinton, D.M. Memory B cells: Effectors of long-lived immune responses. *Eur. J. Immunol.* 2009, 39, 2065–2075.
45. Hendrikx, L.H.; Felderhof, M.K.; Öztürk, K.; de Rond, L.G.; van Houten, M.A.; Sanders, E.A.; Berbers, G.A.; Buisman, A.-M. Enhanced memory B-cell immune responses after a second acellular pertussis booster vaccination in children 9 years of age. *Vaccine* 2011, 30, 51–58.
46. Crotty, S.; Felgner, P.; Davies, H.; Glidewell, J.; Villarreal, L.; Ahmed, R. Cutting edge: Long-term B cell memory in humans after smallpox vaccination. *J. Immunol.* 2003, 171, 4969–4973.
47. Hendrikx, L.H.; Öztürk, K.; De Rond, L.G.; Veenhoven, R.H.; Sanders, E.A.; Berbers, G.A.; Buisman, A.-M. Identifying long-term memory B-cells in vaccinated children despite waning antibody levels specific for *Bordetella pertussis* proteins. *Vaccine* 2011, 29, 1431–1437.
48. Botafogo, V.; Pérez-Andres, M.; Jara-Acevedo, M.; Bárcena, P.; Grigore, G.; Hernández-Delgado, A.; Damasceno, D.; Comans, S.; Blanco, E.; Romero, A. Age Distribution of Multiple Functionally Relevant Subsets of CD4+ T Cells in Human Blood Using a Standardized and Validated

- 14-Color EuroFlow Immune Monitoring Tube. *Front. Immunol.* 2020, 11, 166.
49. Linskens, E.; Diks, A.M.; Neirinck, J.; Perez-Andres, M.; De Maertelaere, E.; Berkowska, M.A.; Kerre, T.; Hofmans, M.; Orfao, A.; van Dongen, J.J.M.; et al. Improved Standardization of Flow Cytometry Diagnostic Screening of Primary Immunodeficiency by Software-Based Automated Gating. *Front. Immunol.* 2020, 11, 584646. <https://doi.org/10.3389/fimmu.2020.584646>.
  50. Flores-Montero, J.; Grigore, G.; Fluxá, R.; Hernández, J.; Fernandez, P.; Almeida, J.; Muñoz, N.; Böttcher, S.; Sedek, L.; van der Velden, V. EuroFlow Lymphoid Screening Tube (LST) data base for automated identification of blood lymphocyte subsets. *J. Immunol. Methods* 2019, 475, 112662.
  51. Giammanco, A.; Taormina, S.; Chiarini, A.; Dardanoni, G.; Stefanelli, P.; Salmaso, S.; Mastrantonio, P. Analogous IgG subclass response to pertussis toxin in vaccinated children, healthy or affected by whooping cough. *Vaccine* 2003, 21, 1924–1931.
  52. Vesikari, T.; Karvonen, A.; Prymula, R.; Schuster, V.; Tejedor, J.C.; Thollot, F.; Garcia-Corbeira, P.; Damaso, S.; Han, H.-H.; Bouckennooghe, A. Immunogenicity and safety of the human rotavirus vaccine Rotarix™ co-administered with routine infant vaccines following the vaccination schedules in Europe. *Vaccine* 2010, 28, 5272–5279.
  53. Plotkin, S.; Plotkin, S.; Plotkin, S.; Orenstein, W.; Offit, P. *Vaccines (Section 1, Chapter 2)* 6th ed.; Saunders Elsevier: Philadelphia, Pennsylvania, 2008; pp. 17–36.
  54. van der Lee, S.; Sanders, E.A.; Berbers, G.A.; Buisman, A.-M. Whole-cell or acellular pertussis vaccination in infancy determines IgG subclass profiles to DTaP booster vaccination. *Vaccine* 2018, 36, 220–226.
  55. van der Maas, N.A.T.; de Melker, H.E.; Heuvelman, C.J.; van Gent, M.; Mooi, F.R.. Kinkhoestsurveillance in 2013 en 2014—RIVM Briefrapport 2014-0165; Rijksinstituut voor volksgezondheid en milieu (RIVM), Bilthoven, 2014; p. 36.
  56. Cherry, J.D. Epidemic pertussis in 2012—The resurgence of a vaccine-preventable disease. *N. Engl. J. Med.* 2012, 367, 785–787.
  57. Subissi, L.; Rodeghiero, C.; Martini, H.; Litzroth, A.; Huygen, K.; Leroux-Roels, G.; Piérard, D.; Desombere, I. Assessment of IgA anti-PT and IgG anti-ACT reflex testing to improve Bordetella pertussis serodiagnosis in recently vaccinated subjects. *Clin. Microbiol. Infect.* 2020, 26, 645.e1-645.e648.
  58. Hendriks, L.H.; Öztürk, K.; De Rond, L.G.; De Greeff, S.C.; Sanders, E.A.; Berbers, G.A.; Buisman, A.-M. Serum IgA responses against pertussis proteins in infected and Dutch wP or aP vaccinated children: An additional role in pertussis diagnostics. *PLoS ONE* 2011, 6, e27681.
  59. Diavatopoulos, D.A.; Edwards, K.M. What is wrong with pertussis vaccine immunity? Why immunological memory to pertussis is failing. *Cold Spring Harb. Perspect. Biol.* 2017, 9, a029553.
  60. Brüggemann, M.; Williams, G.T.; Bindon, C.I.; Clark, M.R.; Walker, M.R.; Jefferis, R.; Waldmann, H.; Neuberger, M.S. Comparison of the effector functions of human immunoglobulins using a matched set of chimeric antibodies. *J. Exp. Med.* 1987, 166, 1351–1361.
  61. Weiss, A.A.; Patton, A.K.; Millen, S.H.; Chang, S.-J.; Ward, J.I.; Bernstein, D.I. Acellular pertussis vaccines and complement killing of Bordetella pertussis. *Infect. Immun.* 2004, 72, 7346–7351.
  62. Odendahl, M.; Mei, H.; Hoyer, B.F.; Jacobi, A.M.; Hansen, A.; Muehlinghaus, G.; Berek, C.; Hiepe, F.; Manz, R.; Radbruch, A. Generation of migratory antigen-specific plasma blasts and mobilization of resident plasma cells in a secondary immune response. *Blood* 2005, 105, 1614–1621.
  63. Nanan, R.; Heinrich, D.; Frosch, M.; Kreth, H.W. Acute and long-term effects of booster immunisation on frequencies of antigen-specific memory B-lymphocytes. *Vaccine* 2001, 20, 498–504.
  64. Lau, D.; Lan, L.Y.-L.; Andrews, S.F.; Henry, C.; Rojas, K.T.; Neu, K.E.; Huang, M.; Huang, Y.; DeKosky, B.; Palm, A.-K.E. Low CD21 expression defines a population of recent germinal center graduates primed for plasma cell differentiation. *Sci. Immunol.* 2017, 2, eaai8153.
  65. Koutsakos, M.; Wheatley, A.K.; Loh, L.; Clemens, E.B.; Sant, S.; Nüssing, S.; Fox, A.; Chung, A.W.; Laurie, K.L.; Hurt, A.C. Circulating TFH cells, serological memory, and tissue compartmentalization shape human influenza-specific B cell immunity. *Sci. Transl. Med.* 2018, 10, eaan8405.
  66. Andrews, S.F.; Wilson, P.C. The anergic B cell. *Blood J. Am. Soc. Hematol.* 2010, 115, 4976–4978.
  67. Isnardi, I.; Ng, Y.-S.; Menard, L.; Meyers, G.; Saadoun, D.; Srdanovic, I.; Samuels, J.; Berman, J.; Buckner, J.H.; Cunningham-Rundles, C. Complement receptor 2/CD21—Human naive B

## Chapter 3.2

---

cells contain mostly autoreactive unresponsive clones. *Blood J. Am. Soc. Hematol.* 2010, 115, 5026–5036.

68. Lin, A.; Apostolovic, D.; Jahnmatz, M.; Liang, F.; Ols, S.; Tecleab, T.; Wu, C.; Van Hage, M.; Solovay, K.; Rubin, K. Live attenuated pertussis vaccine BPZE1 induces a broad antibody response in humans. *J. Clin. Investig.* 2020, 130, 2332–2346.

69. Thorstensson, R.; Trollfors, B.; Al-Tawil, N.; Jahnmatz, M.; Bergström, J.; Ljungman, M.; Törner, A.; Wehlin, L.; Van Broekhoven, A.; Bosman, F. A phase I clinical study of a live attenuated *Bordetella pertussis* vaccine-BPZE1; a single centre, double-blind, placebo-controlled, dose-escalating study of BPZE1 given intranasally to healthy adult male volunteers. *PLoS ONE* 2014, 9, e83449.

70. Boehm, D.T.; Wolf, M.A.; Hall, J.M.; Wong, T.Y.; Sen-Kilic, E.; Basinger, H.D.; Dziadowicz, S.A.; de la Paz Gutierrez, M.; Blackwood, C.B.; Bradford, S.D. Intranasal acellular pertussis vaccine provides mucosal immunity and protects mice from *Bordetella pertussis*. *NPJ Vaccines* 2019, 4, 40.

71. De Graaf, H.; Gbesemete, D.; Gorringer, A.R.; Diavatopoulos, D.A.; Kester, K.E.; Faust, S.N.; Read, R.C. Investigating *Bordetella pertussis* colonisation and immunity: Protocol for an inpatient controlled human infection model. *BMJ Open* 2017, 7, e018594.

72. Preston, A.; de Graaf, H.; Ibrahim, M.; Hill, A.; Gbesemete, D.; Vaughn, A.; Gorringer, A.; Buisman, A.-M.; Faust, S.; Kester, K. Controlled human infection with *Bordetella pertussis* induces asymptomatic, immunising colonisation. *Clin. Infect. Dis.* 2020, 71, 403–411.



## Chapter 3.3

### **Longitudinal dynamics of human B-cell response at the single-cell level in response to Tdap vaccination**

Indu Khatri<sup>1 2</sup>, Annieck M. Diks<sup>1</sup>, Erik B. van den Akker<sup>2 3</sup>, Liesbeth E. M. Oosten<sup>4</sup>, Jaap Jan Zwaginga<sup>4</sup>, Marcel J. T. Reinders<sup>2 5</sup>, Jacques J. M. van Dongen<sup>1,\*</sup> and Magdalena A. Berkowska<sup>1</sup>

<sup>1</sup>Department of Immunology, Leiden University Medical Center, 2333 ZA Leiden, The Netherlands; i.khatri@lumc.nl (I.K.); A.M.Diks@lumc.nl (A.M.D.); M.A.Berkowska@lumc.nl (M.A.B.)

<sup>2</sup>Leiden Computational Biology Center, Leiden University Medical Center, 2333 ZC Leiden, The Netherlands; e.b.van\_den\_akker@lumc.nl (E.B.v.d.A.); M.J.T.Reinders@tudelft.nl (M.J.T.R.)

<sup>3</sup>Department of Molecular Epidemiology, Leiden University Medical Center, 2333 ZC Leiden, The Netherlands

<sup>4</sup>Department of Hematology, Leiden University Medical Center, 2333 ZA Leiden, The Netherlands; L.E.M.Oosten@lumc.nl (L.E.M.O.); j.j.zwaginga@lumc.nl (J.J.Z.)

<sup>5</sup>Delft Bioinformatics Lab, Delft University of Technology, 2628 CD Delft, The Netherlands

**Vaccines, November 2021**

**<https://doi.org/10.3390/vaccines9111352>**



### **Abstract**

To mount an adequate immune response against pathogens, stepwise mutation and selection processes are crucial functions of the adaptive immune system. To better characterize a successful vaccination response, we performed longitudinal (days 0, 5, 7, 10, and 14 after Boostrix vaccination) analysis of the single-cell transcriptome as well as the B-cell receptor (BCR) repertoire (scBCR-rep) in plasma cells of an immunized donor and compared it with baseline B-cell characteristics as well as flow cytometry findings. Based on the flow cytometry knowledge and literature findings, we discriminated individual B-cell subsets in the transcriptomics data and traced over-time maturation of plasmablasts/plasma cells (PB/PCs) and identified the pathways associated with the plasma cell maturation. We observed that the repertoire in PB/PCs differed from the baseline B-cell repertoire e.g., regarding expansion of unique clones in post-vaccination visits, high usage of IGHG1 in expanded clones, increased class-switching events post-vaccination represented by clonotypes spanning multiple IGHC classes and positive selection of CDR3 sequences over time. Importantly, the Variable gene family-based clustering of BCRs represented a similar measure as the gene-based clustering, but certainly improved the clustering of BCRs, as BCRs from duplicated Variable gene families could be clustered together. Finally, we developed a query tool to dissect the immune response to the components of the Boostrix vaccine. Using this tool, we could identify the BCRs related to anti-tetanus and anti-pertussis toxoid BCRs. Collectively, we developed a bioinformatic workflow which allows description of the key features of an ongoing (longitudinal) immune response, such as activation of PB/PCs, Ig class switching, somatic hypermutation, and clonal expansion, all of which are hallmarks of antigen exposure, followed by mutation & selection processes.

**Keywords:** B-cell receptor repertoire; Tdap vaccine; pertussis; single cell; vaccination

## Introduction

The adaptation of the immune system to recognize antigenically distinct epitopes of pathogens is a critical feature of the antibody (Ab) -mediated immunity in response to infection/vaccination. Abs are products of terminally differentiated B cells, plasma cells (PCs), and are the secreted forms of B-cell receptors (BCRs). Generation of a highly diverse BCR repertoire (BCR-rep) starts during precursor B-cell development in bone marrow, where developing B cells assemble immunoglobulin heavy (IGH) and light chain genes in the process of V(D)J recombination. B cells with a functional BCR leave the bone marrow and are ready to recognize antigens in the peripheral immune system. Following antigen recognition, the BCR undergoes affinity maturation in the germinal centers (GCs) through introduction of somatic hypermutations (SHM) and subsequent selection processes for B cells with high-affinity BCR [1]. The introduction and subsequent selection of SHM are critical steps in raising the appropriate immune response. Typically, through positive selection, SHM accumulate in so called complementarity-determining regions (CDRs) because CDRs are in direct contact with the antigen, while SHM in the framework regions (FWR) are less frequently selected, because FWRs are responsible for maintaining receptor structure. Additionally, B cells optimize their effector functions by exchanging the initial C $\mu$  constant region by other downstream IGH constant regions. This process is known as class-switch recombination (CSR). Memory B cells that have recognized pathogen/antigen circulate through the peripheral lymphoid system, differentiate into plasmablasts and re-enter bone marrow to become long-lived Ab-producing PCs. The immune response to a booster vaccination or a re-encounter of the same antigen would lead to the use of pre-existing Abs as the first line of defense [2]. The encounter with an antigen will initiate the processes of SHM and affinity maturation where new Abs are generated from the pool of the pre-existing memory B cells [3,4]. Using flow cytometry, we have recently shown that in booster vaccination settings (Boostrix), an increase in circulating PC numbers, associated with their phenotypical maturation, occurs as early as five days post-vaccination, with a peak in expansion and maturation at day seven post-vaccination [5]. However, the dynamics of the over-time changes in the BCR-rep after Boostrix vaccination in humans are not known yet. Therefore, we performed longitudinal measurements and analysis of single-cell transcriptomics and single-cell BCR-rep (scBCR-rep) in PCs derived from an individual vaccinated with a Tdap Booster vaccine (Boostrix®, GlaxoSmithKline), and compared them with the total BCR-rep at baseline. Along with understanding the dynamics of scBCR-rep after Boostrix vaccination, with this pilot study, we aimed to assess the differences between the flow cytometry and single-cell transcriptomics data at the level of protein vs. transcript expression level and develop a bioinformatics workflow to identify key features of an ongoing (longitudinal) immune response. Furthermore, we also tracked the footprints of the selection processes e.g., V(D)J usage, level of SHMs in FWRs and CDRs and CSR events in B-cell clonotypes to understand the immune responses in a booster vaccination.

As the Boostrix vaccine contains multiple antigens i.e., diphtheria toxoid (DT),

tetanus toxoid (TT), three *Bordetella pertussis* proteins i.e., filamentous hemagglutinin (FHA), pertactin (Prn) and pertussis toxoid (PT), and aluminum hydroxide as an adjuvant [6], we obtained receptor repertoire information against all components of the vaccine. Although it is known that majority of PCs in the response peak at day 7 (d7) are Ag-specific [7,8], we aimed to dissect the immune response against each component. This was, however, subjected to the known pool of Abs against the antigens of Boostrix vaccine. Knowing limitations of the available anti-toxoid Abs for toxoids in vaccine, we developed a method to search the known Ab CDR3 sequences for these vaccine components in our data.

Here, we have analyzed the longitudinal single-cell transcriptomics and scBCR-rep data in PCs derived from an individual vaccinated with Boostrix vaccine and compared them with the total B cells and/or plasma cells at baseline. Using transcriptomics data, we have identified additional membrane markers for flow cytometry that can be used to identify the B-cell subtypes and maturation of plasma cells. With the scBCR-rep data, we have clustered functionally similar receptors and assessed different components of the repertoire for associations between visits and to baseline. Importantly, we found BCRs associated with the vaccine components in scBCR-rep data.

### Methods

#### **Inclusion Criteria and Informed Consent from the Subject**

The donor used in this study was a 28-year-old female, who was recruited as one of 10 healthy adults in a vaccination study where volunteers received Boostrix and wherein their immune responses were monitored over-time by means of flow cytometry (registration number: P16-214, EUDRACT: 2016-002011-18). This longitudinal study aimed at understanding the (Ag-specific) cellular immune responses post-Boostrix vaccination and was approved by the Medical Ethics Committee Leiden-Den Haag-Delft. Inclusion and exclusion criteria were previously published [5]. In short, the donor had to be generally healthy, had completed a vaccination schedule according to the Dutch National Immunization program ([www.rivm.nl/en/national-immunisation-programme](http://www.rivm.nl/en/national-immunisation-programme); accessed on 31 August 2020) and had no known or suspected exposure to pertussis infection nor vaccination in the past 10 years. She also provided an informed consent prior to the inclusion. The individual was selected for the current single-cell study as she had a representative increase in plasma cells at the peak of the plasma cell response (i.e., day 7 (d7)). EDTA-blood samples for single-cell transcript sequencing were collected at baseline and d5, d7, d10 and d14 post-vaccination, which based on the parent study, corresponded to the plasma cell expansion (d5-d10) and contraction of plasma cell response [5] (**Figure S1**). The sequencing of the samples of only one individual were performed as a pilot study to optimize the pipeline to sort cells from the frozen samples, to make comparative assessment of the flow cytometry and transcriptomics data and to develop a pipeline for downstream processing the BCR-rep data and identify toxoid specific BCRs from total B cells.

### High Throughput B-Cell and Plasmablast/Plasma Cell Sorting

Prior to the sort, 78.2 million PBMCs from five different time-points were individually (per time-point) stained with an Ab cocktail for surface markers for 30 min at RT in the dark (CD19 BV786, CD24 BV650, CD27 BV421, CD38 Per-CP-Cy5.5), followed by a live/dead staining (Zombie NIR Fixable Viability kit, Biolegend) according to the manufacturer's protocol. Next, samples were prepared for multiplexing according to the protocols provided on the 10x Genomics website ([www.10xgenomics.com](http://www.10xgenomics.com); accessed on 9 January 2019). In short, Fc block was added and after a 10 min incubation at 4 °C, unique cell hashing Abs (10x Genomics) were added to each sample separately (per time-point). After incubation for 20 min at 4 °C, cells were washed three times and resuspended in PBS. Next, all post-vaccination samples were pooled and sorted on a high-speed cell sorter (BD FACSAria III, BD Biosciences at the flow cytometry core facility of LUMC) using an 85µm nozzle and a pressure of 45PSI, while the baseline sample was sorted separately, but in the same collection tube, to ensure an enrichment of plasmablasts/plasma cells (PB/PCs) in the sorted sample. Cells were collected in a BSA-coated Eppendorf tube filled with an RPMI + 10% FCS solution to avoid excessive cell loss. At baseline, the first 10,000 total CD19+ B cells were sorted, and after adjusting the sorting gate to exclusively sort PB/PCs, another 1201 CD19+CD38++CD24+CD27+ PB/PCs were sorted. For subsequent visits, all available PB/PCs were sorted (11,051 cells). In total, we sorted 22,252 cells. Directly after the sort, samples were spun down and resuspended into the recommended volume (RPMI + 10% FCS). Further sample processing took place at the Leiden genome technology center (LGTC) in the LUMC according to the 10x Genomics protocols (**Figure S1**).

### 10x CITE-Seq Transcriptomics and scBCR-Rep Sequencing

Nearly 22,000 B cells enriched in PB/PCs from different time-points were processed into single cells in a Chromium Controller (10x Genomics) (**Figure S1**). During this process, individual cells were embedded in Gel Beads-in-Emulsion (GEMs) where all generated cDNAs share a common 10x oligonucleotide barcode. Reverse transcription PCR and library preparation were carried out under the Chromium Single Cell 3' v3 protocol (10x Genomics) per manufacturer's recommendations. After amplification of the cDNA, a 5' gene expression library and paired heavy and light chain library were generated from cDNA of the same cell using Chromium Single Cell VDJ reagent kit (scBCR-rep library; v1.1chemistry, 10x Genomics). After library preparation, quality control was performed using a bioanalyzer (Agilent 2100 Bioanalyzer; Agilent Technologies). The libraries were sequenced in the NovaSeq6000 sequencer (Illumina) using the v1.0 sequencing reagent kit (read length: 2 × 150 bp).

### Unsupervised Clustering of Single-Cell Transcriptomics Data

The raw sequencing data from different visits were processed using Cell Ranger (v3.1.0) against the GRCh38 human reference genome with default parameters. Single-cell RNA-seq data were processed in R with Seurat (v3.2.3) [9]. Raw UMI count matrices for both expression and hashtags oligos (HTO) generated from

the Cell Ranger 10x Genomics pipeline (<https://www.10xgenomics.com/>; accessed on 27 August 2019) were loaded into a single Seurat object. Cells were discarded if they met any of the following criteria: percentage of mitochondrial counts >25; the number of unique features <100 or >5000. Furthermore, mitochondrial genes, non-protein-coding genes, and genes expressed in fewer than 3 cells were discarded. Moreover, the immunoglobulin V genes were removed from the counts for clustering analysis. The scaled counts of the constant genes were added to the metadata of the Seurat object. We used MULTISEQDemux [10] with default parameters to demultiplex the data to independent visits (corresponding to HTO1-HTO5 tags) and eliminated doublets and negatives among the cells (**Figure S2**). We found a few T cells (~20–30 cells) in our data which clustered separately and we removed them from further analysis.

After retaining 5010 singlets, we log normalized the gene counts for each cell using the ‘NormalizeData()’ function of Seurat with the default parameters. The normalized data were scaled again using ‘ScaleData()’. The G2M and S phase scores were regressed out from the Seurat object. Principal component analysis (PCA), selecting the 10 most varying principal components, and t-distributed stochastic neighbor embedding (tSNE) dimension reduction were performed. A nearest-neighbor graph using the 10 dimensions of the PCA reduction was calculated using ‘FindNeighbors()’, followed by clustering using ‘FindClusters()’ with a resolution of 0.6. FACS-like plots were generated using transcript average cell scoring implemented in ‘TACSplot()’ [11].

### **Differential Gene Expression Analysis**

For comparisons between expression values, the Seurat function ‘FindMarkers()’ was used with the ‘Wilcox method’. Cell type markers were obtained using the ‘FindAllMarkers()’ function with a Wilcoxon signed-rank test. The fold changes of the mean expression level of genes between the selected cell populations were calculated. The pathway analysis of the relevant genes was performed using ‘ClueGO’ [12].

### **Identification of V(D)JC Genes in the Reconstructed BCRs**

Demultiplexing, gene quantification and BCR contig and clonotype assignment were performed using the Cell Ranger 3.0.2 V(D)J pipeline with GRCh38 as reference. In order to get the BCR of a single cell, we obtained high-confidence contig sequences for each cell and kept the contigs with productive BCR rearrangements. The assembled filtered BCRs from 6437 cells were submitted to IMGT HighV-Quest for the V(D)J annotation. The constant gene annotation of the BCRs was obtained from the Cell Ranger output. The usage of constant gene in this individual was identified from the single-cell data and was compared with the constant gene usage identified by the flow cytometry. All chains (single, pairs, threes or fours) were retained. Of 6437 cells with BCRs, 4051 single cells had one heavy chain recorded in the Seurat object. The repertoire analysis was performed on both the sets (6437 and 4051 cells) and the discussed set is implicitly mentioned in the text or figure legends. In case two or more in-frame/productive



heavy chains were recorded from one cell, both the chains were included in the repertoire analysis.

### Identification of B-Cell Clonotypes

Multiple files obtained from the IMGT HighV-Quest were combined using an in-house Python script. The B cell clonotypes were identified with the same V family, J gene, and 80% nucleotide identity in IG heavy chain CDR3 as computed by Levenshtein distance {Python}. As V gene assignment might be flawed by the assignment methods, we used the V family to call clonotypes which avoids inaccurate grouping of the clones in the first place. Also, a comparative assessment was performed of the clonotypes obtained when using V genes versus V family in assigning B cell clonotypes.

### Analysis of scBCR-Rep and Clonotypes

The Circos plots of VJ usage were made using circlize {R}. To plot identified clonotypes, IGHC usage, class-switching events and CDR3 length usage, ggplot2 {R} was used. We used bcRep {R} [13] to plot the amino acid usage in the amino acid sequence of the junction. BCellMA {R} [14] was used to plot the replacement amino acid mutations from IMGT HighV-Quest output tables. Clonal lineages were built using alakazam [15] and plotted using igraph {R}. The clonal lineages were built based on the SHMs introduced in the V gene sequence. The V genes were compared to the germline V gene in the IMGT database and the number of mutations in the clonal group was used to build these lineages. In case two different mutation lineages were detected in a clonal group and an intermediate BCR was missing, the tool alakazam incorporated an inferred node suggesting a missing BCR that could not have been sampled and/or sequenced.

3.3

### Query Tool to Identify Anti-Toxoid BCRs

The currently profiled BCRs comprise of all the PB/PCs raised in response to the vaccine which comprises of multiple components. To identify the contribution of each component of the vaccine, we developed an in-house tool using Python. To show its functionality, junction sequences related to anti-TT, anti-DT, anti-FHA, anti-Prn and anti-PT were searched in the literature. We could only identify the CDR3 sequences for anti-TT, anti-DT and anti-PT. These sequences were searched in the Boostrix-specific BCR-rep obtained in this study. The search was not only performed based on the percentage identity, but a parameter of length flexibility was also incorporated; i.e., the search space will include junction sequences that are longer or shorter by a user defined length. The sequence similarity is calculated based on the Levenshtein distance of the junction sequences.

## Results

### Single-Cell Transcriptome Landscape of the Cells from a Vaccinated Individual

#### *Majority of the PB/PCs Derived from d5 and d7 Post-Vaccination*

We measured the transcriptomics and BCR-rep data at the single-cell level from the longitudinal samples obtained from an individual following Boostrix vacci-



nation. After applying quality checks to the transcriptomics data from 10,000 total CD19+ B cells and 12,252 CD19+CD38++CD24+CD27+ PB/PCs from five pre-defined time-points (**Figure S1**), we obtained 5010 singlets (**Figure S2**). Unsupervised clustering using Seurat distinguished seven different cell clusters based on their transcription profile (**Figure 1A**). CD19, CD38, CD24 and CD27 markers used to define the cells by flow cytometry allowed discrimination between B cells (**Figure 1A**; Clusters B1-B3) and PB/PCs (**Figure 1A**; Clusters P1-P4). Based on the tag mapping we could identify the sampling time-point of individual cells. The highest number of cells was obtained from d0 when both total B cell and PB/PCs were sorted. At follow-up visits, more PB/PCs were obtained at d5 and d7 and clearly less at d10 and d14 (**Figure 1B** and **Figure S2B**). This reflected the number of sorted cells (**Figure S1B**), but mostly post-vaccination fluctuations in the number of PB/PCs (**Figure S1C**), which were also observed in the flow cytometry data obtained from this donor previously [5].

### *Proliferating Cells Are Clustered in One Cluster*

Despite having regressed out cell cycle influence, the P4 cluster separated based on the expression of the cell cycle genes (**Figure 1C**). A majority of the cells in all the clusters, except P3 and P4, were in G1 with a few cells in S phase, whereas P3 and P4 clusters were heavily comprised of the cells belonging to S and G2M phase (**Figure 1C**), suggesting that most proliferating cells are clustered in P4. The cells present in G1 phase are the mature PB/PCs deemed to produce Abs which are mostly present in P1 and P2 clusters.

### *B1-B3 Clusters Correspond to Naive, Memory and Activated Memory B Cells, Respectively*

The B-cell clusters i.e., B1-B3 were assigned individual identities based on the differentially expressed genes among these clusters and the classical markers and/or literature. The B1 cluster expressed classical markers of naive B cells i.e., IGHD, CXCR4<sup>high</sup> [16] and FOXP1 [17] (**Figure 1D**). Cluster B2 was defined as memory B cells based on overexpressed of unique markers e.g., BANK1, REL. The genes BCL3 and LTB, that promote Ab production, were also highly expressed in cluster B2 [18]. The SOX5, ZBTB32 are markers for activated memory B cells which were also representative markers for cluster B3, hence the 124 cells in cluster B3 were identified as activated memory B cells [19]. The decreasing expression of CXCR4 marker from naive to memory to activated memory B cells was observed in clusters B1 to B3, which was also mentioned in the similar subsets identified from an influenza vaccination study [19]. Overall, we could discriminate between naive B cells (cluster B1), memory B cells (cluster B2), activated memory B cells (cluster B3) and PB/PCs (clusters P1-P4) based on markers unique to these cell types (**Figure 1A, D**).

## **Flow Cytometry Guided Plasma Cell Maturation in the Single-Cell Transcriptome**

### *Staging of PB/PCs Based on Flow Cytometry Markers*

Previously, we used longitudinal flow cytometry data from 10 vaccinated donors

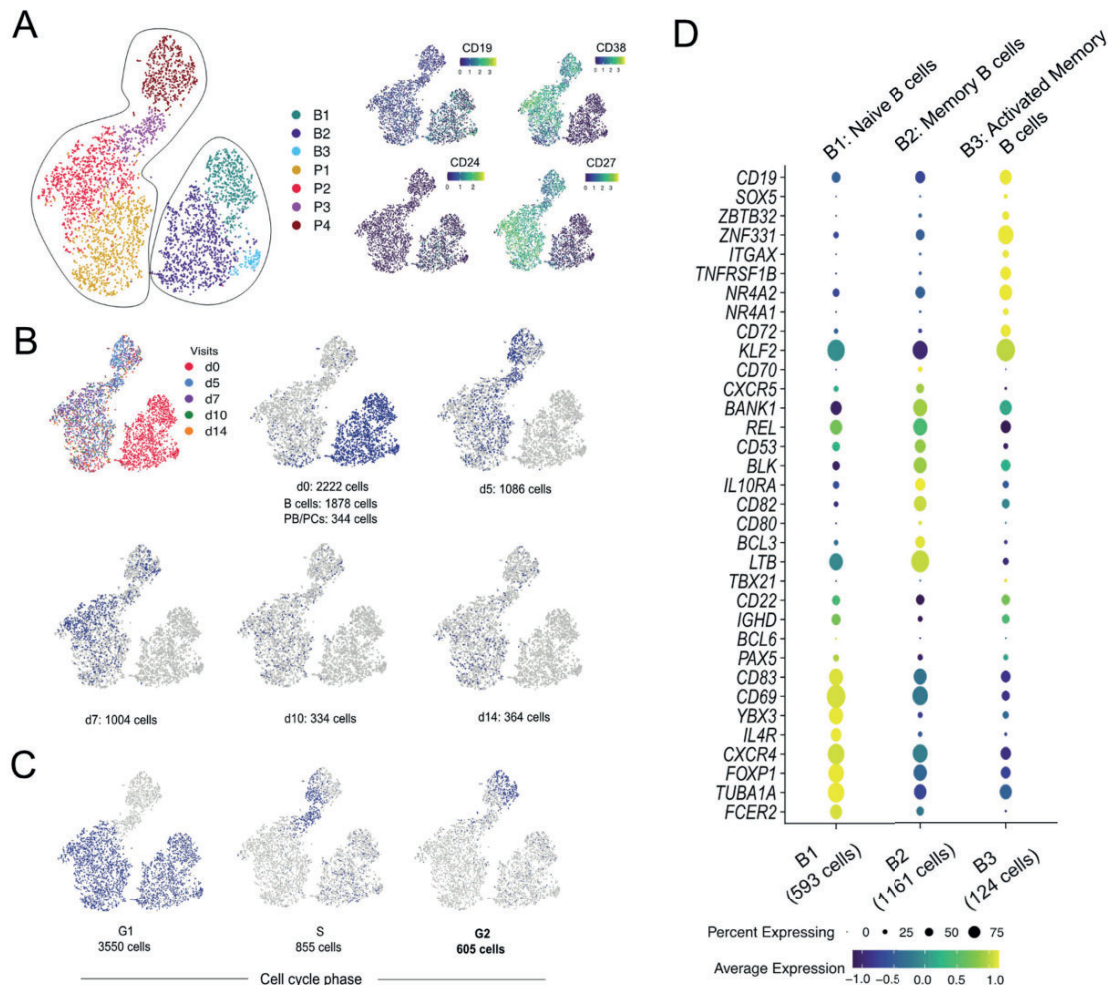


**Figure 1. Identification of B-cell subpopulations by single cell-transcriptomics analysis.** (A) The clusters of cells are represented on a tSNE plot based on the highly variable genes. The clusters are named as B1-B3 for B cells and P1-P4 for PB/PCs. The expression of the markers used for sorting the cells in the study is plotted on the tSNE plot. High expression of CD38 and CD27 marks the clusters P1-P4 as the PB/PCs. (B) Plotting tag information on the tSNE plot. The cells are assigned to each visit and cells at d0 are assigned to B cells and PB/PCs based on their location in B1-B3 and P1-P4 clusters, respectively. (C) Visualizing cell cycle scores on tSNE plot. G1, S and G2M cell-cycle scores are represented on the tSNE plot where P3 and P4 clusters comprise of S and G2M phase cells. (D) Dot plot of the gene markers used for identifying the B-cell subpopulations. B1: Naive B cells; B2: Memory B cells; B3: Activated memory B cells.

to establish how expression of selected cell surface markers changes during maturation of PB/PCs [5]. To visualize the plasma cell maturation in the here studied donor, the PB/PCs data from days 0, 5, 7, 10 and 14 were merged in the Infinicyt software (Infinicyt™ Software v2.0, Cytognos) and the maturation was defined by the downregulation of CD20 and upregulation of CD138 (**Figure 2A** left panel). The most mature cells exhibited CD20-CD138+ phenotype. Then we traced changes in expression of four additional markers i.e., CD19, CD27, CD62L, and CD38. Based on the expression of all six markers, we drew new maturation pathways and divided it into six continuous maturation stages (**Figure 2A** right panel). Similar to flow cytometry staging, after removing B cells, PB/PCs

were clustered based on all the genes and arranged with phenotype ranging from CD20+CD138- (less mature) to CD20-CD138+ (most mature) (**Figure 2B**). However, the cells from different clusters were mixed and the maturation based on P1-P6 clusters could not be drawn. Therefore, we clustered the PB/PCs again based on the expression of only 6 genes SELL (CD62L), TNFRSF7 (CD27), SDC1 (CD138), ADPRC1 (CD38), MS4A1 (CD20) and B4 (CD19)) and used the expression of CD20 and CD138 to align the clusters with the maturation pathway of the PB/PCs. Herein, based on the maturation pathway defined by CD20 and CD138 markers, a trajectory from the blue-colored clusters (Pa1) to the dark red ones (Pa10) can be drawn (**Figure 2C**). Based on the maturation of clustered cells the staging of the PB/PCs was performed from Pa1-Pa10 and the expression of other markers was assessed (**Figure 2D**).

### *Pathways and Additional Membrane Markers Identified in Relation to the Maturation of PB/PCs*

Based on the 10 clusters/stages of the plasma cell maturation, we identified additional markers that might be changing during the maturation of the PB/PCs (**Figure 2E**). Genes with similar expression to the six maturation markers were selected from the single-cell transcriptomics data (**Table S1; Figure 2E**). The HLA locus-specific genes were not included in the analysis. Several of these genes are involved in the regulation of immunoglobulin production, molecular mediation of immune responses, N-glycosylation, antigen processing and presentation, protein folding and cytokine production (**Figure 2F**). The majority of these pathways directly suggest the role of these genes in the Ig secretion, post-translational modifications to ensure correct folding of the proteins and henceforth an optimum response of the immune system to the vaccines. This is in line with the preparation for immunoglobulin secretion, which is the major role of most mature PB/PCs.

### **Characteristics of V(D)J Usage over Time upon Vaccination**

#### *Identification of Ig Heavy and Light Chains in Majority of the Sequenced Cells*

Additional to transcriptomics profiling, we measured the BCRs of the cells from the longitudinal samples obtained from an individual after Boostrix vaccination. The barcode mapped BCR information for each cell was obtained from the Cell Ranger output. We filtered out the unproductive rearrangements and could map at least one heavy or light chain for 4175 cells (**Figure S3A**). No chain was recorded for 835 cells (of which 818 cells were collected at do) (**Figure S3A**), most likely owing to the low expression of BCR in non-plasma cells. We also observed that the cells comprised multiple chains varying from three to five heavy and/or light chains (~8%). Therefore, we filtered out additional chains that were supported by a low number of reads as compared to the other chains from the same cell. In case multiple productive chains were supported by similar number of reads, we included them all in our analysis. After filtering, we found varying chain numbers (1, 3 or 4 chains) mostly for B cells identified at do (**Figure S3A**), which partly could be related to the low expression of BCR or possible doublets. The BCRs with 3 or 4 chains comprised of completely different V, D, J and C genes for



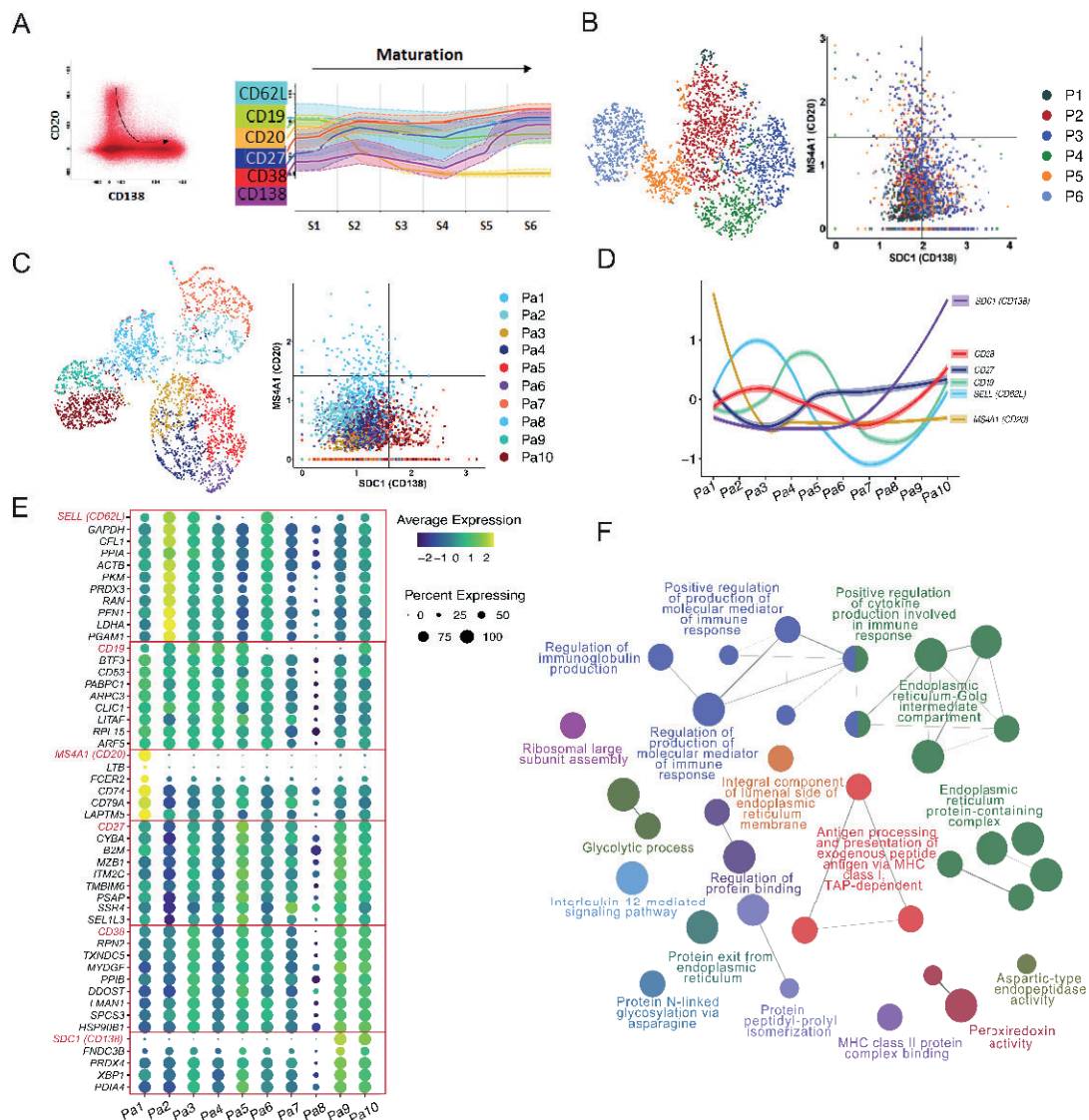


**Figure 2. Plasmablast/plasma cell maturation using flow cytometry and single-cell transcriptomics data over time following vaccination.** (A) Flow cytometric evaluation of cell surface markers in maturing PB/PCs. Plasma cell maturation pathway was drawn in the Infinicyt software based on the surface expression of CD20 and CD138. The least mature PB/PCs were defined as CD20+CD138- and the most mature as CD20-CD138+. Dot plot in the left panel shows all PB/PCs from the same donor and time-points used in the sequencing, and black arrow indicates the direction of plasma cell maturation. Each dot represents one cell. Subsequently, the entire maturation pathway was divided into 10 maturation stages (S1–S6), for which expression of additional cell surface markers was evaluated (right panel). (B) FACS-like plot to arrange PB/PCs clusters P1–P6 in the maturation pathway defined by the expression of CD20 and CD138. (C) Redefining stages of PB/PCs in single-cell transcriptome data using six markers pre-selected based on flow cytometry. The PB/PCs were clustered using six pre-defined maturation markers and FACS-like plotting is used to stage the plasma cell clusters based on the maturation pathway. Ten clusters i.e., Pa1–Pa10 were obtained. (D) The spaghetti plot of all six markers visualized after staging the PB/PCs. (E) Additional maturation markers identified using single-cell transcriptomics data based on the Pa1–Pa10 plasma cell clusters and corresponding stages. Genes following similar expression patterns were identified using the TACSplot function. (F) The important pathways identified based on the top 20 similar genes to each of the six maturation genes. The GO terms based on biological processes, molecular pathways, cellular components, and immunological processes were merged. The pathways with  $<0.05$  corrected  $p$  values were selected for visualization.

both heavy and light chains, which might be related to the doublets that could not be removed in the filtering steps or the production of multiple chains in B cells [20]. For further comparisons in the manuscript, the BCRs from do B cells and PB/PCs were considered independently and post-vaccination BCRs were compared with do PB/PCs. Also, the expression of BCRs in B cells for both heavy and light chains was lower as compared to plasma cells.

### *Cells with Different IGHV and IGHJ Are Dominant at Different Time Points*

The single cells with paired heavy and light chain information revealed preferential pairing between IGHV genes and IGKV1 and IGKV3 gene families (**Figure S3B**). IGLV genes mostly belonged to the IGLV1, IGLV2 and IGLV3 gene families. Also, over time, IGKV1, IGKV3, IGLV1, IGLV and IGLV3 gene families remained the most abundant, with minor variations in the usage which can be due to the limited number of cells or expansion of individual clones. However, no strong selection for a particular light chain was observed. On the contrary, we did observe changes in the usage of the IGHV genes over time (**Figure S3B**). Overall, the IGHV3 was the most used gene family, however, the usage of IGHV1, IGHV2, IGHV4 gene families increased in PB/PCs collected at d5 and d7 (around the peak of plasma cell response). To better understand the dynamics of the gene usage in IGH chains, we looked into the V(D)J gene usage. We found that IGHD3 genes were used the most over all time-points, whereas the usage of IGHV and IGHJ genes changed over time (**Figure S3C**). We observed that the increased usage of IGHV1, IGHV2, IGHV4 gene families was accompanied by an increased usage of IGHJ2, IGHJ3 and IGHJ6 genes post-vaccination.

### *IGHV3 and IGHJ4 Genes Predominant in do PB/PCs*

As we observed increased usage of several IGHV and IGHJ gene families, we examined the usage of IGHV and IGHJ gene families in all cells across different visits at baseline and post-vaccination. We observed more restricted scBCR-rep in do PB/PCs as compared to do B cells (**Figure S3D**). While 55 unique of 158 VJ pairs were observed in do B cells, only 16 unique usage of 118 VJ pairs were present in do PB/PCs. The IGHV3-23 and IGHJ4 were the most used pairs in both do B cells and PB/PCs. The majority of the recombination events observed in do B cells used IGHV1, IGHV3, IGHV4, IGHV5 families recombining with IGHJ4, however, it was highly selective in do PB/PCs, i.e., the IGHV3 family genes and IGHJ4 gene were used the most.

### *Few Clonotypes Expand with Delay at d10*

While comparing the PB/PCs from post-vaccination visits to do PB/PCs, we observed that the overall diversity increased at all the time-points post-vaccination (**Figure 3A**). We observed 50 and 65 new VJ pairs at d5 and d7 post-vaccination, respectively. Despite comparable numbers of sorted PBMCs and plasma cell counts at d10 and d14, we observed 24 new VJ pairs at d10 post-vaccination as compared to 35 new VJ pairs used at d14. Overall, we observed high usage of the IGHV3-23 gene and the IGHV4 gene family at all time-points including baseline. A clear expansion of IGHV1 and IGHV4 family genes especially IGHV1-2, IGHV1-

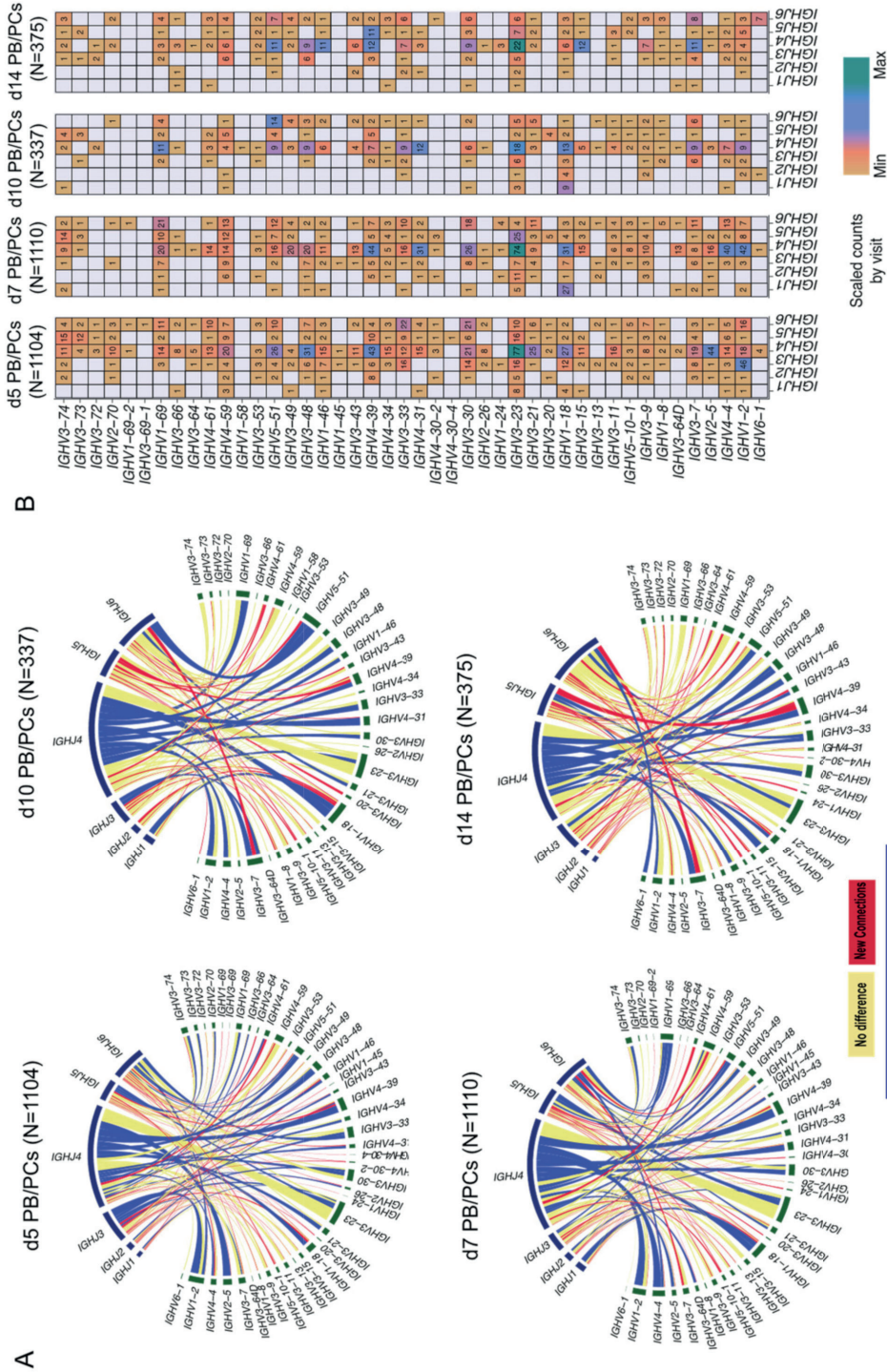


**Figure 3. VJ gene usage in PB/PCs from all the post-vaccination visits relative to baseline.** (A) Circos plot of VJ gene usage in PB/PCs from all the post-vaccination visits relative to baseline. Each ribbon represents a specific pairing between V and J genes, and the ribbon width represents the confidence bounds of the plotted data using the LOESS method. Ribbons color shows no change (yellow) or expanded links (dark blue) or new recombination events (red) as compared to do PB/PCs. (B) Heatmap plot of VJ gene usage in PB/PCs from all the post-vaccination visits.



18, IGHV3-33, IGHV4-39, IGHV4-31 gene can be observed around the peak of plasma cell expansion (**Figure 3A**; d5, d7 and d10). IGHV5-51 usage was also observed to be expanding at d10. The expansion of selected few V(D)J genes at the later time-points suggested the expansion of few clones with a delay. When comparing the relative usage of IGHV and IGHJ genes between visits post-vaccination, we observed that the usage of majority of the genes is comparable between visits with few exceptions, for example, the usage of IGHV1-69 increased at d5 and d7 post-vaccination (**Figure 3B**). Furthermore, IGHV1-2 and IGHJ3 were used the most at d5, whereas IGHV1-2 and IGHJ4 were used at d7, while at d10 and d14 the usage of IGHV1-2 was minimal.

### **Constant Gene Usage over Time upon Vaccination**

#### *IGHG1 Constant Gene Predominant at the Peak of the PB/PCs*

Assessment of the constant gene usage helps in understanding the raised effector function post-vaccination. To identify the usage of the constant genes in the profiled BCRs, we grouped the receptors based on the constant genes.IGHM was the most used constant chain in do B cells (**Figure 4A**), followed by IGHD. It was in line with the abundance of naive/pre-germinal center B cells in the pre-vaccination scBCR-rep. However, IGHA1 was the most used constant gene in the do PB/PCs (**Figure 4A**). The composition of the constant chains changed after vaccination and IGHG1 became the most used chain. The percentage of cells utilizing IGHA1 decreased at the peak of the plasma cell response i.e., d5 and d7, but at d10 and d14 returned to the levels comparable to baseline. The usage of IGHD was negligible in the PB/PCs post-vaccination. On the other hand, IGHM usage reduced at the peak of PB/PCs response which returned to original levels at d14. We observed a similar trend in the flowcytometry data, wherein the 67% of PB/PCs expanded at d7 was IgG1+ and the relative usage of IgA1 was reduced (**Figure 4B**). The IGHD expression was relatively low in the single-cell data limiting identification of the IgM+IgD+ B cells, which we could indeed identify in the flow cytometry data (data not shown). With the paired chain information from single cells, we observed that the IGKC gene was the most used gene followed by IGLC2 in all the post-vaccination visits. The high usage of the IGKC gene is in line with our previous results specifying high usage of IGKV gene families (**Figure 4C**). Interestingly, in do PB/PCs, IGLC1, IGLC2 and IGLC3 genes were used more frequently than other IGLC genes.

### **BCR Clonotypes over Time upon Vaccination**

#### *Identification of Clonotypes Based on V Family Grouping*

The BCRs were clustered into clones/clonotypes with a slight deviation from the classical definition of clonotypes; instead of genes, we used V family and J gene for grouping. Irrespective of the definition used, results of the clustering were highly similar (rand index of 0.99). The differences in the number of clusters were caused by the fact that several singletons clustered with other singletons with similar BCRs when the V gene definition was relaxed by V family (**Table S2**). Of 3334 clonotypes, 662 clonotypes could not be assigned any visit, 575 of which were singletons (8 clones with >10 BCRs; the largest clone comprises 129

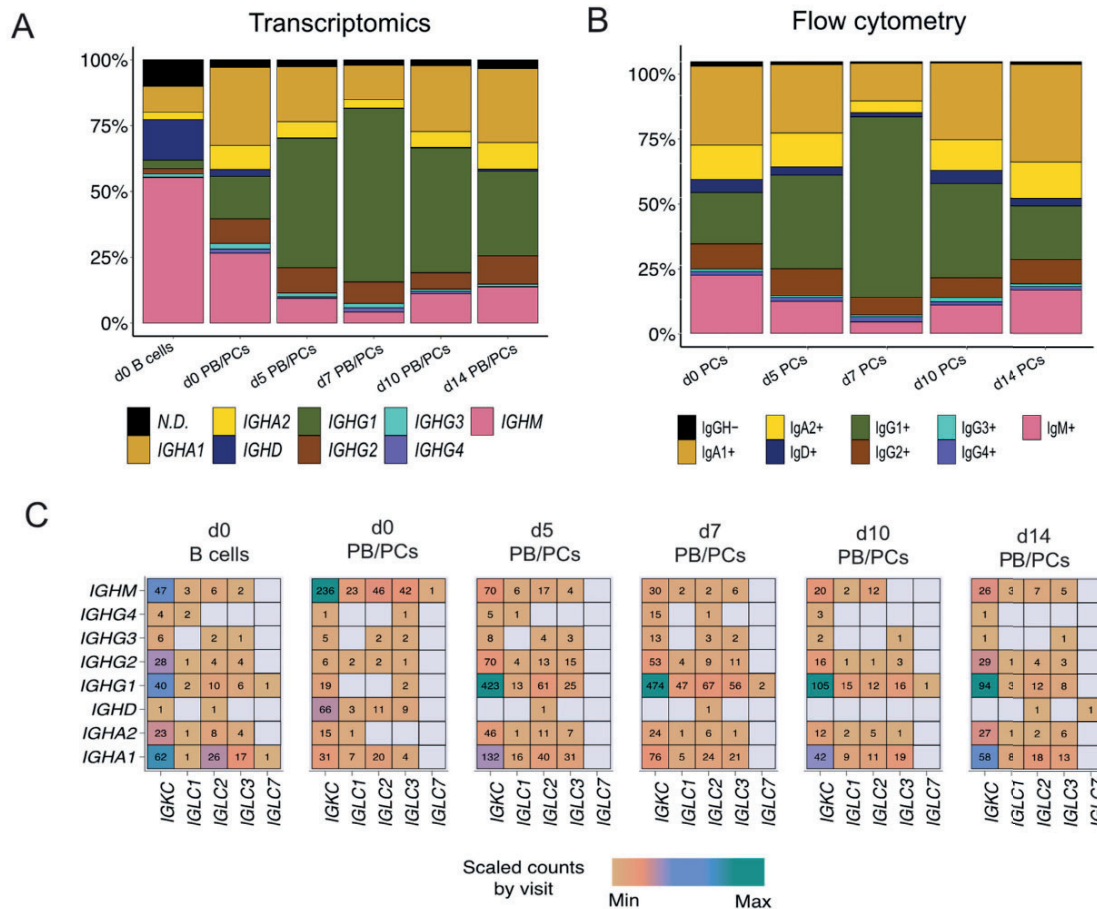


**Figure 4. The dynamics of heavy and light constant gene usage in the BCRs over different time-points pre- and post-vaccination.** (A) Usage of IGH constant genes in single-cell BCRs over time. The PB/PCs and B cells at the d0 are considered separately. (B) Over time usage of constant genes in the PB/PCs as identified by flow cytometry (based on membrane and intracellular Ig expression). (C) The usage of heavy and light constant genes across different visits. The numbers in the heatmap are the number of chains using a given pair and the colors are ranged based on the scaled counts for each visit.

BCRs). Overall, 936 of 3334 clonotypes had at least 2 cells. 369 of 936 clonotypes were shared between at least two visits of which 145 clonotypes had cells present on d0. For the 4051 cells derived from the known visits and with a rearranged productive heavy chain, **Figure 5A** shows the origin of the top 30 (449 BCRs) of 145 (2075 BCRs) clonotypes. The largest clone comprised of 46 B cells and was present in all visits but d14 (**Figure 5A**; C115). However, 30 additional B cells belonged to the same clonotype, but could not be assigned any visit (**Figure S4A**; the top second clone). The clonotype C115, consisting of only the IGHG1 isotype, had an expansion of identical sequences across multiple visits including baseline as visualized by the largest pie in **Figure 5B**. This largest node comprises of 58 individual BCR sequences wherein 34 of them are derived from d5 and 20 BCRs could not be assigned to any visit.

#### CSR Events within the Clonotypes

We investigated the clonotypes for the CSR events by querying clones with dif-

ferent IGHC chains. Of 369 clonotypes shared between different visits, 191 clonotypes used the same constant gene and do not represent clonotypes with CSR. Interestingly, a majority of clonotypes (53%; 101 of 191) only used the IGHG1 gene, 21% clonotypes used IGHA1 followed by 10% using IGHM and 8% using IGHG2. Thus, clonotypes followed the same trend as constant gene usage. Of 178 clonotypes that used multiple constant genes, 17% used IGHG1 and IGHA1 (**Figure 5C**). IGHG1 is clustered with IGHM three times more (74%) as compared to IGHG2 clustering with IGHM. Similarly, IGHA1 is clustered with IGHM three times more than IGHA2, suggesting high CSR between IGHM and IGHA1. Overall, we found that 45% of these clonotypes contained IGHM and IGHG isotypes, followed by IGHM and IGHA (29%). The usage of multiple constant genes in the clonotypes suggest a high IGHG1 response followed by IGHA1.

### *Clonal Lineages of the Clonotypes with CSR Events*

We selected a few of the large clonotypes to visualize the class-switching process via lineage construction. While some of the clones (e.g., clone 660, utilizing almost exclusively IGHG1 with one IGHA1) were highly mutated and diverse (**Figure S4B**), others (e.g., clone 1980) showed a more conserved mutation pattern with very few mutations separating the clone members (**Figure 5D**). Clone 1980 is the 20th largest clone where the IGHA and IGHG constant genes expanded with identical sequence in the V genes, which were only one to four mutations away from the IGHM harboring BCR (**Figure 5D**). This is an example of a receptor wherein the BCRs at later time-points harbor fewer mutations as compared to the germline than the BCRs sampled on do. This suggests that this clone is derived from memory responses generated during previous antigen encounters.

### *Comparable Length of Most of the Junctions*

Similarly, CDR3 length distribution was plotted for all the cells grouped by clonotype at baseline and each visit post-vaccination. We observed a larger proportion of clonotypes with CDR3 lengths of 12 amino acids at d5 (mean length of CDR3:  $15.8 \pm 3.8$  amino acid residues) and 15 amino acids at d7 (mean length of CDR3:  $15.6 \pm 3.1$  amino acid residues). We also observed a few clonotypes with longer junction region at d5 and d7 post-vaccination (**Figure S4C**).

### **Mutation Load in BCRs upon Vaccination**

The selection process for higher affinity Abs during the GC response also leaves an imprint on the IGHV genes, in terms of the type of amino acid substitutions observed in the cells which have successfully passed selection. Analysis of such mutation patterns at the nucleotide level allows us to understand the adaptability of the immune system to the antigens encountered during vaccination.

### *Positively Correlated Mutations in Heavy and Light Chain Genes*

The majority of the BCRs in the activated memory B cells used the IGHM (34 cells) gene followed by the IGHA1 (6 cells) constant genes. As expected, the mutation load between memory B cells (cluster B2) and activated memory B cells (cluster B3) was not significantly different. We observed that the IGHG1 and IGHM BCRs

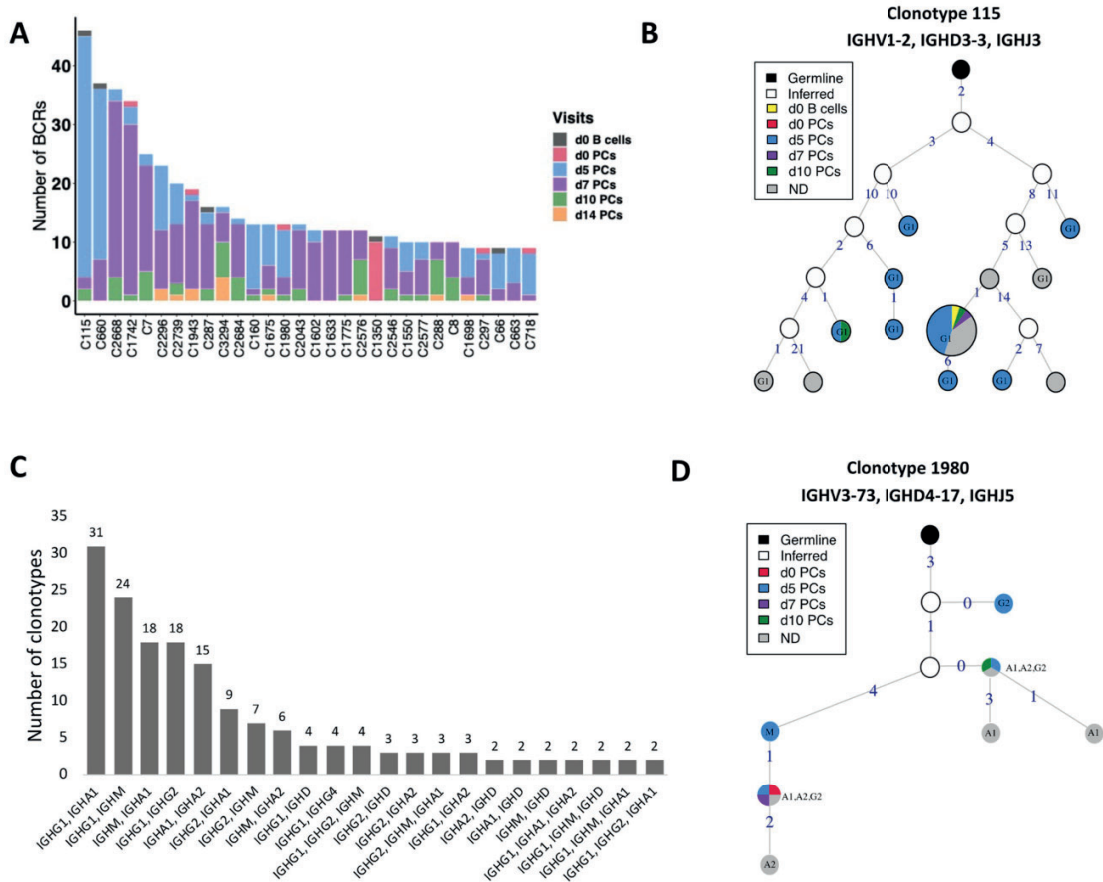


**Figure 5. BCR clonotypes over different time-points.** (A) 30 most numerous clonotypes over different time-points pre- and post-vaccination. Contribution of different visits to the total size of a clone is indicated by colors. (B) Clonal lineage of clonotype 115. The graph is constructed using V gene germline sequence as the root node. The size of each node is scaled and directly related to the number of BCRs for that particular sequence. The nodes are colored based on the visits from which sequences are derived. The unique sequences present across multiple visits are also grouped and colored differently as mentioned in the legend. Germline is colored black and the inferred nodes are colored white. The edge label indicates the number of different nucleotides as compared to the previous node. (C) A bar plot indicating the >2 clonotypes containing cells with multiple constant genes. For example; each of 31 clonotypes consist of sequences using IGHG1 and IGHA1 constant genes. The number of clonotypes for each combination is mentioned on the top of bar. (D) Clonal lineage of clonotype 1980 with class-switch recombination events. Additional inferred nodes were added to correctly represent the order of class-switching.

in PB/PCs had significantly more mutations ( $p < 0.05$ ;  $< 0.001$ ) in the complete V gene as compared to the memory and activated memory B cells sampled at d0 (**Figure 6A**). The mutations in V region in sequences using IGHG1 constant gene are also accounted for in the CDR1 and FR3 region whereas for IGHM the significant differences were also observed in FR2, CDR2 and FR3 regions. We observed that IGHV of BCRs utilizing IGHG1, in general, harbored more mutations in post-vaccination visits as compared to other constant genes in all V regions (**Figure 6A**), which might be associated with the expansion in the IGHG1 BCRs post-vaccination. Moreover, we found that the mutations in heavy chains were positively correlated with the mutations in the light chain in all the regions with significant p values (**Figure 6B**).



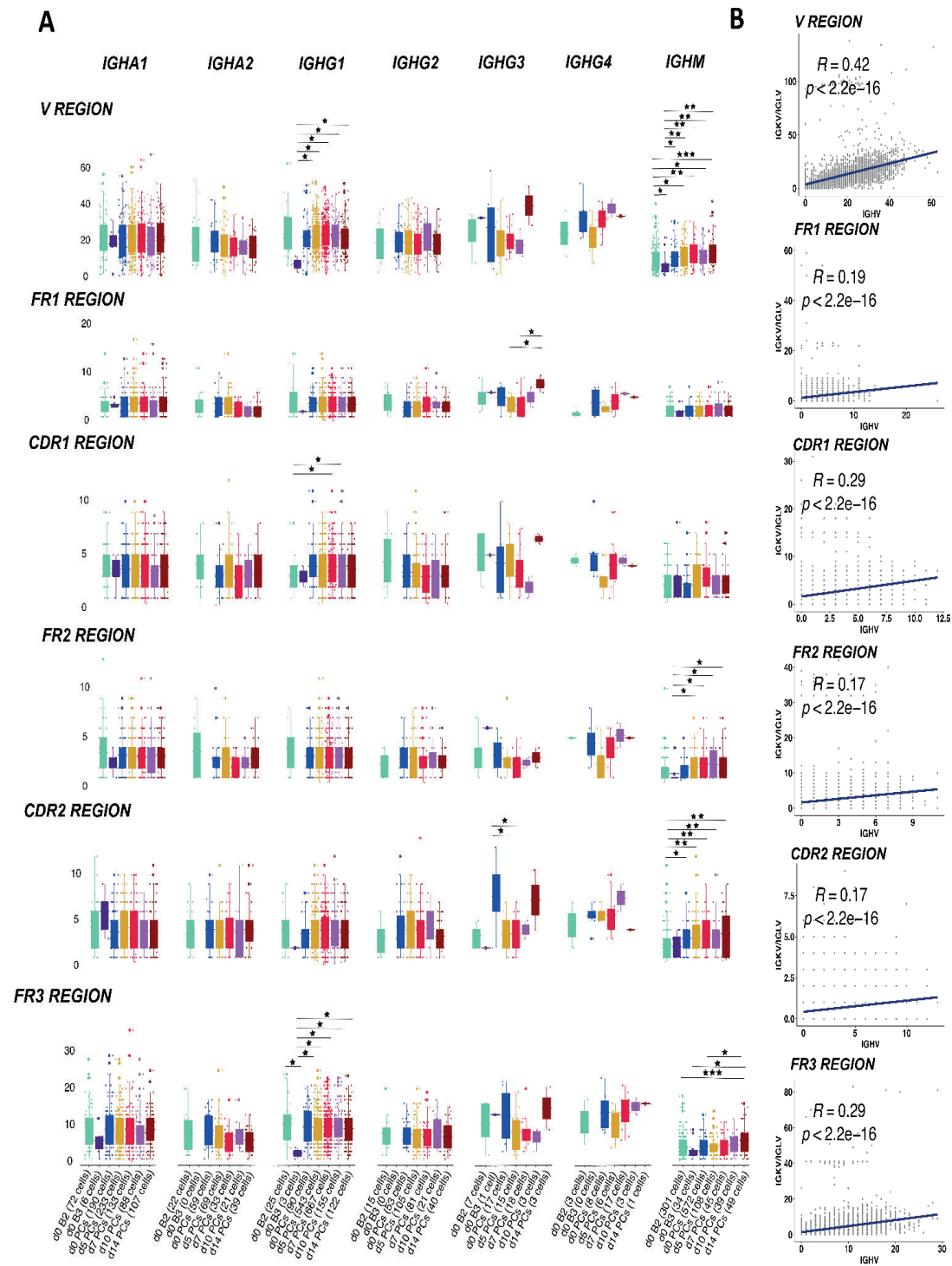


**Figure 6. SHM levels in the V genes in heavy and light chains.** (A) The boxplot representing the number of mutations in the V genes of BCRs over different time-points pre- and post-vaccination per different constant gene. The mutations have been identified in each cell over framework and complementarity determining regions in the V region. The cells at do are divided over naive B cells, memory B cells, activated memory B cells and PB/PCs. Each dot is a sequence from a single cell. The significant mean differences as calculated by the t-test are highlighted by asterix as \*: 0.05–0.01, \*\*: 0.01–0.001 and \*\*\* < 0.001. (B) The correlation of mutation numbers in all the V regions between heavy and light variable genes for all cells with known paired constant BCRs. The regression line is fitted and the correlation and p values are indicated on top.



### *Positive Selection of Mutations in the CDR Region over Time*

To further confirm that the mutations in PB/PCs were antigen driven, we employed BASELINE [21] to detect the selection by analyzing mutation patterns in experimentally derived Ig sequences. We observed a negative/neutral selection in framework regions and slightly positive selection in the CDRs (**Figure S5**). The differences between the selection estimates in both FWR and CDR regions were highly significant ( $p \leq 0.03$ ) except in FWR region at visit d10 ( $p = 0.25$ ). The positive selection of mutations in CDRs and negative selection in FWRs correspond with normal antigen-specific B cells [22]. Moreover, we did not observe a varying trend i.e., increasing or decreasing selection pressure in CDRs over time suggesting that the selected receptors were already available at the beginning of the response and these were recruited over time for optimum immune response.

### **BCRs Specific to Vaccine Toxoids**

To identify toxoid-specific lineages in the scBCR-rep, we searched literature for the CDR3 sequences known to be specific to antigens present in the Boostrix vaccine. We used the CDR3 amino acid sequences of the (mono-)clonal Abs for the anti-DT [23], anti-TT [24] and anti-PT [25] to query the related BCRs in our data (**Figure S6**). To account for individual-specific variability in the CDR3 sequences (as a result of SHM and affinity maturation processes specific to the individuals), we allowed a certain level of flexibility in our search. Apart from relaxing the identity of the CDR3 sequence at the amino acid level to 60–70%, the length of the CDR3 sequences was also allowed to vary by 1-3 amino acid residues.

### *Identification of Conserved Anti-TT BCRs*

We could not identify any relevant BCR sequence highly related to the anti-DT Ab sequences previously published. However, we identified 54 BCRs from 25 clonotypes that were highly similar to anti-TT Ab query sequences. 65% of the observed anti-TT BCR clones used the IGHG1 constant gene followed by the IGHA1 (13%), IGHM (15%) and IGHA2 (6%) genes. IGHG1 was observed at all time-points, whereas IGHA1, IGHA2 and IGHM were observed only until d7 post-vaccination. Clone 288 and 291 are 82% and 88% identical to the query anti-TT Ab sequence (**Figure 7A**). Similarly, clone 681 and 2083 are 80% and 86% identical to their respective anti-TT Ab query sequences. Clone 288 was the largest expanded clone with anti-TT specific BCRs (**Figure 7B**). This clone was present mostly at the later time-points post-vaccination. The presence of highly conserved BCR clones to the queried anti-TT Ab sequences suggests the BCRs can be highly conserved among different individuals. Furthermore, it also suggests that the immune response against TT is memorized efficiently by the immune system for secondary responses.

### *Identification of BCRs (Un-)Likely Related to Anti-PT BCRs*

Analogously, we identified 20 BCRs that were similar to the anti-PT Ab query sequences, however the BCRs were not conserved as compared to the query sequences. This might suggest that the selected BCRs may be specific to antigens other than PT. 55% of the hits used the IGHG1 gene sampled from all visits, fol-

lowed by 30% IGHM BCRs sampled from the memory B cells (cluster B3) at baseline. Unlike the anti-TT BCR sequences, we also observed a few BCRs using the IGHD constant gene. One clone with maximum identity (~70%) to the anti-PT Ab query sequence was found (**Figure 7C**). This clone used the IGHG1 constant gene. Clone 2450 is 73% identical to its respective anti-PT Ab query sequence. We did not observe highly conserved (>80%) CDR3 sequences to the anti-PT Ab query sequences suggesting either a unique individual-specific repertoire or recurrent adaptability of the immune response to the subsequent encounter of the antigen i.e., PT.

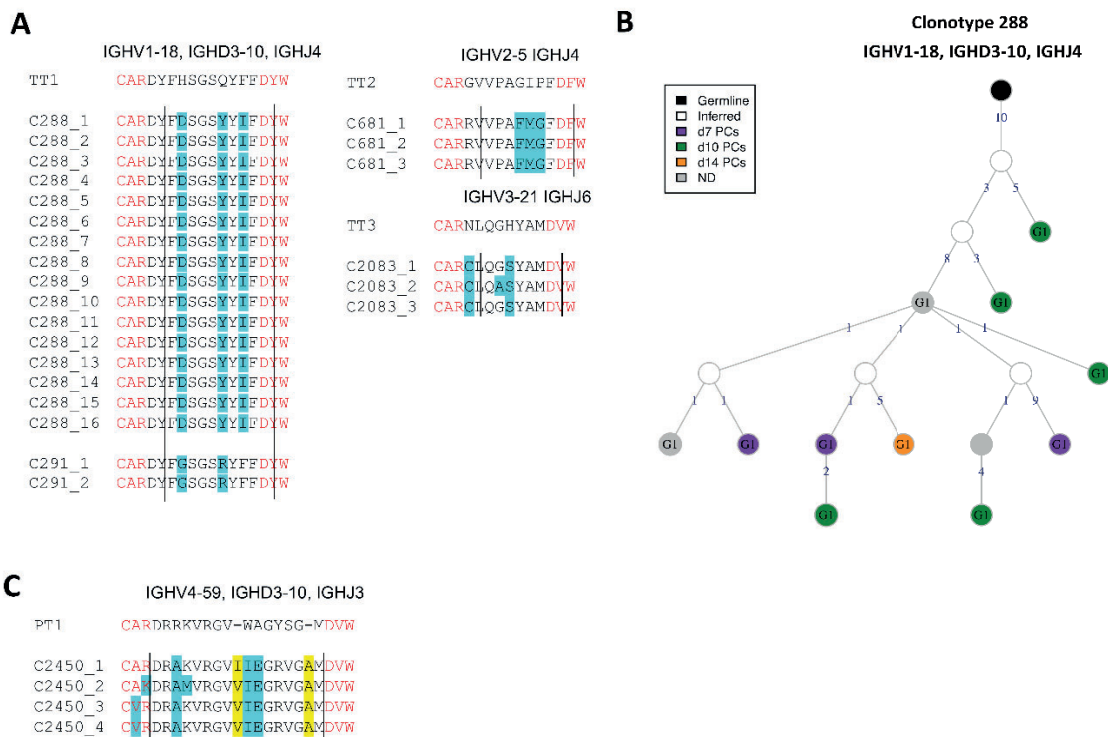


**Figure 7. Toxoid-specific lineages upon Boostrix vaccination.** (A) Highly conserved anti-tetanus toxoid BCR clonotypes. Four clonotypes with >80% identity are aligned to the anti-TT Ab query sequences. The changed residues are highlighted in cyan and clonotype IDs are mentioned. The V and J gene residues are highlighted in red and demarcated by straight lines. (B) BCR lineage of anti-tetanus toxoid clonotype 288. The largest anti-TT BCR clonotype is visualized. (C) (Un-)likely related anti-pertussis toxoid BCR clonotypes. One clonotype with >70% identity is aligned to the respective anti-PT Ab query sequences. The length flexibility allowed the identification of these clonotypes. The changed residues are highlighted in cyan and the insertions are highlighted in yellow. Clonotype IDs are mentioned.

## Discussion

Understanding human B-cell immune responses to infections is critical for vaccine development and assessment [26]. The repertoire of antigen receptor sequences changes during an encounter with foreign antigen from pathogens/vaccination [19,27]. Identifying the signatures of effective responses from the repertoire data is challenging and systematic analysis of the repertoire together with the dynamics of clonal lineages during infection/vaccination is crucial. Here, we systematically characterized the cell types in sorted B cells and PB/PCs using sin-

gle-cell transcriptomics data and developed a robust workflow to capture the longitudinal changes (do, 5, 7, 10, and 14 after Boostrix vaccination) in the BCRs and clonal lineages using repertoire data from the same cells. Moreover, we accorded our results with previously acquired flow cytometry data from the same individual [5]. We identified additional membrane markers that could be used in flow cytometry to dissect the maturation of PB/PCs. Furthermore, using one individual, we developed a bioinformatic workflow as a proof-of-principle to compare the BCR-rep in PB/PCs with the baseline B-cell repertoire and reported expansion of unique clones in post-vaccination visits, high usage of IGHG1 in expanded clones, increased class switching events post-vaccination and positive selection of CDR3 sequences over time. We also found that the Variable gene family-based clustering of BCRs improved the clustering of BCRs. Finally, the query tool developed in the study dissect the immune response to the components of Boostrix vaccine is unique to this study. Albeit that this pilot study contains only one individual, this study still allows us to select for the right processes to be evaluated in a larger series. Additionally, the analysis performed in one individual could impact the biological findings in our study, especially, the V(D)J gene usage and clonal lineage analysis, which should be assessed in larger studies.

The classical markers used in phenotyping by flow cytometry are not always captured in the sparse single-cell transcriptomics data which makes it challenging to define uniform populations in both the technologies. Therefore, the identification of naive B cells, memory B cells, activated memory B cells and plasma cell clusters was made using a combination of classical CD markers and other gene-based markers known in the literature. For example, CXCR4, a chemokine receptor, turned out to be an important marker for the identification of the naive B cells [16], whereas the classical markers IGHD, CD19 were dimly expressed in this cell subset. Also, CXCR4 is known to be progressively downregulated in transition from naive B cells to memory B cells to activated memory B cells [19], which we also observed in clusters B1, B2 and B3 (Figure 1D). The activated memory B-cell state displays a hallmark of an effector B-cell response and shares several markers with previously defined aged/autoimmunity-associated B cells, e.g., high expression of ITGAX (CD11c) [28]. Another activated memory B-cell marker, i.e., ZBTB32, is known to modulate the duration of memory B-cell recall responses in mice [29]. Defining the B-cell populations accurately helps in better understanding of the molecular processes e.g., immunoglobulin production, antigen processing and presentation and glycolysation in vaccination/infection (Figure 2F), which in turn might be helpful in identifying therapeutic targets in pathogen immunity. Moreover, among all activated memory B-cell markers, ITGAX, CD72 and TNFRSF1B are membrane markers, that in addition to the classical B-cell markers can be used to sort activated memory B cells.

Despite regressing out cell cycle genes, we still observed a high score for the G2+S genes in the P4 cluster, suggestive of the most proliferating PB/PCs. Although we did not consider the cell cycle genes for lineage tracing, the P4 plasma cell cluster was the endpoint of the trajectory, which suggests the role of developmental ge-

nes other than cell cycle genes in the plasma cell development and proliferation. Interestingly, these P1-P4 clusters of PB/PCs do not accurately depict the developmental stages of PB/PCs as defined by the CD20 and CD138 markers in flow cytometry [5]. We showed that using flow cytometry data as a reference, the stages of plasma cell maturation could be tracked accurately and additional plasma cell maturation markers, contributing from the early to late plasma cell maturation pathway, were identified. For example, peroxiredoxin PRDX3 (similar expression as SELL (CD62L)) suffices the metabolic requirements of PCs in early phase of development that are destined to secrete massive amounts of Ig [30]. PPIA, peptidyl-prolyl isomerase A, catalyzes the protein folding and might play an important role in folding the Abs in the early phase of plasma cell development. Additionally, PABPC1 (expression similar to CD19) mediates the regulation of the switching from membrane IgH to secreted IgH isoform in PCs [31]. CD74 (expression similar to MS4A1 (CD20)) is directly involved in shaping the scB-CR-rep by initiating a cascade that results in proliferation of B cells and rescues the cells from apoptosis [32,33]. MZB1 (expression similar to CD27) is an important co-chaperone in plasma cell differentiation [34]. Loss of this gene can affect migratory properties of the Ab secreting cells and their trafficking and retention to the bone marrow [34]. Similarly, the SSR4 gene plays an important role in protein assembly and trafficking [35]. Its high expression is related to IgG4-related diseases [36]. The markers DDOST and PPIB (expression similar to CD38) are involved in protein glycosylation and unfolded protein responses in the plasma cell development process as also identified in the pathway analysis. Finally, XBP1 (similar expression as SDC1 (CD138)) is responsible for late events i.e., increased protein synthesis in plasma cell differentiation [37,38]. Herein, 32% of 104 genes were found to express membrane bound proteins and hence can be used in flow cytometry to dissect additional stages of plasma cell maturation and/or sort specific populations e.g., Ab-secreting cells. A few of these markers e.g., CD74 [39] and CD22 [40] have already been used in quantitative flow cytometry studies to distinguish normal B cells from the B-cell related malignancies.

The repertoire in response to infection/vaccination has generally preference for specific V, D or J genes. For example, anti-hemagglutinin clones have been shown to use the IGHV1-69 gene [35,41] and IGHV4-34 gene [19] is abundant in influenza vaccination/infection studies. However, the usage of the IGHV3-7 gene increased after Hepatitis B vaccination [42]. Also, the abundance of the IGHV4-59, IGHV4-39, IGHV3-23, IGHV3-53, IGH3-66, IGHV2-5, and IGHV2-70 genes was found in SARS-CoV2 infection studies [43,44,45,46]. Similarly, we observed an increased usage of the IGHV3-23 gene on all visits post-vaccination; the usage of the IGHV1-2, IGHV1-18, IGHV3-33, IGHV4-39, IGHV4-31 genes increased at d5, d7 and d10 post-vaccination; and IGHV5-51 was highly used at d10 post-vaccination. We found that none of the specific classes of the IGHV genes has driven the overall response. Moreover, we identified high usage of the IGHD3 family and the IGHJ6 gene, which is in general abundantly used in the general repertoire [47,48,49], most likely owing to the perfect recombination signal sequences [50,51]. In the light chains, we also observed a high usage of the IGK genes as



compared to the IGL loci gene, reflecting the normal 3:2 ratio observed in humans at baseline [52,53,54], which was skewed to a ~8:3 ratio at d5, suggesting selection mechanisms due to the antigen exposure.

We identified ~900 of ~3500 clonotypes with >1 BCR clustered together. The majority of them were present on d5 and d7 post-vaccination. Although, the PB/PCs expanded after vaccination are enriched for vaccine-specificity, we cannot rule out that some of the PCs may have a different specificity [55,56]. Approximately, 70% of the Ab-secreting cells in the influenza vaccination study have been shown to be influenza-vaccine specific, previously [8]. The clonotype classification allowed us to identify class-switching events, the majority of which contained IGHM and IGHG, followed by IGHM and IGHA. It is known from previous studies that ~85% of the switches from IgM commonly comprises of IgG1, IgA1 and IgG2 in decreasing order [57]. Higher usage of the IgG subclasses (48% IgG1, 22% IgG2, and 9% IgG3) has been known previously from influenza vaccine responsive clones [19], which was also observed in our study. Altogether, the highest usage of the IGHG1 gene and the highest number of clonotypes containing IgM and IgG suggest the vaccine target IgG-based immune response, common immune response in intramuscular vaccine administration.

The selection processes and molecular events affect the V gene of IG heavy chain differently than the light chains [58,59] resulting in less diversity in the light chain repertoire [60]. Although we observed significant correlations between the mutations in V regions in heavy and light chain genes, the correlation was <45%. The high mutation rate in IGHV BCRs utilizing the IGHM class has been proposed as a mechanism of the immune system to maintain long-term memory to the vaccine [61]. Moreover, the high number of mutations in IGHG1 and IGHM genes in CDR and FR3 regions might also be associated with the maturation of IgG affinity during the response to the Boostrix vaccine. As the vaccine is a booster and only one individual was used for the pilot study, it might be difficult to assess the role of booster in affinity maturation processes.

The dissection of the immune response to all the antigens and/or separate components of a vaccine, when cells are not pre-sorted based on their reactivity, can be helpful to estimate the response to each of the antigens. We identified a few clonotypes related to anti-TT and anti-PT BCRs, suggesting the public nature of the queried sequences. Identification of highly conserved anti-TT BCRs suggests an optimal repertoire for strong immunodominant epitopes. However, we observed that the anti-PT BCRs were not highly conserved which could be explained by either a unique private repertoire to the antigen or that each encounter with this antigen shapes the repertoire with additional mutations. The number of identified anti-TT and anti-PT clones are not directly related to the complexity of the proteins in the vaccine but related to the number of epitopes found in the literature. Additional support to this observation can be obtained with repertoire data obtained from antigen-specific B cells from multiple individuals.



## Chapter 3.3

---

Overall, we identified B-cell populations and additional plasma cell maturation pathway biomarkers based on the transcriptomics data. Importantly, we used the longitudinal scBCR-rep data to understand the V(D)JC gene usage, clonal expansion and SHM events post-vaccination and their role in shaping immune responses. Together, we were able to dissect the immune responses to the components of the Boostrix vaccine.

### Conclusions

To conclude, we have characterized the PB/PCs response of an immunized donor by performing longitudinal analysis (d0, 5, 7, 10, and 14 after Boostrix vaccination) of the single-cell transcriptome as well as the B-cell receptor (BCR) repertoire (scBCR-rep) data and comparing them with the flow cytometry data from the same donor. We report that the conventional membrane protein markers for cell type identification in flow cytometry do not match transcript expression levels. Hence, proper B-cell subsetting based on gene expression profile requires use of additional parameters. Also, the flowcytometry data guided us to trace the maturation pathway of the PB/PCs, which was not feasible with the single-cell transcriptomic data, owing to differences in the transcript level expression. However, after tracing the maturation pathway, we could find multiple additional membrane markers e.g., CD37, CD52, CD22, CD53, FCER2 that could be used in flow cytometry to dissect the maturation of PB/PCs. Furthermore, in this study, we developed a methodology to compare the BCR-rep in PB/PCs with the baseline B-cell repertoire and reported expansion of unique clones in post-vaccination visits, high usage of IGHG1 in expanded clones, increased class-switching events post-vaccination and positive selection of CDR3 sequences over time. We also found that the Variable gene family-based clustering of BCRs improved the clustering of BCRs. Finally, the query tool developed in the study to dissect the immune response to the components of the Boostrix vaccine is unique to this study.

### Author Contributions

I.K., A.M.D., E.B.v.d.A., M.J.T.R., J.J.M.v.D. and M.A.B.: concept and design of the study. A.M.D. and M.A.B.: Processed samples for single-cell sequencing and organized clinical part of the study. I.K.: Analyzed the data. I.K. and M.A.B.: Interpreted the results. L.E.M.O. and J.J.Z. coordinated the clinical part of this study. All authors have read and agreed to the published version of the manuscript.

### Funding

This project has received funding from the PERISCOPE program. PERISCOPE has received funding from the Innovative Medicines Initiative 2 Joint Undertaking under grant agreement No 115910. This Joint Undertaking receives support from the European Union's Horizon 2020 research and innovation program and European Federation of Pharmaceutical Industries and Associations (EFPIA) and Bill and Melinda Gates Foundation (BMGF). IK received personal funding for this work from the European Union's Horizon 2020 research and innovation program under the Marie Skłodowska-Curie grant agreement No 707404.

**Institutional Review Board Statement**

The study was conducted according to the guidelines of the Declaration of Helsinki, and approved by the Medical Ethics Committee Leiden-Den Haag-Delft (protocol code P16-214, EUDRACT:2016-002011-18, approved on 11-01-2017).

**Informed Consent Statement**

Informed consent was obtained from all subjects involved in the study.

**Data Availability Statement**

Raw and processed data have been deposited at Gene Expression Omnibus and are available via GEO accession GSE185427. The codes are made available via the GitHub repository <https://github.com/InduKhatri/Single-cell-BCR>.

**Acknowledgments**

The authors gratefully acknowledge the Flow cytometry Core Facility at LUMC (coordinated by K. Schepers, M. Hameetman, run by operators S. van de Pas, D. Lowie, J. Jansen, IJ. Reyneveld and former operators E. de Haas and G. de Roo) for their support. We are grateful to the subject, who volunteered to contribute to clinical study. We would also like to acknowledge Rick J. Groenland and Bas de Mooij, who helped in acquiring and sorting cells for the study. We would like to acknowledge Susan Kloet and the personnel from the Leiden genome technology center (LGTC) at the LUMC for providing the sequencing support. Finally, the authors would like to thank the team of Liesbeth Oosten and Jaap-Jan Zwaginga from the Dept. of Hematology, LUMC, for their help with the clinical part of this study.

**Conflicts of Interest**

J. J. M. van Dongen is the founder of the EuroClonality Consortium and one of the inventors on the EuroClonality-owned patents and EuroFlow-owned patents, which are licensed to Invivoscribe, BD Biosciences or Cytognos; these companies pay royalties to the EuroClonality and EuroFlow Consortia, respectively, which are exclusively used for sustainability of these consortia. J. J. M. van Dongen reports an Educational Services Agreement with BD Biosciences and a Scientific Advisory Agreement with Cytognos, with honorarium fees paid to LUMC. The rest of the authors declare that they have no other relevant conflicts of interest.

**Supplementary Materials**

The Supplementary Material for this article can be found online at: <https://www.mdpi.com/article/10.3390/vaccines9111352/s1>

or using the following QR code:

**References**

1. Eisen, H.N. Affinity enhancement of antibodies: How low-affinity antibodies produced early in immune responses are followed by high-affinity antibodies later and in memory B-cell responses. *Cancer Immunol. Res.* 2014, 2, 381–392.

## Chapter 3.3

---

2. Hammarlund, E.; Thomas, A.; Amanna, I.J.; Holden, L.A.; Slayden, O.D.; Park, B.; Gao, L.; Slifka, M.K. Plasma cell survival in the absence of B cell memory. *Nat. Commun.* 2017, 8, 1781.
3. Imani, F.; Kehoe, K.E. Infection of human B lymphocytes with MMR vaccine induces IgE class switching. *Clin. Immunol.* 2001, 100, 355–361. 4. Pan-Hammarström, Q.; Zhao, Y.; Hammarström, L. Class Switch Recombination: A Comparison Between Mouse and Human. *Adv. Immunol.* 2007, 93, 1–61.
5. Diks, A.M.; Khatri, I.; Oosten, L.E.; De Mooij, B.; Groenland, R.J.; Teodosio, C.; Perez-Andres, M.; Orfao, A.; Berbers, G.A.M.; Zwaginga, J.J.; et al. Highly sensitive flow cytometry allows monitoring of changes in circulating immune cells in blood after Tdap booster vaccination. *Front. Immunol.* 2021, 12, 2091.
6. GlaxoSmithKline. BOOSTRIX (Tetanus Toxoid, Reduced Diphtheria Toxoid and Acellular Pertussis Vaccine, Adsorbed) Injectable Suspension, for Intramuscular Use; GlaxoSmithKline: Research Triangle Park, NC, USA, 2020.
7. Ellebedy, A.H.; Jackson, K.J.L.; Kissick, H.T.; Nakaya, H.I.; Davis, C.W.; Roskin, K.M.; McElroy, A.K.; Oshansky, C.M.; Elbein, R.; Thomas, S.; et al. Defining antigen-specific plasmablast and memory B cell subsets in human blood after viral infection or vaccination. *Nat. Immunol.* 2016, 17, 1226–1234.
8. Wrammert, J.; Smith, K.; Miller, J.; Langley, W.A.; Kokko, K.; Larsen, C.; Zheng, N.Y.; Mays, I.; Garman, L.; Helms, C.; et al. Rapid cloning of high-affinity human monoclonal antibodies against influenza virus. *Nature* 2008, 453, 667–671.
9. Stuart, T.; Butler, A.; Hoffman, P.; Hafemeister, C.; Papalexi, E.; Mauck, W.M.; Hao, Y.; Stoeckius, M.; Smibert, P.; Satija, R. Comprehensive Integration of Single-Cell Data. *Cell* 2019, 177, 1888–1902.e21.
10. Mylka, V.; Aerts, J.; Matetovici, I.; Poovathingal, S.; Vandamme, N.; Seurinck, R.; Hulselmans, G.; Van Den Hoecke, S.; Wils, H.; Reumers, J.; et al. Comparative analysis of antibody- and lipid-based multiplexing methods for single-cell RNA-seq. *bioRxiv* 2020.
11. Kernfeld, E.M.; Genga, R.M.J.; Neherin, K.; Magaletta, M.E.; Xu, P.; Maehr, R. A Single-Cell Transcriptomic Atlas of Thymus Organogenesis Resolves Cell Types and Developmental Maturation. *Immunity* 2018, 48, 1258–1270.e6.
12. Bindea, G.; Mlecnik, B.; Hackl, H.; Charoentong, P.; Tosolini, M.; Kirilovsky, A.; Fridman, W.H.; Pagès, F.; Trajanoski, Z.; Galon, J. ClueGO: A Cytoscape plug-in to decipher functionally grouped gene ontology and pathway annotation networks. *Bioinformatics* 2009, 25, 1091–1093.
13. Bischof, J.; Ibrahim, S.M. bcRep: R Package for Comprehensive Analysis of B Cell Receptor Repertoire Data. *PLoS ONE* 2016, 11, e0161569.
14. Zuckerman, N.S.; Hazanov, H.; Barak, M.; Edelman, H.; Hess, S.; Shcolnik, H.; Dunn-Walters, D.; Mehr, R. Somatic hypermutation and antigen-driven selection of B cells are altered in autoimmune diseases. *J. Autoimmun.* 2010, 35, 325–335.
15. Stern, J.N.H.; Yaari, G.; Vander Heiden, J.A.; Church, G.; Donahue, W.F.; Hintzen, R.Q.; Huttner, A.J.; Laman, J.D.; Nagra, R.M.; Nylander, A.; et al. B cells populating the multiple sclerosis brain mature in the draining cervical lymph nodes. *Sci. Transl. Med.* 2014, 6, 248ra107.
16. Berkowska, M.A.; Schickel, J.-N.; Grosserichter-Wagener, C.; de Ridder, D.; Ng, Y.S.; van Dongen, J.J.M.; Meffre, E.; van Zelm, M.C. Circulating Human CD27 – IgA + Memory B Cells Recognize Bacteria with Polyreactive Igs. *J. Immunol.* 2015, 195, 1417–1426.
17. Toellner, K.M. FOXP1 inhibits plasma cell differentiation. *Blood* 2015, 126, 2076–2077.
18. Hövelmeyer, N.; Wörns, M.A.; Reissig, S.; Adams-Quack, P.; Leclaire, J.; Hahn, M.; Wörtge, S.; Nikolaev, A.; Galle, P.R.; Waisman, A. Overexpression of Bcl-3 inhibits the development of marginal zone B cells. *Eur. J. Immunol.* 2014, 44, 545–552.
19. Horns, F.; Vollmers, C.; Dekker, C.L.; Quake, S.R. Signatures of selection in the human antibody repertoire: Selective sweeps, competing subclones, and neutral drift. *Proc. Natl. Acad. Sci. USA* 2019, 116, 1261–1266.
20. Shi, Z.; Zhang, Q.; Yan, H.; Yang, Y.; Wang, P.; Zhang, Y.; Deng, Z.; Yu, M.; Zhou, W.; Wang, Q.; et al. More than one antibody of individual B cells revealed by single-cell immune profiling. *Cell Discov.* 2019, 5, 64.
21. Yaari, G.; Uduman, M.; Kleinstein, S.H. Quantifying selection in high-throughput Immunoglobulin sequencing data sets. *Nucleic Acids Res.* 2012, 40, e134.
22. Fang, L.; Lowther, D.E.; Meizlish, M.L.; Anderson, R.C.E.; Bruce, J.N.; Devine, L.; Huttner, A.J.; Kleinstein, S.H.; Lee, J.Y.; Stern, J.N.H.; et al. The immune cell infiltrate populating meningo-

- mas is composed of mature, antigen-experienced T and B cells. *Neuro. Oncol.* 2013, 15, 1479–1490.
23. Sevigny, L.M.; Booth, B.J.; Rowley, K.J.; Leav, B.A.; Cheslock, P.S.; Garrity, K.A.; Sloan, S.E.; Thomas, W.; Babcock, G.J.; Wang, Y. Identification of a human monoclonal antibody to replace equine diphtheria antitoxin for treatment of diphtheria intoxication. *Infect. Immun.* 2013, 81, 3992–4000.
  24. Lavinder, J.J.; Wine, Y.; Giesecke, C.; Ippolito, G.C.; Horton, A.P.; Lungu, O.I.; Hoi, K.H.; DeKosky, B.J.; Murrin, E.M.; Wirth, M.M.; et al. Identification and characterization of the constituent human serum antibodies elicited by vaccination. *Proc. Natl. Acad. Sci. USA* 2014, 111, 2259–2264.
  25. Acquaye-Seedah, E.; Reczek, E.E.; Russell, H.H.; DiVenere, A.M.; Sandman, S.O.; Collins, J.H.; Stein, C.A.; Whitehead, T.A.; Maynard, J.A. Characterization of individual human antibodies that bind pertussis toxin stimulated by acellular immunization. *Infect. Immun.* 2018, 86, e00004-18.
  26. Wec, A.Z.; Haslwanter, D.; Abdiche, Y.N.; Shehata, L.; Pedreño-Lopez, N.; Moyer, C.L.; Bornholdt, Z.A.; Lilov, A.; Nett, J.H.; Jangra, R.K.; et al. Longitudinal dynamics of the human B cell response to the yellow fever 17D vaccine. *Proc. Natl. Acad. Sci. USA* 2020, 117, 6675–6685.
  27. Nourmohammad, A.; Otwinowski, J.; Łuksza, M.; Mora, T.; Walczak, A.M.; Leitner, T. Fierce Selection and Interference in B-Cell Repertoire Response to Chronic HIV-1. *Mol. Biol. Evol.* 2019, 36, 2184–2194.
  28. Hao, Y.; O’neill, P.; Naradikian, M.S.; Scholz, J.L.; Cancro, M.P. A B-cell subset uniquely responsive to innate stimuli accumulates in aged mice. *Blood J. Am. Soc. Hematol.* 2011, 118, 1294–1304.
  29. Jash, A.; Wang, Y.; Weisel, F.J.; Scharer, C.D.; Boss, J.M.; Shlomchik, M.J.; Bhattacharya, D. ZBTB32 Restricts the Duration of Memory B Cell Recall Responses. *J. Immunol.* 2016, 197, 1159–1168.
  30. Masciarelli, S.; Sitia, R. Building and operating an antibody factory: Redox control during B to plasma cell terminal differentiation. *Biochim. Biophys. Acta-Mol. Cell Res.* 2008, 1783, 578–588.
  31. Peng, Y.; Yuan, J.; Zhang, Z.; Chang, X. Cytoplasmic poly(A)-binding protein 1 (PABPC1) interacts with the RNA-binding protein hnRNPLL and thereby regulates immunoglobulin secretion in plasma cells. *J. Biol. Chem.* 2017, 292, 12285–12295.
  32. Cohen, S.; Shachar, I. Cytokines as regulators of proliferation and survival of healthy and malignant peripheral B cells. *Cytokine* 2012, 60, 13–22.
  33. Gil-Yarom, N.; Radomir, L.; Sever, L.; Kramer, M.P.; Lewinsky, H.; Bornstein, C.; Blecher-Gonen, R.; Barnett-Itzhaki, Z.; Mirkin, V.; Friedlander, G.; et al. CD74 is a novel transcription regulator. *Proc. Natl. Acad. Sci. USA* 2017, 114, 562–567.
  34. Andreani, V.; Ramamoorthy, S.; Pandey, A.; Lupar, E.; Nutt, S.L.; Lämmermann, T.; Groschedl, R. Cochaperone Mzb1 is a key effector of Blimp1 in plasma cell differentiation and  $\beta$ 1-integrin function. *Proc. Natl. Acad. Sci. USA* 2018, 115, E9630–E9639.
  35. Lingwood, D.; McTamney, P.M.; Yassine, H.M.; Whittle, J.R.R.; Guo, X.; Boyington, J.C.; Wei, C.J.; Nabel, G.J. Structural and genetic basis for development of broadly neutralizing influenza antibodies. *Nature* 2012, 489, 566–570.
  36. Lin, W.; Zhang, P.; Chen, H.; Chen, Y.; Yang, H.; Zheng, W.; Zhang, X.; Zhang, F.; Zhang, W.; Lipsky, P.E. Circulating plasmablasts/plasma cells: A potential biomarker for IgG4-related disease. *Arthritis Res. Ther.* 2017, 19, 25.
  37. Shaffer, A.L.; Shapiro-Shelef, M.; Iwakoshi, N.N.; Lee, A.H.; Qian, S.B.; Zhao, H.; Yu, X.; Yang, L.; Tan, B.K.; Rosenwald, A.; et al. XBP1, downstream of Blimp-1, expands the secretory apparatus and other organelles, and increases protein synthesis in plasma cell differentiation. *Immunity* 2004, 21, 81–93.
  38. Todd, D.J.; McHeyzer-Williams, L.J.; Kowal, C.; Lee, A.H.; Volpe, B.T.; Diamond, B.; McHeyzer-Williams, M.G.; Glimcher, L.H. XBP1 governs late events in plasma cell differentiation and is not required for antigen-specific memory B cell development. *J. Exp. Med.* 2009, 206, 2151–2159.
  39. Bergmann, H.; Yabas, M.; Short, A.; Miosge, L.; Barthel, N.; Teh, C.E.; Roots, C.M.; Bull, K.R.; Jeelall, Y.; Horikawa, K.; et al. B cell survival, surface BCR and BAFFR expression, CD74 metabolism, and CD8– dendritic cells require the intramembrane endopeptidase SPPL2A. *J. Exp. Med.* 2013, 210, 31.
  40. Jasper, G.A.; Arun, I.; Venzon, D.; Kreitman, R.J.; Wayne, A.S.; Yuan, C.M.; Marti, G.E.; Stetler-Stevenson, M. Variables affecting the quantitation of CD22 in neoplastic B cells. *Cytom. Part B Clin. Cytom.* 2011, 80B, 83–90.
  41. Pappas, L.; Foglierini, M.; Piccoli, L.; Kallewaard, N.L.; Turrini, F.; Silacci, C.; Fernan-



## Chapter 3.3

---

- dez-Rodriguez, B.; Agatic, G.; Giacchetto-Sasselli, I.; Pellicciotta, G.; et al. Rapid development of broadly influenza neutralizing antibodies through redundant mutations. *Nature* 2014, 516, 418–422.
42. Galson, J.D.; Trück, J.; Clutterbuck, E.A.; Fowler, A.; Cerundolo, V.; Pollard, A.J.; Lunter, G.; Kelly, D.F. B-cell repertoire dynamics after sequential hepatitis B vaccination and evidence for cross-reactive B-cell activation. *Genome Med.* 2016, 8, 68.
43. Montague, Z.; Lv, H.; Otwinowski, J.; Wu, N.C.; Nourmohammad, A.; Ka, C.; Mok, P.; De-witt, W.S.; Isacchini, G.; Yip, G.K.; et al. Dynamics of B cell repertoires and emergence of cross-reactive responses in patients with different severities of COVID-19. *Cell Rep.* 2021, 35, 109173.
44. Pinto, D.; Park, Y.J.; Beltramello, M.; Walls, A.C.; Tortorici, M.A.; Bianchi, S.; Jaconi, S.; Culap, K.; Zatta, F.; De Marco, A.; et al. Cross-neutralization of SARS-CoV-2 by a human monoclonal SARS-CoV antibody. *Nature* 2020, 583, 290–295.
45. Rogers, T.F.; Zhao, F.; Huang, D.; Beutler, N.; Burns, A.; He, W.T.; Limbo, O.; Smith, C.; Song, G.; Woehl, J.; et al. Isolation of potent SARS-CoV-2 neutralizing antibodies and protection from disease in a small animal model. *Science* 2020, 369, 956–963.
46. Brouwer, P.J.M.; Caniels, T.G.; van der Straten, K.; Snitselaar, J.L.; Aldon, Y.; Bangaru, S.; Torres, J.L.; Okba, N.M.A.; Claireaux, M.; Kerster, G.; et al. Potent neutralizing antibodies from COVID-19 patients define multiple targets of vulnerability. *Science* 2020, 369, 643–650.
47. Li, A.; Rue, M.; Zhou, J.; Wang, H.; Goldwasser, M.A.; Neuberg, D.; Dalton, V.; Zuckerman, D.; Lyons, C.; Silverman, L.B.; et al. Utilization of Ig heavy chain variable, diversity, and joining gene segments in children with B-lineage acute lymphoblastic leukemia: Implications for the mechanisms of VDJ recombination and for pathogenesis. *Blood* 2004, 103, 4602–4609.
48. Yamada, M.; Wasserman, R.; Reichard, B.A.; Shane, S.; Caton, A.J.; Rovera, G. Preferential utilization of specific immunoglobulin heavy chain diversity and joining segments in adult human peripheral blood B lymphocytes. *J. Exp. Med.* 1991, 173, 395–407. [Google Scholar] [CrossRef]
49. Hong, B.; Wu, Y.; Li, W.; Wang, X.; Wen, Y.; Jiang, S.; Dimitrov, D.S.; Ying, T. In-depth analysis of human neonatal and adult IgM antibody repertoires. *Front. Immunol.* 2018, 9, 128.
50. Khatri, I.; Berkowska, M.A.; van den Akker, E.B.; Teodosio, C.; Reinders, M.J.T.; van Dongen, J.J.M. Population matched (pm) germline allelic variants of immunoglobulin (IG) loci: Relevance in infectious diseases and vaccination studies in human populations. *Genes Immun.* 2021, 22, 172–186.
51. Hesse, J.E.; Lieber, M.R.; Mizuuchi, K.; Gellert, M. V(D)J recombination: A functional definition of the joining signals. *Genes Dev.* 1989, 3, 1053–1061.
52. Belessi, C.; Stamatopoulos, K.; Hadzidimitriou, A.; Hatzi, K.; Smilevska, T.; Stavroyianni, N.; Marantidou, F.; Paterakis, G.; Fassas, A.; Anagnostopoulos, A.; et al. Analysis of expressed and non-expressed IGK locus rearrangements in chronic lymphocytic leukemia. *Mol. Med.* 2005, 11, 52–58.
53. Bräuninger, A.; Goossens, T.; Rajewsky, K.; Küppers, R. Regulation of Immunoglobulin Light Chain Gene Rearrangements during Early B Cell Development in the Human. *Eur. J. Immunol.* 2001, 31, 3631–3637.
54. Korsmeyer, S.J.; Hieter, P.A.; Ravetch, J.V.; Poplack, D.G.; Waldmann, T.A.; Leder, P. Developmental hierarchy of immunoglobulin gene rearrangements in human leukemic pre-B-cells. *Proc. Natl. Acad. Sci. USA* 1981, 78, 7096–7100.
55. Odendahl, M.; Mei, H.; Hoyer, B.F.; Jacobi, A.M.; Hansen, A.; Muehlinghaus, G.; Berek, C.; Hiepe, F.; Manz, R.; Radbruch, A.; et al. Generation of migratory antigen-specific plasma blasts and mobilization of resident plasma cells in a secondary immune response. *Blood* 2005, 105, 1614–1621.
56. Galson, J.D.; Trück, J.; Fowler, A.; Clutterbuck, E.A.; Münz, M.; Cerundolo, V.; Reinhard, C.; van der Most, R.; Pollard, A.J.; Lunter, G.; et al. Analysis of B Cell Repertoire Dynamics Following Hepatitis B Vaccination in Humans, and Enrichment of Vaccine-specific Antibody Sequences. *EBio-Medicine* 2015, 2, 2070–2079.
57. Horns, F.; Vollmers, C.; Croote, D.; Mackey, S.F.; Swan, G.E.; Dekker, C.L.; Davis, M.M.; Quake, S.R. Lineage tracing of human B cells reveals the in vivo landscape of human antibody class switching. *Elife* 2016, 5, e16578.
58. Neuberger, M.S.; Milstein, C. Somatic hypermutation. *Curr. Opin. Immunol.* 1995, 7, 248–254.
59. Storb, U.; Peters, A.; Klotz, E.; Rogerson, B.; Hackett, J. The mechanism of somatic hypermutation studied with transgenic and transfected target genes. *Semin. Immunol.* 1996, 8, 131–140.
60. Collins, A.M.; Watson, C.T. Immunoglobulin light chain gene rearrangements, receptor



- editing and the development of a self-tolerant antibody repertoire. *Front. Immunol.* 2018, 9, 2249.
61. Moticka, E.J.; Streilein, J.W. Hypothesis: Nonspecific polyclonal activation of memory B cells by antigen as a mechanism for the preservation of long term immunologic anamnesis. *Cell. Immunol.* 1978, 41, 406–413.
62. Blanco, E.; Pérez-Andrés, M.; Arriba-Méndez, S.; Contreras-Sanfeliciano, T.; Criado, I.; Pelak, O.; Serra-Caetano, A.; Romero, A.; Puig, N.; Remesal, A.; et al. Age-associated distribution of normal B-cell and plasma cell subsets in peripheral blood. *J. Allergy Clin. Immunol.* 2018, 141, 2208–2219.e16.



## Chapter 3.4

### **Distinct cellular kinetics in participants protected from colonization upon *B. pertussis* challenge**

A.M. Diks<sup>1\*</sup>, H. de Graaf<sup>2 3\*</sup>, C. Teodosio<sup>1 4</sup>, R.J. Groenland<sup>1</sup>, B. de Mooij<sup>1</sup>, M. Ibrahim<sup>3</sup>, A.R. Hill<sup>3</sup>, R.C. Read<sup>3</sup>, J.J.M. van Dongen<sup>1 4</sup>, M.A. Berkowska<sup>1</sup> on behalf of the IMI-2 PERISCOPE Consortium

<sup>1</sup> Department of Immunology, Leiden University Medical Center, Albinusdreef 2, 2333 ZA, Leiden, the Netherlands

<sup>2</sup> Faculty of Medicine, University Hospital Southampton NHS Foundation Trust, Southampton, UK

<sup>3</sup> NIHR Southampton Biomedical Research Centre, University of Southampton, University Hospital Southampton NHS Foundation Trust, Southampton, UK

<sup>4</sup> Centro de Investigación del Cáncer-Instituto de Biología Molecular y Celular del Cáncer (CIC-IBMCC, USAL-CSIC-FICUS) and Department of Medicine, University of Salamanca, Salamanca, Spain

\* These authors contributed equally to this manuscript

**Manuscript in preparation**

### Summary

The authors apply high-dimensional flow cytometry to monitor the cellular immune response in a human *Bordetella pertussis* challenge model. These cellular studies show that participants protected from colonization have a distinct early cellular immune response, likely reflecting effective immunological memory.

### Abstract

**Background:** Limited data is available on the mechanisms of protection against colonization with *Bordetella pertussis* in humans.

**Methods:** Cellular responses to *Bordetella pertussis* challenge were monitored longitudinally using high-dimensional EuroFlow-based flow cytometry, allowing quantitative detection of >250 different immune cell subsets in blood.

**Results:** Participants who were protected from colonization showed different early cellular responses compared to colonized participants. Especially prominent for non-colonized participants were the early expansion of (CD36-) non classical monocytes at day 1 (d1), NK cells (d3), follicular T helper cells (d1/d3) and plasma cells (d3). Plasma cell expansion at d3 correlated negatively with the CFU load at d7 and d9 post-challenge. Participants that seroconverted showed increased plasma cell maturation at d11-14.

**Conclusion:** These early cellular immune responses following experimental infection can now be further characterized and potentially linked to an efficient mucosal immune response, preventing colonization. Ultimately, their presence may be used to evaluate whether new *Bordetella pertussis* vaccine candidates are protective against *Bordetella pertussis* colonization.

## Introduction

The introduction of vaccines has significantly reduced the amount of infectious disease-related deaths.[1] However, many vaccines are based on empirical results, and the mechanisms of protection and underlying immunological processes are not completely understood. For vaccines/diseases for which no clear correlate of protection is defined, as is the case for pertussis, increased insight into the immunological processes associated with infection may be an important step forward. Pertussis is a disease of the respiratory tract, caused by the bacterium *Bordetella pertussis* (Bp). Infection with Bp occurs via respiratory droplets. Although the whole cell pertussis (wP) vaccine and the acellular pertussis (aP) vaccine are known to protect against disease, the incidence of pertussis has been rising in the past decennia.[2] Several animal models have been established to study pertussis infection and vaccination. These models resulted in valuable insights into the different immune responses induced by aP and wP vaccination, new vaccine candidates, different routes of administration, and infection.[3-5] In baboons, aP vaccination induced a T helper (Th) 1/Th2 response, protecting animals from severe disease, but did not prevent colonization and transmission to naive vaccinated animals.[3] In contrast, natural infection with Bp and -to a lesser extent- wP vaccination induced a Th1/Th17 memory response. Moreover, wP vaccinated animals were protected from severe disease, and although not protected against colonization, they cleared the infection significantly quicker than aP-vaccinated and naive animals. Lastly, previously infected animals were protected from colonization and disease.[3] The question remains to what extent animal models resemble the course of Bp infection and the accompanying immune response in humans. This topic can only be addressed in human vaccination and challenge studies.

Data on humans in the pre-pertussis vaccine era indicated that although natural infection does not result in complete lifelong protection, reinfection is much milder than primary infection.[6] Moreover, protection after natural infection was estimated to last longer compared to aP or wP vaccine-induced protection.[6] This implies that despite high vaccination coverage, the carriage and transmission of pertussis persist, which may explain the reported resurgence of pertussis in the last decades.[7-9] Improved protection against transmission is an important aspect for the development of future vaccines/vaccination strategies against pertussis.

Currently, modifications of existing pertussis vaccines as well as new vaccine candidates are being investigated.[4] Yet limited data is available on the mechanisms and immune signatures associated with protection against colonization. Moreover, it is difficult to extrapolate data from intramuscular vaccination to other routes of administration, such as intranasal delivery, which more resembles the 'natural way' of Bp encounter. For pertussis, the live-attenuated BPZE1 vaccine -which is delivered intranasally- is currently one of the most advanced vaccine candidates in clinical development also aiming to reduce the transmission of pertussis.[4,10]



In 2017, a human challenge model for Bp (controlled bacterial infection) was established at the National Health Institute for Health Research Clinical Research Facility (CRF) Southampton, UK by the University of Southampton as part of the IMI-2 PERISCOPE Consortium.[11,12] In this model, asymptomatic colonization of participants can be established in a safe way. A major advantage of using this human challenge model is that one can define more clearly whether a participant is protected against colonization by measuring serum antibodies and culturing bacteria from throat and nasal samples. Moreover, in contrast to sampling from pertussis patients, the exact moment of infection is known, and the synchronized sampling in multiple participants enables us to find shared patterns arising after bacterial challenge. The analysis of the cellular immune response following bacterial challenge may yield new insights in the cellular kinetics important for early removal of bacteria from the mucosal layers and protection against colonization. Comparison of similarities and differences between the immune responses launched after vaccination or bacterial challenge may help to identify why current pertussis vaccines do not fully protect against infection and what should be changed to induce protection against carriage. Identification of immune signatures associated with protection against colonization may be of importance in the evaluation of vaccines that aim at reduction/prevention of carriage and transmission. In this exploratory study, we monitored the cellular kinetics in humans after intranasal challenge with Bp. All participants were wP-primed and had no known recent contact with Bp. We monitored the immune responses in these participants and identified cellular changes that were unique for participants protected from colonization.

### Results

#### **10/15 participants colonized after challenge with B1917 strain**

Samples from 15 participants were collected between November 2017 and September 2018. Five participants were challenged intranasally with  $10^4$  colony forming units (CFU) and ten participants were challenged intranasally with  $10^5$  CFU. As reported previously, participants challenged with  $10^5$  CFU more frequently reported mild symptoms of cough, rhinorrhea and nasal congestion than participants challenged with  $10^4$  CFU.[12] None of the participants developed pertussis disease or required rescue medication. No serious adverse events were reported. In the here-presented study, no differences in immune cell kinetics were found between participants challenged with  $10^4$  or  $10^5$  CFU, unless indicated specifically. One participant withdrew from the study after day (d) 14, and one participant withdrew after d28, both not related to the study. Samples collected until the moment of withdrawal were used.

To determine the colonization status after challenge, nasal washes were performed from d4 onwards as described previously (**Fig 1A-B**).[12] Challenge with  $10^4$  CFU and  $10^5$  CFU resulted in Bp positive culture in 2/5 and 8/10 participants, respectively. Of the 10 colonized participants, four participants showed low-density colonization (defined as  $<1000$  CFU/mL at any time point during the study), and six participants showed high-density colonization ( $>1000$  CFU/mL at

any time point during the study). In further analyses, we divided the participants based on colonization and seroconversion status and searched for unique immune signatures associated with these readouts.

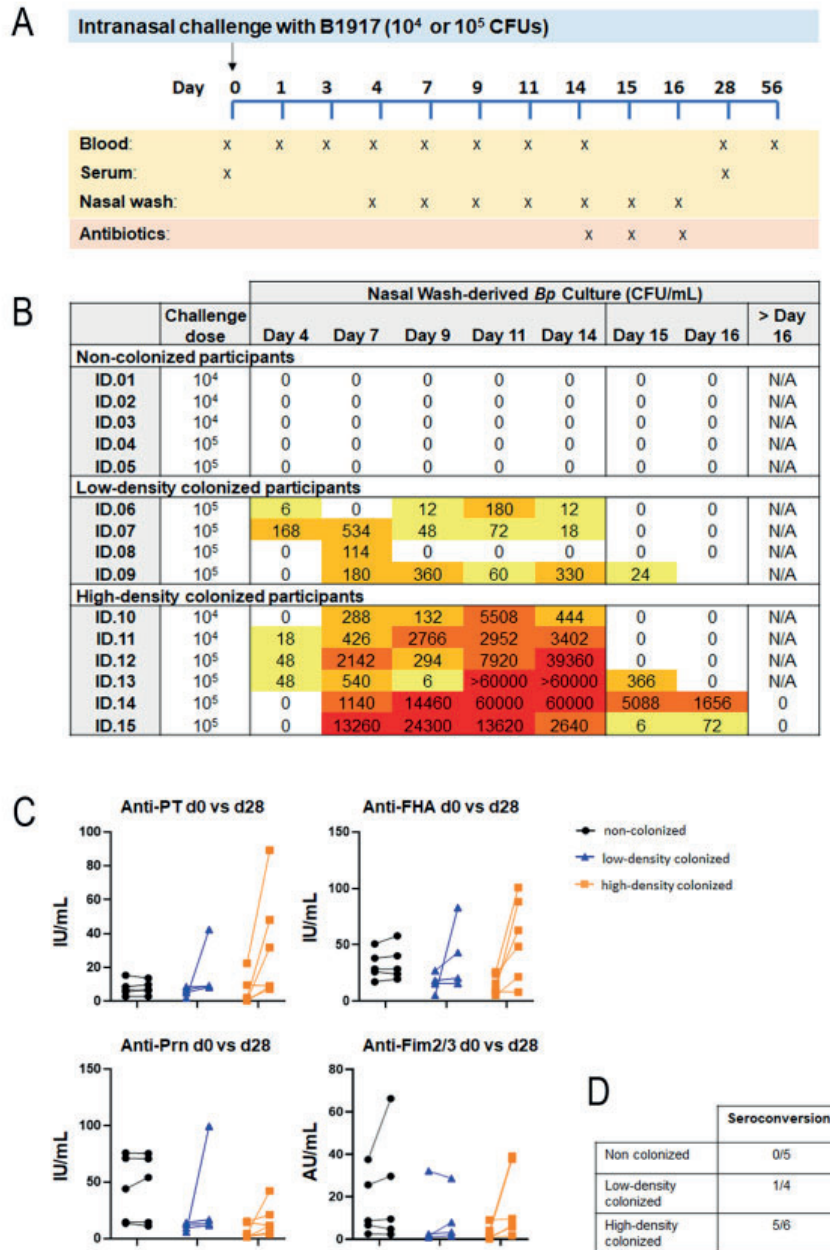


**Figure 1. Study and cohort description and clinical readout.** A. Overview of intervention and sampling time points used in this study, including the mandatory antibiotics treatment for all participants at d14, d15 and d16 after bacterial challenge. B. Overview of participants clustered based on the clinical readout (colonized/not colonized) and degree of colonization: no colonization, low-density colonization, and high-density colonization, based on the cultures derived from nasal washes and the anti-PT IgG values at baseline and 1 month after challenge. C. Ag-specific serum IgG levels at baseline and 28 days after challenge, as evaluated by multiplex immunoassay. Data are arranged according to degree of colonization. D. Number of non-colonized, low-density colonized, and high-density colonized participants that seroconverted. PT= pertussis toxin, FHA= filamentous hemagglutinin, Prn= pertactin, Fim2/3= Fimbriae 2 and 3.

Ag-specific serum IgG levels (against PT, FHA, Prn and Fim2/3) were determined at baseline and d28 (**Fig 1C**). Comparison of baseline Ag-specific serum IgG levels of the 15 participants evaluated in this study versus all participants included in the overarching bacterial challenge study showed no differences (data not shown). Six participants showed signs of seroconversion (one low-density and five high-density colonized participants), non-colonized participants showed no sign of seroconversion (**Fig 1D**). On top of increased anti-PT IgG serum levels, colonized participants also showed generally higher increases in other Ag-specific Igs than non-colonized participants. As only an >2-fold increase of anti-PT serum IgG was used as cut-off for seroconversion, we also investigated if any participant had an >2-fold increase for another antigen, but not for PT. This was not observed. Lastly, the absolute increase in Ag-specific serum IgG was most prominent in high-density colonized participants, especially for anti-PT and anti-FHA IgG.

### **Fluctuations in circulating innate immune cells after bacterial challenge**

During natural encounter or challenge, the bacterium itself triggers innate immunity at the site of infection (mucosal surfaces). Thus, a fast (and local) innate response may be important to control Bp directly upon encounter. As recruitment of innate cells to and from tissues may be detected in the blood early after challenge, we evaluated the cellular changes of innate immune cell subsets after bacterial challenge.

Early after challenge, total circulating leukocyte numbers (expressed as ratio of baseline) did not change. However, at d11, d28 and d56 post-challenge, circulating leukocyte numbers decreased (**Fig 2A**). Circulating neutrophils decreased significantly at d1, d4 and d11 post-challenge (ratio of baseline) (**Fig 2B**). Interestingly, when dividing into mature and immature neutrophils, this decrease was only observed for mature neutrophils (not shown). Circulating eosinophils decreased at d3, d4, d28 and d56 post-challenge (**Fig 2C**). The most prominent changes were observed in circulating monocyte populations. Monocytes mature from classical monocytes (cMo), via intermediate (iMo) to nonclassical monocytes (ncMo) and can be further subdivided into different functional subsets or activation stages.[13,14] Fluctuations in total cMo were limited, with only a minor reduction in circulating cMo at d1, d11 and d28 (data not shown). However, within cMo subsets, decreased numbers (ratio of baseline) were observed for CD62L+ cMo at d1, d4, d9, d11, d14, d28 and d56 post-challenge, whereas increased numbers (ratio of baseline) were observed for CD62L- cMo at d1, d4, d7, d9, d28 and d56 post-challenge (**Fig 2D+E**). CD62L, also known as L-selectin, is shed upon activation and CD62L- cMo are considered activated and possibly more mature.[15] Moreover, an increase in intermediate monocytes (iMo) was observed at d3 and d4 post-challenge (ratio of baseline) (**Fig 2F**). No consistent early fluctuations were observed for ncMo, although their numbers decreased at d11 post-challenge (ratio of baseline) (**Fig 2G**). Within the dendritic cell (DC) compartment no early consistent changes were observed, although both plasmacytoid DCs (pDC) and myeloid DCs (mDC) showed a decrease in cells from d28

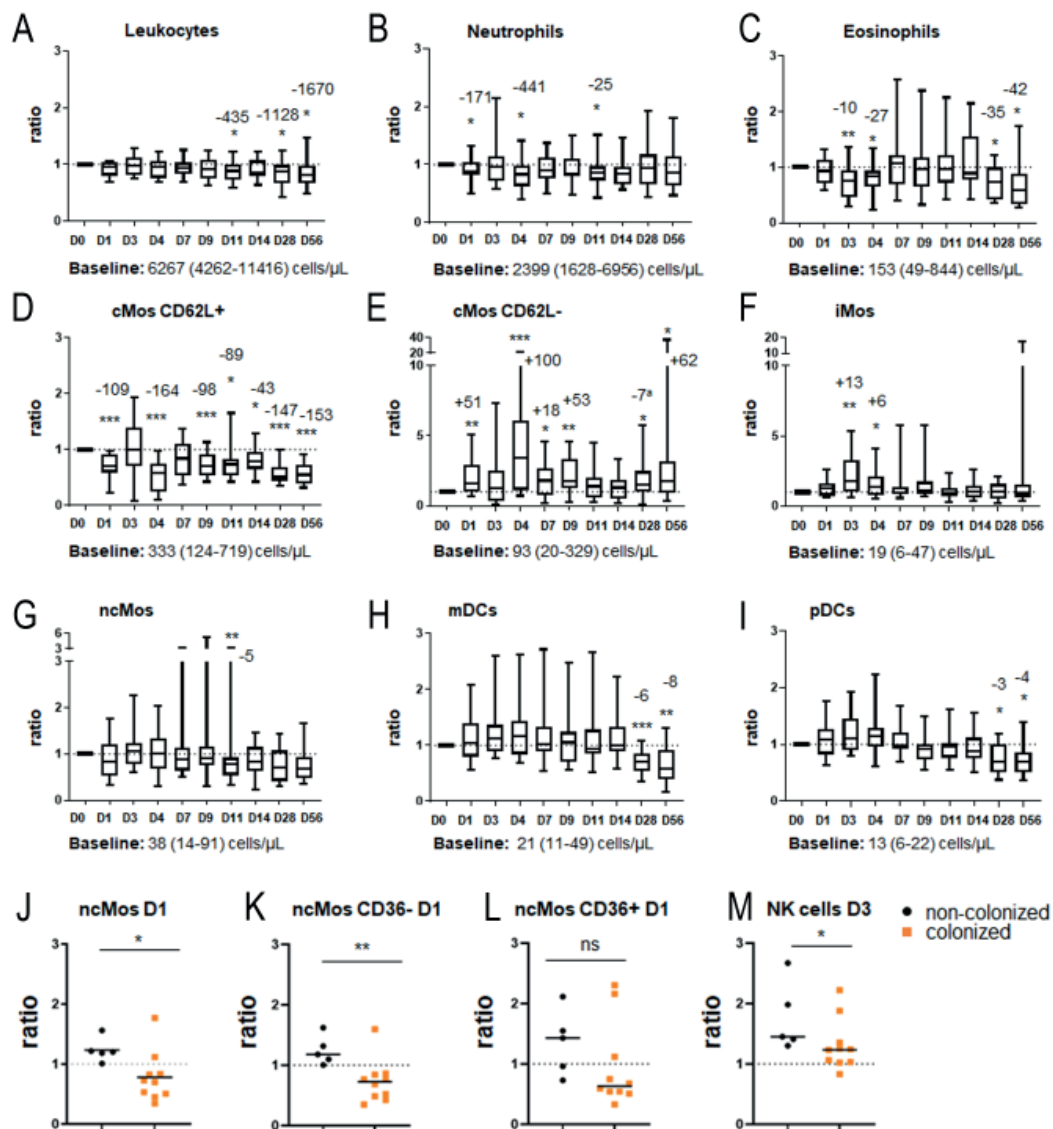


**Figure 2. Fluctuations of cell numbers in the innate immune cell compartment after bacterial challenge.** Boxplots (median, Q1, Q3, min-max) showing the kinetics of major innate immune cell subsets (A-I) expressed as ratio compared to baseline. N=15. Dashed line indicates a ratio of 1.0 (baseline value). Baseline cell counts, median (min-max) in cells/ $\mu$ L are indicated below each graph. Longitudinal changes were evaluated using Wilcoxon test and ratio of baseline. In case of significant differences in ratio compared to baseline, the median increase or decrease in cells/ $\mu$ L is indicated on top of the bar. (J-M) Increase or decrease of cell numbers expressed as ratio compared to baseline in colonized and non-colonized participants. N=15. Statistical test performed; Mann-Whitney on ratio of baseline. \* Indicates  $p < 0.05$ , \*\* indicates  $p < 0.01$ , \*\*\* indicates  $p < 0.001$ . D=days post-challenge. cMo= classical monocyte. iMo= intermediate monocyte. ncMo= non-classical monocyte. mDC= myeloid dendritic cell. pDC = plasmacytoid dendritic cell. a Although in panel E the ratio versus baseline was increased, the median cell count at d28 vs median cell count at baseline was lowered (-7 cells/ $\mu$ L).

onwards (**Fig 2H+I**).

To investigate whether the kinetics of innate immune cells are associated with colonization, we compared the numbers of circulating innate immune cells in

participants who were colonized and non-colonized. No consistent differences between colonized and non-colonized participants were observed for leukocytes, eosinophils, iMo, cMo and dendritic cells. For circulating neutrophils, the decrease in mature neutrophils was visible as a trend in non-colonized individuals at d1 ( $p=0.125$ ), d4 ( $p=0.0625$ ), and d11 ( $p=0.0625$ ), but was less prominent in colonized individuals. An increase in circulating ncMo (ratio of baseline), especially CD36- ncMo, was found at d1 post-challenge in non-colonized participants (**Fig 2J-L**), while these were decreased in colonized participants. Finally, at d3 post-challenge, non-colonized participants had higher NK-cell expansion (ratio of baseline) than colonized participants (**Fig 2M**).

Next, we divided the colonized participants based on colonization density (low- or high-density colonization). Here, we found that the decrease in (especially CD36-) ncMo was most prominent for low-density colonized participants (**Suppl. Fig 1A-C**). cMo maturation (represented by shedding of CD62L) did not differ between low- and high-density colonized participants (data not shown). However, we did observe a decrease in a circulating mDC subset in low-density colonized participants (CD1c+ CD14dim mDC, **Suppl. Fig 1D**). Lastly, NK cells in high-density colonized participants did not expand, whereas the NK cell expansion in low-density colonized participants -to some extent- resembled that of the non-colonized participants (**Suppl. Fig 1E**).

To summarize: we observed fluctuations in innate cell numbers in the early days after bacterial challenge. Decreased cell numbers may indicate migration of cells into the tissue, and the shedding of CD62L may indicate a shift towards a more activated phenotype in the cMo compartment. Cellular kinetics differed between non-colonized and colonized participants, and between high- and low-density colonized participants. The colonization density did not reflect the magnitude of cellular changes, as these were usually more prominent in low-density colonized participants.

### **Limited fluctuations of T-cell populations post-challenge**

Activation of T cells is required for cellular immunity and the activation of humoral immunity by providing T-cell help to B cells in the germinal center reaction. As there are different T-cell responses generated after vaccination with aP or wP and (natural) infection [16,17], we set out to determine changes in circulating T cells after experimental exposure to Bp.

Within circulating total T cells, CD4 T cells, CD4 T helper (Th) and regulatory T cells, no changes occurred until d28 and d56, when a significant decrease compared to baseline was observed (**Fig 3A-C**). However, an expansion of follicular T helper (FTH) cells was observed at d3 post-challenge (ratio of baseline) (**Fig 3D**). This expansion of FTHs was not polarized to any specific FTH cell type. Additionally, no consistent changes were observed in CD4 Th cell fluctuations (**Fig 3E-I**) or Th cell maturation/activation.



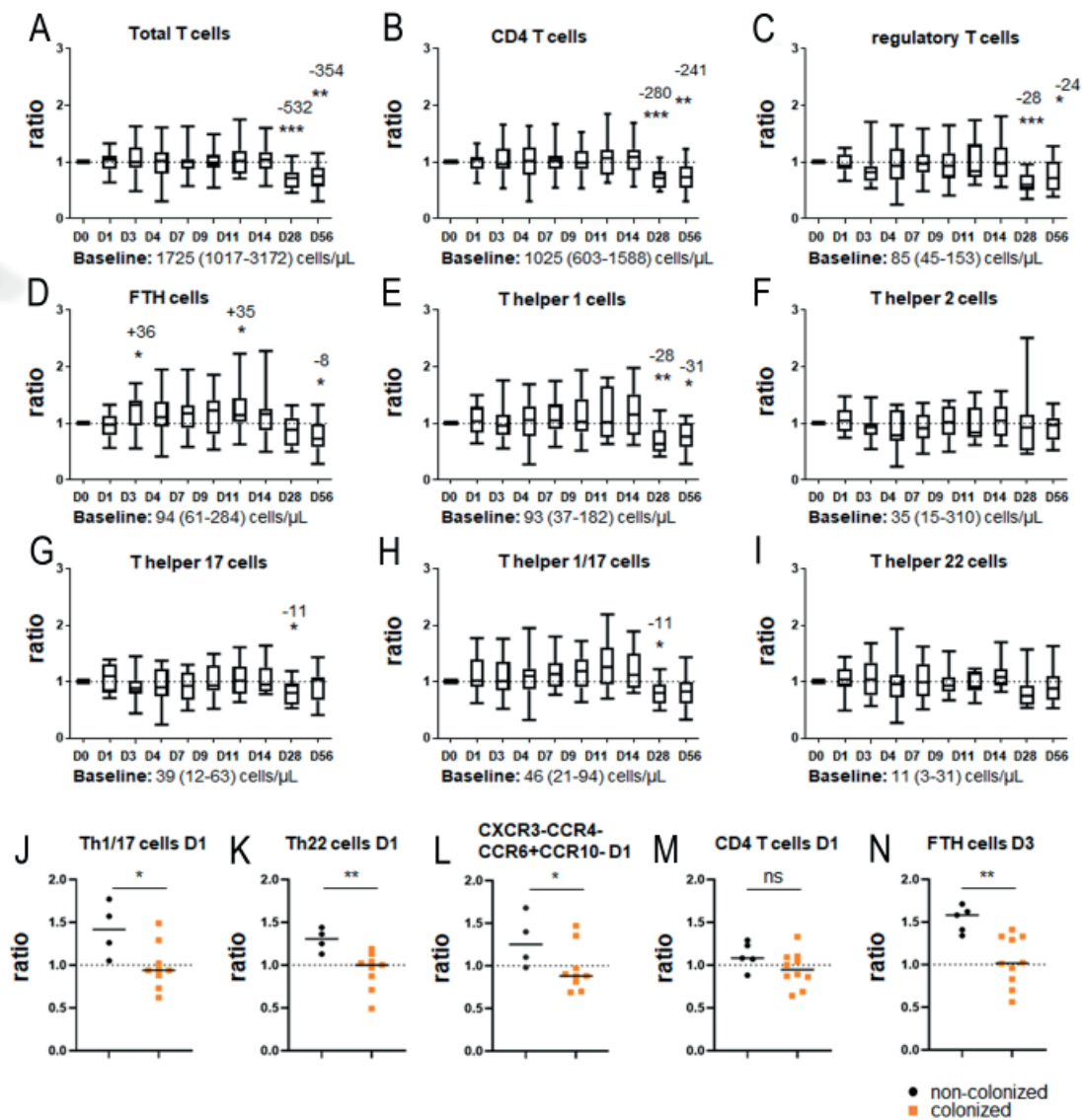


**Figure 3. Fluctuations of cell numbers in the T-cell compartment after bacterial challenge.** Boxplots (median, Q1, Q3, min-max) showing the kinetics of major innate immune cell subsets (A-I) expressed as ratio compared to baseline. N=15. Dashed line indicates a ratio of 1.0 (baseline value). Baseline cell counts, median (min-max) in cells/ $\mu$ L are indicated below each graph. Longitudinal changes were evaluated using Wilcoxon test and ratio of baseline. In case of significant differences in ratio compared to baseline, the median increase or decrease in cells/ $\mu$ L is indicated on top of the bar. (J-N) Increase or decrease of cell numbers expressed as ratio compared to baseline in colonized and non-colonized participants. N=13 (J-L) or N=15 (M, N). Statistical test performed; Mann-Whitney on ratio of baseline. \* Indicates  $p < 0.05$ , \*\* indicates  $p < 0.01$ , \*\*\* indicates  $p < 0.001$ . D= Days post-challenge. FTH= follicular T helper cells, Th= T helper cell, CXCR3-CCR4-CCR6+CCR10- = recently defined Th subset with phenotype CXCR3-CCR4-CCR6+CCR10-.

When grouping the participants based on colonization status, three different CD4 Th subsets increased significantly in non-colonized participants (ratio of baseline) compared to colonized participants at d1 post-challenge (**Fig 3J-L**). A small expansion in Th1/17 cells was observed at d1 post-challenge. Additionally, we found an expansion of Th22 cells and of a recently defined Th subset (phenotype:

CXCR3-CCR4-CCR6+CCR10-) at d1 in non-colonized participants.[18] The difference between colonized and non-colonized participants was not fully explained by total CD4 T-cell kinetics (**Fig 3M**). An increase in total FTH cells at d3 was primarily found in non-colonized participants (**Fig 3N**). Due to technical and biological reasons (missing antibody in a surface stain ‘master mix’ and/or a CD45RA polymorphism [19]), at this time point FTH subsets could only be defined in 9/15 participants. Nevertheless, we observed a trend towards increased naive FTHs, Th1-like, Th1/17-like and Th17-like FTHs at d3 post-challenge in non-colonized participants. This increase was significant for Th2-like FTH cells (**Suppl. Fig 2**). When looking at the impact of colonization density, comparison between non-colonized and low-density colonized participants resulted in significant differences for Th-cell subsets at d1 (**Suppl. Fig 3A-D**). Moreover, FTH expansion at d3 was higher in non-colonized participants compared to both low- and high-density colonized participants (**Suppl. Fig 3E**). No consistent changes were observed in maturation/activation of Th subsets.

Thus, although we observed consistent changes in the Th cell compartment at d1 after bacterial challenge, the most prominent change was the expansion of circulating FTH cells at d3 post-challenge. This expansion was only observed in non-colonized participants and not polarized to any subset.

### **Increased plasma cell numbers at d3 and d11-14 post-challenge**

T-cell help, given by FTH cells in the secondary lymphoid organs, is required to activate B cells after antigen encounter.[20] Activation of B cells leads to the formation of memory B cells and plasma cells, and consequently to the production of (protective) antibodies. After (booster) vaccination with aP, skewing towards IgG1 plasma cells was reported, whereas natural encounter is thought to induce IgA memory, as shown by the positive correlation between age and IgA responses against Bp.[21-24]

Upon challenge, fluctuations in the naive and memory B-cell compartment were limited and not consistent in-between participants (**Fig 4A**). However, plasma cells expanded at d11-14 post-challenge and were significantly increased at d14 post-challenge (ratio of baseline) (**Fig 4B, Suppl. Fig 4A**). In participants inoculated with  $10^5$  CFU, a trend towards higher plasma cell expansion was observed at d11-14 post-challenge (**Suppl. Fig 4B, ns**). At d14 post-challenge, IgG2, IgA1 and IgA2 plasma cells were significantly increased compared to baseline, and for IgG1 this was observed as a trend ( $p= 0.121$ ) (**Fig 4C-I**). Finally, despite clear expansion, no consistent changes were observed in the distribution of maturation stages of total plasma cells, which were primarily defined by the loss of CD20 and gain of CD138 markers (**Suppl. Fig 4D**).

Next, we grouped the participants based on colonization status. Here, we detected an expansion of plasma cells at d3, which was most prominent in non-colonized participants, but found in seven participants in total (**Fig 5A, ns**). Among all plasma cell subsets, expansion at d3 seemed slightly more prominent for IgG1

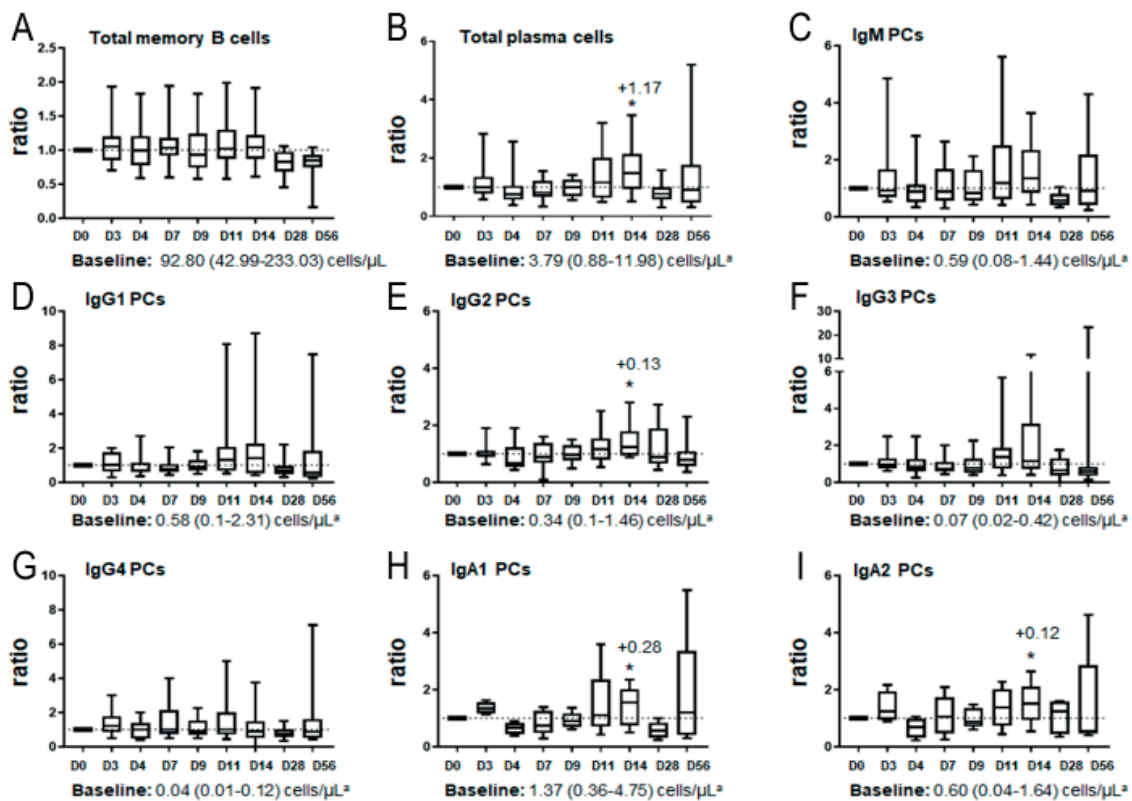


**Figure 4. Kinetics in the plasma cell compartment upon bacterial challenge.** A. Boxplot (median, Q1, Q3, min-max) showing the expansion of total memory B cells post-challenge. N=15. B-I. Boxplots (median, Q1, Q3, min-max) showing the expansion of total (B), IgM (C), IgG1-4 (D-G), and IgA1-2 (H-I) plasma cells post-challenge expressed as ratio compared to baseline (B-I; N=14). Dashed line indicates a ratio of 1.0 (baseline value). Shown are medians and range. Dashed line indicates a ratio of 1.0 (baseline value). Baseline cell counts, median (min-max) in cells/ $\mu\text{L}$  are indicated below each graph. Longitudinal changes were evaluated using Wilcoxon test on ratio of baseline. In case of significant differences in ratio compared to baseline, the median increase in cells/ $\mu\text{L}$  is indicated on top of the bar. \* Indicates  $p < 0.05$ . PC = plasma cell, d= days post-challenge. a Participant ID.12 showed strongly elevated (IgM) plasma cell counts at baseline, which were about 5x (total plasma cells) and 25x (IgM plasma cells) higher compared to counts measured at day 28 and 56. Therefore, this participant was excluded in panel B-I.

(ns), IgG4 (ns) and IgA1 (ns). Plasma cell expansion at d11-14 seemed unrelated to colonization status (**Fig 5B**). Next, we investigated the maturation patterns of IgG1 and IgA1 plasma cells in colonized and non-colonized participants (**Fig. 5C+D**). We observed that in non-colonized participants the expansion of IgG1 at d3 post-challenge mostly comprised the least and most mature IgG1 plasma cells, whereas for IgA1 this expansion comprised the least and intermediate mature IgA1 plasma cells. For IgG4 plasma cells, cell counts were generally too low to reliably monitor all three plasma cell maturation stages. When assessing the distribution of total plasma cells over different maturation stages, we found a relative increase in more immature plasma cells at d3 and d4 post-challenge in non-colonized participants, but not in colonized participants (**Fig 5C**).

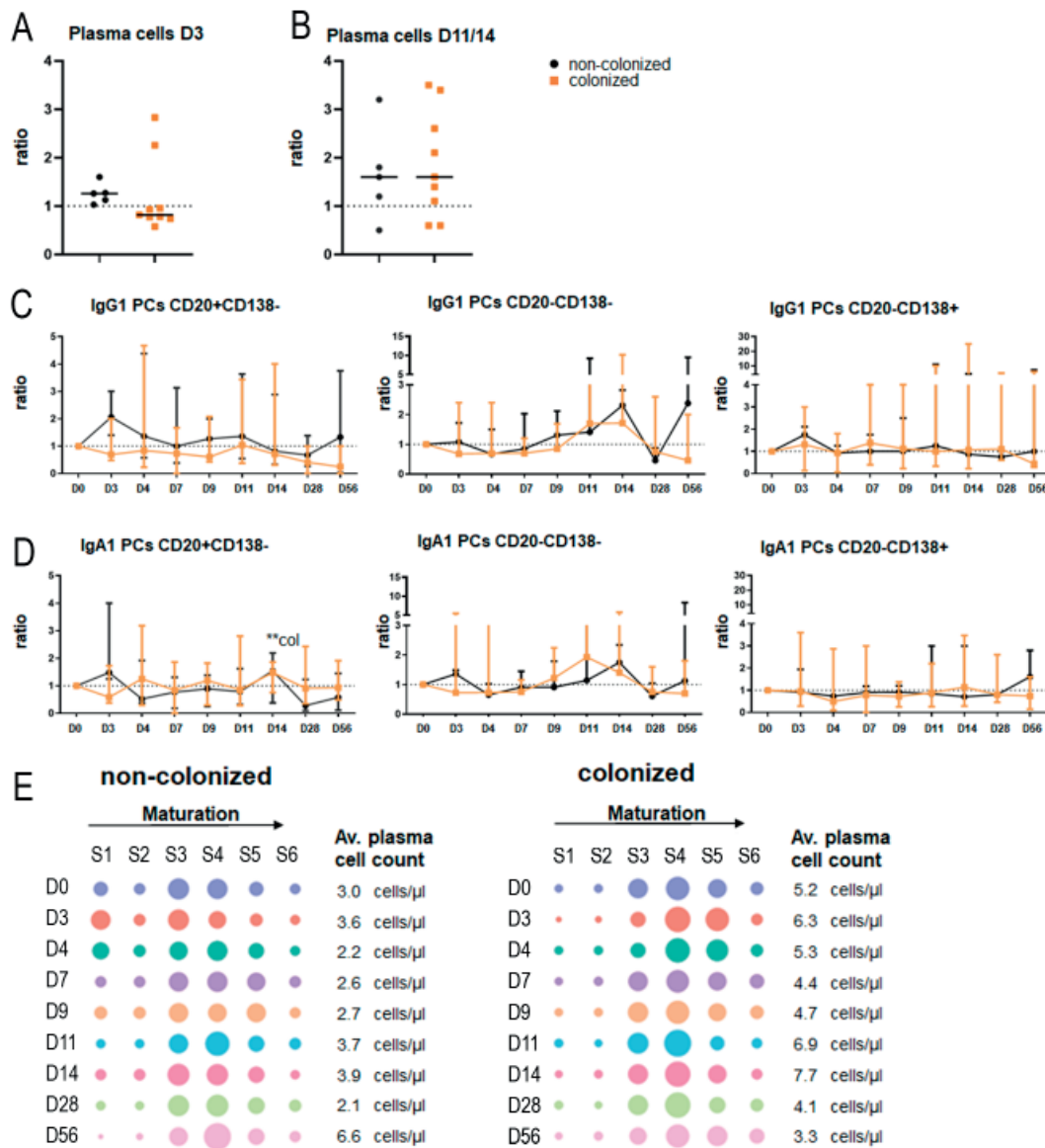


**Figure 5. Different kinetics in the plasma cell compartment colonized and non-colonized participants.** Of note: due to different normalization of plasma cells in participant ID.12, this participant was not included in the analysis of total plasma cells (panel A, B and E; N=14). A. Plasma cell expansion at d3 post-challenge, expressed as ratio compared to baseline. B. Plasma cell expansion d11-14 post-challenge expressed as ratio compared to baseline (of d11 and d14, the day of maximum expansion was used for each participant). N=14 C+D. Longitudinal changes in IgG1 (C) and IgA1 (D) plasma cell maturation stages expressed as ratio compared to baseline. N=15. Dashed line indicates a ratio of 1.0 (baseline value). E. Distribution of total plasma cells over six different maturation stages (MS1-6), expressed as percentage of total plasma cell population. Average plasma cell counts are indicated at the right side of each plot. N=15 Statistical test performed for longitudinal analysis, Wilcoxon test on ratio of baseline. Statistical test for comparison between groups per time point; Mann-Whitney on ratio of baseline. \*\* Indicates  $p < 0.01$ .

Then, we divided participants based on colonization density. Aside from non-colonized participants, the plasma cell expansion at d3 was observed in 1 low- and 1 high-density colonized participant (**Suppl. Fig 5A**). Expansion of plasma cells at d11-14 post-challenge was not specific for colonization density (**Suppl. Fig 5B**).

Upon inspection of IgG1 and IgA1 plasma cells, we found that at d3 post-challenge, non-colonized participants had significantly higher numbers of least mature IgA1 plasma cells, as compared to low-density colonized participants. Moreover, both high-density and non-colonized participants showed an increase in intermediate mature IgG1 and IgA1 plasma cells at d11-14 post-challenge (**Suppl. Fig 5C+D**, ns). When assessing the distribution of total plasma cells over different maturation stages, the differences between low-density colonized and non-colonized participants were most prominent at early time points (d0, d3 and d4) (**Suppl. Fig 5E**).

As the expansion of plasma cells at d3 post-challenge seemed more prominent in non-colonized participants, we correlated the plasma cell expansion at d3 with the maximum CFU load and the CFU load at each day post-challenge until the first day of azithromycin treatment. No correlation was found between the plasma cell expansion and the maximum CFU load. Instead, we found a negative correlation between plasma cell expansion at d3 and CFU load at d7 (Spearman  $R = -0.5773$ ,  $p=0.0269$ ) and CFU load at d9 (Spearman  $R = -0.6215$ ,  $p= 0.0157$ ). Plasma cell expansion at d3 did not correlate with CFU load at d11 or d14. Finally, as T-cell help is required for B-cell activation, we correlated the plasma cell expansion at d3 with Th-cell expansion at d1 and FTH expansion at d3, but no correlation was observed.

Thus, within the B-cell compartment, we observed most changes within the IgG and IgA plasma cell subsets. An early expansion of plasma cells at d3 post-challenge was primarily observed in non-colonized participants, whereas plasma cells at d11-14 post-challenge expanded irrespective of colonization status. A negative correlation was observed between CFU load and plasma cell expansion at d7 and d9 post-challenge. Lastly, maturation of the IgG1 and IgA1 plasma cells was observed to some extent, especially towards to intermediate mature phenotype at d11-14 post-challenge.

### **Plasma cell expansion and maturation are predictors of seroconversion**

As Ag-specific serum Ig levels are routinely used as a readout for vaccine efficacy and/or protective immunity, we also investigated cellular changes associated with seroconversion. Here, we found that all participants who seroconverted (1 low-density and 5 high-density colonized participants) had a more prominent expansion of total plasma cells at d14 post-challenge compared to non-seroconverting participants ( $p<0.05$ ) (**Fig 6A**). This expansion was clearest in IgM, IgG1 and IgA1 plasma cells ( $p<0.05$ ). In participants who seroconverted, the number of intermediate (d14) and most mature (d11 and d14) IgG1 plasma cells was significantly higher compared to non-seroconverting participants (**Fig 6B**). For IgA1 plasma cells, slight differences between seroconverting and non-seroconverting participants were found for the least mature plasma cells (d4 and d9), and a trend towards higher intermediate mature plasma cells was found in seroconverting participants at d11 and d14 (**Fig 6C**). When observing the distribution in matu-



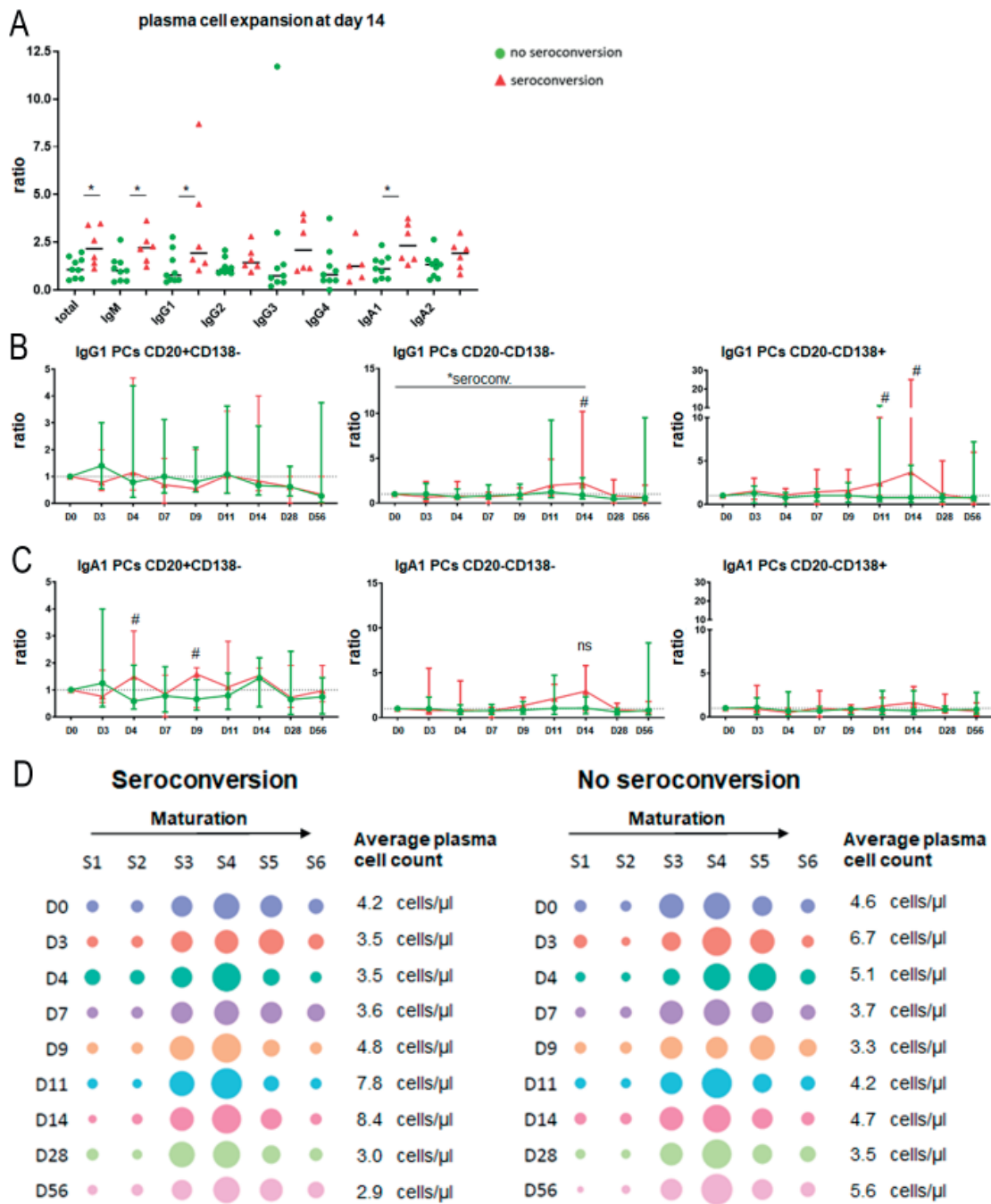


**Figure 6. Different plasma cell kinetics in participants that did or did not seroconvert.**

A. Expansion of plasma cell numbers at d14 post-challenge. Expansion is expressed as ratio compared to baseline. N=15 B+ C. Longitudinal changes in IgG1 (B) and IgA1 (C) plasma cell maturation stages expressed as ratio compared to baseline. N=15. Dashed line indicates a ratio of 1.0 (baseline value). D. Distribution of total plasma cells over six different maturation stages (MS1-6), expressed as percentage of total plasma cell population. Average plasma cell counts are indicated at the right side of each plot. N=15 Statistical test performed for longitudinal analysis, Wilcoxon test on ratio of baseline. Statistical test for comparison between groups per time point; Mann-Whitney on ratio of baseline. \* Indicates  $p < 0.05$  (longitudinal change), # indicates  $p < 0.05$  (difference between cohorts).

ration stages in the total plasma cell compartment, we again observed the increase in intermediate mature plasma cells in seroconverting participants at d11-d14 post-challenge (**Fig 6D**). In non-seroconverting participants, a slight increase in more mature plasma cells was observed at d3-4 post-challenge.

Evaluation of other immune cell subsets did not reveal any additional cellular changes specific for seroconversion. Lastly, we investigated the correlation between maximum colonization density in CFU during the study and the absolute increase in serum IgG (d28-d0) directed against PT, FHA, Prn and Fim2/3. We found a positive correlation for anti-PT IgG (Spearman  $R = 0.6486$ ,  $p = 0.0109$ ) and anti-FHA (Spearman  $R = 0.5684$ ,  $p = 0.0296$ ), but not for anti-Prn or anti-Fim2/3 IgG.

### **Baseline Bp-specific serum IgG levels correlate with maximum CFU count**

It is known that baseline status can impact the immune response. Therefore, we correlated the number of plasma cells at baseline and the Bp-specific IgG serum levels with the maximum CFU load. As anti-PT IgG serum levels  $>20$  IU/mL were used as exclusion criteria, we did not correlate baseline anti-PT IgG with maximum CFU count. Still, we found a negative correlation between Bp-specific IgG levels and maximum CFU counts for anti-FHA (Spearman  $R = -0.5292$ ,  $p = 0.0447$ ), anti-Prn (Spearman  $R = -0.6170$ ,  $p = 0.0166$ ) and anti-Fim2/3 (Spearman  $R = -0.5210$ ,  $p = 0.0487$ ), possibly indicating pre-existing immunity in several participants. No correlations were found between baseline plasma cell numbers and the maximum CFU load.

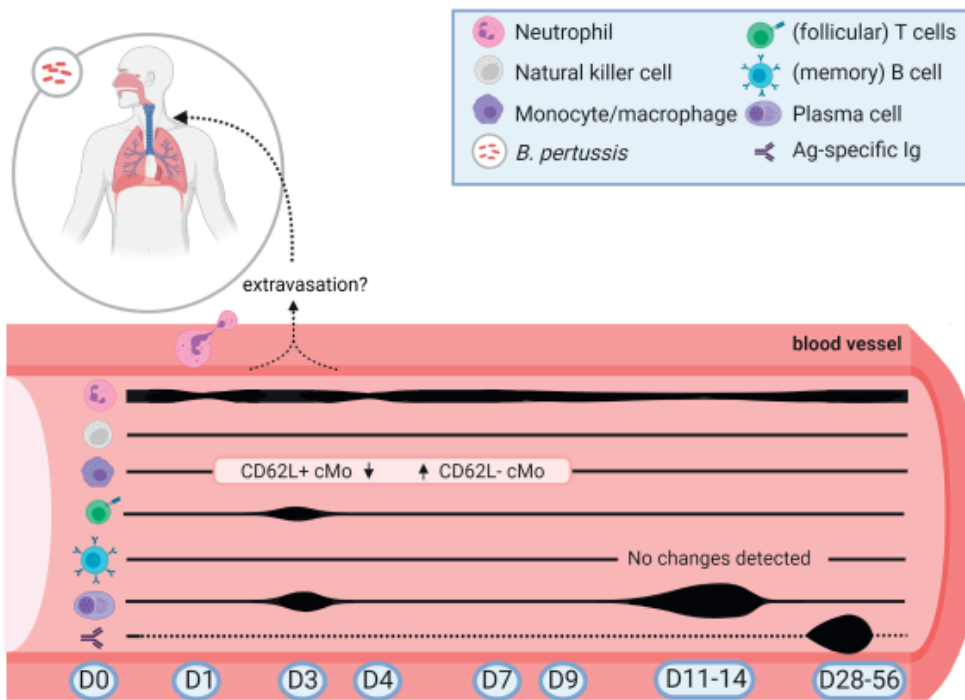
### **Most informative time points and cell populations associated with protection against colonization.**

The here presented study identified the immune cell populations and sampling time points that are most informative for follow-up studies. Especially in the early days after bacterial challenge (d1, d3 and d4), changes in the innate immune compartment are detected. Changes in the adaptive immune response can be monitored at various time points during the two weeks after challenge, with d1, d3, d11 and d14 being most informative in our hands. The most informative time points and cell populations to follow up on after bacterial challenge are summarized in **Figure 7A** (general kinetics post-challenge) and **7B** (kinetics specific for non-colonized participants).

### **Discussion**

This study describes cellular immune responses following bacterial challenge and evaluates which features of this response correlate with protection against colonization and/or seroconversion status. First, we evaluated the general immune cell kinetics post-challenge. Next, we assessed differences in immune signature based on colonization status, density, or seroconversion status. We found that in the early days (d1, 3, 4) after bacterial challenge, multiple cellular changes can be observed in the blood, especially in the neutrophils, monocyte compartments,

A General kinetics post-challenge



B Kinetics non-colonized participants

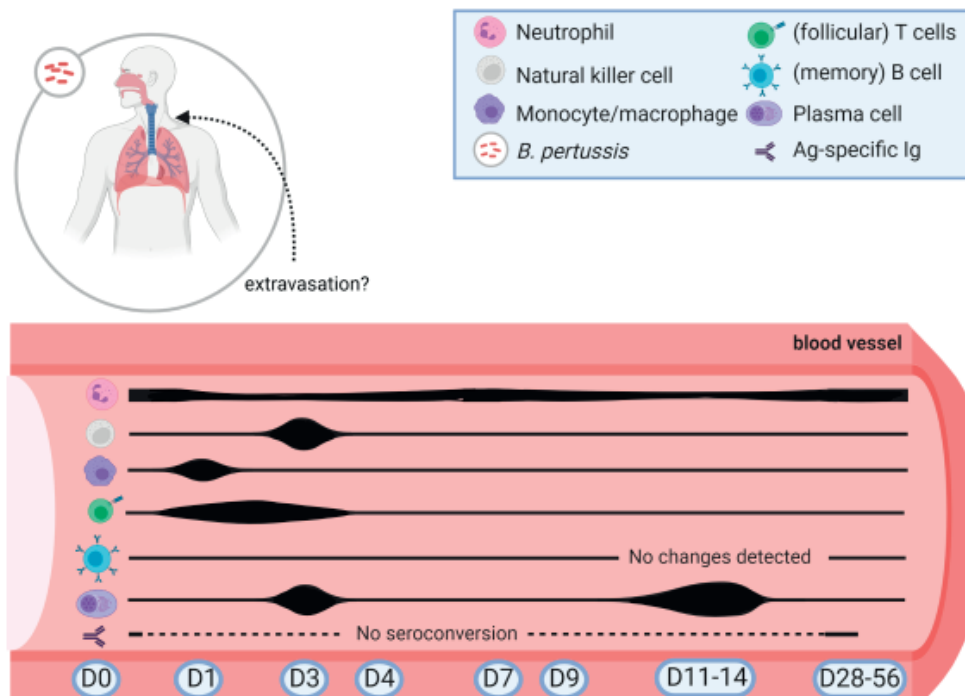


**Figure 7. Overview of most informative time points and cell populations after bacterial challenge.** A. General cellular kinetics post-challenge irrespective of clinical readout. B. Cellular kinetics unique to participants protected against colonization, possibly indicating pre-existing immunity in these participants.

FTH cells and plasma cells. Kinetics of these subsets differed between colonized and non-colonized participants, and surprisingly, the most prominent differences were found in the response between low-density colonized and non-colonized participants. Interestingly, the d3 plasma cell expansion negatively correlated with CFU load at d7 and d9 post-challenge. Later, at d11-14 post-challenge, expansion of various plasma cell subsets was observed, and increased plasma cell maturation was found in participants who showed seroconversion. Although this exploratory study comprised of only 15 participants, which were clustered based on their colonization status (leading to low statistical power), we detected consistent kinetics related to clinical readouts (colonization and seroconversion status). An important aspect in vaccine evaluation and improvement is understanding the underlying immune response. Cellular immunity against Bp colonization is never studied before in human, but comparisons can be made with vaccination studies, where protection against pertussis is achieved through intramuscular vaccination. Indeed, there are multiple studies describing antibody responses, and some studies also describe cellular responses induced by intramuscular vaccination against pertussis.[17,21-23,25] The major differences between current Bp vaccines and natural infection are the location of antigen encounter (intramuscular vs. mucosal) and the variety and concentration of antigens (aP vaccines contain purified Bp antigens usually combined with other bacterial/viral compounds like tetanus, diphtheria, polio). Although Bp vaccines confer protection against disease, they do not seem to prevent colonization and transmission of the bacterium.[3,26,27] Therefore, it is of critical importance to understand what is required to prevent colonization, translocation, and transmission of Bp. The benefit of reduced carriage has already been demonstrated for meningococcal disease and *Haemophilus influenzae* type b, where reduced carriage resulted in lowered transmission and increased herd immunity. This is most likely related to better mucosal immunity.[28-30]

In two previous vaccination studies, we explored the cellular responses to intramuscular aP booster vaccination in various cohorts using highly similar methods (aP-primed children, aP- or wP-primed adolescents, wP-primed young adults, and wP-primed older adults).[21,31] Both studies pointed towards the d7 plasma cell expansion and maturation as the major cellular change post-vaccination. One of these studies also investigated the innate and T-cell kinetics in 10 wP-primed participants who received an aP booster.[21] There, we observed 'late' monocyte kinetics at d3 post-vaccination (mostly iMo and ncMo) in approximately half of the participants. No consistent changes were observed post-vaccination in the numbers or composition of the CD4 T-cell, CD8 T-cell, or NK cell compartment. Comparing these studies with the here presented controlled infection study, we found clear differences between the kinetics post-challenge and post-vaccination, which are discussed in more detail below. Interestingly, several of the findings in this challenge model were in line with in a recent study evaluating the immune responses after intranasal vaccination with an attenuated Bp strain.[10]

Of all evaluated innate immune cells, especially monocyte subsets hold promise

for future evaluation. The decrease of CD62L<sup>+</sup> cMo and increase of CD62L<sup>-</sup> cMo implies activation and maturation of the cMo. This activation was seen in all challenged participants irrespective of clinical readout. However, the early expansion of (especially) CD36<sup>-</sup> ncMo was found exclusively in participants protected against colonization. Currently, information about the exact role of CD36<sup>-</sup> ncMo is scarce. However, part of the CD36<sup>-</sup> ncMos are SLAN<sup>+</sup> ncMos. SLAN<sup>+</sup> ncMos were recently reviewed by Ahmad et al [32] and are known to be circulating and tissue myeloid cells with high plasticity and a pro-inflammatory function. *In vitro* studies showed that SLAN<sup>+</sup> ncMos could rapidly differentiate into macrophages [13,33,34] or acquire DC functions, [35,36] and had a greater capacity to prime naive T cells towards Th1/Th17 cells when compared to CD1c<sup>+</sup> DCs.[32,36-38] Although these findings were not obtained in the context of Bp infection, the ability to promote Th1 and Th17 responses is relevant in the case of Bp infection, implying that SLAN<sup>+</sup> ncMos may contribute to the (protective) immune response. Consequently, we believe that monocyte subsets should be included in future immune monitoring studies.

In our previously published vaccination study, we did not observe the activation of cMo or the expansion of CD36<sup>-</sup> ncMo, although an expansion of overall iMo and ncMo was found.[21] This may be explained by the lack of early time points after vaccination or by the different mode of antigen encounter. Recent work on intranasal vaccination with a life attenuated Bp (BPZE1) did not observe consistent changes or maturation in cMo, iMo or ncMo either.[10] This may be attributed to differences in methodology, such as depth of evaluation, (number of) evaluated time points or the use of an attenuated Bp strain. Interestingly, the authors reported the production of several proinflammatory cytokines by purified monocytes upon stimulation with BPZE1, implying that upon contact with Bp, the monocytes start a local inflammation response.

We observed a decrease in circulating mature neutrophils several days post-challenge, which was a bit more prominent in the participants protected against colonization. The decrease in mature neutrophils may imply that these cells have been recruited into the tissue. Recent mouse studies indicated a role for IL-17, secreted by tissue-resident CD4 T cells (Trm cells), which is expected to play a role in the recruitment of neutrophils and enhancing Bp clearance.[39,40] Of note, those studies primarily focused on neutrophils present in (nasal) tissue, which may not be easily integrated in human studies due to the more invasive nature of sampling of tissue-resident cells (e.g. via nasal scrapings). As the decreased number of circulating mature neutrophils observed in this study may imply neutrophil extravasation, this (mature) population should be considered in future investigations.

The expansion of NK cells seemed to have an inverse relation with colonization density. This expansion was not observed upon booster vaccination with aP, neither did the intranasal study report on NK cell kinetics.[10,21] Animal studies have shown a role for NK cells in Bp infection, where they are thought to be the



initial source of IFN $\gamma$  (reviewed by Higgs et al., [41]). The production of IFN $\gamma$  is essential for containment of the infection and promotion of the Th1 response. Although we did not monitor IFN $\gamma$  secretion, we did find an early specific NK-cell signature (expansion) in the non-colonized participants.

Interestingly, we found that low-density colonized donors showed more prominent innate immune cell kinetics compared to high-density colonized participants. A possible explanation might be the presence of some pre-existing immunological memory, yet not as high as in participants protected from colonization. This pre-existing memory might result in a more targeted innate immune response (influenced by pre-existing memory cells or antibodies) and faster control of bacterial growth as compared to donors without any noteworthy pre-existing immunological memory.

We found an increase in FTH cells at d3 post-challenge, which was especially prominent in non-colonized participants. Although we did not find such expansion after aP booster vaccination, the flow cytometric analysis of FTH cells after intranasal pertussis vaccination (with BPZE1) did report an expansion of activated (as measured by expression of PD-1 and ICOS) Th1-like FTH cells starting at d4 post-vaccination.[10] We did not assess activation status of the FTH cells, but did observe an expansion of FTH cells at d3 post-challenge. Activation and/or expansion of FTH cells can support formation of germinal centers, and thus initiate humoral responses, leading to the generation of (protective) antibodies. Moreover, we found increased numbers of circulating T-helper cells of the Th1/17, TH22 and CXCR3-CCR4-CCR6+CCR10- phenotype at d1 and d3 post-challenge. These changes were not observed after an aP booster vaccination, and are much earlier than the T-cell readout that was used in the evaluation of BPZE1 vaccination, where a Th1-response was found in stimulated PBMCs at d28 post-vaccination.<sup>10</sup> In this study, we observed expansion of several IgG and IgA plasma cell subsets at d3 (mostly in non-colonized participants) and at d11-14 post-challenge. This is different compared to post-vaccination kinetics, where we observed a prominent and homogeneous expansion and maturation of (primarily IgG1) plasma cells at d7 post-vaccination. This difference may be explained by the way that the antigen is administered. During the booster vaccination, a high dose of antigen (+ adjuvant) is injected into the muscle, and thus all participants will be exposed to the antigen at the same time (d0), resulting in a synchronized induction of the immune response in vaccinated donors. Upon intranasal bacterial challenge, all participants are challenged with Bp at d0, but there may be differences in bacterial growth between participants. Therefore, the plasma cell peak may differ in timing between participants and thus not be as homogenous as after receiving a booster vaccination. Like in the post-challenge data, the expansion of plasma blasts (total, no subsets identified) after intranasal vaccination peaked at d14.[10] Interestingly, in that same set of data, in 2/12 participants an expansion of plasma blasts/plasma cells seemed present already at d4 post-vaccination, although the authors did not comment on this.

## Chapter 3.4

---

The observed IgG response is most likely the result of previous vaccine-induced immunity against Bp and natural boosting, whereas the IgA response can be mainly attributed to previous natural infections. It should be noted that once generated, both IgG and IgA memory B cells may be triggered by vaccination and/or infection. As natural infection occurs via the respiratory tract, local mucosal immunity (i.e., secretory IgA antibodies) is of importance in the rapid removal/neutralization of Bp upon infection. Increased mucosal immunity should be an important aspect for future Bp vaccine candidates, as this may reduce transmission. However, we believe that before this can be evaluated, the cellular responses preventing colonization and transmission should be understood. Of course, the question is to what extent the circulating IgA plasma cells represent mucosal IgA responses. Additional analysis of surface or intracellular markers may give insight in the destination of these plasma cells, for example, the use of markers that allow to differentiate between circulating and mucosa-oriented plasma cells (such as adhesion molecule  $\beta$ 7 integrin, J-chain or C-C motif receptor 10 (CCR10) [42-44]), may help to understand the destination of the expanding plasma cells. Expression of the J-chain would be of special interest for the peak of plasma cells that was observed at d3 post-challenge in the participants who were protected from colonization, as expression of mucosal homing markers may be lost when these cells are recruited from mucosal layers into the circulation. Moreover, repertoire studies comparing the (Ag-specific) B-cell receptor (BCR) repertoire between B cells at baseline, the plasma cells at d3 and at d11-14, and memory B cells at later time points may yield valuable insights in the relationship of these cells. Such repertoire studies could give insights in the breadth of the antibody response between challenged and vaccinated individuals. Additionally, (Ag-specific) BCR repertoire studies may also identify differences in antibody reactivity between high-density, low-density, and non-colonized participants, possibly showing selection towards a shared (protective) response to specific antigens/epitopes in participants protected against colonization. Lastly, it may be of interest to determine the clonal relationship between the plasma cells at d3 and the plasma cells that arise at d11/14, to see whether these d3 plasma cells are indeed derived from pre-existing immunity.

In this study, all participants were inoculated with predefined doses of a well-characterized Bp strain. We acknowledge that a controlled experimental infection is not the same as a natural infection model. The mode of infection, the dose and circumstances are designed to be standardized and this might be a limitation to translate these findings to natural pertussis infection. Nevertheless, we clearly observed shared kinetics within the total cohort, and when stratifying based on colonization status.

Not all participants who were colonized, showed signs of seroconversion. Perhaps translocation of Bp is required to initiate seroconversion. In that case, although these participants were colonized, the bacteria did not fully translocate into the tissue in all participants, leading to seroconversion only in the participants where bacteria had translocated. It may be of interest to compare the kine-

tics of antibodies in the mucosal lining fluid of the nose in participants who did and did not seroconvert and their colonization density. Additionally, it may be of interest to study whether the mucosal antibodies and the early plasma cell peak are associated with each other (e.g. by comparing BCRs). Moreover, it may be interesting to investigate whether participants can transmit Bp to others, as this would confirm that asymptomatic infection results in transmission of Bp. Such finding would imply that the presence/absence of symptoms and the serology status may not correctly reflect carriage/transmission state, and thus that serological surveillance studies, although valuable, may still underestimate the number of Bp infections.

In this cellular immune monitoring study, we evaluated the overall immune cell kinetics. We previously showed that there is a fair correlation between Ag-specific ELISpot data and plasma cell flow cytometry data in post-vaccination settings [45]. Although no ELISpot experiments were performed in the here-reported study, we did observe an increased number of (total and more mature) plasma cells at d14 post-challenge in donors showing seroconversion. The latter is in line with the ELISpot data that was previously reported on the total cohort used in the dose-finding study of this human challenge model.[12] There, increased numbers of Ag-specific Ig producing plasma cells were observed in multiple colonized participants (n=16) at d14 post-challenge, but not in participants protected from colonization (n=9). In both studies seroconversion was only observed in colonized participants. Given the relationship between Ag-specific Ig producing plasma cells and the serum Ig levels, the participants showing increased number of Ag-specific Ig producing plasma cells are likely the donors with seroconversion. Aside from ELISpot, an Ag-specific approach combined with mucosal-tracing markers may be informative, possibly helping us to find (surrogate) biomarkers of protection in the blood. An antigen-specific approach would be especially relevant to monitor kinetics of specific memory B- and T- cells.

One remaining question is whether the early response observed in participants protected from colonization is indeed protective, and to what extent this information can be used in future studies. To confirm whether a protective response is observed in participants, in fact a rechallenge would be required (e.g., an infection-reinfection cohort). As we know that natural infection gives the best protection (compared to wP and aP vaccination) [3,6], it may be that this controlled infection leads to a similar level of protection. Based on our data, we hypothesize that the initial decrease in mature neutrophils, and early expansion of CD36- nc-Mos, NK cells, FTH T cells and plasma cell in the non-colonized participants may be associated with an efficient mucosal immune response, preventing colonization. When re-challenging the same group of individuals, we would expect a higher number of participants to be protected against colonization, and thus to show this same early cellular response.

To the extent of our knowledge, we are one of the first to investigate such in-depth cellular immune responses in a Bp human challenge model. Here, we report which

cell populations and time points can yield valuable information about the colonization status and how this compares to vaccine-induced cellular kinetics. Because of the low incidence of pertussis and the difficulty to diagnose it early, there is a lack of information on cellular responses upon Bp infection in humans. Increased insight, especially in the protective immune signature, is crucial to the development of novel pertussis vaccines, which should aim to prevent colonization and transmission of Bp. This study increases insights in the cellular responses in individuals with varying degree of colonization upon controlled bacterial challenge. As we only investigated 15 participants, these findings should be corroborated in future studies. When fully established, this human challenge model can not only be used to study Bp infection, colonization, translocation, transmission and/or shedding in challenged individuals, but also to dissect the induced immune responses: early vs late responses, mucosal vs systemic responses, and protective vs non-protective responses. More importantly, controlled bacterial challenge could be an important step to evaluate the efficacy of novel Bp vaccine candidates with respect to protection against colonization and transmission.

### **Experimental methods**

#### **Inclusion criteria and sample collection**

Peripheral blood (PB) samples were collected during a dose-finding controlled infection study using Bp (NCT03751514, ethical committee reference 17/SC/0006), which aimed to determine the dose required to colonize at least 70% of participants, and was reported by De Graaf et al. [11,12] Participants (wP-primed) were eligible for the study when they were healthy, aged 18-45 years, available for the 16-day admission period and scheduled visits, vaccinated against Bp at least 5 years before enrollment, did not use antibiotics within 4 weeks before enrollment of the study, had no contraindication to azithromycin (administered at d14, d15, and d16) and had no contact with individuals vulnerable to pertussis (full eligibility criteria were reported before [12]). Participants with recent exposure to Bp, defined as baseline serum anti-PT IgG of >20 IU/mL (determined by ELISA), were excluded. Participants were challenged and admitted to the National Health Institute for Health Research Clinical Research Facility in Southampton, UK. A total of 34 participants were challenged with various doses of Bp. This paper describes 15 healthy participants who were challenged intra-nasally with  $10^4$  (n=5) or  $10^5$  (n=10) CFU of Bp strain B1917 (n=15, m/f ratio: 8/7, age range: 18-43 years old).

Colonization was assessed by culture of nasal wash samples on Bp-specific media at d4, d5, d7, d9, d11, d14, d15 and d16 post-challenge.[12] Colonization was defined as any Bp-positive culture at any time point post-challenge. Colonization density was stratified into 3 categories: non-colonized (0 CFU/mL), low-density colonized (< 1000 CFU/mL) and high-density colonized (> 1000 CFU/mL) at any time point.

PB was collected in EDTA blood collection tubes at d0, d1, d3, d4, d7, d9, d11, d14, d28 and d56 post-challenge. PB was taken early morning and transported

to Leiden University Medical Center (LUMC), the Netherlands, where flow cytometric evaluation was performed within 12h after donation. In two participants (ID.08 and ID.13), the expression of CD45RA on lymphocytes was found to be unusual, most likely caused by a CD45RA-related polymorphism<sup>19</sup>, hampering reliable identification of most T-cell subsets in these two participants. Aside from the anti-PT ELISA used for initial screening, serum IgG against PT, Prn, FHA and Fim2/3 was measured at baseline and d28 using multiplex immune assay (MIA) [46] at the National Institute for Public Health and the Environment (RIVM, The Netherlands). In this study, seroconversion is defined as an >2-fold increase in anti-PT IgG compared to baseline.

### **Blood processing and staining – immune monitoring panels and absolute count determination**

All PB samples were subjected to high-throughput EuroFlow-based flow cytometric immunophenotyping with four multicolor immune monitoring panels (or their direct prototypes). These panels allow monitoring the kinetics of over 250 circulating immune cell subsets. In short, the B-cell and plasma cell tube (BIGH) allows identification of up to 115 B- and plasma cell subsets, that are distinguished based on expressed Ig subclasses and their maturation stage-associated phenotype.[45,47] The CD4 T-cell panel (CD4T) allows identification of >89 CD4 T-cell subsets with different functionalities and maturation stages.[18] The CD8 cytotoxic T-cell panel (CYTOX) allows identification of up to 50 subsets within the CD8 T-cell and natural killer (NK) cell compartment.[47] Lastly, the dendritic cell-monocyte panel (DC-Monocyte) allows identification of up to 19 different (sub)populations within the myeloid compartment, including subsets of monocytes and dendritic cells [van der Pan et al., manuscript submitted].

All blood samples were processed according to the EuroFlow standard operating protocol (SOP) as reported previously (protocols available at [www.EuroFlow.org](http://www.EuroFlow.org)).[21,45] Two adjustments of the previously reported methods concerned the addition of surface marker CD45 to the BIGH, CD4T and CYTOX panel, and the cytoplasmic staining with a CD154 antibody in the CD4T and the CYTOX panel. The latter resulted in an additional intracellular staining step for the CYTOX panel.

In short, for CD4T and CYTOX panel 100µL PB was used for a membrane and intracellular staining using the Fix and Perm kit (Sanbio). For the BIGH and DC-Monocyte panel, high cell numbers were required, and thus a bulk lysis was performed on whole blood, then 10 million cells were stained for membrane markers. For the BIGH panel, this was followed by intracellular staining for immunoglobulins (again, using the Fix and Perm kit). For the DC-Monocyte panel, the surface staining was followed by a 10 min incubation with BD FACS lysing solution (BD Biosciences, San Jose, CA, USA), washed and acquired on the flow cytometer.

Absolute cell counts were determined with the use of Perfect-Count Microspher-



## Chapter 3.4

---

res™ (Cytognos, Spain) according to the EuroFlow SOP ([www.EuroFlow.org](http://www.EuroFlow.org)). In short, exactly 50µL of PB was stained with antibodies directed against CD19, CD3 and CD45, and samples were incubated for 30 min in the dark. Next, 500µL of NH<sub>4</sub>CL was added, and after 10 min incubation exactly 50µl of Perfect-Count Microspheres™ were added. Samples were acquired immediately after. This procedure allowed for accurate assessment of absolute cell counts of leukocytes, lymphocytes, B-, T- and NK cells.

All samples were measured on a BD FACS LSR Fortessa 4L or on a BD FACS LSR Fortessa X-20 4L (BD Biosciences, San Jose, CA, USA). Flow cytometer performance was assessed daily according to the EuroFlow guidelines as previously described.[48,49] Staining with all antibody panels was performed at every time point, with exception of d1 post-challenge, at which the BIGH panel was not applied.

### **Data analysis and statistics**

All data were analyzed manually in the Infinicyt™ Software (v2.0, Cytognos, Spain) according to the EuroFlow gating strategies.[18,45,47] [Van der Pan et al, manuscript submitted] Plasma cell maturation stages were defined using the maturation pathway tool in the Infinicyt software, as previously described.[21]

Differences in cell counts between multiple (>2) conditions were assessed with Kruskal-Wallis, followed by Dunn's test. Differences between cell counts/ratios in two tested conditions were assessed with Mann-Whitney test. A p-value <0.05 was considered statistically significant. GraphPad Prism 8.0 software (GraphPad, San Diego, CA, USA) was used for statistical tests. Correlations between two parameters were assessed using Spearman's ranking correlation.

### **Acknowledgements**

The authors would like to thank the nurses for their help in this study, Suzanne Comans for her help with data analysis and all participants for their participation in this study. We thank Indu Khatri for her help in constructing the Bubble Plots in Python. Moreover, we are thankful for Anna De Schutter, Sarah Horswill, Rosy Haig, and FlyBe Airlines for their help in transferring the samples from UK to the Netherlands. The authors gratefully acknowledge the Flow cytometry Core Facility (FCF) of Leiden University Medical Center (LUMC) in Leiden, the Netherlands (<https://www.lumc.nl/research/facilities/fcf>), coordinated by M. Hameetman, run by the FCF Operators, D.M. Lowie, S. van de Pas, G.I.J. Reyneveld, and former FCF coordinator dr. K Schepers and former operators J.P. Jansen, E.F.E de Haas, G.M. De Roo, R.J. McLaughlin and S.A.J. Veld (Directors: Prof. F.J.T. Staal and Prof. J.J.M. van Dongen) for their technical support. The data safety and monitoring committee: Dr. Stephen Gordon, Dr. Wei Shen Lim, Dr. Patrick Lillie. The nurses and coordinating staff of the NIHR Clinical Research Facility Southampton (director: Prof. S.N. Faust). The scientific advisory committee: Prof Andrew Gorringe, Dr. Kent Kester and Dr. Dimitri Diavotopoulos.

### **Funding**

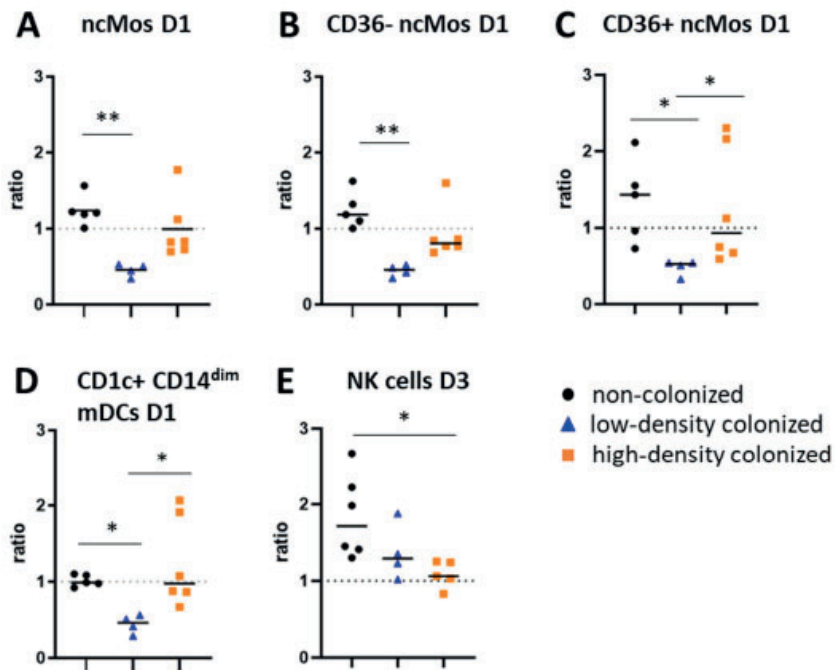
This PERISCOPE project has received funding from the Innovative Medicines Initiative 2 Joint Undertaking under grant agreement No 115910. This Joint Undertaking receives support from the European Union's Horizon 2020 research and innovation program and EFPIA and BMGF. This manuscript only reflects the author's views. The Joint Undertaking is not responsible for any use that may be made of the information this manuscript contains. The flow cytometric studies were supported by the EuroFlow Consortium, which received support from the FP6-2004-LIFESCIHEALTH-5 program of the European Commission (grant LSHB-CT-2006-018708) as Specific Targeted Research Project (STREP).

### **Conflict of interest**

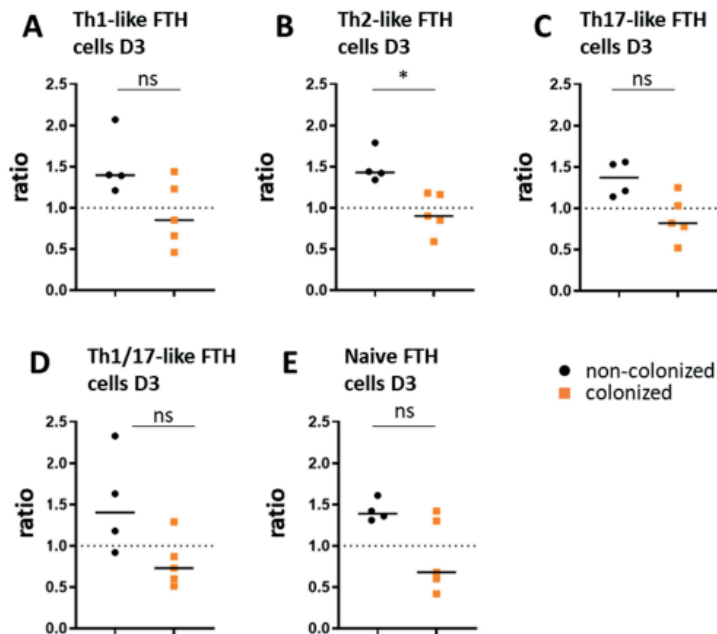
J.J.M. van Dongen is chairman of the EuroFlow scientific consortium, which was initially supported by the FP6-2004-LIFESCIHEALTH-5 program of the European Commission (grant LSHB-CT-2006-018708) as Specific Targeted Research Project (STREP); now the EuroFlow consortium receives royalties from licensed patents, which income is solely used for continuation of the collaboration within the consortium. In addition, J.J.M. van Dongen has an Educational Service Agreement with BD Biosciences and a Scientific Advisory Agreement with Cytognos; income from these agreements goes to LUMC. Lastly, J.J.M. van Dongen, M.A. Berkowska, C.I. Teodosio and A.M. Diks are listed as (co)inventors on the patent issued by the EuroFlow scientific consortium, which describes the flow cytometry panels used in this study. Other authors declare no conflict of interest.

### **Supplemental Materials**

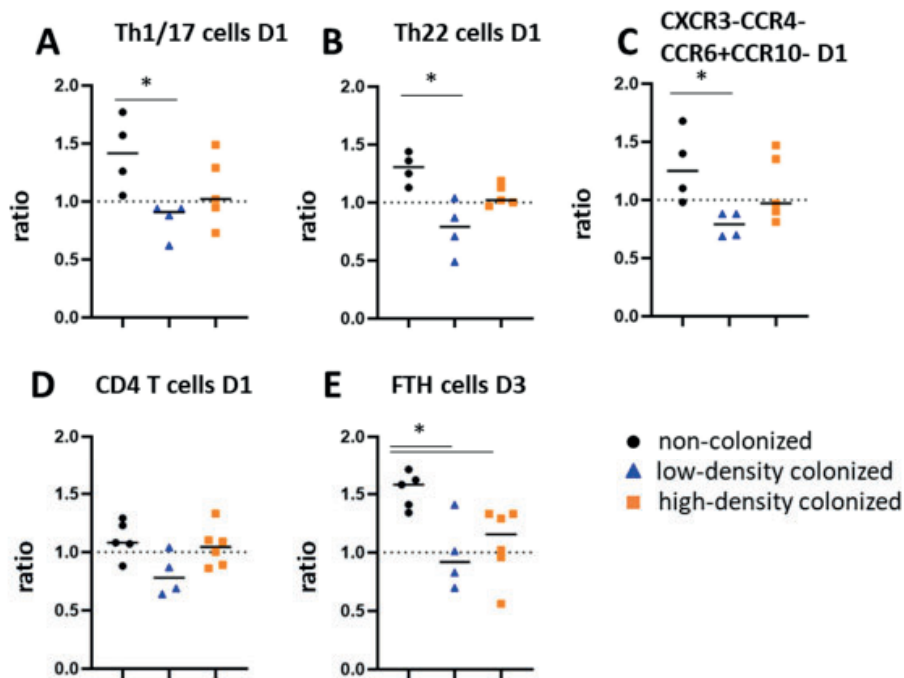
This work is still a manuscript in preparation. Therefore, all supplemental material is shown on the following pages.



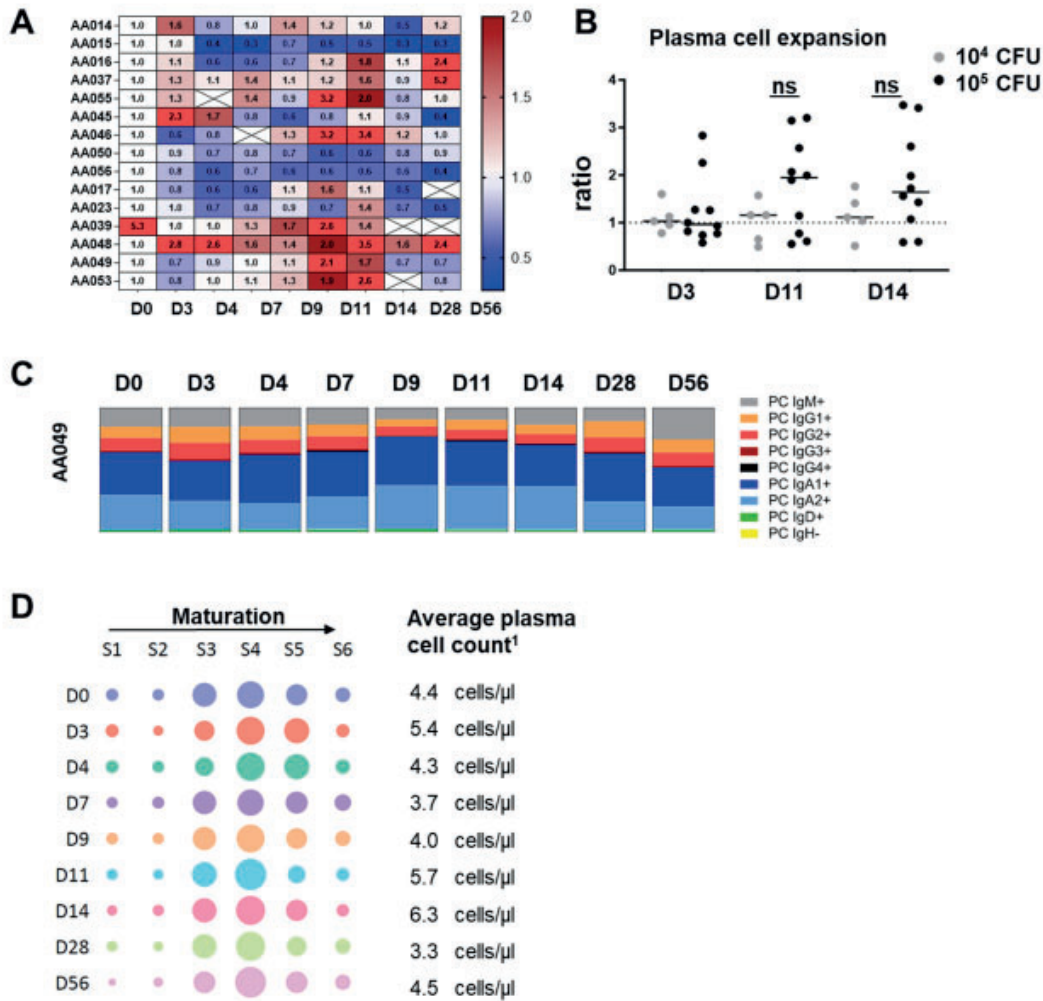
**Supplemental Figure 1. Different kinetics in the innate immune cell compartment based on colonization density.** Differences are presented as ratio of baseline. Dashed line indicates a ratio of 1.0 (baseline value). Kruskal-Wallis followed by Dunns' test was used to assess differences. D= days after challenge. \*  $p < 0.05$ , \*\*  $p < 0.01$ .



**Supplemental Figure 2. Expansion of follicular T helper (FTH) cells in participants protected from colonization.** Expansion of FTH subsets at d3 post-challenge expressed as ratio of baseline. Dashed line indicates a ratio of 1.0 (baseline value). Of note, due to technical limitations, in 6/15 participants no FTH subsets could be defined. N=9. Differences between groups were assessed using Mann-Whitney test. \*  $p < 0.05$ . D= days after challenge.

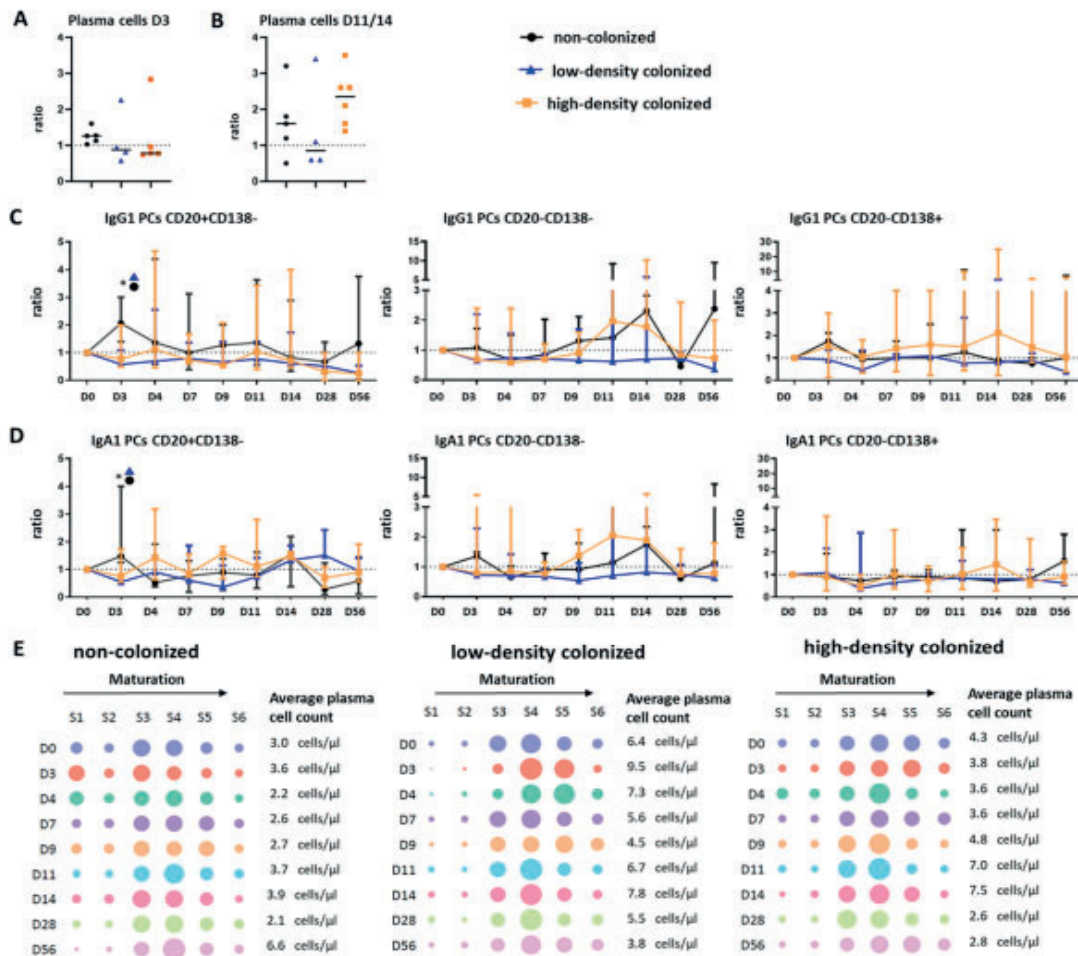


**Supplemental Figure 3. Kinetics of T helper cells in participants grouped upon colonization density.** Expansion or reduction of circulating cells was expressed as ratio of baseline. Dashed line indicates a ratio of 1.0 (baseline value). Kruskal-Wallis followed by Dunns' test was used to assess differences. \*  $p < 0.05$ . D= days after challenge, FTH= follicular T helper cells, Th cell= T helper cell.



**Supplemental Figure 4. Kinetics in the plasma cell compartment upon bacterial challenge.** A. Heatmap representing the expansion of plasma cells in ratio compared to baseline ranked based on colonization status. NB: Participant ID.12 showed a strongly elevated number of IgM plasma cells at baseline. Dashed line indicates a ratio of 1.0 (baseline value). Therefore, it was decided to normalize the plasma cell numbers of this participant to d3 instead of baseline. B. Expansion of plasma cell in ratio compared to baseline. The cohort is split based on initial CFU dosage ( $10^4$  or  $10^5$  CFU of BP1917) received at the day of challenge. Each dot represents one participant, the bar indicates the median value of all participants in each cohort. C. Fluctuations in the distribution of the plasma cell compartment over time. One representative participant is shown. D. Per time point the percentage of plasma cells in each maturation stage was plotted (total plasma cells in donors that were or were not colonized, grouped per time point). The size of the dot indicates the % of plasma cells in each maturation stage (average of participant). Cell count is shown at the right side of the plot (average of participants). Bubble plots were generated using plotly python graphing library.<sup>1</sup> Participant ID.12 was not included in panel D due to deviating baseline IgM plasma cell counts, possibly hinting at an ongoing immune response at time of challenge. D= Days after challenge.





**Supplemental Figure 5. Plasma cell kinetics in participants that were non-colonized, low-density colonized, or high-density colonized.** A. Plasma cell expansion at d3 post-challenge. Expansion expressed as ratio compared to baseline. Each dot represents one participant, the bar indicates the median value of all donors each cohort. B. Plasma cell expansion at d11/14 post-challenge. Expansion expressed as ratio compared to baseline. For panel A and B, Kruskal-Wallis followed by Dunns' test was used to assess differences. C+D. Total plasma cells were divided into three different maturation stages (CD20+CD138-, CD20-CD138-, CD20-CD138+). Per maturation stage, the ratio compared to baseline was compared between donors of the three groups for IgG1 (C) and IgA1 (D) plasma cells. E. Per time point the percentage of plasma cells in each maturation stage was plotted (total plasma cells in donors that that were or were not colonized, grouped per time point). The size of the dot indicates the % of plasma cells in each maturation stage (average of donors). Cell count is shown at the right side of the plot (average of participants). Bubble plots were generated using plotly python graphing library. Dashed line indicates a ratio of 1.0 (baseline value). Statistical test performed for longitudinal analysis: Wilcoxon. Statistical test for comparison between groups per time point; Mann-Whitney. D= days after challenge.

### References

1. Roush SW, Murphy TV, Group V-PDTW. Historical comparisons of morbidity and mortality for vaccine-preventable diseases in the United States. *Jama*. 2007;298(18):2155-2163.
2. Clark TA. Changing pertussis epidemiology: everything old is new again. *The Journal of infectious diseases*. 2014;209(7):978-981.
3. Warfel JM, Zimmerman LI, Merkel TJ. Acellular pertussis vaccines protect against disease but fail to prevent infection and transmission in a nonhuman primate model. *Proceedings of the National Academy of Sciences*. 2014;111(2):787-792.
4. Loch C. Will we have new pertussis vaccines? *Vaccine*. 2018;36(36):5460-5469.
5. Roberts R, Moreno G, Bottero D, et al. Outer membrane vesicles as acellular vaccine against pertussis. *Vaccine*. 2008;26(36):4639-4646.
6. Wendelboe AM, Van Rie A, Salmaso S, Englund JA. Duration of immunity against pertussis after natural infection or vaccination. *The Pediatric infectious disease journal*. 2005;24(5):S58-S61.
7. Tan T, Dalby T, Forsyth K, et al. Pertussis across the globe: recent epidemiologic trends from 2000 to 2013. *The Pediatric infectious disease journal*. 2015;34(9):e222-e232.
8. De Greeff SC, De Melker HE, Van Gageldonk PG, et al. Seroprevalence of pertussis in The Netherlands: evidence for increased circulation of *Bordetella pertussis*. *PLoS one*. 2010;5(12):e14183.
9. Heininger U, André P, Chlibek R, et al. Comparative epidemiologic characteristics of pertussis in 10 central and eastern European countries, 2000-2013. *PLoS One*. 2016;11(6):e0155949.
10. Lin A, Apostolovic D, Jahnmatz M, et al. Live attenuated pertussis vaccine BPZE1 induces a broad antibody response in humans. *The Journal of Clinical Investigation*. 2020;130(5).
11. De Graaf H, Gbesemete D, Gorringer AR, et al. Investigating *Bordetella pertussis* colonisation and immunity: protocol for an inpatient controlled human infection model. *BMJ open*. 2017;7(10):e018594.
12. de Graaf H, Ibrahim M, Hill AR, et al. Controlled human infection with *Bordetella pertussis* induces asymptomatic, immunizing colonization. *Clinical Infectious Diseases*. 2020;71(2):403-411.
13. Ziegler-Heitbrock L, Ancuta P, Crowe S, et al. Nomenclature of monocytes and dendritic cells in blood. *Blood*. 2010;116(16):e74-e80.
14. Damasceno D, Almeida J, Teodosio C, et al. Monocyte Subsets and Serum Inflammatory and Bone-Associated Markers in Monoclonal Gammopathy of Undetermined Significance and Multiple Myeloma. *Cancers*. 2021;13(6):1454.
15. Damasceno D, Teodosio C, van den Bossche WB, et al. Distribution of subsets of blood monocytic cells throughout life. *Journal of Allergy and Clinical Immunology*. 2019;144(1):320-323. e326.
16. Bancroft T, Dillon MB, da Silva Antunes R, et al. Th1 versus Th2 T cell polarization by whole-cell and acellular childhood pertussis vaccines persists upon re-immunization in adolescence and adulthood. *Cellular immunology*. 2016;304:35-43.
17. Lambert EE, Corbière V, van Gaans-van den Brink J, et al. Uncovering Distinct Primary Vaccination-Dependent Profiles in Human *Bordetella Pertussis* Specific CD4+ T-Cell Responses Using a Novel Whole Blood Assay. *Vaccines*. 2020;8(2):225.
18. Botafogo V, Pérez-Andres M, Jara-Acevedo M, et al. Age distribution of multiple functionally relevant subsets of CD4+ T cells in human blood using a standardized and validated 14-color euroflow immune monitoring tube. *Frontiers in immunology*. 2020;11:166.
19. Schwinzer R, Wonigeit K. Genetically determined lack of CD45R-T cells in healthy individuals. Evidence for a regulatory polymorphism of CD45R antigen expression. *The Journal of experimental medicine*. 1990;171(5):1803-1808.
20. Gatto D, Brink R. The germinal center reaction. *Journal of Allergy and Clinical Immunology*. 2010;126(5):898-907.
21. Diks AM, Khatri I, Oosten LE, et al. Highly Sensitive Flow Cytometry Allows Monitoring of Changes in Circulating Immune Cells in Blood After Tdap Booster Vaccination. *Frontiers in Immunology*. 2021;12:2091.
22. Versteegen P, Pinto MV, Barkoff AM, et al. Responses to an acellular pertussis booster vaccination in children, adolescents, and young and older adults: A collaborative study in Finland, the Netherlands, and the United Kingdom. *EBioMedicine*. 2021;65:103247.
23. van der Lee S, Sanders EA, Berbers GA, Buisman A-M. Whole-cell or acellular pertussis vaccination in infancy determines IgG subclass profiles to DTaP booster vaccination. *Vaccine*. 2018;36(2):220-226.
24. Prince HE, Lieberman JM, Cherry JD. Age-related differences in patterns of increased Bor-

- detella pertussis antibodies. *Clinical vaccine immunology*. 2012;19(4):545-550.
25. Van Der Lee S, Hendrikx LH, Sanders EA, Berbers GA, Buisman A-M. Whole-cell or acellular pertussis primary immunizations in infancy determines adolescent cellular immune profiles. *Frontiers in immunology*. 2018;9:51.
  26. Wendelboe AM, Njamkepo E, Bourillon A, et al. Transmission of *Bordetella pertussis* to young infants. *The Pediatric infectious disease journal*. 2007;26(4):293-299.
  27. Bolotin S, Harvill ET, Crowcroft NS. What to do about pertussis vaccines? Linking what we know about pertussis vaccine effectiveness, immunology and disease transmission to create a better vaccine. *Pathogens disease*. 2015;73(8).
  28. Balmer P, Burman C, Serra L, York LJ. Impact of meningococcal vaccination on carriage and disease transmission: a review of the literature. *Human Vaccines & Immunotherapeutics*. 2018;14(5):1118-1130.
  29. Takala A, Santosham M, Almeida-Hill J, Wolff M. Vaccination with *Haemophilus influenzae* type b meningococcal protein conjugate vaccine reduces. *Pediatric Infectious Disease Journal*. 1993;12:593-599.
  30. Zhang Q, Choo S, Everard J, Jennings R, Finn A. Mucosal immune responses to meningococcal group C conjugate and group A and C polysaccharide vaccines in adolescents. *Infection immunology*. 2000;68(5):2692-2697.
  31. Diks AM, Versteegen P, Teodosio C, et al. Age and Primary Vaccination Background Influence the Plasma Cell Response to Pertussis Booster Vaccination. *Vaccines*. 2022;10(2):136.
  32. Ahmad F, Döbel T, Schmitz M, Schäkel K. Current concepts on 6-sulfo LacNAc expressing monocytes (slanMo). *Frontiers in Immunology*. 2019;10:948.
  33. van Leeuwen-Kerkhoff N, Lundberg K, Westers TM, et al. Transcriptional profiling reveals functional dichotomy between human slan+ non-classical monocytes and myeloid dendritic cells. *Journal of leukocyte biology*. 2017;102(4):1055-1068.
  34. Calzetti F, Tamassia N, Micheletti A, Finotti G, Bianchetto-Aguilera F, Cassatella MA. Human dendritic cell subset 4 (DC4) correlates to a subset of CD14dim/- CD16++ monocytes. *Journal of Allergy Clinical Immunology*. 2018;141(6):2276-2279. e2273.
  35. Vermi W, Micheletti A, Finotti G, et al. slan+ monocytes and macrophages mediate CD20-dependent B-cell lymphoma elimination via ADCC and ADCP. *Cancer research*. 2018;78(13):3544-3559.
  36. Toma M, Wehner R, Kloß A, et al. Accumulation of tolerogenic human 6-sulfo LacNAc dendritic cells in renal cell carcinoma is associated with poor prognosis. *Oncoimmunology*. 2015;4(6):e1008342.
  37. Schäkel K, Kannagi R, Kniep B, et al. 6-Sulfo LacNAc, a novel carbohydrate modification of PSGL-1, defines an inflammatory type of human dendritic cells. *Immunity*. 2002;17(3):289-301.
  38. Hänsel A, Günther C, Ingwersen J, et al. Human slan (6-sulfo LacNAc) dendritic cells are inflammatory dermal dendritic cells in psoriasis and drive strong TH17/TH1 T-cell responses. *Journal of Allergy Clinical Immunology*. 2011;127(3):787-794. e789.
  39. Borkner L, Curham LM, Wilk MM, Moran B, Mills KH. IL-17 mediates protective immunity against nasal infection with *Bordetella pertussis* by mobilizing neutrophils, especially Siglec-F+ neutrophils. *Mucosal immunology*. 2021;1-20.
  40. Dubois V, Chatagnon J, Thiriard A, et al. Suppression of mucosal Th17 memory responses by acellular pertussis vaccines enhances nasal *Bordetella pertussis* carriage. *Vaccines*. 2021;6(1):1-10.
  41. Higgs R, Higgins S, Ross P, Mills K. Immunity to the respiratory pathogen *Bordetella pertussis*. *Mucosal immunology*. 2012;5(5):485-500.
  42. Mei HE, Yoshida T, Sime W, et al. Blood-borne human plasma cells in steady state are derived from mucosal immune responses. *Blood*. 2009;113(11):2461-2469.
  43. Kunkel EJ, Kim CH, Lazarus NH, et al. CCR10 expression is a common feature of circulating and mucosal epithelial tissue IgA Ab-secreting cells. *The Journal of clinical investigation*. 2003;111(7):1001-1010.
  44. Castro CD, Flajnik MF. Putting J chain back on the map: how might its expression define plasma cell development? *The Journal of Immunology*. 2014;193(7):3248-3255.
  45. Diks AM, Versteegen P, Teodosio C, et al. Evaluation of B-Cell Kinetics After Acellular Pertussis Vaccination in Four Cohorts of Different Age and Priming Background. 2021.
  46. van Gageldonk PG, van Schaijk FG, van der Klis FR, Berbers GA. Development and validation of a multiplex immunoassay for the simultaneous determination of serum antibodies to *Bordetella pertussis*, diphtheria and tetanus. *Journal of immunological methods*. 2008;335(1-2):79-89.

## Chapter 3.4

---

47. van Dongen JJM, Orfao de Matos Correia E Vale JA, Goncalves Grunho Teodosio CI, et al., Inventors; PCT/NL2020/050688. Means and methods for multiparameter cytometry-based leukocyte subsetting. priority date: 05-11-2019, 2019.
48. Kalina T, Flores-Montero J, Lecrevisse Q, et al. Quality assessment program for EuroFlow protocols: Summary results of four-year (2010–2013) quality assurance rounds. *Cytometry Part A*. 2015;87(2):145-156.
49. Kalina T, Flores-Montero J, Van Der Velden V, et al. EuroFlow standardization of flow cytometer instrument settings and immunophenotyping protocols. *Leukemia*. 2012;26(9):1986-2010.

## Chapter 4

### ***PLCG2* variant p.P522R -associated with healthy aging- may reduce the aging of the human immune system**

A.M. Diks<sup>1 2</sup>, C. Teodosio<sup>13</sup>, B. De Mooij<sup>1</sup>, R.J. Groenland<sup>1</sup>, B.A.E. Naber<sup>1</sup>, I.F. de Laat<sup>1</sup>, A.A. Vloemans<sup>1</sup>, S. Rohde<sup>2</sup>, M.I. de Jonge<sup>4</sup>, L. Lorenz<sup>2</sup>, D. Horsten<sup>2</sup>, J.J.M. van Dongen<sup>1 3</sup>, M.A. Berkowska<sup>1\*</sup>, H. Holstege<sup>2\*</sup>

<sup>1</sup> Department of Immunology, Leiden University Medical Center, Albinusdreef 2, 2333 ZA, Leiden, the Netherlands

<sup>2</sup> Department of Human Genetics, Vrije Universiteit Amsterdam, Amsterdam UMC, Amsterdam, the Netherlands

<sup>3</sup> Translational and Clinical Research Program, Cancer Research Center (IBMCC; University of Salamanca - CSIC); Cytometry Service, NUCLEUS; Department of Medicine, University of Salamanca and Institute of Biomedical Research of Salamanca (IBSAL), Spain

<sup>4</sup> Laboratory of Medical Immunology, Radboud Institute for Molecular Life Sciences, Radboud University Medical Centre, Nijmegen, The Netherlands

\* These authors contributed equally to this manuscript

**Manuscript submitted**



### Abstract

**Background:** Phospholipase C gamma 2 (PLC $\gamma$ 2) is encoded by the *PLCG2* gene. A single-nucleotide polymorphism (p.P522R) associates with protection against several dementia subtypes and with increased likelihood of longevity. Cell lines and animal models indicated that p.P522R is a functional hypermorph. We aimed to confirm this in human peripheral immune cells.

**Methods:** We compared effects of p.P522R on immune system function between carriers and non-carriers (aged 59-103y), using in-depth immunophenotyping, functional B-cell and myeloid-cell assays, and *in vivo* SARS-CoV-2 vaccination.

**Results:** As expected, effects of p.P522R on immune cell function were small. Immune cell numbers in p.P522R carriers better resembled a younger reference cohort than those of non-carriers. Moreover, carriers expressed lower levels of Fc $\epsilon$ RI on several immune cell subsets and elevated CD33 levels on classical monocytes. Upon B-cell stimulation, PLC $\gamma$ 2 phosphorylation and calcium release were increased in carriers compared to non-carriers. Normalized ROS production in myeloid cells was higher upon PLC $\gamma$ 2-dependent stimulation, but lower upon PLC $\gamma$ 2-independent stimulation. Carriers and non-carriers had similar serological responses to SARS-CoV-2 vaccination.

**Conclusion:** Compared to non-carriers, immune profiles from carriers more closely resembled those from younger individuals, suggesting that p.P522R associates with resilience against immunological aging.

**Keywords:** Phospholipase C gamma 2, PLC $\gamma$ 2 p.P522R, *PLCG2* rs72824905, healthy aging, immunosenescence, flow cytometry, functional studies

## Background

The average human lifespan has greatly expanded in the past decennia. In most individuals, increase in age coincides with a decline in cognitive and physical health. Many age-related impairments, such as lowered resistance to infection, dementia, osteoporosis, atherosclerosis, and diabetes are directly or indirectly related to the aging immune system, especially to the low grade inflammation that is frequently observed in older individuals (inflamm-aging).(1, 2)

Upon aging, the output of naive B and T cells from the bone marrow into the periphery decreases, leading to lower numbers of naive lymphocytes in the circulation. Additionally, B and T-cell receptor (BCR, TCR) diversity decreases upon aging, leaving aged individuals less equipped to deal with neo-antigens.(1, 3, 4) Human and animal models have shown impaired germinal center (GC) formation, reduced affinity maturation, reduced memory B-cell (MBC) differentiation and lowered levels of plasma cells in the bone marrow.(3) Additionally, the functioning of innate immune cells declines. In neutrophils derived from aged individuals, a lowered capacity to phagocytose opsonized particles and decreased production of reactive oxygen species (ROS) was reported.(4, 5) Likewise, monocytes derived from older adults showed reduced phagocytic capacity, lowered ROS production and lower anti-tumor properties.(1, 6, 7)

Each individual is uniquely vulnerable to the effects of aging. Therefore, several studies have searched for (biomolecular) elements and pathways associated with resilience to the effects of aging, i.e. that optimally maintain both physical and cognitive functions during the aging process.(8-10) One of the factors identified is a single-nucleotide polymorphism (SNP) in the Phospholipase C gamma 2 (*PLCG2*) gene (p.P522R, rs72824905).(8)

PLC $\gamma$ 2 is an enzyme with a critical regulatory role in various immune and inflammatory pathways. It is involved in downstream receptor signaling where, upon receptor stimulation, it hydrolyses PIP<sub>2</sub> (phosphatidylinositol 4,5-bisphosphate) to generate IP<sub>3</sub> (inositol 1,4,5-triphosphate) and DAG (diacylglycerol), which are second messenger molecules that further transmit the activation signal, leading to the release of intracellular calcium.(11, 12) Amongst others, PCL $\gamma$ 2 is expressed downstream of several members of the immunoglobulin superfamily, such as the B-cell receptor on B cells, but also downstream of Fc receptors (FcR) in innate cells, such as Fc $\gamma$ III and 2B<sub>4</sub> on NK cells, Fc $\epsilon$ RI on mast cells, TREM (Triggering Receptors Expressed on Myeloid cells) on macrophages and microglia, and FcR-involving collagen receptors on platelets.(12-14)

We previously observed that the p.P522R variant was associated with a lower risk of several forms of age-related neurodegenerative diseases, including Alzheimer's disease, frontotemporal dementia, dementia with Lewy Bodies, and progressive supranuclear palsy.(9, 15) Recently, multiple sclerosis was added to this list.(16) This p.P522R variant simultaneously associates with increased likelihood of ex-

treme longevity.(9) In fact, a recent study suggested that the p.P522R variant may maintain cognitive function during aging by mitigating the accumulation of toxic tau pathology in the brain, when this co-occurs with the accumulation of amyloid pathology, both hallmarks of Alzheimer's disease.(17) The same study suggested that the cognitive decline observed in individuals who carry the APOE- $\epsilon$ 4 allele, the strongest genetic risk factor for Alzheimer's disease, in combination with the p.P522R *PLCG2* variant, was slower and less compared to individuals who carried the APOE- $\epsilon$ 4 allele without the protective p.P522R variant.(9, 17) Together, this suggests that the effect of p.P522R associates with maintaining an aspect of the immune system that, when compromised, increases the risk of these neurodegenerative diseases. Many studies have therefore investigated the effect of this variant in the innate immune cells of the brain, the microglia. However, *PLCG2* is most prominently expressed in peripheral immune cells, suggesting that this variant may also affect human peripheral immune system function. Furthermore, it might well be that the peripheral immune system function also influences brain function.

The p.P522R variant was shown to be a gain-of-function variant (functional hypermorph) in transfected COS7, HEK293T and BV2 cells, a p.P522R mouse model, and gene-edited human iPSCs.(13, 18, 19) In the current study, we investigated the impact of p.P522R carriership on the human immune system and its implications for healthy aging. To the best of our knowledge, an in-depth evaluation of the PLC $\gamma$ 2 expression in circulating immune cells between p.P522R carriers and non-carriers has not yet been performed. We hypothesized that the immune system of p.P522R carriers translates to an increased resilience to the effects of aging compared to age-matched non-carriers. To this end, we investigated the quantities, immunophenotypes, and functions of circulating immune cells in p.P522R carriers and non-carriers from 9 different nuclear families, in which one parent reached 100 years with high levels of cognitive performance and carried the p.P522R variant. We evaluated phosphorylation of PLC $\gamma$ 2 and calcium release upon BCR stimulation and analyzed the replication history in B-cell subsets. *In vivo* B-cell responses were assessed by measuring the serum Ig response to SARS-CoV-2 vaccination. Lastly, myeloid cell subsets were exposed to opsonized *Escherichia coli*, after which phagocytosis and ROS production were monitored.

## Methods

### Experimental design

A total of 36 individuals from the 100 plus study cohort, as previously described by Holstege et al (20), were selected for this study (METC number: 2016.440, approved by the Medical Ethics Committee of the VU University Medical Center, Amsterdam, the Netherlands). In short, volunteers either had to be  $\geq 100$  years, and self-reported as cognitively healthy, which was confirmed by a family member of close relation (20), or to be the offspring or a sibling of such individuals. When including offspring, the parent had to be a confirmed p.P522R carrier. After inclusion, peripheral blood (PB) was collected at one or multiple

occasions in K3EDTA collection tubes (PB-EDTA), sodium heparin collection tubes (PB-HEP), and serum collection tubes (BD Vacutainer, BD Biosciences, San Jose, Ca, USA). To avoid influence of circadian rhythm on cell counts, samples were always collected in the morning. p.P522R carriership was determined by Sanger sequencing or Illumina Genome Screening Array (GSA, GSAshared-CUSTOM\_20018389\_A2, v1, human genome build 37) as described elsewhere. (21) In the current study, we investigated quantities, immunophenotypes, and functions of circulating immune cells in three overlapping cohorts (Cohort I, II and III), described in **Table 1**. Immunophenotyping was performed on all individuals included in Cohort I (n=33). Calcium flux measurements were performed on cells from donors included in Cohort I and II, with exception of two donors that showed B-cell aberrancies (n=33). Functional evaluation (phosphorylation of PLCy2, KREC analysis, phagocytosis assay and ROS production) was performed on Cohort II (n=14). Lastly, vaccination responses were evaluated in Cohort III (n=22). Family composition can be found in **Table S1**.

### **Settings of flow cytometers**

For all flow cytometers (available at the Flow cytometry Core Facility at LUMC) there was a daily quality control (QC). QC for Cytex Aurora flow cytometers (Cytex Biosciences, Fremont, Ca, USA) was performed using SpectroFlo QC Beads (Cytex Biosciences). BD FACS LSR Fortessa 4L and BD FACS Canto II 3L (BD Biosciences, San Jose, CA, USA) were calibrated according to EuroFlow guidelines and daily QC was performed using BD™ Setup and Tracking (CS&T) beads (BD Biosciences) and Perfect-Count Microspheres™ (Cytognos, Spain), as described before.(22, 23)

### **Immunophenotyping of circulating immune cells**

PB-EDTA from Cohort I was used <12h after collection for immunophenotyping. In-depth analysis of circulating innate and adaptive immune cells was performed using previously published flow cytometry panels, or their direct prototypes, and gating strategies (**Table S2**).

The dendritic cell-monocyte (DC-monocyte) panel allows identification of up to 19 different (sub)populations in the myeloid compartment.(24, 25) The CD4-T cell panel (CD4T) allows identification of at least 89 (sub)populations within the CD4 T-cell compartment, which comprise of different functionalities and maturation stages.(25, 26) The CD8 cytotoxic T-cell (CYTOX) panel allows identification of up to 50 (sub)populations within the CD8 T-cell and the natural killer (NK) cell compartments.(25) Lastly, the B-cell and plasma cell (BIGH) panel allows identification of up to 115 populations of B and plasma cells, distinguished based on their maturation stage-associated phenotype and the expressed Ig subclasses. (25, 27, 28)

Depending on the antibody combination, samples were either processed according to the bulk lysis protocol for staining of  $10 \times 10^6$  cells (DC-monocyte and BIGH) or prepared using the EuroFlow stain-lyse-wash protocol (CD4T,

## Chapter 4

CYTOX); both protocols available on [www.EuroFlow.org](http://www.EuroFlow.org). For BIGH and CYTOX tubes, surface staining was followed by intracellular staining with the Fix & Perm reagent kit (Nordic MUBio, Susteren, The Netherlands) according to manufacturer's protocol. In brief, 100µl of washed sample was fixed with 100µl of Solution A (15 min in the dark at RT), washed, and permeabilized by adding 100µl of Solution B (15 min in the dark at RT) and antibodies against intracellular markers. After washing, cells were re-suspended in PBS for immediate acquisition (or stored for max ~3h at 4°C).

**Table 1. Description of the cohorts used in this study; Cohort I, II, III.**

| <b>Cohort I: Extensive immunophenotyping</b> |                    |                        |            |
|--|--------------------|------------------------|------------|
|  | <b>Min-max age</b> | <b>Mean/median age</b> | <b>M/F</b> |
| <b>Carriers (18)</b>                         | 59-103 y           | 75.1/71 y              | 7/11       |
| <b>Non-carriers (15)</b>                     | 61-83 y            | 73.1/74 y              | 8/7        |

- Cognitively healthy individuals
- p.P522R carrying centenarian; or a child/sibling of such centenarian
- 33 donors from 7 families
  - Blood collection
  - Immunophenotyping of >100 circulating immune cell subsets
  - PBMCs storage

| <b>Cohort II: Functional assays</b> |                    |                        |            |
|-------------------------------------|--------------------|------------------------|------------|
|                                     | <b>Min-max age</b> | <b>Mean/median age</b> | <b>M/F</b> |
| <b>Carriers (8)</b>                 | 59-78 y            | 69.5/69 y              | 6/2        |
| <b>Non-carriers (6)</b>             | 71-83 y            | 77.3/77.5y             | 4/2        |

- Healthy individuals (based on clinical records and current medication use)
- 14 donors from 8 families (12/14 donors selected from Cohort I)
  - Blood collection for:
    - B-cell activation
    - Replication history of B-cell subsets
    - Phagocytic capacity

| <b>Cohort III: <i>in vivo</i> evaluation</b> |                    |                        |            |
|--|--------------------|------------------------|------------|
|  | <b>Min-max age</b> | <b>Mean/median age</b> | <b>M/F</b> |
| <b>Carriers (10)</b>                         | 62-82 y            | 73.1/71.5 y            | 6/4        |
| <b>Non-carriers (12)</b>                     | 64-87 y            | 76.3/76.5y             | 8/4        |

- Vaccinated against SARS-CoV-2
- 22 donors from 9 families (entire cohort II + 7 donors from Cohort I + 1 additional donor)
  - Serum collection 7-14 weeks after second vaccination
    - Detection of serum IgG, IgA and IgM responses against:
      - Receptor Binding Domain
      - Spike protein
      - Nucleocapsid protein

Carrier: carrier of PLCG2 p.P522R, non-carrier; not a carrier of PLCG2 p.P522R. PBMCs; peripheral blood mononuclear cells, Ig; Immunoglobulin



An additional flowcytometry panel was used to evaluate expression of non-phosphorylated PLC $\gamma$ 2 in various cell populations (**Table S2**). Here, samples were processed according to the bulk lysis protocol for staining of  $2.5 \times 10^6$  cells ([www.EuroFlow.org](http://www.EuroFlow.org)).

For precise enumeration of cells, we used Perfect-Count Microspheres<sup>™</sup> (Cytognos) according to the EuroFlow SOP (protocol available on [www.EuroFlow.org](http://www.EuroFlow.org)). In short, 50 $\mu$ l of well-mixed Perfect Count Microspheres were added to 50 $\mu$ l of peripheral blood. This mixture was incubated for 30 min with antibodies directed against CD19, CD3 and CD45. Next, 500 $\mu$ l of NH<sub>4</sub>Cl was added to lyse the red blood cells. After a 10 min incubation with NH<sub>4</sub>Cl, samples were immediately acquired on a BD FACS LSR Fortessa 4L, or a BD FACS LSR Fortessa X-20 4L (both BD Biosciences, San Jose, CA, USA).

### Measurement of phosphorylated PLC $\gamma$ 2

For in vitro stimulation assays, PB-HEP from Cohort II was used <12h after collection. Intracellular expression of phosphorylated PLC $\gamma$ 2 (pPLC $\gamma$ 2) was measured to assess B-cell activation upon stimulation with IgM or IgG Fabs (being F(ab)<sub>2</sub> fragment Goat anti-human IgM Heavy Chain secondary antibody (Southern Biotech), and F(ab)<sub>2</sub> fragment Goat anti-human IgG (Jackson ImmunoResearch), respectively). First, PB-HEP was subjected to a bulk lysis to remove red blood cells (protocol at [www.EuroFlow.org](http://www.EuroFlow.org)). Then, cells were incubated with an antibody cocktail for surface staining (45 min, RT in the dark) (**Table S2**), washed with PBS, incubated with 1 $\mu$ l 1:10 Zombie NIR<sup>™</sup> Fixable Viability Dye (BioLegend) for 30 min at RT and washed again. Subsequently, cells were resuspended in 230 $\mu$ L PBS+0.5% BSA and incubated with 10 $\mu$ g anti-IgM F(ab)<sub>2</sub> or anti-IgG F(ab)<sub>2</sub> fragments (10 min at 37°C in a shaking water bath). The reaction was stopped by adding 62.5 $\mu$ l Inside fix (Cell signaling buffer set A; Miltenyi) and incubating for 10 min in the dark. Afterwards, cells were washed and permeabilized (Cell signaling buffer set A, Miltenyi), washed again and resuspended in PBS+0.5% BSA. Next, antibodies to detect pPLC $\gamma$ 2 and immunoglobulins were added (30 min at RT in the dark). After a final washing step, cells were resuspended in PBS and acquired on a BD FACS Canto II 3L. Integrated MFI (iMFI) was calculated according to the following equation (**E1**):(29)

$$\mathbf{E1:} \quad \text{integrated MFI} = \% \text{ pPLC}\gamma 2 \text{ positive cells} \times \text{MFI pPLC}\gamma 2 \text{ positive cells}$$

As the stimulated B-cell receptor could not be targeted for antibody stain to identify cells, the following marker combinations were used to identify B-cell subsets: For IgM stimulation: pre-GC B cells, CD20+CD27-IgG-IgA-; unswitched MBCs, CD20+CD27+IgG-IgA-; class-switched MBCs, CD20+CD27+IgG+ or CD20+CD27+IgA+. For IgG stimulation: pre-GC B cells, CD20+CD27-IgD-IgA-; unswitched MBCs, CD20+CD27+IgD+IgA-; class-switched IgG MBCs, CD20+CD27+IgD-IgA-.

### **Calcium flux assay**

Peripheral blood mononuclear cells (PBMCs) from Cohort I and II were isolated from fresh PB-HEP by means of a density gradient (in-house; Ficoll-amidotrizoate, density 1.077g/mL) and stored in liquid nitrogen (freeze medium; RPMI + 40%FCS + 10% DMSO). At the day of analysis, PBMCs were thawed and washed twice with loading buffer (HBSS + 10mM HEPES + 5% FCS). Next, cells ( $10 \times 10^6$  PBMCs/mL) were loaded with Indo-1 Calcium Sensor Dye (Fisher Scientific, final concentration 2 $\mu$ g/mL) for 30 min at 37°C, labeled with antibodies directed against cell surface markers and incubated for additional 15 min at 37°C (**Table S2**). Subsequently, cells were washed with 10-20x labeling volume in Flux buffer (HBSS + 10mM HEPES + 5% FCS + 1mM CaCl<sub>2</sub>) and resuspended in 500 $\mu$ l Flux buffer. Samples were measured immediately on a Cytex Aurora 5L flow cytometer.

After establishing a ~2.5 min baseline, cells were stimulated with 20 $\mu$ L (10  $\mu$ g) anti-IgM F(ab)<sub>2</sub> Fragments (Southern Biotech) or 8.3 $\mu$ l (10  $\mu$ g) anti-IgG F(ab)<sub>2</sub> Fragments (Jackson ImmunoResearch) and measured for ~10 min. Finally, ionomycin was added (5 $\mu$ l, 1mg/mL in DMSO) and samples were measured for ~2.5 minutes. Acquisition was performed at medium speed (~30 $\mu$ l/min). During stimulation and measurement, samples were kept at 37°C in a tube heating device. Indo-Free and Indo-Bound signal was detected in the UV7 and UV1 detector, respectively. Samples were analyzed by dividing the sample into 30 time slots (of equal time, ~30 sec) with the Infinicyt Software (Cytognos) and determining the UV1/UV7 ratios in each time slot. Time slots 1-5 represent baseline signal, time slots 6-25 represent Fab-stimulated signal, and time slots 26-30 represent ionomycin-stimulated signal. MFIs of all time slots were used to plot a curve per B-cell population, from which the area under the curve (AUC) was determined for each individual sample using the GraphPad PRISM Software (v8.1.1). To calculate AUC for the 'total Fab stimulation', time slots 6-25 were used. When calculating the AUC for the 'peak of Fab stimulation', time slots 7-12 were used, as these were the highest values in all donors and presented the peak of calcium release. 'Ionomycin stim' AUC was calculated using time slots 26-30. In all cases, AUC was only calculated for points higher than baseline signal (unstimulated sample). As the stimulated B-cell receptor could not be targeted for antibody stain to identify cells, the following marker combinations were used to identify B-cell subsets: For IgM stimulation: pre-GC B cells, CD20+CD27-IgG-IgA-; unswitched MBCs, CD20+CD27+IgG-IgA-; class-switched MBCs, CD20+CD27+IgG+ or IgA+, and for IgG stimulation: pre-GC B cells, CD20+CD27-IgD+IgA-; unswitched MBCs, CD20+CD27+IgD+IgA-; class-switched IgG MBCs, CD20+CD27+IgD-IgA-.

### **KREC analysis to determine cell proliferation history**

PB-HEP from Cohort II was used <24h after collection for high-speed cell sorting of pre-GC B cells (CD19+CD27-IgM+IgG-IgA-), unswitched MBCs (CD19+CD27+IgM+IgG-IgA-) and class-switched MBCs (CD19+CD27+IgM-IgG+ or CD19+CD27+IgM-IgA+) using a BD FACS Aria III 4L (BD Biosciences, San Jose, CA, USA). On average, a purity of at least 98% was reached for pre-GC B

cells, unswitched MBCs, and class-switched MBCs, respectively. KREC numbers were determined as previously described.<sup>(30, 31)</sup> In short, DNA of sorted populations and the KREC control cell line (DBO1) was isolated with a QIAmp microkit (QIAGEN) and DNA concentrations were determined by NanoDrop 2000 (Thermo Fisher Scientific). Next, we performed qPCR (Quantstudio qPCR Machine, Thermo Fisher Scientific) to quantify the average amount of coding joints (Cj), signal joints (Sj) and Albumin (Alb) in each B-cell population and the control cell line (DBO1), using the primers that were previously described by van Zelm and colleagues.<sup>(30)</sup> The number of cell divisions ( $\Delta Ct$ ) for each B-cell population was calculated with the following equation (**E2**):

$$\mathbf{E2:} \quad \Delta Ct = Ct(Sj) - Ct(cj) - \Delta Ct(\text{control})$$

Where  $\Delta Ct$  (control) is a standard correction for primer efficacy based on the  $Ct(sj)$  and  $Ct(cj)$  from DNA from the DBO1 control cell line.

### **Phagocytosis of pHRodo™ Green *E. coli* Bioparticles**

Assessment of the phagocytic capacity was performed with opsonized *E. coli* (pHRodo™ Green *E. coli* Bioparticles, ThermoFisher). Polystyrene FACS tubes (4mL) were filled with 200 $\mu$ L PB-HEP (Cohort II, <12h after collection) and placed on ice for at least 10 minutes. Then, 40 $\mu$ L of pHRodo™ Green *E. coli* was added, samples were mixed and incubated at 37°C for exactly 20 min. All further steps were performed on ice or at 4°C to stop the reaction. Cells were washed and stained (30 min on ice in the dark) with an antibody cocktail (**Table S2**). Next, samples were lysed with BD lyse (10 min, rolling at 4°C). Lastly, cells were washed, resuspended in cold PBS with 0.5% BSA and acquired at a Cytex Aurora 3L flow cytometer. To prevent shedding of CD62L, TAPI-2 (final concentration of 20 $\mu$ M) was always present. To account for background activation or signal, several control tubes were measured in addition to the sample tubes (**Table S3**).

### **Production of reactive oxygen species (ROS)**

Production of ROS upon stimulation was assessed with the phagoBURST kit (PHAGOBURST™ CE/IVD kit, BD Biosciences) according to manufacturer's protocol with some modifications, as described further in this paragraph. In short, each tube was filled with 200 $\mu$ L PB-HEP (Cohort II, <12h after collection) and placed on ice for at least 10 minutes. Then, 20 $\mu$ L of wash buffer (reagent A), Phorbol 12-Myristate 13-acetate (PMA) (Sigma, P8139-1mg, final concentration 600ng/mL), or *E. coli* (reagent B, well-mixed by pipetting) was added to each tube. After proper mixing, tubes were incubated for exactly 10 min at 37°C in a shaking water bath. Next, 20 $\mu$ L of substrate (dihydrorhodamine -DHR123, reagent E) was added to each tube and mixed. Tubes were incubated for another 10 min at 37°C. Subsequently, the assay was stopped by lysing the cells (reagent F, 15 min, RT, dark). Cells were washed twice, stained for 15 min in the dark at RT with antibody cocktail (Table S2) and PBS with 0.5% BSA, washed again, resuspended in PBS with 0.5% BSA and stored on ice until acquisition on a Cytex Aurora 3L flow cytometer (<1h). To prevent shedding of CD62L, TAPI-2 (final

concentration of 20 $\mu$ M) was always present. The rhodamine 123 (R123) signal was used as a readout for ROS production (conversion from DHR123 to R123). To account for background activation or signal, several control tubes were measured in addition to the sample tubes (**Table S4**).

### **Data integration phagocytosis and ROS production**

The phagocytosis assay and the ROS production were considered complementary assays in which we evaluated three aspects of phagocytosis. First, we evaluated the percentage of phagocytosing cells, then we combined this – together with the pHRedo™ Green signal- into the integrated MFI (iMFI)(29), which was used as a measure of how many particles each cell has phagocytosed (**E3**). For ease of interpretation, this value was divided by 100,000.

**E3:**     integrated MFI=% E.coli positive cells  $\times$  MFI E.coli positive cells

Lastly, we measured the production of ROS upon phagocytosis and combined this with the iMFI into one output; the normalized ROS production, which was defined as the ROS generation per given number of phagocytosed particles (**E4**).

**E4:**     normalized ROS production= (R123 MFI)/(integrated MFI)

### ***In vivo* evaluation**

We collected additional blood samples from donors (Cohort III), 7-14 weeks after their second vaccination against SARS-CoV-2. Serum antibodies directed against the Spike (S) protein, Receptor Binding Domain (RBD) and Nucleocapsid (N) protein were determined by a fluorescent-bead-based multiplex immunoassay (MIA), as previously described.(32) In short, the stabilized pre-fusion conformation of the ectodomain of the Spike protein, the receptor binding domain of the S-protein (RBD) and the Nucleocapsid (N) protein were each coupled to beads or microspheres with distinct fluorescence excitation and emission spectra. Serum samples were diluted and incubated with the antigen-coupled microspheres. Following incubation, the microspheres were washed and incubated with phycoerythrin-conjugated goat anti-human, IgG, IgA, and IgM. The data were acquired on the Luminex FlexMap3D System and MFI was converted to international units per milliliter (IU/ml), using Bioplex Manager 6.2 (Bio-Rad Laboratories) software.

### **Data analysis and statistical analysis**

Flow cytometry data was analyzed with Infinicyt software (version 2.0.3.a. and 2.0.4.b., Cytognos, Spain). Statistical analysis was performed in GraphPad Prism 8.1.1 software (GraphPad, San Diego, CA, USA). Differences between p.P522R carriers and non-carriers, were evaluated using the Mann-Whitney test. Impact of age was assessed using Spearman's correlation.  $P < 0.05$  was considered significant.

## Results

### Numbers of circulating immune cells in the study cohort are representative for healthy aged adults

Upon aging, the composition of the immune system changes. The median age of the studied cohort was 72 years (range: 59 -103 years), as most of the donors were children of a centenarian who carried the p.P522R variant, and only a few were centenarians or siblings from a centenarian (details provided in **Methods section** and **Table 1**). To assess to what extent this cohort represented the general (age-matched) population, we first compared absolute counts of multiple innate and adaptive cell populations with reference values from healthy age-matched cohorts.(24, 26, 27) (ref 22: van der Pan et al, manuscript in revision) Overall, innate, CD4 T- and B-cell counts in the donors were representative of their age category, with exception of IgG3, IgG4 and IgA2 plasma cells, which were slightly elevated in several donors. In three donors (carriers, one family), a subclinical B-cell expansion was observed. Additionally, two donors (non-carriers, different families) in whom we observed B-cell aberrancies were excluded from all further analyses and referred to a hemato-oncologist for further evaluations (the expanded B-cell phenotypes observed in the initial research-based screening were: CD19+CD20+CD5+CD21+CD27+IgM+IgD-/dim and CD19+CD20+CD5+CD-21dimCD27+IgG1dim). For CD8 T- and NK-cell subsets no age-matched reference values were available. No impact of sex on cell counts was observed. An impact of age on cell counts was found for several subpopulations. To reduce impact of sex or age on the comparison between p.P522R carriers and non-carriers, cohorts were sex- and age-matched as much as possible. Lastly, we observed a pronounced effect of pedigree, as in several subsets cell counts from all first-degree family members tended to cluster together, even when individuals were living at different locations for many years (**Figure S1**).

### Several parameters in p.P522R carriers resemble younger healthy donors

To evaluate the impact of PLC $\gamma$ 2 carriership on cell counts in innate and adaptive immune cell subsets, we related this information to the carriership status. Overall, p.P522R carriers tended to have higher total and immature B-cell numbers, and significantly more CD20++CD21-CD24+ naive and IgG1+ MBCs (**Figure 1A**). This pattern was observed in at least half of the families with mixed carriership (CD20++CD21-CD24+ naive B cells; 3/6, IgG1+ MBCs; 5/6 families). Interestingly, upon comparing median cell counts carriers and non-carriers with an internal reference cohort (n=25, 9 females, aged 18-54, median age: 27 years), the carrier cell counts more closely resembled the counts of the younger cohort than the non-carriers (**Figure 1A**). Interestingly, for the CD20++CD21-CD24+ naive B cells, the median cell count was slightly higher in carriers than in the younger cohort.

Next, we evaluated expression of several surface markers: HLA-DR, CD62L, CD16, CD33 and Fc $\epsilon$ RI on innate immune cells, CD45RA, CD27, CD28 and CD3 on T cells, and CD20 and CD21 on B cells. Interestingly, we found a reduced ex-



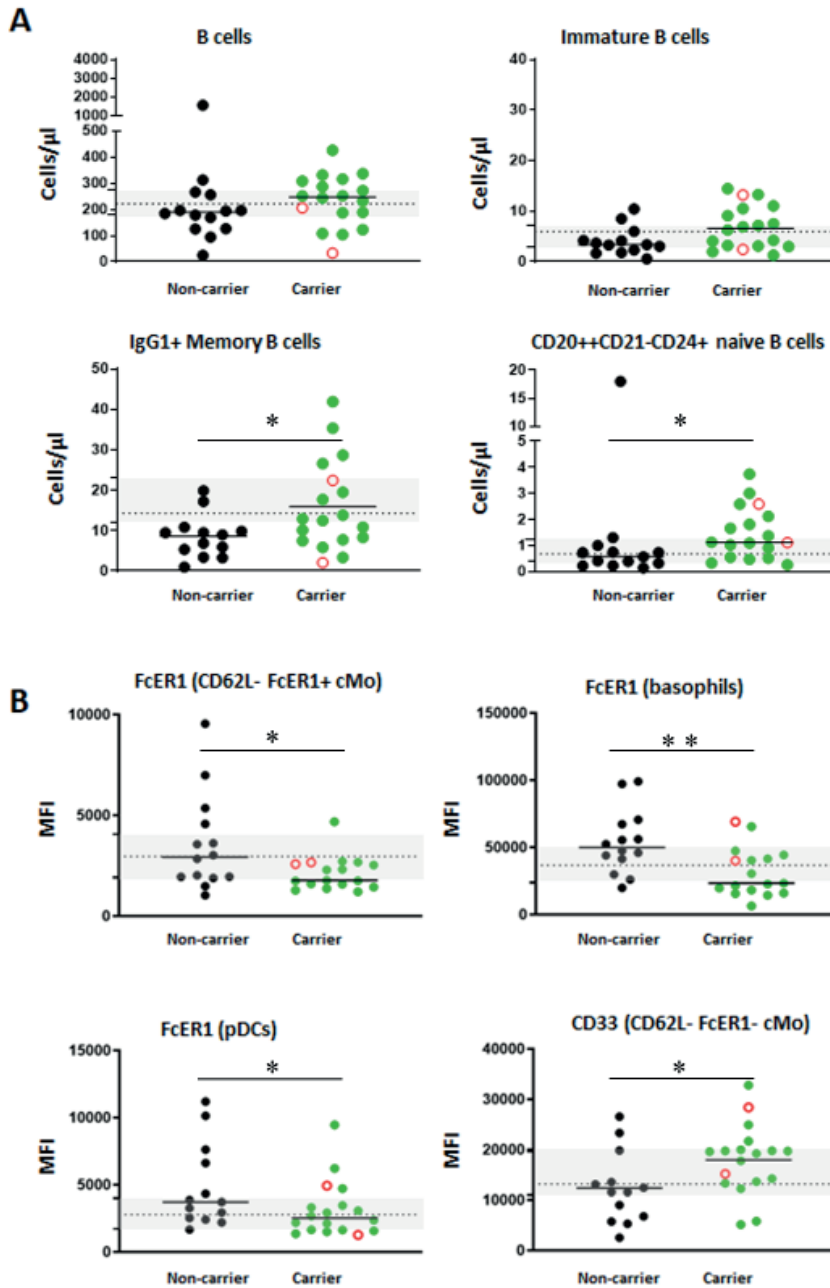


**Figure 1. Main differences between PLC $\gamma$ 2 p.P522R carriers and non-carriers in Cohort I.** (A) Major differences in absolute immune cell counts between carriers and non-carriers. (B) Major differences in activation marker expression between carriers and non-carriers. Mean fluorescence intensity (MFI) was corrected by subtraction of background signal on a negative reference population. Differences between cohorts were determined using the Mann-Whitney test. Green circles indicate p.P522R carriers, and black circles indicate non-carriers. Centenarian data points are indicated in the graphs as an open red circle. Grey boxes indicate the 95%CI and dashed lines indicate the median cell count or MFI from a younger reference cohort (n=25, average age: 31 years old), whose data was collected in the same laboratory, using identical methods and equipment. N=31, \* p<0.05, \*\* p<0.01.

pression of FcεRI on CD62L- FcεRI+ classical monocytes (CD62L- FcεRI+ cMo), basophils and plasmacytoid dendritic cells (pDCs) in p.P522R carriers with a median age of 71 years (range 59-103 years) versus non-carriers with a median age of 74 years (range 61-83 years) (Figure 1B). Median FcεRI expression in carriers was below, or in the lower range, of the young reference cohort (n.s.). In contrast to FcεRI expression, the expression of CD33 on CD62L- FcεRI- cMos was increased in the p.P522R carriers, and in the high range of the 95% confidence interval of the younger reference cohort, while non-carriers resided on the lower end of the 95% confidence interval of the younger reference cohort (n.s.) (**Figure 1B**).  
Higher PLCγ2 expression in immune cells of p.P522R carriers

Then, we evaluated the PLCγ2 expression levels in different leukocyte populations in the total cohort (irrespective of carriership). The highest PLCγ2 expression was found in eosinophils, with high variation between individuals, and, more consistently, in antigen-experienced B cells (**Figure 2A**). When comparing carriers with non-carriers, the levels of PLCγ2 in all evaluated B-cell subsets were consistently higher in p.P522R carriers than in non-carriers (**Figure 2BC**). Likewise, innate cells tended to have slightly higher median values for PLCγ2 expression in p.P522R carriers compared to non-carriers (**Figure 2BC**).

To summarize our findings in this first analysis (e.g. Cohort I): based on cell counts, Cohort I seemed representative for healthy individuals of this age group. Whenever differences in cell counts were found between p.P522R carriers and non-carriers, carriers more closely resembled the younger control cohort. Lastly, PLCγ2 expression tended to be higher in carriers, mostly on antigen-experienced B cells.

### **Higher levels of phosphorylated PLCγ2 in stimulated B cells from p.P522R carriers**

In a second analysis (Cohort II), we evaluated the effect of p.P522R on PLCγ2 activity in several B-cell subsets derived from 14 healthy older adults (6 non-carriers, 8 carriers) (**Table 1, Text S1**). As PLCγ2 is located downstream of the BCR, we assessed whether specific elements of the signaling pathway were affected by the carriership status. The BCR was stimulated with IgM (stimulation with IgG Fabs was also tested, but results were considered unreliable due to high background signal). In the steady state, we observed no significant difference between the levels of phosphorylated PLCγ2 (pPLCγ2) in B cells from p.P522R carriers and non-carriers (Figure 3A). Upon BCR stimulation with IgM Fabs, a similar percentage of unswitched MBCs was activated, but the integrated mean fluorescent intensity (iMFI) of PLCγ2 was almost two-fold higher in carriers than in non-carriers (3667 vs 2051, respectively), implying a stronger activation in carriers (**Figure 3A**). Moreover, levels of pPLCγ2 tended to be higher in stimulated pre-GC B cells in carriers. According to expectations, no increase in pPLCγ2 was observed upon IgM stimulation in the (IgM-) class-switched MBCs in either group.

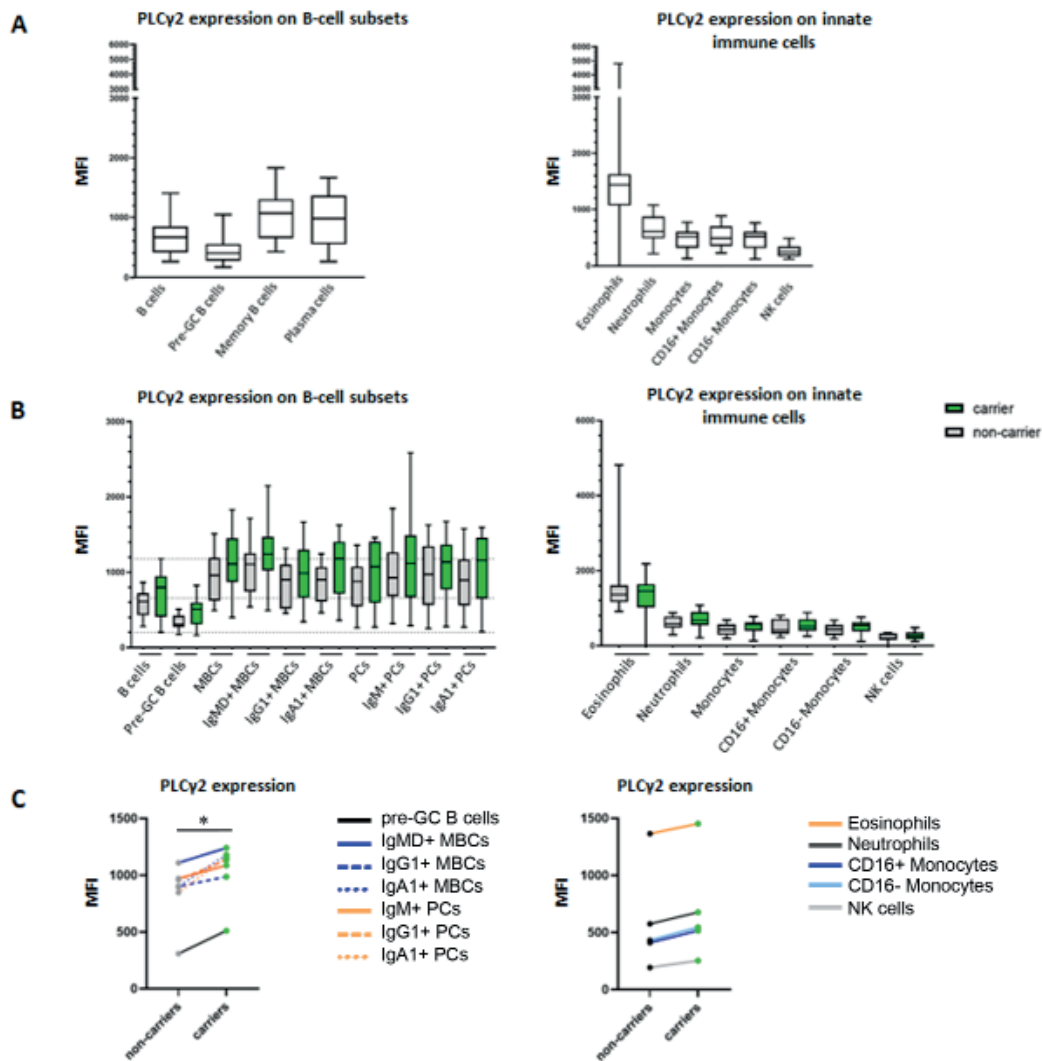


**Figure 2. PLCy2 expression in different populations of circulating immune cells.** (A) PLCy2 expression measured as mean fluorescence intensity (MFI) and corrected for background signal by subtracting the MFI signal of a negative reference population (T cells) of the total cohort (irrespective of p.P522R carriership). N= 31. (B) PLCy2 expression on B-cell and myeloid cell subsets in p.P522R carriers (green) and non-carriers (grey). Dashed lines represent the median (min-max) of PLCy2 expression of B cells of the total cohort. (C) PLCy2 expression on B-cell and myeloid cell subsets between carriers (green) and non-carriers (grey). The median of each subset is plotted, medians of the same subset are connected with lines. Differences were evaluated with Mann-Whitney test. MBC; memory B cell, IgMD+ MBC; unswitched memory B cell, Pre-GC; pre-Germinal Center B cells, PC; plasma cells, NK cells; Natural Killer cells. \*  $p < 0.05$ .

### **Higher calcium flux in B cells upon BCR stimulation in p.P522R carriers**

Next, we evaluated the effect of p.P522R further downstream of the BCR by measuring the calcium release ('calcium flux') upon BCR stimulation using IgM Fabs. After a pilot experiment using IgM and IgG Fab stimulation in 12 donors, we found IgM stimulation to be most robust (**Figure S2**). We observed no differences in calcium flux in pre-GC B cells derived from Cohort II donors (**Figure 3B**), but there was a trend towards more robust calcium flux in p.P522R carriers vs non-carriers upon Fab stimulation in unswitched MBCs ('Total flux' and 'Flux at peak') (**Figure 3C**). However, this trend was not observed when comparing the calcium flux of all donors included in cohort I and II (**Figure S3**). Again, stimulation with IgM Fabs did not result in calcium release in class-switched MBCs, thus confirming that the measured calcium flux is truly due to BCR-specific stimulation (**Figure 3D**).

### **No difference in number of cell divisions between carriers and non-carriers**

Stronger B-cell activation upon stimulation in p.P522R carriers may result in more robust proliferation upon antigen encounter. To test this hypothesis, we evaluated B-cell replication history with the KREC (kappa-recombination excision circle) assay. Despite generally low cell counts, we were able to determine that pre-GC B cells measured in all 14 individuals in Cohort II had undergone on average 1.58 cell divisions, while unswitched MBCs measured in 8/14 individuals, had undergone on average 7.82 cell divisions (**Figure 3E**). These findings are in line with previous publications.<sup>(31)</sup> We observed no clear difference in replication history of B-cell subsets between p.P522R carriers and non-carriers, possibly due to the limited number of donors in the non-carrier cohort (replication history in pre-GC B cells: 1.43 vs 1.64; in unswitched MBCs: 7.12 vs 7.82 (**Figure 3F**)). Lastly, although class-switched MBC samples were collected as well, the obtained cell numbers were generally too low to determine the number of undergone cell divisions.

### **Serum Ig responses to SARS-CoV-2 vaccination comparable between p.P522R carriers and non-carriers**

To test whether the effect of p.P522R on B-cell activation as observed in our *in vitro* experiments also translates to an *in vivo* effect (e.g. effect on antibody production), we recognized a window of opportunity in the current global vaccination efforts against SARS-CoV-2. We collected serum samples from 22 individuals (Cohort III), 7-14 weeks after receiving a second vaccination against SARS-CoV-2. Donors were vaccinated with Comirnaty® (Pfizer/BioNTech, 9 carriers, 9 non-carriers); Spikevax® (Moderna, 1 carrier); Vaxzevria® (AstraZeneca, 1 non-carrier), or did not indicate vaccine type (2 non-carriers). All donors developed prominent IgG responses against the viral Receptor Binding Domain (RBD) and Spike (S)-protein. Antibody responses against the viral Nucleocapsid (N)-protein – indicative of viral infection- were predominantly IgM responses (**Figure 4A, B**). No differences were observed between p.P522R car-

# Chapter 4

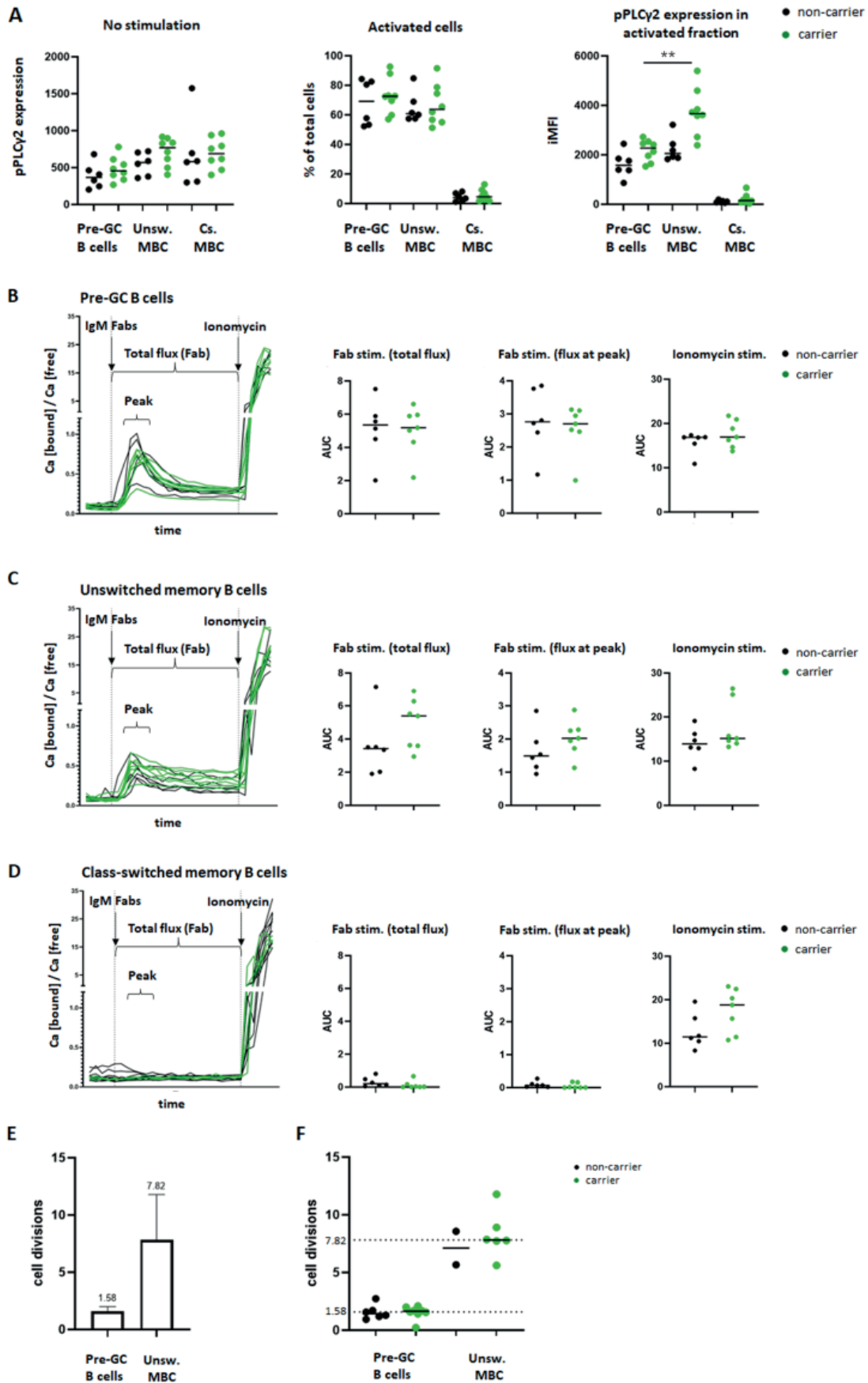




**Figure 3 (previous page). Assessment of B-cell activation upon IgM Fab stimulation and B-cell replication history in p.P522R carriers and non-carriers.** (A) Expression of phosphorylated PLC $\gamma$ 2 (pPLC $\gamma$ 2) in B cells before and after stimulation of the B-cell receptor with IgM Fabs. Detection of pPLC $\gamma$ 2 was used as a direct measure of B-cell receptor activation after IgM Fab stimulation. N=14. (B-D) Measurement of calcium release ('flux') after B-cell stimulation with IgM Fabs of pre-GC B cells (CD27-IgG-IgA-) (B), unswitched memory B cells (CD27+IgG-IgA-) (C), or class-switched memory B cells (CD27+IgG+ or CD27+IgA+) (D) in cohort II. Differences between carriers and non-carriers were evaluated by comparing the area under the curve (AUC) of the total Fab stimulation (from stimulation until the moment ionomycin was added, ~ 10 min, flux intensity and duration), the peak of the response after Fab stimulation (the 5 highest points after the Fabs were added to the cells; flux intensity), and after ionomycin was added (to determine the maximum flux). AUC was calculated only for points that were higher than baseline value (unstimulated sample). N=13 (one sample was lost due to technical failure). (E+F) Measurement of the average number of undergone cell divisions by total pre-GC B cells (CD27-IgM+IgG-IgA-) or unswitched memory B cells (CD27+IgM+IgG-IgA-) by means of qPCR based KREC assay in the total cohort (E) or separated into carriers and non-carriers (F). For pre-GC B cells; n=14. Due to low DNA concentration, for unswitched MBC; n=8. Differences were evaluated by Mann-Whitney test. Pre-GC; pre-Germinal Center, MBC; memory B cells, IMFI; integrated mean fluorescence intensity (for calculation, see Methods) Unsw. MBC; unswitched memory B cells, Cs. MBC; class-switched memory B cells. \*\* p<0.01.

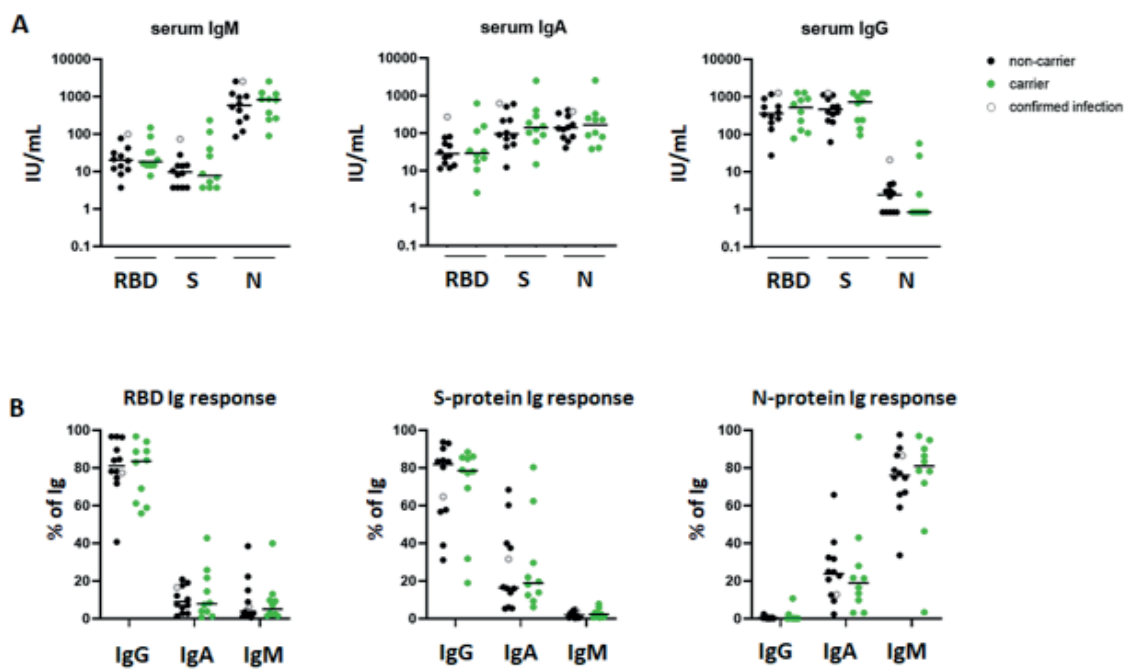


**Figure 4. Response to SARS-CoV-2 vaccination in p.P522R carriers and non-carriers.** Samples were donated 7-14 weeks after second vaccination. Type of vaccine received by donors: Comirnaty® (Pfizer/BioNTech) – 9 carriers, 9 non-carriers; Spikevax® (Moderna) - 1 carrier, 0 non-carriers; Vaxzevria® (AstraZeneca) – 0 carriers, 1 non-carrier; vaccine type not indicated- 0 carriers, 2 non-carriers. One donor reported a confirmed SARS-CoV-2 infection, this donor is indicated with an open grey circle. (A) Serum IgM, IgA, and IgG response against the receptor binding domain (RBD), spike protein (S-protein) and nucleocapsid protein (N-protein), expressed in IU/mL. (B) Composition of the serum Ig response per antigen, expressed as % of total antigen-specific Ig response.

riers and non-carriers.

Summarizing our (B-cell related) findings in Cohort II/III: PLC $\gamma$ 2 in unswitched MBCs from p.P522R carriers is more strongly phosphorylated upon stimulation compared to non-carriers. Moreover, the calcium flux in p.P522R carriers was increased relative to non-carriers, at least in individuals from Cohort II, who were selected based on fewer comorbidities. Due to technical limitations, we were unable to obtain reliable results for class-switched memory cells, such that it is currently unclear to what extent these data can be extrapolated to other MBC subsets. Despite clear differences between p.P522R carriers and non-carriers in the multiple *in vitro* functional experiments, *in vivo* antibody responses raised against SARS-CoV-2 vaccine were comparable between carriers and non-carriers.

### **Increased ROS production upon FcR-mediated stimulation of innate immune cells in p.P522R carriers**

Besides being located downstream of the BCR, PLC $\gamma$ 2 is also located downstream of FcRs, which are present on many cells of the innate immune system, including the microglia of the brain. Therefore, we evaluated ROS production and phagocytic activity upon FcR-mediated stimulation in several cell types of the innate immune system: neutrophils, classical, intermediate, and non-classical monocytes (cMos, iMos and ncMos, and their subsets), and myeloid and plasmacytoid dendritic cells (mDCs, pDCs, and their subsets).

Although the percentage of phagocytosing cells did not differ between p.P522R carriers and non-carriers (**Figure 5A**), the iMFI, reflecting the amount of phagocytosed *E. coli* particles per cell (phagocytic capacity), tended to be lower in carriers. This trend was especially prominent in classical and non-classical monocyte subsets, less prominent in CD14<sup>-</sup> mDC subsets and iMos, and not observed in CD14<sup>dim</sup> mDCs (**Figure 5A**, **Figure S4**).

In addition to phagocytosis, we evaluated ROS production upon phagocytosis of opsonized *E. coli* particles (PhagoBURST assay). No difference between p.P522R carriers and non-carriers was observed in the amount of ROS produced (**Figure 5A**, **Figure S4**). To combine information from both assays, we investigated ROS production relative to the number of phagocytosed particles. We observed that this ‘normalized ROS production’ was increased in carriers, which was especially evident in CD62L<sup>-</sup>cMos (**Figure 5A**). Also, we observed that the ROS production relative to number of phagocytosed particles tended to be increased (n.s.) in carriers across all evaluated monocyte subsets and neutrophils (**Figure 5B**, **Figure S4A-C**). Lastly, we observed increased normalized ROS production in CD14<sup>-</sup> mDCs, but not in CD14<sup>dim</sup> mDCs (**Figure S4D-E**). Thus, the ROS generation per particle tends to be somewhat higher in several cell populations in p.P522R carriers compared to non-carriers.

Additionally, we stimulated samples with Phorbol 12-Myristate 13-acetate (PMA), which results in FcR-independent ROS generation. Surprisingly, we observed

a trend towards decreased ROS production in p.P522R carriers compared to non-carriers, which was seen for neutrophils, monocyte subsets and DC subsets (**Figure S5**). This effect was the strongest in monocytes, especially in CD62L+ and CD62L- cMos, where p.P522R carriers showed a significantly lowered ROS production compared to non-carriers.

Thus, upon stimulation with opsonized *E. coli*, we observed that p.P522R carriers had a lower phagocytic capacity despite overall similar ROS production upon phagocytosis of *E. coli* and thus had increased ROS production relative to the number of opsonized particles. Nevertheless, the total FcR-independent ROS generation was lower in these same carriers. In general, differences were most prominent in the monocyte subpopulations.

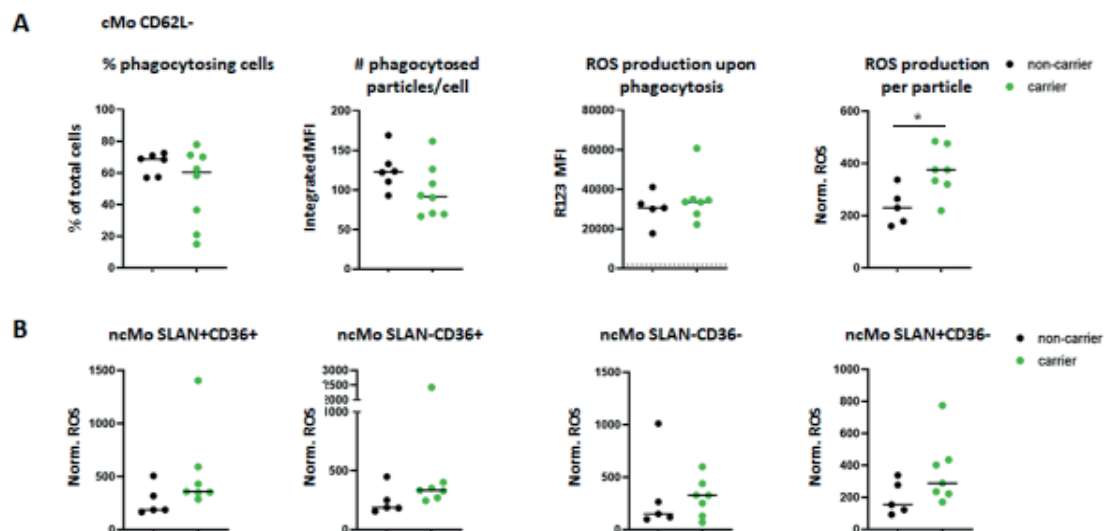


**Figure 5. Detection of phagocytosis and ROS production in monocyte subsets after stimulation with pHRedo™ Green *E. coli* bioparticles.** (A) To evaluate the outcome of the phagocytosis assays, three different readouts were used per population; % of cells that were phagocytosing, the average amount of particles phagocytosed per cell, and the ROS production upon phagocytosis (as measured by conversion of DHR123 into R123). The average amount of particles phagocytosed per cell and the ROS production were further combined into one value; the ROS produced per particle, or the ‘normalized ROS’ (calculations are indicated in the Methods). The values are presented for the CD62L- classical monocyte (cMo) subset (B) The normalized ROS of all four defined non-classical monocyte (ncMo) subsets, based on expression of CD36 and SLAN. Differences were evaluated by means of Mann-Whitney test. All readouts were corrected for background/baseline activation by subtracting the value of the control (ice) from the activated (37°C) sample. \*  $p < 0.05$ .

## Discussion

In this study, we investigated the impact of PLC $\gamma$ 2 variant p.P522R on the immune system in older adults. We showed that p.P522R carriers had higher numbers of circulating CD20++CD21-CD24+ naive B cells and IgG1+ MBCs, lower expression of Fc $\epsilon$ RI on several innate immune cells (pDCs, basophils and CD62L-

FcεRI+ cMos), and higher expression of CD33 on CD62L- FcεRI- cMos. Overall PLCγ2 expression tended to be higher in p.P522R carriers. Upon BCR stimulation, the levels of phosphorylated PLCγ2 were significantly higher in unswitched MBCs derived from in p.P522R carriers compared to non-carriers, and we observed a trend towards higher calcium flux. This suggests that B-cell stimulation in p.P522R carriers leads to a stronger activation compared to non-carriers. The number of cell divisions undergone by pre-GC B cells and unswitched MBCs was not different between p.P522R carriers and non-carriers. Upon vaccination against SARS-CoV-2, vaccine-specific antibody levels did not differ between p.P522R carriers and non-carriers. We also evaluated phagocytosis and ROS production in myeloid cells and found the most prominent differences in the monocyte subsets, where upon FcR-dependent stimulation, (normalized) ROS production was increased in carriers. In contrast, FcR-independent ROS generation was lowered in these same carriers. Across all experiments, the observed effects are small, which is in full accordance with our expectations: the molecular interplay that makes up a robust immune system function has evolved under high evolutionary pressure, such that only subtle changes will be tolerated to have an advantageous effect.

To our knowledge, this is the first study that investigates the effect of the PLCγ2 variant p.P522R in the human immune system ex-vivo and in-vivo. Previous studies have reported that -amongst others- the genetic constellation, unique to all individuals, has a profound influence on cell counts.(33, 34) In line with these previous studies, we observed an effect of pedigree on the numbers of circulating immune cells. Using human subjects means accepting to sample in individuals from a heterogenous genetic background compared to inbred animals or cell lines. To minimize genetic heterogeneity, we set out to select samples of p.P522R carrier and non-carrier siblings. These siblings (~71/72-year-old) were children from a parent who participated in the 100-plus Study, who reached at least 100 years and carried the protective p.522R PLCγ2 variant.(20) We acknowledge that, next to the protective variant in PLCγ2, these individuals, both p.P522R carrier and non-carrier siblings, may be enriched with additional advantageous genetic elements associated with prolonged health which may positively affect immune system function. Nevertheless, comparison with age-matched reference cohorts confirmed that cell counts were representative for the general older adult population.

Upon BCR-stimulation, B cells in p.P522R carriers showed a stronger activation. This was most prominent for unswitched MBCs. Due to technical limitations, we were unable to confirm whether the same holds true for class-switched MBCs. In vitro studies that investigated the activation levels of unswitched and class-switched MBCs reported conflicting data, and thus indicate that future studies are required.(35) Nonetheless, the in vitro stimulation of B cells from the homogenous and healthy individuals in Cohort II suggested that the activation signal in carriers was stronger, which is in line with the suggestion that the p.P522R variant is a functional hypermorph, as previously observed in cell lines and mouse models.

(13, 18, 19) However, this pattern was lost upon the combination of Cohort II with Cohort I. Cohort I was a more heterogeneous cohort including individuals with diverse comorbidities or medication use that may influence the immune responses, such as (undiagnosed) autoimmune disease, use of steroids, or use of non-steroid anti-inflammatory drugs (NSAIDs).

While our analysis of post-vaccination serum responses did not reveal a beneficial effect of p.P522R in terms of generated serum levels of IgG, IgM or IgA, the complexity of the generated response (e.g., B-cell repertoire) may differ between p.P522R carriers and non-carriers. Previous studies indicated that with increasing age the diversity of the B-cell repertoire decreases(36, 37), therefore, an in-depth evaluation of the Ag-specific B-cell repertoire, especially their VDJ regions, may reveal differences between p.P522R carriers and non-carriers. Although we did not investigate repertoire in this study, the higher numbers of circulating CD20<sup>++</sup>CD21-CD24<sup>+</sup> naive B cells in carriers may represent a broader available B-cell repertoire. This may leave carriers better equipped to deal with neoantigens.

Innate immune cells in p.P522R carriers had a lower expression of FcεRI which, upon activation, contributes to the production of important immune mediators that promote inflammation (cytokines, interleukins, leukotrienes, and prostaglandins).(38, 39) Allergy-related expression of IgE associates with an upregulation of FcεRI expression(40), but since 5/7 reported allergies were in p.P522R carriers the frequency of a reported allergy could not explain the decreased FcεRI expression among carriers.

While the current study was ongoing, two studies were published that evaluated the impact of p.P55R on phagocytosis. Takalo et al reported increased phagocytic activity of opsonized *E. coli* (as determined by pHRodo™ Green signal and percentage of phagocytosing cells) in murine p.P522R microglia-like cells (BV2 cell-line) and knock-in murine macrophages.(13) In functional analyses between, macrophages derived from homozygous knock-in mice and wild type littermates, Takalo et al revealed that the p.P522R variant potentiates the primary function of PLCγ2 as a PIP2-metabolizing enzyme.(13) This was associated with improved survival and increased acute inflammatory responses of the knock-in macrophages. Maguire et al showed that -although P522R showed hypermorphic activity in Ca-release and endocytosis experiments-, phagocytosis of opsonized *E. coli* was reduced in mouse microglia and macrophages and in human iPSC-derived microglia. However, they indicated that reduction of phagocytosis may have been due to substrate deprivation (PIP2) upon prolonged stimulation.(19) The discrepancies between the study of Takalo and Maguire might be explained by differences in experimental setup, such as in the timeframe used for phagocytosis, the type of evaluated readout, concentration of substrate, and the cell types evaluated.

In our study of primary human cells, the number of phagocytosed particles per



cell seemed somewhat reduced in p.P522R carriers, which aligns with our observation that innate immune cells in p.P522R carriers had a higher expression of CD33 which, upon stimulation by any molecule with sialic acid residues (such as glycoproteins or glycolipids), results in a cascade that inhibits phagocytosis in the cell.(41) Importantly, previous studies suggested an association between CD33 levels and the etiology and pathology of Alzheimers' disease: the common CD33 risk allele (rs3865444, associated with increased chance of developing Alzheimers' disease in GWAS) was associated with higher CD33 expression too. (41, 42) However, carriers of the risk allele had a 7-fold increased expression of CD33 on peripheral monocytes.(42) In our study we see a much lower increase in CD33 surface expression in one particular monocyte subset (~1.67-fold, CD62L- FcεRI- cMo). Additionally, our results indicated that the ROS production per phagocytosed particle seemed increased in p.P522R carriers, although overall ROS production between carriers and non-carriers was similar. These findings suggest that p.P522R carriers have a more efficient ROS production per particle. This more efficient ROS production (per particle) may contribute to an increased resilience to age-related decline of immune function as previous studies indicated that with increasing age, both the phagocytic capacity (# particles ingested/neutrophil) and oxidative burst are reduced.(5, 43, 44) The higher ROS production per phagocytosed particle might translate to increased degradation capacity -and thus more effective clearance- within the phagocyte. This capacity has been reported to be decreased in aged individuals as well as Alzheimers' disease patients.(45) While we cannot exclude that other advantageous (genetic) elements carried by these donors also contribute to this phenotype, this more efficient ROS production in p.P522R carriers may protect these individuals from infection and can thus contribute to a long-term maintenance of healthy immune function.

PLCy2 is not the only molecule expressed on peripheral immune cells that has been shown to associate with protection against neurodegenerative diseases. A recent preprint suggested an association between HLA-variant DRBI\*04 and protection against neurodegenerative diseases (HLA-DR is mainly expressed on antigen-presenting cells).(46) In this study we cannot answer the question whether the protective effect of the p.P522R variant on neurodegenerative diseases is translated, perhaps in part, through the peripheral immune system. However, a recent study by Prongpreecha et al suggested that reduced activation of PLCy2 in PMBCs is a molecular characteristic of Alzheimers' disease.(47) Our findings clearly indicate that both adaptive and innate circulating human primary cells of the peripheral system are subtly changed in carriers of the p.P522R variant. The more efficient ROS production we observed upon FcR-mediated stimulation in peripheral monocytes may translate directly to the microglia in the *in vivo* human brain, which also express FcR. Therefore, the p.P522R variant may protect the brain with a mechanism similar to that observed in peripheral immune cells. Although there is discussion on whether phagocytosis is beneficial or detrimental during Alzheimers' disease (19, 48), a more efficient clearance of tissue damage and debris in the brain may be beneficial at least in the initial stages of Alzheimers' disease. To what extent a more sensitive B-cell response has

a protective effect on the brain remains to be investigated. However, (natural) antibodies against brain amyloid or tau have been observed not only in Alzheimer's disease patients, but also in cognitively healthy elderly individuals.(49, 50) In fact, in brain proteinopathies, antibodies can enter the brain parenchyma and effectively remove the aberrant proteins, making these antibodies promising candidates for intervention strategies for several types of dementia.(51-53) We may thus speculate that a sensitive B-cell system, such as observed in the p.P522R carriers, through increased activity in the periphery, may contribute to the long-term maintenance of brain health.

### Conclusions

Our study confirmed the hypermorphic activity of PLC $\gamma$ 2 p.P522R in circulating immune cells, which provides a low-invasive source of primary cells for future studies. It would be interesting to evaluate whether p.P522R benefits carriers early in life, or whether its protective effect plays a role mostly later in life by, for example, delaying immunosenescence, both in the soma and in the central nervous system. More insight in the functioning of p.P522R may help design future therapies and better define the therapeutic window of PLC $\gamma$ 2.

### List of abbreviations

Phospholipase C gamma 2 (PLC $\gamma$ 2)  
 B and T-cell receptor (BCR, TCR)  
 germinal center (GC)  
 memory B-cell (MBC)  
 reactive oxygen species (ROS)  
 single-nucleotide polymorphism (SNP)  
 Phospholipase C gamma 2 gene (PLCG2)  
 phosphatidylinositol 4,5-bisphosphate (PIP2)  
 inositol 1,4,5-triphosphate (IP3)  
 diacylglycerol (DAG)  
 Fc receptors (FcR)  
 Triggering Receptors Expressed on Myeloid cells (TREM)  
 peripheral blood (PB)  
 Genome Screening Array (GSA)  
 quality control (QC)  
 Setup and Tracking beads (CS&T beads)  
 Dendritic cell-monocyte (DC-monocyte)  
 CD4-T cell panel (CD4T)  
 CD8 cytotoxic T-cell panel (CYTOX)  
 B-cell and plasma cell panel (BIGH)  
 Peripheral blood mononuclear cells (PBMCs)  
 area under the curve (AUC)  
 coding joints (Cj)  
 signal joints (Sj)  
 Albumin (Alb)  
 dihydrorhodamine (DHR123)

## Chapter 4

---

classical, intermediate, and non-classical monocytes (cMos, iMos and ncMos)  
phosphorylated PLC $\gamma$ 2 (pPLC $\gamma$ 2)  
integrated mean fluorescent intensity (iMFI)  
kappa-recombination excision circle (KREC)  
Receptor Binding Domain (RBD)  
Spike protein (S protein)  
Nucleocapsid protein (N protein)  
myeloid and plasmacytoid dendritic cells (mDCs, pDCs)  
Phorbol 12-Myristate 13-acetate (PMA)  
non-steroid anti-inflammatory drugs (NSAIDs)

### **Declarations**

Ethics approval and consent to participate: In this study, we selected 36 individuals from the 100 plus study cohort, as previously described by Holstege et al (METC number: 2016.440, approved by the Medical Ethics Committee of the VU University Medical Center, Amsterdam, the Netherlands). Informed consent was obtained from each study participant.

**Consent for publication:** not applicable.

**Availability of data and materials:** The datasets used and/or analysed during the current study are available from the corresponding authors on reasonable request. Questions and requests about the clinical data should be submitted to H. Holstege. Questions and requests for the experimental data discussed in this manuscript should be submitted to J.J.M. van Dongen.

**Funding/Competing interests:** This work was supported by the HorstingStuit Foundation, the Hans und Ilse Breuer Foundation and Stichting VUmc Fund; and by the ABOARD project, Project number: ZonMW (#73305095007 and Health~Holland, Topsector Life Sciences & Health (PPP-allowance; #LSHM20106).

AMD, CT, JJMvD and MAB report inventorship of the patent “Means and methods for multiparameter cytometry-based leukocyte subsetting” (NL2844751, PCT/NL2020/050688, filing date 5 November 2019), owned by the EuroFlow Consortium. In addition, JJMvD reports to be chairman of the EuroFlow scientific foundation, which receives royalties from licensed patents, which are collectively owned by the participants of the EuroFlow Foundation. These royalties are exclusively used for continuation of the EuroFlow collaboration and sustainability of the EuroFlow consortium. JJMvD reports an Educational Services Agreement from BD Biosciences (San José, CA) and a Scientific Advisor Agreement with Cytognos; all related fees and honoraria are for the Immunology department at Leiden University Medical Center. All other authors declare they have no competing interests.

**Authors' contributions:** Conceptualization, HH, JJMvD; Data curation, DH,

LL, SR, AMD; Formal analysis, BN, BdM, RJG, AAV, MdJ, CT, MAB, AMD; Funding acquisition, HH; Investigation, BN, BdM, RJG, IFL, AAV, MdJ, AMD; Methodology, CT; Project administration, DH, LL, AMD; Resources; DH, LL, SR, HH; supervision, HH, JJMvD, MAB, CT; Visualization, AMD; writing – original draft preparation, MAB, AMD; writing – review and editing, all authors read the manuscript, provided feedback and agree with the final manuscript.

**Acknowledgments:** The authors would like to thank the participants of the 100-plus Study and their family members for providing the blood samples analyzed in this work. Further, we thank the LUMC Vrijwillige Donoren Service (LuVDS), who provided healthy blood samples for optimization of all assays, E. Simonetti (Radboudumc, Laboratory of Medical Immunology) for running the multiplex immunoassay, and the LUMC technical support team for the design and production of the tube heating device used in this study. The authors gratefully acknowledge the Flow cytometry Core Facility at LUMC (coordinated by M. Hameetman, run by operators S. van de Pas, D. Lowie, IJ. Reyneveld and former FCF members dr. K. Schepers, J. Jansen, E. de Haas, and G. de Roo) for their support.

**Supplementary Materials:** The Supplementary Material for this article can be found online at: <https://assets.researchsquare.com/files/rs-1929710/v1/107d2012-dd37-43b1-b2cb-966265d906bf.pdf?c=1661362356>

Or using the following QR code:



## References

1. Castelo-Branco C, Soveral I. The immune system and aging: a review. *Gynecological Endocrinology*. 2014;30(1):16-22.
2. Franceschi C, Bonafè M, Valensin S, Olivieri F, De Luca M, Ottaviani E, De Benedictis G. Inflamm-aging: an evolutionary perspective on immunosenescence. *Annals of the new York Academy of Sciences*. 2000;908(1):244-54.
3. Cancro MP, Hao Y, Scholz JL, Riley RL, Frasca D, Dunn-Walters DK, Blomberg BB. B cells and aging: molecules and mechanisms. *Trends in immunology*. 2009;30(7):313-8.
4. Frasca D, Diaz A, Romero M, Garcia D, Blomberg BB. B cell immunosenescence. *Annual review of cell developmental biology*. 2020;36:551-74.
5. Fortin CF, McDonald PP, Lesur O, Fülöp Jr T. Aging and neutrophils: there is still much to do. *Rejuvenation research*. 2008;11(5):873-82.
6. McLachlan JA, Serkin CD, Morrey KM, Bakouche O. Antitumoral properties of aged human monocytes. *The Journal of Immunology*. 1995;154(2):832-43.
7. Hearps AC, Martin GE, Angelovich TA, Cheng WJ, Maisa A, Landay AL, Jaworowski A, Crowe SM. Aging is associated with chronic innate immune activation and dysregulation of monocyte phenotype and function. *Aging cell*. 2012;11(5):867-75.
8. Sims R, Van Der Lee SJ, Naj AC, Bellenguez C, Badarinarayan N, Jakobsdottir J, Kunkle BW, Boland A, Raybould R, Bis JC. Rare coding variants in *PLCG2*, *ABI3*, and *TREM2* implicate microglial-mediated innate immunity in Alzheimer's disease. *Nature*

genetics. 2017;49(9):1373-84.

9. van der Lee SJ, Conway OJ, Jansen I, Carrasquillo MM, Kleineidam L, van den Akker E, Hernández I, Van Eijk KR, Stringa N, Chen JAJAn. A nonsynonymous mutation in *PLCG2* reduces the risk of Alzheimer's disease, dementia with Lewy bodies and fronto-temporal dementia, and increases the likelihood of longevity. 2019;138(2):237-50.
10. Wagner K-H, Cameron-Smith D, Wessner B, Franzke BJN. Biomarkers of aging: from function to molecular biology. 2016;8(6):338.
11. Wilde JI, Watson SP. Regulation of phospholipase C  $\gamma$  isoforms in haematopoietic cells: why one, not the other? Cellular signalling. 2001;13(10):691-701.
12. Wang D, Feng J, Wen R, Marine J-C, Sangster MY, Parganas E, Hoffmeyer A, Jackson CW, Cleveland JL, Murray PJ. Phospholipase  $Cy2$  is essential in the functions of B cell and several Fc receptors. Immunity. 2000;13(1):25-35.
13. Takalo M, Wittrahm R, Wefers B, Parhizkar S, Jokivarsi K, Kuulasmaa T, Mäkinen P, Martiskainen H, Wurst W, Xiang XJMn. The Alzheimer's disease-associated protective *Plcy2*-P522R variant promotes immune functions. 2020;15(1):1-14.
14. Andreone BJ, Przybyla L, Llapashtica C, Rana A, Davis SS, van Lengerich B, Lin K, Shi J, Mei Y, Astarita GJNN. Alzheimer's-associated *PLCy2* is a signaling node required for both *TREM2* function and the inflammatory response in human microglia. 2020;23(8):927-38.
15. Strickland SL, Morel H, Prusinski C, Allen M, Patel TA, Carrasquillo MM, Conway OJ, Lincoln SJ, Reddy JS, Nguyen TJAnc. Association of *ABI3* and *PLCG2* missense variants with disease risk and neuropathology in Lewy body disease and progressive supranuclear palsy. 2020;8(1):1-12.
16. Chen F, Zhang Y, Wang L, Wang T, Han Z, Zhang H, Gao S, Hu Y, Liu GJJoAsD. *PLCG2* rs72824905 Variant Reduces the Risk of Alzheimer's Disease and Multiple Sclerosis. 2021(Preprint):1-7.
17. Kleineidam L, Chouraki V, Próchnicki T, van der Lee SJ, Madrid-Marquez L, Wagner-Thelen H, Karaca I, Weinhold L, Wolfsgruber S, Boland A. *PLCG2* protective variant p. P522R modulates tau pathology and disease progression in patients with mild cognitive impairment. Acta neuropathologica. 2020;139(6):1025-44.
18. Magno L, Lessard CB, Martins M, Lang V, Cruz P, Asi Y, Katan M, Bilsland J, Lashley T, Chakrabarty PJAsr, therapy. Alzheimer's disease phospholipase C-gamma-2 (*PLCG2*) protective variant is a functional hypermorph. 2019;11(1):16.
19. Maguire E, Menzies GE, Phillips T, Sasner M, Williams HM, Czubala MA, Evans N, Cope EL, Sims R, Howell GRJTEj. *PIP2* depletion and altered endocytosis caused by expression of Alzheimer's disease-protective variant *PLCy2* R522. 2021;40(17):e105603.
20. Holstege H, Beker N, Dijkstra T, Pieterse K, Wemmenhove E, Schouten K, Thiesens L, Horsten D, Rechtuijt S, Sikkes SJEjoe. The 100-plus Study of cognitively healthy centenarians: rationale, design and cohort description. 2018;33(12):1229-49.
21. Tesi N, van der Lee SJ, Hulsman M, Jansen IE, Stringa N, van Schoor N, Meijers-Heijboer H, Huisman M, Scheltens P, Reinders MJJEJoHG. Centenarian controls increase variant effect sizes by an average twofold in an extreme case-extreme control analysis of Alzheimer's disease. 2019;27(2):244-53.
22. Kalina T, Flores-Montero J, Lecrevisse Q, Pedreira CE, Velden VH, Novakova M, Mejstrikova E, Hrusak O, Böttcher S, Karsch D. Quality assessment program for EuroFlow protocols: Summary results of four-year (2010–2013) quality assurance rounds. Cytometry Part A. 2015;87(2):145-56.
23. Kalina T, Flores-Montero J, Van Der Velden V, Martin-Ayuso M, Böttcher S, Ritgen M, Almeida J, Lhermitte L, Asnafi V, Mendonca A. EuroFlow standardization of flow cytometer instrument settings and immunophenotyping protocols. Leukemia. 2012;26(9):1986-2010.



24. Pan Kvd, Bruin-Versteeg Sd, Damasceno D, Hernández-Delgado A, Sluijs-Gelling AJvd, Bossche WBvd, Laat IFd, Diez P, Naber BA, Diks AM, Berkowska MA, Mooij Bd, Groenland RJ, Bie FJd, Khatri I, Kassem S, Jager ALd, Louis A, Almeida J, Gaans Jv, Bar-koff A-M, He Q, Ferwerda G, Versteegen P, Berbers GA, Orfao A, Dongen JJMv, Teodosio C. Development of a standardized and validated flow cytometry approach for monitoring of innate myeloid immune cells in human blood. in review at *Frontiers at Immunology*. 2022.
25. van Dongen JJM, OdmCEV, J.A. ; Goncalves Grunho Teodosio, C.I.; Perez Y Andres, M.; Almeida Parra, J.M.; Van den Bossche, W.B.L.; Botafogo Goncalves, V.D.; Berkowska, M.A.; Van der Pan, K.; Blanco Alvarez, E.; Diks, A.M. , inventor; P119646NLOO, assignee. Means and methods for multiparameter cytometry-based leukocyte subsetting. The Netherlands 2019 priority date 5 November 2019.
26. Botafogo V, Pérez-Andres M, Jara-Acevedo M, Bárcena P, Grigore G, Hernández-Delgado A, Damasceno D, Comans S, Blanco E, Romero A. Age Distribution of Multiple Functionally Relevant Subsets of CD4+ T Cells in Human Blood Using a Standardized and Validated 14-Color EuroFlow Immune Monitoring Tube. *Frontiers in Immunology*. 2020;11:166.
27. Blanco E, Pérez-Andrés M, Arriba-Méndez S, Contreras-Sanfeliciano T, Criado I, Pelak O, Serra-Caetano A, Romero A, Puig N, Remesal A. Age-associated distribution of normal B-cell and plasma cell subsets in peripheral blood. *Journal of Allergy and Clinical Immunology*. 2018;141(6):2208-19. e16.
28. Diks AM, Versteegen P, Teodosio C, Groenland RJ, de Mooij B, Buisman A-M, Torres-Valle A, Pérez-Andrés M, Orfao A, Berbers GAM, van Dongen JJM, Berkowska MA, Consortium obotI-P. Age and Primary Vaccination Background Influence the Plasma Cell Response to Pertussis Booster Vaccination. 2022;10(2):136.
29. Darrah PA, Patel DT, De Luca PM, Lindsay RW, Davey DF, Flynn BJ, Hoff ST, Andersen P, Reed SG, Morris SL. Multifunctional TH 1 cells define a correlate of vaccine-mediated protection against *Leishmania major*. *Nature medicine*. 2007;13(7):843-50.
30. Van Zelm MC, Van Der Burg M, Langerak AW, Van Dongen JJ. PID comes full circle: applications of V (D) J recombination excision circles in research, diagnostics and newborn screening of primary immunodeficiency disorders. *Frontiers in immunology*. 2011;2:12.
31. Van Zelm MC, Szczepański T, Van Der Burg M, Van Dongen JJ. Replication history of B lymphocytes reveals homeostatic proliferation and extensive antigen-induced B cell expansion. *The Journal of experimental medicine*. 2007;204(3):645-55.
32. Fröberg J, Gillard J, Philipsen R, Lanke K, Rust J, van Tuijl D, Teelen K, Bousema T, Simonetti E, van der Gaast-de Jongh CJNc. SARS-CoV-2 mucosal antibody development and persistence and their relation to viral load and COVID-19 symptoms. 2021;12(1):1-11.
33. Garner C, Tatu T, Reittie J, Littlewood T, Darley J, Cervino S, Farrall M, Kelly P, Spector T, Thein SJB, *The Journal of the American Society of Hematology*. Genetic influences on F cells and other hematologic variables: a twin heritability study. 2000;95(1):342-6.
34. Hall M, Ahmadi K, Norman P, Snieder H, MacGregor A, Vaughan R, Spector T, Lanchbury JJG, *Immunity*. Genetic influence on peripheral blood T lymphocyte levels. 2000;1(7):423-7.
35. Kurosaki T, Aiba Y, Kometani K, Moriyama S, Takahashi YJr. Unique properties of memory B cells of different isotypes. 2010;237(1):104-16.
36. Kolibab K, Smithson SL, Rabquer B, Khuder S, Westerink MJJI, *immunity*. Immune response to pneumococcal polysaccharides 4 and 14 in elderly and young adults: analysis of the variable heavy chain repertoire. 2005;73(11):7465-76.
37. Ademokun A, Wu YC, Martin V, Mitra R, Sack U, Baxendale H, Kipling D, Dunn-Walters DKJAc. Vaccination-induced changes in human B-cell repertoire and pneu-

- mococcal IgM and IgA antibody at different ages. 2011;10(6):922-30.
38. Spiegelberg H, Melewicz F, Ferreri N, editors. IgE Fc receptors on monocytes and allergy. *Annales de l'Institut Pasteur/Immunologie*; 1986: Elsevier.
39. Plaut M, Pierce JH, Watson CJ, Hanley-Hyde J, Nordan RP, Paul WEJN. Mast cell lines produce lymphokines in response to cross-linkage of FcεRI or to calcium ionophores. 1989;339(6219):64-7.
40. Gould HJ, Sutton BJJNRI. IgE in allergy and asthma today. 2008;8(3):205-17.
41. Jiang T, Yu J-T, Hu N, Tan M-S, Zhu X-C, Tan LJMn. CD33 in Alzheimer's disease. 2014;49(1):529-35.
42. Bradshaw EM, Chibnik LB, Keenan BT, Ottoboni L, Raj T, Tang A, Rosenkrantz LL, Imboywa S, Lee M, Von Korff AJNn. CD33 Alzheimer's disease locus: altered monocyte function and amyloid biology. 2013;16(7):848-50.
43. Fülöp Jr T, Foris G, Worum I, Leövey A. Age-dependent alterations of Fc gamma receptor-mediated effector functions of human polymorphonuclear leucocytes. *Clinical and experimental immunology*. 1985;61(2):425.
44. Butcher S, Chahal H, Nayak L, Sinclair A, Henriquez N, Sapey E, O'mahony D, Lord J. Senescence in innate immune responses: reduced neutrophil phagocytic capacity and CD16 expression in elderly humans. *Journal of leukocyte biology*. 2001;70(6):881-6.
45. Gabandé-Rodríguez E, Keane L, Capasso MJJonr. Microglial phagocytosis in aging and Alzheimer's disease. 2020;98(2):284-98.
46. Guen YL, Luo G, Ambati A, Damotte V, Jansen I, Yu E, Nicolas A, de Rojas I, Leal TP, Miyashita A, Bellenguez C, Lian MM, Parveen K, Morizono T, Park H, Grenier-Boley B, Naito T, Küçükali F, Talyansky SD, Yogeshwar SM, Sempere V, Satake W, Alvarez V, Arosio B, Belloy ME, Benussi L, Boland A, Borroni B, Bullido MJ, Caffarra P, Clarimon J, Daniele A, Darling D, Debette S, Deleuze J-F, Dichgans M, Dufouil C, During E, Düzel E, Galimberti D, Garcia-Ribas G, García-Alberca JM, García-González P, Giedraitis V, Goldhardt O, Graff C, Grünblatt E, Hanon O, Hausner L, Heilmann-Heimbach S, Holstege H, Hort J, Jung YJ, Jürgen D, Kern S, Kuulasmaa T, Ling L, Masullo C, Mecocci P, Mehrabian S, de Mendonça A, Boada M, Mir P, Moebus S, Moreno F, Nacmias B, Nicolas G, Nordestgaard BG, Papenberg G, Papma J, Parnetti L, Pasquier F, Pastor P, Peters O, Pijnenburg YAL, Piñol-Ripoll G, Popp J, Porcel LM, Puerta R, Pérez-Tur J, Rainero I, Ramakers I, Real LM, Riedel-Heller S, Rodriguez-Rodriguez E, Luís Royo J, Rujescu D, Scarmeas N, Scheltens P, Scherbaum N, Schneider A, Seripa D, Skoog I, Solfrizzi V, Spalletta G, Squassina A, van Swieten J, Sánchez-Valle R, Tan E-K, Tegos T, Teunissen C, Thomassen JQ, Tremolizzo L, Vyhnaek M, Verhey F, Waern M, Wiltfang J, Zhang J, Zetterberg H, Blennow K, Williams J, Amouyel P, Jessen F, Kehoe PG, Andreassen O, Van Duin C, Tsolaki M, Sánchez-Juan P, Frikke-Schmidt R, Sleegers K, Toda T, Zettergren A, Ingelsson M, contributors E, group GAs, consortium D, DemGene, EADI, GERAD, consortium APsDG, Okada Y, Rossi G, Hiltunen M, Gim J, Ozaki K, Sims R, Foo JN, van der Flier W, Ikeuchi T, Ramirez A, Mata I, Ruiz A, Gan-Or Z, Lambert J-C, Greicius MD, Mignot E. Protective association of *HLA-DRB1*\*04 subtypes in neurodegenerative diseases implicates acetylated Tau PHF6 sequences. 2021:2021.12.26.21268354.
47. Phongpreecha T, Fernandez R, Mrdjen D, Culos A, Gajera CR, Wawro AM, Stanley N, Gaudilliere B, Poston KL, Aghaeepour N. Single-cell peripheral immunoprofiling of Alzheimer's and Parkinson's diseases. *Science advances*. 2020;6(48):eabd5575.
48. D'Andrea MR, Cole GM, Ard MDJNoa. The microglial phagocytic role with specific plaque types in the Alzheimer disease brain. 2004;25(5):675-83.
49. Britschgi M, Olin C, Johns H, Takeda-Uchimura Y, LeMieux M, Rufibach K, Rajadas J, Zhang H, Tomooka B, Robinson W. Neuroprotective natural antibodies to assemblies of amyloidogenic peptides decrease with normal aging and advancing Alzheimer's disease. *Proceedings of the National Academy of Sciences*. 2009;106(29):12145-50.

50. Rosenmann H, Meiner Z, Geylis V, Abramsky O, Steinitz M. Detection of circulating antibodies against tau protein in its unphosphorylated and in its neurofibrillary tangles-related phosphorylated state in Alzheimer's disease and healthy subjects. *Neuroscience letters*. 2006;410(2):90-3.
51. Sevigny J, Chiao P, Bussière T, Weinreb PH, Williams L, Maier M, Dunstan R, Salloway S, Chen T, Ling Y. The antibody aducanumab reduces A $\beta$  plaques in Alzheimer's disease. *Nature immunology*. 2016;537(7618):50-6.
52. Tolar M, Abushakra S, Hey JA, Porsteinsson A, Sabbagh M. Aducanumab, gantenerumab, BAN2401, and ALZ-801—the first wave of amyloid-targeting drugs for Alzheimer's disease with potential for near term approval. *Alzheimer's research therapy*. 2020;12(1):1-10.
53. Congdon EE, Sigurdsson EM. Tau-targeting therapies for Alzheimer disease. *Nature Reviews Neurology*. 2018;14(7):399-415.



## **Chapter 5**

### **General Discussion**



Immune monitoring is a process in which a diverse set of tools is applied to allow evaluation of the immune system. Monitoring of the immune system, both when an active response is ongoing and when in homeostasis, can yield valuable information about the immune status of an individual or a group. Vaccination is an example of an active response. Here, monitoring can yield information about the efficacy of applied vaccination/immunization method, or it can give information about the functioning of the immune system in one or more individuals (for example when using a neoantigen). The importance of immune monitoring is well-recognized and various efforts are made to harmonize/standardize protocols, yet further improvements are still needed to facilitate direct comparisons between different laboratories and between different clinical studies.

In this thesis, we addressed multiple topics related to immune monitoring. First, we investigated the impact of various pre-analytical and analytical factors on the data quality and robustness of analysis (**Chapter 2**). We formulated a list of guidelines to improve reliability and reproducibility of data regarding immune cell quantity and phenotype. These guidelines find application both in research utilizing human blood, but also in patient diagnostics or industry, e.g., in evaluation of new treatments or vaccination strategies.

Next, we evaluated the longitudinal immune response following a pertussis booster vaccination, or after bacterial challenge with *Bordetella pertussis* (*Bp*) (**Chapter 3**). In case of booster vaccination, we investigated the immune response not only in a 'standard' cohort of healthy adults, but also in a cohort of children, adolescents, and older adults. Additionally, we extended our flow cytometry studies with antigen (Ag)-specific assays, such as serology and ELISpot, and showed that they can complement each other.

In **Chapter 3.1**, we investigated kinetics of >250 circulating immune cell subsets after booster vaccination. We observed the most prominent changes in the plasma cell compartment. Consequently, we focused on kinetics in the B-cell compartment in **Chapter 3.2** and found that irrespective of age and primary vaccination background, the expansion and maturation of (primarily) IgG1 plasma cells was the most prominent feature of an immune response initiated by acellular pertussis (aP) booster vaccination. Despite these similarities, specific differences in plasma cell responses appeared to be associated with age and primary vaccination background.

Conclusions drawn from flow cytometry can not only be supplemented by techniques such as ELISpot and serology, but also by more exploratory techniques such as B-cell receptor (BCR) repertoire analysis. In **Chapter 3.3**, we investigated the BCR repertoire of plasma cells by means of single cell sequencing techniques and evaluated to what extent the distribution of plasma cell subsets in this data was reflecting the flow cytometry data. Moreover, we built a query tool to help search for BCRs specific to individual vaccine components.

As diverse cell populations and timepoints can be of importance in different models, we compared the cellular kinetics (within innate immune cells, T cells, and B cells) between Bp booster vaccination or bacterial challenge in **Chapter 3.1** and **3.4**. Here, we found that the expansion and maturation of plasma cells was less prominent and was delayed in time in the bacterial challenge model, but more heterogeneous with respect to used plasma cell isotypes. Using the data gathered in **Chapter 3**, we identified informative timepoints and cell populations that could be monitored in future vaccination/challenge studies. This data emphasizes the importance of pilot (time point finding) studies.

Finally, we set out to use immune monitoring to evaluate the immune system in homeostasis to get in-depth information on the leukocyte composition and function in a group of individuals carrying a specific genetic variant, which is associated with decreased risk of developing dementia, and increased chance of longevity (**Chapter 4**). This was supplemented with SARS-CoV-2 vaccination studies to evaluate the induced immune responses.

Several of the conclusions drawn from the here-presented work have implications for future studies and/or experiments. These implications and highlights will be discussed further in this chapter.

### **The need for (increased) standardization in immune monitoring**

Standardization of the pre-analytical, analytical, and post-analytical processes is crucial to improve data quality and reproducibility. The importance of standardization is well-recognized, with many scientific articles, guidelines, protocols and tools being published in the past years, not only for flow cytometry, but also for immune monitoring in general.[1-10] Thus, when designing a clinical trial, there are multiple guidelines available to make informed decisions about the logistics and how to keep the pre-analytical phase as controlled and optimal as required for the type of study.

### **Pre-analytical factors**

To understand the impact of storage and transportation after sample collection, we first determined the optimal storage time and condition. In our case, storage of whole blood at room temperature for <24h, but ideally <6h, was the best for PB-EDTA. Storage from 6h onwards resulted in decreasing absolute cell counts (**Chapter 2.1**). In this entire thesis, we attempted to store samples as short as possible (ideally <6-12h, with exception of the storage experiments in **Chapter 2**) and samples were always kept at room temperature as whole blood until the moment of processing. To avoid introducing any bias in longitudinal data, we aimed to keep storage conditions and used anti-coagulant as similar as possible. In this thesis we only investigated the impact of the pre-analytical factors on the primary immunodeficiency screening and orientation tube (PIDOT). However, the EuroFlow Consortium has further investigated the impact of several pre-analytical factors on other EuroFlow panels (such as tube 1 from the acute myeloid leukemia/myelodysplastic syndrome (AML/MDS) panel, the acute leukemia

orientation tube (ALOT), and the lymphoid screening tube (LST) and published their findings recently.[11]

### **Analytical and post-analytical factors**

In this thesis, the guidelines and protocols as proposed by the EuroFlow Consortium have been applied to all experiments executed on a BD FACS Canto II 3L, a BD FACS LSR Fortessa 4L, or a BD FACS LSR X-20 Fortessa 4L (BD Biosciences, San Jose, CA, USA).[4, 5] In short, this means that standardized protocols were used whenever available, and that CS&T beads (BD Biosciences) as well as SPHERO™ Rainbow calibration particles (Cytognos, Salamanca, Spain) were run daily to check machine performance.

One strategy that could help reporting the data in a more harmonized and standardized manner is the use of database-driven analysis (Automated Gating & Identification; AGI), possibly combined with comparison with reference cell counts and/or automated reporting of findings. The AGI tool makes use of algorithms that cluster flow cytometry data based on an established reference database.[8] Although events that cannot be automatically assigned still require manual checking, we and others have shown that the use of AGI strongly reduced the variability as compared to manual analysis, where each operator introduces subjectivity (**Chapter 2.2**).[12-14]

The calibration and daily quality control (QC) of instruments, and the use of standardized protocols for sample preparation and acquisition are a prerequisite for a successful automated analysis. When using the database-driven approach, it is of importance that evaluated samples have undergone similar preparation/treatment as the samples in the reference database. When sample treatment or used anti-coagulant deviates from the samples used to construct the reference database, this may influence the scatter properties or fluorescence of the acquired sample. As a result, automated analysis may be suboptimal, with many events requiring a manual check.

In case no database-driven approach is available, which is often the case for (highly) exploratory research, the use of highly standardized analysis strategies can be a solution. In this thesis, we started with manual analysis of flow cytometry data acquired in strictly controlled settings. In the meantime, a database-driven approach, using a highly similar gating strategy, became available. In two consecutive clinical trials (one using manual gating and one using AGI, **Chapter 3.1** and **3.2**, respectively), we found that (major) findings were reproducible between the two approaches, confirming that the degree of standardization was sufficiently high.

Additionally, several commercially available databases contain not only fully annotated flow cytometry datafiles of healthy individuals, but also fully annotated patient material or reference values, which aid clinical laboratories to establish a diagnosis. For example, when staining a (suspected) patient sample with the

ALOT panel and using the automated analysis in the Infinicyt Software, the Compass Tool performs immunophenotypic diagnosis and classification in patients with acute leukemia (AL). Based on the outcome, consecutive steps can be taken to finalize the diagnosis.[15] Another example is the inclusion of well-annotated files of patients with PIDs in the reference database for the PIDOT.[16]

### **Cohort selection and definition**

Cohort selection is inherently related to clinical trials. While selecting a cohort, the aim is to make it representative of the total target group. In the introduction of this thesis, we referred to a systematic review that we conducted.[17] Here, we found that the extent of cohort description varied between evaluated studies, even though the reported metadata (such as comorbidities, age range, number of individuals, sex distribution, ethnicity, current health status, etc.) is an important factor showing how well the cohort represents the total target population.

One example of the importance of the cohort definition became apparent in **Chapter 4** of this thesis, where we determined the calcium release in memory B cells (MBCs) upon BCR stimulation. This assay was performed for a set of the healthiest individuals ('Cohort II'), but also in the total cohort ('Cohort I'), which had far less strict inclusion criteria, and more reported comorbidities. Results differed between the two cohorts. Non class-switched MBCs from Cohort I showed no difference in calcium flux upon stimulation between *PLCG2* p.P522R carriers and non-carriers. However, when only selecting Cohort II (the healthiest individuals, whose cells were used for several functional experiments), we observed a clear trend towards a more robust calcium flux in stimulated non class-switched MBCs in carriers. This marks the importance of clearly stating the inclusion criteria. Thus, standardization of cohort description should be an ongoing effort.

To gain more confidence in the representativeness of a cohort, it is a good practice to compare baseline parameters of the cohort to available reference values. With the introduction of high dimensional flow cytometers, the number of reported cell populations (percentages and cell counts) is growing. It would be highly beneficial to establish and keep updating such 'reference values' for healthy controls of different age categories as distribution of multiple leukocyte subsets changes during lifetime. Several of such reference values in healthy controls of several age ranges have already been published, both as tables and as database-implemented reference values, e.g. for diagnostic purposes.[12, 16, 18, 19] [van der Pan et al, manuscript accepted] Importantly, reference values may also be impacted by other factors such as sex and ethnicity.[20, 21] Therefore, these factors should ideally be included as metadata as well.

It is not unimaginable that in the (near) future, reference ranges of various studies reporting on the same cell populations and subsets will be merged into large databases. In fact, such efforts are already ongoing, and tools are being developed. For example, in 2018 Hu and colleagues introduced a bioinformatic tool for automated meta-analysis of mass and flow cytometry files.[20] Of note, the

heterogeneity between studies was marked as a challenge. To facilitate such meta-analysis, it is important that cohort description is clearly stated. Moreover, the used antibody cocktail, phenotypic identification of cell populations and mode of reporting (e.g., IU/mL, ratio compared to baseline, % of total cells, or cells/ $\mu$ L blood) should be clearly stated to enable merging of (sub)data, although the latter may be less of an issue when raw data files are used. This clarity is as important when comparing or merging data in-between different studies to draw valid conclusions. In an era where bioinformatics play an important role in handling these high-dimensional datafiles, consistency and transparency is becoming increasingly important.

In addition to clearly stated methods, it is becoming more standard to deposit raw data (or to provide this upon request) in repositories such as ImmPort (Immport.org).[22] This results in increased data transparency, and enables comparison or alignment of data analysis strategies between studies where initially different approaches were used. Additionally, guidelines outlining the minimal required information are available.[1] Although we mainly focus on flow cytometry data here, this statement also applies for other fields, such as mass cytometry or single-cell sequencing data.

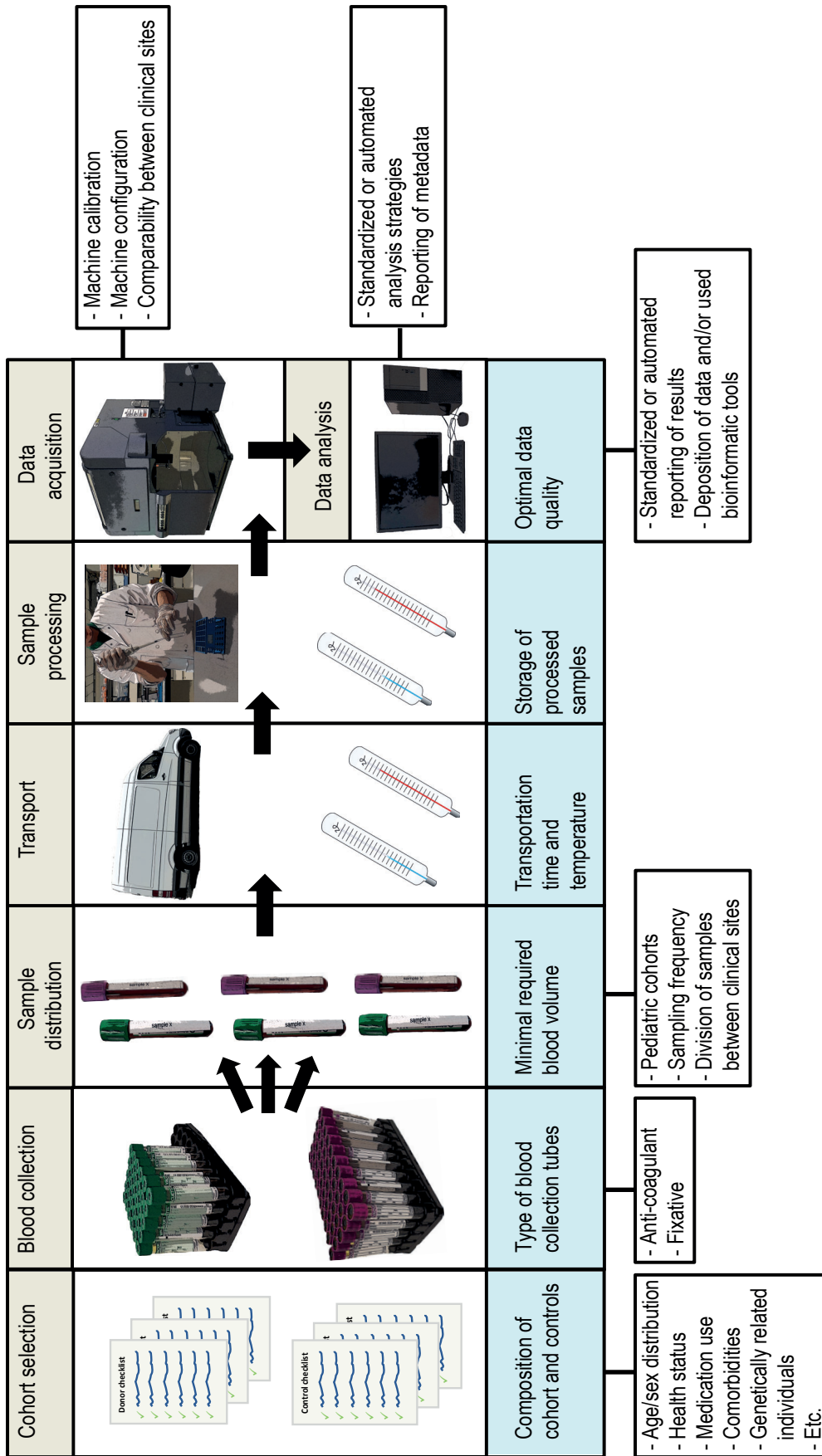
Based on the findings in this thesis, I highly encourage other researchers to be as complete and consistent as possible when describing their methods, data, and readouts. In **Figure 1**, I indicated which pre-analytical, analytical, and post-analytical factors can influence the results of (meta-)analysis and should thus be carefully decided (please beware that this figure does not aim to give a complete overview of all factors known to influence results of the (meta-)analysis). To provide a better overview of the experimental procedure used in individual studies throughout this thesis, I have included a comprehensive list of used gating strategies, used flow cytometry panels and list of population definitions as appendices in this thesis.

### **Role of bioinformatic tools in analysis**

With the ever-increasing size and dimensionality of experimental data, bioinformatics is becoming an important tool in the objective interpretation of data. Especially the spectral flow cytometers and mass cytometers yield high-dimensional data that may require specialized software for objective analysis.[23-27] Various software and analysis packages are available to attune to everyone's needs. In this thesis we primarily used (direct) prototypes of flow cytometry panels of which standardized gating strategies and databases for automated analysis were developed in the Infinicyt Software. Some of these were developed specifically

**Figure 1 (next page). Overview of factors in the pre-analytical, analytical, and post-analytical process that can influence the quality of results and should ideally be decided before start of large experiments, such as a clinical trial.** To increase transparency and help re-use of data (e.g., meta-analysis or to construct a database), a clear cohort definition and data availability statement are of importance. Figure modified from Diks et al (this thesis).





for the PERISCOPE program in a collaboration with Cytognos, the company that developed the Infinicyt Software. Therefore, we used the Infinicyt software for all flow cytometry analysis in this thesis. Yet we recognize that there are many different analysis software packages/analysis methods (such as instrument-packages software FACS Diva, stand-alone software FlowJo or FSC Express, or methods such as t-SNE, vi-SNE, FlowSOM, SPADE or PhenoGraph), all with their own strengths.[27] Although several of these approaches are relatively accessible, not all are equally user-friendly, therefore collaboration and crosstalk with bioinformaticians is highly encouraged. In this thesis, we aimed for objective analysis by means of applying (bio)informatic strategies, such as correlation networks and the use of database-driven analysis.

In addition to the flow cytometry data, other techniques, such as single-cell sequencing, require a certain level of expertise in bioinformatic approaches. In **Chapter 3.3**, our bioinformatician developed an analysis pipeline to evaluate and interpret the whole transcriptome and BCR sequencing data. Moreover, the PLCG2 variant investigated in **Chapter 4** was a result of a large genome-wide association study (GWAS) by Sims et al., where researchers from different fields and institutes worked together to identify rare coding variants associated with Alzheimer's Disease, which again emphasizes the need for inter-field collaboration.[28] Although I acknowledge that it may be challenging for both parties to meet at 'the border of their comfort zone', I believe this is how we can advance objective analysis of big data and -in fact- science in general. Therefore, I highly recommend researchers to collaborate with one another, and learn from and with each other.

In-depth immune monitoring to evaluate the functioning of the immune system Although majority of this thesis focused on the immune system during an antigen challenge, there are many cases where monitoring of the immune system in homeostasis is performed. For example, to confirm or exclude an immunological disorder (e.g., with the PIDOT panel as discussed in **Chapter 2**) or to diagnose hematological malignancies. Aside from diagnostics, the immune system can also be monitored in more exploratory settings, as was done in **Chapter 4**. There, we investigated the immune system both in presence and absence of stimulation in carriers of a genetic variant of the PLCG2 gene (variant p.P522R/ rs72824905), which was associated with decreased risk of several forms of age-related neurodegenerative diseases, including Alzheimer's Disease.[29-31] Moreover, this variant was associated with increased chance of longevity.[29] As the immune system is (in)directly involved in several of these diseases, we hypothesized that evaluation of the immune system may give information about the (protective) mechanism of action.

Age is an important risk factor in many neurodegenerative diseases, and individuals of the same metric age can present with differently pronounced signs of biological aging. Based on the findings presented in **Chapter 4**, we speculate that p.P522R carriers are somehow more resilient to the effect of biological aging.

There are many markers that can be used as marker of aging, and the function and composition of the immune system is one of them. Even though most disease-related pathologies in dementia occur in the brain, immune cells -isolated from the blood- can provide valuable information about aging processes. There are several similarities between blood phagocytes and microglia, such as the expression of *PLCG2* and the mechanisms used to remove damaged cells, pathogens, or (cellular) debris. Therefore, some findings in the blood phagocytes might give insight in the microglia of the same individual as well. Moreover, a recent conference abstract from the 63rd ASH Annual Meeting described the tracing of somatic mutations (occurring in blood or bone marrow), and found these mutations in cells that resided in the brain and could not be distinguished from microglia. [32] This may suggest that during lifetime, (progenitor) cells originating from the blood and bone marrow can find their way into the brain and contribute to the microglial pool. Thus, insights into the functional capacities of circulating immune cells (mainly phagocytes) may translate in part to neurodegenerative diseases and possibly the functioning of microglia in these individuals. The clear advantage of blood is that it can be obtained in a minimally invasive way, whereas human microglia can generally only be obtained post-mortem or from brain biopsies. Of note, iPSC-derived human microglia are an alternative to primary human-derived microglia and have been shown to have a highly similar transcriptomic profile, protein expression, and functional ability to their brain-derived counterpart. [33] Lastly, immunoglobulins (Igs) are also able to enter the brain and exert their functions there, making them potential candidates for intervention strategies for several types of dementia.[34-36]

Certain *PLCG2* variants can be associated with the pathological conditions. For example, there is a condition called *PLCG2* associated antibody deficiency and immune dysregulation (PLAID),[37] which is generally associated with loss- or gain-of-function deletions in *PLCG2*. Most patients are thought to have a deletion in the autoregulatory domain, which leaves the active site of the enzyme continuously exposed.[38] To the best of our knowledge p.P522R, which is a gain of function variant, has not been associated with any disease/disorders, but in fact reduces the chance to develop several neurodegenerative diseases.[29-31] It should however be noted that this is a rare variant that only recently gained attention, and data on human subjects are still limited. Thus, it may be wise to further characterize p.P522R carriers (e.g., the prevalence of malignancies, immune disorders and/or other morbidities). Here, immune monitoring can play an important role by combining immunophenotyping with an *ex vivo* functional analysis using blood as a minimally invasive source of material.

### **Immune monitoring to evaluate ongoing immune responses - complementarity of different approaches**

The efficacy of vaccines has been demonstrated by the reduction of infectious-disease related deaths since their introduction.[39] In addition to neutralizing Igs, cellular responses play an important role in the protective immunity generated by vaccines.[40, 41] However, not all underlying cellular mechanisms are fully

understood. Generally, serology is considered the golden standard to assess vaccine efficacy. Serological tests may evaluate the bactericidal activity of produced Igs, their neutralization or inhibition activity, or the level of Ag-specific Igs in the serum.[40]

In many (exploratory) vaccination studies, serology is complemented with other readouts, such as ELISpot and flow cytometry.[42-45] Occasionally, approaches such as DNA/RNA sequencing or mass cytometry are used.[46, 47] Although these various techniques can complement each other, one can wonder to what extent these assays are redundant or unique in their findings, and which assays should be included in a certain setup. Aside from costs associated with each technique, the required time and expertise for analysis of raw data, as well as the extent of standardization may play a role, especially when application in clinical trials or diagnostic purposes is the end goal.

In this thesis, we applied various techniques to measure vaccine-induced responses. In all Bp studies, we measured the increase in Ag-specific serum Ig levels and the longitudinal changes in circulating immune cells, with a special focus on the B-cell compartment. Although in **Chapter 3.1** we found that the maximum expansion of total IgG1 MBCs (between d7 and 28) positively correlated with the increase in Ag-specific serum Ig, we could not confirm this in **Chapter 3.2**. A possible explanation for this can be that in **Chapter 3.1**, we were able to choose maximum expansion from several close timepoints, whereas in **Chapter 3.2** only 1 or 2 timepoints were available. Here, we may have missed the peak of IgG1 MBC expansion. Additionally, in **Chapter 3.2**, we correlated the increase in Ag-specific IgG or IgA MBCs (ELISpot) with the increase in total IgG or IgA MBCs (flow cytometry). However, no correlation was observed between these two techniques.

Monitoring of the vaccine-induced kinetics in the MBC compartment seems to require an Ag-specific approach, such as ELISpot or flow cytometry with (fluorescently) labeled antigens. These antigens could comprise of fluorescently labeled pathogens or pathogen-derived molecules, tetramers composed of pathogen-derived molecules, of fluorescently labeled Klickmers (multiple identical antigens coupled to a dextran molecule). Both ELISpot and Ag-specific flow cytometry approaches have been reported in studies before, have high potential to be standardized, and can be optimized relatively fast, provided that (labeled) antigens are readily available or can easily be produced.[48-50] When such Ag-specific flow cytometry panels are established, these allow for longitudinal monitoring and immunophenotyping of Ag-specific cells, but also for more exploratory strategies such as BCR repertoire studies of Ag-specific cells. With regards to the work done in **Chapter 3** of this thesis, it would be of interest to evaluate the Ag-specific B-cell response in individuals of different age groups (**Chapter 3.2**). As individuals are expected to encounter Bp multiple times during life, the specific response may change over the course of our lifetime. From a primarily vaccine-based systemic response in children to a mixed vaccine-based/natural encounter-based res-

ponse in adults, where local mucosal immunity may play an important role too. Moreover, based on the studies discussed in **Chapter 3.1** and **Chapter 3.4**, we could get new insights in the longitudinal Ag-specific B-cell response generated after a booster vaccine or bacterial challenge, respectively.

Expansion of IgG1 MBCs observed in **Chapter 3.1**, which correlated with an increase in Ag-specific serum IgG level, was minor when expressed as ratio over baseline (at most 1.9-fold increase). Similar levels of expansion were observed in the innate compartment and T-cell compartment but varied between donors. It can be debated if such minor expansions are biologically relevant, especially when variable between individuals. Although we kept factors known to influence the numbers of circulating cells, such as circadian rhythm, recent plasma or blood donation, or a vaccination unrelated to this study, tightly controlled, there could still be other factors influencing the fluctuation that may not be controlled that easily, such as the season, subclinical infections, undiagnosed co-morbidities, dehydration, the impact of repetitive blood donation within the time of the study, etc. Understanding natural fluctuations of the immune cells can be achieved by inclusion of a cohort of healthy individuals who donate blood at the exact same timepoints without receiving a Tdap booster vaccine at d0, ideally over a time-span that covers all seasons when vaccinated donors were included. By monitoring the natural fluctuations of cell populations, we can be more certain whether observed fluctuations are vaccine-induced or may simply be natural fluctuations. Immune monitoring to evaluate ongoing immune responses - plasma cell response to vaccination

In contrast to MBC monitoring, which requires an Ag-specific approach, we found that the expansion and maturation of plasma cell subsets does correlate with Ag-specific Ig serum levels. In **Chapter 3.1**, the correlation network analysis showed clear correlations between the kinetics of (especially more mature) IgG1, IgG4, and IgA1 plasma cells and vaccine component-specific serum IgGs and IgAs. However, when correlating the increase in total vaccine-specific Ig levels with the increase in plasma cells, this correlation was not considered significant as it did not pass the FDR (false discovery rate) correction. However, in a next study with fewer variables (**Chapter 3.2**), we observed a correlation between the expansion of IgG1 and IgA1 plasma cells (expressed as ratio over baseline) and the vaccine-component specific serum IgGs and IgAs. Thus, the expansion and maturation of plasma cells may be a good indication of ongoing immune responses and a correlate of serological data. Given the function of plasma cells (massive Ig production), their expansion is not surprising and has been reported before, especially the plasma cell expansion at d7 post booster vaccination is a frequent finding.[49, 51-53] However, their monitoring/description is usually limited to the total plasma cell population, or to major classes (IgG, IgA, and IgM plasma cells). The in-depth approach used in this thesis, allowing us to determine the expressed Ig subclass and maturation stage, yields additional information in the induced immune response and difference between individuals. More in-depth knowledge of the induced plasma cell response may be of added



value during the early/exploratory stages of vaccine research. An example hereof is the generation of IgG1 vs IgG4 plasma cells, although both will be identified as 'IgG' plasma cells, the Igs they secrete have different functional capacities regarding complement fixation and binding of FcRs.[54] This may have consequences for the generated immune responses, e.g. when Ag-specific IgG1 and IgG4 would both be present, this may lead to competition for the antigen, and thus may reduce opsonization- and complement-mediated removal of the pathogen. Likewise, generation of IgA1 or IgA2 plasma cells would both be detected as IgA, although they have different chemical and biological properties.

A clear advantage of using plasma cells as biomarker of ongoing immune responses is that the baseline levels of plasma cells are very low. This makes the plasma cell system a relatively 'clean' system, in which an Ag-specific approach is not strictly required to get a fair impression of the ongoing responses. Indeed, when correlating the absolute increase in Ag-specific plasma cells (as determined by ELISpot) with the absolute increase in total plasma cells (as determined by flow cytometry), we found a clear positive correlation between the two methods (Spearman's Ranking Correlation test,  $r \approx 0.6$ ,  $p < 0.0001$ ), indicating complementarity of the two assays (**Chapter 3.2**). Moreover, ELISpot findings have previously been shown to correlate with the levels of Ag-specific serum Igs, albeit with various degrees of correlation.[43, 49] Based on the findings in this thesis, we believe that flow cytometric evaluation of the plasma cell compartment may serve as a worthy, fast, in-depth alternative of plasma cell ELISpot evaluation. Another important conclusion is that the d7 expansion of plasma cells has been reported in various age groups (e.g., children, adolescents, young and older adults), and after various (booster) vaccinations (e.g., rabies, tetanus, pertussis, influenza, and hepatitis B), indicating that this may be a widely applicable biomarker.[17, 49, 51-53] It should be noted however that in several occasions, such as a primary vaccination, the expansion of plasma cells may be delayed. This was shown for rabies vaccination, where plasma cells after primary vaccination were observed at d10, and for vaccination with life-attenuated yellow-fever virus, where plasma cells were observed at d14 after primary vaccination.[52, 55] In contrast, upon primary vaccination with a life-attenuated *Vibrio cholerae* vaccine, plasmablasts were observed at d7 after vaccination.[56] These findings highlight the importance of an initial time-finding study as pilot before starting a large-scale immune monitoring study.

### **Vaccination vs bacterial challenge – *Bordetella pertussis***

In this thesis, we had the opportunity to evaluate the longitudinal kinetics of immune cells after a booster vaccination against Bp and after bacterial challenge with live bacterium (Bp strain B1917). Evaluation of immune cell kinetics after controlled bacterial infection can mimic natural infection but has several advantages over the (retrospective) monitoring of confirmed pertussis cases. The main advantages are (a) known baseline immune status of the individual, (b) defined inoculum dose and time (c) homogenous infection in all individuals regarding pathogen strain, reducing microbiological variation. Moreover, *in vivo* monitoring

may result in additional insights compared to in vitro stimulation experiments, as in this setting, not only the isolated immune cells, but the entire organism is responding to the pathogen. It is true that a human model is more restricted compared to an animal model, for example regarding the type of sampling, and the degree of disease-related symptoms that are tolerated by ethical protocols (in the human model monitored in **Chapter 3.4**, inducing bacterial carriage without Bp disease was the objective). However, no extrapolation to another species is required, and the cohort will much better represent the human population (broader age-range, genetic diversity, and human). Thus, although the human challenge model may have its own limitations, we do believe that it is the best model for monitoring of the immune response to controlled Bp infection. Once fully established, this human challenge model can not only be used to study the infection, colonization, translocation, transmission and/or shedding of Bp in challenged individuals, but also the induced immune responses (protective vs non-protective). More importantly, controlled bacterial challenge could be an important step to evaluate the efficacy of novel Bp vaccine candidates. Before such studies can be performed, the safety and efficacy of the original challenge model should be established. For this model, it was done by de Graaf and colleagues who have published their findings in 2019.[57] In **Chapter 3.4** of this thesis, we add to these findings and describe the induced immune responses in challenged individuals.

We thoroughly compared the immunological responses between individuals receiving a booster vaccine and those who were challenged. In short, differences observed in the generated immune response concerned three major aspects: *timing*, *magnitude*, and *diversity*.

In short, we found that the fluctuations of immune cell subsets following vaccination and bacterial challenge occurred at different time points. Within the innate immune cells in both cases most prominent changes were found in the monocyte compartment, but timing and type of cells differed (for a full description of kinetics, please refer to **Chapter 3.1** and **Chapter 3.4**). After bacterial challenge, we observed a decrease of CD62L<sup>+</sup> cMos and an increase of CD62L<sup>-</sup> cMos, which may indicate activation and maturation of cMos from d1 onwards.[58] After booster vaccination, the earliest sampling point was only at d3. However, another part of the BERT study (B-cell kinetics were discussed in **Chapter 3.2**) focused on the innate immune response and included d1 in the study. Although not available yet, comparison of the kinetics at d1 after booster vaccination and bacterial challenge could lead to new insights in the early cellular immune response.

Moreover, within the B-cell compartment, differences between bacterial challenge and vaccination were the most visible regarding time, magnitude, and diversity. Plasma cell expansion after bacterial challenge was less pronounced (1.6-fold compared to baseline (**Chapter 3.4**)) compared to the vaccination studies, where we observed a 5.4-fold compared to baseline (**Chapter 3.1**) and a 2.6-, 3.0-, 3.4-, and 5.7-fold compared to baseline (**Chapter 3.2**, children, adolescents, young adults, and older adults, respectively)). Moreover, the plasma cell response

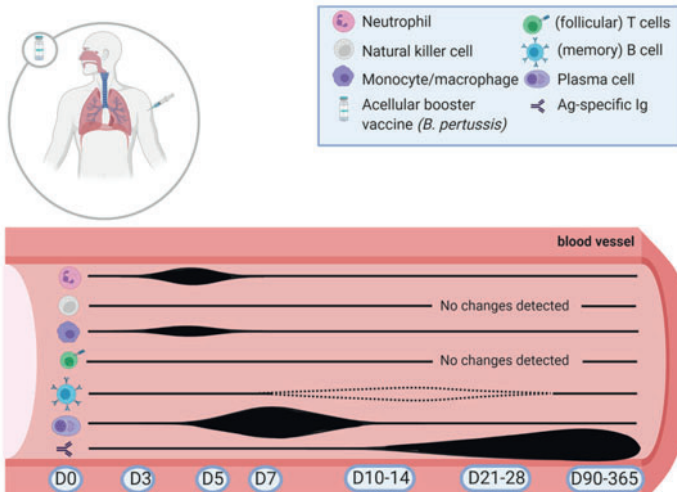
was delayed after bacterial challenge (d11/14) compared to post-vaccination (d7). Lastly, the plasma cell response seemed more diverse (i.e., no strong polarization towards a specific Ig subclass) when compared to the post-vaccination response.

The different kinetics of immune cells between vaccination and bacterial challenge (**Figure 2**) are not surprising, as both models differ in the type of antigen as well as route of administration. In the case of vaccination, a high dose of selected antigens is directly injected into the muscle, which will lead instantly to the recruitment of innate cells and initiate an immune response. In contrast, bacterial challenge may not lead to such instant cell recruitment and activation. In fact, bacterial colonization itself might not be sufficient to induce a systemic (anamnestic) immune response, for which translocation of the bacterium through the mucus layer is required. This may happen at a different pace, or not happen in part of the donors. In **Chapter 3.4** we showed that not all colonized donors showed signs of seroconversion, which may indicate that a systemic response was not initiated (or at least not to the same extent) in every donor with confirmed colonization. Moreover, we found that although the d3 plasma cell peak was most prominent in non-colonized donors, it could also be found in several colonized donors. And the expansion of plasma cells at d11/14 was not unique for colonized donors, although a trend towards higher plasma cell expansion was found in high-density colonized donors. Thus, the link between colonization and systemic immunity may not be as straightforward as we might hope.

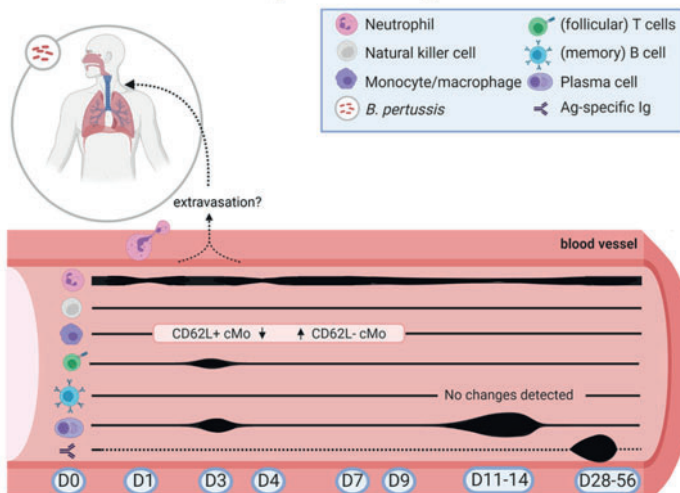
In this thesis, we did not evaluate the (local) mucosal responses. As Bp is transmitted via air droplets and infects the airways, mucosal immunity is expected to play a major role in prevention of infection and transmission. Despite high vaccination coverage the carriage and transmission of Bp persist, which may explain the reported resurgence of pertussis in the last decades.[59-61] I believe that increased mucosal immunity should be an important aim for future Bp vaccine candidates, as this may reduce transmission. The benefit of reduced carriage has already been suggested for other nasopharyngeal-microbe related infectious diseases, such as meningococcal disease and *Haemophilus influenzae* type b.[62, 63] There, intramuscular vaccination resulted in reduced carriage, which was suggested to lead to increased herd immunity/protection because of interrupted transmission. This interrupted transmission was most likely caused by increased mucosal immunity. Indeed, vaccination against meningococcal disease did not

**Figure 2 (next page). Summarizing figure showing the main differences and similarities detected in our studies in a cohort of individuals vaccinated against pertussis or challenged with *Bordetella pertussis*.** (A) Schematic overview of main observed immune cell kinetics in donors that received aP booster vaccination. Of note, in Chapter 3.1 of this PhD thesis, we observed an increase in the number of memory B cells after vaccination, but this was not confirmed in later studies (Chapter 3.2), therefore, this is indicated with dashed lines. Levels of Ag-specific Ig were measured at all time points. (B) Schematic overview of main observed kinetics in donors that were challenged with *Bordetella pertussis*, irrespective of inoculum dose ( $10^4$  or  $10^5$ ). Levels of Ag-specific Ig were only measured at d0 and d28 post-challenge. (C). Schematic overview of main observed kinetics in donors that were not colonized after challenge with *Bordetella pertussis*. Levels of Ag-specific Ig were only measured at d0 and d28 post-challenge.

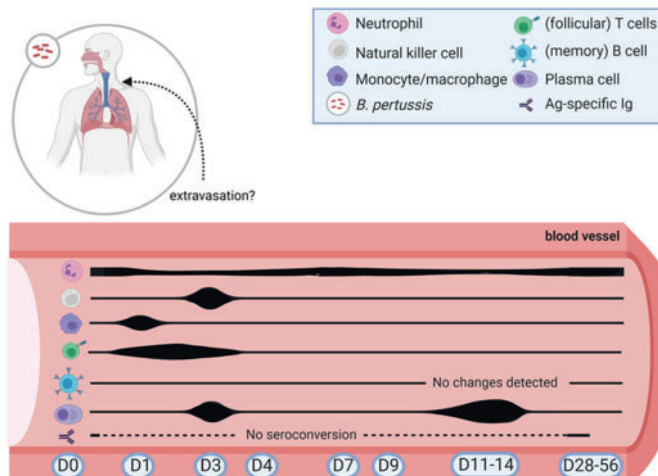
**A Kinetics upon Boostrix vaccination**



**B General kinetics post-challenge**



**C Kinetics individuals not colonized post-challenge**



only reduce carriage, but also lead to an increase in secretory IgG and IgA after booster vaccination, leading to authors to conclude that mucosal immunity was boosted.[64] Although IMI2-PERISCOPE-colleagues have investigated the levels of Igs in the mucosal lining fluid (MLF) of the nose at various time points post bacterial challenge (unpublished data), there was limited overlap between participants, and comparisons between the flow cytometry data and the MLF are yet to be done. Future studies should consider combining both outcomes in the same set of individuals. Aside from data generated in each individual assay, the combination may give insight whether the generated IgA plasma cell response can function as a (surrogate) marker for the generation of local mucosal responses. In addition to this comparison, it would be interesting to add further markers to the flow cytometry panel that increase insight in the origin and/or destination of these generated plasma cells. For example, detection of the joining (J)-chain, which regulates the multimerization of IgM and IgA, could help identify plasma cells that are probably destined to migrate to mucosal surfaces (when associated with J-chain, IgA is secreted as a dimer, which is the typical form in mucosa). [65] Moreover, simultaneous expression of chemokine receptor CCR10 (ligand: CCL28) and integrin receptor  $\alpha 4\beta 1$  (ligand: VCAM1) could indicate homing to the mucosal surfaces.[66] Another way to gain insight in the relationship between the peripheral plasma cells and the mucosal lining Igs, is by comparing the BCR sequences between isolated mucosal Igs and isolated peripheral plasma cells, ideally at several time points following bacterial challenge.

One remaining question is whether the early response observed in donors protected from colonization is indeed protective, and to what extent this information can be used in future studies. To confirm whether a protective response is observed in these individuals, in fact a rechallenge would be required (e.g., an infection-reinfection cohort). As we know that natural infection gives the best protection (compared to wP and aP vaccination)[67, 68], it may be that this controlled infection leads to a similar level of protection. Based on our data, we assume that the early expansion of plasma cell/T cells in the non-colonized donors is associated with protection. When re-challenging the same group of individuals, we would expect a higher number of participants to be protected against colonization, and thus to show this same early expansion of plasma cells/T cells. Moreover, we could compare the BCRs of d11/14 after primary challenge with the BCRs at d3 after re-challenge. If these plasma cells are indeed protective, we would expect (highly) similar BCRs at d3 after re-challenge.

Moreover, although environmental sampling did not reveal any shedding of Bp from the colonized individuals [57], it would be extremely insightful to know if challenged individuals transmit Bp to others. Such efforts are ongoing within the PERISCOPE. These studies may be performed in the clinic or as outpatient study, where challenged individuals are ‘co-housed’ with non-challenged individuals (e.g., housemate or partner, but without contacts with vulnerable individuals, such as the elderly or (unvaccinated) infants). Naturally, the non-challenged individuals should be screened beforehand and give informed consent. By moni-



toring both the challenged and non-challenged individuals, we could investigate whether transmission takes place.

When this challenge model has been fully defined, the next step would be to evaluate (novel) pertussis vaccines in a vaccination-infection model. In such a model, healthy donors would be vaccinated with a new pertussis vaccine candidate, and 1-2 months later they would be challenged with Bp to evaluate the level of protection induced by the vaccine. When combined with immune monitoring, this would lead to better understanding of the mode of action and protection of the vaccine candidate. Aside from the human challenge model that has been established by de Graaf et al., similar efforts are made by Halperin et al. at the Dalhousie University (Nova Scotia, Canada), where a study was initiated in Jan 2022, and is expected to be completed in Nov 2023 (ClinicalTrials.gov identifier (NCT number): NCT05136599). When writing this thesis, no findings have been published on this latter model yet. Both challenge models use a different well-defined clinical isolate (Bp B1917 by de Graaf et al., and Bp D420 by Halperin et al.). These strains are genetically close and a small comparative study in baboons did not observe major differences after challenge with B1917 or D420.[69] To summarize: establishment of a safe and effective human (re)challenge model can have great potential in the evaluation of future pertussis candidate vaccines, as this can be the ultimate way to evaluate the vaccine efficacy and blocking of transmission in a safe, controlled, and ethical manner.

### **Future of vaccines against respiratory diseases – towards induction of mucosal immunity**

In the past years the induction of mucosal immunity to reduce transmission and carriage has been mentioned repeatedly to improve the pertussis vaccines and to reduce the circulation of Bp in the population.

The induction of mucosal immunity may lead to rapid clearance of the pathogen, and thus reduce the replication and transmission of the bacterium. Although this increased clearance may not be a direct benefit for the individual itself (the current vaccines are already effectively preventing disease and mucosal immunity is generated during natural encounters), the transmission to vulnerable groups, such as the elderly, the immunocompromised, and unvaccinated children, may be strongly reduced from the moment of vaccination. Thus, by inducing mucosal immunity already at priming, one is not dependent on natural encounter to generate mucosal immunity and reduce transmission. This may lead to a much faster reduction in circulation of the pathogen.

Multiple studies investigated the induction of mucosal immunity against pertussis in mouse and/or humans (reviewed in [70]). Of these, several candidate vaccines are already being evaluated in humans in phase I/II clinical trials. With the data gathered in this thesis, we hope to provide researchers currently working on novel and improved (pertussis) vaccines with informative timepoints and populations to monitor. I would like to emphasize:

- The importance of time-finding pilot studies, as our data suggested that the induced immune response and its kinetics depend on the route of vaccine administration.
- The potential of longitudinal flow cytometry-based immunophenotyping for in-depth investigation of the ongoing cellular immune responses to supplement current approaches
- That in the case of vaccination studies, especially monitoring of the innate immune cells and the plasma cell compartment may be a quick and informative tool, whereas monitoring of MBCs and T cells would require an Ag-specific approach.

Lastly, I strongly recommend researchers to make efforts to increase the (sample, and thus final) quality and reproducibility of their work, for example by introducing standardized (multi-center validated) SOPs and to be transparent in their cohort selection and data analysis strategies.

### References

1. Lee JA, Spidlen J, Boyce K, et al. MIFlowCyt: the minimum information about a Flow Cytometry Experiment. *Cytometry Part A: the journal of the International Society for Analytical Cytology* 2008; 73: 926-930.
2. Amir E-aD, Lee B, Badoual P, et al. Development of a comprehensive antibody staining database using a standardized analytics pipeline. *Frontiers in immunology* 2019; 1315.
3. Kalina T, Bakardjieva M, Blom M, et al. EuroFlow standardized approach to diagnostic immunophenotyping of severe PID in newborns and young children. *Frontiers in immunology* 2020; 11: 371.
4. Kalina T, Flores-Montero J, Van Der Velden V, et al. EuroFlow standardization of flow cytometer instrument settings and immunophenotyping protocols. *Leukemia* 2012; 26: 1986-2010.
5. Kalina T, Flores-Montero J, Lecomte Q, et al. Quality assessment program for EuroFlow protocols: Summary results of four-year (2010–2013) quality assurance rounds. *Cytometry Part A* 2015; 87: 145-156.
6. Pitoiset F, Cassard L, El Soufi K, et al. Deep phenotyping of immune cell populations by optimized and standardized flow cytometry analyses. *Cytometry Part A* 2018; 93: 793-802.
7. Finak G, Langweiler M, Jaimes M, et al. Standardizing flow cytometry immunophenotyping analysis from the human immunophenotyping consortium. *Scientific reports* 2016; 6: 1-11.
8. Pedreira C, da Costa ES, Lecomte Q, et al. From big flow cytometry datasets to smart diagnostic strategies: The EuroFlow approach. *Journal of immunological methods* 2019; 475: 112631.
9. Streitz M, Miloud T, Kapinsky M, et al. Standardization of whole blood immune phenotype monitoring for clinical trials: panels and methods from the ONE study. *Transplantation research* 2013; 2: 1-15.
10. Alexander T, Bondanza A, Muraro P, et al. SCT for severe autoimmune diseases: consensus guidelines of the European Society for Blood and Marrow Transplantation for immune monitoring and biobanking. *Bone marrow transplantation* 2015; 50: 173-180.
11. Sędek Ł, Flores-Montero J, van der Sluijs A, et al. Impact of Pre-Analytical and Analytical Variables Associated with Sample Preparation on Flow Cytometric Stainings Obtained with EuroFlow Panels. *Cancers* 2022; 14: 473.
12. Botafogo V, Pérez-Andres M, Jara-Acevedo M, et al. Age distribution of multiple function-

nally relevant subsets of CD4+ T cells in human blood using a standardized and validated 14-color euroflow immune monitoring tube. *Frontiers in immunology* 2020; 11: 166.

13. Flores-Montero J, Grigore G, Fluxá R, et al. EuroFlow Lymphoid Screening Tube (LST) data base for automated identification of blood lymphocyte subsets. *Journal of immunological methods* 2019; 475: 112662.
14. Lhermitte L, Barreau S, Morf D, et al. Automated identification of leukocyte subsets improves standardization of database-guided expert-supervised diagnostic orientation in acute leukemia: a EuroFlow study. *Modern Pathology* 2021; 34: 59-69.
15. Lhermitte L, Mejstrikova E, Van Der Sluijs-Gelling A, et al. Automated database-guided expert-supervised orientation for immunophenotypic diagnosis and classification of acute leukemia. *Leukemia* 2018; 32: 874-881.
16. Van der Burg M, Kalina T, Perez-Andres M, et al. The EuroFlow PID orientation tube for flow cytometric diagnostic screening of primary immunodeficiencies of the lymphoid system. *Frontiers in immunology* 2019; 10: 246.
17. Diks AM, Overduin LA, Van Leenen LD, et al. B-Cell Immunophenotyping to Predict Vaccination Outcome in the Immunocompromised-A Systematic Review. *Frontiers in immunology* 2021: 3524.
18. Blanco E, Pérez-Andrés M, Arriba-Méndez S, et al. Age-associated distribution of normal B-cell and plasma cell subsets in peripheral blood. *Journal of Allergy and Clinical Immunology* 2018; 141: 2208-2219. e2216.
19. Besci Ö, Başer D, ÖĞÜLÜR İ, et al. Reference values for T and B lymphocyte subpopulations in Turkish children and adults. *Turkish journal of medical sciences* 2021; 51: 1814-1824.
20. Hu Z, Jujjavarapu C, Hughey JJ, et al. MetaCyto: a tool for automated meta-analysis of mass and flow cytometry data. *Cell reports* 2018; 24: 1377-1388.
21. Troussard X, Cornet E, Bardet V, et al. Full blood count normal reference values for adults in France. *Journal of clinical pathology* 2014; 67: 341-344.
22. Bhattacharya S, Dunn P, Thomas CG, et al. ImmPort, toward repurposing of open access immunological assay data for translational and clinical research. 2018; 5: 1-9.
23. Hartmann FJ, Bendall SC. Immune monitoring using mass cytometry and related high-dimensional imaging approaches. *Nature Reviews Rheumatology* 2020; 16: 87-99.
24. Melsen JE, van Ostaijen-Ten Dam MM, Lankester AC, Schilham MW, van den Akker EB. A comprehensive workflow for applying single-cell clustering and pseudotime analysis to flow cytometry data. *The Journal of Immunology* 2020; 205: 864-871.
25. Höllt T, Pezzotti N, van Unen V, et al. Cytosplore: Interactive immune cell phenotyping for large single-cell datasets. *Computer Graphics Forum: Wiley Online Library*; 2016. p. 171-180.
26. Palit S, Heuser C, De Almeida GP, Theis FJ, Zielinski CE. Meeting the challenges of high-dimensional single-cell data analysis in immunology. *Frontiers in immunology* 2019; 10: 1515.
27. Cheung M, Campbell JJ, Whitby L, Thomas RJ, Braybrook J, Petzing J. Current trends in flow cytometry automated data analysis software. *Cytometry Part A* 2021; 99: 1007-1021.
28. Sims R, Van Der Lee SJ, Naj AC, et al. Rare coding variants in PLCG2, ABI3, and TREM2 implicate microglial-mediated innate immunity in Alzheimer's disease. *Nature genetics* 2017; 49: 1373-1384.
29. van der Lee SJ, Conway OJ, Jansen I, et al. A nonsynonymous mutation in PLCG2 reduces the risk of Alzheimer's disease, dementia with Lewy bodies and frontotemporal dementia, and increases the likelihood of longevity. *Acta neuropathologica* 2019; 138: 237-250.
30. Strickland SL, Morel H, Prusinski C, et al. Association of ABI3 and PLCG2 missense variants with disease risk and neuropathology in Lewy body disease and progressive supranuclear palsy. *Acta neuropathologica communications* 2020; 8: 1-12.
31. Chen F, Zhang Y, Wang L, et al. PLCG2 rs72824905 Variant Reduces the Risk of Alzheimer's Disease and Multiple Sclerosis. *Journal of Alzheimer's Disease* 2021: 1-7.
32. Bouzid H, Belk J, Jan M, et al. Clonal Hematopoiesis is Associated with Reduced Risk of Alzheimer's Disease. *Blood* 2021; 138: 5.
33. Abud EM, Ramirez RN, Martinez ES, et al. iPSC-derived human microglia-like cells to study neurological diseases. *Neuron* 2017; 94: 278-293. e279.
34. Sevigny J, Chiao P, Bussière T, et al. The antibody aducanumab reduces A $\beta$  plaques in Alzheimer's disease. *Nature immunology* 2016; 537: 50-56.
35. Tolar M, Abushakra S, Hey JA, Porsteinsson A, Sabbagh M. Aducanumab, gantenerumab,

- BAN2401, and ALZ-801—the first wave of amyloid-targeting drugs for Alzheimer’s disease with potential for near term approval. *Alzheimer's research therapy* 2020; 12: 1-10.
36. Congdon EE, Sigurdsson EM. Tau-targeting therapies for Alzheimer disease. *Nature Reviews Neurology* 2018; 14: 399-415.
  37. Milner JD. PLAID: a syndrome of complex patterns of disease and unique phenotypes. *Journal of clinical immunology* 2015; 35: 527-530.
  38. Ombrello MJ, Remmers EF, Sun G, et al. Cold urticaria, immunodeficiency, and autoimmunity related to PLCG2 deletions. *New England Journal of Medicine* 2012; 366: 330-338.
  39. Roush SW, Murphy TV, Group V-PDTW. Historical comparisons of morbidity and mortality for vaccine-preventable diseases in the United States. *Jama* 2007; 298: 2155-2163.
  40. Plotkin SA. Correlates of protection induced by vaccination. *Clinical vaccine immunology* 2010; 17: 1055-1065.
  41. Plotkin SA. Complex correlates of protection after vaccination. *Clinical infectious diseases* 2013; 56: 1458-1465.
  42. Lin A, Apostolovic D, Jahnmatz M, et al. Live attenuated pertussis vaccine BPZE1 induces a broad antibody response in humans. *The Journal of clinical investigation* 2020; 130: 2332-2346.
  43. Buisman A, De Rond C, Öztürk K, Ten Hulscher H, Van Binnendijk R. Long-term presence of memory B-cells specific for different vaccine components. *Vaccine* 2009; 28: 179-186.
  44. Jackson LA, Anderson EJ, Roupael NG, et al. An mRNA vaccine against SARS-CoV-2—preliminary report. *New England Journal of Medicine* 2020.
  45. Sadoff J, Le Gars M, Shukarev G, et al. Interim results of a phase 1–2a trial of Ad26. COV2. S Covid-19 vaccine. *New England Journal of Medicine* 2021; 384: 1824-1835.
  46. da Silva Antunes R, Soldevila F, Pomaznoy M, et al. A system-view of Bordetella pertussis booster vaccine responses in adults primed with whole-cell versus acellular vaccine in infancy. *JCI insight* 2021; 6.
  47. Querec TD, Akondy RS, Lee EK, et al. Systems biology approach predicts immunogenicity of the yellow fever vaccine in humans. *Nature immunology* 2009; 10: 116-125.
  48. Slota M, Lim J-B, Dang Y, Disis ML. ELISpot for measuring human immune responses to vaccines. *Expert review of vaccines* 2011; 10: 299-306.
  49. Tian C, Chen Y, Liu Y, et al. Use of ELISpot assay to study HBs-specific B cell responses in vaccinated and HBV infected humans. *Emerging Microbes Infections* 2018; 7: 1-10.
  50. Kerkman PF, Fabre E, van der Voort EI, et al. Identification and characterisation of citrullinated antigen-specific B cells in peripheral blood of patients with rheumatoid arthritis. *Annals of the rheumatic diseases* 2016; 75: 1170-1176.
  51. Ellebedy AH, Jackson KJ, Kissick HT, et al. Defining antigen-specific plasmablast and memory B cell subsets in human blood after viral infection or vaccination. *Nature immunology* 2016; 17: 1226-1234.
  52. Blanchard-Rohner G, Pulickal AS, Jol-van der Zijde CM, Snape MD, Pollard AJ. Appearance of peripheral blood plasma cells and memory B cells in a primary and secondary immune response in humans. *Blood, The Journal of the American Society of Hematology* 2009; 114: 4998-5002.
  53. Frölich D, Giesecke C, Mei HE, et al. Secondary immunization generates clonally related antigen-specific plasma cells and memory B cells. *The Journal of Immunology* 2010; 185: 3103-3110.
  54. Vidarsson G, Dekkers G, Rispens T. IgG subclasses and allotypes: from structure to effector functions. *Frontiers in immunology* 2014; 5: 520.
  55. Sandberg JT, Ols S, Löfling M, et al. Activation and kinetics of circulating T follicular helper cells, specific plasmablast response, and development of neutralizing antibodies following yellow fever virus vaccination. 2021; 207: 1033-1043.
  56. Adekunle O, Dretler A, Kauffman RC, Cho A, Roupael N, Wrammert JJPNTD. Longitudinal analysis of human humoral responses after vaccination with a live attenuated *V. cholerae* vaccine. 2021; 15: e0009743.
  57. de Graaf H, Ibrahim M, Hill AR, et al. Controlled human infection with Bordetella pertussis induces asymptomatic, immunizing colonization. *Clinical Infectious Diseases* 2020; 71: 403-411.
  58. Damasceno D, Teodosio C, van den Bossche WB, et al. Distribution of subsets of blood monocytic cells throughout life. *Journal of Allergy and Clinical Immunology* 2019; 144: 320-323. e326.
  59. Tan T, Dalby T, Forsyth K, et al. Pertussis across the globe: recent epidemiologic trends from 2000 to 2013. *The Pediatric infectious disease journal* 2015; 34: e222-e232.
  60. De Greeff SC, De Melker HE, Van Gageldonk PG, et al. Seroprevalence of pertussis in The

- Netherlands: evidence for increased circulation of *Bordetella pertussis*. *PLoS one* 2010; 5: e14183.
61. Heininger U, André P, Chlibek R, et al. Comparative epidemiologic characteristics of pertussis in 10 central and eastern European countries, 2000-2013. *PLoS One* 2016; 11: e0155949.
  62. Balmer P, Burman C, Serra L, York LJ. Impact of meningococcal vaccination on carriage and disease transmission: a review of the literature. *Human Vaccines & Immunotherapeutics* 2018; 14: 1118-1130.
  63. Takala A, Santosham M, Almeida-Hill J, Wolff M. Vaccination with *Haemophilus influenzae* type b meningococcal protein conjugate vaccine reduces. *Pediatric Infectious Disease Journal* 1993; 12: 593-599.
  64. Zhang Q, Choo S, Everard J, Jennings R, Finn A. Mucosal immune responses to meningococcal group C conjugate and group A and C polysaccharide vaccines in adolescents. *Infection immunity* 2000; 68: 2692-2697.
  65. Castro CD, Flajnik MF. Putting J chain back on the map: how might its expression define plasma cell development? *The Journal of Immunology* 2014; 193: 3248-3255.
  66. Kunkel EJ, Butcher EC. Plasma-cell homing. *Nature Reviews Immunology* 2003; 3: 822-829.
  67. Wendelboe AM, Van Rie A, Salmaso S, Englund JA, Tjebk. Duration of immunity against pertussis after natural infection or vaccination. 2005; 24: S58-S61.
  68. Warfel JM, Zimmerman LI, Merkel TJ, Poterucha A. Acellular pertussis vaccines protect against disease but fail to prevent infection and transmission in a nonhuman primate model. 2014; 111: 787-792.
  69. Naninck T, Coutte L, Mayet C, et al. In vivo imaging of bacterial colonization of the lower respiratory tract in a baboon model of *Bordetella pertussis* infection and transmission. *Scientific reports* 2018; 8: 1-11.
  70. Dubois V, Loch C. Mucosal Immunization Against Pertussis: Lessons From the Past and Perspectives. *Frontiers in immunology (Review)*. 2021; 12.





## **Appendices**

**Appendix 1**

**Appendix 2**

**Summary**

**Samenvatting**

**Curriculum Vitae**

**List of Publications**

**Acknowledgements**

**APPENDIX 1. Overview of the EuroFlow panels and versions used in this thesis.**

For transparency within this PhD thesis and convenience of the reader only!  
When citing, please refer to the original publications instead of this appendix!

**Table 1. EuroFlow Primary immunodeficiency orientation tube (PIDOT). Version 1**  
Official references for this panel: van der Burg M, Kalina T, Perez-Andres M, et al. The EuroFlow PID Orientation Tube for Flow Cytometric Diagnostic Screening of Primary Immunodeficiencies of the Lymphoid System. *Frontiers in Immunology* 2019;10:246.

| Marker | Fluorochrome | Clone  | Source          | Cat. number | Volume (µL) | Membrane                       | Intracellular             |
|--------|--------------|--------|-----------------|-------------|-------------|--------------------------------|---------------------------|
| CD27   | BV421        | M-T271 | BD Biosciences  | 562513      | 1           | all added to membrane staining | no intracellular staining |
| CD45RA | BV510        | HI100  | BD Biosciences  | 563031      | 2.5         |                                |                           |
| CD8    | FITC         | SKI    | BD Biosciences  | 345772      | 5           |                                |                           |
| IgD    | FITC         | IA6-2  | BioLegend       | 348205      | 1.25        |                                |                           |
| CD16   | PE           | 3G8    | BD Biosciences  | 555407      | 5           |                                |                           |
| CD56   | PE           | C5-9   | Cytognos        | CYT-56PE    | 5           |                                |                           |
| CD4    | PerCP Cy5.5  | SK3    | BD Biosciences  | 332772      | 7           |                                |                           |
| IgM    | PerCP Cy5.5  | MHM-88 | BioLegend       | 314511      | 2           |                                |                           |
| CD19   | PE-Cy7       | J3-119 | Beckman Coulter | IM3628      | 5           |                                |                           |
| TCRγδ  | PE-Cy7       | 11F2   | BD Biosciences  | 649806      | 1           |                                |                           |
| CD3    | APC          | SK7    | BD Biosciences  | 345767      | 2.5         |                                |                           |
| CD45   | APC-H7       | 2D1    | BD Biosciences  | 641417      | 2           |                                |                           |

**Table 2. EuroFlow Primary immunodeficiency orientation tube (PIDOT). Version 2 – lyophilized version of the PIDOT with 2 drop-in antibodies (CD27 BV421 and CD45RA BV510). In the lyophilized version, different clones were used for CD8, IgD, CD4, TCR $\gamma\delta$ , CD3, and CD45. Fluorochromes stayed the same, with exception of CD45, where APC H7 was replaced by APC C750**

Official references for this panel: van der Burg M, Kalina T, Perez-Andres M, et al. The EuroFlow PID Orientation Tube for Flow Cytometric Diagnostic Screening of Primary Immunodeficiencies of the Lymphoid System. *Frontiers in Immunology* 2019;10:246.

| Marker             | Fluorochrome | Clone  | Source   | Cat. number  | Volume ( $\mu$ L) | Membrane                       | Intracellular             |
|--------------------|--------------|--------|----------|--------------|-------------------|--------------------------------|---------------------------|
| CD27               | BV421        | M-T271 | Cytognos | CYT-PIDOT8-R | 1                 | all added to membrane staining | no intracellular staining |
| CD45RA             | BV510        | HI100  |          |              | 2.5               |                                |                           |
| CD8                | FITC         | UCHT-4 |          |              | 50                |                                |                           |
| IgD                | FITC         | IADB6  |          |              |                   |                                |                           |
| CD16               | PE           | 3G8    |          |              |                   |                                |                           |
| CD56               | PE           | C5.9   |          |              |                   |                                |                           |
| CD4                | PerCP Cy5.5  | RPA-T4 |          |              |                   |                                |                           |
| IgM                | PerCP Cy5.5  | MHM-88 |          |              |                   |                                |                           |
| CD19               | PE-Cy7       | J3-119 |          |              |                   |                                |                           |
| TCR $\gamma\delta$ | PE-Cy7       | TCR-1  |          |              |                   |                                |                           |
| CD3                | APC          | UCHT-1 |          |              |                   |                                |                           |
| CD45               | APC-C750     | HI30   |          |              |                   |                                |                           |

**Table 3. EuroFlow PERISCOPE B-cell and plasma cell panel (BIGH) panel, version 1**

Official references for this panel: Blanco E, Pérez-Andrés M, Arriba-Méndez S, et al. Age-associated distribution of normal B-cell and plasma cell subsets in peripheral blood. *JACI* 2018;141(6):2208-2219. e2216. Diks AM, Versteegen P, Teodosio C, et al. Age and Primary Vaccination Background Influence the Plasma Cell Response to Pertussis Booster Vaccination. *Vaccines*. 2022;10(2):136. Patent filed by Van Dongen et al. Means and Methods for Multiparameter Cytometry-Based Leukocyte Subsetting. P119646NLOO (2019). PCT/NL2020/050688, priority date 5 November 2019.

| Marker | Fluorochrome | Clone   | Source         | Cat. number | Volume (µL)    | Membrane | Intracellular |
|--------|--------------|---------|----------------|-------------|----------------|----------|---------------|
| CD27   | BV421        | M-T271  | BD Biosciences | 562513      | 2              |          |               |
| IgM    | BV510        | MHM-88  | BioLegend      | 314522      | 2              |          | X             |
| CD62L  | BV605        | DREG-56 | BioLegend      | 304833      | 5              |          |               |
| CD24   | BV650        | ML5     | BD Biosciences | 563720      | 5              |          |               |
| CD21   | BV711        | B-Ly4   | BD Biosciences | 563163      | 5              |          |               |
| CD19   | BV786        | SJ25C1  | BD Biosciences | 563163      | 4              |          |               |
| IgG3   | FITC         | SAG3    | Cytognos       | CYT-IGG3F   | 3              |          | X             |
| IgG2   | FITC         | SAG2    | Cytognos       | CYT-IGG2F   | 3              |          | X             |
| IgA2   | PerCP Cy5-5  | SAA2    | Cytognos       | CYT-IGA1C   | 3              |          | X             |
| IgA1   | PerCP Cy5-5  | SAA1    | Cytognos       | CYT-IGA2C   | 3              |          | X             |
| IgG1   | PE           | SAG1    | Cytognos       | CYT-IGG1PE  | 3              |          | X             |
| IgG2   | PE           | SAG2    | Cytognos       | CYT-IGG2PE  | 3              |          | X             |
| IgG4   | APC          | SAG4    | Cytognos       | CYT-IGG4AP  | 3              |          | X             |
| IgA1   | APC          | SAA1    | Cytognos       | CYT-IGA1AP  | 3              |          | X             |
| IgD    | FITC         | IA6-2   | BioLegend      | 348205      | 1.25           |          | X             |
| CD20   | PE CF594     | 2H7     | BD Biosciences | 562295      | 2.5 (1:10 dil) |          |               |
| CD138  | PE-Cy7       | MI15    | BioLegend      | 356513      | 5              |          |               |
| CD5    | PE-Cy7       | LIF7F12 | BD Biosciences | 348810      | 6              |          |               |
| IgD    | APC          | IA6-2   | BD Biosciences | 561303      | 4              |          | X             |
| CD38   | APC H7       | HB7     | BD Biosciences | 656646      | 3              |          |               |



**Table 4. EuroFlow PERISCOPE B-cell and plasma cell panel (BIGH) panel, version 2 – replacement of single/individual Ig antibodies by lyophilized Ig subclass cocktail**

Official references for this panel: Blanco E, Pérez-Andrés M, Arriba-Méndez S, et al. Age-associated distribution of normal B-cell and plasma cell subsets in peripheral blood. *JACI* 2018;141(6):2208-2219. e2216. Dijs AM, Versteegen P, Teodosio C, et al. Age and Primary Vaccination Background Influence the Plasma Cell Response to Pertussis Booster Vaccination. *Vaccines*. 2022;10(2):136. Patent filed by Van Dongen et al. Means and Methods for Multiparameter Cytometry-Based Leukocyte Subsetting. P119646NL00 (2019). PCT/NL2020/050688, priority date 5 November 2019.

| Marker              | Fluorochrome                                    | Clone   | Source         | Cat. number | Volume (µL)    | Membrane                       | Intracellular |
|---------------------|---|---------|----------------|-------------|----------------|--------------------------------|---------------|
| CD27                | BV421   | M-T271  | BD Biosciences | 562513      | 2              |                                |               |
| IgM                 | BV510   | MHM-88  | BioLegend      | 314522      | 2              |                                | X             |
| CD62L               | BV605   | DREG-56 | BioLegend      | 304833      | 5              |                                |               |
| CD24                | BV650   | ML5     | BD Biosciences | 563720      | 5              |                                |               |
| CD21                | BV711   | B-Ly4   | BD Biosciences | 563163      | 5              |                                |               |
| CD19                | BV786   | SJ25C1  | BD Biosciences | 563163      | 4              |                                |               |
| Subclasses cocktail | Fluorochromes and clones identical to version 1 |         | Cytognos       | CYT-IGS-1   | 25             | all added to membrane staining | X             |
| IgD                 | FITC  | IA6-2   | BioLegend      | 348205      | 1.25           |                                | X             |
| CD20                | PE CF594  | 2H7     | BD Biosciences | 562295      | 2.5 (1:10 dil) |                                |               |
| CD138               | PE-Cy7  | MI15    | BioLegend      | 356513      | 5              |                                |               |
| CD5                 | PE-Cy7  | LIF7F12 | BD Biosciences | 348810      | 6              |                                |               |
| IgD                 | APC   | IA6-2   | BD Biosciences | 561303      | 4              |                                | X             |
| CD38                | APC H7  | HB7     | BD Biosciences | 656646      | 3              |                                |               |

**Table 5. EuroFlow PERISCOPE B-cell and plasma cell panel (BIGH) panel, version 3 - addition of CD45 AF700**

Official references for this panel: Blanco E, Pérez-Andrés M, Arriba-Méndez S, et al. Age-associated distribution of normal B-cell and plasma cell subsets in peripheral blood. JACI 2018;141(6):2208-2219. e2216. Diks AM, Versteegen P, Teodosio C, et al. Age and Primary Vaccination Background Influence the Plasma Cell Response to Pertussis Booster Vaccination. Vaccines. 2022;10(2):136. Patent filed by Van Dongen et al. Means and Methods for Multiparameter Cytometry-Based Leukocyte Subsetting. P119646NLOO (2019). PCT/NL2020/050688, priority date 5 November 2019.

| Marker              | Fluorochrome                                    | Clone   | Source         | Cat. number | Volume (µL)    | Membrane                       | Intracellular |
|---------------------|---|---------|----------------|-------------|----------------|--------------------------------|---------------|
| CD27                | BV421   | M-T271  | BD Biosciences | 562513      | 2              |                                |               |
| IgM                 | BV510   | MHM-88  | BioLegend      | 314522      | 2              |                                | X             |
| CD62L               | BV605   | DREG-56 | BioLegend      | 304833      | 5              |                                |               |
| CD24                | BV650   | ML5     | BD Biosciences | 563720      | 5              |                                |               |
| CD21                | BV711   | B-Ly4   | BD Biosciences | 563163      | 5              |                                |               |
| CD19                | BV786   | SJ25C1  | BD Biosciences | 563163      | 4              |                                |               |
| Subclasses cocktail | Fluorochromes and clones identical to version 1 |         | Cytognos       | CYT-IGS-1   | 25             | all added to membrane staining | X             |
| IgD                 | FITC  | IA6-2   | BioLegend      | 348205      | 1.25           |                                | X             |
| CD20                | PE CF594  | 2H7     | BD Biosciences | 562295      | 2.5 (1:10 dil) |                                |               |
| CD138               | PE-Cy7  | MI15    | BioLegend      | 356513      | 5              |                                |               |
| CD5                 | PE-Cy7  | LIF7F12 | BD Biosciences | 348810      | 6              |                                |               |
| IgD                 | APC   | IA6-2   | BD Biosciences | 561303      | 4              |                                | X             |
| CD45                | AF700   | HI30    | BD Biosciences | 560566      | 10             |                                |               |
| CD38                | APC H7  | HB7     | BD Biosciences | 656646      | 3              |                                |               |

**Table 6. EuroFlow PERISCOPE CD4 T-cell (TCD4) panel, version 1**

Official references for this panel: Botafogo V, Pérez-Andrés M, Jara-Acevedo M, et al. Age distribution of multiple functionally relevant subsets of CD4+ T cells in human blood using a standardized and validated 14-color EuroFlow immune monitoring tube. *Frontiers in Immunology*. 2020;11:166. Patent filed by Van Dongen et al. Means and Methods for Multiparameter Cytometry-Based Leukocyte Subsetting. P119646NLOO (2019). PCT/NL2020/050688, priority date 5 November 2019.

| Marker | Fluorochrome   | Clone     | Source         | Cat. number | Volume (µL) | Membrane                       | Intracellular             |
|--------|----------------|-----------|----------------|-------------|-------------|--------------------------------|---------------------------|
| CD27   | BV421          | M-T271    | BD Biosciences | 562513      | 2           | All added to membrane staining | No intracellular staining |
| CD45RA | BV510          | HI100     | BD Biosciences | 563031      | 2.5         |                                |                           |
| CD62L  | BV650          | DREG-56   | BioLegend      | 304832      | 2.5         |                                |                           |
| CD127  | BV711          | HIL7RM21  | BD Biosciences | 563165      | 2.5         |                                |                           |
| CD3    | BV786          | SK7       | BD Biosciences | 563800      | 1           |                                |                           |
| CD25   | FITC VioBright | 4E3       | Miltenyi       | 130-104-323 | 10          |                                |                           |
| CCR10  | PerCP Cy5.5    | 1B5       | BD Biosciences | 564772      | 2.5         |                                |                           |
| CXCR3  | PE             | 1C6/CXCR3 | BD Biosciences | 557185      | 10          |                                |                           |
| CCR6   | PE-CF594       | 11A9      | BD Biosciences | 564816      | 5           |                                |                           |
| CCR4   | PE-Cy7         | L291H4    | BioLegend      | 359410      | 1           |                                |                           |
| CXCR5* | APC            | 51505     | R&D            | FAB190A-100 | 10          |                                |                           |
| CD4    | APC H7         | SK3       | BD Biosciences | 641398      | 5           |                                |                           |

\*EuroFlow PERISCOPE CD4 T-cell (TCD4) panel, version 1a - replacement of CXCR5 from R&D by CXCR5 from Miltenyi (panel switch while studies ongoing)

| Marker | Fluorochrome | Clone  | Source   | Cat. number | Volume (µL) | Membrane | Intracellular |
|--------|--------------|--------|----------|-------------|-------------|----------|---------------|
| CXCR5  | APC          | REA103 | Miltenyi | 130-098-422 | 2.5         | X        |               |

**Table 7. EuroFlow PERISCOPE CD4 T-cell (TCD4) panel, version 2 - addition of CD45 AF700 and CD154 BV605**

Official references for this panel: Botafogo V, Pérez-Andrés M, Jara-Acevedo M, et al. Age distribution of multiple functionally relevant subsets of CD4+ T cells in human blood using a standardized and validated 14-color EuroFlow immune monitoring tube. *Frontiers in Immunology*. 2020;11:166. Patent filed by Van Dongen et al. Means and Methods for Multiparameter Cytometry-Based Leukocyte Subsetting. P119646NL00 (2019). PCT/NL2020/050688, priority date 5 November 2019.

| Marker | Fluorochrome   | Clone     | Source         | Cat. number | Volume (µL) | Membrane                              | Intracellular |
|--------|----------------|-----------|----------------|-------------|-------------|---------------------------------------|---------------|
| CD27   | BV421          | M-T271    | BD Biosciences | 562513      | 2           |                                       |               |
| CD45RA | BV510          | HI100     | BD Biosciences | 563031      | 2.5         |                                       |               |
| CD154  | BV605          | 24-31     | BioLegend      | 310826      | 5           |                                       | X             |
| CD62L  | BV650          | DREG-56   | BioLegend      | 304832      | 2.5         |                                       |               |
| CD127  | BV711          | HIL7RM21  | BD Biosciences | 563165      | 2.5         |                                       |               |
| CD3    | BV786          | SK7       | BD Biosciences | 563800      | 1           |                                       |               |
| CD25   | FITC VioBright | 4E3       | Miltenyi       | 130-104-323 | 10          |                                       |               |
| CCR10  | PerCP Cy5.5    | 1B5       | BD Biosciences | 564772      | 2.5         | All antibodies except for CD154 BV605 |               |
| CXCR3  | PE             | 1C6/CXCR3 | BD Biosciences | 557185      | 10          |                                       |               |
| CCR6   | PE-CF594       | 11A9      | BD Biosciences | 564816      | 5           |                                       |               |
| CCR4   | PE-Cy7         | L291H4    | BioLegend      | 359410      | 1           |                                       |               |
| CXCR5* | APC            | 51505     | R&D            | FAB190A-100 | 10          |                                       |               |
| CD45   | AF700          | HI30      | BD Biosciences | 560566      | 2.5         |                                       |               |
| CD4    | APC H7         | SK3       | BD Biosciences | 641398      | 5           |                                       |               |

\*EuroFlow PERISCOPE CD4 T-cell (TCD4) panel, version 1a - replacement of CXCR5 from R&D by CXCR5 from Miltenyi (panel switch while studies ongoing)

| Marker | Fluorochrome | Clone  | Source   | Cat. number | Volume (µL) | Membrane | Intracellular |
|--------|--------------|--------|----------|-------------|-------------|----------|---------------|
| CXCR5  | APC          | REA103 | Miltenyi | 130-098-422 | 2.5         | X        |               |

**Table 8. EuroFlow PERISCOPE CD8 cytotoxic T-cell (CYTOX) panel, version 1**  
 Official reference for this panel: Patent filed by Van Dongen et al. Means and Methods for Multiparameter Cytometry-Based Leukocyte Subsetting. P119646NL00 (2019). PCT/NL2020/050688, priority date 5 November 2019.

| Marker     | Fluorochrome | Clone   | Source         | Cat. number | Volume (µL) | Membrane | Intracellular |
|------------|--------------|---------|----------------|-------------|-------------|----------|---------------|
| CD27       | BV421        | M-T271  | BD Biosciences | 562513      | 2           | X        |               |
| CD45RA     | BV510        | HI100   | BD Biosciences | 563031      | 2.5         | X        |               |
| CD62L      | BV650        | DREG-56 | BioLegend      | 304832      | 2.5         | X        |               |
| CD16       | BV711        | 3G8     | BD Biosciences | 563127      | 2.5         | X        |               |
| CD3        | BV786        | SK7     | BD Biosciences | 563800      | 1           | X        |               |
| CD57       | FITC         | HNK1    | BD Biosciences | 333169      | 10          | X        |               |
| CD28       | PerCP Cy5.5  | CD28.2  | BioLegend      | 302922      | 5           | X        |               |
| Granzyme B | PE           | GB11    | Sanquin        | M2289       | 15          |          | X             |
| CD8        | PE CF594     | RPAT8   | BD Biosciences | 562282      | 1           | X        |               |
| TCRγδ      | PE Cy7       | 11F2    | BD Biosciences | 655410      | 1           | X        |               |
| CD56       | APC H7       | HCD56   | BioLegend      | 318332      | 5           | X        |               |



**Table 9. EuroFlow PERISCOPE CD8 cytotoxic T-cell (CYTOX) panel, version 2 - addition of CD45 AF700 and CD154 BV605**  
 Official reference for this panel: Patent filed by Van Dongen et al. Means and Methods for Multiparameter Cytometry-Based Leukocyte Subsetting. P119646NL00 (2019). PCT/NL2020/050688, priority date 5 November 2019.

| Marker     | Fluorochrome | Clone   | Source         | Cat. number | Volume (µL) | Membrane | Intracellular |
|------------|--------------|---------|----------------|-------------|-------------|----------|---------------|
| CD27       | BV421        | M-T271  | BD Biosciences | 562513      | 2           | X        |               |
| CD45RA     | BV510        | HI100   | BD Biosciences | 563031      | 2-5         | X        |               |
| CD154      | BV605        | 24-31   | BioLegend      | 310826      | 5           |          | X             |
| CD62L      | BV650        | DREG-56 | BioLegend      | 304832      | 2-5         | X        |               |
| CD16       | BV711        | 3G8     | BD Biosciences | 563127      | 2-5         | X        |               |
| CD3        | BV786        | SK7     | BD Biosciences | 563800      | 1           | X        |               |
| CD57       | FITC         | HNK1    | BD Biosciences | 333169      | 10          | X        |               |
| CD28       | PerCP Cy5.5  | CD28.2  | BioLegend      | 302922      | 5           | X        |               |
| Granzyme B | PE           | GB11    | Sanquin        | M2289       | 15          |          | X             |
| CD8        | PE CF594     | RPAT8   | BD Biosciences | 562282      | 1           | X        |               |
| TCRγδ      | PE Cy7       | 11F2    | BD Biosciences | 655410      | 1           | X        |               |
| CD45       | AF700        | HI30    | BD Biosciences | 560566      | 2.5         | X        |               |
| CD56       | APC H7       | HCD56   | BioLegend      | 318332      | 5           | X        |               |

**Table 10. EuroFlow PERISCOPE DC-Monocyte panel, version 1**

Official references for this panel: Van der Pan et al, Development of a standardized and validated flow cytometry approach for monitoring of innate myeloid immune cells in human blood, *Frontiers in Immunology*, 2022, 5141. Patent filed by Van Dongen et al. Means and methods for multiparameter cytometry-based leukocyte subsetting. P119646NL00 (2019), PCT/NL2020/050688, priority date 5 November 2019.

| Marker          | Fluorochrome | Clone    | Source         | Cat. number | Volume (µL) | Membrane | Intracellular             |
|-----------------|--------------|----------|----------------|-------------|-------------|----------|---------------------------|
| CD141           | BV421        | 1A4      | BD Biosciences | 565321      | 2.5         | X        |                           |
| CD45            | OC515        | GA90     | Cytognos       | CYT-45OC    | 10          | X        |                           |
| CD62L           | BV605        | DREG-56  | BioLegend      | 304833      | 5           | X        |                           |
| HLA DR          | BV711        | G46-6    | BD Biosciences | 563696      | 2.5         | X        |                           |
| CD16            | BV786        | 3G8      | BD Biosciences | 563690      | 5           | X        |                           |
| CD1c            | BB515        | F10/21A3 | BD Biosciences | 565054      | 5           | X        |                           |
| CD36            | PerCP Cy5.5  | CLB-IVC7 | Immunostep     | 36PP5-100T  | 10          | X        |                           |
| SLAN            | PE           | DD.1     | Miltenyi       | 130-093-029 | 10          | X        |                           |
| FceR1           | PE           | EAR-37   | Thermo Fisher  | A18416      | 5           | X        |                           |
| CD33            | PE Cy7       | P67.6    | BD Biosciences | 333952      | 5           | X        | No intracellular staining |
| CD300e (IREM2)  | APC          | UP-H2    | Immunostep     | IREM2A-100T | 10          | X        |                           |
| CD303           | APC          | AC144    | Miltenyi       | 130-090-905 | 10          | X        |                           |
| CD14            | APC H7       | M5E2     | BD Biosciences | 641349      | 5           | X        |                           |
| BV stain buffer |              |          | BD Biosciences | 566349      | 50          | N/A      |                           |

**Table 11. EuroFlow PERISCOPE DC-Monocyte panel, version 2 - replacement of CD45 OC515 by CD45 AF700**  
 Official references for this panel: Van der Pan et al, Development of a standardized and validated flow cytometry approach for monitoring of innate myeloid immune cells in human blood, *Frontiers in Immunology*, 2022, 5141. Patent filed by Van Dongen et al. Means and methods for multiparameter cytometry-based leukocyte subsetting. P119646NL00 (2019), PCT/NL2020/050688, priority date 5 November 2019.

| Marker          | Fluorochrome | Clone    | Source         | Cat. number | Volume (µL) | Membrane | Intracellular             |
|-----------------|--------------|----------|----------------|-------------|-------------|----------|---------------------------|
| CD141           | BV421        | 1A4      | BD Biosciences | 565321      | 2.5         | X        |                           |
| CD62L           | BV605        | DREG-56  | BioLegend      | 304833      | 5           | X        |                           |
| HLA DR          | BV711        | G46-6    | BD Biosciences | 563696      | 2.5         | X        |                           |
| CD16            | BV786        | 3G8      | BD Biosciences | 563690      | 5           | X        |                           |
| CD1c            | BB515        | F10/21A3 | BD Biosciences | 565054      | 5           | X        |                           |
| CD36            | PerCP Cy5.5  | CLB-IVC7 | Immunostep     | 36PP5-100T  | 10          | X        |                           |
| SLAN            | PE           | DD.1     | Miltenyi       | 130-093-029 | 10          | X        |                           |
| FcεR1           | PE           | EAR-37   | Thermo Fisher  | A18416      | 5           | X        |                           |
| CD33            | PE Cy7       | P67.6    | BD Biosciences | 333952      | 5           | X        |                           |
| CD300e (IREM2)  | APC          | UP-H2    | Immunostep     | IREM2A-100T | 10          | X        | No intracellular staining |
| CD303           | APC          | AC144    | Miltenyi       | 130-090-905 | 10          | X        |                           |
| CD45            | AF700        | HI30     | BD Biosciences | 560566      | 10          | X        |                           |
| CD14            | APC H7       | M5E2     | BD Biosciences | 641349      | 5           | X        |                           |
| BV stain buffer |              |          | BD Biosciences | 566349      | 50          | N/A      |                           |

**Table 12. Overview of the panels used in this thesis.**

| Thesis chapter | PIDOT version (V) | BIGH tube version (V) | DC-Monocyte tube version (V) | CD4 T-cell tube version (V) | CD8 cytotoxic T-cell tube version (V) |
|----------------|-------------------|-----------------------|------------------------------|-----------------------------|---------------------------------------|
| Chapter 2.1    | V1, V2            |                       |                              |                             |                                       |
| Chapter 2.2    | V1                |                       |                              |                             |                                       |
| Chapter 3.1    |                   | V1, V2                | V1                           | V1, V1a                     | V1                                    |
| Chapter 3.2    |                   | V3                    | V2                           | V2, V2a                     | V2                                    |
| Chapter 3.4    |                   | V3                    | V2                           | V2, V2a                     | V2                                    |
| Chapter 4.1    |                   | V3                    | V2                           | V2a                         | V2                                    |

## **APPENDIX 2. Phenotypic descriptions used to identify cell populations in samples stained with EuroFlow panels.**

For transparency within this PhD thesis and convenience of the reader only!  
When citing, please refer to the original publications instead of this appendix!

**Gating strategies for the EuroFlow PIDOT panel have been published previously and can be found in the following manuscripts and in Chapter 2.2 of this PhD thesis:**

- van der Burg M, Kalina T, Perez-Andres M, et al. The EuroFlow PID Orientation Tube for Flow Cytometric Diagnostic Screening of Primary Immunodeficiencies of the Lymphoid System. *Frontiers in Immunology* 2019;10;246.
- van der Velden VHJ, Flores-Montero J, Perez-Andres M, et al., Optimization and testing of dried antibody tube: The EuroFlow LST and PIDOT tubes as examples. *Journal of Immunological Methods*. 2019; 475: 112287

**Official reference for the EuroFlow PERISCOPE B-cell and plasma cell panel (BIGH) panel:**

- Blanco E, Pérez-Andrés M, Arriba-Méndez S, et al. Age-associated distribution of normal B-cell and plasma cell subsets in peripheral blood. *JACI* 2018;141(6):2208-2219. e2216.
- Diks AM, Versteegen P, Teodosio C, et al. Age and Primary Vaccination Background Influence the Plasma Cell Response to Pertussis Booster Vaccination. *Vaccines*. 2022;10(2):136.
- Patent filed by Van Dongen et al. Means and Methods for Multiparameter Cytometry-Based Leukocyte Subsetting. P119646NL00 (2019). PCT/NL2020/050688, priority date 5 November 2019.

**Official reference for the EuroFlow PERISCOPE CD4 T-cell (TCD4) panel:**

- Botafogo V, Pérez-Andres M, Jara-Acevedo M, et al. Age distribution of multiple functionally relevant subsets of CD4+ T cells in human blood using a standardized and validated 14-color EuroFlow immune monitoring tube. *Frontiers in immunology*. 2020;11:166.
- Patent filed by Van Dongen et al. Means and Methods for Multiparameter Cytometry-Based Leukocyte Subsetting. P119646NL00 (2019). PCT/NL2020/050688, priority date 5 November 2019.

**Official reference for the EuroFlow PERISCOPE CD8 cytotoxic T-cell (CYTOX) panel:**

- Patent filed by Van Dongen et al. Means and Methods for Multiparameter Cytometry-Based Leukocyte Subsetting. P119646NL00 (2019). PCT/NL2020/050688, priority date 5 November 2019.

**Official references for the EuroFlow PERISCOPE DC-Monocyte panel:**

- Van der Pan et al, Development of a standardized and validated flow cytometry approach for monitoring of innate myeloid immune cells in human blood, *Frontiers in Immunology*, 2022, 5141.
- Patent filed by Van Dongen et al. Means and methods for multiparameter cytometry-based leukocyte subsetting. P119646NL00 (2019), PCT/NL2020/050688, priority date 5 November 2019.



**Table 1. Phenotypic descriptions used to define B-cell subsets stained with EuroFlow PERISCOPE B-cell and plasma cell panel (BIGH) panel by manual analysis.** The removal of debris and doublets is not indicated in the analysis strategy below, but should be performed to ensure high quality data. This table was previously published in: Diks et al. Age and Primary Vaccination Background Influence the Plasma Cell Response to Pertussis Booster Vaccination. *Vaccines*, 2022

| Stepwise approach (gating in 2D plots)  | Phenotypic description  |
|---|---|
| #1. Identification of total plasma cells  | <ul style="list-style-type: none"> <li>• CD45+CD19dimCD38highCD21-CD24-</li> <li>• Light scatter properties are low/medium (between lymphocytes and monocytes).</li> </ul>  |
| #2. Definition of maturation stage  | <ul style="list-style-type: none"> <li>• Least mature plasma cells: CD20+CD138-</li> <li>• Intermediate mature plasma cells: CD20-CD138-</li> <li>• Most mature plasma cells: CD20-CD138+</li> </ul>  |
| #3. Classification of plasma cells based on isotype   | <ul style="list-style-type: none"> <li>• IgM+, no expression of other isotype Igs</li> <li>• IgG1+, no expression of other isotype Igs</li> <li>• IgG2+, no expression of other isotype Igs</li> <li>• IgG3+, no expression of other isotype Igs</li> <li>• IgG4+, no expression of other isotype Igs</li> <li>• IgA1+, no expression of other isotype Igs</li> <li>• IgA2+, no expression of other isotype Igs</li> <li>• IgD+, no expression of other isotype Igs</li> <li>• IgH-, no Ig expression of any isotype Igs</li> </ul> |
| #4. Classification of plasma cells based on CD62L expression  | <ul style="list-style-type: none"> <li>• CD62L-</li> <li>• CD62L+</li> </ul>  |
| #5. Identification of total B cells   | CD45+CD19+CD20+ B cells show low light scatter characteristics (lymphocyte range)   |
| #6. Identification of switched memory B-cell (MBC) subsets based on isotype. Switched MBCs express only one isotype | <ul style="list-style-type: none"> <li>• IgG1+, no expression of other isotype Igs</li> <li>• IgG2+, no expression of other isotype Igs</li> <li>• IgG3+, no expression of other isotype Igs</li> <li>• IgG4+, no expression of other isotype Igs</li> <li>• IgA1+, no expression of other isotype Igs</li> <li>• IgA2+, no expression of other isotype Igs</li> </ul>  |
| #7. Subclassification based on maturation/functional CD markers   | <ul style="list-style-type: none"> <li>• CD20+CD21+<br/>Homogenous CD24 staining</li> <li>• CD20++CD21-/dim<br/>CD24+<br/>CD24-</li> </ul>  |
| #8. Subclassification based on CD62L/CD27 positivity  | <ul style="list-style-type: none"> <li>• CD27+CD62L+</li> <li>• CD27+CD62L-</li> <li>• CD27-CD62L-</li> <li>• CD27-CD62L+</li> </ul>  |
| #9. Identification of non-switched MBCs   | CD27+IgM++IgD+<br>Of note, a minor subset of IgD+IgM- MBCs may be found as well. These can be classified separately.  |

## Appendix 2

|   |  |
|---|--|
| #10. Subclassification based on maturation/functional CD markers                  | <ul style="list-style-type: none"> <li>CD20+CD21+<br/>Homogenous CD24 staining</li> <li>CD20++CD21-/dim<br/>CD24+<br/>CD24-</li> </ul> No further subclassification in these populations.            |
| #11. Classification of pre-germinal center (preGC) B cells                        | CD27-IgM+IgD+  |
| #12. Subclassification based on maturation/functional CD markers                  | <ul style="list-style-type: none"> <li>Immature preGC B cells: CD38+CD24+CD5+CD21-/+</li> <li>Naive CD5+ B cells: CD38-/dim CD24-/dimCD5+</li> <li>Naive CD5- B cells:CD38-/CD24-/dimCD5-</li> </ul> |
| #13. Subclassification of naive B cells based on maturation/functional CD markers | <ul style="list-style-type: none"> <li>CD20+CD21+<br/>Homogenous CD24 staining</li> <li>CD20++CD21-/dim<br/>CD24+<br/>CD24-</li> </ul>   |

**Table 2. Phenotypic descriptions used to define T-cell subsets stained with EuroFlow PERISCOPE CD4 T-cell (TCD4) panel by manual analysis.** The removal of debris and doublets is not indicated in the analysis strategy below, but should be performed to ensure high quality data.

| Stepwise approach (gating in 2D plots)                                   | Phenotypic description   |
|--|--|
| #1 Identification of total CD4 T cells                                   | CD3+CD4+CD45+<br>Light scatter properties are low ('lymphocyte gate'). |
| #2 Identification of regulatory T cells (Tregs) within CD4 T cells       | CD25+CD127dim  |
| #3 Identification of follicular helper T cells (TFHs) within CD4 T cells | CD25-/dim CD185+ CCR10-  |

|  |   |
|--|---|
| <p>#4 Division of total CD4 T cells into T-helper (TH) subsets</p> | <ul style="list-style-type: none"> <li>Divide based on chemokine receptor expression (CD183, CD194, CD196, and CCR10) <ul style="list-style-type: none"> <li>Naive: CD27+CD45RA+CD62L+CD127+CD183-CD194-CD196-CCR10-</li> <li>TH1: CD183+ CD194-CD196-CCR10-</li> <li>TH2: CD183- CD194+CD196-CCR10-</li> <li>TH17: CD183- CD194+CD196+CCR10-</li> <li>TH1/17: CD183+CD194-CD196+CCR10-</li> <li>TH22: CD183- CD194+CD196+CCR10+</li> <li>CD183+CD194+CD196+CCR10+</li> <li>CD183+CD194+CD196+CCR10-</li> <li>CD183+CD194+CD196-CCR10+</li> <li>CD183+CD194+CD196-CCR10-</li> <li>CD183+CD194-CD196+CCR10+</li> <li>CD183+CD194-CD196-CCR10+</li> <li>CD183-CD194-CD196+CCR10-</li> <li>CD183-CD194+CD196-CCR10+</li> <li>Non-naive CD4+CD183-CD194-CD196-CCR10-CD27-/+CD45RA-CD62L-/+</li> </ul> </li> </ul> |
| <p>#5 Division of total Tregs in TH-like subsets</p>               | <ul style="list-style-type: none"> <li>Divide primarily based on chemokine receptor expression (CD183, CD194, CD196, and CCR10) <ul style="list-style-type: none"> <li>Naive Treg: CD27+CD45RA+CD62L+ CD183-CD194-CD196-CCR10-</li> <li>TH1-like: CD183+CD194-CD196-CCR10-</li> <li>TH2-like: CD183-CD194+CD196-CCR10-</li> <li>TH17-like: CD183-CD194+CD196+CCR10-</li> <li>TH22-like: CD183-CD194+CD196+CCR10+</li> <li>CD183+CD194+CD196-CCR10+ Treg</li> <li>CD183+CD194+CD196-CCR10- Treg</li> <li>CD183+CD194+CD196+CCR10- Treg</li> <li>CD183+CD194+CD196+CCR10+ Treg</li> <li>CD183-CD194+CD196-CCR10+ Treg</li> </ul> </li> </ul>  |
| <p>#6 Division of total TFHs in Treg-/TH-like subsets</p>          | <ul style="list-style-type: none"> <li>Divide primarily based on chemokine receptor expression (CD183, CD194, CD196, and CCR10) <ul style="list-style-type: none"> <li>CD185+CD27+CD45RA+CD62L+ T cells (CD183-CD194-CD196-CCR10-)</li> <li>Treg TFH: CD127+/dimCD183-/+CD194-/+CD196-/+CCR10-</li> <li>TH1-like: CD183+CD194-CD196-CCR10-</li> <li>TH2-like: CD183-CD194+CD196-CCR10-</li> <li>TH17-like: CD183-CD194+CD196+CCR10-</li> <li>TH1/17-like: CD183+CD194-CD196+CCR10-</li> <li>CD183+CD194+CD196-CCR10- TFH</li> <li>CD183+CD194+CD196+CCR10- TFH</li> <li>CD183-CD194-CD196+CCR10- TFH</li> <li>CD183+CD194+CD196-CCR10- TFH</li> </ul> </li> </ul>   |
| <p>#7 division of each subset into different maturation stage</p>  | <ul style="list-style-type: none"> <li>Divide based on CD27, CD45RA, and CD62L <ul style="list-style-type: none"> <li>Central memory (CD27+CD45RA-CD62L+)</li> <li>Transitional memory (CD27+CD45RA-CD62L-)</li> <li>Effector memory (CD27-CD45RA-CD62L-/+)</li> <li>Terminal effector (CD27-CD45RA+CD62L-/+)</li> </ul> </li> </ul>  |

## Appendix 2

**Table 3. Phenotypic descriptions used to define T-cell and NK-cell subsets stained with the EuroFlow PERISCOPE CD8 cytotoxic T-cell (CYTOX) panel by manual analysis.** The removal of debris and doublets is not indicated in the analysis strategy below but should be performed to ensure high quality data.

| Stepwise approach (gating in 2D plots)                                       | Phenotypic description   |
|--|--|
| #1 Identification of total T cells   | <ul style="list-style-type: none"> <li>• CD3+CD45+</li> <li>• Light scatter properties are low ('lymphocyte gate').</li> </ul>   |
| #2 Identification of total TCR $\gamma\delta$ + T cells within total T cells | CD3+ TCR $\gamma\delta$ +  |
| #3 Identification of total CD8+ and CD8- T cells within total T cells        | <ul style="list-style-type: none"> <li>• CD8+ T cells: CD8+ TCR<math>\gamma\delta</math>-</li> <li>• CD8- T cells: CD8- TCR<math>\gamma\delta</math>-</li> </ul>   |
| #4 Identification of total NK cells  | CD3- TCR $\gamma\delta$ - CD45+<br>Light scatter properties are low ('lymphocyte gate').<br>CD56-/+<br>CD16-/+ (lower than neutrophils)<br>CD45RA-/+ (most NK cells are CD45RA positive)<br>CD62L-/+   |
| # 5 Identification of additional lymphocytes                                 | Light scatter properties are low ('lymphocyte gate').<br>CD45+CD3-CD4-   |
| #6 Identification of myeloid cells   | Neutrophils: high SSC, CD16+CD45+<br>Eosinophils: high SSC, CD45+, Autofluorescence results in double positive population in CD57 vs cy Granzyme B plot<br>Monocytes: intermediate SSC, CD45+CD16+/-<br>CD45RA-/+ and mostly CD62L+  |
| #7 Subsetting of TCR $\gamma\delta$ + T cells                                | <ul style="list-style-type: none"> <li>• Naive: CD27+CD28+CD45RA+CD62L+GranzB-CD57-</li> <li>• Central memory: CD27+CD28+CD45RA-CD62L+<br/>CD57-cyGranzB-/+<br/>CD57+CyGranzB+</li> <li>• Transitional memory: CD27+CD28-/+CD45RA-<br/>CD62L-/dim<br/>CD57-cyGranzB-<br/>CD57-CyGranzB+<br/>CD57+CyGranzB+</li> <li>• Peripheral memory: CD27-CD28+CD45RA-<br/>CD62L-/+<br/>CD57-cyGranzB-<br/>CD57-CyGranzB+<br/>CD57+CyGranzB+</li> <li>• Early effector: CD27+CD28-CD45RA+CD62L-/+<br/>CD57-CyGranzB+<br/>CD57+CyGranzB+</li> <li>• Terminal effector: CD27-CD28-CD45RA+CD62L-/+<br/>CD57-CyGranzB+<br/>CD57+CyGranzB+</li> </ul> |

|                               |  |
|-------------------------------|--|
| #8 Subsetting of CD8+ T cells | <ul style="list-style-type: none"> <li>• Naive: CD27+CD28+CD45RA+CD62L+ (NB: in some donors the naive population can be divided into CD62Lhigh and CD62Llow)</li> <li>• Central memory: CD27+CD28+CD45RA-CD62L+<br/>CD57-CyGranzB-/+<br/>CD57+ CyGranzB-/+</li> <li>• Transitional memory: CD27+CD28+C-<br/>D45RA-CD62L-/dim<br/>CD57-cyGranzB-<br/>CD57+CyGranzB-<br/>CD57-CyGranzB+<br/>CD57+CyGranzB+</li> <li>• Peripheral memory: CD27-CD28-/+CD45RA-<br/>CD62L-/+<br/>CD57-cyGranzB-<br/>CD57-CyGranzB+<br/>CD57+CyGranzB+</li> <li>• Early effector: CD27+CD28-CD45RA+CD62L-/+<br/>CD57-cyGranzB-<br/>CD57-CyGranzB+<br/>CD57+CyGranzB+</li> <li>• Terminal effector: CD27-CD28-CD45RA+CD62L-/+<br/>CD57-cyGranzB-<br/>CD57-CyGranzB+<br/>CD57+CyGranzB+</li> </ul> |
| #9 Subsetting of NK cells     | <ul style="list-style-type: none"> <li>• CD56+ bright NK cells: CD56brightCD16lo/dim<br/>CD57-cyGranzB-<br/>CD57-CyGranzB+</li> <li>• CD56+dim NK cells: CD56dimCD16+<br/>CD57-cyGranzB-<br/>CD57-CyGranzB+<br/>CD57+CyGranzB+</li> </ul>  |



## Appendix 2

**Table 4. Phenotypic descriptions used to define innate immune cell (sub)sets stained with the EuroFlow PERISCOPE DC-Monocyte panel by manual analysis.** The removal of debris and doublets is not indicated in the analysis strategy below, but should be performed to ensure high quality data.

| Stepwise approach (gating in 2D plots)                 | Phenotypic description  |
|--|---|
| #1 Identify eosinophils                                | SSC high, CD45+ neg. for all other markers in the panel   |
| #2 Identify mature neutrophils                         | SSC high CD45+CD16+   |
| #3 Identify immature neutrophils                       | <ul style="list-style-type: none"> <li>CD45+CD33+CD16-/ +HLA DR-CD14-SLAN&amp;FcER1-<br/>CD62L-<br/>CD62L+</li> </ul>   |
| #4 Identify monocytes                                  | <ul style="list-style-type: none"> <li>SSC intermediate</li> <li>CD45+CD33+CD16-/ +HLA DR+<br/>CD14-/ +SLAN&amp;FcER1-/ +</li> </ul>  |
| # 5 Divide the monocytes based on CD14/CD16 expression | <ul style="list-style-type: none"> <li>ncMo: CD14-/dimCD16+CD62L- SLAN &amp;FcER1-/ +<br/>SLAN+CD36+<br/>SLAN-CD36+<br/>SLAN-CD36-<br/>SLAN+CD36-</li> <li>iMo:CD16+CD14+HLA DR+Slan&amp;FcER1-CD300e&amp;CD303+CD36+</li> <li>cMo:CD16-CD14+62L-/ +<br/>CD62L+FcER1+<br/>CD62L-FcER1+<br/>CD62L+FcER1-<br/>CD62L-FcER1-</li> </ul> |
| #6 Identify the CD1c+ myeloid DCs                      | <ul style="list-style-type: none"> <li>SSC intermediate</li> <li>CD45+CD33+CD141-/dimFcER1+HLA DR+CD16-CD14-/dim<br/>CD14dim<br/>CD14-</li> </ul>   |
| #7 Identify the plasmacytoid DCs                       | SSC intermediate<br>CD45+CD303+CD14-HLA DR+CD16-CD36+   |
| #8 Identify the CD141+ myeloid DCs                     | CD141+CD33+CD300e-CD303-CD14-HLA DR+CD16-   |
| #9 Identify the Axl+ DCs within the plasmacytoid DCs   | CD33hiCD141hiCD36dim  |
| #10 Identify the basophils                             | SSC intermediate<br>CD45dimCD33+CD303-CD300e-CD14-HLA DR-   |
| #11 Identify 'unspecified nucleated cells'             | Left-over CD45+ events that fit the singlet gate  |

## Summary

Our immune system consists out of several complementary layers which all play an important role in defending our body from pathogens and tissue damage. In **Chapter 1**, I explain the immune system and how immune monitoring can be a valuable source of information about the immune status of an individual or a group, both when the immune system is in homeostasis and when an active response is ongoing. An example of an active response is the response triggered/elicited by vaccination. Here, immune monitoring can give us information about the efficacy of applied vaccination/immunization method, or it can give information about the functioning of the immune system in one or more individuals. The importance of immune monitoring is well-recognized and various efforts are made to harmonize or, preferably, standardize the laboratory protocols used in immune monitoring studies.

Standardization in (multi-centre) clinical trials is very important to obtain data that is reliable and comparable in-between study locations. Therefore, we first evaluated the influence of various pre- and post-analytical procedures on the quality of the samples used for immunophenotyping of leukocyte subsets in blood. In **Chapter 2.1**, we assessed the impact of delayed sample processing and acquisition, storage temperature and the impact of fixatives on the quantity and distribution of leukocyte subsets. Based on our findings, we formulated a set of guidelines to improve reliability and reproducibility of data regarding immune cell quantity and phenotype.

Data analysis is part of a post-analytical procedure that requires standardization. Therefore, we evaluated the impact of delayed sample processing on the performance of automated (database-driven) analysis in **Chapter 2.2**. We showed that automated analysis is superior to manual analysis regarding reproducibility and robustness. However, expert revision of database-driven analysed files remains necessary in samples with numerical alterations and aberrant B- and T-cell maturation and/or marker expression profiles.

The knowledge gathered in **Chapter 2** was utilized in several clinical trials where we aimed to dissect the cellular immune responses following controlled pertussis infection or vaccination. These clinical trials were initiated locally at the LUMC or within the IMI-2 PERISCOPE consortium and their major outcomes are summarized in **Chapter 3**.

In **Chapter 3.1**, we investigated kinetics of >250 circulating immune cell subsets after an acellular pertussis (aP) booster vaccination. We observed the kinetics of circulating immune cells at various timepoints post-vaccination and found that the most prominent changes occur in the plasma cell compartment; especially (IgG1) plasma cells showed a homogenous expansion and maturation at day 7 post-vaccination. Consequently, in **Chapter 3.2** we focused on kinetics in the B-cell compartment in different age cohorts of vaccinees, and found that irres-

## Summary

---

pective of age and the related primary vaccination background, the expansion and maturation of (primarily) IgG1 plasma cells was the most prominent feature of an immune response initiated by aP booster vaccination. Despite these similarities, specific differences in plasma cell responses appeared to be associated with age (primarily IgG1, IgG3 and IgA1 responses in adults, and IgG1, IgG3 and IgG4 responses in children) and primary vaccination background (stronger plasma cell responses in those originally primed with wP). The observed difference may be explained by a better protection induced by wP vaccination, or by the fact that older people have most likely encountered Bp multiple times in life, and thus probably had several ‘natural boosters’. In this chapter, we also found that the flow cytometry data corroborated ELISpot data, and both techniques were complementary to each other.

Conclusions drawn from flow cytometry data can not only be supplemented by techniques such as ELISpot and antibody serology, but also by more exploratory transcriptome techniques such as B-cell receptor (BCR) repertoire analysis. Therefore, we further extended our studies on the immune response after aP vaccination in **Chapter 3.3**. Here, we investigated the BCR repertoire and clonal relatedness of plasma cells from different time points by means of single cell sequencing techniques. We observed that the BCR repertoire in plasma cells at day (d) 5, 7, 10, and 14 after vaccination differed from the repertoire at baseline, such as high usage of IGHG1 in expanded clones, increased class-switching events and somatic hypermutation (SHM) patterns, fitting with positive selection of CDR3 sequences over time. In this chapter, we confirmed that the distribution of plasma cell subclasses was highly comparable between the flow cytometry and sequencing data. Moreover, we built a bioinformatic query tool to help searching for BCRs specific to individual vaccine components.

As diverse cell populations and timepoints can be of importance in different models, we compared the cellular kinetics (within innate immune cells, T cells, and B cells) between an aP booster vaccination and a bacterial challenge with *Bordetella pertussis* (strain B1917) in **Chapter 3.4**. We found that the expansion and maturation of plasma cells was less prominent and more delayed in time in the bacterial challenge model, as well as more heterogenous with respect to the isotypes of the expanding plasma cells. Using the data gathered in **Chapter 3**, we identified informative timepoints and cell populations that could be monitored in future vaccination and human challenge studies. Especially prominent for non-colonized participants were the early expansion of (CD36-) non-classical monocytes at d1, natural killer cells (d3), follicular T helper cells (d1-d3) and plasma cells (d3). These populations may be interesting for future monitoring. This data emphasizes the importance of pilot studies (for timepoint finding) and highlights differences in the generated immune response upon vaccination (which has a precise dosage and timing) or controlled infection (which has a more variable exposure in antigen dosage and time, due to the process of colonization and infection through mucosal layers). As current pertussis vaccines do not protect against transmission, unraveling the immune response associated with protecti-

on against infection may help the design of more effective vaccines against pertussis.

Finally, in **Chapter 4**, we set out to use immune monitoring to evaluate the immune system in homeostasis. We investigated the leukocyte composition and function in a group of individuals carrying a specific genetic variant in the *PLCG2* gene (p.P522R). This variant is associated with cognitively healthy aging and longevity. Although it is known that the PLC $\gamma$ 2 protein is involved in signaling downstream of cellular receptors such as the B-cell receptor and the Fc-receptor, the impact of p.P522R on the human immune system remains unknown. We performed an in-depth analysis on the quantity and functionality of the circulating immune cells in (older) adults and supplemented this with the evaluation of and active immune response: the SARS-CoV-2 vaccination responses in a subset of these individuals. Although no differences were observed in the response to SARS-CoV-2 vaccination, carriers of the genetic variant tended to show less signs of immunosenescence compared to age-matched non-carriers.

In this thesis, I evaluated pre- and post-analytical procedures critical for reproducibility of clinical studies and applied them to investigate immune responses to *Bordetella pertussis* and to characterize a polymorphism in healthy older adults. By doing so, I (1) created a set of guidelines for sample handling in clinical trials, (2) showed differences in immune responses to vaccination against *Bordetella pertussis* versus controlled natural infection, and (3) described possible implications of carrying the p.P522R *PLCG2* variant on the human immune system. In **Chapter 5**, I discuss the potential implications of these findings and indicate what next steps can be made in the process of improving pertussis vaccines and in the process of dissecting the impact of the *PLCG2* P522R genetic variant on the immune system and evaluate its potential as a therapeutic target.

### Samenvatting

Ons immuunsysteem bestaat uit verschillende onderdelen, die elk een eigen belangrijke rol spelen in de bescherming van ons lichaam tegen pathogenen (bacteriën, virussen, schimmels, etc.) en tegen weefselschade. In **hoofdstuk 1** van dit proefschrift leg ik uit hoe het immuunsysteem werkt. Daarnaast leg ik uit hoe het monitoren van het immuunsysteem ('immuunmonitoring') waardevolle informatie kan leveren over de immunestatus van een individu of van een groep. Immunmonitoring kan informatie geven over het immuunsysteem wanneer het in balans is, of juist wanneer een afweerreactie bezig is. Dit is bijvoorbeeld na het ontvangen van een vaccinatie. Als je het immuunsysteem na een vaccinatie bestudeert, kan dit informatie geven over het gebruikte middel (de efficiëntie) en over het functioneren van het immuunsysteem van de individu of de groep. Het belang van immunmonitoring wordt algemeen erkend en er wordt vanuit verschillende hoeken gewerkt aan het "harmoniseren" of bij voorkeur "standaardiseren" van de laboratoriumprotocollen die worden gebruikt voor immunmonitoring studies.

Wanneer een klinische studie op meerdere locaties plaatsvindt, is het erg belangrijk dat er vooraf een zorgvuldige standaardisatie tussen deze locaties wordt verkregen. Dit zorgt ervoor dat de geproduceerde data betrouwbaarder zijn en niet worden beïnvloed door gebruik van verschillende (locatie-gebonden) laboratoriumprotocollen. Daarom behandel ik in dit proefschrift eerst het effect van verschillende factoren in het verwerkingsproces (bijv. het pre- en post-analytische proces) op de kwaliteit van de bloedmonsters, die worden gebruikt voor bijvoorbeeld immunfenotypering. In **hoofdstuk 2.1** hebben we onderzocht hoe de gemeten aantallen en de verdeling van de bloedcellen kunnen worden beïnvloed door: (1) vertraging van het verwerken van het bloedmonster, (2) vertraging van het meten van een verwerkt bloedmonster op de flowcytometer, (3) de temperatuur waarop het bloedmonster wordt bewaard, (4) het gebruik van fixerende middelen om het bloedmonster langer houdbaar te maken. Op basis van onze onderzoeksresultaten hebben wij richtlijnen kunnen opstellen. Deze richtlijnen verbeteren de betrouwbaarheid en reproduceerbaarheid van data betreffende de gemeten aantallen en de verdeling van bloedcellen.

Data-analyse is een post-analytische procedure waar standaardisatie ook nodig is. Daarom onderzochten wij in **hoofdstuk 2.2** het effect van vertraagde verwerking van bloedmonsters op de kwaliteit van automatische (= door een database aangestuurde) analyse. We zagen dat, wanneer het aankomt op reproduceerbaarheid en robuustheid, een automatische analyse superieur is aan een handmatige analyse. Desalniettemin is een (handmatige) check door een expert nog altijd nodig wanneer de aantallen van de verschillende afweercellen, de rijping van de verschillende afweercellen, of de expressie van celkenmerken buiten de normale waarden valt.

De kennis verzameld in **hoofdstuk 2** is vervolgens gebruikt in meerdere klinische studies waarin we de cellulaire afweerreacties na een gecontroleerde infectie

met *Bordetella (B.) pertussis* (= de kinkhoest bacterie) of na vaccinatie tegen *B. pertussis* (= de kinkhoestvaccinatie) bestudeerden. De hier besproken klinische studies zijn opgezet in het LUMC of binnen het IMI-2 PERISCOPE consortium. De belangrijkste uitkomsten van deze studies zijn samengevat in hoofdstuk 3 van dit proefschrift.

In **hoofdstuk 3.1** hebben we onderzocht hoe de kinetiek van meer dan 250 verschillende soorten afweercellen in ons bloed veranderen na het toedienen van een niet-cellulair kinkhoest vaccin (aP vaccin; bevat slechts drie specifieke eiwitten van de kinkhoestbacterie). Op verschillende momenten na de vaccinatie zagen we consistente veranderingen in de kinetiek van de afweercellen. De toename en uitrijping van het aantal (IgG1) plasmacellen (= antistof-producerende afweercellen) op dag 7 na vaccinatie was de meest consistente en duidelijke verandering. Vervolgens hebben wij ons in **hoofdstuk 3.2** vooral gericht op de veranderingen in het B-cel gedeelte van het immuunsysteem. Hier keken we naar de veranderingen in het immuunsysteem na toediening van een vaccin binnen verschillende leeftijdsgroepen. Zij verschilden zodanig in leeftijd dat ze als baby verschillende kinkhoestvaccins hebben gekregen (de zogenoemde vaccinatie-achtergrond). Opnieuw zagen we dat de uitrijping van IgG1 plasmacellen en de toename in aantallen plasmacellen de meest duidelijke veranderingen waren. Dit vonden we in elke groep, ongeacht de leeftijd of vaccinatie-achtergrond. Naast de IgG1 respons zagen we wel andere specifieke verschillen tussen mensen met een bepaalde leeftijd of vaccinatie-achtergrond; volwassenen hadden een gemengde IgG1-IgG3 én IgA1 plasmacel-respons, terwijl kinderen en adolescenten een gemengde IgG1-IgG3 en IgG4 plasmacel-respons hadden. Ook hadden mensen die als baby gevaccineerd waren met het cellulaire vaccin (wP; vaccin met de complete dode bacterie) een sterkere toename in het aantal plasmacellen vergeleken met mensen die het niet-cellulaire vaccin (aP) als baby hadden ontvangen. Dit kan erop duiden dat vaccinatie met het oude (cellulaire) vaccin een betere antistofproductie heeft opgewekt, òf dat de oudere mensen vaker contact hebben gehad met de kinkhoest bacterie, bijvoorbeeld doordat ze een lichte infectie hebben gehad. Hierdoor worden er óók IgA antistoffen gemaakt; deze zijn erg belangrijk voor de afweer in de slijmvliezen. De slijmvliezen (bijv. de luchtwegen) zijn nou precies de plekken waar de kinkhoestbacterie probeert het lichaam binnen te komen. Tenslotte vonden we in dit onderzoek dat de resultaten van de flowcytometrie experimenten overeenkwamen met die van de ELISpot experimenten (= kweekexperimenten). Deze technieken geven dus aanvullende informatie over dezelfde personen.

De flowcytometrie resultaten kunnen ook worden uitgebreid door andere technieken dan ELISpot of serologische antistofbepalingen, bijvoorbeeld door meer verkennende RNA technieken te gebruiken om de grote mate van diversiteit van de antistoffen te onderzoeken. Dit noemen we ook wel B-cel receptor (BCR) repertoire-analyse. De BCR zit vast aan de buitenkant van het celoppervlak van de B cel, maar kan ook worden uitgescheiden door de B cel. Wanneer de BCR uitgescheiden is, noemen wij de BCR een antistof. Dit hebben wij gedaan in **hoofdstuk 3.3**. We onderzochten het BCR-repertoire en de klonale relaties tus-



## Samenvatting

---

sen plasmacellen geïsoleerd op verschillende momenten na vaccinatie. Dit deden wij door middel van de zogenoemde ‘single-cell sequencing’ techniek. Het BCR-repertoire van plasmacellen geïsoleerd op 5, 7, 10 en 14 dagen na vaccinatie verschilden van de plasmacellen geïsoleerd op dag 0 (dus vóór de vaccinatie). De verschillen waren vooral zichtbaar in het gebruik van de IgG1 zware keten (= een onderdeel van de BCR), de hoeveelheid ‘class-switching events’ (= het veranderen van antistof-functie), en de positieve selectie in de CDR3 regio over tijd (= het veranderen van de vorm van de grijp-arm van de antistof door mutaties in het DNA te introduceren. Dit heeft als doel om BCRs met verschillende beschermingsgraden te maken en de beste BCRs te selecteren). In dit hoofdstuk zagen we dat de verdeling binnen de plasmacel populaties zoals bepaald met flow cytometrie overeenkwam met die zoals bepaald met single-cell sequencing. Tenslotte hebben we in dit hoofdstuk bioinformatica toegepast om een zogenoemde ‘query tool’ te ontwerpen; deze bioinformatica-techniek helpt bij het zoeken naar BCRs die specifiek zijn gericht tegen onderdelen van het niet-cellulaire pertussis vaccin.

Verskillende celpopulaties en tijdstippen kunnen belangrijk zijn in verschillende studiemodellen. Daarom vergeleken we in **hoofdstuk 3.4** de kinetiek van verschillende celpopulaties (uit het aangeboren en aangeleerde immuunsysteem) na het ontvangen van een vaccin tegen *B. pertussis* of na een infectie met *B. pertussis* (onder gecontroleerde omstandigheden). Vergeleken met de respons na vaccinatie, was de toename en uitrijping van plasmacellen vertraagd en minder uitgesproken. De toename en uitrijping van plasmacellen werd wel in meer verschillende antistof-subgroepen (isotypen) gevonden dan het geval was na vaccinatie.

Met de data uit **hoofdstuk 3** hebben we bepaald welke tijdstippen en welke celpopulaties informatief kunnen zijn om te monitoren in toekomstige vaccinatie-/ infectiestudies. Ook keken we naar de cel kinetiek die geassocieerd werd met bescherming tegen kolonisatie na een infectie met *B. pertussis*. Hieronder vielen de vroege toename in het aantal (CD36-) niet-klassieke monoccyten (dag 1), van de ‘Natural Killer’ cellen (dag 3), de ‘follicular helper T cellen’ (dag 1-3) en de plasmacellen (dag 3). Vanwege die associaties zijn deze afweercelpopulaties mogelijk interessant voor toekomstige monitoring studies.

De resultaten van deze studies benadrukken het belang van pilot-studies, bijvoorbeeld om de juiste tijdstippen of celpopulaties vast te stellen. Verder laat dit onderzoek zien dat er verschillen bestaan in immuunrespons na een infectie of vaccinatie. De huidige kinkhoestvaccins beschermen ons niet goed tegen de aanwezigheid van de kinkhoestbacterie op onze slijmvliezen (= kolonisatie) en daarmee ook minder goed tegen overdracht/verspreiding van de bacterie. Als we beter begrijpen hoe de bescherming tegen bacteriële kolonisatie tot stand komt, kunnen we deze informatie misschien gebruiken om betere vaccins tegen kinkhoest te ontwikkelen.

In **hoofdstuk 4** gebruikten we immuunmonitoring om het immuunsysteem te

bekijken terwijl het in balans is. We bestudeerden de aantallen en de verdeling van afweercellen in het bloed bij een groep mensen die een speciale genetische variant in het *PLCG2* gen bij zich dragen (de variant heet p.P522R), en vergeleken dit met mensen die deze variant niet hebben. *PLCG2* draagt de genetische code voor het eiwit PLC $\gamma$ 2. De p.P522R variant-eiwit wordt geassocieerd met gezond oud worden, zowel geestelijk als lichamelijk. Hoewel we weten dat het PLC $\gamma$ 2 eiwit in afweercellen betrokken is bij het doorgeven van signalen, zodra een BCR of een Fc-receptor wordt geactiveerd, weten we niet veel van de invloed die het p.P522R variant-eiwit heeft op het afweersysteem. Daarom onderzochten we hoe dit variant-eiwit de aantallen en het functioneren van afweercellen in (oudere) volwassenen beïnvloedt. Hierbij maakten we ook gebruik van cel-stimulaties in het laboratorium. Daarnaast bestudeerden we de antistofreactie tegen COVID-vaccinatie in deze groep (oudere) volwassenen; dus hier keken we weer naar het afweersysteem in actie. Hoewel we geen verschillen zagen in respons tegen COVID-vaccinatie bij mensen die de p.P522R variant wel of niet bij zich droegen, zagen we wel dat mensen met de p.P522R variant minder immunologische veroudering leken te hebben ten opzichte van leeftijdsgenoten die de variant niet hadden.

Dus: in dit proefschrift heb ik pre- en post-analytische procedures die belangrijk zijn voor de reproduceerbaarheid van klinische studies geëvalueerd, en heb ik deze toegepast voor monitoring van het immuunsysteem. Hierbij keek ik zowel naar het immuunsysteem in actie (vaccinatie tegen en blootstelling aan *B. pertussis*) en naar het immuunsysteem in balans (om de genetische variant *PLCG2* p.P522R te bestuderen). Hierbij heb ik (1) richtlijnen opgesteld voor het verwerken van (bloed)monsters in klinische studies, (2) de verschillende immuunreacties van het lichaam na vaccinatie tegen *B. pertussis* of infectie met *B. pertussis* bestudeerd, en (3) de mogelijke implicaties van het dragen van genetische variant *PLCG2* p.P522R op het humane immuun systeem beschreven. In het laatste hoofdstuk van dit proefschrift – **hoofdstuk 5**– bediscussieer ik de potentiële implicaties van deze bevindingen. Ook geef ik aan wat ik denk dat de volgende stappen zouden kunnen zijn in de ontwikkeling en/of verbetering van kinkhoest vaccins en in het verder ontrafelen van de gevolgen van *PLCG2* p.P522R op het immuunsysteem en de mogelijkheid om dit als een therapeutisch doelwit te gebruiken.

## Curriculum Vitae

---

### Curriculum Vitae

Annieck Margo Diks was born on May 13th, 1992 in Doetinchem, the Netherlands. She grew up in Gaanderen. In 2010, she completed her secondary school at the Almende college - Isala, Silvolde. After this, she moved to Wageningen (the Netherlands) and enrolled in the BSc Biotechnology program at Wageningen University & Research Center (WUR). The end of her BSc program comprised a thesis at the Laboratory of Monoclonal Antibodies (LMA, Dep. of Nematology, WUR), where she studied the immunomodulating effect of *Agaricus bisporus* varieties under supervision of dr. Ruud Wilbers and associate prof. Arjen Schots. After completing her BSc studies in 2013, she continued with the master program 'Medical Biotechnology'. During her MSc, she took a gap year in which she volunteered as a full-time board member (chairman position) at the local youth association 'Unitas Wageningen'.

For her MSc thesis, Annieck returned to the Laboratory of Monoclonal Antibodies. Here, she worked on the project 'Transient expression of helminthic protein Sm29 and virus induced gene silencing of  $\beta$ -hexosaminidases in *Nicotiana benthamiana*' under supervision of dr. Ruud Wilbers and associate prof. Arjen Schots. The MSc thesis was followed by an internship at Genmab BV (Utrecht, the Netherlands), where she worked for 6 months in The Antibody Sciences cluster.

Upon completion of her MSc (Oct 2016), Annieck started her PhD trajectory at Leiden University Medical Center (LUMC) in Jan 2017. She worked under supervision of dr. Magdalena A. Berkowska and prof. Jacques J.M. van Dongen. One year into her PhD, Annieck also started working as an external PhD candidate at the Alzheimer Centre (Amsterdam UMC), under supervision of dr. Henne Holstege. The red line of Anniecks PhD project was the monitoring of the human immune system by means of (standardized) flow cytometric analysis of human leukocytes. The results of her PhD are described in this thesis.

In September 2022, Annieck returned to Genmab BV, where she started as Scientist Translational Research.

**A.M. Diks**, C. Bonroy, C. Teodosio, R.J. Groenland, B. de Mooij, E. de Maertelaere, J. Neiryneck, J. Philippé, A. Orfao, J.J.M. van Dongen, M.A. Berkowska. "Impact of blood storage and sample handling on quality of high dimensional flow cytometric data in multicenter clinical research." *Journal of immunological methods* 475 (2019): 112616.

E. Linskens, **A.M. Diks**, J. Neirinck, M. Perez-Andres, E. de Maertelaere, M.A. Berkowska, T. Kerre, M. Hofmans, A. Orfao, J.J.M. van Dongen, F. Haerynck, J. Phillipé, C. Bonroy. "Improved Standardization of Flow Cytometry Diagnostic Screening of Primary Immunodeficiency by Software-Based Automated Gating" *Frontiers in immunology* 11 (2020): 584646.

**A.M. Diks**, I. Khatri, L.E.M. Oosten, B. de Mooij, R.J. Groenland, C. Teodosio, M. Perez-Andres, A. Orfao, G.A.M. Berbers, J.J. Zwaginga, J.J.M. van Dongen, M.A. Berkowska "Highly sensitive flow cytometry allows monitoring of changes in circulating immune cells in blood after Tdap booster vaccination." *Frontiers in immunology* 12 (2021): 2091.

I. Khatri, **A.M. Diks**, E.B. van den Akker, L.E.M. Oosten, J.J. Zwaginga, M.J.T. Reinders, J.J.M. van Dongen, M.A. Berkowska. "Longitudinal Dynamics of Human B-Cell Response at the Single-Cell Level in Response to Tdap Vaccination." *Vaccines* 9.11 (2021): 1352.

**A.M. Diks**, P. Versteegen, C. Teodosio, R.J. Groenland, B. de Mooij, A. Buisman, A. Torres-Valle, M. Perez-Andres, A. Orfao, G.A.M. Berbers, J.J.M. van Dongen, M.A. Berkowska. "Age and Primary Vaccination Background Influence the Plasma Cell Response to Pertussis Booster Vaccination." *Vaccines* 10.2 (2022): 136.

**A.M. Diks\***, L.A. Overduin\*, L.D. van Leenen, L. Slobbe, H. Jolink, L.G. Visser, J.J.M. van Dongen, M.A. Berkowska. "B-Cell Immunophenotyping to Predict Vaccination Outcome in the Immunocompromised-A Systematic Review." *Frontiers in immunology* (2021): 3524.

H. Pasmans, M.A. Berkowska, **A.M. Diks**, B. de Mooij, R.J. Groenland, L. de Rond, M.A. Nicolaie, S. H. van den Burg, J.J.M. van Dongen, F.R.M. van der Klis, A. Buisman. "Characterization of the early cellular immune response induced by HPV vaccines" *Frontiers in immunology* 13 (2022)

K. van der Pan, S. de Bruin-Versteeg, D. Damasceno, A.H. Delgado, A.J. van der Sluijs-Gelling, W.B.L. van den Bossche, I.F. de Laat, P. Díez, B.A.E. Naber, **A.M. Diks**, M.A. Berkowska, B. de Mooij, R.J. Groenland, F.J. de Bie, I. Khatri, S. Kassem, A.L. de Jager, A. Louis, J. Almeida, J.A.M. van Gaans-van den Brink, A. Barkoff, Q. He, G. Ferwerda, P. Versteegen, G.A.M. Berbers, A. Orfao, J.J. M van Dongen, C. Teodosio "Development of a standardized and validated flow cytometry approach for monitoring of innate myeloid immune cells in human blood." *Frontiers in immunology* (2022): 5141.

## Acknowledgements

---

### Acknowledgements

With these words I reach the final part of my PhD thesis. I am grateful to the great people that I've met these past years and for all those people that supported me in one way or another during this journey. With all the opportunities for collaborative studies in which I have been involved, I am pretty sure that this thesis could have been twice as thick, if I would.

My special thanks goes out to:

Jacques, thank you for providing me the opportunity to do my PhD in your group. Not only have you guided me during this process, but you also created extra opportunities to extend my PhD with additional projects.

Magda, you were the best supervisor I could have wished for. Thank you so much for your help, guidance, patience, no-mercy-word reductions in the manuscripts, the occasional pep talks, and of course the fun moments we had in daily life and during conferences.

Rick & Bas, guys, without your help I would probably still be analyzing FCS files. Please know I am eternally grateful for all your support and the fun in the lab.

Cristina, thanks for all your input during these past years. You have helped me a lot with understanding the innate part of the studies, and I truly enjoyed the talks we had during these past years, both the science related and unrelated ones.

Sandra V, thank you for your help with the Centenarian study and the PERISCOPE studies. Your knowledge, lab skills, and network made experiments easier and more fun.

Indu, thanks for your help with the bioinformatic part of this thesis. I would be completely lost if it weren't for your help.

Gita and Inge, thank you for your help with the Centenarian study. I am not sure how the phagocytosis experiments would have looked without your support and tips about handling of innate cells.

Kyra, Lisanne, and Anniek, it was so nice to be able to share the pros and cons of the PhD trajectory with you. Thank you for those moments.

All other members, students, guest-employees, and veterans of the IMM team: Mihaela, Paula, Bart, Marieke, Nicole, Fenna, Sara, Alita, Sandra B, Alesha, Rosalie, Demi, Jasmina, Laurens, Laura, Safa, Hella, Mirjam, Sandra H, Fadi, Alyssa and Chatelaïne; being part of this team felt natural from the start. When looking back at these past years, my mind fills up with great memories.

## Acknowledgements

---

Hans, Rob, Pauline, Annemarie and Guy: it was simply a pleasure to work with you. Thanks for the nice collaboration and data discussions.

Not to be forgotten are all members of the LUMC Immunology Department, the FCF team, and the PERISCOPE Consortium (especially the Salamanca team). Thank you for your help, feedback, and the fruitful discussions we've had.

Henne, Debbie, Linda, and Susan -actually, everybody on the 100+ team-; Working with you can only be described as a pleasure. I really appreciate the enthusiasm that surrounds the 100+ team members and the great data discussions that we had.

My colleagues from the Hemapheresis Unit/Hematology, especially Jaap Jan, Liesbeth, Linda and Patricia; thank you so much for your efforts for our local pertussis vaccination trial and your professional input. Please know that it was always a pleasure to go upstairs to pick up study samples; your ever-present smiles were a good start of the experiments every time.

Aside from my colleagues, I want to acknowledge my family who supported me during the past 6 years.

Papa & Mary, Mama & Han, Jeroen & Sylvia. Bedankt voor al jullie interesse in dit project de afgelopen jaren, en voor jullie begrip wanneer mijn tijdschema het even niet toeliet was om langs te komen. Bij jullie kom ik thuis.

Kirsten en Relinde, ontzettend bedankt voor alle support de afgelopen jaren.

Patrick, dankjewel. Voor alles. Ik ben benieuwd wat de toekomst ons brengt.



